SCHOLARLY PUBLICATIONS

A CURRENT AWARENESS BULLETIN
OF RESEARCH OUTPUT

@DTU

(28th Edition)

APRIL 2015

BY: CENTRAL LIBRARY

DELHI TECHNOLOGICAL UNIVERSITY
(FORMERLY *DELHI COLLEGE OF ENGINEERING)*
GOVT. OF N.C.T. OF DELHI
SHAHBAD DAULATPUR, MAIN BAWANA ROAD
DELHI 110042

PREFACE

This is the **Twenty Eight** Issue of Current Awareness Bulletin started by Delhi Technological University, Central Library. The aim of the bulletin is to compile, preserve and disseminate information published by the faculty, students and alumni for mutual benefits. The bulletin also aims to propagate the intellectual contribution of Delhi Technological University (DTU) as a whole to the academia.

The bulletin contains information resources available in the internet in the form of articles, reports, presentations published in international journals, websites, etc. by the faculty and students of DTU. The publications of faculty and student which are not covered in this bulletin may be because of the reason that the full text either was not accessible or could not be searched by the search engine used by the library for this purpose.

The learned faculty and students are requested to provide their uncovered publications to the library either through email or in CD, etc to make the bulletin more comprehensive.

This issue contains the information published during **April 2015**. The arrangement of the contents is alphabetical. The full text of the article which is either subscribed by the university or available in the web is provided in this bulletin.

Central Library

CONTENTS

9. Crystal structure and mechanical properties of spark plasma sintered Cu2Se: Anefficient photovoltaicandthermoelectricmaterial, Kriti Tyagi, Bhasker Gahtori, ***3.Sivaiah Bathula, 3.M.Jayasimhadri***, Sakshi Sharma, Niraj Kumar Singh, D. Haranath, A.K. Srivastava and Ajay Dhar, Applied Physics, DTU

10. Day Ahead Load Forecast in ISO New England Market and Ontario Market using a Novel ANN A K Pandey, K B Sahay, D Chandra and ***3.M M Tripathi***, DTU

11. Design and Development of Solar Electric Vehicles at Delhi Technological University, ***3.Rajat Sharma*** and ***3.Dr. J.P. Kesari***, Mechanical Engineering,, DTU

12. Design of all optical logic gates in photonic crystal wave guides ***3.Preeti Rani, 3.Yogita Kalra*** and ***3.R.K. Sinha***, Applied Physics, DTU

13. Design of Current-Mode Sinusoidal Oscillators Using Single FTFN, ***8.1Mukesh Kumr***, Dharam Vir, Dr. Pradeep Dimri, Electronics and Communication, DTU

14. Determining the Water Quality Index of an Urban Water Body Dal Lake, Kashmir, India, ***6.Raj Shailesh Kanakiya***, S.K. Singh, J.N. Sharma, Environmental Engineering, DTU

15. Digital Watermarking of Audio in Time Domain Multiple Bit Plane based on Chaotic Scrambling***, 3.Jeebananda Panda, 8.Indu Kumari*** and ***8.Nitish Goel***, ECE, DTU

16. Effect of different carrier gases and their flow rates on the growth of carbon nanotubes, ***3.Aarti Tewari*** and ***3.Suresh C. Sharma***, Applied Physics, DTU

17. Failure analysis of Magneto rheological Brake, Lijesh K.P. and ***3.Chiranjit Sarkar***, Mechanical, DTU

18. Frictional Characteristics of Brake Pads using Inertia Brake Dynamometer, ***3.Chiranjit Sarkar*** and Harish Hirani, Mechanical, DTU

19. Impact of Temperature Gradient on the Indian Major Carp Catla catla Larvae, ***3.J. G. Sharma***, S. P. Singh, P. Mittal and R. Chakrabarti, Biotechnology, DTU

20. mit-o-matic: A Comprehensive Computational Pipeline for Clinical Evaluation of Mitochondrial Variations from Next-Generation Sequencing Datasets, Sham sudheen Karuthedath Vellarikkal, Heena Dhiman, Kandarp Joshi, ***3.Yasha Hasija***, Sridhar Sivasubbu, and Vinod Scaria, Biotechnology, DTU

21. International Conference On Recent Trends In Engineering Science And Management (CURRENT TRENDS IN DOMESTIC SOLAR WATER HEATING - CPC AN AMICABLE ALTERNATIVE, A PROPOSED DISTINCT DESIGN (from page no. 52 onwards), Jaji Varghese, ***3.Dr.Samsher*** and ***3.Dr.Manjunath.K***, Mechanical Engineering, DTU

22. Shear Behavior of Magnetorheological Fluid and its effect on MR brake performance ***3.Chiranjit Sarkar***, Mechanical Engineering, DTU

23. Software Design and Hardware Realisation of Single Phase to Single Phase Step Down Cycloconverter, Shweta Sethi, Prof. G.K. Jindal and ***3.Prof. Madhusudan Singh***, Electrical Engineering, DTU

24. TARGETED SURVEILLANCE SYSTEM FOR HIGHLY MANEUVERABLE OBJECTS USING FUZZY KALMAN FILTER, ***3.Rajesh Rohilla, 3.Vasundhara Dehiya*** and ***3.Rajiv Kapoor***, Electronics and Communication, DTU

25. The potential of Canna lilyfor wastewater treatment under Indian conditions, ***3.A. K. Haritasha, 3.Ashish Sharma*** and ***3.Kanika Bahela***, Environmental Engineering, DTU

26. Thermo Analysis of Hydrogen Liquefaction System, ***3.Devender Kumar*** and ***3.R. S. Mishra***, Mechanical, DTU

27. Thermodynamic (Exergy-Energy) Analysis of a Low Pressure Kaptiza Claude System for Liquefaction of Gases, ***3.Devender Kumar*** and ***3.R. S. Mishra***, Mechanical, DTU

28. Microalgae as Future Fuel: Real Opportunities and Challenges***, 3.Monica Sharma, 3.Nitin Thukral, 3.Navneet Kaur Soni*** and ***3.Sagar Maji***, Biotechnology and Mechanical, DTU

1. Vice Chancellor	***1.1. Ex Vice Chancellor***
2. Pro Vice Chancellor	***2.1. Ex Pro Vice Chancellor***
3. Faculty	***3.1. Ex Faculty***
4. Teaching-cum-Research Fellow	
5. Alumni	
6. Research Scholar	***6.1. Ex Research Scholar***
7. PG Scholar	***7.1. Ex PG Scholar***
8. Undergraduate Student	***8.1. Ex Undergraduate Student***

ISSN NO. 2320-5407

Journal homepage:http://www.journalijar.com

INTERNATIONAL JOURNAL OF ADVANCED RESEARCH

RESEARCH ARTICLE

Air Quality Assessment: A Statistical Approach to Stationary Air Monitoring Stations

Allaa M. Aenab[1], S. K. Singh[2], Ali Jabir Lafta[3]

1. PhD student, Environmental Engineering Department, Delhi Technological University (DTU), Delhi, India
2. Professor, Environmental Engineering Department, Delhi Technological University (DTU), Delhi, India
3. Manager of Air Quality Monitoring Division, Ministry of Environment, Baghdad, Iraq

Manuscript Info *Abstract*

Manuscript History:

Received: 15 January 2015
Final Accepted: 20 February 2015
Published Online: March 2015

Key words:
Air Quality, Air Pollution, Environmental Monitoring Station, ANOVA two way test, t-test and Baghdad City.

Corresponding Author

Allaa M. Aenab

Air pollution has become an increasingly important environmental issue in Iraq. High levels of suspended particulates have become a common parameter of many regions. Air pollution is a serious environmental health threat to humans. Adverse effects range from nausea, difficulty in breathing and skin irritations, to birth defects, immuno-suppression and cancer. The pollutants for which sampling and analytical techniques discussed are O_3, CO_2 and Temperature. Samples were collected from two stations in Baghdad city for 2 years (2012 & 2013). The study assesses levels and variations of Ozone (O_3), carbon Dioxide (CO_2) and the Temperature, using stationary environmental monitoring stations in Baghdad, Iraq. Analysis of variance (ANOVA) Two way confirmed significant variations in monthly observations. Also, t-test for difference of means as two independent samples showed that except for CO_2 in Al-Andulis air monitoring station all the other air quality parameters do not show significant difference. The study shows a need for constant urban air quality monitoring in Baghdad, Iraq.

INTRODUCTION

The rapid growth of Baghdad city in last years has resulted in significant increase in environmental pollution. Hence, effective and coordinated measures for controlling pollution need to be put in place without delay for the city (Salah, 2011). At the end of the 2003 war, Baghdad's infrastructure was seriously degraded (Allaa et al., 2012 (a)). That of the causes of increased concentrations of heavy metals in the air is the occurrence of dust storms which carry dust storms amounts of dust containing heavy metals from the surface of land passing through, causing high concentrations of total suspended particles and that was mostly exceeding the specific national proposal and thus increasing the concentrations of heavy metals (Allaa et al., 2013). Baghdad's dusty atmosphere is resulting air pollution caused by drought that continued for several seasons (ODD, 2010). Air pollution describes the concentrations that cause damage to humans, plant, animal life, human-made materials and structures. According to US EPA the air pollution and air pollutant are defined (US EPA, 2009). With respect to Urban Air Pollution, the meteorological conditions that effect transport and dispersion take place in the so-called planetary boundary layer (Ekman layer), roughly the lower 1000 m of the atmosphere. Within this layer, wind speed and wind direction are influenced by the roughness of the surface and the vertical height of flows (Seinfeld and Pandis, 1998). The United Nations Environment Programme (UNEP) also says air pollution, resulting from burning oil and aggravated by war, is cause for concern (Allaa et al., 2012 (b)).

Ozone is a highly oxidative compound formed in the lower atmosphere from gases (originating to a large extent from anthropogenic sources) by photochemistry driven by solar radiation. Owing to its highly reactive chemical properties, ozone is harmful to vegetation, materials and human health. In the troposphere, ozone is also an efficient greenhouse gas (WHO, 2008). Ground-level ozone is a public health concern. Prolonged exposure to low-level ozone concentrations is as harmful to human health as exposure to higher levels for shorter durations. It inflames lung tissues

and can cause coughing, chest pains, and asthma. Children are most at risk from exposure to ozone because they play and exercise outdoors during the months ozone concentrations are highest. The elderly are also susceptible (ADEQ, 2013). Most important among these processes is combustion of fossil fuels and biomass which produces carbon dioxide (CO_2), carbon monoxide (CO), nitrogen oxides (NO_x), volatile organic compounds (VOCs), black carbon (BC) aerosols, and sulfur oxides (SO_x, comprised of some sulfate aerosols, but mostly SO_2 gas which subsequently forms white sulfate aerosols) (Ronald et al., 2005).
Surface temperature inversions play a major role in air quality, especially during the winter when these inversions are the strongest. The warm air above cooler air acts like a lid, suppressing vertical mixing and trapping the cooler air at the surface. As pollutants from vehicles, fireplaces, and industry are emitted into the air, the inversion traps these pollutants near the ground, leading to poor air quality (EPA, 1947).

2. Objectives and Approach

The objective of this study is to assess Baghdad's air quality. This comprised an assessment of Baghdad's air pollution levels by O_3, CO_2 and Temperature and evaluates air quality in Baghdad City.

- To evaluate air quality in Baghdad City.
- To assess air pollution in Baghdad City.
- To Define standards or guidelines for allowable concentration of these pollutants, consistent with public health protection.

3. Study area

Baghdad city is located in central of Iraq within the sector of flat sedimentary plain. The borders of the municipality of Baghdad encompass fourteen an administrative unit, eight in Rusafa (east of Tigris river) and six in Karkh (west of Tigris river), and area of the municipality of Baghdad (870 km^2). Advantage of the characteristics of study area is essential extremism great in temperature, few precipitations, few relative humidity and high brightness of the sun. Baghdad population is more than (6 millions) with governmental statistics (Bassim et al., 2010). According to UN figures, around 150 million tons of dust and gas pollutants, various other spread annually in the air, and the transport is the main source of air pollution, where a 40% of all sources of air pollution and this percentage can be up to more than 60% for a city like Baghdad with increase the number of vehicles operating with gasoline and traffic congestion large harmful emissions will result in accumulation to a deterioration is evident in the quality of air, as well as the accumulation of the amount of greenhouse gases that cause global warming, all that damage the ecological balance of the ecosystem, while can be an industrial pollution and emissions resulting from the use of generators for more than 30% (Allaa et al., 2013). The trends of ozone are assumed to be due photochemical ozone production from anthropogenic trace gases and biomass in Iraq and several researchers are investigated (Al-Saadi, 1999) which founded that the concentrations of carbon dioxide are higher than the acceptable levels especially in the industrial regions around Baghdad city, also (Affaj, 2000) studied the distributions of the concentrations of polluted gases such as CO_2 and hydrocarbons and found that the concentrations of these gases are higher than the international and national permission levels.
An additional challenge in Iraq is that electricity demand is seasonal, with the highest peak occurring in the summer months as a result of very high temperatures in much of the country. During the summer, peak hourly electricity demand could be expected to reach levels around 50% above the average demand level, increasing the gap between grid-based electricity supply (operating at capacity) and demand (UN, 2012 & World Bank, 2012). The generation providers from household and shared generator sources are difficult to quantify. Most of these generators are using diesel engines especially the higher power generators. Diesel engines yield relatively considerable levels of hydrocarbons (HCs), carbon monoxide (CO), and volatile organic compounds (VOCs). Diesel engines are relatively high emitters of oxides of nitrogen (NOx) and particulate matter (PM) (Chaichan, 2013). Sanchez reported that non-road heavy-duty engines (primarily diesel engines) accounted for approximately 40% of inhalable ambient particulate (PM_{10}), and 60–80% of fine particulate ($PM_{2.5}$) inventory (Sanchez, 1997).

4. Data procurement

Samples were collected from two stations in central of Baghdad city as shown in Fig. 1, the stations is:

- **Ministry of Transport in Al-Allawi:** It is located under the influence of pollutants from vehicle exhaust due to being at the center of the capital city; also it's so close from the central terminal for passenger inside Baghdad and to other cities out of Baghdad. In this location are measured concentrations of total suspended

particles and concentrations of dust falling.

- **Baghdad Environmental Directorate in A-Andulis Square:** It is location in service and trade area in addition to residential area and a number of other activities. Also the most important sources of pollution here is exhaust of vehicles due to traffic density and the presence of Highway at a distance (800 m) from the monitoring station, which is increasing pressure in the load pollution affecting the quality of ambient air, especially in working days. Located near of the monitoring station the city centre (Bab Al Sharqi) largest area for shopping. Where is measured in total suspended particles and dust falling on this location (Allaa et al., 2013).

5. Methodologies

5.1 Estimation of significant difference by Student's t-test

A *t*-test is any statistical hypothesis test in which the test statistic has a Student's t-distribution if the null hypothesis is true. It is applied when sample sizes are small enough that using an assumption of normality and the associated z-test leads to incorrect inference.

Suppose we want to test if two independent samples x_i (i=1, 2... n_1) and y_j, (j=1, 2… n_2) of sizes n_1 and n_2 have been drawn from two normal populations with means μ_x and μ_y respectively (Allaa et al., 2012 ©; Gupta et al., 2000).

$$t = \frac{x' - y'}{s\sqrt{\frac{1}{n_1} + \frac{1}{n_2}}}$$

Where: $x' = \frac{1}{n_1}\sum_{i=1}^{n} x_i \quad , y' = \frac{1}{n_2}\sum_{j=1}^{n} y_j$

And $S^2 = \frac{1}{n_1 + n_2 - 2}\left[\sum (x_i - x')^2 + \sum (y_j - y')^2\right]$

If

$$|t| \text{ p } t_{0.05, n_1 + n_2 - 2}$$

Then the means do not differ significantly

The student's t-test is performed at 95% significance level. The value of $t_{0.05, n-1}$ is evaluated from the t-distribution tables and then compared with the t value obtained from the formula given above. If $|t| < t_{0.05, n-1,}$ then it is concluded that the two means i.e. the sample mean and the population mean do not differ significantly.

5.2 Estimation of variability by ANOVA – 2 way (space and time)

The ANOVA test is used to test the equality of variances of several normal populations. Let X_{ij} (j=1,2,…,n) be a random sample of size n_i from the normal population N(μ_i, σ_i^2), i=1,2,…,k. We want to test the null hypothesis (Allaa et al., 2012 ©; Gupta et al., 2000):

$H_0 = \sigma 1^2 = \sigma 2^2 = \sigma^2$ (unspecified), with μ_1, μ_2 (unspecified) against the alternative hypothesis:

H1: σ_i^2 (i=1, 2) are not equal; μ_1, μ_2 unspecified

$F = (m(n-1)s_1^2)/(n(m-1)s_2^2)$_ $F(m-1,n-1)$

$F1 = F_{m-1,n-1}(1-\alpha/2)$ and $F2 = F_{m-1,n-1}(\alpha/2)$

If F2<F<F1

Thus the variances do not differ significantly.

6. Results

The student t-test shows in the table (1) for the Al-Andulis air quality monitoring station, except for CO_2 samples all the air quality parameters show no significant differences.
The student t-test shows in the table (2) for the Al-Allawi air quality monitoring station, all the air quality parameters show no significant differences.

The ANOVA test is done for the parameters (O_3, CO_2 and Temperature) for the years 2012 and 2013. For all the cases where F2<F<F1 the variance has consistent values and for any other condition the test fails.

Fig. (1) Baghdad map with air quality monitoring stations.

Table (1) Al-Andulis air quality monitoring (2012-2013)

	2012			2013		
Months	**O_3**	**CO_2**	**Temp.**	**O_3**	**CO_2**	**Temp.**
WHO	**0.08**	**250**	**-**	**0.08**	**250**	**-**
Standard	**PPM in 8-hrs**	**PPM**	**°C**	**PPM in 8-hrs**	**PPM**	**°C**
January	0.01	378	13.9	0.02	401	15.3
February	0.02	399	14.6	0.03	420	15.2
March	0.03	398	17.3	0.03	410	19.1
April	0.04	397	29.6	0.05	405	30.5
May	0.03	398	34.3	0.02	411	35.7
June	0.03	402	37.9	0.04	415	40.2
July	0.04	391	40.6	0.04	408	42.4
August	0.02	394	37.7	0.03	410	42.2
September	0.03	401	36.2	0.04	420	38.7
October	0.02	448	31.3	0.03	460	35.3
November	0.02	447	22.4	0.04	455	25.6
December	0.02	450	17.7	0.03	465	18.5
Mean	0.026	408.583	27.792	0.033	423.333	29.892
Std	0.009	24.777	10.005	0.009	22.869	10.654
t_test	-1.920	-5.936	-0.5	/	/	/
t0.95,22	2.075	2.075	2.075	/	/	/
ltl	$t< t_{0.05,22}$	$t> t_{0.05,22}$	$t< t_{0.05,22}$	/	/	/

Table (2) Al-Allawi air quality monitoring (2012-2013)

	2012			2013		
Months	**O_3**	**CO_2**	**Temp.**	**O_3**	**CO_2**	**Temp.**
WHO	**0.08**	**250**	**-**	**0.08**	**250**	**-**
Standard	**PPM in 8-hrs**	**PPM**	**°C**	**PPM in 8-hrs**	**PPM**	**°C**
January	0.03	450	15.1	0.04	465	14.1
February	0.03	460	16.3	0.03	478	15.3
March	0.05	435	18.4	0.04	450	20.2
April	0.05	445	32.1	0.05	455	32.5
May	0.04	429	36.7	0.04	448	37.4
June	0.04	457	39.3	0.05	464	40.2
July	0.05	459	42.4	0.05	486	48.5
August	0.04	455	41.7	0.04	478	45.3
September	0.05	460	38.5	0.05	468	42.4
October	0.04	478	34.2	0.04	475	35.3
November	0.03	535	25.5	0.05	466	26.3
December	0.04	520	18.9	0.04	476	15.5
Mean	0.041	465.250	29.925	0.043	467.417	31.083
Std	0.008	31.858	10.462	0.007	11.889	12.424
t_test	-0.27	-0.22	-0.25	/	/	/
t0.95,22	2.075	2.075	2.075	/	/	/
ltl	$t< t_{0.05,22}$	$t< t_{0.05,22}$	$t< t_{0.05,22}$	/	/	/

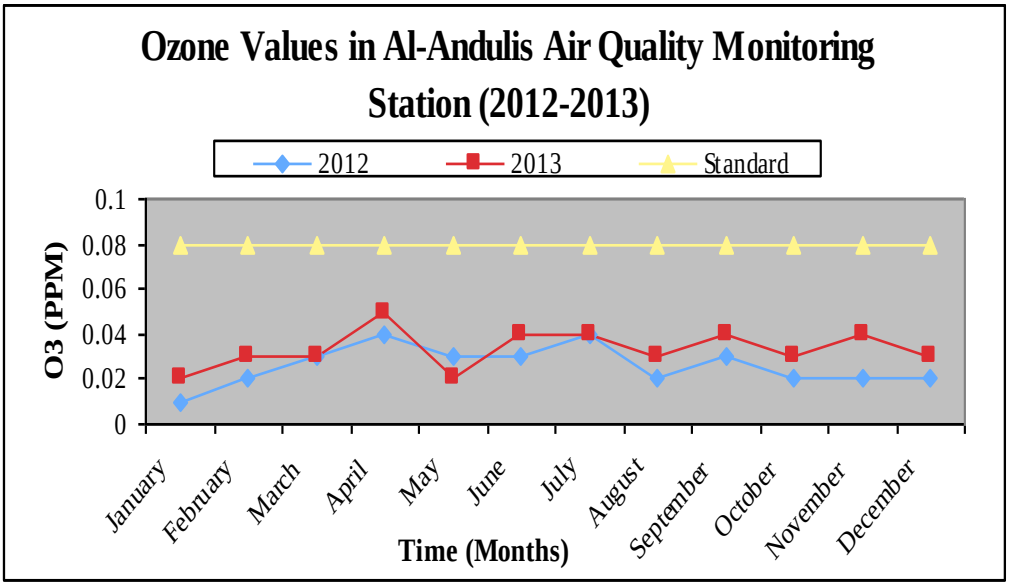

Fig. (2) Ozone values in Al-Andulis air quality monitoring station (2012-2013)

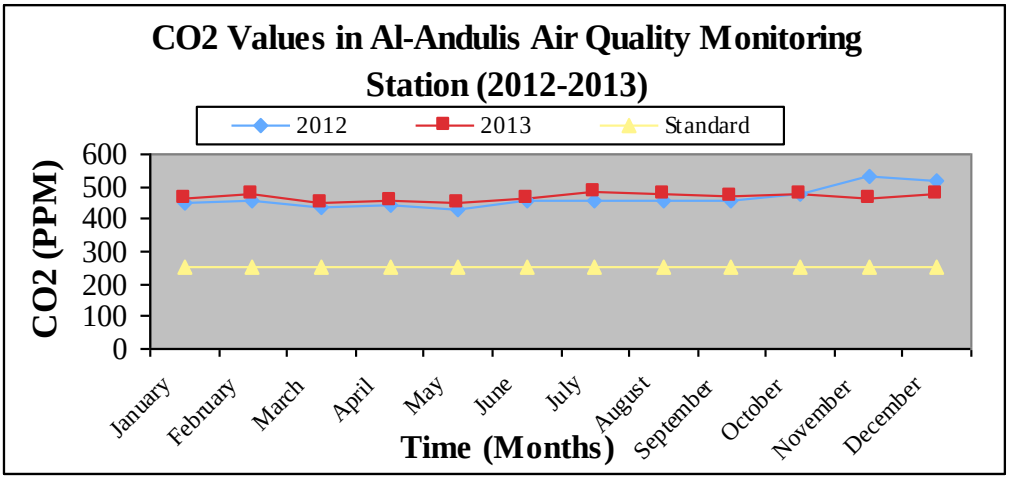

Fig. (3) CO_2 values in Al-Andulis air quality monitoring station (2012-2013)

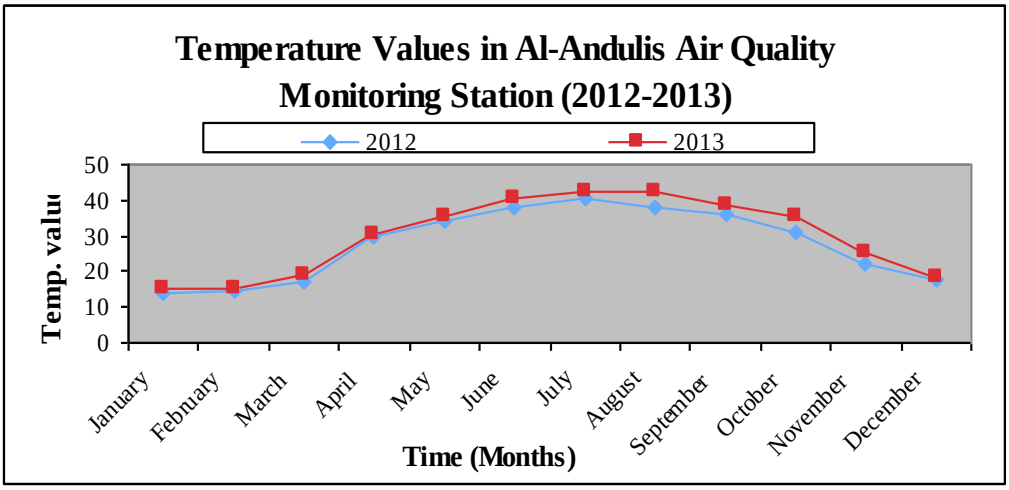

Fig. (4) Temperature values in Al-Andulis air quality monitoring station (2012-2013)

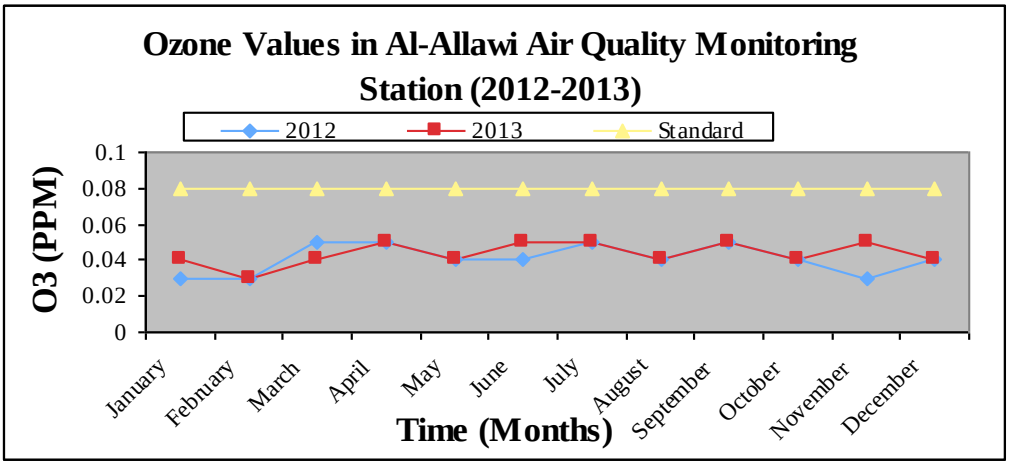

Fig. (5) Ozone values in Al-Allawi air quality monitoring station (2012-2013)

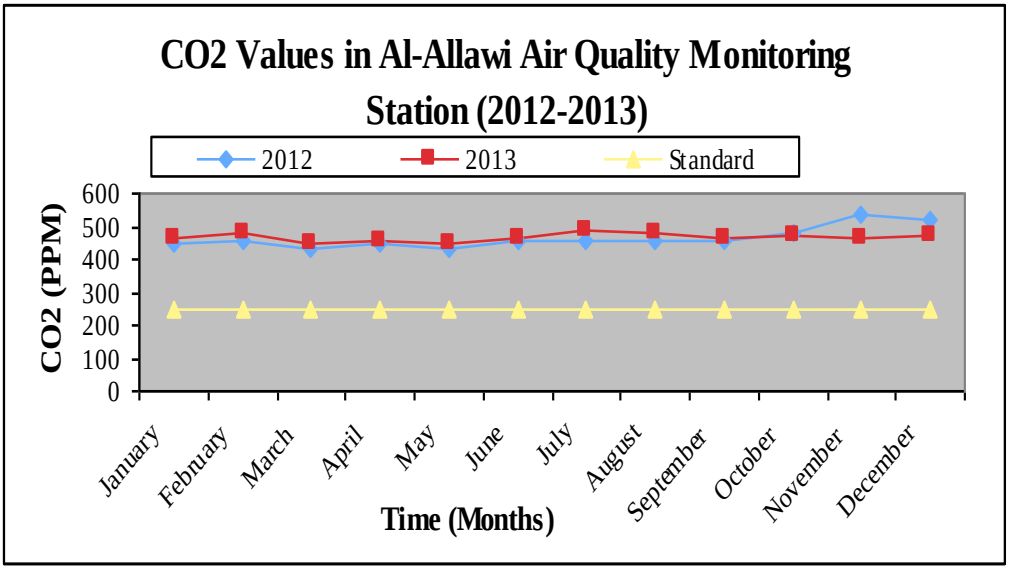

Fig. (6) CO_2 values in Al-Allawi air quality monitoring station (2012-2013)

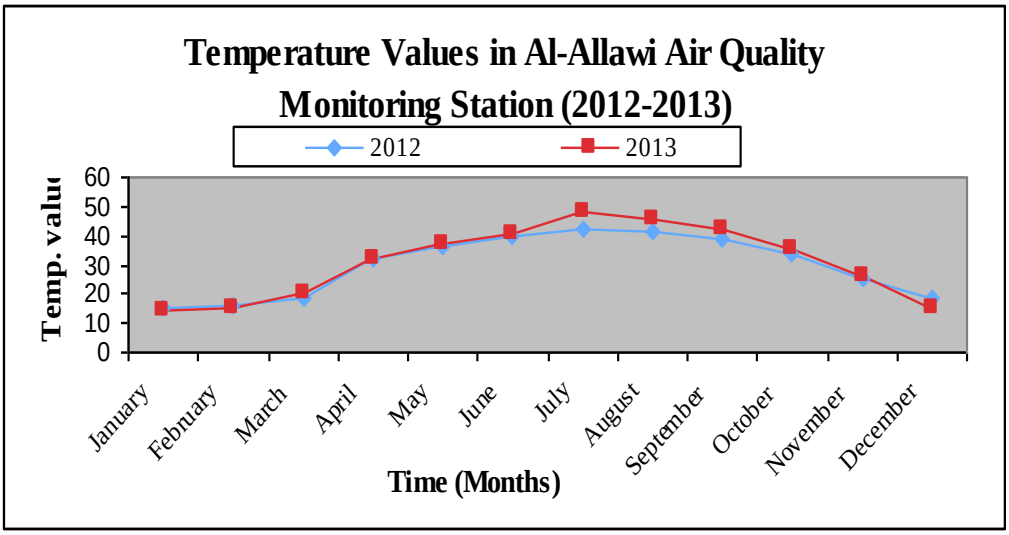

Fig. (7) Temperature values in Al-Allawi air quality monitoring station (2012-2013)

Table (3) ANOVA test for O_3 values for the year 2012

Station	Jan	Feb	Mar	Apr	May	June	July	Aug	Sep	Oct	Nov	Dec	std	Sy	F	F1	F2	
Al-Andulis	0.01	0.02	0.03	0.04	0.03	0.03	0.04	0.02	0.03	0.02	0.02	0.02	0.01	0.0	1.29	2.69	0.37	F2<F< F1
Al-Allawi	0.03	0.03	0.05	0.05	0.04	0.04	0.05	0.04	0.05	0.04	0.03	0.04	0.01	0.0	/	/	/	/
std	0.014	0.007	0.014	0.007	0.007	0.007	0.007	0.014	0.014	0.014	0.007	0.01	/	/	/	/	/	/
Sx	0.000	0.000	0.000	0.000	0.000	0.000	0.000	0.000	0.000	0.000	0.000	0.00	/	/	/	/	/	/
F	4.00	0.25	4.00	1.00	1.00	1.00	0.25	1.00	1.00	4.00	0.25	/	/	/	/	/	/	/
F1	3.825	3.825	3.825	3.825	3.825	3.825	3.825	3.825	3.825	3.825	3.825	/	/	/	/	/	/	/
F2	0.26	0.26	0.26	0.26	0.26	0.26	0.26	0.26	0.26	0.26	0.26	/	/	/	/	/	/	/
	F2<F>F1	F2>F<F1	F2<F>F1	F2<F<F1	F2<F<F1	F2<F<F1	F2>F<F1	F2<F<F1	F2<F<F1	F2<F>F1	F2>F<F1	/	/	/	/	/	/	/

Table (4) ANOVA test for O_3 values for the year 2013

Station	Jan	Feb	Mar	Apr	May	June	July	Aug	Sep	Oct	Nov	Dec	std	Sy	F	F1	F2	
Al-Andulis	0.02	0.03	0.03	0.05	0.02	0.04	0.04	0.03	0.04	0.03	0.04	0.0	0.01	0.0	1.76	2.69	0.37	F2<F<F1
Al-Allawi	0.04	0.05	0.04	0.06	0.04	0.05	0.05	0.04	0.05	0.04	0.05	0.0	0.01	0.0	/	/	/	/
std	0.014	0.014	0.007	0.007	0.014	0.007	0.007	0.007	0.007	0.007	0.007	0.01	/	/	/	/	/	/
Sx	0.00	0.00	0.00	0.00	0.00	0.00	0.00	0.00	0.00	0.00	0.00	0.00	/	/	/	/	/	/
F	1.00	4.00	1.00	0.25	4.00	1.00	1.00	1.00	1.00	1.00	1.00	/	/	/	/	/	/	/
F1	3.825	3.825	3.825	3.825	3.825	3.825	3.825	3.825	3.825	3.825	3.825	/	/	/	/	/	/	/
F2	0.26	0.26	0.26	0.26	0.26	0.26	0.26	0.26	0.26	0.26	0.26	/	/	/	/	/	/	/
	F2<F<F1	F2<F>F1	F2<F<F1	F2>F<F1	F2<F>F1	F2<F<F1	F2<F<F1	F2<F<F1	F2<F<F1	F2<F<F1	F2<F<F1	/	/	/	/	/	/	/

Table (5) ANOVA test for CO_2 values for the year 2012

Station	Jan	Feb	Mar	Apr	May	June	July	Aug	Sep	Oct	Nov	Dec	std	Sy	F	F1	F2	
Al-Andulis	378	399	398	397	398	402	391	394	401	448	447	450	25	670	0.60	2.69	0.37	F2<F<F1
Al-Allawi	450	460	435	445	429	457	459	455	460	478	535	520	32	1107	/	/	/	/
std	50.9	43.1	26.2	33.9	21.9	38.9	48.1	43.1	41.7	21.2	62.2	49.5	/	/	/	/	/	/
Sx	5184	3721	1369	2304	961	3025	4624	3721	3481	900	7744	4900	/	/	/	/	/	/
F	1.39	2.72	0.59	2.40	0.32	0.65	1.24	1.07	3.87	0.12	1.58	/	/	/	/	/	/	/
F1	3.825	3.825	3.825	3.825	3.825	3.825	3.825	3.825	3.825	3.825	3.825	/	/	/	/	/	/	/
F2	0.26	0.26	0.26	0.26	0.26	0.26	0.26	0.26	0.26	0.26	0.26	/	/	/	/	/	/	/
	F2<F<F1	F2<F<F1	F2<F<F1	F2<F<F1	F2<F<F1	F2<F<F1	F2<F<F1	F2<F<F1	F2<F>F1	F2>F<F1	F2<F<F1	/	/	/	/	/	/	/

Table (6) ANOVA test for CO_2 values for the year 2013

Station	Jan	Feb	Mar	Apr	May	June	July	Aug	Sep	Oct	Nov	Dec	std	Sy	F	F1	F2	
Al-Andulis	401	420	410	405	411	415	408	410	420	460	455	465	23	571	3.70	2.69	0.37	F2<F>F1
Al-Allawi	465	478	450	455	448	464	486	478	468	475	466	476	12	154	/	/	/	/
std	45.3	41.0	28.3	35.4	26.2	34.6	55.2	48.1	33.9	10.6	7.8	7.8	/	/	/	/	/	/
Sx	4096	3364	1600	2500	1369	2401	6084	4624	2304	225	121	121	/	/	/	/	/	/
F	1.22	2.10	0.64	1.83	0.57	0.39	1.32	2.01	10.24	1.86	1.00	/	/	/	/	/	/	/
F1	3.825	3.825	3.825	3.825	3.825	3.825	3.825	3.825	3.825	3.825	3.825	/	/	/	/	/	/	/
F2	0.26	0.26	0.26	0.26	0.26	0.26	0.26	0.26	0.26	0.26	0.26	/	/	/	/	/	/	/
	F2<F<F1	F2<F<F1	F2<F<F1	F2<F<F1	F2<F<F1	F2<F<F1	F2<F<F1	F2<F<F1	F2<F>F1	F2<F<F1	F2<F<F1	/	/	/	/	/	/	/

Table (7) ANOVA test for Temperature values for the year 2012

Station	Jan	Feb	Mar	Apr	May	June	July	Aug	Sep	Oct	Nov	Dec	std	Sy	F	F1	F2	
Al-Andulis	13.9	14.6	17.3	29.6	34.3	37.9	40.6	37.7	36.2	31.3	22.4	17.7	10	109	0.91	2.69	0.37	F2<F<F1
Al-Allawi	15.1	16.3	18.4	32.1	36.7	39.3	42.4	41.7	38.5	34.2	25.5	18.9	10	119	/	/	/	/
std	0.85	1.20	0.78	1.77	1.70	0.99	1.27	2.83	1.63	2.05	2.19	0.85	/	/	/	/	/	/
Sx	1.44	2.89	1.21	6.25	5.76	1.96	3.24	16.00	5.29	8.41	9.61	1.44	/	/	/	/	/	/
F	0.50	2.39	0.19	1.09	2.94	0.60	0.20	3.02	0.63	0.88	6.67	/	/	/	/	/	/	/
F1	3.825	3.825	3.825	3.825	3.825	3.825	3.825	3.825	3.825	3.825	3.825	/	/	/	/	/	/	/
F2	0.26	0.26	0.26	0.26	0.26	0.26	0.26	0.26	0.26	0.26	0.26	/	/	/	/	/	/	/
	F2<F<F1	F2<F<F1	F2>F<F1	F2<F<F1	F2<F<F1	F2<F<F1	F2>F<F1	F2<F<F1	F2<F<F1	F2<F<F1	F2<F<F1	/	/	/	/	/	/	/

Table (8) ANOVA test for Temperature values for the year 2013

Station	Jan	Feb	Mar	Apr	May	June	July	Aug	Sep	Oct	Nov	Dec	std	Sy	F	F1	F2	
Al-Andulis	15.3	15.2	19.1	30.5	35.7	40.2	42.4	42.2	38.7	35.3	25.6	18.5	11	124	0.68	2.69	0.37	F2<F<F1
Al-Allawi	14.1	15.3	20.2	32.5	37.4	45.6	48.5	45.3	42.4	37.5	26.3	15.5	13	183	/	/	/	/
std	0.85	0.07	0.78	1.41	1.20	3.82	4.31	2.19	2.62	1.56	0.49	2.12	/	/	/	/	/	/
Sx	1.44	0.01	1.21	4.00	2.89	29.16	37.21	9.61	13.69	4.84	0.49	9.00	/	/	/	/	/	/
F	144	0.01	0.30	1.38	0.10	0.78	3.87	0.70	2.83	9.88	0.05	/	/	/	/	/	/	/
F1	3.825	3.825	3.825	3.825	3.825	3.825	3.825	3.825	3.825	3.825	3.825	/	/	/	/	/	/	/
F2	0.26	0.26	0.26	0.26	0.26	0.26	0.26	0.26	0.26	0.26	0.26	/	/	/	/	/	/	/
	F2<F>F1	F2>F<F1	F2<F<F1	F2<F<F1	F2>F<F1	F2<F<F1	F2<F>F1	F2<F<F1	F2<F<F1	F2<F>F1	F2>F<F1	/	/	/	/	/	/	/

7. Conclusions

The following conclusions have been made based on the study:

- The Ozone (O_3) was with the limits of WHO and Iraqi standards and the student t-test shows in Al-Andulis air quality monitoring station and Al-Allawi air quality monitoring station no significant differences. Also Ozone shows in ANOVA two-way test (space and time) in 2012, except for the months of January, February, March, July, October and November all the other months show consistent values. All the results are consistent with respect to time. In 2013 shows, except for the months of February, April and May all the other months show consistent values. All the results are consistent with respect to time.
- The carbon Dioxide (CO_2) was out of the limits of WHO and Iraqi standards and the student t-test shows in Al-Andulis air quality monitoring station significant differences and Al-Allawi air quality monitoring station no significant differences. In ANOVA two-way test in 2012 shows except for the months of September and October and all the other months show consistent values. All the results are consistent with respect to time. In 2013 shows, except September all the other months show consistent values. The results are inconsistent with respect to time.
- Also after exam the temperature by student t-test shows in Al-Andulis air quality monitoring station and Al-Allawi air quality monitoring station no significant differences. And by ANOVA two way test shows in 2012, except for the months of March and July, all the other months show consistent values. All the results are consistent with respect to time. And in 2013 shows, except for the months of January, February, May, July, October and November, all the other months show consistent values. All the results are consistent with respect to time.

References

1. Salah A. H. Saleh, 2011. Air Quality Over Baghdad City Using Earth Observation And Landsat Thermal Data. Journal of Asian Scientific Research, 1(6), pp.291-298
2. Allaa M. Aenab, S. K. Singh, 2012 (a). Environmental Assessment of Infrastructure Projects of Water Sector in Baghdad, Iraq. Journal of Environmental Protection, 2012, 3, 1-10 doi:10.4236/jep.2012.31001 Published Online January 2012 (http://www.SciRP.org/journal/jep)
3. Allaa M. Aenab, S. K. Singh, 2012 (b). Evaluation of Drinking Water Pollution and Health Effects in Baghdad, Iraq. Journal of Environmental Protection, 2012, 3, 533-537 doi:10.4236/jep.2012.36064 Published Online June 2012 (http://www.SciRP.org/journal/jep)
4. Allaa M. Aenab, S.K. Singh, Ali Jabir Lafta, 2013. Critical assessment of air pollution by ANOVA test and human health effects. Atmospheric Environment 71 (2013) 84-91
5. ODD, 2010. 10 Most Polluted Cities in The World.
6. US EPA (2009): Air pollution definition:
7. Seinfeld, J. H. and Pandis, S. N. (1998): Atmospheric Chemistry and Physics: From Air Pollution to Climate Change. John Wiley and Sons, New York.
8. WHO, 2008. Health risks of ozone from long-range transboundary air pollution. Publications WHO Regional Office for Europe, Scherfigsvej 8, DK-2100 Copenhagen, Denmark. ISBN 978 92 890 42895.
9. ADEQ, 2013, Ozone and Air Pollution, Arizona Department of Environmental Quality 1110 W. Washington Street Phoenix, AZ 85007 (602) 771-2300
10. Ronald G. Prinn, John Reilly, Marcus Sarofim, Chien Wang and Benjamin Felzer, 2005. Effects of Air Pollution Control on Climate. MIT Joint Program on the Science and Policy of Global Change. Report No. 118 January 2005.
11. EPA, 1947. Temperature Inversions Impact Air Quality. EPA courtesy of Yolo-Solano Air Quality Management District 1947 Galileo Court, Suite 103 Davis, CA 95616
12. Bassim Mohammed Hashim, Dr.Maitham Abdullah Sultan, 2010. Using remote sensing data and GIS to evaluate air pollution and their relationship with land cover and land use to Baghdad city. The 1st International Applied Geological Congress, Department of Geology, Islamic Azad University Mashhad Branch, Iran, 26-28 April 2010.
13. AL-Saadi A.N. Air pollution at Baghdad city by carbon monoxide. M.Sc thesis, college of science, Baghdad university,1999.
14. Afaaj A.H. Study of air pollution at Bayje city, environmental researches office, Iraqi Organization of Atomic Energy, Tech report, 2000.
15. UN, 2012. Inter-Agency Information and Analysis Unit, Landmines and unexploded ordnances factsheet in

Iraq, United Nations, New York, 2012.
16. World Bank, 2012. Doing Business 2012: Doing business in a more transparent world, World Bank, Washington, DC, 2012.
17. Diaz-Sanchez D, The role of diesel exhaust particles and their associated poly-aromatic hydrocarbons in the induction of allergic airway disease, Allergy, vol. 52, pp: 52–56, 1997.
18. Allaa M. Aenab, S. K. Singh, 2012©. Critical Assessment of Environmental Quality of Baghdad, Iraq. Journal of Environmental Engineering, Vol. 138, No. 5, May 1, 2012. ©ASCE, ISSN 0733-9372/2012/5-0–0/$25.00.
19. Gupta S. and Kapoor V., 2000. Fundamentals of Mathematical Statistics. Tenth revised edition :August 2000.

2015 IEEE International Conference on Computational Intelligence & Communication Technology

Analysis of Memristor Behavior in presence of Harmonics

Ramanpreet Singh Chhina
Electrical Department
Delhi Technological University
Delhi
rpschhina@gmail.com

***Abstract*—Memristor is the fourth basic passive circuit element after resistor, capacitor and inductor. It was proposed in 1971 by Leon Chua using symmetry arguments but was clearly experimentally demonstrated in 2008. Since then a number of models for the device have been proposed, this paper reviews two of these models namely Numerical Model and Fully Symbolic Homotopy based Model. Further, these two models are used to analyze the behavior of Memristor in presence of voltage and current time harmonics in addition to the fundamental component.**

***Index Terms*—Memristor, Mathematical Modelling** *(key words)*

INTRODUCTION

Memristor is the fourth basic passive circuit element, it was proposed by Leon Chua in 1971[1]. Each one the existing passive circuit elements i.e. R,L and C link two out of the four basic circuit variables i.e. V, I, Q and Φ. Where
V - Voltage, I – Current, Q- Charge and Φ - Flux.
So, a hypothetical device was formulated relating the only remaining pair of charge and flux. Researchers at HP labs realized an actual physical memristor in 2008[2].

Memristor realized by HP is represented by two coupled variable resistors having resistances

$$R_{ON}\,{}^{w}/_{D} \text{ And } R_{OFF}\left(1-{}^{w}/_{D}\right)$$

Where w is function of current

$$w(t) = \mu_V\,{}^{R_{ON}}/_{D}\int_0^t i(\tau)\,d\tau \qquad (1)$$

So it's total resistance or as it called memristance is given by

$$M(t) = R_{ON}\,{}^{w(t)}/_{D} + R_{OFF}\left(1-{}^{w(t)}/_{D}\right) \qquad (2)$$

Solving these two equations, a mathematical model of memristor is developed. Numerical model is obtained by solving simply the two equation. Solution by Homotopy Method leads to a fully symbolic model.

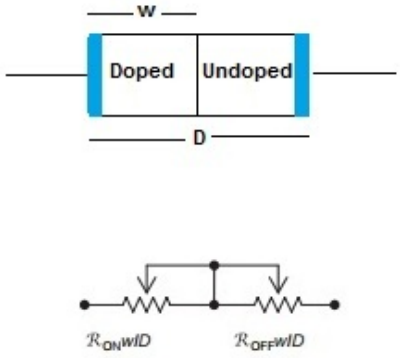

Fig.1 Coupled variable Resistor Model

NUMERICAL MODEL

Width w(t) of the doped material is determined by the quantity of current flown. It can be expressed as the function of charge as

$$w(t) = \mu_V\,{}^{R_{ON}}/_{D}\,q(t) + w_0 \qquad (3)$$

Where w_0 is the width of the doped material at time zero.

Solving eqns. (2) and (3) Memristance can be written as a function charge q as

$$M(q) = M_0 - \left({}^{\mu R_{ON} R_D}/_{D^2}\right)q(t) \qquad (4)$$

Where

$$M_0 = R_{ON}\,{}^{w_0}/_{D} + R_{OFF}\left(1-{}^{w_0}/_{D}\right) \qquad (5)$$

978-1-4799-6023-1/15 $31.00 © 2015 IEEE
DOI 10.1109/CICT.2015.70

Memristance as a function of flux is

$$M^2 = {M_0}^2 - \left({}^{2\mu R_{ON} R_D}/_{D^2}\right)\varphi(t) \qquad (6)$$

M is bounded by R_{ON} and R_{OFF}, i.e.

$$M \in (R_{ON}, R_{OFF})$$

And

$$\varphi(t) = \int_0^t v(\tau)d(\tau) \qquad (7)$$

Using eqns. (6) and (7), Memristor response for any voltage signal can be analyzed. So, this provides as a complete mathematical model for Memristor.

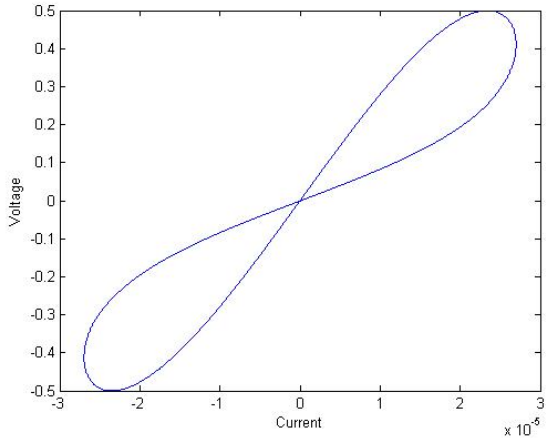

Fig.2 IV characteristics of Memristor obtained by simulating the Numerical Model in MATLAB

FULLY SYMBOLIC MODEL

A model for memristor was obtained by solving the differential equation, governing the physical functioning of the device, by using a homotopy formulation in [3].

Homotopy Perturbation Method was used to obtain a model of memristor when only a sinusoidal current signal is applied and it resulted in a form [3]

$$M = (\alpha - 1)\left(\begin{array}{l} \left[\begin{array}{c} -\frac{3}{4}\left(\frac{\mu {A_p}^2 a_1}{D^2\omega}\right)^2 X_0(5{X_0}^2-1)(X_0-1)^3(X_0+1)^3 R_{ON}^3 \\ -\left(\frac{\mu A_p a_1}{D^2\omega}\right)X_0(X_0-1)^2(X_0+1)^2 R_{ON}^2 \\ +X_0\frac{[1+(X_0^{-1}-1)\alpha]}{(\alpha-1)}R_{ON} \end{array}\right] \\ +\left[\begin{array}{c} \left(\frac{\mu {A_p}^2 a_1}{D^2\omega}\right)^2 X_0(5X_0^2-1)(X_0-1)^3(X_0+1)^3 R_{ON}^3 \\ +\left(\frac{\mu A_p a_1}{D^2\omega}\right)X_0(X_0-1)^2(X_0+1)^2 R_{ON}^2 \end{array}\right]\cos(\omega t) \\ +\left[\frac{1}{4}\left(\frac{\mu {A_p}^2 a_1}{D^2\omega}\right)^2 X_0(5{X_0}^2-1)(X_0-1)^3(X_0+1)^3 R_{ON}^3\right]\cos(2\omega t) \end{array}\right)$$

With this as basis in the next section a model is developed where current signal can take any general form and a mathematical expression is provided for w(t) derived using HPM method for a case where an Additional component is present along with the fundamental one.

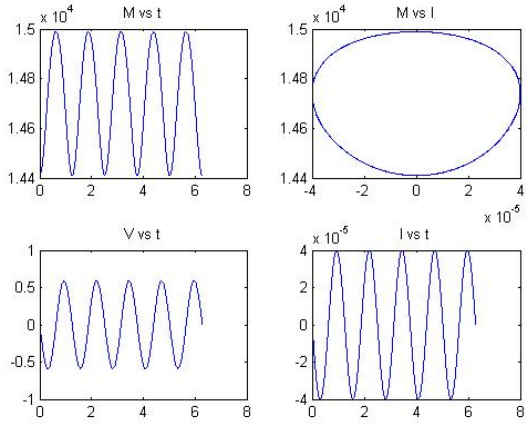

Fig.3 The various plots obtained by simulating the Fully Symbolic Homotopy based Model in MATLAB.

BEHAVIOR IN PRESENCE OF HARMONICS

In this section the response of memristor is studied in presence of time harmonics, additional to the fundamental voltage and current components. Simulation experiments were independently carried on the two models using MATLAB.

For Current Harmonics Fully Symbolic Homotopy Based Model was used.

In general terms w(t) obtained from Fully Symbolic Model can be written as

$$w(t) = A + B\int_0^t i(\tau)d\tau + C\int_0^t i(\tau)\theta(\tau)d\tau \qquad \ldots(8)$$

Where

$$A = X_0$$
$$B = -\delta X_0(X_0-1)^2(X_0+1)^2$$
$$C = \delta^2 X_0(5{X_0}^2-1)(X_0-1)^3(X_0+1)^3$$

And

$$\theta(t) = \int_0^t i(\tau)d\tau \qquad (9)$$

So for two components let

$$i(t) = A_{p1}sin\omega t + A_{p2}sin2\omega t$$

$$\theta(t) = \frac{1}{\omega}\left(A_{p1}cos\omega t + \frac{A_{p2}}{2}cos2\omega t - (A_{p1} + \frac{A_{p2}}{2})\right)$$

$$\int_0^t i(\tau)\theta(\tau)d\tau = \frac{1}{\omega^2}\left(\frac{{A_{p2}}^2}{8}(cos4\omega t - 1) + \frac{A_{p1}A_{p2}}{4}(cos3\omega t - 1) + \frac{1}{2}\left(\frac{{A_{p1}}^2}{2} - \frac{{A_{p2}}^2}{2} - A_{p1}A_{p2}\right)(cos2\omega t - 1) - \left({A_{p1}}^2 + \frac{A_{p1}A_{p2}}{4}\right)(cos\omega t - 1)\right) \quad (10)$$

The highest frequency term is four times the fundamental component. If there are n components then the highest frequency term will be 2n times the fundamental.

For more than two components analysis using Homotopy based method becomes very cumbersome and time consuming. So, simulations were carried out for current signal having only two components. R_{ON}=100Ω, a=160,X_0=0.1,D=10^{-8}m, μ=$10^{-10}$$cm^2s^{-1}V^{-1}$

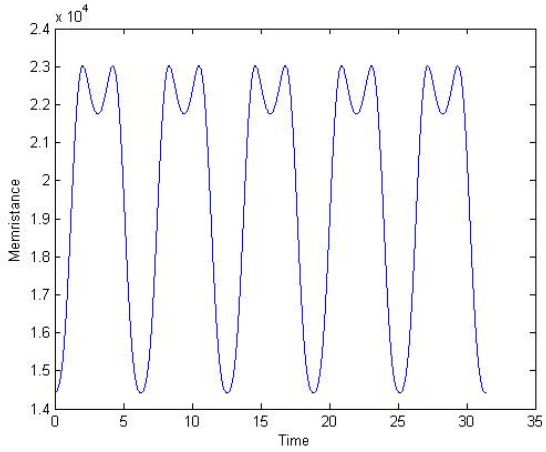

Fig.4 Memristance as a function of time when one additional harmonic is present

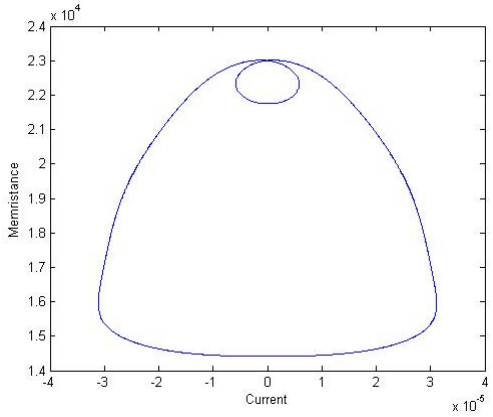

Fig.5 Current Vs Memristance

Using Numerical Model the memristor behavior was studied when only Voltage harmonics are present. This expression is presented for the first time in this paper.

$${M_{eff}}^2 = M^2 + {M_1}^2 - {X_0}^2 \quad (11)$$

Where

M is the resistance at time t when only Fundamental component is applied.

M1 is the resistance at time t when only first harmonic is applied.

M_{eff} is the resistance at time t when both fundamental and first harmonic are applied simultaneously.

For in general

$${M(t)_{eff}}^2 = M(t)^2 + M_1(t)^2 + M_2(t)^2 \dots\dots\dots M_n(t)^2 - n{X_0}^2 \quad (12)$$

Where M_n is the resistance when only nth harmonic is applied.

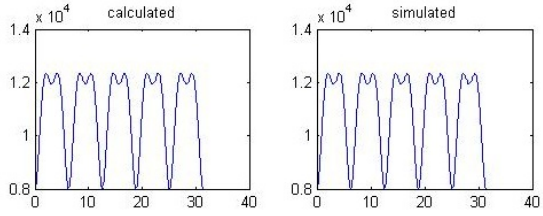

Fig.6 Calculated and simulated values of Memristance vs time

The figure shows the agreement between the values calculated from the above presented relation and the values from simulation model

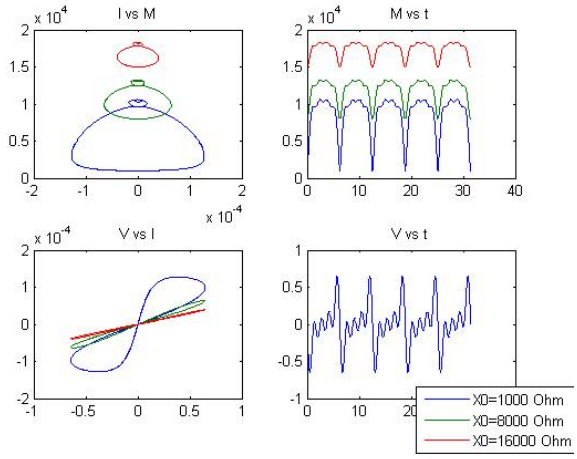

Fig.6 Various plots using Numerical Model

Various plots for voltage signal having fundamental component of frequency ω and three additional harmonics with same amplitude but frequencies as 2ω, 3ω and 4ω respectively were obtained from simulation and are presented here.

CONCLUSION

In presence of additional Harmonics the behavior of the device becomes complicated and it becomes difficult to predict the response due to nonlinear variations in memristance with respect to voltage and frequency. Usage of Fully Symbolic Model was extended from simple sinusoidal source to more complex sources.

REFERENCES

[1] ," Chua, L.O., "Memristor-The missing circuit element" , *Circuit Theory, IEEE Transactions on* , vol.18, no.5, pp.507,519, Sep 1971

[2] DB Strukov, GS Snider, DR Stewart, RS Williams.,"The missing memristor found" , Nature, vol. 453 pp. 80-83,April 2008

[3] Sarmiento-Reyes, A; Hernandez-Martinez, L.; Hernandez Mejia, C.; Diaz Arango, G.U.; Vazquez-Leal, H., "A fully symbolic homotopy-based memristor model for applications to circuit simulation", Circuits and Systems (LASCAS), 2014 IEEE 5th Latin American Symposium on , vol., no., pp.1,4, 25-28 Feb. 2014

[4] Raja, T.; Mourad, S., "Digital Logic Implementation in Memristor-Based Crossbars - A Tutorial", *Electronic Design, Test and Application, 2010. DELTA '10. Fifth IEEE International Symposium on* , vol., no., pp.303,309, 13-15 Jan. 2010

[5] Radwan, AG.; Zidan, M.A; Salama, K.N., "On the mathematical modeling of memristors", Microelectronics (ICM), 2010 International Conference on , vol., no., pp.284,287, 19-22 Dec. 2010

APPLICATION OF FUZZY BASED METHODOLOGY IN SELECTION OF VEHICLE ACCORDING TO FUEL TYPE

Kiran Pal[1] ,Surendra Tyagi[2], Manish Jain[3]
[1]Assistant Professor, Department of Mathematics, Delhi Institute of Tool Engineering, Delhi,
[2]Research Scholar, Department of Computer Science, Delhi Technological University, Delhi,
[3]Department of Mechanical Engineering,RJIT, BSF Academy, Takenpur, Gwalior, India
Email: kiranpaldite@gmail.com, surendratyagi2000@gmail.com, manish_jn@rediffmail.com

Abstract: Number of Private vehicles in India is growing very rapidly. Poor public transportation system in most of the urban cities has enforced many middle class to switch to own a vehicle for their daily commuting of family commuting. This paper is an attempt to choose suitable vehicle according to fuel type using fuzzy based methodology. Time is changing rapidly; climatic condition due to vehicular pollution is going to worst. So in addition to economy a number of other important factors should be considered at the time of buying vehicle. Using the proposed methodology a new customer can easily choose a proper fuel type for his individual requirement.

Index term: Fuzzy, Hybrid, Petrol, Fuel, Diesel

I. INTRODUCTION

Our fossil fuel sources are limited and depleting quickly. Petrol and diesel will eventually get all used up. Atop this are concerns regarding burning exhaust gases and particulate matter from vehicles adding to air pollution. Considering all these factors, the recent focus has shifted towards the use of alternative fuel sources for mobility. India still falls short in terms of awareness though. A number of options are at hand, Electric Vehicles, Hybrid technology and Hydrogen fuel cells. Hydrogen fuel cell powered vehicles are the most sensible source, but unfortunately it will take years to install the infrastructure in place. Hybrids and electric cars are the only clever option, however due to the complexities of engine construction they cost a fortune [1]

II. CONCEPT OF FUZZY LOGIC

Fuzzy logic has rapidly become one of the most successful of today's technologies for complex decision making applications. The reason for which is very simple. Fuzzy logic addresses such applications perfectly as it resembles human decision making with an ability to generate precise solutions from certain or approximate information. While other approaches require accurate equations to model real-world behaviors, fuzzy design can accommodate the ambiguities of real-world in human language and logic. Although genetic algorithms and neural networks can perform just as well as fuzzy logic in many cases, fuzzy logic has the advantage that the solution to the problem can be cast in terms that human operators can understand, so that their experience can be used in the design of the controller. This makes it easier to mechanize tasks that are otherwise already successfully performed by humans. [2]
In a broad sense, fuzzy logic refers to fuzzy sets - a set with unclear boundaries. Examples of fuzzy sets are “hot,” “tall,” “medium,” etc. In a narrow sense, fuzzy logic is a logical system that aims to formalize approximate reasoning .In fuzzy logic a fuzzy symbol can take any truth

values from the closed set [0, 1] of real numbers thus generalizing the Boolean truth values. As the technology was further embraced, fuzzy logic was used in more useful applications.

III. FUZZY SETS BACKGROUND

The precision of mathematics owes its success in large part to the efforts of Aristotle and the philosophers who preceded him. In their efforts to devise a concise theory of logic, and later mathematics, the so-called "Laws of Thought" were posited. One of these, the "Law of the Excluded Middle," states that every proposition must either be True or False. Even when, Parmenides proposed the first version of this law around 400 B.C.E. There were strong and immediate objections: for example, Heraclitus proposed that things could be simultaneously, True and not True. It was Plato who laid the foundation for what would become fuzzy logic, indicating that there was a third region (beyond True and False) where these opposites "tumbled about." Other, more modern philosophers echoed his sentiments, notably Hegel, Marx, and Engels.[3] But it was Lukasiewicz who first proposed a systematic alternative to the bi-valued logic of Aristotle.

In the early 1900's, Lukasiewicz described a three-valued logic, along with the mathematics to accompany it. The third value he proposed can best be translated as the term "possible" and he assigned it a numeric value between True and False. Eventually, he proposed an entire notation and axiomatic system from which he hoped to derive modern mathematics. Later, he explored four-valued logics, five-valued logics, and then declared that in principle there was nothing to prevent the derivation of an infinite-valued logic.

Lukasiewicz felt that three- and infinite-valued logics were the most intriguing, but he ultimately settled on a four-valued logic because it seemed to be the most easily adaptable to Aristotelian logic.

IV. FUZZY BRIEFS

The mechanisms which make fuzzy logic machines work, it is important to realize what fuzzy logic actually is. Fuzzy logic is a superset of conventional (Boolean) logic that has been extended to handle the concept of partial truth-truth values between "completely true" and "completely false". As its name suggests, it is the logic underlying modes of reasoning which are approximate rather than exact. The importance of fuzzy logic derives from the fact that most modes of human reasoning and especially common sense reasoning are approximate in nature.The essential characteristics of fuzzy logic are as follows.

Knuth proposed a three-valued logic similar to Lukasiewicz's, from which he speculated that mathematics would become even more elegant than in traditional bi-valued logic.[4] His insight, apparently missed by Lukasiewicz, was to use the integral range 12alternative failed to gain acceptance, and has passed into relative obscurity. It was not until relatively recently that the notion of an infinite-valued logic took hold. In 1965 Lotfi A. Zadeh published his seminal work "Fuzzy Sets" which described the mathematics of fuzzy set theory, and by extension fuzzy logic [5] This theory proposed making the membership function (or the values False and True) operate over the range of real numbers [0.0, 1.0]. New operations for the calculus of logic were proposed, and showed to be in principle at least a generalization of classic logic. It is this theory which we will now discuss.

- In fuzzy logic, exact reasoning is viewed as a limiting case of approximate reasoning.
- In fuzzy logic everything is a matter of degree.
- Any logical system can be fuzzified
- In fuzzy logic, knowledge is interpreted as a collection of elastic or, equivalently, fuzzy constraint on a collection of variables.
- Inference is viewed as a process of propagation of elastic constraints.

The third statement hence, defines Boolean logic as a subset of Fuzzy logic.

V. FUZZY SETS THEORY

Fuzzy Set Theory was formalised by Professor Lofti Zadeh at the University of California in 1965. [6] What Zadeh proposed is very much a paradigm shift that first gained acceptance in the Far East and its successful application has ensured its adoption around the world. A paradigm is a set of rules and regulations which

defines boundaries and tells us what to do to be successful in solving problems within these boundaries. For example the use of transistors instead of vacuum tubes is a paradigm shift - likewise the development of Fuzzy Set Theory from conventional bivalent set theory is a paradigm shift. Bivalent Set Theory can be somewhat limiting if we wish to describe a 'humanistic' problem mathematically

VI. SELETION OF VEHICLE BASED ON FUELTYPE

To buy a vehicle is an important time to general person. He should keep each and every fact in mind. Present day demand of petrol and gas cars is increasing and demand of diesel car is going to decrease because of likely same prices of diesel and petrol. [6] Figure 1 and 2 shows the comparisons of diesel and petrol vehicles market share. And it is clear from these figures but there are many factors which affect the choice for a vehicle according to fuel type. These factors are discussed in table 1 and 2.These factors may be suitably modified according to their applicability in a particular situation

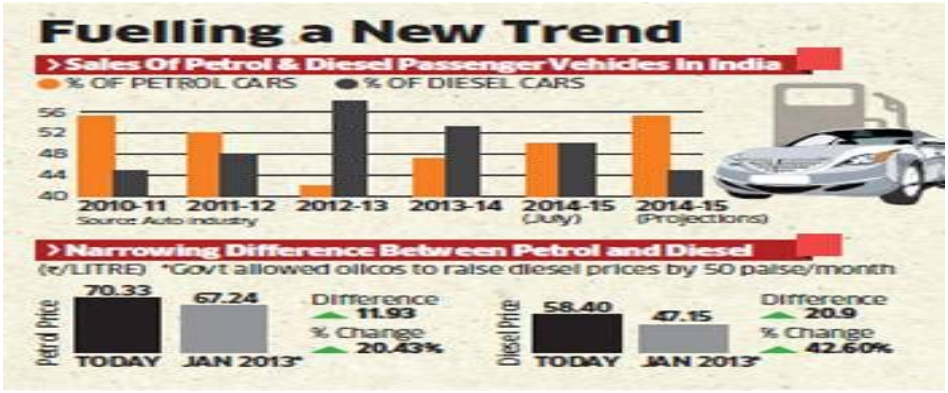

Figure 1: Sales trend of Petrol and diesel cars [7]

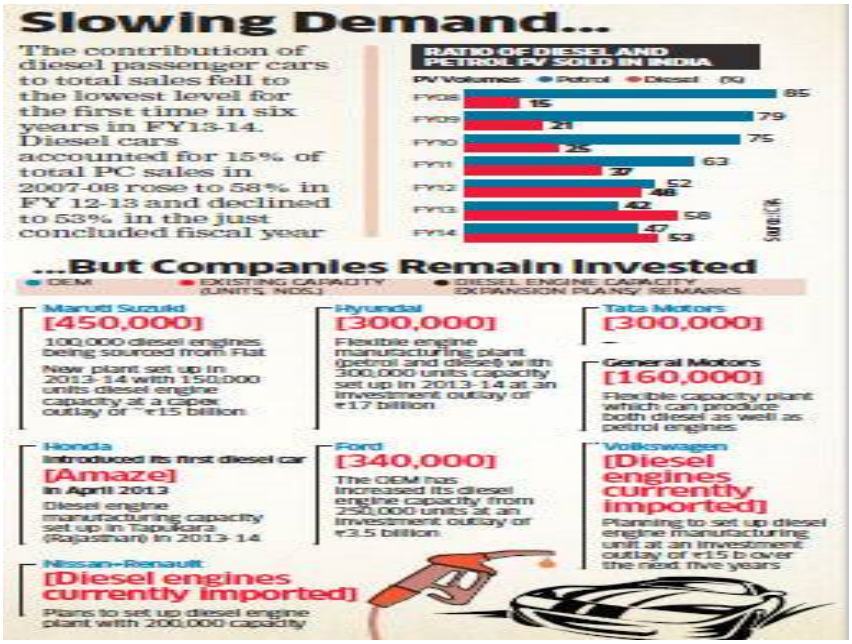

Figure 2: Reduction of the demand of Diesel Cars in India [8]

VII. SELECTION CRITERIA:

Selection of vehicle for a person is an important factor. In this paper, there are following 7 representative factors have been considered, though nit can be modified to incorporate any other factor.

1. Price
2. Environment Impact
3. Availability of fuel
4. Daily Running requirement
5. Load
6. Climate condition
7. Maintenance

Price: if a person does not have money, he cannot arrange his requirements but has to manage all things for his family in limited resources. In case of buying vehicle, he has to see all the aspects related to money and post expenses in fuel so price of fuel is important factor for a person who is buying vehicle.

Environment Impact: To keep clean environment is our responsibility. We should keep in mind this factor, when we do any work. So Environment Impact factor is also important in present scenario while pollution has become more discussion issue.

Availability of fuel: Friends indeed, friends in need, whether a fuel why not a so good but this is not available, it is meaningless for us. So we have to choose that fuel which is easily available.

Daily Running requirement: A person travel daily from one place to other, his requirement depends on this.

Load: According his purpose, vehicle has to bear that load.

Climate condition: Temperature, pressure, road condition are also factor , which has to keep in mind while buying vehicle.

Maintenance: To buy a vehicle is easy but, it is very difficult of its maintenance.

Table 1:Fuel Selection criteria and respective weight factors

S. No.	Selection factor	Notation	Weight factor	Person's Rating	Weighted rating
1	Price	P	W_1	R_1	$W_1 * R_1$
2	Environment Impact	E	W_2	R_2	$W_2 * R_2$
3	Availability of fuel	A	W_3	R_3	$W_3 * R_3$
4	Daily Running requirement	R	W_4	R_4	$W_4 * R_4$
5	Load	L	W_5	R_5	$W_5 * R_5$
6	Climatic condition	C	W_6	R_6	$W_6 * R_6$
7	Maintenance	M	W_7	R_7	$W_7 * R_7$
	Total weightage		$\sum Wi$	$\sum Ri$	$\sum Ri * Wi$

$$Membeship\ value = \sum(Ri * Wi)/(\sum Wi * Rmax)$$

Illustrative example

Table 2: *Illustrative example*

			S.I.(Petrol & CNG)		C.I.(Diesel)		EL(SOLAR & HYBRID)	
S. No.	Selection factor	Weight factor	Person's Rating for C1	Weighted rating C1	Person's Rating for C2	Weighted rating C2	Person's Rating for C3	Weighted rating C3
1	Price	***0.55***	***6***	***3.3***	***8***	***4.4***	***9***	***4.95***

2	Environment Impact	***0.9***	***6***	***5.4***	***5***	***4.5***	***9***	***8.1***
3	Availability of fuel	***0.7***	***7***	***4.9***	***7***	***4.9***	***5***	***3.5***
4	Daily Running requirement	***0.85***	***6***	***5.1***	***8***	***6.8***	***4***	***3.4***
5	Load	***0.75***	***7***	***5.25***	***8***	***6***	***4***	***3***
6	Climatic condition	***0.7***	***6***	***4.2***	***4***	***2.8***	***7***	***4.9***
7	Maintenance	***0.5***	***7***	***3.5***	***9***	***4.5***	***8***	***4***
	Total	4.95		***31.65***		***33.9***		***31.85***
	Membership value		0.639394		0.684848		0.643434	

VIII. CONCLUSION:

Selection of the fuel type for the vehicle is a very complex problem for the first time vehicle buyers. Present fuzzy based approach is an attempt to help the vehicle buyer in the selection of type of fuel , It takes care of the environmental, availability of the fuel, climatic factors etc. Thus it is a suitable method for this problem.

IX. REFERENCES:

[1] http://www.business-standard.com/article/news-cd/union-budget-why-should-electric-and-hybrid-cars-get-more-subsidies-114070801032_1.html

[2] http://www.dortmundintelligence.com/index.php/technology_ci_fuzzy_systems.html

[3] Fukumi S., Mizurnoto M., Tanaka K., **Some considerations of fuzzy conditional inference,** Fuzzy Sets and Systems, 4 (1980), pp. 243–273

[4] Zadeh, L.A. (1971), "Similarity relations and fuzzy ordering", Information Sciences, 3, 177--200.

[5] Zadeh, L.A. (1965), "Fuzzy sets", Information and control, 8, 338--353.

[6] http://articles.economictimes.indiatimes.com/2014-08-20/news/53029171_1_petrol-cars-petrol-models-two-fuels

[7] http://articles.economictimes.indiatimes.com/2014-07-05/news/51092090_1_diesel-vehicles-diesel-engines-new-diesel-plant

[8] http://www.moneycontrol.com/news/business/buyingcar-why-petrol-vehicles-make-more-economic-sense_1180157.html.

International Journal of Software Engineering and Its Applications
Vol. 9, No. 3 (2015), pp. 29-40
http://dx.doi.org/10.14257/ijseia.2015.9.3.04

Applying Machine learning for configuring Agile Methods

Rinky Dwivedi and Daya Gupta

Delhi Technological University, New Delhi, INDIA
rinkydwivedi@gmail.com, daya_gupta2006@yahoo.in

Abstract

Situational method for satisfying organisation configuration definitions has become an important activity for many modern organisations. In the last few decades many situational method models have been developed but no model has proved to be successful at effectively deliver the customized light-weight methods fulfilling the organisation requirements. The paper introduces an Agile Method engineering approach to find the degree of suitability of agile methods for a particular situation. The introduced process uses associative clustering for finding the cluster of appropriate methods against the organisational requirements-in-hand. The specially designed fuzzy logic controller is used to extract the most appropriate methods from the cluster of appropriate methods. Fuzzy logic controller works in coordination with the databases that have been formed using the previous results and is being trained with the new knowledge. Finally two practical case studies have been discussed to describe how these concepts are applied in practice with industry specified requirements and results are being explored.

Keywords- *Agile methods, method configuration, situational method for current organisational requirement*

1. Introduction

Agile methods for software development emerged in mid 1990s [3], they intend to improve the software quality and responsiveness to changing customer requirements. Twelve golden principles have been defined in an agile alliance meeting conducted in 2001[4]. These principles provide support for the software development however; there is no guidance about how to configure agile methods for the situation-in-hand [19, 20]. This extends a need to develop a configuration process for agile methods that supports to select some practices of different agile methods for the current organisational requirements.

Method Engineering (ME) is a related stream of research that has been focused on tailoring of software development methods to the actual need of development context. ME has proved to be benefited for number of projects [14, 15]. In the present research we focus to introduce a Agile Method Engineering(AME) process to form situation specific agile method, the method thus formed is a blend of more than one configured method assembled together to form the desired method that fulfils the current organisation requirement.

AME process supports an Essentiality attribute for agile methods; this essentiality attribute can take two values either essential or variable. A similar type of proposal for traditional methods had been put forward in [9, 10] the proposal contained in that paper is static in nature (*i.e.*, the methods stored in the method base are in the form of pre-made method configurations). Whereas, for agile methods, there is a requirement of a dynamic approach to configure (*i.e.*, the essentialities within the method are decided dynamically for every organisational requirement) [11-13].

Given the above, we were interested in investigating the use and tailoring of agile methods in actual practice. Specifically, our research objective is to investigate

ISSN: 1738-9984 IJSEIA

- How suitable agile methods are being selected (among the pool of all agile methods) for the current organisational requirement.
- Assigning weights to all suitable methods using fuzzy logic controller.
- Customizing highly weighted or most suitable agile methods found.
- How the individual customized methods needs to be assembled to form situated methods.

For the purpose, the proposed Agile Method Engineering process is divided into sub-processes that independently handle the task of method retrieval, finding suitable method and deciding the essential practices of the methods(or customizing the method) as per the situation-in-hand. The process flows as first finding the associative discovery cluster rules on the information stored in the databases, further retrieving the most suitable methods found, the retrieved methods are then assigned weights using the upper layer of fuzzy Logic Controller. The lower layer of Fuzzy Logic Controller is used to assign the weights to the practices of the methods; here the term 'weight' refers to the degree of suitability of the method for the specified set of requirements. The essence of the method customization process is to find essentialities in the methods that led to form organisational specific method.

The paper is organised in 5 sections, including this opening section. In the following section, we discuss basic concepts used in this paper, in order to understand the proposed Agile Method engineering process section three contains the step-by-step procedure required to form situated method. In fourth section we show the case studies utilizing the proposed Agile Method Engineering process. Finally the paper closes with the fifth section, containing a discussion and a conclusion.

Motivation for the proposed agile method engineering process

Although the introduction of agile development methods is an improvement over the traditional system development methods but since requirements of organisation vary and there is no single agile method that fulfils the entire set of requirements.

This motivates to create a blend of different agile methods based on the rich knowledge of the past usage of these methods under different requirement sets. The applicability of the method thus formed will be significantly improved than the existing methods because the assembled method thus formed contains the essentials of each constituent method.

2. Basic Concepts of the Process

The proposed Agile Method Engineering (AME) process is presented based on a set of concepts. These concepts build the foundation of the whole process. In the next subsections, the brief introductions of these concepts are given; the discussion provides the black-boxing of its contents. Internal view will be described in the subsequent sections.

2.1 Defined Requirement

The present method engineering approaches are anchored with several assumptions major ones are, it is possible for project members to explicitly specify the required situational method upfront and successfully communicate these requirements to the method engineer and these requirements do not change over the lifetime of a project[1,2]. However, in practice requirements are often 'evolutionary' in nature; a commonly cited method for these system requirements is the user-centred agile approach that helps in bridging between end users and systems developers. Another major problem with the requirements is 'vagueness'-requirements are often vague and difficult to understand. To handle these, a support system is provided in the present research that converts the elicited vague requirements into a specific format that can be easily input to any tool support

designed for the method configuration. The entire set of converted requirements is termed as 'defined requirements' for our process. The process and the format of the defined requirements will be discussed in the white boxing of the process.

2.2 Method Configuration

Since projects differ in various dimensions, for example, with respect to development context, situation, complexity and granularity. Different proposals for how to create a situational method that fits the unique project have been put forth, ranging from formalized meta-methods [14] to architectural based [7] and further extended to more formal guidelines [8]. Present research reveals an Agile Method Engineering approach that uses method configuration process to configure individual agile methods, these configured agile methods assembles to satisfy the current organisational requirement definition. The process introduce the Essentiality attribute for agile methods, the essentiality attribute can take two values either essential or variable.

The method configuration process designed for agile method engineering is dynamic in nature, the presence of essential practices are purely dependent on the current requirements. In other words, Method configuration means to configure a particular agile method to various situated factors [16, 17, 18].

2.3 Situated Agile Method Formed

The heavily weighted or most suitable configured Methods are assembled to form the situated method. Situated method comprises of Method Part and Method Extension Part. **Method part** primarily contains the essentials of the first configured method, and may also contain the essentials of the other configured method (s), discussed in detail in later sections. The length of the method part is obtained by the MAX function applied on all the configured methods. The appended part that is, **method extension part** contains all the remnant essentials of the configured methods.

3. The Agile Method Engineering Process

The agile method engineering process is defined as a two part process (two sub-processes), this is introduced to make the process more understandable and less complex. Former is to obtain suitable methods for the situation-in-hand and later is to configure them by finding the essential practices for the most-suitable or highly weighted configured methods. The configured methods are put together to form the situated method.

The following section will discuss the white boxing of the process.

3.1. Selection Sub-Process

The first sub-process deals with finding the suitable methods and assigning weights to them, represented by Figure 1 and described as follows:

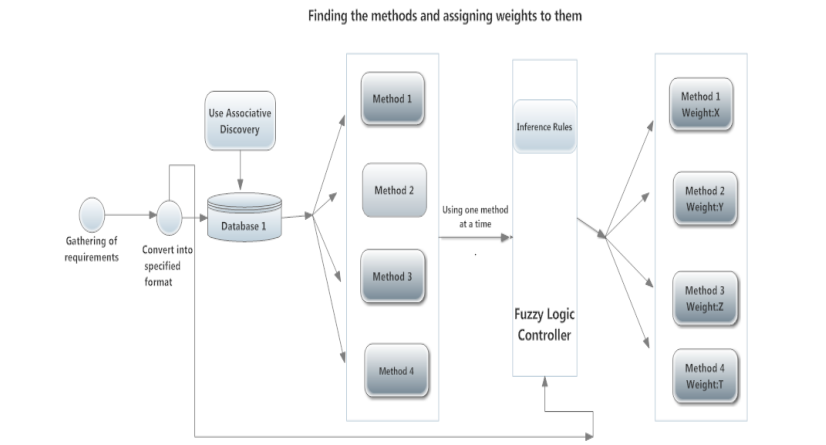

Figure 1. Finding Methods and Assign Weights to them

3.1.1 Gathering of the Requirements:

The process begins with the elicitation of the method requirements, the elicited requirements are often vague and difficult to understand. To handle this 'vagueness' requirements are converted into a standard format, specified by the framewok. The formatted requirements are fed into the Database that serves two purposes: it creates a repository of requirements for future use and for generating the associative discovery clustering rules to find the cluster of suitable methods using some datamining tool like WEKA.

3.1.2 Format for Specifying the Requirements:

The elicited requirements are first represented in a format for further processing, these formatted requirements are then act as a keywords for method search or cluster operation. The format specifies that every keyword should have at least 2 words or should be split into 2 words where the first word should be an adjective and next one will be noun.

Like:

- Small followed by team : small team
- Complex followed by technology: complex technology

3.1.3 Finding the Suitable Methods

The step followed by gathering of the requirements is the methods retreival and methods selection. For method retreival operation, associative clustering is used to find the cluster of appropriate methods.

Associative Clustering for method retreival

Clustering is basically unsupervised learning it finds "natural" grouping of instances given unlabeled data. Associative clustering is based on associative discovery rules that discover the presence of an object with respect to another object. It is used in market analysis basically where the vendors decide the placing of the items in the vicinity of the other items.

Association rules are if/then statements that help uncover relationships between

seemingly unrelated data in a relational database or other information repository. An example of an association rule would be "If a customer buys a dozen eggs, he is 80% likely to also purchase milk." An association rule has two parts, an antecedent (if) and a consequent (then). An antecedent is an item found in the data. A consequent is an item that is found in combination with the antecedent. The project extends the concept of clustering, for generating the associations or relationships between the requirements and put forward the suitable methods from the cluster generated.

Example: If the set of requirements are ‘R1, R3, R4', the suitable methods may be 'M2', ‘M6’ or ‘M8’.

A special set of database is designed for the process that contains the set of keywords and the methods that suit the combination of those keywords, this database is a standard which has been made out of exhaustive study and research on various set of requirements and is always enriched with updated data with the usage of system.

Database Schema

Database 1:

Keywords: P*ermutations and combinations of the keywords*

Cluster of Methods: *The method names suitable for the combination of the keywords.*

3.1.4 Method Selection-selecting Suitable Methods

Out of all the selected methods which are lined up after the previous step, the task is to select the most suitable ones-this is being carried out using fuzzy logic controller. It assigns membership to each of the methods depicting the degree of perfectness of the particular method for the defined requirements. In progress the highly weighted methods are selected for further processing.

Fuzzy logic controller assigns the membership degree to the agile methods (found from clustering operation) for the specified set of requirements. It takes the defined requirements and the suitable methods found, as its input and assigns the weight to the method. Rule Base here will be in the form of IF-Then Rules .Say if the set of keywords is “X” and method for this is “Y”, and then Value is “High”. Value tells the suitability of the respective method for the given set of defined requirements.

The value will be one of the Keywords: Low, Average, and High. The Range for keywords has been decided by the experts. Here the input will directly be in the fuzzified form that is in the linguistic terms. The rule base is applied to the fuzzified terms that fall under the work of inference engine. The output of the inference engine will be defuzzified to assign the crisp value.

One important thing is that it is not necessary that every time the same value is assigned to a method and further to its practices. As there is a range that is being fed into the fuzzy inference system so for the same set of defined requirements value may vary in the specified range.

3.2. Configuration Process

The next sub-process describes the procedure for assigning the weights to the practices of the highly weighted methods. Specifically it categorises the essential practices for the current organisational requirement.

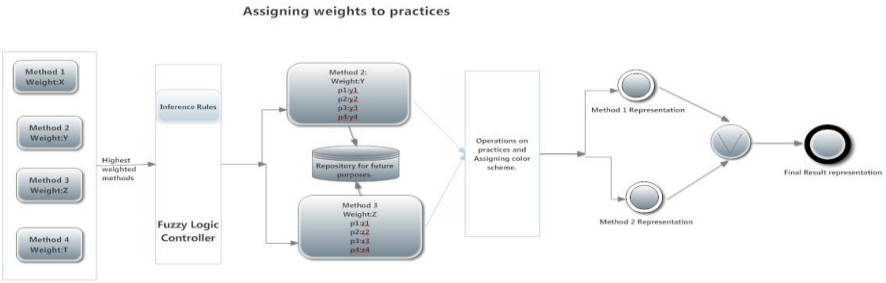

Figure 2. Assigning Weights to Practices

3.2.1 Assigning Weights to the Practices

Finding the essential practices is the basis for our method configuration process. The frame work provides the space for finding the membership of the practices for the most-suitable agile methods found for the situation-in-hand, using the lower layer of FLC. The process filters out the unwanted methods by selecting the highly weighted methods for further operation for example the methods with highest weights are discovered and are given as input with the set of requirements to find the membership degree of the practices of the method. The outcome is then fed into the Database 2 - a repository that can be used in future if the similar set of defined requirements came across and these databases will be updated periodically.

Database schema
Database 2:
Keywords: ***Permutations and combinations of the keywords.***
Weighted Methods: ***Retrieved Agile methods with their respective weights.***
Weighted Practices: ***Weighted practices of the highly-weighted agile methods for the situation in hand.***

The output of the FLC is stored in the second database; third column stores the weights of the practices for the highly weighted methods. FLC will be updated after every usage.
Example: If the set of defined requirements is X={} and Method is Y with weight A then Practice 1 is “Low”, Practice 2 is “Average”, Practice 3 is “Low”, Practice 4 is “High”. These “Low”, “High”, “Average” keywords will be assigned numerical values after the process of defuzzification.

3.2.2 Finding Essentiality in the Method for the Set of Defined Requirements

This subpart describes the operations performed on the weighted practices to find the essentiality pattern. For each highly weighted method, the mean of weight for all the practices is calculated separately. This is executed in order to find the essentiality pattern for the practices. Essentials are those that are mandatory to consider for the situated agile method. Assign ‘1’to those practices, whose weights are greater than the nominal value, these are termed as essentials, ‘0’to remnant practices whose weights are lesser than the nominal value these are termed as variables.

3.2.3 Assigning the Colour Scheme

In order to differentiate between the highly weighted configured methods, a different colour is assigned to each method. Say ‘red’ colour to method 1 and ‘green’ colour to method 2 and so on.

3.2.4 Assembling the Individual Highly Weighted Configured Methods

This process requires to perform logical OR operation but with an exception that if there are two 1's of different colour both will be considered and will be appended to the result. If the numbers of practices are not same a 'don't care condition(X)' is applied. The obtained outcome is the final situated method formed by assembling the individual configured method.

Consider ' 1' as representation for essential practices of method 1 and '1' for essential practices of method 2. A 0 represents the variable practice of either method.

There may arise 4 cases during the OR operation:

1. 1 OR 0: output will be 1 in method part.
2. 1 OR 0: output will be 1 in method part.
3. 0 OR 0: output will be 0 in method part.
4. 1 OR 1: output will be 1 in the method part and 1 in the method extension part.

3.2.5 Method Representation

Final output of the above step is represented into two parts: method part and method extended part. **Method part** includes the actual part that comes out of the OR operation whose length is the length of the maximum of the two method representations M1 and M2 and rest of the appended part which is called **method extension part** that falls under the 4th case of OR operation discussed in later sections, where it is required to keep the essential practices of both the methods, so this part contains the essentials of the second practice as essentials of the first method had already been included in the method part.

4 Empirical Grounding: The Illustrations

In order to evaluate the usefulness of the proposed methodology, case studies are used as a research method. Two case studies have been chosen for the same. These case studies are based on two projects carried out by two different organisations.

Case Study 1: A large software project developed by a software company to produce a stock market investment and analysing tool for analysing the fluctuations in the stock market and intelligently studies the areas for the investment in the market. It involves a huge team for its development which are further isolated into small teams with a self organising feature. The project uses the complex technology for the implementation. The average duration of the project was 1 year. The software involves the changing requirement nature from the customer's side. There is a need for documented requirements, to track the progress of the project and further to help during the testing phase.

Extracting the Requirements and converting into a specific format. Converting into the specified format (Table 1):

Table 1. Extracted Requirements for Case Study 1

Number	*Requirements*
R1	*Large Software*
R2	*Changing Requirements*
R3	*Complex Technology*
R4	*Small teams*
R5	*Isolated teams*
R6	*Documented Requirements*
R7	*Iterative Developments*
R8	*Self-Organising Team*

Feed these requirements to the database as a query, and it will give set of the best possible methods. Here set of the methods means more than one set; it will contain those methods also that are used only 10% percent of the times and such methods will be filtered out using FLC. For fresh requirements, rules will be generated using associative clustering. The general format will be "If 'combination of keywords' is X, then method is Y.

Further, the requirements and the retrieved methods are fed to the fuzzy logic controller to find their membership degree for the situation-in-hand. For the current situation, the two most suitable methods (method with high membership degree) found are shown in Table 2:

Table 2. Retrieved Methods

Number	*Method*	*Weight*
M1	*Feature Driven Development*	*0.8*
M2	*Scrum*	*0.7*

The retrieved suitable methods and set of requirements are again fed to FLC, to find the weights of the practices of these methods for the current organisational requirement. The output will be shown in Table 3 and 4:

For Feature Driven Development:

Table 3. Weighted Practices of Retrieved Method 1

Number	*Practice*	*Weight*
P1	*Domain object modelling*	*0.8*
P2	*Developing by Feature*	*0.8*
P3	*Inspection*	*0.4*
P4	*Individual class ownership*	*0.7*
P5	*Feature teams*	*0.9*
P6	*Regular builds*	*0.3*
P7	*Configuration Management*	*0.2*
P8	*Progress report*	*0.4*

For Scrum:

Table 4. Weighted Practices of Retrieved Method 2

Number	*Practice*	*Weight*
P1	*Product Backlog*	*0.8*
P2	*Sprint Backlog*	*0.4*
P3	*Effort Estimation*	*0.9*
P4	*Sprint*	*0.8*
P5	*Daily Scrum meeting*	*0.3*
P6	*Sprint Review meeting*	*0.5*

Since, the method configuration process, is centred around the 'identification of essential practices' the next step is to find the mean (nominal) weight of the practices of individual method. The mean weight is considered as the nominal value-above which the practices are considered as essentials for the current situation-in-hand.

For Feature Driven Development:
Mean= (0.8+0.8+0.4+0.7+0.9+0.3+0.2+0.4)/8= 4.5/8= 0.5625 rounded off to 0.6.

For Scrum:
Mean=(0.8+0.4+0.9+0.8+0.3+0.5)/7= 37/7=0.528 rounded off to 0.5

A'1' in the configured method representation, shows that particular practice is essential and it should be included in the situated method whereas, a '0' represents the variability in the configured method. Separate colour schemes are assigned to the methods

for clear identification say, RED colour to the method Feature Driven Development and Green to the method Scrum.

Method M1 (Feature Driven Development) representation after all the calculations is:

1	1	0	1	0	0	0	0

Method M2 (Scrum) representation after all the calculations is:

1	0	1	1	0	0	1	X

In the above representation, notice a 'don't care' condition is appended at the end of the second one, the purpose is to make equal length of considered methods. The final situated method is formed by performing the ORing operation on the considered methods

There may arise 4 cases during the OR operation:

1. 1 OR 0: output will be 1 in method part.
2. 1 OR 0: output will be 1 in method part.
3. 0 OR 0: output will be 0 in method part.
4. 1 OR 1: output will be 1 in the method part and 1 in the method extension part.

Output after ORing is

1	1	1	1	0	0	1	0	1	1

There is no colour assign to '0'in the situated method formed because of the fact that neither of the practices of the suitable methods has been selected in the output sequence.

Understanding the output

After all the calculations the final method representation shows the practices of the methods that should be considered according to the set of requirements given by the customer.
Considering the above illustration's output

1	1	1	1	0	0	1	0	1	1
1	2	3	4	5	6	7	8	1	2

|------Method part---------||----Method Extension part------|

Second row represents the position of every bit in the output sequence. The output method has two parts namely:

1. Method part
2. Method extended part

Method part includes the actual part that comes out of the OR operation whose length is the length of the maximum of the two method representations M1 and M2, which is 8 here and rest of the appended part which is called **method extension part** that falls under the 4th case of OR operation , where it is required to keep the essential practices of both the methods, so this part contains the essentials of the second practice as essentials of the first method had already been included in the method part.

The Red colour represents the practices of method 1 and green colour represents the practices of the method 2. Only important point to consider is sequencing of the practices.

The above output can be explained as:

Position 1st and 2nd of the method part in the situated method signifies the presence of 1st and 2nd practices of the method 1; consider the value at position 3rd of the method part, which implies that 3rd practice of the method 2 has to be considered. Position 4 of the method part represents the presence of practice number 4th of the method 1. Then there are '0's till position 8 that represents the variables-those practices which may or may not become a part of situated method. Further in the method extension part, the position number again starts from 1 and followed till the required length according to the OR operation. So 1 in green colour at position 1 of the method extension part represents the presence of 1st practice of the method 2 and similarly 1 in green colour at position 2 of method extended part represents the 2nd number practice of method 2.

Case Study 2: Case study 2 is a project that involves the upgrading of the existing code and it a large software project. It was being developed for a University which has many colleges located at various different places and each college administration used the software for the academy management placement management of the students. It involved the iterative and incremental development of the software, but on the other side it was a rapid development project. The project had seen an active user involvement during the development of the project because of the ever changing requirements of the customer. Since it was needed by colleges at different locations so teams were also spread at different locations for the software development so it was a distributed development project.

Extracting and converting the requirements into a specified format as shown in Table 5.

Table 5. Extracted Requirements for Case Study 2

Number	*Requirement*
R1	*Upgrading code*
R2	*Large project*
R3	*Active user-involvement*
R4	*Iterative Development*
R5	*Changing requirements*
R6	*Rapid development*
R7	*Distributed development*
R8	*Object-oriented approach*
R9	*Incremental development*

Take the two most suitable (or three best methods) with the highest weights for further processing.

Table 6. Retrieved Methods

Number	*Method*	*Weight*
M1	*Dynamic System Development Method(DSDM)*	*0.9*
M2	*Feature Driven Development(FDD)*	*0.8*

Weighted method practices for the current situation-in-hand.

For DSDM

Table 7. Weighted Practices of Retrieved Method 1

Number	*Practice*	*Weight*
P1	*Active User involvement*	*1.0*
P2	*Empowered team*	*0.9*
P3	*Frequent delivery of products*	*0.8*
P4	*Fitness for business purpose*	*0.7*
P5	*Iterative and incremental delivery*	*1.0*
P6	*Reversible changes*	*0.5*
P7	*Requirements are base lined at high level*	*0.4*
P8	*Integrated Testing*	*0.3*
P9	*Collaborative and cooperative approach shared by stakeholders*	*0.9*

For FDD

Table 8. Weighted Practices of Retrieved Method 2

Number	*Practice*	*Weight*
P1	*Domain object modelling*	*0.8*
P2	*Developing by feature*	*0.9*
P3	*Inspection*	*0.4*
P4	*Individual class ownership*	*0.4*
P5	*Feature teams*	*0.5*
P6	*Regular builds*	*0.9*
P7	*Configuration management*	*0.4*
P8	*Progress reporting*	*0.8*

Identification of essential practices - for DSDM:

Mean=1.0+0.9+0.8+0.7+1.0+0.5+0.4+0.3+0.9=6.5/9=0.72 rounded off to 0.7

For FDD:

Mean=0.8+0.9+0.4+0.4+0.5+0.9+0.4+0.8=5.1/8=0.635 rounded off to 0.6

Method representation after all the calculations is

Method M1 (DSDM)

1	*1*	*1*	*1*	*1*	*0*	*0*	*0*	*1*

Method M2 (FDD)

1	*1*	*0*	*0*	*0*	*1*	*0*	*1*	*X*

Performing OR operation on the two method equivalents.

1	*1*	*1*	*1*	*1*	*0*	*0*	*0*	*1*
1	*1*	*0*	*0*	*0*	*1*	*0*	*1*	*X*

Output:

1	*1*	*1*	*1*	*1*	*1*	*0*	*1*	*1*	*1*	*1*
1	*2*	*3*	*4*	*5*	*6*	*7*	*8*	*9*	*1*	*2*

|--- ------Method part----------||---Method Extension part---

5. Conclusion

An agile method engineering approach has been developed to find the degree of veracity of agile methods for the specified set of requirements. This evolutionary

approach opens the paths to utilize the revolution brought by the concept of agility. Such a method can be used under the circumstances when a single agile method does not fulfils the complete set of requirements of the customer, so there is a need for the blend of parts of more than one agile method, which the introduced method process helps to achieve. The process supports to specify the requirements in laymen language and finds the suitable agile methods for the same with the practices that need to be followed. The aim is to deliver situation specific agile method for the current organisation requirement.

In the introduced method, there is a dependency on the sequencing of the practices and if there is any change in their sequencing, the situated method formed will turn out to be useless. It can be improved to remove this dependency in the future and make this method more flexible to work upon.

References

[1] M. Rizwan and J. Qureshi, "Agile software development methodology for medium and large projects", In IET Software, **(2011)**.
[2] D. Zhang, "Machine learning and software engineering", Software Quality Journal, vol. 11, **(2003)**, pp. 87–119.
[3] Agile Manifesto, (2001). Manifesto for agile software development.
[4] K. Beck and C. Andres, "Extreme programming explained: embrace change", 2nd ed., Addison-wesley, **(2004)**.
[5] K. Schwaber and M. Beedle, "Agile software development with scrum", Nouvelle editions, **(2002)**.
[6] J. Hunt, "Feature Driven Development", Agile software construction, Springer, **(2006)**, pp. 161-182.
[7] Ahamed, "Performing Assembly-Based Method Engineering by Architecture-Centric Method Engineering Approach", Second UKSIM European Symposium on Computer Modeling and Simulation, IEEE, **(2008)**.
[8] B. Henderson-Sellers, R. France, G. Georg and R. Reddy, "A method engineering approach to developing aspect-oriented modelling processes based on the OPEN process framework", Information and software technology, vol. 49, **(2007)**, pp. 761-773.
[9] D. Gupta and R. Dwivedi, "Configuration from Situational Method Engineering", ACM SIGSOFT, Software Engineering Notes, vol. 37, no. 3, **(2012)**, pp. 1-11.
[10] D. Gupta and R. Dwivedi, "A Step towards Method Configuration from Situational Method Engineering", Software Engineering: An International Journal (SEIJ), vol. 2, no. 1, **(2012)**, pp. 51-59.
[11] R. Dwivedi and D. Gupta, "Customizing agile methods using genetic algorithm", Proceedings of International Conference on Advances in Communication, Network and Computing, Elsevier, **(2014)**.
[12] R. Dwivedi, "Configuration Issues and Efforts for Configuring Agile Approaches-Situational based Method Engineering", International Journal of Computer Applications, vol. 61, no. 17, **(2013)**, pp. 23-27.
[13] D. Gupta and R. Dwivedi, "Domain specific priority based implementation of mobile services- an agile way", International Conference on Software Engineering Research and Practice, Las Vegas, USA, **(2012)** July.
[14] D. Gupta and N. Prakash, "Engineering Methods from their Requirements Specification", Requirements Engineering Journal, vol. 6, **(2001)**, pp. 135-160.
[15] B. Henderson-Sellers and J. Ralyte, "Situational Method Engineering: State-of-the-Art Review", Journal of Universal Computer Science, vol. 16, no. 3, **(2010)**, pp. 424-478.
[16] F. Karlsson and P. J. Ågerfalk, "Method Configuration: Adapting to Situational Characteristics While Creating Reusable Assets", Information and Software Technology, vol. 46, no. 9, **(2004)**, pp. 619-633.
[17] J. Cameron, "Configurable development processes", Communications of the ACM, vol. 45, no. 3, **(2002)**, pp. 72-77.
[18] B. Fitzgerald, G. Hartnett and K. Conboy, "Customizing agile methods to software practices at Intel Shannon", European Journal of Information Systems, vol. 15, no. 2, **(2006)**, pp. 197-210.
[19] F. Karlsson and P. J. Ågerfalk, "Exploring Agile Values in Method Configuration", European Journal of Information Systems, vol. 18, no. 4, **(2009)**, pp. 300-316.
[20] A. Qumer and B. Henderson-Sellers, "crystallisation of agility-back to basics", ICSOFT, vol. 2, **(2006)**, psp. 121-126.

International Journal of Innovative Research in Advanced Engineering (IJIRAE) ISSN: 2349-2163
Issue 3, Volume 2 (March 2015) www.ijirae.com

APPROACH OF FUZZY LOGIC FOR EVALUATION OF GREEN BUILDING RATING SYSTEM

Sunita Bansal[1]; Dr. Srijit Biswas, FIE[2]; Dr. S. K. Singh[3]
[1]*Assoc. Professor, Department of Civil Engineering, Manav Rachna International University, Faridabad, India,*
[2]*Professor , Department of Civil Engineering, Manav Rachna International University, Faridabad, India,* [3]*Professor, Department of Environmental Engineering, Delhi Technological University, Delhi, India*

Abstract: - For rating of a green building in India, the tool 'Green Rating for Integrated Habitat Assessment (GRIHA)' has a great role for evaluation process. Using the guidelines of GRIHA, overall rating of a green building is done based on the acquired points out of 104 after evaluation of a set of thirty four criterias by different experts independently[4]. Each criteria is well defined in terms of points and provision is kept to award the full point only after full satisfaction of the expert on the quality of works under that criteria. Naturally the membership value (μ(x)) is considered as either 1 or 0 when the experts is either fully satisfied or not. So assessment in between 'acceptable and not acceptable'; 'best and poor'; 'efficient and not efficient'; 'more and less'; 'high and low'; 'good and bed' is not possible within [1,0] due to the involvement of uncertainty. Every expert hesitates more or less on every evaluation activity in between of all the above conditions because some part of his perception contributes to truthness and some part to falseness when he allots the points against different criterias. Thus uncertainty is an integral part of the accuracy of the assessments of each criterion which can be solved by the approach of fuzzy logic [6]. In this paper a flexible rating system is developed to address wide range of projects data with degree of certainty which is only the solution of the present day problem of GRIHA.

Keywords: fuzzy logic, GRIHA, rating system, uncertainty, weighted rating, etc.

1. Introduction:

India, like other developing countries, is going through a revolution in construction sector, which is the result of expanding population, growing urbanization and an increasing awareness about saving the environment. Building rating systems have been quite effective in raising awareness about energy efficient and green building design [1]. The site, design and operation of a building has to be such that the working and living environment is comfortable and the building has zero adverse effect on the environment. To facilitate the design, construction and operation of a green buildings, the tool 'GRIHA' developed by 'The Energy and Resources Institute (TERI)' and Ministry of New and Renewable Energy (MNRE) together has a great role in India for assessment of "greenness" of a green building in terms of rating like 1star, 2star, 3star, 4star & 5star[2,5]. There is a set of 34 criterias with differential weightage which gives total 104 points and after evaluation of each criteria by different experts, star rating will be awarded on the basis of total earned points out of 104, with minimum 50 points required for rating certification[4]. No points are granted for partial compliance i.e. if an evaluated criterion is satisfied then full point is awarded and if criteria is partially or not satisfied then 0 point is awarded. There is no provision of intermediate points in between for corresponding to partially satisfied or partially acceptable cases. If the membership value (μ(x)) of satisfaction is considered as 1 then for not satisfaction it will be 0, nothing will be in between 1 and 0. Whereas it is seldom possible that a criteria is fully satisfied but can be complied to a certain degree of satisfaction for which the membership value (μ(x)) of satisfaction can be any value within [1,0] due to involvement of uncertainty in between two zones of satisfaction and not-satisfaction of the expert. Thus it is very difficult to make genuine assessment based only on full points allotted logic. Instead we will have to consider all degree of perceptions of expert within [1,0].

There are total 34 criterias in GRIHA for rating of greenness of a building and for all cases evaluation is done by human being where there is certainly a limitation of knowledge or intellectual functionaries. The statistical observations or data so obtained for rating of a green building against 34 criterias are not always crisp or precise. Most of the data are non-numeric or unreliable statistical data rather linguistic and hedges viz. "good site", "very good water quality", "less noisy", "less landscape", "well designed", "more renewable energy", "highly acceptable", etc. to list a few only out of infinity. Such types of imprecise data are fuzzy in nature [3,6]. Evaluation of many criteria here is not always possible with numerical valued description for which basis we awarded the full point as per GRIHA. All the out put evaluation results of criterias are 100% based on the satisfaction level and the perception level of the experts which can never be same for all the situations, indoor as well as outdoor environment. Consequently it is ideal to adopt a proper mathematical tool to do a proper and genuine judgment and rating of a green building and certainly fuzzy logic is the most suitable for the purpose. Because of this obvious reason we adopt fuzzy logic in the present work.

2. Methodology

Now we propose a methodology of fuzzy assessment for rating of a green building based on criterias by GRIHA. For better understanding the proposed fuzzy based methodology, few useful preliminaries are discussed below.

2.1 Crisp Set

A crisp set can be described by a characteristic function or discrimination function by which individuals from the universal set X are determined to be either members or nonmembers of a set. Suppose for a given set A, this function assign a value $_A(x)$ to every x X such that

$_A(x) = 1$ iff x A , and $_A(x) = 0$ iff x A

In crisp set theory, a very precise boundary is there to determine whether an element belongs to a set or not. Accordingly the membership value in favour of the truthness of belongingness of an element/attribute is considered as 1 or 0. For example, if A is the sub set of universal set U membership values of the elements of the universe with respect to it's subset are $_A(x) = 1$, $_A(y) = 1$, and $_A(z) = 0$.

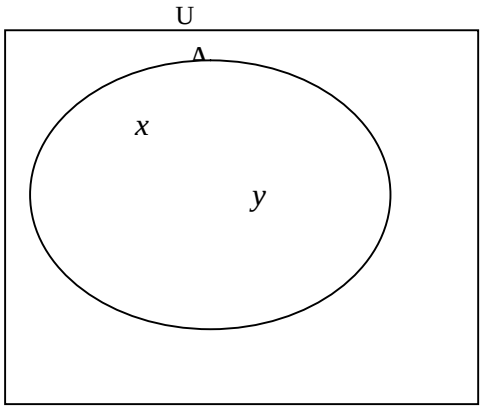

(Fig-1: Crisp Set A and elements x, y and z of Universal Set U)

2.2 Fuzzy Set [6]

This crisp characteristic function can now be generalized such that the values assigned to the elements of the universal set fall within a specified range [0,1] and indicate the membership grade of these elements in the set in question. There is no clear boundary in between set A and it's universal set U and thus we can not draw it. Such a function is called membership function and the set defined as fuzzy set. The membership function for fuzzy sets can take any value from the closed interval [0,1] instead of either 0 or 1 like crisp set[3]. Fuzzy set A is defined as the set of ordered pairs A = { (x_1, $_A(x_1)$) , (x_2, $_A(x_2)$) , ….. , (x_n, $_A(x_n)$) }, where $_A(x)$ is the grade of membership of element *x* in set A. Greater the $_A(x)$, greater is the truthness of the statement that element *x* belongs to set A[6].

Example: Let us consider a set X = {2, 5, 9,18,21,25}, whose elements denote the number of vehicles waiting in line at a signal. Set B consists of the fuzzy set "small number of vehicles in line." Fuzzy set B can be shown as: B = { (2, 0.95), (5, 0.55), (9, 0.20), (18, 0.10), (21, 0.05), (25, 0.01) }. The grades of membership 0.95, 0.55,…, 0.01 are subjectively determined and indicate the "strength" of membership of individual elements in fuzzy set B.

2.3 Attribute of the Assessment [3]

The assessment is done by collecting information or values for certain attributes which are called the attributes of the assessment. For example, consider a project of "Rating of Green Building", for which some relevant attributes could be "good site selection", "less building water use", "more resource recovery" etc.

2.4 Universe of the Assessment [3]

Collection of all attributes of the assessment is called the Universe of the Assessment.

2.5 Total Weighted Rating of a Fuzzy Set

Let μ be a fuzzy set of a finite set X. Suppose that to each element x X, there is an associated weight W_x *R+* (set of all non-negative real numbers).

Then the 'weighted rating' of the fuzzy set μ is the non-negative number a(μ) given by

$$a(\mu) = \sum_{i=1}^{n} \{\mu(x_i) W_{xi}\}$$

2.6 Grading of Fuzzy Assessment Output

In order to achieve the GRIHA certification a project must achieve minimum 50 points out of 100. Depending upon the value of a(μ), the grading of overall output for award the GRIHA certificate could be temporarily proposed as below : -

grade A = 5 Star rated building ,	if	90	a (μ)	100
grade B = 4 Star rated building ,	if	80	a (μ)	90
grade C = 3 Star rated building ,	if	70	a (μ)	80
grade D = 2 Star rated building ,	if	60	a (μ)	70
grade E = 1 Star rated building ,	if	50	a (μ)	60

In next section we present the methodology of assessment of GRIHA rating scale by a case study.

3. Case Study

Consider a project 'ASSESSMENT OF RATING OF A GREEN BUILDING'. To assess the rating of green building, we consider all criterias of GRIHA as attributes (x_i) of proposed methodology except criteria no-32 & 34 as both have no direct influence in the overall rating of the building. We also consider all the points of GRIHA assigned against each criterion as weightage (W_i) of that particular attribute. Considering favourable aspects of green building, suppose the 32 attributes with their weightage are:-

x_1 = good site selection (W_1=1)
x_2 = well preserved and protected landscape during construction (W_2=5)
x_3 = good soil conservation (post construction) (W_3= 4)
x_4 = well designed to include existing site features (W_4=2)
x_5 = good reduction in hard paving on site(W_5=2)
x_6 = good enhanced outdoor lighting system efficiency (W_6=3)
x_7 = well planned and optimised utilities circulation efficiency(W_7=3)
x_8 = good provision of sanitation/safety facilities for construction workers (W_8=2)
x_9 = less air pollution during construction (W_9=2)
x_{10} = less landscape water requirement(W_{10}=3)
x_{11} = less building water use(W_{11}=2)
x_{12} = less wastage of water during construction(W_{12}=1)
x_{13} = good building design to reduce conventional energy demand(W_{13}=6)
x_{14} = good energy performance of building within specified comfort(W_{14}=12)
x_{15} = good use of fly ash in building structure(W_{15}=6)
x_{16} = good use of efficient construction technology (W_{16}=4)
x_{17} = less use of low-energy material in interiors(W_{17}=4)
x_{18} = more renewable energy utilization(W_{18}=5)
x_{19} = more renewable energy based hot water system(W_{19}=3)
x_{20} = good waste water treatment process(W_{20}=2)
x_{21} = good water re-cycle and re-use (including rainwater) (W_{21}=5)
x_{22}= less waste during construction(W_{22}=2)
x_{23} = good waste segregation(W_{23}=2)
x_{24} = good storage and disposal of waste(W_{24}=2)
x_{25} = more resource recovery from waste(W_{25}=2)
x_{26} = less use of low VOC paints / adhesive/sealants(W_{26}=4)
x_{27} = less ozone depleting substances(W_{27}=3)
x_{28} = good water quality(W_{28}=2)
x_{29} = high acceptable outdoor and indoor noise level(W_{29}=2)
x_{30}= good tobacco and smoke control(W_{30}=1)
x_{31} = high universal accessibility(W_{31}=1)
x_{32} = good operations and maintenance protocol (W_{32}=2)

Naturally, all independent expert's views for individual attribute will lead to a fuzzy set of the universe U, where U = { x_1, x_2, x_3, x_4, x_5, ……, x_{32} }.

Now the job is to assign values to these attributes. This can be done either by direct observation or by collecting views from all the stakeholders. Let us suppose that the data collected for an attribute x_i reveals that more or less 70 % are in support of the truthness of the attribute and the rest 30% are in support of falseness then the membership value of fuzzy set will be $\mu_A(x_i)$ = 0.7. Suppose the membership values of each attribute judged by different experts are as below:

attribute	in support of truthness μ(x)	in support of falseness = (1-μ(x))	weight of the attribute W_x	weighted Rating
x_1	.75	.25	1	0.75
x_2	.65	.35	5	3.25
x_3	.5	.5	4	2.0
x_4	.6	.4	2	1.2
x_5	.8	.2	2	1.6
x_6	.7	.3	3	2.1
x_7	.9	.1	3	2.7
x_8	.45	.55	2	0.9
x_9	.9	.1	2	1.8
x_{10}	.75	.25	3	2.25
x_{11}	.55	.45	2	1.1
x_{12}	.85	.15	1	0.85
x_{13}	.45	.55	6	2.7
x_{14}	.55	.45	12	6.6
x_{15}	.85	.15	6	5.1
x_{16}	.4	.6	4	1.6
x_{17}	.55	.45	4	2.2
x_{18}	.45	.55	5	2.25
x_{19}	.6	.4	3	1.8
x_{20}	.75	.25	2	1.5
x_{21}	.85	.15	5	4.25
x_{22}	.5	.5	2	1
x_{23}	.6	.4	2	1.2
x_{24}	.85	.15	2	1.7
x_{25}	.8	.2	2	1.6
x_{26}	.9	.1	4	3.6
x_{27}	.45	.55	3	1.35
x_{28}	.9	.1	2	1.8
x_{29}	.75	.25	2	1.5
x_{30}	.85	.15	1	0.85
x_{31}	.5	.5	1	0.5
x_{32}	.6	.4	2	1.2
		Total Weighted Rating (a(μ)) =		**64.8**

From the result of fuzzy assessment, the 'Total Weighted Rating (a(μ))' value is = **64.8** and thus the grade is to be awarded as **"D"**

Result: The building is **2 Star** rated green building.

4. Conclusion

GRIHA rates the greenness of a building by awarding points based on a set of criteria evaluated by experts. There is no scope for fluctuations of experts' perceptions or insufficient and unreliable statistical data, while taking decision towards evaluation of any criteria. Every expert as a human being will feel uncomfortable to assess a criteria by linguistic variables like good, bad, best, low, high etc for which he has to award points allocated against it.

The proposed fuzzy model based on GRIHA criterias has tremendous powers to minimize the uncertainty that arises due to experts' perceptions. Even the most minimal compliance of criteria can be accounted for in the Fuzzy analysis making the rating process more precise. The Green Rating thus obtained in the overall output result has more degree of certainty than from the present guidelines of GRIHA.

References:

[1] Abair, Jesse W. : " Green buildings : what it means to be 'green' and the evolution of green building laws ; Recent developments in land use, planning and zoning " , The urban lawyer 40.3 (Summer 2008) : 623(10).
[2] ADaRSH, Ministry of New and Renewable Energy (MNRE), Govt. of India : "The national rating system for green building- The little book of GRIHA rating".
[3] Bansal, Sunita; Biswas. Srijit ; Singh, S.K. : "Selection of Most Economical Green Building out of n-Alternatives : Approach of Vague Fuzzy Logic" ; ' International Journal of Engineering and Technology' Vol-4, No-2, pp 164-168 (Feb-2015).
[4] Ministry of New and Renewable Energy (MNRE) , Govt. of India and The Energy and Research Institute (TERI), New Delhi : "GRIHA Manual (Volume-I)".
[5] Siva, Kishan. ; ADaRSH, GRIHA, Ministry of New and Renewable Energy (MNRE) , Govt. of India and The Energy and Research Institute (TERI), New Delhi
[6] Zadeh, L., Fuzzy Sets, Inform. Control., 8(1965), 338-353.

This article has been accepted for publication in a future issue of this journal, but has not been fully edited. Content may change prior to final publication. Citation information: DOI 10.1109/JLT.2015.2418993, Journal of Lightwave Technology

Broadband mid-infrared supercontinuum spectra spanning 2 – 15 μm using As_2Se_3 chalcogenide glass triangular-core graded-index photonic crystal fiber

Than Singh Saini, *Member OSA*, Ajeet Kumar, *Member OSA*, Ravindra Kumar Sinha., *Member IEEE*

Abstract— **In this paper, we report analysis, design and numerical modeling of mid-infrared supercontinuum generation across 2 – 15 μm molecular 'fingerprint region' using a new design of triangular-core graded-index photonic crystal fiber pumped with 50 fs laser pulses of peak power of 3.5 kW at 4.1 μm. Proposed photonic crystal fiber design offers the nonlinear coefficient as high as 1944 $W^{-1}\times Km^{-1}$ at pump wavelength. To the best of our knowledge the supercontinuum in PCF with such broadband spectra has been reported first time. Proposed photonic crystal fiber design has potential applications in gas sensing, food quality control and early cancer diagnostics.**

Index Terms—**Nonlinear optics, highly nonlinear photonic crystal fiber, mid-infrared supercontinuum.**

I. Introduction

DURING the last decade white-light supercontinuum generation (SCG) in optical fibers has emerged as an active and exciting research field. Various types of new light sources have been created which are finding applications in a diverse range of fields such as optical coherence tomography [1, 2], optical communications [3], frequency metrology [4], fluorescence lifetime imaging [5], gas sensing [6, 7], food quality control [8] and early cancer diagnostics [9]. Supercontinuum is formed when a large number of nonlinear processes such as self phase modulation (SPM), stimulated Raman scattering, cross-phase modulation and four-wave mixing act together upon a pump beam in order to cause extensive spectral broadening of the original pump beam. The breakthroughs in recent years have raised scientific concerns to understand and model how all these nonlinear processes interact together to generate supercontinuum and how parameters can be engineered to control and enhance the supercontinuum (SC) spectra.

The mid-infrared region is important because the fundamental molecular vibration absorption bands are stronger than the overtones and combination vibration absorption bands situated in the near-infrared region. Mid-infrared spectroscopy is able to provide thorough understanding of the molecular structure of matter and to perform non-intrusive diagnostics of composite systems of physical, chemical and biological interest. SC spectra spanning visible to near-infrared in silica based fibers have been generated previously for various applications [10-12]. However, the broadening of SC spectra in silica fibers is limited by the strong material absorption beyond 2.5 μm wavelength, which effectively limits the spectral evolution into the mid-infrared region. For this reason a large number of non-silica glasses such as tellurite, ZBLAN, bismuth, fluoride and chalcogenide have been proposed for SCG in mid-infrared region [13-19].

Among all non-silica glasses, the chalcogenide glasses are excellent candidates for mid-infrared region because some of its compositions possess optical transparency upto 25 μm in this region [20]. The As_2Se_3 glass has shown excellent optical transparency between 0.85 – 17.5 μm with attenuation coefficient of less than 1 cm^{-1} [20]. In addition to broadband mid-infrared transmission window, chalcogenide glasses have also very large linear and nonlinear refractive indices which make them promising candidates for mid-infrared SCG [21]. *Shaw et al.* [22] presented an experimental demonstration of SCG in the spectral range from 2.1 to 3.2 μm using hexagonal structure of As_2Se_3 based chalcogenide photonic crystal fiber (PCF). Recently, *Hu et al.* [23] gave a design procedure, which can be used to maximize the band-width of supercontinuum generation in As_2Se_3 chalcogenide PCFs, for more than 4 μm band-width of SC. *Kubat et al.* [24] presented a numerical design optimization of ZBLAN fibers for mid-infrared SC sources using direct pumping with 10 ps pulses from mode-locked Yb and Er lasers to obtain broad spectra ranging from 1– 4.5 μm. *Klimczak et al.* [25] achieved SC

The authors gratefully acknowledge the (i) initiatives and support towards establishment of the "TIFAC-Center of Relevance and Excellence" in Fiber Optics and Optical Communication at Delhi Technological University (Formerly Delhi College of Engineering) Delhi, through the "Mission REACH" program of Technology Vision-2020 of the Government of India and (ii) TUN-IND bilateral research project "Design, modeling and characterization of highly nonlinear fibers for all-optical high bit-rate network," funded by Ministry of Higher Education and Scientific Research of Republic of Tunisia and Department of Science and Technology, Govt. of India.

Authors are with the TIFAC-Center of Relevance and Excellence in Fiber Optics and Optical Communication, Department of Applied Physics, Delhi Technological University, Delhi- 110042, INDIA

T. S. Saini (e-mail: tsinghdph@gmail.com), A. Kumar (e-mail: ajeetdph@gmail.com); R. K. Sinha (e-mail: dr_rk_sinha@yahoo.com).

This article has been accepted for publication in a future issue of this journal, but has not been fully edited. Content may change prior to final publication. Citation information: DOI 10.1109/JLT.2015.2418993, Journal of Lightwave Technology

broadening between 930 nm to 2170 nm spectral range using all-solid soft glass microstructured optical fiber. In Ref. [26] the authors have experimentally demonstrated the SCG covering 0.9 − 9 μm with the help of commercially available ZBLAN fiber and commercially available chalcogenide PCF. Recently, *Kubat et al.* [27] presented numerical modelling of broadband mid-infrared SCG spanning from 3 – 12.5 μm in step-index fiber pumped at 4.5 μm with 0.75 kW pump power. *Petersen et al.* [28] demonstrated broadband mid-infrared supercontinuum spectra covering the range of 1.4 – 13.3 μm in mid-infrared regime using ultra-high NA chalcogenide step-index fiber.

In comparison to SCG in standard optical fibers, PCF requires input laser pulses with very less initial peak power. The higher order dispersion effects are stronger in PCF and play a much more significant role in pulse propagation. The dramatic spectral broadening with relatively low-intensity laser pulses in PCF is very interesting phenomena and can be used in various fascinating applications such as frequency metrology.

The broadening mechanism of supercontinuum spectrum mainly depends upon the dispersion profile of optical fiber structure as well as input pulse characteristics. In the anomalous group velocity dispersion regime when highly intense laser pulse incident on nonlinear medium it evolves towards the higher-order solitons [29]. For the femtosecond pumping, the higher-order solitons are affected by the higher-order dispersion and stimulated Raman scattering. Consequently, the higher order solitons become unstable and breakup into several fundamental solitons through the fission process. Such chaotic soliton fission process causes shot-to-shot noise in the supercontinuum spectrum [30, 31]. But in case of normal group velocity dispersion regime, for femtosecond pulses SPM is the only reason for ultra wide spectral broadening [31]. This makes such broad-band SC suitable for time-resolved applications such as optical coherence tomography, pump-probe spectroscopy and nonlinear microscopy. One of the possibilities for generating SC in the normal dispersion regime is to pump the fiber far below the zero dispersion wavelength (ZDW), so that the generated spectrum does not extend into the anomalous dispersion region. However, this would require high power or very short pulses to overcome the short effective interaction length due to high value of dispersion. It is worthwhile to mention here that the broadening of SC demonstrated in [28] is the largest achieved in fiber geometry till date. However, possibility of broadening of SC spectra beyond 20 μm is being discussed in scientific news and views [32].

Mid-infrared domain in the range of 2 – 15 μm of electromagnetic spectrum is of particular importance because of the molecular fingerprint of biological tissue lie within this domain. This domain is useful to determine a tissue spectral map which provides very important information about the existence of diseases such as cancer. Therefore, it is necessary to develop broadband supercontinuum sources in mid-infrared domain. The chalcogenide glasses have this potential to provide such broadband mid-infrared supercontinuum sources.

In this paper we present analysis, design and numerical modeling for achieving ultra broadband mid-infrared supercontinuum spectra spanning 2 – 15 μm using As_2Se_3 based chalcogenide-glass triangular-core graded-index (TCGI) PCF. To obtain efficient broadband supercontinuum spectrum in mid-infrared regime, proposed TCGI PCF has been specifically designed for all-normal dispersion characteristic. Such broadband mid-infrared supercontinuum spectrum is obtained in relatively short length (*i.e.* 5 mm) of PCF, using a sub-harmonic generation source of the mode-locked thulium 50 fs pulsed fiber laser at 4.1μm [33].

This paper is organized in five sections. Section-I provides a brief introduction and overview of previous works on SCG in photonic crystal fibers. In section-II, detailed description of method of analysis is given. Section-III explains the design of proposed triangular-core graded-index PCF. Section-IV is devoted to the results and discussion. Finally, conclusion of this work is summarized in section-V.

II. METHOD OF ANALYSIS

A. Linear Characteristics of PCF structure

To simulate the effective index of fundamental mode propagating through proposed triangular-core graded-index photonic crystal fiber, a full vectorial finite element method (FEM) based software 'COMSOL Multiphysics' has been employed. For calculating the wavelength dependent refractive index of As_2Se_3 based chalcogenide material following two terms Sellmeier equation has been used [34].

$$n^2 - 1 = A_0 + \sum_{n=1}^{2} \frac{A_n \lambda^2}{\lambda^2 - a_n^2} \qquad (1)$$

In above Eq. (1) A_0, A_n and a_n are the sellmeier coefficients with A_0=3.3344, a_1=0.43834 μm, a_2=41.395 μm, A_1=3.3105 and A_2=0.89672 for As_2Se_3 based chalcogenide glass which we have used as a fiber material in this work.

The group velocity dispersion plays an important role in SCG because it determines the extent to which different spectral components of an ultra-short pulse propagate at different phase velocities in the photonic crystal fiber. The group velocity dispersion $D(\lambda)$ is calculated from wavelength dependent effective indices of propagating mode using the following relation [29]

$$D(\lambda) = -\frac{\lambda}{c}\frac{\partial^2 Re(n_{eff})}{\partial \lambda^2} \qquad (2)$$

where, c is the velocity of light in free space, $Re(n_{\text{eff}})$ is the real part of the effective index. Both material and waveguide dispersion are included in the above equation as Sellmeier equation is taken into account while calculating n_{eff}.

The effective area of propagating mode in the PCF is calculated using the relation given below [27, 29].

$$A_{eff} = \frac{\left(\iint_{-\infty}^{\infty} |E|^2 \, dx \, dy\right)^2}{\left(\iint_{-\infty}^{\infty} |E|^4 dx \, dy\right)} \qquad (3)$$

This article has been accepted for publication in a future issue of this journal, but has not been fully edited. Content may change prior to final publication. Citation information: DOI 10.1109/JLT.2015.2418993, Journal of Lightwave Technology

where, *E* is the electric field distribution derived by solving the eigenvalue problem drawn from Maxwell's equations.

B. Nonlinear Characteristics of PCF structure

Nonlinearity in PCF is the most important parameter which must be studied more rigorously in order to get accurate results. The nonlinear coefficient (γ), offered by PCF structure, related to the nonlinear refractive index of material of PCF and the effective area of propagating mode as follows [29].

$$\gamma = \frac{2\pi n_2}{\lambda A_{eff}(\lambda)} \quad (4)$$

where, n_2 is the nonlinear refractive index of material (n_2 = 5.2×10^{-18} m^2/W at 4.5 μm wavelength [27]), λ is the pump wavelength and A_{eff} is the effective area of fundamental mode and its value depends on the wavelength. For broader supercontinuum spectra the nonlinear refractive index (*i.e.* n_2) should be as high as possible and A_{eff} should be as small as possible. Wavelength dependent effective mode area is obtained using Eq.(3) as mentioned in Ref. [27]. The value of γ can be enhanced by taking material with high non linear refractive index and/or by designing a PCF with lower effective mode area.

To simulate SC, the following generalized nonlinear Schrodinger equation (GNLSE) has been solved for output pulse envelope, *A* (z, t) using split-step Fourier method [10]

$$\frac{\partial A}{\partial z} + \frac{\alpha}{2}A - \left(\sum_{n\geq 2}\beta_n \frac{i^{n+1}}{n!}\frac{\partial^n A}{\partial t^n}\right) = i\gamma\left(1+\frac{i}{\omega_o}\frac{\partial}{\partial t}\right)\left[A(z,t)\int_{-\infty}^{\infty} R(t')\ |A(z,t-t')|^2 dt'\right] \quad (5)$$

The left hand side of Eq. (5) deals with linear propagation effects while the right hand side of this deals with nonlinear effects of PCF structure. α represents the power losses in the PCF as the light travels through it. We have included both the material and confinement losses in all the simulations. A constant material loss coefficient of 0.6 cm^{-1} has been considered for 2 – 15 μm spectral range [20]. For designed TCGI PCF the typical value of simulated confinement loss is ~3.9×10^{-5} dB/mm at 4.1 μm. The propagation constant (β) at any frequency (ω), relative to pulse central frequency(ω_0), can be expanded as Taylor series expansion [10]

$$\beta(\omega) = \beta(\omega_0) + \beta_1(\omega_0)(\omega-\omega_0) + \frac{1}{2!}\beta_2(\omega_0)(\omega-\omega_0)^2 + \frac{1}{3!}\beta_2(\omega_0)(\omega-\omega_0)^3 + \cdots \quad (6)$$

where, $\beta_n(\omega_0) = \frac{d^n\beta}{d\omega^n}$, first term in the right hand side of Eq. (6) gives the effective refractive index of the propagating mode and the second and third terms are related to the group velocity and the group velocity dispersion (GVD) of the pulse respectively. We have evaluated higher order dispersion up to the order of 9th from the group velocity dispersion curve.

R (t') is the nonlinear response function and takes account of the electronic and nuclear contributions and expressed as follows:

$$R(t') = (1-f_R)\delta(t'-t_e) + f_R\, h_R(t') \quad (7)$$

where, f_R is the fractional contribution of the Raman response to the total linear response. For As_2Se_3 chalcogenide glasses the fractional contribution f_R=0.115 [35]. The electronic contribution is treated in this analysis as occurring instantaneously because $t_e \approx 1$ fs. $h_R(t')$ is the Raman response function and contains information on the vibration of material molecules as light passes through the fiber.

The Raman response function $h_R(t')$ can be calculated by most common and approximate analytic form which is given by the following relation:

$$h_R(t') = \frac{\tau_1^2+\tau_2^2}{\tau_1\tau_2} exp\left(-\frac{t'}{\tau_2}\right)\sin\left(\frac{t'}{\tau_1}\right) \quad (8)$$

where, Raman period τ_1=23.1fs and life time τ_2=195 fs for As_2Se_3 based glasses [35].

In our study, we consider the hyperbolic secant pulse as input pulse which is expressed as the relation given below:

$$A(z=0,t) = \sqrt{P_0}.sech\left(\frac{t}{t_o}\right) \quad (9)$$

where, $t_0=T_{FWHM}/1.7627$ and P_0 is peak power of input pulse.

III. DESIGN OF PROPOSED TCGI PCF

We present a novel triangular-core graded-index PCF structure with four layers of air holes arranged in triangular lattice pattern in As_2Se_3-based chalcogenide glass. As shown in Fig. 1 (*a*) three air holes have been removed from the centre to construct a triangular-core of the PCF. The center to center distance of air holes is taken as constant and represented by Λ. The diameters of air holes in first, second, third and fourth ring are d_1, d_2, d_3 and d_4 respectively. For our design $d_1 < d_2 < d_3 < d_4$, *i.e.* the air filling fraction (d_n/Λ, n = 1, 2, 3, 4) of cladding increases with *'n'*. Where '*n*' is the number of rings of air holes. In other words the effective refractive index of cladding successively decreases for first, second, third and fourth rings of air holes. That is why the structure of PCF is named as 'graded-index'. The structure is surrounded by the cylindrical perfectly matched layer (PML) for eliminating the back reflection effect at the boundary. The reason of designing triangular-core graded index PCF is to get all-normal and nearly zero dispersion characteristic at desired pump wavelength. Triangular shaped core and Graded index profile of air holes increase the confinement of field and thus increase the nonlinearity. Gradually increasing shape of air holes effectively generates an equivalent refractive index profile of monotonically decreasing refractive index. Such a design is having strong control in achieving the ultra broadband flatted dispersion [36] which is essential for achieving ultra broadband SCG. Simulated electric field distribution of propagating mode in proposed triangular-core graded-index PCF at 4.1 μm has been illustrated in Fig.1 (*b*).

This article has been accepted for publication in a future issue of this journal, but has not been fully edited. Content may change prior to final publication. Citation information: DOI 10.1109/JLT.2015.2418993, Journal of Lightwave Technology

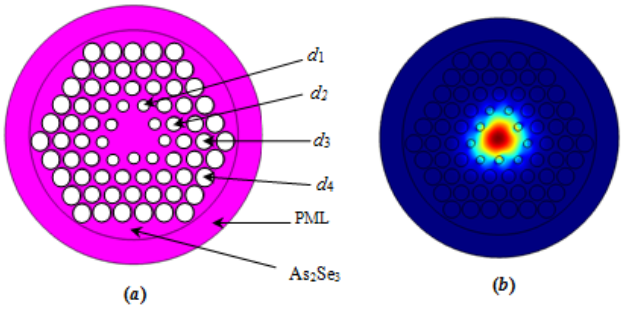

Fig.1: (a) Transverse cross-section of proposed TCGI PCF; (*b*) the electric field distribution of propagating mode in PCF at 4.1 µm.

IV. Results and Discussion

In order to obtain ultra broadband SC in proposed PCF structure, we have optimized the structural parameters (*i.e.* Λ, d_1, d_2, d_3 and d_4) to achieve all-normal chromatic dispersion profile. The effect of various values of air hole diameter in first ring, d_1 on dispersion characteristic, while keeping other parameters fixed, is illustrated in Fig. 2. Similarly the effect of diameter of air holes in second ring on the dispersion profile of proposed triangular-core PCF is shown in Fig.3. It is to be noted here that we have simulated the effect of the diameters of air holes in third and fourth ring and found that they are relatively less sensitive on dispersion characteristic of proposed PCF structure (not shown in figure). For optimized geometrical parameters (as shown in table I), the chromatic dispersion profile of proposed triangular-core graded-index PCF is shown in Fig.4. The proposed PCF structure offers flat dispersion across 3.35 – 4.20 µm spectral range within the dispersion value of approximately –2 ps/(nm×Km). Confinement loss is very improtant parameter for generating SC spectra in fibers. We have simulated the confinement loss of our proposed PCF structure and shown in Fig.5. Proposed PCF structure offers low confinement loss of ~ 3.9×10^{-5} dB/mm at pump wavelength (*i.e.* 4.1µm). However, the loss at 10 µm is ~14 dB/mm. Since the higher wavelengths (>8 µm) generate at 5 mm length of the PCF, the broadening of supercontinumm spectrum would not be affected by higher losses at higher wavelengths.

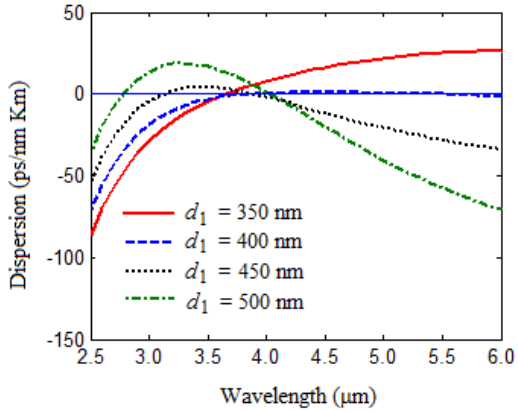

Fig.2: The effect of the diameter of the air holes in first ring (*i.e.* d_1) on chromatic dispersion profile while keeping other parameters fixed as: d_2 = 700 nm, d_3 = 800 nm, d_4 = 900 nm, and Λ = 1000 nm.

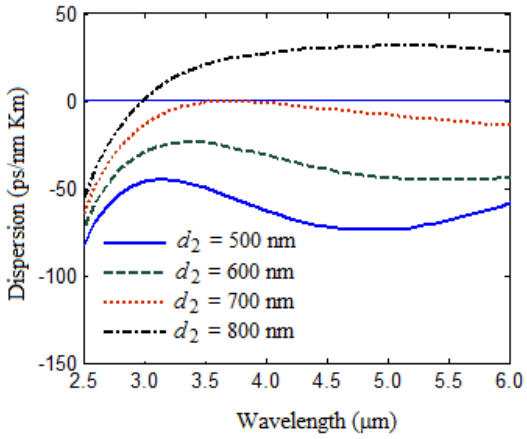

Fig.3: The effect of the diameter of the air holes in second ring (*i.e.* d_2) on chromatic dispersion profile while keeping other parameters fixed as: d_1 = 420 nm, d_3 = 800 nm, d_4 = 900 nm, and Λ = 1000 nm.

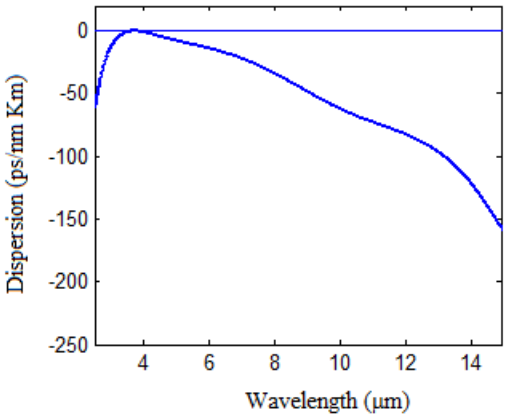

Fig.4: The chromatic dispersion characteristic of proposed triangular-core graded-index photonic crystal fiber structure with optimized parameters (*i.e.* d_1 = 420 nm, d_2 = 700, d_3 = 800 nm, d_4 = 900 nm, and Λ = 1000 nm).

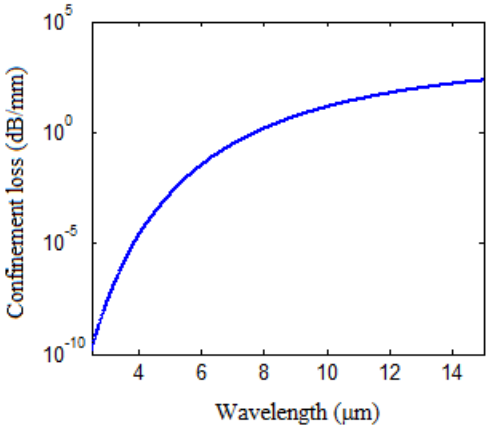

Fig.5: The confinement loss of proposed triangular-core graded-index photonic crystal fiber structure with optimized parameters (*i.e.* d_1 = 420 nm, d_2 = 700, d_3 = 800 nm, d_4 = 900 nm, and Λ = 1000 nm).

The wavelength dependent effective-mode-area of propagating mode and corresponding nonlinear coefficient has been illustrated in Fig.6. Simulated results show that the proposed triangular-core graded-index PCF structure offers

This article has been accepted for publication in a future issue of this journal, but has not been fully edited. Content may change prior to final publication. Citation information: DOI 10.1109/JLT.2015.2418993, Journal of Lightwave Technology

nonlinear coefficient (γ) as high as 1944 $W^{-1}\times Km^{-1}$ with effective mode area of 4.1 μm^2 at 4.1 µm input pump wavelength.

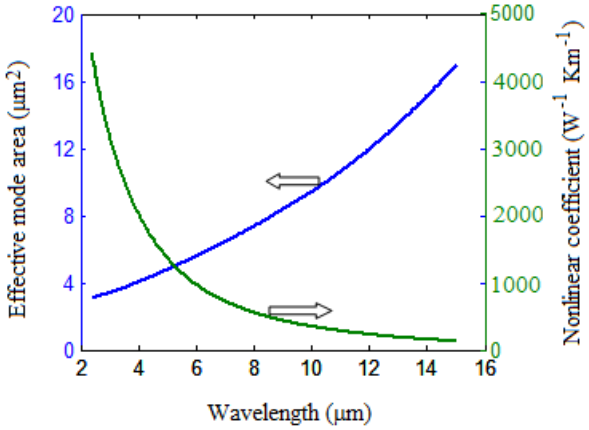

Fig.6: The variation of effective mode area of propagating mode and corresponding nonlinear coefficient of proposed triangular-core graded-index photonic crystal fiber with optimized parameters (*i.e.* d_1 = 420 nm, d_2 = 700, d_3 = 800 nm, d_4 = 900 nm, and Λ = 1000 nm).

As illustrated in Fig.7, by launching the laser pulses of proper parameters (pulse parameters are shown in table II) we are able to obtain broadband spectra ranging 2 – 15 µm in only 5 mm length of proposed triangular-core graded-index photonic crystal fiber. The calculated values of nonlinear length ($L_{NL} = 1/\gamma P_0$) and dispersion length ($L_D = \frac{T_0^2}{\beta_2}$; $T_0 = T_{FWHM}/1.763$), for proposed PCF are 1.47×10^{-4} m and 5.2×10^{-2} m respectively for 50 fs laser pulse at 4.1 µm. The solitons order, $N \approx \sqrt{L_D/L_{NL}}$ is 18 for proposed PCF structure. The solitons fission length, $L_{fiss} = L_D/N$ is equal to 2.76 mm. Within 5 mm length of the TCGI PCF an ultra-broadband SC extending from 2 – 15 µm has been generated with 50 fs laser pulses of peak power of 3.5 kW. As shown in Fig.7, beyond 5 mm length of the PCF the broadening of SC spectra does not increase significantly. This is because of the lower nonlinearity and higher losses at wavelengths greater than 15 µm for proposed TCGI PCF structure.

Finally, the influence of the input pulse width *i.e.* full width at half maximum (T_{FWHM}) on the bandwidth of output spectrum in 5 mm long TCGI PCF has been revealed in Fig. 8. The input peak power is fixed at 3.5 kW. When the value of T_{FWHM} increases the output spectra start to get narrower. This is due to the SPM effect. It is to be noted here that the short pulse is better to get broader SC spectra. The optimized values of input pulse are summarized in table II.

Proposed triangular-core graded-index PCF structure can be fabricated by standard extrusion and stacking based methods. For fabrication purposes it is also very important to investigate the tolerance of the proposed structure with respect to the various design parameters. After investigating the effect of small variations in the values of d_1, d_2, d_3, d_4 and Λ we have found that the magnitude of dispersion and the effective mode area of propagating mode are less sensitive to the structural parameters. For example, at 4.1 µm wavelength 1% variation in d_1 changes the dispersion value by ~ 4 % and changes the effective mode area by 0.8%. These changes produce only ~1% changes in the spectral broadening of SC spectra.

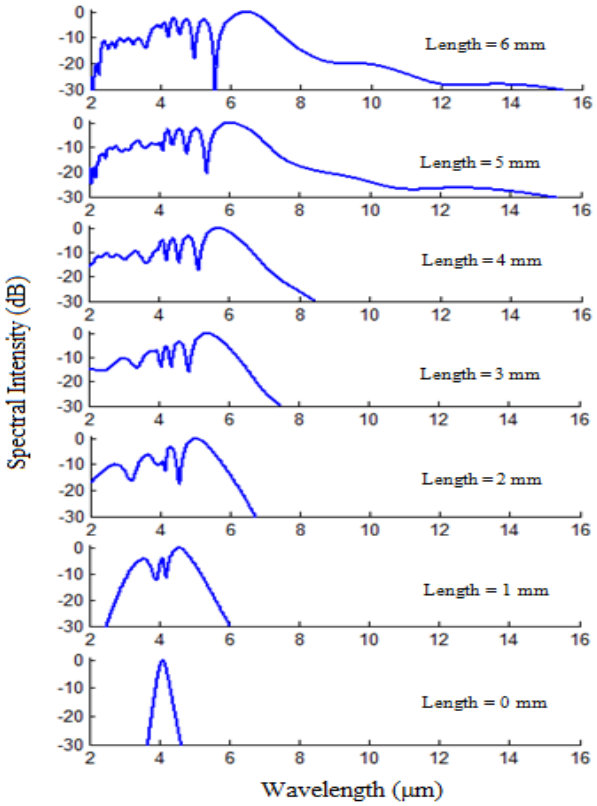

Fig.7: Spectral broadening of supercontinuum spectra from various length of PCF; when 50 fs laser pulses with peak power of 3.5 kW launched at proposed triangular-core graded-index PCF structure.

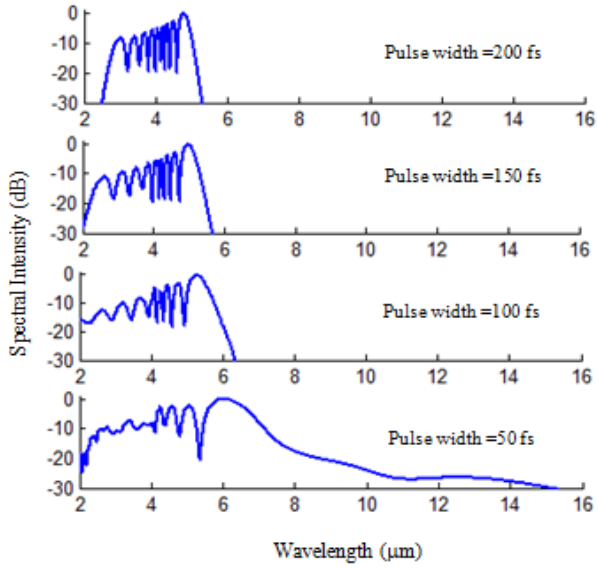

Fig.8: Broadening of output spectra from 5 mm long TCGI PCF obtained at various values of pulse width (T_{FWHM}) when peak power of incident pulses = 3.5 kW.

This article has been accepted for publication in a future issue of this journal, but has not been fully edited. Content may change prior to final publication. Citation information: DOI 10.1109/JLT.2015.2418993, Journal of Lightwave Technology

TABLE I
GEOMETRICAL PARAMETERS OF PROPOSED TCGI PCF

Parameter name	Pitch	d_1	d_2	d_3	d_4
Parameter value	1000 nm	420 nm	700 nm	800 nm	900 nm

TABLE II
OPTIMIZED INPUT PULSE PARAMETERS

Parameter name	Peak power	T_{FWHM}	Pulse shape
Parameter value	3.5 kW	50 fs	hyperbolic secant

V. CONCLUSIONS

A new design of triangular-core graded-index PCF for ultra-broadband SCG in mid-infrared regime covering atmospheric transparent windows (*i.e.* 3 – 5 μm, and 8 – 13 μm of spectrum region) and the molecular 'fingerprint region' from 2 – 15 μm, is reported in this paper. Such broadband mid-infrared spectrum is achieved by launching 50 fs laser pulses from mode-locked Tm-doped fiber laser with peak power of 3.5 kW on a very small length (*i.e.* 5 mm) of proposed PCF. Simulated results indicate that the proposed PCF structure offers nonlinear coefficient as high as 1944 $W^{-1}\times Km^{-1}$ at 4.1 μm pump wavelength with effective mode area of 4.1 μm^2. This new type of photonic crystal fiber can be a good candidate for generating efficient supercontinuum which is applicable for various nonlinear applications such as gas sensing, food quality control and early cancer diagnostics.

REFERENCES

[1] I. Hartl, X. D. Li, C. Chudoba, R. K. Ghanta, T. H. Ko, J. G. Fujimoto, J. K. Ranka, and R. S. Windeler, "Ultrahigh-resolution optical coherence tomography using continuum generation in an air-silica microstructure optical fiber," *Opt. Lett.* ***26***, 608–610 (2001).

[2] P. Hsiung, Y. Chen, T. H. Ko, J. G. Fujimoto, C. J. S. de Matos, S. V. Popov, J. R. Taylor, and V. P. Gapontsev, "Optical coherence tomography using a continuous-wave, high-power, Raman continuum light source," *Opt. Express* ***12***, 5287–5295 (2004).

[3] H. Takara, T. Ohara, T. Yamamoto, H. Masuda, M. Abe, H. Takahashi, and T. Morioka, "Field demonstration of over 1000-channel DWDM transmission with supercontinuum multi-carrier source," *Elect. Lett.* ***41***, 270–271 (2005).

[4] J. Ye, H. Schnatz, and L. Hollberg, "Optical frequency combs: from frequency metrology to optical phase control," *IEEE J. Sel. Topics Quant. Elect.* ***9***, 1041–1058 (2003).

[5] C. Dunsby, P. M. P. Lanigan, J. McGinty, D. S. Elson, J. Requejo-Isidro, I. Munro, N. Galletly, F. McCann, B. Treanor, B. Onfelt, D. M. Davis, M. A. A. Neil, and P. M. W. French, "An electronically tunable ultrafast laser source applied to fluorescence imaging and fluorescence lifetime imaging microscopy," *J. Phys. D: Applied Physics* ***37***, 3296–3303 (2004).

[6] S. Sanders, "Wavelength-agile fiber laser using group-velocity dispersion of pulsed super-continua and application to broadband absorption spectroscopy," *Appl. Phys. B: Lasers and Optics* ***75***, 799–802 (2002).

[7] M. Ere-Tassou, C. Przygodzki, E. Fertein, and H. Delbarre, "Femtosecond laser source for real-time atmospheric gas sensing in the UV - visible," *Opt. Commun.* ***220***, 215–221 (2003)

[8] J. Wegener, R. H. Wilson and H. S. Tapp, "Mid-infrared spectroscopy for food analysis: recent new applications and relevant developments in sample presentation methods," *Trends Anal. Chem.* ***18***, 85-93 (1999).

[9] A. B. Seddon "A prospective for new mid-infrared medical endoscopy using chalcogenide glasses," *Int. J. Appl. Glass Sci.* ***2***, 177-191 (2011).

[10] J. M. Dudley, G. Genty, and S. Coen, "Supercontinuum generation in photonic crystal fiber," *Rev. Mod. Phys.* ***78***, 1135–1184 (2006).

[11] J. Swiderski and M. Michalska, "Mid-infrared supercontinuum generation in a single-mode thulium-doped fiber amplifier," *Laser Phys. Lett.* ***10***, 035105(2013).

[12] J. K. Ranka, R. S. Windeler and A. J. Stentz, "Visible continuum generation in air silica microstructured optical fibers with anomalous dispersion at 800 nm," *Opt. Lett.* ***25(1)***, 25-27 (2000).

[13] T. S. Saini, A. Baili, V. Dahiya, A. Kumar, R. Cherif, M. Zghal, R. K. Sinha, "Design of equiangular spiral photonic crystal fiber for supercontinuum generation at 1550 nm," *Proc. SPIE 9200, Photonic Fiber and Crystal Devices: Advances in Materials and Innovations in Device Applications VIII*, 920012 (September 5, 2014).

[14] T. S. Saini, A. Kumar, R. K. Sinha, "Highly Nonlinear Triangular core photonic crystal fiber with all normal dispersion for supercontinuum generation," *Frontier in Optics (FiO)*, Oct. 19-23, 2014, paper: FW1D-4

[15] M. El-Amraoui, G. Gadret, J. C. Jules, J. Fatome, C. Fortier and J. Troles, "Microstructured chalcogenide optical fibers from As_2S_3 glass: towards new IR broadband sources," *Opt. Express* ***18***, 26655-26665 (2010).

[16] L. Liu, G. Qin, Q.Tian, D. Zhao, and W. Qin, "Numerical investigation of mid-infrared supercontinuum generation up to 5 μm in single mode fluoride fiber," *Opt. Express* ***19,*** 10041-10048 (2011).

[17] W. Yuan "2–10 μm mid-infrared supercontinuum generation in As_2Se_3 photonic crystal fiber," *Laser Phys. Lett.* ***10(9),*** 095107 (2013).

[18] P. Yan, R. Dong, G. Zhang, H. Li, S. Ruan, H. Wei, J. Luo, " Numerical simulation on the coherent time-critical 2-5 μm supercontinuum generation in an As_2S_3 microstructured optical fiber with all-normal flat-top dispersion profile," *Opt. Commun.* ***293***, 133-138 (2013).

[19] T. S. Saini A. Kumar, and R. K. Sinha, "Broadband mid-IR supercontinuum generation in As_2Se_3 based chalcogenide photonic crystal fiber: A new design and analysis," *Opt. Commun.* ***347***, 13 – 19 (2015).

[20] V. Shiryaev and M. Churbanov, "Trends and prospects for development of chalcogenide fibers for mid-infrared transmission," *J. Non-Cryst. Solids* ***377***, 225 – 230 (2013).

[21] R. E. Slusher, G. Lenz, J. Hodelin, J. Sanghera, L. B. Shaw, and I. D. Aggarwal, "Large Raman gain and nonlinear phase shift in high-purity As_2Se_3 chalcogenide fibers," *J. Opt. Soc. Am. B* ***21***, 1146–1155 (2004).

[22] L. B. Shaw, V. Q. Nguyen, J. S. Sanghera, I. D. Aggarwal, P. A. Thielen, and F. H. Kung, "IR supercontinuum generation in As-Se photonic crystal fiber," *Proc. Advanced Solid State Photonics*, paper TuC5 (2005).

[23] J. Hu, C. R. Menyuk, L. B. Shaw, J. S. Sanghera, and I. D. Aggarwal, "Maximizing the bandwidth of supercontinuum generation in As_2Se_3 chalcogenide fibers," *Opt. Express* ***18(7),*** 6722-6739 (2010).

[24] I. Kubat, C. S. Agger, P. M. Moselund, O. Bang, "Mid-infrared supercontinuum generation to 4.5 μm in uniform and tapered ZBLAN step-index fibers by direct pumping at 1064 or 1550 nm," *J. Opt. Soc. Am. B 30* ***(16),*** 2743-2757 (2013).

[25] M. Klimczak, B. Siwicki, P. Skibinski, D. Pysz, R. Stepien, A. Heidt, C. Radzewicz, and R. Buczynski, "Coherent supercntinuum generation up to 2.3 μm in all-solid soft-glass photonic crystal fibers with flat all-normal dispersion," *Opt. Exp.* ***22(15),*** 18824 – 18832 (2014).

[26] I. Kubat, C. R. Petersen, U. V. Moller, A. Seddon, T. Benson, L. Brilland, D. Mechin, P. M. Moselund, and O. Bang, "Thulium pumped mid-infrared 0.9-9 μm supercontinuum generation in concatenated fluoride and chalcogenide glass fibers," *Opt. Express* ***22 (4),*** 3959 - 3969 (2014).

[27] I. Kubat, C. S. Agger, U. Moller, A. B. Seddon, Z. Tang, S. Sujecki, T. M. Benson, David Furniss, S. Lamrini, K. Scholle, P. Fuhrberg, B. Napier, M. Farries, J. Ward, P. M. Moselund, and O. Bang, "Mid-infrared supercontinuum generation to 12.5μm in large NA chalcogenide step-index fibres pumped at 4.5μm," *Opt. Exp.* ***22(16),*** 19169-19182 (2014).

[28] C. R. Petersen, U. Moller, I. Kubat, B. Zhou, S. Dupont, J. Ramsay, T. Besson, S. Sujecki, N. Abdel-Moneim, Z. Tang, D. Furniss, A. Seddon, and O. Bang, "Mid-infrared supercontinuum covering the 1.4 – 13.3 μm molecular fingerprint region using ultra-high NA chalcogenide step-index fibre," *Nature Photon.* Sept. (2014)

[29] G. P. Agrawal, "Nonlinear Fiber Optics," 5th ed., Elsevier Academic Press, 2013.

[30] W. Liu, L. Pang, X. Lin, R. Gao, and X. Song, "Observation of soliton fission in microstructured fiber," Appl. Opt. 51(34), 8095 – 8101 (2012)

[31] A. V. Husakov and J. Herrmann, "Supercontinuum generation of higher order solitons by fission in photonic crystal fibers," *Phys. Rev. Lett.* ***87,*** 203901 (2001).
[32] G. Steinmeyer and J. S. Skibina, "Entering the mid-infrared," *Nature Photon. (news & views)* ***8(11)***, 814-815 (2014).
[33] N. Leindecker, A. Marandi, R. L. Byer, K. L. Vodopyanov, J. Jiang, I. Hartl, M. Fermann, and P. Schunemann, "Octave-spanning ultrafast OPO with 2.6 – 6.1 μm instantaneous bandwidth pumped by femtosecond Tm-fiber laser," Opt. Express 20, 7046- 7053 (2012).
[34] H. G. Dantanarayana, N. Abdel-Moneim, Z. Tang, L. Sojka, S. Sujecki, D. Furniss, A. B. Seddon, I. Kubat, O. Bang, and T. M. Benson, "Refractive index dispersion of chalcogenide glasses for ultra-high numerical-aperture fiber for mid-infrared supercontinuum generation," *Opt. Mat. Exp.* ***4(7),*** 1444-1455 (2014)
[35] B. Ung and M. Skorobogatiy, "Chalcogenide microporous fibers for linear and nonlinear applications in the mid-infrared," *Opt. Exp.* ***18(8),*** 8647-8659 (2010).
[36] B. Hooda and V. Rastogi, "Segmented-core single mode optical fiber with ultra-large-effective-area, low dispersion slop and flattened dispersion for DWDM optical communication systems," *Progress Electrom. Res. B* **51**, 157-175 (2013)

Than Singh Saini was born in the year of 1984 in Aligarh, India. He received the B. Sc (PCM) and M. Sc. (Physics) degrees in the year of 2004 and 2006 respectively from Dr. B. R. A. University, Agra, India. Currently, He is pursuing Ph.D (Optics & Photonics) from Delhi Technological University, Delhi, India. His area of research interest includes specialty optical fibers and waveguides for high power applications, supercontinuum generation in PCF, slow-and-fast light generation in PCF. He received three best paper presentation awards in three international conferences. He has published 20 research papers in international journals and conference proceedings. He is the student member of SPIE and OSA.

Ajeet Kumar was born in 1983 in India. He received the B. Sc degree from Deen Dayal Upadhayay Gorakhpur University, Gorakhpur, India in 2002, the M. Sc degree from Indian Institute of Technology Roorkee, Roorkee, India in 2004, and the Ph.D degree from the Indian Institute of Technology Roorkee, Roorkee, India in 2009. He worked as a postdoctoral fellow in Gwangju Institute of Science and Technology (GIST), Korea. In July 2010 he joined the Delhi Technological University, Delhi, where he is currently working as an assistant professor. He has published more than 70 research articles in journal and conferences. His current research interests are novel large mode area single-mode fibers, segmented cladding fibers, fiber optic sensors, large-core fiber for solar delivery system and waveguide long period gratings. Dr. Kumar is also recipient of Young Scientist award by Uttarakhand Goverenment, India. He is member of OSA and IEEE.

R. K. Sinha received M. Sc. degree in Physics from the Indian Institute of Technology (IIT), Kharagpur, India, in 1984, and Ph.D. degree in the area of Fiber Optics and Optical Communication Technology from the IIT, Delhi, India, in 1990. He had held various research and academic positions at Indian Institute of Science (IISc), Bangalore during 1991, Birla Institute of Technology and Science (BITS) Pilani during 1992-1994, REC (now NIT) Hamirpur during 1994-1998 and at Delhi College of Engineering-DCE (now Delhi Technological University-DTU), University of Delhi during 1998 to till date. He is currently a Professor of Applied Physics, Dean (Academic-UG) & Chief Coordinator of Technology Information, Forecasting and Assessment Council (TIFAC)–Centre of Relevance and Excellence (CORE) in Fiber Optics and Optical Communication at DTU, Delhi. He is a recipient of Fulbright-Nehru, National Science Council Taiwan, Indo-Swiss Bilateral, Royal Academy of Engineering (UK) and Japan Society for Promotion of Science fellowships and Japanese Government Scholarship in addition to assignment of Visiting Scientist at ICTP-Trieste, Italy, IROST (Iran) and University of Campinas, Brazil. He is also a recipient of Biman-Behari Sen Memorial award 2012, CEOT Optoelectronics Technology award 2004 and S.K.Mitra Memorial Award 2002 from Institution for Electronics and Telecommunication Engineers (IETE) - India, for his outstanding research work in the area of Photonic Crystal Fibers and Photonic Crystal based Nanophotonic Devices. He is a Fellow of International Society for Optical Engineers (SPIE), a Fellow of IETE and a Fellow of Optical Society of India. He has published over 220 research papers in the leading journals and conference proceedings. Prof. Sinha has also served numerous administrative responsibilities like Head of Department of Applied Physics, Dean (Industrial Research and Development), Chairman of many academic and advisory bodies related to education, research and product development in the areas of Optics and Photonics.

International Journal of Current Engineering and Technology
E-ISSN 2277 – 4106, P-ISSN 2347 – 5161

Available at http://inpressco.com/category/ijcet

Research Article

Conceptual Design of Magnetorheological Brake using TK Solver

Chiranjit Sarkar†* and Harish Hirani‡

†Mechanical Engineering Department, Delhi Technological University, Shahbad Daluatpur, Bawana Road, Delhi – 110042, India
‡Mechanical Engineering Department, Indian Institute of Technology Delhi, Hauz Khas, New Delhi – 110016, India

Accepted 01 April 2015, Available online 06 April2015, **Vol.5, No.2 (April 2015)**

Abstract

The aim of this paper is to design a magnetorheological brake (MRB) system, which has potential to replace the existing automobile mechanical shoe-pedal brake system. The proposed brake system consists of rotary disks immersed in a MR fluid and enclosed in an electromagnet. The yield stress of the fluid varies as a function of magnetic field created by electric current passing through the electromagnet. The instantaneous increase in yield stress of fluid significantly increases the friction on the surfaces of rotating disks; thus generating a retarding braking torque. Unfortunately, MR fluids do not show linear increment in shear strength with increase in applied magnetic field, and finally shear strength gets saturated. Therefore in the present study, the non-linear behavior of shear strength and its saturation limits to estimate the braking torque exercised by MR brake have been incorporated. A parametric study considering various configurations of rotating disk and MR gap has been presented. Finally, based on analysis, merits of the multidisc MR brake have been highlighted.

Keywords:*MR fluid, MR brake, Multi disk MR Brake.*

1. Introduction

Magnetorhelogical (MR) suspensions are known for dramatic change in their apparent viscosity. Due to their variable viscosity, MR fluids are used in engineering applications requiring controllable dynamic performance. One such application is magnetorheological brake in which MR fluid is treated as a brake lining material. This material does not wear-away and provides desirable friction resistance by just controlling the magnetic field passing through it. As MR brake involves electromagnetism and magnetisable friction material, this system can be named as "electromagnetic brake" (Gupta and Hirani, 2011).

A typical MR fluid consists of 20-40 volume percentage of pure-iron (purity > 99%) particles (size: Ø3-10 micrometers), suspended in a carrier liquid such as mineral oil, synthetic oil, water or glycol. A variety of proprietary additives to avoid gravitational settling, to elude wear and to promote particle suspension, are added to MR fluids. To model the behavior of MR fluids, the Bingham plastic model (Ginder and Davis, 1994) is used. MR fluids exhibit maximum yield strengths of 50-100 kPa for applied magnetic fields of 150-250 kA/m. The performance of MR-based devices is relatively insensitive to temperature over a broad temperature range (Ginder and Davis,1994).

The design of MR brake starts with the maximum shear strength, τ_{max}, achievable by the available MR fluid. The control on the shear stress (between zero to τ_{max}) of MR fluid is achieved by regulating the magnitude and direction of the magnetic field. The field density is a function of permeability and saturation of materials through which magnetic field passes, brake geometry, number of turns in electromagnetic coil, and current supplied to electromagnetic coil (Sarkar and Hirani, 2015), (Sarkar and Hirani, 2013), (Sukhwani, *et al*, 2009), (Sukhwani and Hirani, 2008), (Sukhwani and Hirani, 2008), (Hirani and Manjunatha, 2007), (Sukhwani, *et al*, 2007), (Sukhwani, *et al*, 2006), (Gupta and Hirani, 2011), (Muzakkir and Hirani, 2015), (Muzakkir, *et al*, 2015). Unfortunately, MR fluids do not show linear increment in shear strength with increase in applied magnetic field, and finally shear strength gets saturated. Therefore in the present study, the non-linear behavior of shear strength and saturation limits to estimate the braking torque exercised by MR brake have been incorporated.

2. Conceptual Design and Development of MR Brake

The MR brake consisting of MR fluid, disk and brake pad as shown in figure 1. Four configurations of MR Brake, considered in the present study, are shown in figure 2.

In configuration 1, brake pad inner radius is r1, its outer radius is r2. The brake pad material is ferromagnetic. When the electric current is supplied to

*Corresponding author: **Chiranjit Sarkar**

the central electromagnet, the MR fluid in the hollow cylindrical area having bore-radius as r1 and outer radius as r2 gets magnetized. The configuration 2 is similar to configuration 1, but the only the difference is radius of rotor is almost equal to the bore radius of housing. This especially is required to minimize the leakage of MR fluid from the brake. In configuration 3, along with the presence of MR fluid at side surfaces of disk, MR fluid is placed on the periphery of the rotating disk. Therefore, when the magnetic field is applied, additional braking due to the MR fluid in the annular region o defined by radius r2, (r2+h) and width w1 is achieved. The configuration 4 shows multi-disk MR brake. Here three rotating disks have been used, which increase the MR effect in the presence of magnetic field.

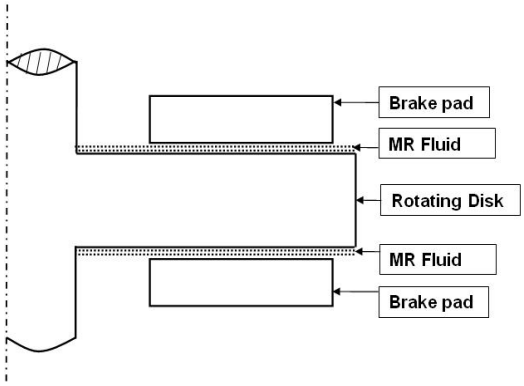

Fig.1 Block diagram of MR Brake

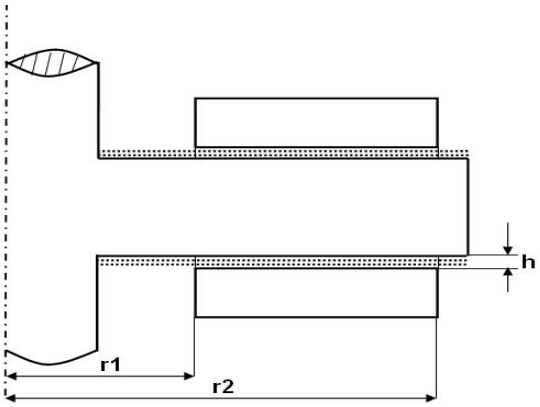

Configuration 1

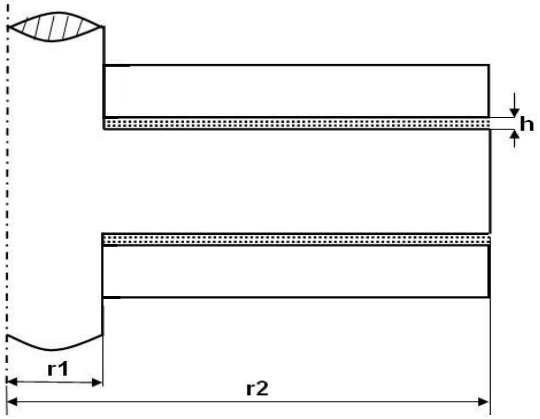

Configuration 2

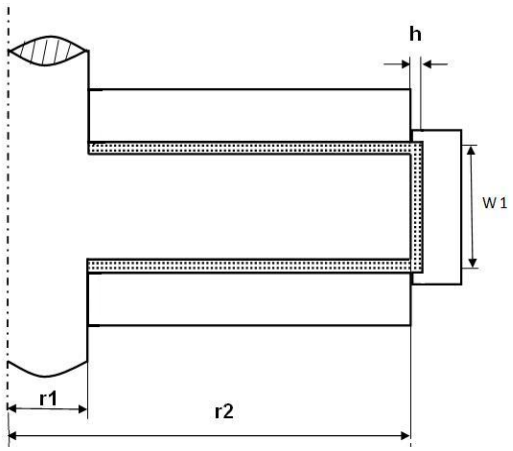

Configuration 3

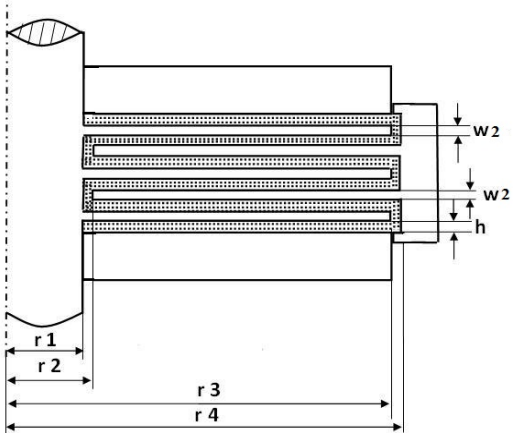

Configuration 4

Fig.2 Four Different Configurations of MR brake

3. Mathematical Modeling

The shear stress of MR fluid is often modeled using Bingham model equation,

$$\tau = \tau_{yd} + \eta\dot{\gamma} \quad (1)$$

Where, $\tau_{yd}$is field induced yield stress, η is viscosity of the MR Fluid and Shear rate, $\dot{\gamma} = \frac{\omega^* r}{h}$.
Here h is gap between disk and brake pad, r is radius and $\omega$is angular speed. Therefore,

$$\tau = \tau_{yd} + \eta \cdot \frac{\omega^* r}{h} \quad (2)$$

Expression of brake torque for MR brake configuration 1 and configuration 2 are same and can be expressed as

$$T_1 = T_2 = 2\pi h(r_2^2 - r_1^2)\tau_{yd} + \frac{4}{3}\eta\pi\omega(r_2^3 - r_1^3) \quad (3)$$

Expression of brake torque for MR brake configuration 3 can be expressed as

$$T_3 = 2\pi h\tau_{yd}(r_2^2 - r_1^2) + \frac{4}{3}\pi\eta\omega(r_2^3 - r_1^3) + \pi w_1\tau_{yd}(r_3^2 - r_2^2) + \frac{2\pi w_1\eta\omega}{3h}(r_3^3 - r_2^3) \quad (4)$$

Expression of brake torque for MR brake configuration 4 can be expressed as

$$T_4 = 6\left\{2\pi h\tau_{yd}(r_3^2 - r_1^2) + \frac{4\pi\eta\omega}{3}(r_3^3 - r_1^3) + \pi w_1\tau_{yd}(r_4^2 - r_3^2) + \frac{2\pi w_1\eta\omega}{3h}(r_4^3 - r_3^3) + \pi w_1\tau_{yd}(r_2^2 - r_1^2) + \frac{2\pi w_1\eta\omega}{3h}(r_2^3 - r_1^3)\right\} \quad (5)$$

As, with increase in magnetic field, the yield stress MR fluid increases, the logarithmic relation (Sarkar and Hirani, 2013)between the yield stress (τ_{yd}) and magnetic field (H) is as follows.

$$\log(\tau_{yd}(B)) = A_1(\log(H))^3 - B_1(\log(H))^2 + C_1\log(H) - D_1 \quad (6)$$

In this equation (6) coefficients A_1, B_1, C_1 and D_1 are specific to the MR fluid.

Equations (3) to (5) show the brake torque output of MR brake of given configuration increases with increase of yield stress but the maximum value of yield stress is governed by saturation magnetization of magnetic material as given by Equation (6) and will put an upper limit on the maximum value of braking torque. Therefore magnetic saturation should be accounted while calculating brake torque output. In this research work, LORD MRF-336AG silicone-based MR fluid (Lord, 2006) (Sukhwani and Hirani, 2008)has been taken for theoretical torque calculations of the MR brake. The magnetic field intensity (H) generated by an electromagnet (17) of MR brake can be expressed by Equation (7).

$$H = \frac{NI}{2h} \quad (7)$$

4. Results and Discussion

For configuration 1, torque in terms of control current and speed has been derived by substituting values of τ_{yd} (Eq. 8) in Equation (3).Here, N=1000,$r_1 = 0.121\ m, r_2 = 0.206\ m, \omega = 43.77\frac{rad}{sec}, \eta = 0.09\ Pas$.

The perform parametric study three values of h 0.25 mm, 0.75 mm and 1.25 mm were selected. The variation in torque T as function of gap h and control current is plotted in the Figure 5. To consider the saturation, the maximum value of $\tau_{yd}$was restricted to 56 kPa. Torque values obtained using this constraint $\tau_{yd} \leq 56$ kPa is plotted in Figure 6.These results indicate on accounting saturation, the braking torque increases with increase in MR gap.

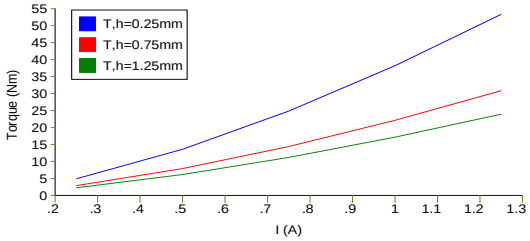

Fig. 5 Torque vs. Current for configuration 1 without saturation

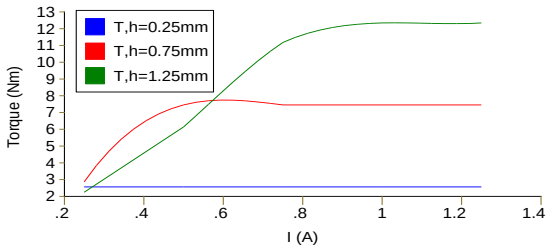

Fig. 6 Torque vs. Current for configuration 1 withsaturation

In configuration 2, r_1 = 0.063 m and r_2 = 0.2135 m. The MR gap, h varies from 0.50 mm to 1 mm. The variation of torque T with the gap h atdifferent control currents is listed in the Table 1. The braking torque saturates at 7.38 Nm and 14.67 Nm for MR gap (h) 0.5 mm and 1 mm respectively.

Table1 Maximum Torque produced at different current at configuration 2.

I, current (A)	Maximum torque at configuration 2			
	Without saturation		With saturation	
	h = 0.5mm	h = 1.0mm	h = 0.5mm	h = 1.0mm
0.25	5.1944	3.7118	5.1944	3.7188
0.50	14.4061	10.2325	7.3479	10.2325
0.75	26.3349	18.6674	7.3479	14.6689
1.0	40.4608	28.6559	7.3479	14.6689
1.25	56.4835	39.9857	7.3479	14.6689

In configuration 3, width W_1 is taken as $0.045m$. The values of torque T as a function of h and control currents are plotted in Figure 7. Figure 8 shows the saturation at h=0.25mm, 0.75mm and 1.25 mm. Therefore, the values of maximum braking torque are 144.01 Nm, 60.51 Nm and 42.49 Nm for MR gap (h) 0.25 mm, 0.7 mm and 1.25 mm respectively. The braking torque saturates at 7.84 Nm, 14.73 Nm and 21.96 Nm for the corresponding MR gaps. These results indicate that the braking torque increases with increase in MR gap.

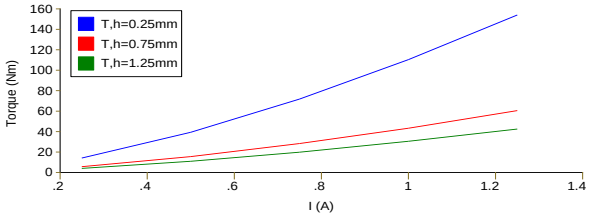

Fig.7 Torque vs. Current for configuration 3 without saturation

In case of configuration 4, $w_2 = 0.003m, r_1 = 0.063m, r_2 = 0.064m, r_3 = 0.213m, and\ r_4 = 0.215m$. The variation of torque T with the gap h for different control currents is shown in Table 2. It shows the saturation of braking torque for MR gaps, h = 0.5mm and h = 1 mm. The braking torque saturates at 43.10 Nm and 86.20 Nm for MR gap (h) 0.5 mm and 1 mm respectively. Theoretical estimations show that the multi disk MR brake provides better torque as compared to single disk MR brake.

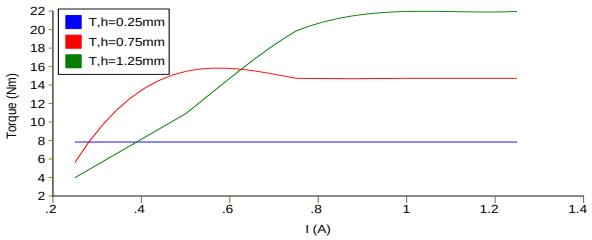

Fig.8 Torque vs. Current for configuration 3with saturation

Table 2 Maximum Torque produced at different current at configuration 4.

I, current (A)	Maximum torque at configuration 4			
	Without saturation		With saturation	
	h = 0.5mm	h = 1.0mm	h = 0.5mm	h = 1.0mm
0.25	32.4710	22.7973	32.4710	22.7973
0.50	90.0481	62.7273	43.1000	62.7272
0.75	164.6077	114.4345	43.1000	86.2000
1.0	252.9000	175.6660	43.1000	86.2000
1.25	353.0495	245.1195	43.1000	86.2000

Conclusions

- In this study performance of a MR fluid brake has been evaluated to investigate its brake torque characteristics. Following conclusions can be drawn from this study:
- Analytical equation to estimate torque resistance offered by brake in terms of direct current and rotational speed has been derived.
- Multidisc MR brake is the best conceptual design as far as maximum torque is concerned.
- It is necessary to account the saturation of MR fluids. MR fluid having high saturation magnetic value shall be selected for the design of MR brakes.

References

C.Sarkar, H.Hirani, (2013), Theoretical and experimental studies on a magnetorheological brake operating under compression plus shear mode, *Smart Materials and Structures*, 22, art. no. 115032.

C.Sarkar, H.Hirani, (2013), Synthesis and characterization of antifriction magnetorheological fluids for brake, *Defence Science Journal*, 63, pp. 408-412.

C.Sarkar, H. Hirani, (2013), Design of a squeeze film magnetorheological brake considering compression enhanced shear yield stress of magnetorheologicalfluid, *Journal of Physics: Conference Series*, 412, 012045.

C. Sarkar, H. Hirani, (2015), Transient thermoelasticanalysis of disk brake, International Journal of Current Engineering and Technology, 5, pp. 413-418.

C. Sarkar, H. Hirani, (2015), Magnetorheological smart automotive engine mount, International Journal of Current Engineering and Technology, 5, pp. 419-428.

C. Sarkar, H. Hirani, (2015), Finite element analysis of magnetorheological brake using ANSYS, International Journal of Current Engineering and Technology, 5, pp. 725-732.

C. Sarkar, H. Hirani, (2015), Design of Magnetorheological Brake using Parabolic Shaped Rotating Disc, International Journal of Current Engineering and Technology, 5, pp. 719-724.

C. Sarkar, H. Hirani, (2015), Synthesis and characterization of nano-copper-powder based magnetorheological fluids for brake, International Journal of Scientific Engineering and Technology, 4, pp. 76-82.

C.Sarkar, H.Hirani, (2015), Effect of particle size on shear stress of magnetorheological fluids, *Smart Science,* (in press).

C.Sarkar, H.Hirani, (2015), Development of magnetorheological brake with slotted disc, *Proc. IMechE, Part D: Journal of Automobile Engineering*, pp.1-18. DOI: 10.1177/0954407015574204.

H.Hirani, C. S. Manjunatha, (2007), Performance evaluation of magnetorheological fluid variable valve, *Proc. of the Institution of Mechanical Engineers, Part D, Journal of Automobile Engineering*, 221, pp. 83-93.

J. M. Ginder, L. C. Davis,(1994), Shear Stresses in Magnetorheological fluids: Role of Magnetic Saturation, Applied Physics Letters, 65, pp. 3410-3412.

S. Gupta, H. Hirani, (2011), Optimization of magnetorheological brake, *ASME/STLE 2011 International Joint Tribology Conference*, pp 405-406.

S. M. Muzakkir, H. Hirani (2015), A Magnetorheological Fluid Based Design of Variable Valve Timing System for Internal Combustion Engine using Axiomatic Design, *International Journal of Current Engineering and Technology*, 5, pp. 603-612.

S. M. Muzakkir, M. G. Patil, H. Hirani (2015), Design of Innovative Engine Valve: Background and Need, *International Journal of Scientific Engineering and Technology*, 4, pp. 178-181.

S. M. Muzakkir, M. G. Patil, H. Hirani (2015), Design of Innovative Engine Valve, *International Journal of Scientific Engineering and Technology*, 4, pp. 212-217.

V.K.Sukhwani, V.Lakshmi, H. Hirani, (2006), Performance evaluation of MR brake: an experimental study, *Indian Journal of Tribology*, pp. 67-52.

V.K.Sukhwani,H.Hirani,T.Singh,(2007), Synthesis of magnetorheologicalgrease,*Greasetech India*.

V.K.Sukhwani, H.Hirani, (2007), Synthesis and characterization of low cost magnetorheological (MR) fluids, *The 14th International Symposium on: Smart Structures and Materials & Nondestructive Evaluation and Health Monitoring*, 65262R-65262R-12.

V.K.Sukhwani, H.Hirani, (2008), A comparative study of magnetorheological-fluid-brake and magnetorheological-grease-brake, *Tribology Online*, 3, pp. 31-35.

V.K.Sukhwani, H.Hirani, T.Singh, (2008), Synthesis and performance evaluation of MR grease, *NLGI Spokesman*,71.

V.K.Sukhwani, H. Hirani, (2008), Design, development and performance evaluation of high speed MR brake, *Proc. Institute Mech. Engineers., Part L, Journal of Materials: Design and Applications*, 222,pp.73-82.

V.K.Sukhwani, H.Hirani, T. Singh, (2009), Performance evaluation of a magnetorheological grease brake, *Greasetech India*, 9,pp. 5-11.

ARTICLE IN PRESS
+ MODEL
IIMB Management Review (2015) xx, 1–13
available at www.sciencedirect.com
ScienceDirect
journal homepage: www.elsevier.com/locate/iimb

ROUND TABLE

Critical success factors for implementation of supply chain management in Indian small and medium enterprises and their impact on performance

Ravinder Kumar [a,*], Rajesh K. Singh [b], Ravi Shankar [c]

[a] Maharaja Agarsen Institute of Technology, Sector-22, Rohini, Delhi, India
[b] Mechanical & Production Engineering Department, Delhi Technological University, Delhi, 110042, India
[c] Department of Management Studies, Indian Institute of Technology (IIT), Hauzkhas, Delhi, India

KEYWORDS
Supply chain management;
Performance;
Critical success factors;
Small and medium enterprises

Abstract Globalization of the economy, e-business, and introduction of new technologies pose new challenges to all organizations especially for small and medium enterprises (SMEs). In this scenario, successful implementation of supply chain management (SCM) can give SMEs an edge over their competitors. However, SMEs in India and other developing countries face problems in SCM implementation due to lack of resources and direction. Against this backdrop, this paper identified 13 critical success factors (CSFs) for implementation of SCM in SMEs and studied their impact on performance of Indian SMEs. Top management commitment, long-term vision, focus on core strengths, devoted resources for supply chain, and development of effective SCM strategy emerged as the most pertinent CSFs. To measure improvement in performance, the authors considered different measures related to customer service and satisfaction, innovation and growth, financial performance, and internal business. Results are analysed by testing research propositions using standard statistical tools.

Introduction

To effectively compete in the global market, small scale organizations should focus on improving the effectiveness of operational functions with effective supply chain management (Singh, Garg, & Deshmukh, 2010). Prior to the 1990s,

* Corresponding author. Tel.: +91 9868387251.
E-mail address: ravi_1_kumar@yahoo.com (R. Kumar).
Peer-review under responsibility of Indian Institute of Management Bangalore.

http://dx.doi.org/10.1016/j.iimb.2015.03.001

Please cite this article in press as: Kumar, R. et al., Critical success factors for implementation of supply chain management in Indian small and medium enterprises and their impact on performance, IIMB Management Review (2015), http://dx.doi.org/10.1016/j.iimb.2015.03.001

Indian organizations operated in a protected environment. There was little competition even among domestic players. Business was driven by almost monopolistic strategies. However the deregulation of the Indian economy in the 1990s has attracted global players in every industrial sector and has unleashed a new competitive spirit in Indian organizations (Saxena & Sahay, 2000). Statistics reveal that India, the fifth largest country in terms of gross national product (GNP) and purchasing power parity (PPP) (World Bank, 1999) and a consumer base of over a billion (CMIE, 2000), constitutes one of the fastest growing markets in the world. India is also counted among the richest with regard to cheap skilled labour, scientific and technological resources and entrepreneurial talents. However, Indian small and medium enterprises (SMEs) find global competition very challenging (Singh, Garg, & Deshmukh, 2008a) To face competition in global markets, SMEs should have effective collaboration with their customers and suppliers, and should be competitive in terms of cost, quality, innovation, and delivery. Successful implementation of supply chain management (SCM) can play a significant role in meeting these challenges and SMEs should have an effective supply chain strategy. Critical success factors (CSFs) of SCM represent a wide variety of strategies devoted to improving operational efficiency and competitiveness of SMEs. In this paper, the authors have identified 13 CSFs for SCM from literature (Table 1). The authors have further attempted to study the effects of the SCM initiatives taken by Indian SMEs on their performance. For this study, issues of performance have been considered based on the balanced score card method. The performance measures included are customer service and satisfaction, innovation and growth, financial performance, and internal business. Previous studies have not analysed the impact of CSFs on different performance measures in a holistic manner like the present study does. This paper has been organised as follows: The second section discusses the literature review and identification of CSFs. The third section discusses research objectives and methodology. The fourth section discusses the findings from the questionnaire-based survey. The fifth section discusses correlation and regression analysis for testing of research propositions. Finally, the sixth section discusses concluding remarks.

Table 1 Assessment of critical success factors in literature.

S.No.	Critical success factors (CSFs)	References
1.	Top management commitment	Fisher (1997), Shin, Collier, and Wilson (2000), Arshinder, Kanda, and Deshmukh (2008), Singh et al. (2008c), Stanley et al. (2009), Sandberg and Abrahamsson (2010), Singh (2011), Singh (2013)
2.	Development of effective SCM strategy	Lee (2000), Cao, Zhang, To, and Ng (2008), Soroor, Tarokh, and Shemshadi (2009), Singh et al. (2010), Singh et al. (2012), Kumar, Singh, and Shankar (2014)
3.	Devoted resources for supply chain	Shin et al. (2000), Gunasekaran, Mcneil, Mcgaughey, and Ajasa (2001), Singh et al. (2010), Singh (2013)
4.	Logistics synchronization	Bowersox (1990), Simatupang, Wright, and Sridharan (2002), Thakkar, Kanda, and Deshmukh (2008), Singh et al. (2012), Kumar, Singh, and Shankar (2013), Kumar, Singh, and Shankar (2015)
5.	Use of modern technologies	Lee, Padmanabhan, and Whang (1997), Arshinder et al. (2008), Thakkar et al. (2008), Singh (2013)
6.	Information sharing with SC members	Ramdas and Spekman (2000), Ozer (2003), Stanley et al. (2009), Singh et al. (2012)
7.	Forecasting of demand on point of sale (POS)	Francesca et al. (2008), Arshinder et al. (2008), Marek and Malyszek (2008)
8.	Trust development in SC partners	Anderson and Narus (1990), Morgan and Hunt (1994), Sahay (2003), Bianchi and Saleh (2010), Singh (2013), Tejpal, Garg, and Sachdeva (2013)
9.	Developing just in time (JIT) capabilities in system	Grittel and Weiss (2004), Arshinder, Kanda, and Deshmukh (2007), Othman and Ghani (2008), Singh (2013)
10.	Development of reliable suppliers	Olorunniwo and Hartfield (2001), Petersen, Handfield, and Ragatz (2005), Othman and Ghani (2008), Singh, Garg, and Deshmukh (2008c), He, Zhao, Zhao, and He (2009), Kumar et al. (2013), Kumar et al. (2015)
11.	Higher flexibility in production system	Das (2001), Olhager and West (2002), Arshinder et al. (2007), Singh (2013)
12.	Focus on core strengths	Singh, Garg, and Deshmukh (2008b), Thakkar et al. (2008), Kumar, Singh, and Shankar (2012), Kumar et al. (2014)
13.	Long-term vision for survival and growth	Ganesan (1994), Morgan and hunt (1994), Thakkar et al. (2008), Singh et al. (2012), Kumar et al. (2013)

Please cite this article in press as: Kumar, R. et al., Critical success factors for implementation of supply chain management in Indian small and medium enterprises and their impact on performance, IIMB Management Review (2015), http://dx.doi.org/10.1016/j.iimb.2015.03.001

Literature review and identification of CSFs

To effectively compete in the global market, SMEs must have effective supply chain management. Conflicting objectives and lack of coordination between supply chain partners may cause uncertainties in supply and demand. Therefore effective SCM is required to streamline the supply chain of SMEs. A number of studies have attempted to identify the CSFs of SCM, Electronic Data Interchange (EDI), and Enterprise Resource Planning (ERP) systems. Bauer (2000) suggested that there are four CSFs in e-business for the automotive industry – understanding and working with diverse social and business cultures around the globe, physical internet infrastructure, understanding the state of the physical infrastructure of the suppliers, and the changing internal management processes and points of view. Power, Sohal, and Rahman (2001) examined the critical factors that influence the agility of organizations in managing their supply chains; in their study, the authors determined seven CSFs in agile SCM using factor analysis. Umble, Haft, and Umble (2003) identified the CSFs for the implementation of ERP systems. Angeles, Corritore, Choton Basu, and Nath (2001) reported 13 EDI implementation success factors that are considered relevant in implementing an inter-organizational system.

The importance of effective strategy for improving competitiveness of SMEs has been stressed in the literature (Singh et al. 2008a). Singh et al. (2008a) further observed that SMEs in general are not able to implement SCM to its full extent, mainly because they depend on bigger customers and follow the norms stipulated by them. Arend and Winser (2005) stated that larger companies consider SMEs as being easy to replace and buyers are reluctant to form partnerships with them. There are significant differences between SMEs and large companies in terms of systems, tools, supply chain and methods of electronic interface adoption. Wagner, Fillis, and Johansson (2003) observed that larger companies have the resources and technical budgets to implement e-business and e-supply strategies but SMEs continue to be challenged by resource limitations.

In SMEs, decisions are generally centrally governed by top management. Resources such as money, time, technology, manpower, and material are controlled and managed by top management. According to Ganesan and Saumen (2005) top management support is very much necessary for cross-functional training, integration of departments within the organization and vendor development for a responsive supply chain.

Studies have observed the importance of top management commitment in areas such as the successful implementation of EDI (Angeles et al. 2001), information systems (IS) (Bruwer, 1984) and ERP systems (Umble et al. 2003). The primary responsibility of the top management is to provide sufficient financial support and adequate resources for building a successful system. Further, the support of the top management will ensure that SCM implementation has high priority within the organization and that it will receive the required resources and attention. Apart from such primary support, psychological or behavioural support is also important for the smooth implementation of SCM, especially if there is significant resistance from the staff involved. Use of information technology such as internet, intranet, software applications packages and decision support systems can be applied to facilitate the information flow within the supply chain, between the members (Stanley, Cynthia, Chad, & Gregory, 2009).

Trust among supply chain partners is another important aspect for improving coordination between the partners. Anderson and Narus (1990) stated that trust is a favourable attitude that exists when one supply chain member has confidence in other supply chain members. Trust is required for flow of information in the supply chain. Risk and reward sharing influence an individual supply chain member's behaviour and his interaction with other supply chain members. Conflicts of interest are likely to occur when one supply chain member gets more benefits when compared to other members from an existing risk and reward sharing process (Cachon & Lariviere, 2005). Bianchi and Saleh (2010) stated that trust and commitment are essential for enhancing importer performance in developing countries. Arshinder, Kanda, and Deshmukh (2006) posit that conflicts in vision and goals of supply chain members result in the individual's profit maximization in place of profit maximization of all the supply chain members.

Mehrjerdi (2009) stressed long-term orientation which was expected to have three specific outcomes i.e. increased relational behaviour, decreased conflicts, and increased satisfaction. Collaborative decision making by supply chain members results in better forecasting of demand, trust between the supply chain members, and flow of information. According to Francesca, Bianco, and Mauro (2008) availability of point of sales (POS) data is important for a responsive supply chain. Since SMEs are under intense pressure to reduce cost, an appropriate inventory management system at every node of the supply chain minimizes the inventory at supply chain nodes (Marek & Malyszek, 2008). Singh, Kumar, and Shankar (2012) observed that effectiveness of Indian construction SMEs can be improved if they focus on product customization, waste reduction, housekeeping, and IT applications to reduce time lag in various processes. Ozer (2003) observed that information sharing is sharing of the inventory data, demand data, and product quality data. Periodic ordering in large batches between the manufacturer and retailer could distort original demand information due to large variance (Ozer, 2003).

Information technology (IT) has gained a lot of importance in SCM implementation in recent years. Increasingly, supply chain operations are changing from electronic data interchange systems and enterprise resource planning systems to internet/intranet to support SCM (Pant, Sethi, & Bhandari, 2003). Lancioni, Smith, and Oliva (2000) observed that use of modern technologies in SCM can lead to advantages such as cost saving, quality improvement, delivery and support, and greater competitive advantage.

Ngai, Cheng, and Ho (2004) observed that the successful implementation of web-based SCM system often requires a substantial amount of investment and intensive research. The need for such research to support a supply chain has not been fully recognized by industry practitioners. This may be due to a lack of awareness of the technologies and their benefits, and of the kind of support that a web based SCM system can provide.

Please cite this article in press as: Kumar, R. et al., Critical success factors for implementation of supply chain management in Indian small and medium enterprises and their impact on performance, IIMB Management Review (2015), http://dx.doi.org/10.1016/j.iimb.2015.03.001

Research objectives and methodology

This paper is an empirical study for identification of CSFs for implementation of SCM and focusses on their effects on the performance of Indian SMEs. Thirteen CSFs are identified from extensive literature review and experts' opinions, (see Table 1) and their effect has been studied on different categories of performance measures; these categories are customer service and satisfaction, innovation and growth, financial performance, and internal business of Indian SMEs. Based on this, the study has attempted to test the following four research propositions:

P1: There is a significant relationship between CSFs and SME performance in terms of customer service and satisfaction.
P2: There is a significant relationship between CSFs and SME performance in terms of innovation and growth.
P3: There is a significant relationship between CSFs and SME performance in terms of financial performance.
P4: There is a significant relationship between CSFs and SME performance in terms of internal business parameters.

To study the effect of different CSFs on performance of Indian SMEs, the authors studied different frameworks from literature but found none that were perfectly related. So the authors developed the following framework and tried to validate it in the current study. As the balanced score card (BSC) approach is the most prevalent, in this study the BSC model was taken as the base while developing the framework (Fig. 1). According to this framework, CSFs of SCM implementation leads to performance improvement of Indian SMEs on different categories based on the BSC approach.

In order to test research propositions and for analysis of different issues related to SCM and performance, a survey instrument was developed. The survey was conducted among Indian SMEs from the auto component, plastic, light engineering and electronics sectors from December 2010 to December 2012. Most of the SMEs were located in semi-urban areas. All of them had investments in plant and machinery as per the definition of SMEs in India. Out of the total responding SMEs, 76% were located in urban areas, 14% in semi-urban areas and 10% in rural areas. Sector wise distribution shows that out of the total responding SMEs, 34% were from the auto-sector, 40% were from light engineering/others sector, 17% from the plastic sector and 9% from the electronic/electrical sector. The authors conducted a pilot survey of 40 SMEs from different sectors to finalize the questionnaire; of the SMEs, in, 20 were from the auto component sector, 5 from the plastic sector, 10 from light engineering, and 5 from the electronics sector. Although the questionnaire was sent by post or e-mail for the final survey, most of the SMEs for the pilot survey were contacted on a personal basis for interview (through office meeting and plant visit) by making an appointment with the management. Most of the responses to the detailed survey were collected by the authors on personal visits to the SME plants since all the SMEs did not respond within the specified time limit,. An annexure was given at the end of questionnaire which contained guidelines for responses and terminology to avoid unknown biases. Most of the respondents were at the level of production manager or business head. At the end of the survey questionnaire, respondents were requested to fill their profile details, but it was optional.

The questionnaire contained two sections: Section A focussed on CSFs for implementation of SCM in Indian SMEs and Section B focussed on performance improvement (on criteria of balanced score card approach) in the past three years on the basis of different initiatives taken towards SCM implementation by Indian SMEs.

In this study, executives were asked to rate the intensity of each attribute for their respective organization on a five-point Likert scale (1 — lowest, 5 — highest). About 1500 SMEs from all parts of India were contacted for collecting responses. These organizations were selected from directories available at Confederation of Indian Industries

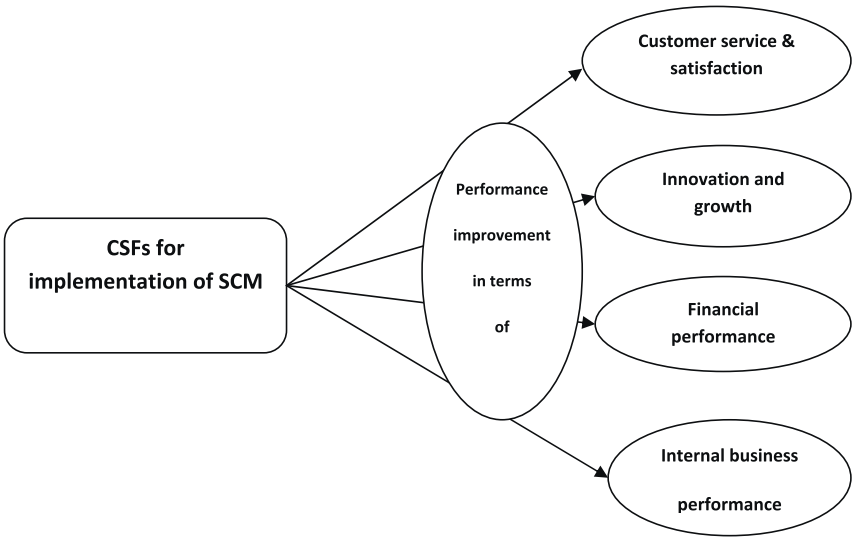

Figure 1 Framework for the study.

Please cite this article in press as: Kumar, R. et al., Critical success factors for implementation of supply chain management in Indian small and medium enterprises and their impact on performance, IIMB Management Review (2015), http://dx.doi.org/10.1016/j.iimb.2015.03.001

(CII), Auto Component Manufacturers Association, Federation of Indian Chambers of Commerce and Industries and Directorate of Industries (Government of NCT Delhi). For this study, respondents were selected based on criteria for SMEs and those belonging to manufacturing and engineering sectors. A total of 251 complete responses were obtained. SPSS 17 software has been used to analyse the collected responses. Of the 251 responding SMEs, 80% did not have a separate SCM department. Issues related to SCM were handled by top management in collaboration with the purchase and the marketing departments. Ten percent of SMEs had a separate SCM department and dedicated team to handle different supply chain issues. The remaining 10% of SMEs had little awareness of SCM,. About 30—40% of the SMEs were aware of the micro, small and medium enterprises development Act (MSMED Act, 2006) and. they were availing the benefits of all Government policies and schemes for MSME. Responses from the rest of the SMEs revealed very little knowledge about the act. The authors observed that either they were not aware of the MSMED Act and the policies and schemes intended for them or they were not in a situation to take advantage of them in the current market situation.

Findings from questionnaire-based survey

Inter-item analysis was used to check the scales for internal consistency or reliability. Cronbach's coefficient was calculated for each scale, as recommended for empirical research in operations management (Flynn, Sakakibara, Schroeder, Bates, & Flynn, 1990). The coefficients of Cronbach's α for all constructs were in the range of 0.854—0.896. These values exceed the minimum requirements of 0.5 for an exploratory study such as this one (Nunnally, 1978). Data acquired from the survey of Indian SMEs were analysed by statistical tests such as one sample t-test, correlation and regression analysis.

CSFs for SCM implementation

Bullen and Rockart (1986) observed that CSFs are few key areas where things must go right for the business to flourish and for the manager's goals to be attained. On the basis of a literature review and a pilot survey, 13 CSFs were identified for Indian SMEs to focus on during implementation of SCM. These are top management commitment, development of effective SCM strategy, devoted resources for supply chain, logistics synchronization, use of modern technologies, information sharing with supply chain members, forecasting of demand based on point of sales (POS), trust development in supply chain partners, developing just in time (JIT) capabilities in the system, development of reliable suppliers, higher flexibility in production system, focus on core strengths, and long-term vision for survival and growth. The results of this study for various CSFs for SCM implementation by Indian SMEs on a Likert scale of five (1 — lowest, 5 — highest) are shown in Table 2. It is observed that the most important factor is top management commitment with mean values of (4.2430), followed by long term vision for survival and growth (4.1355), focus on core strengths (3.9960) and devoted resources for supply chain (3.9402). These results suggest that in Indian SMEs major decisions are taken by the top management.

Sandberg and Abrahamsson (2010) also stated that top management commitment is a key enabler for effective supply chain management. Implementation of SCM proves to be very useful for long term survival. But SCM implementation requires committed management and devoted resources. Usually it is observed that SMEs do not have the time, knowledge or resources to conduct detailed analysis for implementing SCM. In the absence of a plan for long term growth, SMEs often do not understand the full implications of SCM to the organization. The other important CSFs that emerged are development of effective SCM strategy (3.8606), development of reliable suppliers (3.6414), information sharing with supply chain members (3.4343) and logistics synchronisation (3.3745). Usually SMEs work in isolation and involve middlemen in their supply chain, often losing benefits to them. . By establishing close partnerships with their suppliers and customers, SMEs could better achieve product, process and technology innovations. To improve coordination and responsiveness of the supply chain, information sharing with all members of the chain is very important. Supply chain coordination relies on the availability of prompt and accurate information

Table 2 Critical success factors for SCM implementation by Indian SMEs.

S.No	Critical success factors	Mean	Rank	S.D.	t-values	p-values	Cronbach's Alpha
1.	Top management commitment	4.2430	1	.90813	21.685	.000	.896
2.	Long-term vision for survival and growth	4.1355	2	.72497	24.814	.000	
3.	Focus on core strengths	3.9960	3	.80746	19.543	.000	
4.	Devoted resources for supply chain	3.9402	4	.79020	18.851	.000	
5.	Development of effective SCM strategy	3.8606	5	.83455	16.337	.000	
6.	Development of reliable suppliers	3.6414	6	.75823	13.403	.000	
7.	Information sharing with SC members	3.4343	7	.74744	9.205	.000	
8.	Logistics synchronization	3.3745	8	.79195	7.492	.000	
9.	Use of modern technologies	3.3108	9	.71487	6.887	.000	
10.	Higher flexibility in production system	3.2789	10	.82092	5.382	.000	
11.	Forecasting of demand on point of sale (POS)	3.1520	11	.65315	3.680	.000	
12.	Trust development in SC partners	3.1275	12	.66909	3.019	.003	
13.	Developing JIT capabilities in system	3.1116	13	.71239	2.481	.014	

Please cite this article in press as: Kumar, R. et al., Critical success factors for implementation of supply chain management in Indian small and medium enterprises and their impact on performance, IIMB Management Review (2015), http://dx.doi.org/10.1016/j.iimb.2015.03.001

that is visible to all actors in the supply chain. Coordination improves by close partnership with customers and suppliers and helps in joint development of new products, joint effort in reducing purchase lead-time, and cross training of workforces. Coordination also helps in reducing late change of design and orders, which subsequently affects the delivery/logistics performance of the companies. Coordination and responsiveness will not only benefit the suppliers and the customers, but will improve the profits of the overall supply chain.

Logistics synchronisation will help SMEs in optimising their transportation and warehousing costs. Customers' orders and the services of the organization can be effectively connected by a good logistics system.

The other CSFs that emerged in the study are use of modern technologies (3.3108), higher flexibility in production system (3.2789), forecasting of demand based on point of sales data (3.1520), trust development in supply chain partners (3.1275) and developing JIT capabilities in the system (3.1116). Use of modern technologies such as internet, electronic data interchanges, web sites, radio frequency identification (RFID) technologies and ERP helps in better management of information. Accurate, timely, and easily accessible information can improve decision making and forecasting in supply chain. Forecasting of demand based on point of sales data helps in making more accurate forecasts of customer requirements. In the context of SCM, a supplier is able to better match inventory with demand when accurate information is available about the buyer's inventory status. Flexibility in production system (3.2789) helps in dealing with changing product design and demand of customers. From the coordination point of view, trust development in supply chain partners (3.1275) is also very important. Due to a perceived lack of security, a trust deficit exists between SMEs and their partners. Developing JIT capabilities in the system ensures better utilization of resources or helps in reducing waste in different forms.

CSFs for SCM implementation (sector wise observations)
During the study, the authors observed that in the auto and light engineering sectors, the most preferred CSF while implementing SCM was top management commitment with a mean of (4.52) and (4.28) respectively. On the other hand, the plastic sector stressed on devoted resources for supply chain (4.00), and the electronic sector on long term vision for survival and growth (4.00). These results imply that while implementing SCM, different SME sectors have different preferences. . Results of the study show that Indian SMEs in the plastic sector are more concerned with resources for supply chain while making policies for SCM, while SMEs of the electronic/electrical sector pay more attention to long term vision for survival and growth. In the auto and light engineering sectors, top management commitment assumes more importance. The top five CSFs of each sector are shown in Table 3.

Further, the authors observed that in the auto sector the other significant CSFs are long-term vision for survival and growth (4.01), devoted resources for supply chain (3.88), and development of effective SCM strategy (3.81). The least preferred CSF for auto sector is forecasting of demand on point of sale (3.22). This implies that SMEs should consider the actual demand of customers according to sale data while doing forecasting of demand.

In the plastic sector, the authors observed that other important CSFs are development of effective SCM strategy (3.96), development of reliable suppliers, and focus on core strength. The least preferred CSF for the plastic sector is trust development in supply chain partners (3.15). This implies that Indian SMEs in the plastic sector should focus on trust development among its customers and suppliers to excel in the current scenario.

Table 3 Sector wise list of top five critical success factors for SCM implementation by Indian SMEs.

Sectors	S.No.	Top five CSFs	Mean
Auto sector	1.	Top management commitment	4.52
	2.	Long-term vision for survival and growth	4.01
	3.	Devoted resources for supply chain	3.88
	4.	Development of effective SCM strategy	3.81
	5.	Information sharing with SC members/Development of reliable suppliers	3.75
Plastic	1.	Devoted resources for supply chain	4.00
	2.	Development of effective SCM strategy	3.96
	3.	Top management commitment	3.93
	4.	Long-term vision for survival and growth	3.87
	5.	Logistics synchronization	3.75
Electronic/Electrical	1.	Long-term vision for survival and growth	4.00
	2.	Focus on core strengths	3.90
	3.	Development of effective SCM strategy/Devoted resources for supply chain	3.75
	4.	Development of reliable suppliers	3.45
	5.	Information sharing with SC members	3.30
Light engineering/Other	1.	Top management commitments	4.28
	2.	Development of effective SCM strategy	4.07
	3.	Devoted resources for supply chain	4.05
	4.	Long-term vision for survival and growth/Focus on core strengths	4.00
	5.	Logistics synchronization	3.41

Please cite this article in press as: Kumar, R. et al., Critical success factors for implementation of supply chain management in Indian small and medium enterprises and their impact on performance, IIMB Management Review (2015), http://dx.doi.org/10.1016/j.iimb.2015.03.001

In the electronic and electrical sector, other important CSFs are focus on core strengths and top management commitment (3.90). The authors opine that this sector should pay more attention toward development of JIT capabilities in system and forecasting of demand on point of sale (POS).

In the light engineering sector, the other CSFs are development of effective SCM strategy and long term vision for survival and growth. The authors opine that SMEs of light engineering sector should pay more attention toward developing JIT capabilities in the system.

Performance measures

Performance measurement can be defined as the process of quantifying the effectiveness of various processes being followed by the organization. Performance measurement provides the information necessary for decision makers to plan, control, and direct the activities of the organization. Performance measures allow managers to measure performance, to signal and educate employees (and suppliers) on the important dimensions of performance, and to direct improvement activities by identifying deviations from standards. Based on the balanced score card approach, this study has selected the performance measures customer service and satisfaction, innovation and growth, financial performance, and internal business parameters for assessment of performance.

Average improvement in performance in the past three years was measured on a Likert scale of five (1 — lowest, 5 — highest). This scale took care of decreasing, constant, as well as increasing percentage changes (Singh, Garg, & Deshmukh, 2006).

Performance improvement in terms of customer service and satisfaction

On the basis of extensive literature review and expert opinion, 10 parameters of customer service and satisfaction are identified. These parameters are: ability to resolve customer complaints, ability to deliver product on time, ability to follow up customer enquiries, ability to determine future expectations of customer, improvement of order fill rate, ability to reduce customer response time, ability to reduce shipping error, ability to reduce cost continuously, ability to customize the product, and application of ethical standards. In this section, respondents were asked to mention the level of improvement on performance measures related to customer service and satisfaction in the last three years for Indian SMEs on a Likert scale of five (1 — lowest, 5 — highest). Results are shown in Fig. 2. From the analysis of surveyed data it is observed that in the past three years highest improvement has been observed in ability to resolve customer complaints (with mean value of 3.7052). This is followed by ability to deliver product on time (3.6295), ability to follow up customer enquiries (3.6016), and ability to determine future expectations of customer (3.4382). The market is now more customer oriented and in order to satisfy customers, it is important to resolve their complaints, follow enquiries, and predict future demands. Further analysis yielded improvement in order fill rate (3.4343), ability to reduce customer response time (3.3386), ability to reduce shipping error (3.1155), ability to reduce cost continuously (3.0916), ability to customise the product (3.0797) and application of ethical standards (2.7769). To make a supply chain responsive it is advisable for SMEs to have a higher order fill rate with quicker response to customer orders. Delivery of the right product to the right customer at the right time is very important for achieving coordination and responsiveness in the supply chain. Small and medium enterprises have to reduce shipping error for smooth functioning of supply chain processes. For customization of products, the production system of the organization should be adequately flexible. On the other hand there is continuous pressure for cost reduction on SMEs by other members of the supply chain. So, SMEs need to develop expertise in which a balance can be maintained between customer service and cost.

Performance improvement in terms of innovation and growth parameters

In the present study, eight innovation and growth parameters have been identified. Respondents were asked to mention the level of improvement of performance in the past three years in their organization on a Likert scale of five (1 — very low, 5—very high). Results are shown in Fig. 3. It is observed that ability to implement new technologies (4.2430) has highest improvement, followed by ability to respond well to customer demand for new features (3.9402) and ability to compete based on quality (3.8606). To beat the intense competition from global competitors, Indian SMEs have to implement new technology in all fields; they

Figure 2 Performance improvement in terms of customer service and satisfaction.

Please cite this article in press as: Kumar, R. et al., Critical success factors for implementation of supply chain management in Indian small and medium enterprises and their impact on performance, IIMB Management Review (2015), http://dx.doi.org/10.1016/j.iimb.2015.03.001

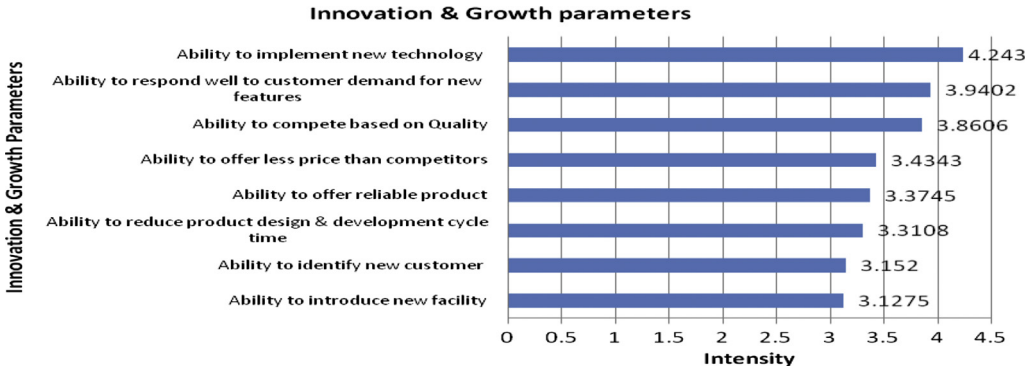

Figure 3 Performance improvement in terms of innovation and growth parameters.

have to improve quality and cut costs. This is also borne out by our study. The authors further observed improvement in ability to offer lower prices than competitors (3.4343), ability to offer reliable products (3.3745), reduce product design and development cycle time (3.3108), identify new customers (3.1520) and ability to introduce new facilities (3.1275). Changing facilities with time and adopting new technology will help SMEs adapt to changing business environments. Offering new products with improved design at cheaper cost will also help them to sustain amidst global competition.

Performance improvement in terms of financial parameters

Financial parameters were measured in terms of average percentage change in the past three years on market share, sales turnover, reduction of inventory cost, export, and return on investment on a Likert scale of five (1 — lowest, 5 — highest). In this study, nine financial parameters have been identified. Results are shown in Fig. 4.

Net profit (3.9004) has the highest improvement followed by return on investment (3.8845) and revenue growth (3.8765). Export share (3.1037) of Indian SMEs has improved least among all measures. These findings imply that performance of Indian SMEs has improved least in term of exports. This may be due to various constraints mentioned in the literature, and which also emerge in this study. The authors observed that without sufficient resources, trained and qualified manpower, and state-of-the-art technology, Indian SMEs could not compete with their counterparts in developed countries, or, especially, with emerging and newly industrializing economies such as Singapore, Hong Kong, South Korea, Taiwan, Mexico and Malaysia. These challenges have forced a majority of the SMEs to focus on local markets and have rendered them unable to compete successfully in the global market. Therefore, a major challenge for Indian SMEs is to broaden their product range and work towards world class quality.

Performance improvement in terms of internal business parameters

On the basis of literature review and pilot survey of the market, eight internal business parameters have been identified. These parameters were measured in terms of average percentage change in the past three years on a Likert scale of five (1 — lowest, 5 — highest). The parameters are: level of teamwork and coordination among internal departments, use of modern quality control techniques, development of cross functional team, ability to reduce the product cycle time, improvement in labour productivity, ability to reduce wastage, ability to reduce inventory, and reduction in breakdown of machines. Results are shown in Fig. 5. To face challenges of global competition, SMEs should have internally and externally coordinated supply chains. This study observed that teamwork and coordination among departments (with mean value of 3.4781) have highest improvement followed by modern quality control techniques (3.3386) and development of cross functional team (3.3068). Forming cross functional teams with members from different departments and different fields makes problem solving easy and more effective. Further in this study it is observed that performance of Indian SMEs has not

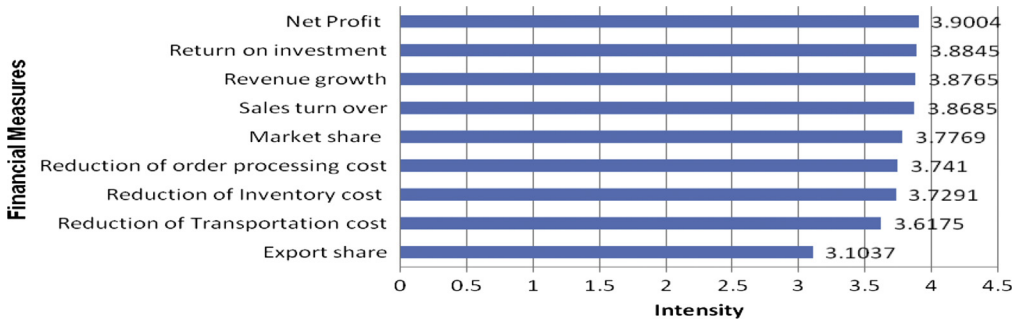

Figure 4 Performance improvement in terms of financial performance measures.

Please cite this article in press as: Kumar, R. et al., Critical success factors for implementation of supply chain management in Indian small and medium enterprises and their impact on performance, IIMB Management Review (2015), http://dx.doi.org/10.1016/j.iimb.2015.03.001

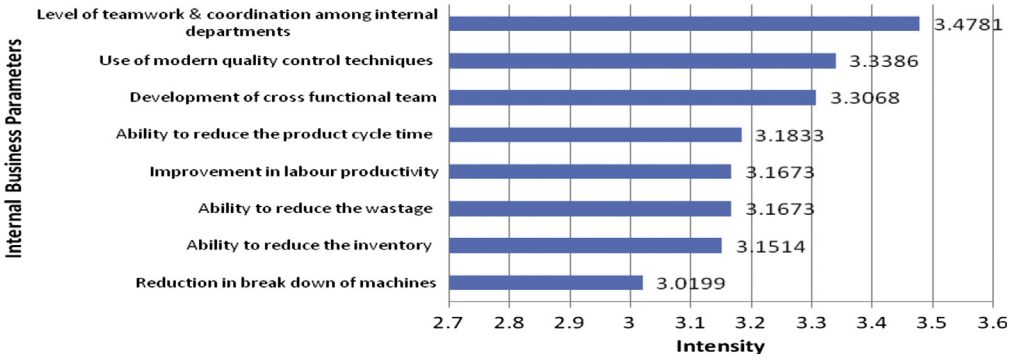

Figure 5 Performance improvement in terms of internal business parameters.

improved significantly on the parameters ability to reduce product cycle time (3.1833), improvement in labour productivity (3.1673), reducing wastage (3.1673), reducing inventory (3.1514) and reduction in breakdown of machines (3.0199). These findings imply that SMEs have to make concerted efforts for improvement in areas of inventory management, maintenance, and productivity.

Correlation and regression analysis for testing of research propositions

In earlier sections, the study has tried to address issues related to critical success factors and business performance of Indian SMEs. The main research propositions in the present study are concerned with the relationship between CSFs and improvement in performance on different categories. For testing of research propositions made in this study, correlation and regression analysis has been carried out in this section. The results are given in Table 4. Some of the observations on the basis of this analysis are as follows:

- Critical success factors for supply chain implementation have significant correlation with performance in terms of customer service and satisfaction, thereby supporting the first proposition. This implies that CSFs for supply chain, if taken into consideration while implementing SCM, can significantly improve performance of Indian SMEs.
- Critical success factors for supply chain implementation have significant correlation with performance in terms of innovation and growth, thereby supporting the second proposition. It means CSFs help in performance improvement in terms of innovation and growth.
- Critical success factors are significantly correlated with financial performance, thereby supporting the third proposition. It means CSFs play an important role in improving financial performance of SMEs.
- Critical success factors for supply chain implementation have significant correlation with performance in terms of internal business, thereby supporting the fourth proposition.

Table 4 Correlation and regression analysis of CSFs with performance issues.

S.No.	CSFs	Correlation coefficient for Perfm.1	Correlation coefficient for Perfm.2	Correlation coefficient for Perfm.3	Correlation coefficient for Perfm.
1	Top management commitment	.353**	.483**	.607**	.264**
2	Development of effective SCM strategy	.296**	.461**	.564**	.051
3	Devoted resources for supply chain	.294**	.490**	.591**	.113
4	Logistics synchronization	.326**	.536**	.579**	.184**
5	Use of modern technologies	.419**	.441**	.456**	.480**
6	Information sharing with SC members	.484**	.418**	.395**	.363**
7	Forecasting of demand on point of sale (POS)	.544**	.380**	.320**	.429**
8	Trust development in SC partners	.480**	.363**	.253**	.453**
9	Developing JIT capabilities in system	.455**	.415**	.279**	.454**
10	Development of reliable suppliers	.389**	.343**	.231**	.265**
11	Higher flexibility in production system	.402**	.428**	.414**	.304**
12	Focus on core strengths	.298**	.597**	.556**	.173**
13	Long-term vision for survival and growth	.460**	.617**	.543**	.195**
14	Average/overall value of CSFs	0.591** (R2 = 0.349)	.693** (R2 = 0.480)	.680** (R2 = 0.462)	.418** (R2 = 0.174)

Notes: Correlation is significant at the 0.01 level (2-tailed); CSFs-Critical success factors; Perfm.1-Performance in terms of customer service and satisfaction; Perfm.2- Performance in terms of innovation and growth criterion; Perfm.3- Performance in terms of financial performance; Perfm.4- Performance in terms of internal business parameters.
Significance levels show you how likely a pattern in your data is due to chance. For example, a value of ".01" means that there is a 99% (1−.01 = .99) chance of it being true.

Please cite this article in press as: Kumar, R. et al., Critical success factors for implementation of supply chain management in Indian small and medium enterprises and their impact on performance, IIMB Management Review (2015), http://dx.doi.org/10.1016/j.iimb.2015.03.001

- Detailed analysis of correlation of different CSFs with different performance issues is shown in Table 4. Top management commitment has significant correlation with all issues related to performance, while CSFs such as development of effective SCM strategy and devoted resources for supply chain do not have significant correlation with performance parameters of internal business. It implies that performance of Indian SMEs can be improved on all issues such as customer service and satisfaction, innovation and growth, and financial and internal business parameters if the management commits to implement SCM. On the other hand, management must pay attention to strategy development for SCM and enough resources should be devoted to it.
- Regression analysis of CSFs as independent variable and performance in terms of customer service and satisfaction as dependent variable ($R^2 = 0.349$) explains 34.9 percent of variability of performance of Indian SMEs. This means that in addition to these independent variables, other factors related to supply chain implementation play a significant role in performance improvement in terms of customer service and satisfaction in the Indian scenario. During analysis and survey, the authors observed that for Indian SMEs cost reduction, quality improvement and on time delivery of goods have more influence on performance. The authors opine that to utilize resources effectively and to maximize benefits of SCM, SMEs should take help from professionals and consultants.
- Regression analysis of CSFs as independent variable and performance in terms of innovation and growth as dependent variable ($R^2 = 0.480$) explains 48 percent of variability of performance of Indian SMEs. This implies that in addition to these independent variables, other factors related to supply chain implementation play a significant role in performance improvement of Indian SMEs in terms of innovation and growth.
- Regression analysis of CSFs as independent variable and performance in terms of finance as dependent variable ($R^2 = 0.462$) explains 46.2 percent of variability of performance of Indian SMEs. This means that in addition to these independent variables, other factors related to supply chain implementation play a significant role in improvement of performance of SMEs in terms of finance. The authors opine that Indian SMEs should take help of professionals and consultants for this.
- Regression analysis of CSFs as independent variable and performance in terms of internal business as dependent variable ($R^2 = 0.174$) explains 17.4 percent of variability of performance of Indian SMEs. It implies that in addition to these independent variables, other factors related to supply chain implementation, play a significant role in performance improvement of Indian SMEs, in terms of internal parameters.

Sector wise correlation and regression analysis

In this section, the authors have tried to analyse the relationship between different CSFs and performance of Indian SMEs of different sectors such as auto, plastic, electronic/electrical, and light engineering. Some of the observations on the basis of this analysis are as follows:

- During sector wise correlation and regression analysis of CSFs with performance, the authors observed that different factors have different effect on performance in different sectors. For instance, in the auto sector top management commitment shows a significant correlation for performance improvement in terms of innovation and growth criterion, financial performance and internal business parameters, but is not significant in terms of customer service and satisfaction (Table 5). This implies that top management of Indian SMEs in the auto sector should focus more on customer service and satisfaction.
- In the plastic sector, top management commitment shows significant correlation for performance improvement in terms of customer service and satisfaction, innovation and growth and financial performance, but is not significant in terms of internal business parameters. It implies that top management of SMEs of the plastic sector should pay more attention to improving internal business standards.
- In the auto sector, developing JIT capabilities in system has significant correlation with all the performance criteria (Table 5), while in the plastic sector this CSF has significant correlation with performance in terms of customer service and satisfaction only. It does not show significant correlation with other criteria of performance. This implies that SMEs of the plastic sector should focus more on developing JIT capabilities to improve their performance.

Limitations of the study

This research is subject to the normal limitations of survey research. The study uses perceptual data provided by production managers or quality managers and business heads, which may not provide clear measures of performance. Continued scepticism within SMEs about the impact of CSFs for SCM on performance is one of the fundamental limitations this research faces. Indian SMEs are, therefore, not very willing to provide useful and timely information and data, for further investigations.

Concluding remarks

The objective of this study was to identify the impact of CSFs for SCM on the performance of Indian SMEs in the context of emerging global market. From this study it is observed that the critical success factors (CSFs) have positive impact on different categories of performance such as customer service and satisfaction, innovation and growth, financial performance, and internal business of Indian SMEs. Further, when analysed sector wise, different CSFs show different impacts on different performance criteria in different sectors. It is also observed that to face the challenges of a global market, SMEs in India are now recognizing the importance of SCM implementation on a larger scale.

On the basis of this study, some of the concluding observations are as follows:

Please cite this article in press as: Kumar, R. et al., Critical success factors for implementation of supply chain management in Indian small and medium enterprises and their impact on performance, IIMB Management Review (2015), http://dx.doi.org/10.1016/j.iimb.2015.03.001

Table 5 Sector wise correlation and regression analysis of CSFs with performance.

S.No.	CSFs	Sectors	Correlation coefficient for Perfm.1	Correlation coefficient for Perfm.2	Correlation coefficient for Perfm.3	Correlation coefficient for Perfm.4
1	Top management commitment	Auto	.140	.458**	.586**	.326*
		Plastic	.490**	.600**	.619**	.150
		Electronic/Electrical	.116	.627**	.612**	.196
		Light engg./Others	.126	.439**	.588**	.339*
2	Development of effective SCM strategy	Auto	.221	.444**	.595**	.150
		Plastic	.186	.463**	.521**	−.274
		Electronic/Electrical	.176	.572**	.734**	.289
		Light engg./Others	.140	.431**	.589**	.231
3	Devoted resources for supply chain	Auto	.104	.425**	.634**	.175
		Plastic	.082	.286	.401*	−.258
		Electronic/Electrical	.106	.604**	.734**	.319
		Light engg./Others	.042	.381**	.530**	.202
4	Logistics synchronization	Auto	.193	.484**	.630**	.255
		Plastic	.183	.968**	.860**	−.070
		Electronic/Electrical	.269	.325	.555*	.545*
		Light engg./Others	.463**	.529**	.630**	.681**
5	Use of modern technologies	Auto	.146	.525**	.568**	.500**
		Plastic	.408*	.121	.105	.009
		Electronic/Electrical	.547*	.555*	.699**	.789**
		Light engg./Others	.370**	.315*	.338*	.646**
6	Information sharing with SC members	Auto	.203	.517**	.489**	.413**
		Plastic	.541**	.199	.282	−.035
		Electronic/Electrical	.603**	.386	.544*	.753**
		Light engg./Others	.290*	.262	.345*	.386**
7	Forecasting of demand on point of sale (POS)	Auto	.579**	.499**	.273*	.521**
		Plastic	.832**	.062	−.035	.348
		Electronic/Electrical	.613**	.595**	.660**	.507*
		Light engg./Others	.740**	.305*	.383**	.701**
8	Trust development in SC partners	Auto	.413**	.594**	.296*	.584**
		Plastic	.661**	.394*	.315	.058
		Electronic/Electrical	.410	.168	.296	.505*
		Light engg./Others	.576**	.101	.284*	.459**
9	Developing JIT capabilities in system	Auto	.656**	.437**	.289*	.612**
		Plastic	.391*	.093	.034	−.093
		Electronic/Electrical	.057	.307	.022	.268
		Light engg./Others	.619**	.261	.316*	.562**
10	Development of reliable suppliers	Auto	.311*	.517**	.292*	.325*
		Plastic	.186	.463**	.521**	−.274
		Electronic/Electrical	.117	−.261	−.195	.198
		Light engg./Others	.628**	.065	.298*	.600**
11	Higher flexibility in production system	Auto	.295*	.400**	.354**	.356**
		Plastic	.407*	.224	.255	−.093
		Electronic/Electrical	.234	.363	.227	−.068
		Light engg./Others	.379**	.277*	.467**	.576**
12	Focus on core strengths	Auto	.296*	.580**	.264	.195
		Plastic	.496**	.559**	.602**	.208
		Electronic/Electrical	.273	.663**	.772**	.164
		Light engg./Others	.306*	.758**	.792**	.531**
13	Long-term vision for survival and growth	Auto	.232	.506**	.368**	.284*
		Plastic	.394*	.802**	.740**	−.090
		Electronic/Electrical	.297	.554*	.428	.148
		Light engg./Others	.529**	.639**	.655**	.562**

Notes: **. Correlation is significant at the 0.01 level (2-tailed), *. Correlation is significant at the 0.05 level (2-tailed); CSFs-Critical success factors; Perfm.1-Performance improvement in terms of customer service and satisfaction; Perfm.2- Performance improvement in terms of innovation and growth criterion; Perfm.3- Performance improvement in terms of financial performance; Perfm.4-Performance improvement in terms of internal business parameters.

Please cite this article in press as: Kumar, R. et al., Critical success factors for implementation of supply chain management in Indian small and medium enterprises and their impact on performance, IIMB Management Review (2015), http://dx.doi.org/10.1016/j.iimb.2015.03.001

- Top management commitment, long-term vision for survival and growth, focus on core strengths, devoted resources for supply chain and development of effective SCM strategy are the main CSFs for implementation of SCM in Indian SMEs.
- In the auto sector, the main CSFs for implementation of SCM are top management commitment, long-term vision for survival and growth, devoted resources for supply chain, and development of effective SCM strategy.
- In the plastic sector, the main CSFs for implementation of SCM are devoted resources for supply chain, development of effective SCM strategy, development of reliable suppliers, and focus on core strength.
- In the electronic/electrical sector, main CSFs for implementation of SCM are long term vision for survival and growth, focus on core strengths, and top management commitment.
- In the light engineering sector, main CSFs for implementation of SCM are top management commitment, development of effective SCM strategy, and long-term vision for survival and growth.
- In customer service and satisfaction category of performance, in the last three years improvement has been observed in terms of ability to resolve customer complaints, ability to deliver product on time, ability to follow up customer enquiries and ability to determine future expectations of customers.
- In innovation and growth category of performance, in the last three years improvement has been observed in terms of ability to implement new technology, ability to respond well to customer demand for new features, ability to compete based on quality, and ability to offer lower prices than competitors.
- Indian SMEs have performed better in the last three years in terms of net profit, return on investment, and revenue growth.
- In the internal business perspective of performance, in the last three years improvement has been observed in terms of teamwork and coordination among internal departments, use of modern quality control techniques, development of cross functional team and ability to reduce the product cycle time.

Findings of the study have many crucial implications for SMEs while implementing SCM, and for academia as well. A major implication is that SMEs should develop their supply chain strategies effectively after analysing the business environment and their future plans. While developing strategies for implementation of SCM in SMEs, they should give due importance to CSFs and keep them in mind while deciding their priorities.

This study can be further extended for comparing SMEs with larger enterprises in terms of different supply chain practices and performance. The findings from this study may be beneficial for SMEs outside India as well.

References

Anderson, J. C., & Narus, J. A. (1990). A model of distributor firm and manufacturer firm working partnerships. *Journal of Marketing, 54*, 42—58.

Angeles, R., Corritore, C. L., Choton Basu, S., & Nath, R. (2001). Success factors for domestic and international electronic data interchange (EDI) implementation for US firms. *International Journal of Information Management, 21*, 329—347.

Arend, R. J., & Winser, J. D. (2005). Small business and supply chain management: is there a fit? *Journal of Business Venturing, 20*, 403—436.

Arshinder, Kanda, A., & Deshmukh, S. G. (2008). Supply chain coordination: perspectives, empirical studies and research directions. *International Journal of Production Economics, 115*, 316—335.

Arshinder, K., Kanda, A., & Deshmukh, S. G. (2006). A graph theoretic approach to evaluate supply chain coordination. *International Journal of Logistics and Systems Management, 2*(4), 329—341.

Arshinder, Kanda, A., & Deshmukh, S. G. (2007). Supply chain coordination issues: an SAP-LAP framework. *Asia Pacific Journal of Marketing and Logistics, 19*(3), 240—264.

Bauer, M. J. (2000). The effect of the Internet on supply chain & logistics. *World Trade, 13*, 71—78.

Bianchi, C., & Saleh, A. (2010). On importer trust and commitment: a comparative study of two developing countries. *International Marketing Review, 27*(1), 55—86.

Bowersox, D. J. (1990). The strategic benefits of logistics alliances. *Harvard Business Review, 68*(4), 36—43.

Bruwer, P. J. S. (1984). A descriptive model of success for computer-based information systems. *Information & Management, 7*, 63—67.

Bullen, C. V., & Rockart, J. F. (1986). A primer on critical success factors. In C. V. Bullen, & J. F. Rockart (Eds.), *The rise of managerial computing: the best of the Center for Information System Research* (383—423). Homewood, Illinois: Dow Jones-Irwin.

Cachon, G. P., & Lariviere, M. A. (2005). Supply chain coordination with revenue sharing contracts: strengths and limitation. *Management Science, 51*(1), 30—44.

Cao, N., Zhang, Z., To, K. M., & Ng, K. P. (2008). How are supply chains coordinated? An empirical observation in textile-apparel business. *Journal of Fashion Marketing & Management, 12*(3), 384—397.

Center for Monitoring Indian Economy (CMIE). (2000). *CMIE: Economic overview 2000*. New Delhi: CMIE.

Das, A. (2001). Towards theory building in manufacturing flexibility. *International Journal of Production Research, 39*(18), 4153—4177.

Fisher, M. (1997). What is the right supply chain for your product? *Harvard Business Review, 75*(2), 105—116.

Flynn, B. B., Sakakibara, S., Schroeder, R. G., Bates, K. A., & Flynn, J. B. (1990). Empirical research methods in operations management. *Journal of Operations Management, 9*, 250—284.

Francesca, M., Bianco, F., & Mauro, C. (2008). Internet and supply chain management: adoption modalities for Italian firms. *Management Research News, 31*(5), 359—374.

Ganesan, S. (1994). Determinants of long-term orientation in buyer-supplier relationships. *Journal of Marketing, 58*, 1—19.

Ganesan, K., & Saumen, B. (2005). Corporate turnaround through effective supply chain management: the case of a leading jewellery manufacturer in India. *Supply Chain Management: An International Journal, 10*(5), 340—348.

Grittell, J. H., & Weiss, L. (2004). Coordination networks within and across organizations: a multi-level framework. *Journal of Management Studies, 41*(1), 127—153.

Gunasekaran, A., Mcneil, R., Mcgaughey, R., & Ajasa, T. (2001). Experience of small to medium size enterprise in the design and implementation of manufacturing cells. *International Journal of Computer Integrated Manufacturing, 14*(2), 212—223.

Please cite this article in press as: Kumar, R. et al., Critical success factors for implementation of supply chain management in Indian small and medium enterprises and their impact on performance, IIMB Management Review (2015), http://dx.doi.org/10.1016/j.iimb.2015.03.001

He, Y., Zhao, X., Zhao, L., & He, J. (2009). Coordinating a supply chain with effort and price dependent stochastic demand. *Applied Mathematical Modeling, 33*, 2777–2790.
Kumar, R., Singh, R. K., & Shankar, R. (2012). Supply chain management issues in an Indian SME: a Sap-Lap analysis. *Journal of Supply Chain Management Systems, 1*(2), 34–44.
Kumar, R., Singh, R. K., & Shankar, R. (2013). Study on coordination issues for flexibility in Supply chain of SMEs: a case study. *Global Journal of Flexible Systems Management, 14*(2), 81–92.
Kumar, R., Singh, R. K., & Shankar, R. (2014). Strategy development by Indian SMEs for improving coordination in supply chain: an empirical study. *Competitiveness Review, 24*(5), 414–432.
Kumar, R., Singh, R. K., & Shankar, R. (2015). Study on collaboration and information sharing practices for SCM in Indian SMEs. *International Journal of Business Information Systems* (in press).
Lancioni, R. A., Smith, M. F., & Oliva, T. A. (2000). The role of the Internet in supply chain management. *Industrial Marketing Management, 29*, 45–56.
Lee, H. L. (2000). Creating value through supply chain integration. *Supply Chain Management Review, 4*(4), 30–36.
Lee, H. L., Padmanabhan, V., & Whang, S. (1997). The bullwhip effect in supply chain. *Sloan Management Review, 38*(3), 93–102.
Marek, P., & Malyszek, E. (2008). A local collaboration as the most successful co-ordination scenario in the supply chain. *Industrial Management & Data Systems, 108*(1), 22–42.
Mehrjerdi, Y. Z. (2009). Excellent supply chain management. *Assembly Automation Journal, 29*(1), 52–60.
Morgan, R. M., & Hunt, S. D. (1994). The commitment-trust theory of relationship marketing. *Journal of Marketing, 58*(3), 20–38.
MSMED Act. (2006). *Micro,small and medium enterprises development Act No.27, Ministry of Law and Justice*. Government of India.
Ngai, E. W. T., Cheng, T. C. E., & Ho, S. S. M. (2004). Critical success factors of web-based supply chain management system using exploratory factor analysis. *Production, Planning & Control, 5*(6), 622–630.
Nunnally, J. C. (1978). *Psychometric methods*. New York, NY: McGraw-Hill.
Olhager, J., & West, B. M. (2002). The house of flexibility: using the QFD approach to deploy manufacturing flexibility. *International Journal of Operations & Production Management, 22*(1), 50–79.
Olorunniwo, F. O., & Hartfield, T. (2001). Strategic partnering when supply base is limited – a case study. *Industrial Management & Data Systems, 101*(1), 47–52.
Othman, R., & Ghani, R. A. (2008). Supply chain management and suppliers' HRM practice. *Supply Chain Management: An International Journal, 13*(4), 259–262.
Ozer, O. (2003). Replenishment strategies for distribution system under advanced demand information. *Management Science, 49*(3), 255–272.
Pant, S., Sethi, R., & Bhandari, M. (2003). Making sense of the e-supply chain landscape: an implementation framework. *International Journal of Information Management, 23*, 201–221.
Petersen, K. J., Handfield, R. B., & Ragatz, G. L. (2005). Supplier integration into new product development: coordinating product, process and supply chain design. *Journal of Operations Management, 23*(3/4), 371–388.
Power, D. J., Sohal, A. S., & Rahman, S. U. (2001). Critical success factors in agile supply chain management. *International Journal of Physical Distribution & Logistics Management, 31*, 247–265.
Ramdas, K., & Spekman, R. E. (2000). Chain or shackles? Understanding what drives supply chain performance. *Interface, 30*(4), 3–21.
Sahay, B. S. (2003). Understanding trust in supply chain relationships. *Industrial Management & Data Systems, 103*(8), 553–563.
Sandberg, E., & Abrahamsson, M. (2010). The role of top management in supply chain management practices. *International Journal of Retail & Distribution Management, 38*(1), 57–69.
Saxena, K. B. C., & Sahay, B. S. (2000). Managing IT for world class manufacturing: the Indian scenario. *International Journal of Information Management, 20*, 29–57.
Shin, H., Collier, D. A., & Wilson, D. D. (2000). Supply management orientation and supplier/buyer performance. *Journal of Operations Management, 18*(3), 317–333.
Simatupang, T. M., Wright, Alan C., & Sridharan, R. (2002). The knowledge of coordination of supply chain integration. *Business Process Management Journal, 8*(3), 289–308.
Singh, R. K. (2011). Developing the framework for coordination in supply chain of SMEs. *Business Process Management Journal, 17*(4), 619–638.
Singh, R. K. (2013). Prioritizing the factors for coordinated supply chain using analytic hierarchy process (AHP). *Measuring Business Excellence, 17*(1), 80–98.
Singh, R. K., Garg, S. K., & Deshmukh, S. G. (2006). Strategy development by Indian SMEs in plastic sector: an empirical study. *Singapore Management Review, 28*(2), 65–83.
Singh, R. K., Garg, S. K., & Deshmukh, S. G. (2008a). Challenges and strategies for competitiveness of SMEs: a case study. *International Journal for Services and Operations Management, 4*(2), 181–200.
Singh, R. K., Garg, S. K., & Deshmukh, S. G. (2008b). Competency and performance analysis of Indian SMEs and large organizations: an exploratory study. *Competitiveness Review: An International Business Journal, 18*(4), 308–321.
Singh, R. K., Garg, S. K., & Deshmukh, S. G. (2008c). Strategy development by SMEs for competitiveness: a review. *Benchmarking: An International Journal, 15*(5), 525–547.
Singh, R. K., Garg, S. K., & Deshmukh, S. G. (2010). Strategy development by Indian SSIs. *Industrial Management & Data Systems, 110*(7), 1073–1093.
Singh, R. K., Kumar, R., & Shankar, R. (2012). Supply chain management in SMEs: a case study. *International Journal of Manufacturing Research, 7*(2), 165–180.
Soroor, J., Tarokh, J. M., & Shemshadi, A. (2009). Theoretical and practical study of supply chain Coordination. *Journal of Business and Industrial Marketing, 24*(2), 131–142.
Stanley, E. F., Cynthia, W., Chad, A., & Gregory, M. (2009). Supply chain information-sharing: benchmarking a proven path. *Benchmarking: An International Journal, 16*(2), 222–246.
Tejpal, G., Garg, R. K., & Sachdeva, A. (2013). Trust among supply chain partners: a review. *Measuring Business Excellence, 17*(1), 51–71.
Thakkar, J., Kanda, A., & Deshmukh, S. G. (2008). A conceptual role interaction model for supply chain management in SMEs. *Journal of Small Business and Enterprise Development, 15*(1), 74–95.
Umble, E. J., Haft, R. R., & Umble, M. M. (2003). Enterprise resource planning: implementation procedures and critical success factors. *European Journal of Operational Research, 146*, 241–257.
Wagner, B. A., Fillis, I., & Johansson, U. (2003). E-business and e-supply in small and medium sized businesses. *Supply Chain Management: An International Journal, 8*(4), 343–354.
World Bank. (1999). *World bank economic review*. Oxford: Oxford University Press.

Please cite this article in press as: Kumar, R. et al., Critical success factors for implementation of supply chain management in Indian small and medium enterprises and their impact on performance, IIMB Management Review (2015), http://dx.doi.org/10.1016/j.iimb.2015.03.001

Solid State Communications 207 (2015) 21–25

Contents lists available at ScienceDirect

Solid State Communications

journal homepage: www.elsevier.com/locate/ssc

Crystal structure and mechanical properties of spark plasma sintered Cu_2Se: An efficient photovoltaic and thermoelectric material

Kriti Tyagi [a], Bhasker Gahtori [a], Sivaiah Bathula [a,b], M. Jayasimhadri [b], Sakshi Sharma [a], Niraj Kumar Singh [a], D. Haranath [a], A.K. Srivastava [a], Ajay Dhar [a,*]

[a] CSIR-Network of Institutes for Solar Energy, CSIR-National Physical Laboratory, Dr. K. S. Krishnan Road, New Delhi 110012, India
[b] Department of Applied Physics, Delhi Technological University, Delhi, India

ARTICLE INFO

Article history:
Received 13 December 2014
Received in revised form
23 December 2014
Accepted 5 February 2015
Communicated by T. Kimura
Available online 12 February 2015

Keywords:
A. Semiconductor
C. Scanning and transmission electron microscopy
D. Mechanical properties
D. Phase transitions

ABSTRACT

Copper selenide (Cu_2Se) based materials are currently being investigated globally for efficient photovoltaic and thermoelectric (TE) device applications. Despite having enormous device potential its crystal structure and mechanical properties are still not fully explored owing to its complex behavior. Stereographic projection is one of such useful tools to estimate the crystallography of the material conclusively. In the current study, the crystal structure of α and β-phases of Cu_2Se was determined by its stereographic projections in reciprocal space. Further, mechanical properties of Cu_2Se are highly important to avoid catastrophic failure and ensure longevity of the TE devices made out of these materials. Cu_2Se exhibited the compressive strength of $\sim$45 MPa with $\sim$3% of plastic strain and a fracture toughness value of $\sim 2 \pm 0.02$ MPa$\sqrt{m}$, the latter being significantly higher than that of the other known TE materials. Finally, thermal shock resistance, which is one of the crucial parameters for the stability and longevity of the device applications, was calculated to be $\sim 281 \pm 12$ W m^{-1}. Superior mechanical properties coupled with highly reported thermoelectric behavior makes Cu_2Se as a potential candidate for green energy generation.

1. Introduction

The development of promising power generation methods that are eco-friendly in nature require special attention to meet the global needs of large power usage [1]. The direct conversion of heat into electrical energy based on thermoelectric (TE) effect without moving parts in the device is an attractive alternative for power generation [2]. The performance of a thermoelectric device depends on its *figure-of-merit* (ZT), a dimensionless quantity of the material defined as $ZT=(\alpha^2\sigma T/\kappa)$, where α, σ, T and κ are Seebeck coefficient, electrical conductivity, temperature and thermal conductivity, respectively. The optimization of ZT clearly demands high TE power and electrical conductivity but having low thermal conductivity values. It is known that these three physical quantities (α, σ and T) of materials are correlated in such a way that the optimization of one adversely affects the other. Among several other available TE materials, Cu_2Se has been designated as one of the most promising materials for TE power generation, due to its high ZT value [2–8] in spite of its complex crystal structure. Further, it has been reported in literature that phase transition in Cu_2Se occurs from monoclinic (α)→cubic (β) at $\sim$413 K [2,9]. But, all the available literature on Cu_2Se unanimously confirms that the high temperature phase exists as β [3,9,10], while quandary still exists over the low temperature α-phase of Cu_2Se. Various groups [2,3,9] have already reported different crystal structures for Cu_2Se predicting that the low temperature phase is either monoclinic, orthorhombic or tetragonal at room temperature ($\sim$25 °C). But still there are many debates unresolved over the crystal structure of Cu_2Se. Hence, there is a need to address the existence of α-phase in Cu_2Se at low temperature with suitable supporting characterization techniques. Moreover, in the β-phase of Cu_2Se, the surface migration of Cu ions as well as evaporation of elemental Se limits the precise control over the final composition. Furthermore, it is desired to have complete crystallographic information of state-of-art TE materials prior to device fabrication to ensure that these materials are strong enough to operate in the temperature range 500–600 K useful for automobiles. Consequently, these materials have to withstand high internal thermal stresses created due to rapid temperature cycling gradients of two ends of the same TE element. Many of the existing TE materials are strong enough in thermoelectric performance, but poor at their mechanical strength. Hence, the mechanical facets of these TE materials are also to be addressed properly. Very few reports are available on mechanical properties of other state-of-the art TE materials, such as, n-type nanostructured SiGe alloys [11], Co_4Sb_{12} [12], $In_{0.1}Co_4Sb_{12}$ [12] and Bi_2Te_3+0.1 vol% SiC [13]. But for Cu_2Se,

* Corresponding author. Tel.: +91 11 4560 9455x9456; fax: +91 11 4560 9310.
E-mail address: adhar@nplindia.org (A. Dhar).

http://dx.doi.org/10.1016/j.ssc.2015.02.004
0038-1098/

there is no comprehensive study available in the literature either on stereographic microstructural interpretations of its crystal structure or mechanical properties. Therefore, in the current study, we report the crystal structure determination employing stereographic projections in reciprocal space for Cu_2Se with respect to temperature dependent $\alpha \rightarrow \beta$ phase transformations. The current study will surely be a guideline for other researchers in the photovoltaic and thermoelectric fields to interpret the crystallographic information for other novel TE materials. Additionally, mechanical properties, such as, fracture toughness; thermal shock resistance and compressive strength have also been investigated in the context of TE device fabrication.

2. Experimental details

Cu_2Se samples were synthesized by thorough grinding of Copper (Cu, 99.99%, Alfa Aesar) and Selenium (Se, 99.99%, Alfa Aesar) powders in respective chemical stoichiometric ratio in a glove box, under a high-purity argon atmosphere and these powders were subsequently pelletized and vacuum-sealed (10^{-5} Torr) in quartz tubes. The sealed quartz ampoules were heat-treated at 1000 °C for 24 h, and then naturally cooled to room temperature. The powder samples of Cu_2Se were subsequently consolidated and sintered under vacuum (~4 Pa) using spark plasma sintering (SPS Syntex, 725) technique at identical optimized process parameters of pressure 60 MPa and temperature 600 °C for 3 min (soaking time) at a heating rate of 400 °C/min using graphite die and punches. Mechanical properties such as fracture toughness measurements were carried out employing the indentation-crack technique using Vickers microhardness tester (FM-e7) with a load of 4.9 N for 10 s of indentation time. Also, compression tests at room temperature were performed as per ASTM standard (ASTM: E9-09) with an aspect ratio of ~2.5 under uniaxial loading with a strain rate of 2×10^{-5} s^{-1} (INSTRON 4204).

3. Results and discussion

3.1. Crystal structure determination by stereographic projections

The microscopy results in conjunction with X-ray diffraction patterns clearly shown in Fig. 1(a,b). It is evident from the Fig. 1(a) $\alpha \rightarrow \beta$ transition takes place as the system loses its monoclinic structure and begins to behave as cubic after ~413 K, which is supported by disappearance of (090) peak in the XRD pattern Fig. 1(b). It has been reported in literature [3] that $\alpha \rightarrow \beta$ phase transition is reversible in Cu_2Se around 413 K. In the current study, we have observed that Cu_2Se has a structural metamorphosis at about 400 ($\pm$10) K. Moreover, it could be noted that, this is a reversible phase transformation. There are several reports on different crystal structures of Cu_2Se [9,14,15]. A review on literature pertaining to various crystalline phases delineates that presumably the composition and also the processing conditions influence the final crystal symmetry of the product. A few crystalline phases, including the current investigation, are summarized in Table 1. However, it is to be noted that there exists no evidence about the formation of different crystalline phases and their phase transformations. Hence, we have employed stereographic interpretations in reciprocal space to determine the structural transitions.

With these stereographic projections, the α-phase (monoclinic) and β-phase (cubic) have been drawn to understand the important zone axes of two different crystal structures in reciprocal space. This methodology has been opted to give an idea of movement of atoms (crystallographic planes) during reversible transformation between $\alpha \rightarrow \beta$ and vice versa in case of Cu_2Se. For this symmetry elements and lattice constants for α-phase (space group: $C2/c$, lattice constants: a=7.14 Å, b=12.39 Å, c=27.33 Å, β=94.40°) and β-phase

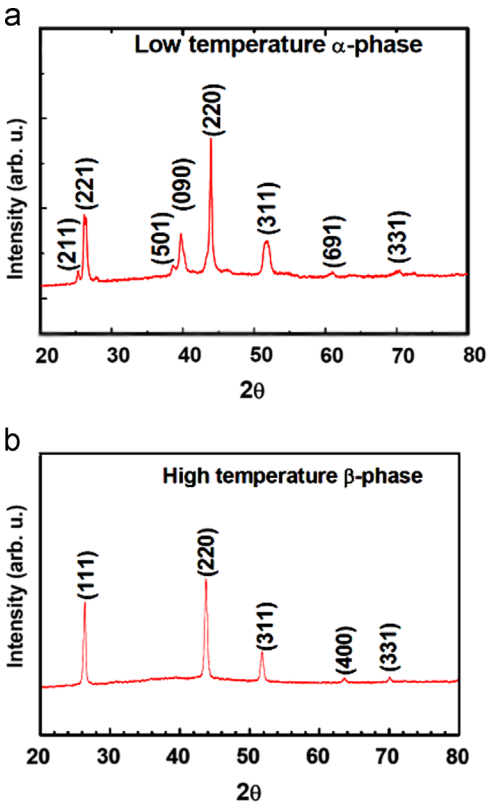

Fig. 1. X-ray diffraction pattern for (a) low temperature monoclinic (α) phase and (b) high temperature cubic (β) phase.

(space group: $Fm\bar{3}m$, a=5.787 Å) are recalled from the literature [15]. The stereographic projection along (010) for monoclinic (α-phase) crystal with space group C2/c has been displayed in Fig. 2. The stereogram shows the presence of important planes in the structure located with respect to the angular distances between the two planes. It is important to mention that a section of 45° (as marked with a white dotted line) is sufficient to exhibit the entire crystal symmetry of a given structure. Keeping this in view the repeatability of 45° section of the stereogram, a zone axes map has been plotted and the reciprocal space calculated diffraction patterns are appended with stereographic projection as shown in Fig. 3. In a similar way stereographic projection along (010) for cubic (β-phase) crystal with space group $Fm\bar{3}m$ has been displayed in Fig. 4. Further, the stereogram of β-phase (lattice constants: a=5.787 Å) has been calculated and plotted for a 45° section along 010 zone axis of face centered cubic lattice. Correspondingly the reciprocal space calculated diffraction patterns are appended with stereographic projection as shown in Fig. 5. The idea of putting the important diffraction patterns of both α and β-phases together to realize about the important planes that are probably involved in thermally reversible transformations during cyclic low to high between these crystalline structures. The structure of Cu_2Se makes a reversible phase transformation around 413 K. Based on the understanding of crystal structure employing stereographic interpretations and XRD experiments [2,3], the final structure is classified in terms of the sub-lattice of selenium, for the reason that copper sub-lattice turns into a super-ionic state at high temperature. However, the structure of copper in the low temperature regime has ever been considered to be random [2,3].

3.2. Mechanical properties

3.2.1. Fracture toughness analysis

It is well known that, most of the research has been focused on thermal and electrical transport properties of Cu_2Se, primarily

Table 1
Lattice parameters and space groups of Cu_2Se available in literature are compared to the current study.

Materials	Phase	Space group	Unit cell details	Reference
Cu_2Se	Monoclinic (low temperature)	$C2/c$	$a=14.087$ Å, $b=20.481$ Å, $c=4.145$ Å, $\beta=90.38^\circ$	Murray et al. [14]
Cu_2Se	Cubic (high temperature)	$Fm-3m$	$a=5.787$ Å	Milat et al. [15]
Cu_2Se	Monoclinic	$C2/c$	$a=7.1379$ Å, $b=12.3823$ Å, $c=27.3904$ Å, $\beta=94.308^\circ$	Gulay et al. [9]
Cu_2Se	**Monoclinic**	***C2/c***	**$a=7.14$ Å, $b=12.39$ Å, $c=27.33$ Å, $\beta=94.40^\circ$**	**This work**

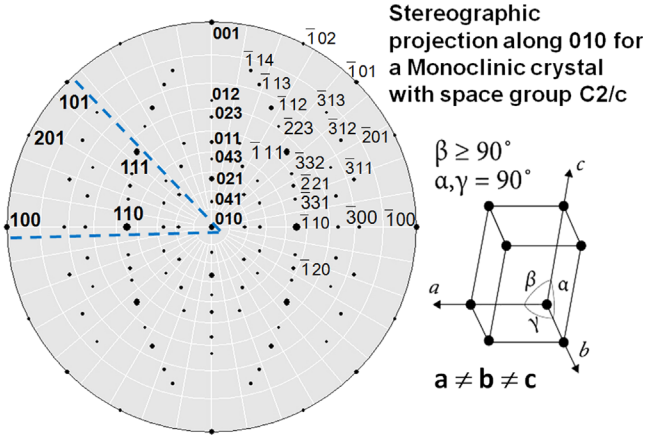

Fig. 2. Stereographic projection along 010 for a monoclinic crystal with space group $C2/c$.

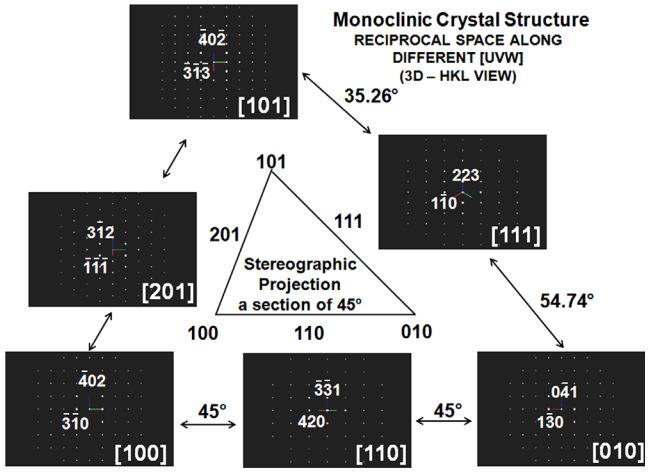

Fig. 3. Reciprocal space along different UVW for a monoclinic crystal structure.

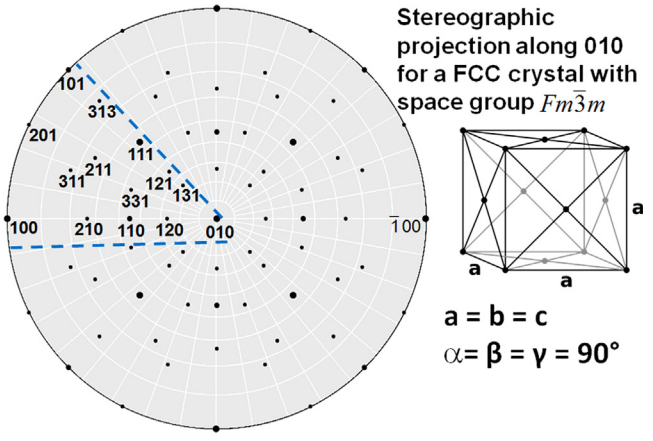

Fig. 4. Stereographic projection along 010 for a face centered cubic crystal structure with space group $Fm\bar{3}m$.

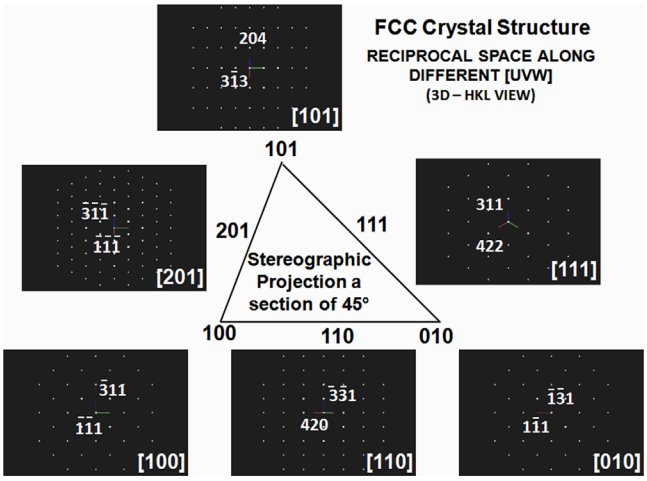

Fig. 5. Reciprocal space along different UVW for a face centered cubic crystal structure.

aimed towards enhancing their thermoelectric performance and efficiencies of state-of-art novel TE materials [1,16–19]. However, their mechanical properties are equally important for the long term reliability of TE modules, as these materials are known to be brittle with low fracture toughness. Further, there is no comprehensive report available for the mechanical properties of this material, which is equally important, for the in-service application of TE modules to avoid catastrophic failure. Hence, in the current study, we report some of the mechanical properties of Cu_2Se samples.

Fracture toughness (K_{IC}) of TE materials is often estimated using Vicker's indentation-Crack (VIF) technique as this method was outlined by Antis et al. [20] for brittle solids for radial mean crack systems, as described:

$$K_{IC} = 0.016\left(\frac{E}{H}\right)^{1/2} \times \frac{P}{l^{3/2}} \quad (1)$$

where P is the load in Newton's, a is the half-diagonal of Vicker's indentation mark in meters, E is Young's modulus in GPa [21] and H is Vickers hardness ~0.43 GPa. As sintered Cu_2Se samples exhibited near theoretical density and these samples were indented with a Vicker's diamond shaped indenter at a load of 4.9 N with a dwell time of 10 s, enough to generate cracks without any spill out of material, as shown in Fig. 6. Subsequently, the observed cracks were in radial mean type cracks as it was reported for other brittle solids [22]. Crack lengths were measured using field emission scanning electron microscope (FESEM) for estimating the fracture strength. The radial mean crack length (c) on the material surface has been measured to be ~46 μm after removal of indenter. The calculated fracture toughness of Cu_2Se alloy after spark plasma sintering (SPS) was found to be $\sim 2.0 \pm 0.02$ MPa$\sqrt{m}$ by VIF method employing Eq. (1). It has been reported that low temperature (<500 K) operating applications of $Bi_2Te_3+0.1$ vol% SiC exhibited a fracture toughness of 1.35 MPa$\sqrt{m}$ [13]. Whereas Co_4Sb_{12}, and $In_{0.1}Co_4Sb_{12}$ at high operating temperatures (>500 K) exhibited a fracture toughness of 0.82 ± 0.11, 0.46 ± 0.13 and 1 ± 0.02 MPa$\sqrt{m}$, respectively

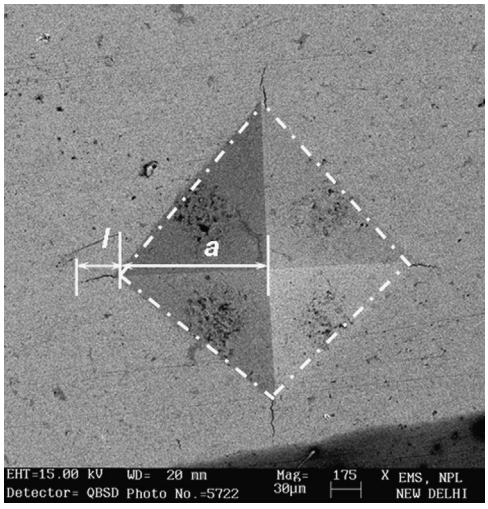

Fig. 6. FESEM image of Vicker's-indentation cracks developed at a load of 4.9 N, *a* is the half-diagonal of indentation mark and *c* is the radial-median crack length.

[12]. Recently, for nanostructured SiGe alloys a fracture toughness value of 1.6 ± 0.05 MPa$\sqrt{\text{m}}$ has been reported by our group [11]. However, these SiGe materials can be operated only at high (≥ 1173 K) temperature. In the current study, Cu_2Se sample finds applications in the temperature range of 500–600 K and most of the automobile exhaust systems fall in this category. Further from the literature, it is to be noted that the fine grain size in nanostructured alloys help to minimize the dislocation pile-up stresses resulting in improvement in fracture toughness [23,24]. Moreover, nanostructured materials containing low crystallite size is expected to enhance the localized fracture processes [25], which generally occur during crack extension [26,27]. On the other hand, the fine nanocrystallites in nanostructured materials would certainly enhance the fracture toughness [28] because during the steady state of crack initiation [29,30], work done by an applied stress is considered to be dissipated as heat by specific rotational deformation, grain boundary sliding and diffusion process [28,31,32]. Hence, the fracture toughness of Cu_2Se could be improved by nanostructuring the Cu_2Se sample.

3.2.2. Compressive strength analysis

Compressive strength test of as-sintered Cu_2Se (α-phase) has been conducted at room temperature (25 °C) under uniaxial compressive loading and a typical stress–strain curve is plotted as shown in Fig. 7. Further, it has been observed that compressive strength of the p-type Cu_2Se found to be 45 MPa with almost 3% of plastic strain, which is significantly higher than other reported values of nearly similar alloy composition [33]. Micro-hardness of the bulk Cu_2Se measured to be 0.43 GPa and these values are comparable with the existing state-of-the art materials, such as Bi_2Te_3 and PbTe, which have the hardness values of 0.62 and 0.23 GPa, respectively [34]. Also, it has been reported in literature that high temperature β-phase (cubic) of Cu_2Se shows the super plastic deformation behavior after $\alpha \rightarrow \beta$ phase transition at 413 K, which in turn resulted a lower (0.0325 GPa) values of compressive strength [33]. However, higher compressive strength values associating with moderate ductility of the Cu_2Se assumes that this could be a reliable TE candidate material in the temperature range of 500–800 K, whereas this material also possesses highest *ZT* among all the available polycrystalline bulk TE materials [3]. It is also to be noted that, strength and ductility of these alloys could also be improved further by nanostructuring approach, where dislocation pinning for slip movement and grain boundary strengthening result the enhancement of compressive strength [35–37].

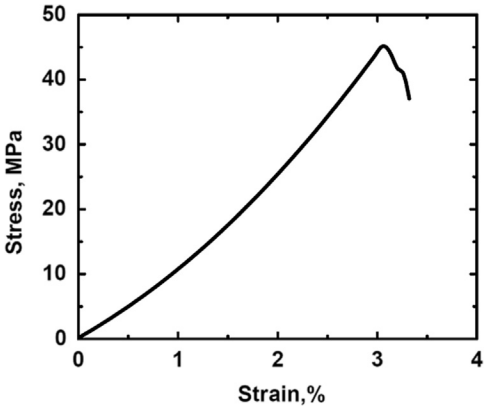

Fig. 7. Stress–strain curve of bulk p-type Cu_2Se tested under uniaxial compression mode with a strain rate of 2×10^{-5} s^{-1}.

3.2.3. Thermal shock resistance

Many of the novel TE materials are sensitive to thermal shock in-service TE devices applications [38–40]. Thermal shock resistance parameter can be defined as a sudden temperature change between hot and cold ends of the TE device legs that can lead to failure due to internal mechanical stress induced by temperature gradients [41–43]. Moreover, structural reliability of TE modules become important and should possess high thermal shock resistance in order to seize resistance to different kinds of thermal stresses under actual operating conditions [23,44–46]. The thermal shock resistance parameter (R_T), is given by the expression [41],

$$R_T = \frac{\sigma(1-\nu)\kappa}{\alpha E} \tag{2}$$

where ν is Poisson's ratio, κ is thermal conductivity and α is the coefficient of thermal expansion. The value of R_T for Cu_2Se has been calculated using Eq. (2) with experimentally determined values of $\sigma = 0.045$ GPa, $\kappa = 2.6$ W/m K and α [2], ν [47] and E [21] from the literature. Thermal shock resistance of current Cu_2Se sample was found to be $\sim 281 \pm 12$ W m^{-1}. This value a bit higher than the other state-of-art TE materials such as, PbTe alloy, which exhibited a value of 140 W m^{-1} [48]. This suggests that Cu_2Se sample prepared in the current study has a very high resistance to thermal shock without compromising their thermoelectric performance. Also, the high value of R_T is attributed to high compressive strength and thermal conductivities for Cu_2Se sample. In general, many of the known TE materials represent high *ZT* due to their low thermal conductivities [49–51]. But, for higher R_T, the materials should have high thermal conductivity to reduce sudden failure in practical applications. Hence, there is need to optimize these transport properties and R_T to get longer life periods for TE materials in device applications. Further, substantial improvement in R_T may be realized through better control and understanding of the microstructure at high temperatures. Also, temperature dependence of the mechanical properties of TE materials has to be evaluated thoroughly since these materials are highly prone to changes in their microstructure with change in temperature.

4. Conclusions

In summary, we have successfully demonstrated the crystal structure determination for both α and β-phases of spark plasma sintered Cu_2Se in reciprocal space by stereographic projections. Further, fracture toughness of Cu_2Se exhibited a value of $\sim 2 \pm 0.02$ MPa$\sqrt{\text{m}}$, which is significantly higher than that of other existing thermoelectric materials at similar operating temperature. Consequently, the compressive strength was found to be 45 MPa with $\sim$3% of plastic strain. Moreover, thermal shock resistance of Cu_2Se was found to be $\sim 281 \pm 12$ W m^{-1}

and we take the credit of reporting for the first time for Cu_2Se system. Mechanical properties of Cu_2Se could be improved further by nanostructuring methodology. Superior mechanical properties coupled with high photovoltaic and thermoelectric performances of Cu_2Se makes it as a potential candidate material for green energy generation.

Acknowledgments

This work was supported by CSIR-TAPSUN (CSIR-NWP 54) programme entitled *"Novel approaches for solar energy conversion under technologies and products for solar energy utilization through networking"*. The authors are grateful to the Director, Prof. R.C. Budhani, for his constant mentoring and support for this project. The technical support rendered by Mr. Radhey Shyam and Mr. Naval Kishor Upadhyay is also gratefully acknowledged.

References

[1] M. Martín-González, O. Caballero-Calero, P. Díaz-Chao, Renew. Sustain. Energy Rev. 24 (2013) 288–305.
[2] H. Liu, X. Shi, F. Xu, L. Zhang, W. Zhang, L. Chen, Q. Li, C. Uher, T. Day, G.J. Snyder, Nat. Mater. 11 (2012) 422–425.
[3] B. Yu, W. Liu, S. Chen, H. Wang, H. Wang, G. Chen, Z. Ren, Nano Energy 1 (2012) 472–478.
[4] S. Ballikaya, H. Chi, J.R. Salvador, C. Uher, J. Mater. Chem. A 1 (2013) 12478–12484.
[5] C. Wadia, A.P. Alivisatos, D.M. Kammen, Environ. Sci. Technol. 43 (2009) 2072–2077.
[6] S. Deka, A. Genovese, Y. Zhang, K. Miszta, G. Bertoni, R. Krahne, C. Giannini, L. Manna, J. Am. Chem. Soc. 132 (2010) 8912–8914.
[7] Q. Guo, G.M. Ford, H.W. Hillhouse, R. Agrawal, Nano Lett. 9 (2009) 3060–3065.
[8] D. Lu, B. Sang, Y. Deng, B.J. Stanbery, L. Eldada, in: Proceedings of 35th IEEE Photovoltaic Specialists Conference (PVSC), IEEE, 2010, pp. 000175–000178.
[9] L. Gulay, M. Daszkiewicz, O. Strok, A. Pietraszko, Chem. Mater. Alloy 4 (2011) 200–205.
[10] H. Liu, X. Yuan, P. Lu, X. Shi, F. Xu, Y. He, Y. Tang, S. Bai, W. Zhang, L. Chen, Adv. Mater. 25 (2013) 6607–6612.
[11] S. Bathula, B. Gahtori, M. Jayasimhadri, S.K. Tripathy, K. Tyagi, A.K. Srivastava, A. Dhar, Appl. Phys. Lett. 105 (2014).
[12] J. Eilertsen, M. Subramanian, J. Kruzic, J. Alloy. Compd. 552 (2013) 492–498.
[13] L.-D. Zhao, B.-P. Zhang, J.-F. Li, M. Zhou, W.-S. Liu, J. Liu, J. Alloy. Compd. 455 (2008) 259–264.
[14] R.M. Murray, R.D. Heyding, Can. J. Chem. 53 (1975) 878–887.
[15] O. Milat, Z. Vučić, B. Ruščić, Solid State Ion. 23 (1987) 37–47.
[16] D.M. Rowe, CRC Handbook of Thermoelectrics, CRC press, USA, 1995.
[17] A. Minnich, M. Dresselhaus, Z. Ren, G. Chen, Energy Environ. Sci. 2 (2009) 466–479.
[18] P.H. Ngan, D.V. Christensen, G.J. Snyder, L.T. Hung, S. Linderoth, N.V. Nong, N. Pryds, Phys. Status Solidi (a) 211 (2014) 9–17.
[19] A.P. Gonçalves, C. Godart, Eur. Phys. J. B 87 (2014) 1–29.
[20] G. Anstis, P. Chantikul, B.R. Lawn, D. Marshall, J. Am. Ceram. Soc. 64 (1981) 533–538.
[21] O.L. Anderson, J. Phys. Chem. Solids 24 (1963) 909–917.
[22] C.-M. Lin, C.-M. Chang, J.-H. Chen, W. Wu, Mater. Sci. Eng.: A 527 (2010) 5038–5043.
[23] A. Kallel, G. Roux, C. Martin, Mater. Sci. Eng.: A 564 (2013) 65–70.
[24] J.-F. Li, W.-S. Liu, L.-D. Zhao, M. Zhou, NPG Asia Mater. 2 (2010) 152–158.
[25] M. Ke, S. Hackney, W. Milligan, E. Aifantis, Nanostruct. Mater. 5 (1995) 689–697.
[26] J.R. Sootsman, J. He, V.P. Dravid, S. Ballikaya, D. Vermeulen, C. Uher, M.G. Kanatzidis, Chem. Mater. 22 (2009) 869–875.
[27] T. Zhu, J. Li, Prog. Mater. Sci. 55 (2010) 710–757.
[28] E. Lavernia, B. Han, J. Schoenung, Mater. Sci. Eng.: A 493 (2008) 207–214.
[29] Y. Wang, M. Chen, F. Zhou, E. Ma, Nature 419 (2002) 912–915.
[30] K. Kumar, H. Van Swygenhoven, S. Suresh, Acta Mater. 51 (2003) 5743–5774.
[31] D. Hasselman, J. Am. Ceram. Soc. 52 (1969) 600–604.
[32] L. Freund, J. Hutchinson, J. Mech. Phys. Solids 33 (1985) 169–191.
[33] M. Korzhuev, V. Bankina, I. Korolkova, G. Sheina, E. Obraztsova, Phys. Status Solidi (a) 123 (1991) 131–137.
[34] F. Ren, E. Case, E. Timm, H. Schock, J. Alloy. Compd. 455 (2008) 340–345.
[35] J. Wang, I. Beyerlein, C. Tomé, Int. J. Plast. 56 (2014) 156–172.
[36] B. Murty, P. Shankar, B. Raj, B. Rath, J. Murday, Nanostructured materials with high application potential, Textbook of Nanoscience and Nanotechnology, Springer (2013) 176–213.
[37] C.A. Handwerker, T.M. Pollock, JOM, pp. 1–21.
[38] K. Masumoto, I. Nishida, in: Google Patents, 1986.
[39] X. Huang, Y. Miyazaki, T. Kajitani, Solid State Commun. 145 (2008) 132–136.
[40] M. Estili, W.-W. Wu, M. Khazaei, Y. Sakka, Sci. Technol. Adv. Mater. 15 (2014) 014201.
[41] J.R. Salvador, J. Yang, A.A. Wereszczak, H. Wang, J.Y. Cho, Sci. Adv. Mater. 3 (2011) 577–586.
[42] K. Bartholomé, B. Balke, D. Zuckermann, M. Köhne, M. Müller, K. Tarantik, J. König, J. Electron. Mater. 43 (2014) 1775–1781.
[43] F. Ren, H. Wang, P.A. Menchhofer, J.O. Kiggans, Appl. Phys. Lett. 103 (2013) 221907.
[44] J. Gladden, G. Li, R. Adebisi, S. Firdosy, T. Caillat, V. Ravi, Phys. Rev. B 82 (2010) 045209.
[45] V. Ravi, S. Firdosy, T. Caillat, E. Brandon, K. Van Der Walde, L. Maricic, A. Sayir, J. Electron. Mater. 38 (2009) 1433–1442.
[46] T.-J. Ha, M.-H. Hong, C.-S. Park, H.-H. Park, Sens. Actuators B: Chem. 181 (2013) 874–879.
[47] J.B. Goodenough, A. Hamnett, G. Huber, F. Hullinger, M. Leiß, S. Ramasesha, H. Werheit, Physics of Non-Tetrahedrally Bonded Binary Compounds III/Physik Der Nicht-tetraedrisch Gebundenen Binären Verbindungen III, Springer, Germany, 1984.
[48] J. Salvador, J. Yang, X. Shi, H. Wang, A. Wereszczak, H. Kong, C. Uher, Philos. Mag. 89 (2009) 1517–1534.
[49] L.-D. Zhao, S.-H. Lo, Y. Zhang, H. Sun, G. Tan, C. Uher, C. Wolverton, V.P. Dravid, M.G. Kanatzidis, Nature 508 (2014) 373–377.
[50] G. JeffreyáSnyder, J. Mater. Chem. A 2 (2014) 3169–3174.
[51] H. Alam, S. Ramakrishna, Nano Energy 2 (2013) 190–212.

Day Ahead Load Forecast in ISO New England Market and Ontario Market using a Novel ANN

A K Pandey[1], K B Sahay [2], D Chandra[3] and M M Tripathi[4]

[1]A K Pandey, UPPCL, Lucknow, India
[1]anvaypandey100@gmail.com
[2]K B Sahay, Delhi Technological University, Delhi, India
[2]kishansahay16@gmail.com
[3]D Chandra, MNNIT, Allahabad, India
[3]dinuchandra@rediffmail.com
[4]M M Tripathi, Delhi Technological University, Delhi, India
[4]mmtripathi@dce.ac.in

ABSTRACT

Accurate short term load forecasting is an essential task in power system planning, operation, and control. This paper discusses significant role of artificial intelligence (AI) in short-term load forecasting (STLF). A new artificial neural network (ANN) has been designed to compute the forecasted load. The ANN model is trained on hourly data from the ISO New England market and Ontario Electricity Market from 2007 to 2011 and tested on out-of-sample data from 2012. Simulation results obtained have shown that day-ahead hourly forecasts of load using proposed ANN is very accurate with very less error in both the markets. However load forecast for ISO New England market & Ontario market is much better with temperature data as input than without taking it. This is due to the fact that temperature and weather data are having high degree of correlation with load of that particular region. This indicates that temperature data is a very important parameter for load forecasting using ANN.

Keywords —Mean Absolute Percentage Error, Mean Absolute Error, Neural Network, Power System, Short-Term Load Forecasting and Electricity Market.

1. INTRODUCTION

With an introduction of deregulation in power industry, many challenges have been faced by the participants of the electricity market. Forecasting electricity parameters such as load and energy price have become a major issue in power systems [1]. The fundamental objective of electric power industry deregulation is to maximize efficient generation and consumption of electricity, and reduction in energy prices. To achieve these goals, accurate and efficient electricity load forecasting is becoming more and more important [2].

Load forecasting is a key task for the effective operation and planning of power systems. Inaccurate forecasting of electricity demand will either lead to the startup of too many units supplying an unnecessary level of reserve or excessive energy purchase, as well as substantial wasted investment in the construction of excess power facilities or may result in a risky operation and unmet demand, persuading insufficient preparation of spinning reserve, and causes the system to operate in a vulnerable region to the disturbance [3].

Load forecasting is categorized as short-term, medium-term, and long-term forecasts, depending on the time scale. The forecasting of hourly-integrated load carried out for one day to week ahead is usually referred to as short-term load forecasting. Short-term load forecasting plays an important role in power systems since the improvement of forecasting accuracy results in the reduction of operating costs and the reliable power system operations [4].

The load at a given hour is dependent not only on previous loads but also on much important weather related variables.

Effective integration of various factors into the forecasting model may provide accurate load forecasts for modern power industries.

Various techniques have been developed for electricity demand forecasting during the past few years. Several research works have been carried out on the application of AI techniques to the load forecasting problem as AI tools have performed better than conventional methods in short-term load forecasting. Various AI techniques reported in literatures are expert systems, fuzzy inference, fuzzy-neural models, neural network (NN). Among the different techniques on load forecasting, application of NN technology for load forecasting in power system has received much attention in recent years [5]-[8]. The main reason of NN becoming so popular lies in its ability to learn complex and nonlinear relationships that are difficult to model with conventional techniques [9].

This paper discusses significant role of artificial intelligence in day-ahead load forecasting, that is, Day-Ahead hourly load forecast over a day, week & month. In this paper, artificial neural network designed using MATLAB R13 has been used to compute the day-ahead hourly load forecast in ISO New England market and Ontario electricity market. Both the hourly temperature and hourly electricity load historical data have been used in forecasting. The temperature variable is included in forecasting of load because temperature has a high degree of correlation with electricity load. The neural network models are trained on hourly data from the ISO New England market, Ontario electricity market from 2007 to 2011 and tested on out-of-sample data from 2012. The simulation results obtained have shown that artificial neural network (ANN) is able to make very accurate short-term load forecast with average errors around 0.85%-3.85% in ISO New England market and 1.07%-3.85% in Ontario electricity market. A box plot [10] of the error distribution of forecasted load has been plotted as a function of hour of the day, day of the week.

This paper has been organized in five sections. Section II presents the overview of neural network used. Section III discusses the selection of various data and model of ANN for day-ahead forecast. Results of simulation are presented and discussed in Section IV. Section V discusses the conclusion and future work.

2. ARTIFICIAL NEURAL NETWORK FOR LOAD FORECASTING

Neural networks are composed of simple elements called neuron, operating in parallel. A neuron is an information processing unit that is fundamental to the operation of a neural network. The three basic elements of the neuron model are (i) set of weights, (ii) an adder for summing the input signals and (iii) activation function for limiting the amplitude of the output of a neuron. A neural network can be trained to perform a particular function by adjusting the values of the connections (weights) between elements. In load forecasting, typically, many input/ target pairs are needed to train a neural network. Neural network is mapped between data set of numeric inputs and a set of numeric targets. The neural network consists of two-layer feed-forward network with sigmoid hidden neurons and linear output neurons. It can fit multi-dimensional mapping problems arbitrarily well, given consistent data and enough neurons in its hidden layer. The neural network is trained with Levenberg-marquardt back propagation algorithm.

3. DATA INPUTS AND ANN MODEL

The models are trained on hourly data from the ISO New England market & Ontario market from 2007 to 2011 and tested on out-of-sample data from 2012. The data used in the ANN model are both the temperature and electricity load hourly historical data. The temperature variable is included because temperature has a close relationship with electricity load. The relationship between demand and average temperature is shown in Fig. 1, where a nonlinear relationship between load and temperature can be observed. For the load forecast, the input parameters include followings.

- Dry bulb temperature
- Dew point temperature
- Hour of day
- Day of the week
- Holiday/weekend indicator (0 or 1)
- Previous 24-hr average load
- 24-hr lagged load
- 168-hr (previous week) lagged load

4. SIMULATION AND RESULTS

In this paper hourly day-ahead load forecasting has been done for sample of each day, week & month of data of year 2012 using neural network tool box of MATLAB R13a. The ANNs are trained with data from 2007 to 2011 and tested on out-of-sample data from 2012. The test sets are completely separate from the training sets and are not used for model estimation or variable selection.

The model accuracy on out-of-sample periods is computed with the Mean Absolute Percent Error (MAPE) metrics. The principal statistics used to evaluate the performance of these models, mean absolute percentage error (MAPE), is defined in eq. 1 below.

$$MAPE\ [\%] = \frac{1}{N}\sum_{i=1}^{N}\frac{|L_A^i - L_F^i|}{L_A^i} \times 100 \qquad (1)$$

Where LA is the actual load, LF is the forecasted load, N is the number of data points.

Various plots of the error distribution as a function of hour of the day, day of the week are generated. Also, the various plots comparing the day ahead hourly actual and forecasted load for every weeks for the year 2012 are also generated. Simulation results of Ontario and ISO New England market are discussed below.

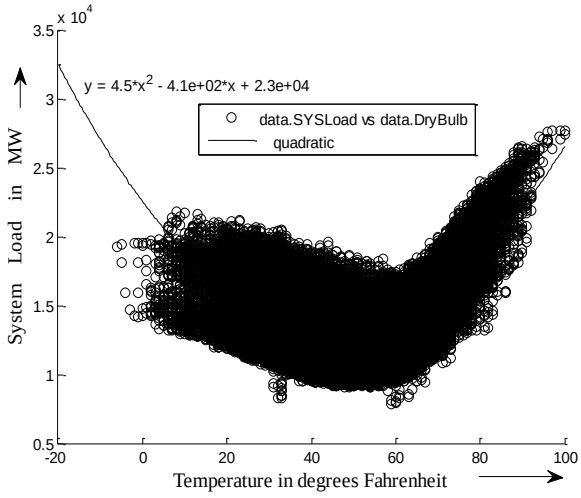

Fig. 1. Scatter plot of system load vs. temperature (degrees Fahrenheit) for ISO England market for year 2007 to 2012 with fitting equation of quadratic.

4.1 Ontario Electricity Market without Considering Temperature Effect

The ANN & improved ANN model used in the forecasting has input, output and one hidden layers. Hidden layer has 50 neurons in ANN, whereas improved ANN consists of a hybrid of 46 & 50 neurons in its hidden layer. Inputs to the input layer are as listed above for load forecast. After simulation the MAPE obtained is 2.90% & 2.85 % for load forecasting for the year 2012 by using ANN & improved ANN respectively as shown in Fig. 2.

The box-plot of the error distribution of forecasted load as a function of hour of the day is presented in Fig. 3. It shows the percentage error statistics of hour of the day in year 2012. It is also evident that the maximum error is for the 6th hour of the day and minimum error for 21th hour of the day in year 2012. The box-plot of the error distribution of forecasted load as a function of day of the week is evaluated in Fig. 4 which shows the percentage error statistics of day of the week in year 2012. The maximum error is for the Monday and minimum error for Friday in year 2012.

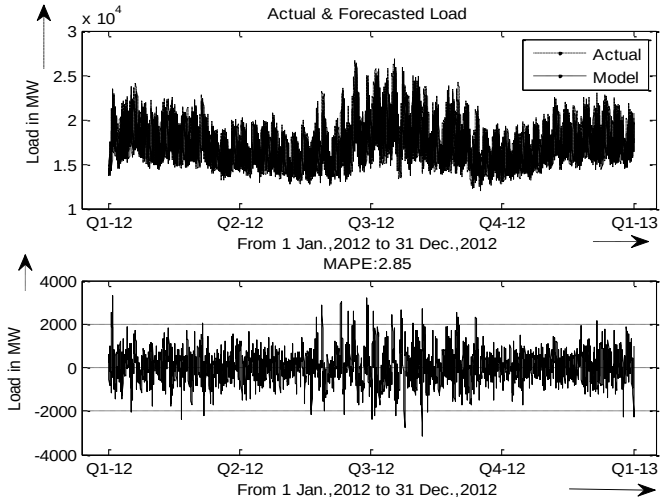

Fig. 2. Multiple series plot between actual load & forecasted load by improved ANN in year 2012 for Ontario electricity market.

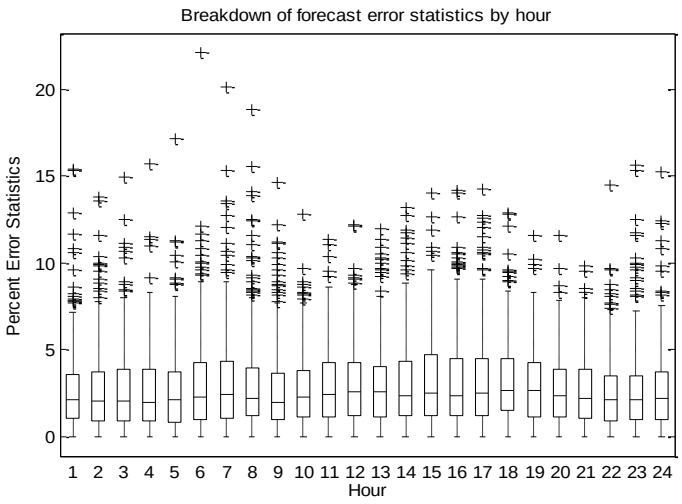

Fig. 3. Error distribution of forecasted load as a function of hour of the day in the year 2012 Ontario electricity market by improved ANN.

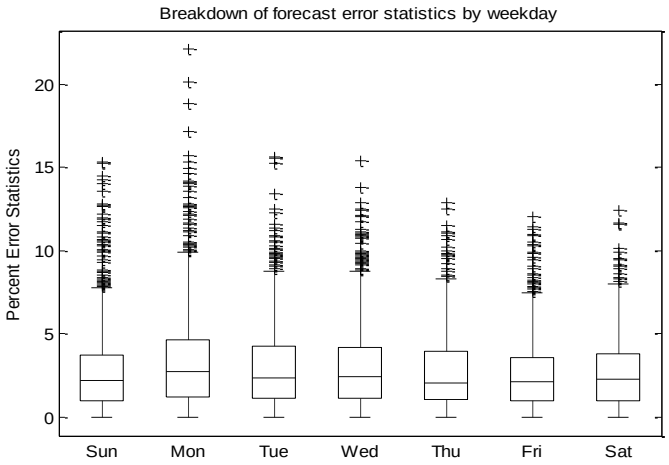

Fig. 4. Error distribution for the forecasted load as a function of day of the week in the year 2012 for Ontario electricity market by improved ANN.

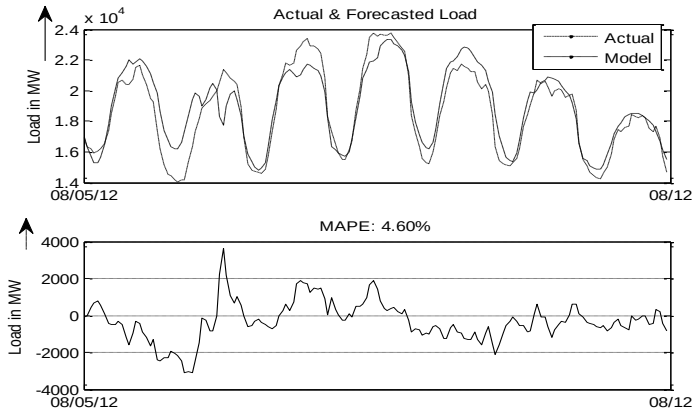

Fig. 5. Maximum MAPE is 4.60 % for the forecast of 05 -11 Aug., 2012 in year 2012 for day ahead hourly weekly forecast by using ANN.

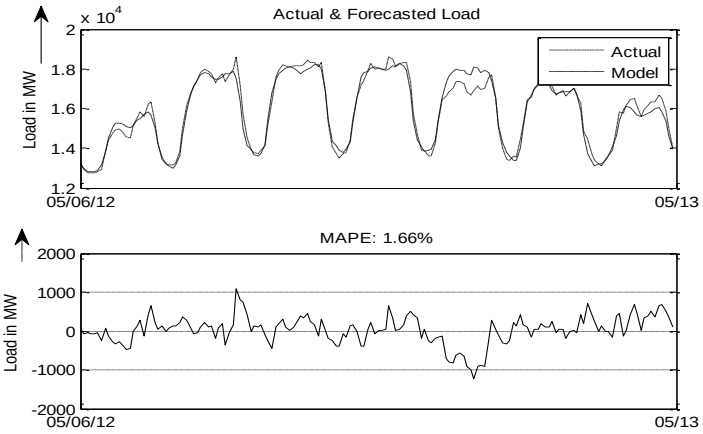

Fig. 6. Minimum MAPE is 1.66% for the forecast of 06-12 May, 2012 for day ahead hourly weekly forecast in the year 2012 by using improved ANN.

Multiple series plots between actual load & forecasted load from 05-11 Aug., 2012 & from 06-12 May, 2012 for Ontario electricity market and also plots of MAPE with maximum error (4.60%) and minimum error (1.66%) for day ahead hourly weekly forecast in year 2012 have been shown in Fig. 5 and Fig. 6 by ANN & improved ANN respectively.

4.2 ISO New England Market

The ANN & improved ANN model used in the forecasting has input, output and one hidden layers. Hidden layer has 52 neurons in ANN, whereas improved ANN has hybrid of 52 & 48 neurons in its hidden layer. Inputs to the input layer as listed above for load forecast with considering temperature data. After simulation the MAPE obtained is 1.55 % & 1.50 % for load forecasting for the year 2012 by ANN & improved ANN respectively.

The box-plot of the error distribution of forecasted load as a function of hour of the day is presented in Fig. 7. It shows the percentage error statistics of hour of the day in year 2012. It is also evident that the maximum error is for the 21st hour of the day and minimum error for 14th hour of the day in year 2012. The box-plot of the error distribution of forecasted load as a function of day of the week is evaluated in Fig. 8 which shows the percentage error statistics of day of the week in year 2012. The maximum error is for the Monday and minimum error for Thursday in year 2012.

Multiple series plots between actual load & forecasted load from 06-12 May, 2012 & from 28 October, 2012 to 03 November, 2012 for ISO New England market and also plots of MAPE with maximum error (3.85%) and minimum error

(0.85%) for day ahead hourly weekly forecast in year 2012 have been shown in Fig. 9 and Fig. 10 by using improved ANN.

Also, an ANN & improved ANN model for forecasting has been developed without considering temperature data (dry bulb & dew point) as an input to input layer. This ANN & improved ANN model used in the forecasting has input, output and one hidden layers. Hidden layer has 38 neurons in ANN, while the improved ANN has hybrid of 42 & 50 neurons in its hidden layer. After simulation the MAPE obtained is 2.90 % & 2.81 % for load forecasting for the year 2012 by using ANN & improved ANN respectively. The MAPE obtained between actual load & forecasted load from 17-23 June & from 06-12 May, 2012 for ISO New England market shows maximum error (5.13%) & minimum error (1.19%) for day ahead hourly weekly forecast in year 2012 by using ANN & improved ANN respectively.

The MAPE & MAE between the forecasted and actual loads for each day, week & month has been calculated and presented from Table I-VI in the year 2012, with & without considering temperature data for both the power market. From the results of Table I-VI it is observed that MAPE & MAE for ISO New England market (with temperature data) is much better than MAPE & MAE for Ontario electricity market. This is due to the fact that temperature and weather data is not been taken as input in Ontario electricity market but it is considered for input in ISO New England market. This indicates that temperature data is a very important parameter for load forecasting using ANN. Also, the MAPE & MAE from Table I-VI of ISO New England market with considering temperature data is much better than without considering temperature data as input to ANN in same market. From the results obtained from Table III, it is clear that maximum MAPE (3.85%) is for July & minimum MAPE (2.17%) is for November, 2012 for Ontario electricity market. Also, it is clear that maximum MAPE (2.02%) is for Dec., 2012 and minimum MAPE (1.4%) is for July, 2012 for ISO New England market (with temperature data),as soon in Fig. 11.

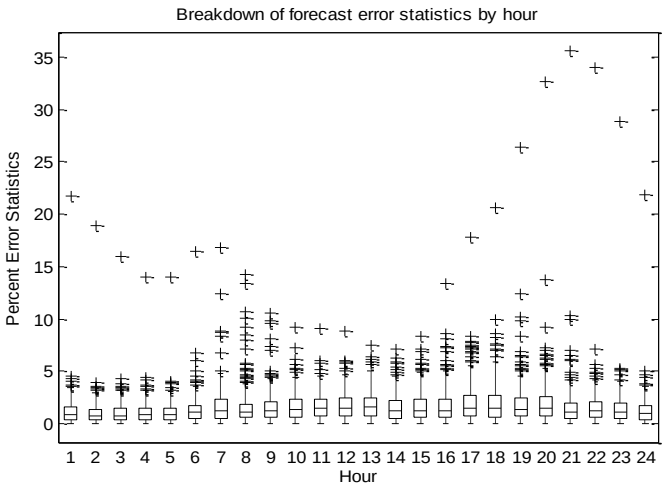

Fig. 7. Error distribution of forecasted load as a function of hour of the day in year 2012 for ISO New England market by improved ANN.

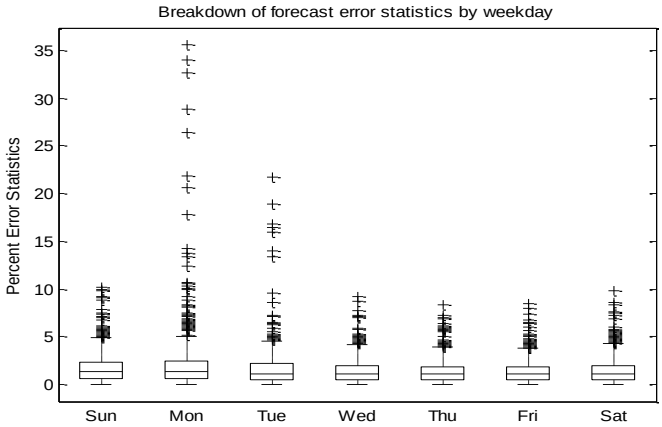

Fig. 8. Error distribution for the forecasted load as a function of day of the week in the year 2012 for ISO New England market by improved ANN.

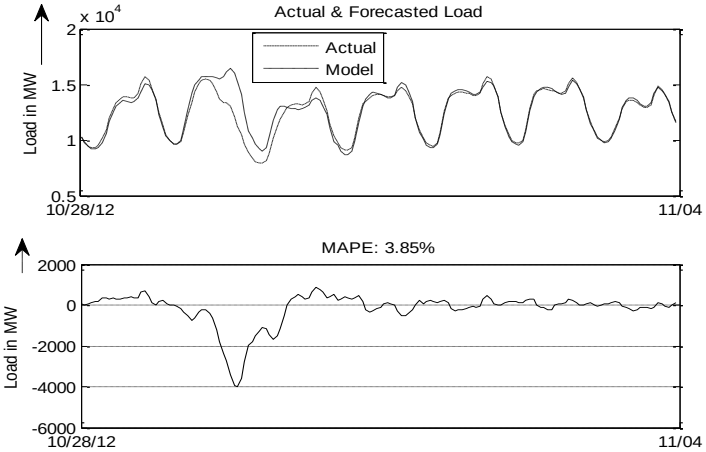

Fig. 9. Maximum MAPE is 3.85% for the load forecast of 28 October, 2012 to 03 November, 2012 for day ahead hourly weekly forecast for year 2012.

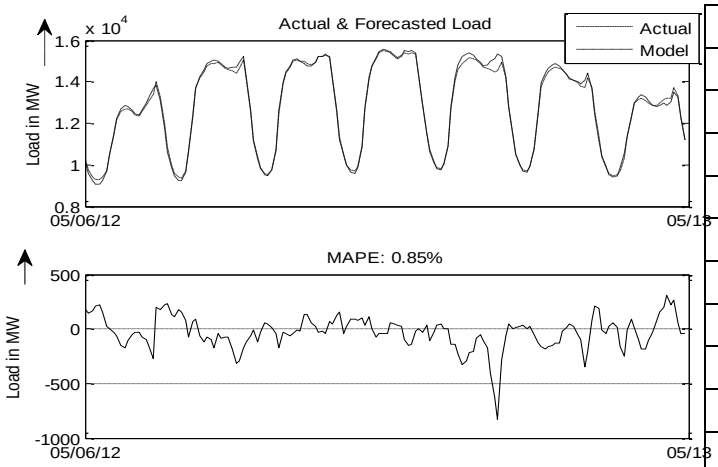

Fig. 10. Minimum MAPE is 0.85% for the load forecast of 06-12 May, 2012 for day ahead hourly weekly forecast for the year 2012.

TABLE I

RESULTS FOR OUT-OF-SAMPLE TEST FOR YEAR 2012

S. N.	Duration (Year 2012) mm/dd - mm/dd	MAPE (%)					
		ISO New England Market				Ontario	
		With Temp. Data		Without temp. data		Without temp. data	
		ANN	Imp. ANN	ANN	Imp. ANN	ANN	Imp. ANN
1	01/01-01/07	2.16	2.04	4.03	3.9	3.9	3.85
2	01/08-01/14	1.32	1.23	2.57	2.45	2.59	2.55
3	01/15-01/21	1.47	1.37	4.13	4.05	2.99	2.86
4	01/22-01/28	1.86	1.8	3.11	3.05	2.07	2.02
5	01/29-02/04	0.9	0.86	2.21	2.02	2.33	2.37
6	02/05-02/11	1.28	1.21	2.62	2.51	2.82	2.82
7	02/12-02/18	1.12	1.08	2.41	2.27	2.77	2.7
8	02/19-02/25	1.47	1.37	2.75	2.58	2.92	2.98
9	02/26-03/03	1.66	1.55	2.85	2.71	2.69	2.64
10	03/04-03/10	1.51	1.52	2.86	2.71	3.43	3.43
11	03/11-03/17	1.94	1.87	2.78	2.76	2.84	2.8
12	03/18-03/24	1.68	1.65	1.57	1.61	2.64	2.61
13	03/25-03/31	1.49	1.28	2.95	2.97	2.43	2.38
14	04/01-04/07	1.58	1.47	2.53	2.44	2.74	2.68
15	04/08-04/14	1.22	1.23	1.99	1.87	2.25	2.3
16	04/15-04/21	1.63	1.65	2.29	2.11	2.4	2.37
17	04/22-04/28	1.32	1.38	2.26	2.12	2.48	2.49
18	04/29-05/05	1.35	1.33	1.55	1.45	2.16	2.1
19	05/06-05/12	0.92	0.85	1.23	1.19	1.68	1.66
20	05/13-05/19	0.99	0.93	1.61	1.59	2.52	2.5
21	05/20-05/26	0.91	0.94	2.06	2.01	2.96	2.96
22	05/27-06/02	1.72	1.71	3.75	3.68	4	3.95
23	06/03-06/09	1.14	1.17	1.96	1.82	2.42	2.27
24	06/10-06/16	0.97	0.92	1.93	1.88	4.21	4.29
25	06/17-06/23	1.84	1.61	5.13	5.38	3.83	3.78
26	06/24-06/30	1.86	1.7	3.96	3.81	3.49	3.38
27	07/01-07/07	2.07	1.8	4.12	4.07	4.34	3.83
28	07/08-07/14	1.26	1.27	3.29	3.51	3.37	3.26
29	07/15-07/21	1.25	1.22	4.46	3.95	4.31	4.27
30	07/22-07/28	1.34	1.27	4.1	3.65	4	4.05
31	07/29-08/04	1.34	1.21	3.11	3.15	3.24	3.27
32	08/05-08/11	1.53	1.53	3.7	3.89	4.6	4.63
33	08/12-08/18	1.54	1.5	3.48	3.17	3.01	2.99
34	08/19-08/25	1.37	1.25	2.61	2.73	2.8	2.74
35	08/26-09/01	1.46	1.49	4.27	4.14	3.71	3.68
36	09/02-09/08	1.71	1.54	3.55	3.57	3.61	3.52
37	09/09-09/15	1.78	1.91	3.84	3.83	4.1	4.06
38	09/16-09/22	1.59	1.58	2.83	2.79	2.25	2.15
39	09/23-09/29	1.26	1.23	1.52	1.48	2.25	2.29
40	09/30-10/06	1.18	1.23	1.42	1.25	1.93	1.89
41	10/07-10/13	1.41	1.44	2.03	2.05	2.95	2.91
42	10/14-10/20	1.5	1.58	1.98	1.89	2.16	2.09
43	10/21-10/27	1.24	1.24	1.32	1.42	1.88	1.87
44	10/28-11/03	3.89	3.85	4.08	4.65	2.23	2.25
45	11/04-11/10	1.96	1.83	3.82	3.86	2.11	2.11
46	11/11-11/17	1.7	1.61	2.57	2.39	1.94	1.91
47	11/18-11/24	1.92	2.04	3.14	2.6	2.17	2.16
48	11/25-12/01	1.19	1.2	3.11	3.07	2.61	2.64
49	12/02-12/08	1.93	1.79	3.58	3.42	2.45	2.43
50	12/09-12/15	1.81	1.76	3.01	2.68	2.74	2.72
51	12/16-12/22	1.77	1.78	2.27	2.24	2.54	2.6
52	12/23-12/29	2.58	2.53	3.89	3.75	3.45	3.46
53	Average	1.55	1.50	2.90	2.81	2.90	2.85

TABLE II

RESULTS FOR OUT-OF-SAMPLE TEST FOR YEAR 2012

SN	Duration (Year 2012) mm/dd-mm/dd	MAE (MW)					
		ISO New England Market				Ontario	
		With Temp. Data		Without temp. data		Without temp. data	
		ANN	Imp. ANN	ANN	Imp. ANN	ANN	Imp. ANN
1	01/01-01/07	321.3	303	606.4	588.2	719.8	709.3
2	01/08-01/14	202.2	187	391.5	368.6	486.3	478.9
3	01/15-01/21	239.6	224	649.8	631.7	589.9	564.3
4	01/22-01/28	287.4	277	457.8	452	382.2	373.7
5	01/29-02/04	134.1	129	330.8	299.2	418.8	424.8
6	02/05-02/11	192.4	183	380.2	366.4	532.1	533.4
7	02/12-02/18	170.4	166	357	335.6	510.8	497.7
8	02/19-02/25	218.3	200	389.5	364.8	530.6	542.1

9	02/26-03/03	248.6	231	408.3	389.3	498.2	488.2
10	03/04-03/10	219.2	222	402.4	378.4	625.4	625.2
11	03/11-03/17	263.9	255	362.5	361.4	467	460.7
12	03/18-03/24	226.2	221	205.6	209	420.3	415.7
13	03/25-03/31	203.8	174	391.5	393.6	415	407.1
14	04/01-04/07	210.5	198	333.7	319.2	470.2	458.7
15	04/08-04/14	155.1	156	255.1	243	382.7	390
16	04/15-04/21	217.5	218	310.9	287.8	400.1	396.4
17	04/22-04/28	172.6	181	290.6	273.1	426.8	427.9
18	04/29-05/05	181.3	177	203.4	188.1	344.6	335.6
19	05/06-05/12	119.4	110	163.5	157.4	272	267.2
20	05/13-05/19	132.4	123	219.6	215	423.1	419.3
21	05/20-05/26	131.1	135	308.9	300.3	525	526.3
22	05/27-06/02	261.1	258	571.8	561.7	713.9	704.6
23	06/03-06/09	158.5	163	271.9	252.2	413.7	391.3
24	06/10-06/16	139.7	131	279.2	270.7	773.6	789.6
25	06/17-06/23	328.9	279	974.1	1008	783.1	774.9
26	06/24-06/30	295.5	272	633.3	605.1	671.1	649.5
27	07/01-07/07	361.8	315	709	692.5	883.5	788.1
28	07/08-07/14	225.7	225	559.8	596.9	644.1	625.1
29	07/15-07/21	227.6	222	772.2	680.4	837.2	829.6
30	07/22-07/28	233.5	218	675.3	615.5	786.4	799
31	07/29-08/04	234.5	212	551	562.3	657.4	665.4
32	08/05-08/11	276	273	675.1	721.1	835.8	843.9
33	08/12-08/18	263.5	255	575.7	526.7	551	547.1
34	08/19-08/25	218.8	199	383.6	396.5	536.8	525.4
35	08/26-09/01	243.7	246	676.1	649.8	700.7	695.1
36	09/02-09/08	273.9	251	545.9	554.5	621.4	604
37	09/09-09/15	255.7	275	520.8	524.1	645.4	643.5
38	09/16-09/22	213.5	213	381.6	369	368	352.2
39	09/23-09/29	167	163	201.5	195.7	360.4	365.6
40	09/30-10/06	164	172	194.2	171	312.7	306.5
41	10/07-10/13	180.8	186	263.4	267.4	475.3	469.8
42	10/14-10/20	202.6	212	271.3	258.1	365	353.6
43	10/21-10/27	164.1	164	174.9	188.9	311.4	309.9
44	10/28-11/03	448.4	444	483.1	555.1	384.2	388.1
45	11/04-11/10	285.3	262	537.7	542.2	392.7	392.9
46	11/11-11/17	239.8	226	354.9	327.8	352.3	347.1
47	11/18-11/24	264.6	279	428.6	355.3	387.4	386.5
48	11/25-12/01	182.7	185	458	454.9	493.7	499
49	12/02-12/08	285.2	266	499.6	472.9	446.2	442
50	12/09-12/15	275.6	269	442.9	391.7	515.5	510.2
51	12/16-12/22	279.2	281	352	343.2	472.4	481.9
52	12/23-12/29	395.5	386	576.8	558.8	613.7	617.5
53	Average	230.6	222	431	419.1	522	516.1

From the results obtained from Table IV-VI, it is clear that highest MAPE (9.14%) is on 06 August & least MAPE (1.01%) is on 26 July, 2012 in Ontario electricity market for day ahead hourly forecast in testing year-2012 & also multiple series plots between actual load & forecasted load with plot of MAPE on 06 August is shown in Fig. 12. Multiple series plots between actual load & forecasted load on 09 May, 2012 for ISO New England market and also plots of MAPE with least error (0.45%) for day ahead hourly forecast in year 2012 have been shown in Fig. 13. Also the highest error for daily forecast is on 29 Oct., 2012 in the year 2012 with MAPE (11.35%) for ISO New England market is presented in Table VI

TABLE III

RESULTS FOR OUT-OF-SAMPLE MONTHLY TEST IN YEAR 2012 BY USING IMPROVED ANN

S.N.	Month	MAPE (%)			MAE(MW)	
		Ontario (Without temp. data)	ISO New England		ISO market (With Temp. data)	Ontario (Without temp. data)
			Without Temp.	With Temp.		
1	Jan	2.86	3.25	1.56	239.03	535.93
2	Feb	2.67	2.47	1.17	175.06	494.5
3	March	2.79	2.52	1.63	226.27	475.86
4	April	2.47	2.11	1.41	186.09	417.56
5	May	2.63	1.91	1.14	160.19	455.23
6	June	3.34	3.17	1.33	207.72	629.5
7	July	3.85	3.84	1.4	243.82	761.38
8	August	3.49	3.41	1.4	240.33	660.34
9	Sept	2.95	2.86	1.54	221.14	481.79
10	Oct	2.22	2.29	1.98	249.9	367.85
11	Nov	2.17	2.88	1.62	229.91	397.61
12	Dec	2.89	3.03	2.02	309.32	527.38

TABLE IV

RESULTS FOR OUT-OF-SAMPLE DAILY TEST FROM JANUARY-APRIL, 2012 BY IMPROVED ANN

Day	MAPE (%) In Different Months of Year 2012							
	Ontario Electrcity Market Without Temp. Data				ISO New England Market With Temp. Data			
	Jan.	Feb.	Mar.	April	Jan.	Feb.	March	April
1	2.29	1.66	1.68	3.56	4.51	0.83	1.18	1.73
2	4.9	1.71	2.83	3.2	2.5	0.71	2.08	1.25
3	7.46	1.07	2.15	1.52	2.43	0.89	2.39	1.62
4	2.96	1.8	2.4	3.13	1.44	0.48	0.79	1.15
5	4.07	1.39	4.61	2.69	1.35	1.64	1.73	0.78

6	2.2	2.32	2.67	2.13	0.97	1.68	1.3	2.63
7	3.09	2.93	6.08	2.51	1.11	0.55	2.36	1.14
8	2.95	3.69	2.68	2.97	1.93	1.06	2.61	2.5
9	2.32	3.05	2.31	1.82	1.2	1.54	0.81	1.5
10	3.36	2.53	3.27	2.34	0.87	1.13	1.06	1.02
11	1.93	3.84	5.04	2.19	1.2	0.84	2.07	0.68
12	1.46	3.44	2.12	2.68	1	0.98	3.2	0.8
13	2.78	4.13	5.31	2	1.28	1.98	2.28	1.13
14	3.06	2.69	1.37	2.11	1.13	1.17	0.8	1
15	3.07	2.92	1.51	2.91	0.73	0.89	1.03	1.07
16	4.32	1.74	1.67	2.42	1.43	0.63	1.38	1.5
17	3.41	2.59	2.56	1.94	1.86	0.99	2.37	2.14
18	2.8	1.39	2.04	2.02	1.41	0.94	2.2	3.54
19	3.42	2.11	3.66	1.77	1.29	1.55	1.91	1.05
20	1.77	5.24	2.4	1.59	1.17	2.07	1.28	1.09
21	1.26	2.73	3.34	3.96	1.7	0.93	0.96	1.15
22	2.63	2.57	2.14	2.13	3.32	1.95	1.78	1.69
23	2.71	1.97	2.88	2.34	2.54	1.05	1.93	1.91
24	1.63	3.77	1.8	2.47	2.34	1.02	1.47	2
25	2.14	2.51	2.56	4.1	0.68	1.02	1.53	1.19
26	1.45	2.89	2.95	2.6	1.17	1.35	1.04	0.59
27	2.21	2.96	2.46	1.74	1.15	1.6	1.77	1.4
28	1.4	2.11	1.5	2.06	1.37	1.47	1.05	0.9
29	3.56	3.86	2.5	3.03	1.15	0.77	0.68	1.46
30	3.16	----	2.08	2.11	0.97	-----	2.01	1.23
31	3.61	-----	2.61	-----	1	------	0.91	-----

TABLE V

RESULTS FOR OUT-OF-SAMPLE DAILY TEST FROM MAY-AUGUST, 2012 BY IMPROVED ANN

Day	MAPE (%) In Different Months of Year 2012							
	Ontario Electrcity Market Without Temp. Data				ISO New England Market With Temp. Data			
	May	Jun.	July	Aug.	May	Jun.	July	Aug.
1	2.99	2.17	2.16	3.89	1.13	1.57	0.96	0.93
2	1.54	2.27	4.81	3.92	1.44	0.71	2.55	1.1
3	1.23	1.09	3.96	2.89	1.33	0.94	1.73	1.08
4	1.49	1.72	6.58	2.64	0.87	1.28	1.69	1.05
5	2.28	2.69	1.44	5.28	1.85	1.85	1.47	1.51
6	1.39	2.59	3.48	9.14	1.16	1.27	1.45	1.02
7	1.49	3.1	4.39	4.27	0.93	1.16	2.75	2.08
8	1.16	2.64	4.6	2.54	0.49	0.82	1.11	1.48
9	1.36	2.07	2.63	5.72	0.45	0.87	1.27	1.15
10	3.06	6.54	2.58	2.65	1.3	1.29	1.77	1.47
11	1.16	2.85	3.09	2.83	0.77	1.01	1.1	1.98
12	1.97	4.83	4.01	1.58	0.88	0.72	0.97	1.26
13	1.94	5.01	3.03	2.84	0.89	0.82	1.27	1.53
14	3.03	2.73	2.89	2.91	0.62	0.83	1.38	1.28
15	2.32	5.78	2.09	3.2	0.66	0.89	0.9	1.06
16	3.58	2.32	4.21	3.26	0.65	0.87	0.67	1.02
17	2.11	2.21	3.47	3.15	1.29	1.11	0.72	1.61
18	2.27	3.4	3.89	4.01	1.02	1.39	1.91	2.71
19	2.21	5.75	6.6	1.26	1.36	1.15	1.12	1.48
20	1.97	4.75	5.27	2.11	0.93	3.23	2.2	1.45
21	4.16	2.68	4.36	2.34	0.96	1.37	1.04	1.27
22	1.75	4.78	6.85	2.91	0.77	1.03	1.21	1.17
23	1.84	2.9	4.76	3.9	0.72	2	1.37	1.24
24	5.07	1.6	5.34	3.32	0.8	1.79	1.21	1.18
25	3.56	4.55	6.06	3.3	1.05	2.71	2.18	0.96
26	2.36	4.09	1.01	2.81	1.35	1.64	1.1	1.69
27	2.39	2.06	2.52	2.63	2.24	1.46	1	1.2
28	6.81	4.8	1.79	3.72	1.03	1.86	0.79	1.53
29	5.27	3.5	2.49	5.07	2.84	1.1	1.01	1.64
30	4.92	3.05	3.63	4.54	2.11	1.36	1.18	1.44
31	3.83	----	3.44	4.06	1.44	-----	2.09	1.65

TABLE VI

RESULTS FOR OUT-OF-SAMPLE DAILY TEST FROM SEPT.-DEC., 2012 BY IMPROVED ANN

Day	MAPE (%) In Different Months of Yaer 2012							
	Ontario Electrcity Market With Temp. Data				ISO New England Market With Temp. Data			
	Sep.	Oct.	Nov.	Dec.	Sep.	Oct.	Nov.	Dec.
1	2.9	2.42	2.74	3.57	1.27	1.35	1.32	1.12
2	3.62	2.44	1.45	1.52	1.49	0.87	1.13	2.76
3	4.94	2.13	2.34	3.12	1.52	1.04	0.85	2.51
4	2.97	1.52	1.23	1.71	1.41	1.3	2.73	1.18
5	3.16	1.6	2.91	3.24	1.78	1.33	1.59	1.79
6	2.01	1.52	2.38	2.7	1.6	1.78	1.13	1.97
7	3.95	2.13	2.9	2.35	1.29	2.27	2.95	1.18
8	3.95	4.47	1.93	2.38	1.72	2.58	0.84	1.15
9	5.19	3.49	1.6	3.44	1.92	1.12	1.7	1.46
10	2.44	2.36	1.81	3.77	2.39	0.87	1.87	1.42
11	3.83	1.52	2.04	2.78	2.04	1.31	2.2	2.03
12	4.49	2.2	1.95	2.46	1.52	0.86	2.66	1.93
13	3.42	4.21	1.99	2.97	1.34	1.09	0.95	1.67
14	3.77	2.14	1.72	1.9	1.83	1.8	1.39	1.96
15	5.25	4.37	2.33	1.73	2.35	2.21	1.28	1.87
16	2.46	1.74	1.4	1.84	2.19	1.69	1.13	2.5
17	2.4	1.34	1.93	3.9	0.99	0.58	1.66	1.37
18	2	1.55	1.39	2.52	1.2	1.22	1.96	1.67
19	2.39	2.02	1.7	2.91	2.23	1.22	1.55	1.53

20	1.98	1.51	1.72	1.92	2.47	2.3	1.04	1.69
21	1.85	2.71	2.56	2.31	0.89	1.96	1.18	1.42
22	1.97	1.44	1.19	2.77	1.1	1.45	2.91	2.28
23	2.72	1.1	2.67	2.62	1.31	0.85	3.54	1.43
24	1.78	2.08	3.88	6.73	1.64	0.79	2.09	6.26
25	3.5	1.79	1.96	2.1	1.73	0.76	2.2	2.71
26	1.86	2.1	2.34	4.2	0.96	1.59	1.3	3.02
27	2.4	1.87	2.29	3.65	1.18	1.3	0.6	1.4
28	1.6	2.88	2.08	2.31	0.56	2.07	0.8	1.67
29	2.14	3	2.74	2.62	1.27	11.35	1.25	1.2
30	1.64	2.28	3.48	2.2	0.96	8.08	1.16	1.28
31	-----	1.07	-----	5.26	-----	2.15	------	4.62

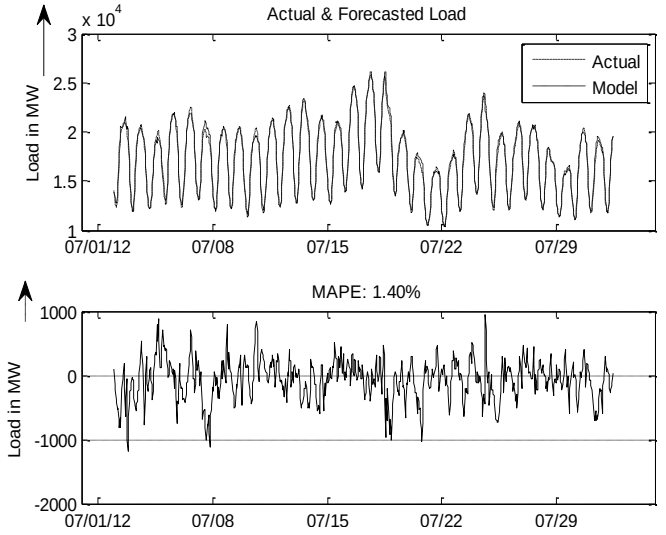

Fig. 11. MAPE is least (1.40%) for day ahead hourly-monthly forecast of July, 2012 of ISO New England market in year 2012.

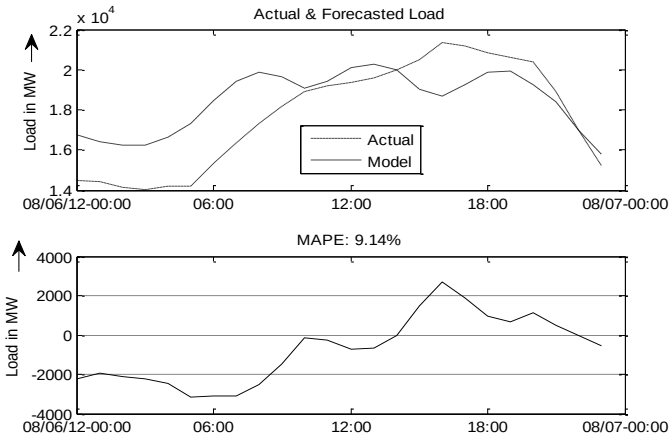

Fig. 12. MAPE is highest (9.14%) for the day ahead hourly forecast on 06 August 2012 in Ontario electricity market in year 2012 by improved ANN.

4.3 For Ontario Electricity Market Considering Temperature Effect

The ANN model used in the forecasting has input, output and one hidden layers. Hidden layer has 56 neurons. Inputs to the input layer as listed above for load forecast. Here temperature & load data of Toronto of Ontario Electricity Market has been considered. After simulation the MAPE obtained is 1.80% for load forecasting for the year 2012. Multiple series plots between actual load & forecasted load from 12-18 February, 2012 and also plots of MAPE with least error (1.07 %) for day ahead hourly weekly forecast in year 2012 have been shown in Fig. 14. The Mean Absolute Percentage Error (MAPE) & Mean Absolute Error (MAE) between the forecasted and actual loads for each week & month has been calculated and presented in the Table VII & Table VIII respectively for the year 2012. From the results obtained from Table VIII, it is clear that maximum MAPE (2.35%) is for July, 2012 and minimum MAPE (1.43%) is for February, 2012. It has been observed that load forecasting of 1-7 July has maximum error with MAPE of 3.85%. From the results obtained in Table I-VIII, it is observed that MAPE in load forecasting for Ontario Electricity Market with temperature data is much better than MAPE without considering it. This is due to the fact that temperature and weather data are having high degree of correlation with load of that particular region. This indicates that temperature data is a very important parameter for load forecasting using ANN.

TABLE VII

RESULTS FOR OUT-OF-SAMPLE TEST FOR YEAR 2012 BY IMPROVED ANN

S. N.	Duration (Year 2012) mm/dd/yy -	Ontario Electricity Market	
		MAPE (%)	MAE(MW)
1	01/01/12-01/07/12	2.92	169.5
2	01/08/12-01/14/12	1.37	83.8
3	01/15/12-01/21/12	1.3	80.73
4	01/22/12-01/28/12	1.16	70.68
5	01/29/12-02/04/12	1.34	81.22
6	02/05/12-02/11/12	1.32	80.52
7	02/12/12-02/18/12	1.07 (min.)	64.62
8	02/19/12-02/25/12	1.87	111.1
9	02/26/12-03/03/12	1.79	107.55
10	03/04/12-03/10/12	1.68	99.33
11	03/11/12-03/17/12	2.07	111.78
12	03/18/12-03/24/12	1.59	88.7
13	03/25/12-03/31/12	1.92	109.57

14	04/01/12-04/07/12	1.6	84.11
15	04/08/12-04/14/12	1.45	77.44
16	04/15/12-04/21/12	1.46	81.3
17	04/22/12-04/28/12	1.34	76.27
18	04/29/12-05/05/12	1.19	65.29
19	05/06/12-05/12/12	1.09	57.08
20	05/13/12-05/19/12	1.23	65.93
21	05/20/12-05/26/12	2.26	125.1
22	05/27/12-06/02/12	2.1	135.3
23	06/03/12-06/09/12	1.51	83.85
24	06/10/12-06/16/12	1.83	115.04
25	06/17/12-06/23/12	1.97	138.06
26	06/24/12-06/30/12	1.73	111.4
27	07/01/12-07/07/12	3.85 (max.)	252.43
28	07/08/12-07/14/12	1.89	130.96
29	07/15/12-07/21/12	1.89	132.6
30	07/22/12-07/28/12	2.22	156.99
31	07/29/12-08/04/12	1.89	132.71
32	08/05/12-08/11/12	3.41	202.7
33	08/12/12-08/18/12	1.44	85.52
34	08/19/12-08/25/12	1.47	93.12
35	08/26/12-09/01/12	1.74	112.72
36	09/02/12-09/08/12	2.6	156.89
37	09/09/12-09/15/12	1.74	103.58
38	09/16/12-09/22/12	1.64	89.74
39	09/23/12-09/29/12	1.27	68.13
40	09/30/12-10/06/12	1.38	76.67
41	10/07/12-10/13/12	2.49	129.27
42	10/14/12-10/20/12	1.59	86.96
43	10/21/12-10/27/12	1.61	89.42
44	10/28/12-11/03/12	3.12	176.45
45	11/04/12-11/10/12	1.42	82.18
46	11/11/12-11/17/12	1.76	98.59
47	11/18/12-11/24/12	1.93	110.94
48	11/25/12-12/01/12	1.23	76.55
49	12/02/12-12/08/12	1.66	97.77
50	12/09/12-12/15/12	1.7	104.64
51	12/16/12-12/22/12	1.81	107.46
52	12/23/12-12/29/12	3.03	162.55
53	Average	1.80	113.90

TABLE VIII

RESULTS FOR OUT-OF-SAMPLE MONTHLY TEST IN YEAR 2012 BY IMPROVED ANN

S.N.	Month	Ontario Electricity Market	
		MAPE (%)	MAE(MW)
1	January	1.65	98.95
2	February	1.43 (min.)	86.39
3	March	1.87	105.22
4	April	1.44	78.6
5	May	1.63	93.67
6	June	1.76	110.87
7	July	2.35 (max.)	161.91
8	August	2.02	125.9
9	September	1.8	104.19
10	October	2.15	118.2
11	November	1.57	90.64
12	December	2.13	122

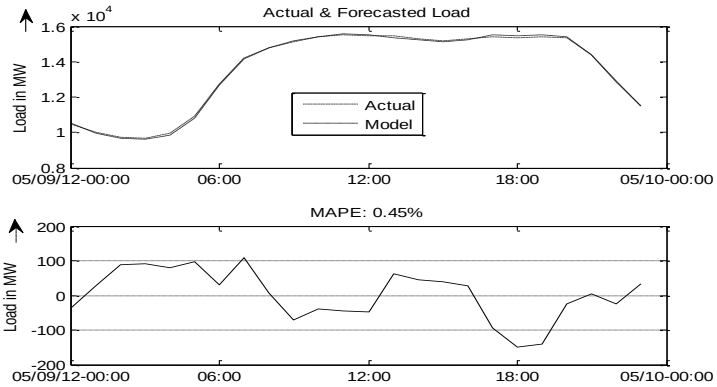

Fig. 13. MAPE is least (0.45%) for day ahead hourly forecast on 09 May, 2012 for ISO New England market in year 2012.

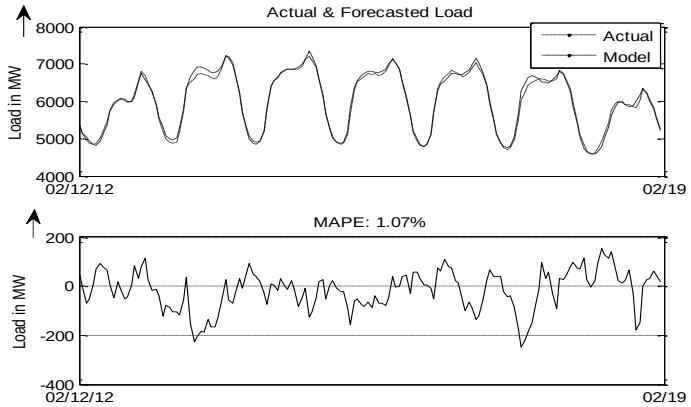

Fig. 14. MAPE is minimum (1.07%) for the load forecast of 12-18 February, 2012 for day ahead hourly weekly forecast.

5. CONCLUSION AND FUTURE WORK

This paper presents an ANN & improved ANN model for day-ahead short-term electricity loads forecasting in ISO New England market and Ontario market. Its forecasting reliabilities were evaluated by computing the MAPE & MAE between the exact and predicted electricity load values. We were able to obtain an MAPE 1.80% for Ontario market and

MAPE 1.50% for ISO New England market in the year 2012 by using improved ANN. The results suggest that improved ANN model with the developed structure can perform well in day ahead load forecasting with least possible error. It has been observed that temperature plays an important role in electricity load forecasting. In future effect of other weather parameters like humidity, precipitation, and wind velocity on short-term load forecasting may be worked out.

REFERENCES

[1] Michael Negnevitsky, Paras Mandal and Anurag K. Srivastava, "An Overview of Forecasting Problems and Techniques in Power Systems," IEEE PES Confernce, pp. 1-4 , ISSN: 1944-9925 ,ISBN: 978-1-4244-4241-6, July 2009.

[2] Paras Mandal, Tomonobu Senjyu, Katsumi Uezato, and Toshihisa Funabashi, "Several-Hours-Ahead Electricity Price and Load Forecasting Using Neural Networks," IEEE PES Conference, vol. 3, pp. 2146-2153, ISBN:0-7803-9157-8 ,June 2005.

[3] Shu Fan and Rob J. Hyndman, "Short-Term Load Forecasting Based on a Semi-Parametric Additive Model," IEEE Trans. Power Syst., vol. 27, Issue 1, pp. 134–141, Feb. 2012.

[4] Paras Mandal, Tomonobu Senjyu, Katsumi Uezato, and Toshihisa Funabashi, "Forecasting Several-Hours-Ahead Electricity Demand Using Neural Network," IEEE Conference on Power Syst., vol. 2,pp. 515–521, April 2004.

[5] M. M. Tripathi, K. G. Upadhyay, S. N. Singh, "Short-Term Load Forecasting using Generalized Regression and Probabilistic Neural Networks in the Electricity Market", The Electricity, Volume 21, Issue 9, November 2008, pp 24-34

[6] M. M. Tripathi, K. G. Upadhyay, S. N. Singh, "Electricity Price Forecasting using General Regression Neural network (GRNN) for PJM Electricity Market", International Review of Modeling and Simulation (IREMOS) ISSN: 1974-9821, Volume 1, No. 2, December 2008, pp 318-324

[7] M. M. Tripathi, K. G. Upadhyay, S. N. Singh, "A novel method of Load forecasting using GRNN and PNN techniques in PJM and Australian Electricity Market using Market pricing signal as input", International Journal of Computer Application in Engineering, Technology and Science (IJ-CA-ETS) ISSN: 0974-3596, Vol. 2, Issue 2, June - December 2009, pp. 604-610.

[8] M. M. Tripathi, S. N. Singh, K. G. Upadhyay, "Price Forecasting in Competitive Electricity Markets: an analysis", Proceedings of International Conference on Energy Engineering (ICEE-2009), Puducherry, India, 7-9 January 2009, paper no. EEE4214.

[9] K. G. Upadhyay, M. M. Tripathi, S. N. Singh, "An Approach to Short Term Load Forecasting using Market Price Signal", International Conference on Distribution (CIRED 2007), Vienna, Austria, 21-24 May 2007, paper 0487.

[10] http://www.mathworks.in

Optik 126 (2015) 950–955

Contents lists available at ScienceDirect

Optik

journal homepage: www.elsevier.de/ijleo

Design of all optical logic gates in photonic crystal waveguides

Preeti Rani, Yogita Kalra, R.K. Sinha*

TIFAC-Centre of Relevance and Excellence in Fiber Optics and Optical Communication, Department of Applied Physics, Delhi Technological University (Formerly Delhi College of Engineering), Bawana Road, Delhi 110042, India

ARTICLE INFO

Article history:
Received 24 February 2014
Accepted 3 March 2015

Keywords:
Photonic crystals
Logic gates
FDTD method
Optical interference effect

ABSTRACT

In this paper, we report the design of all optical logic gates based on two-dimensional photonic crystal (PhC) composed of triangular lattice of air holes in silicon (Si). The proposed structure has been simulated using finite difference time domain (FDTD) method and it has been shown that all optical logic operations can be achieved if an appropriate initial phase is introduced between the input beams so that they may interfere constructively or destructively. The optical logic gates designed in the proposed structure have a response period of 1.024 ps and can operate at a bit rate of 0.976 Tbit/s.

1. Introduction

Logic gates and devices play a basic, critical and important part in modern electronics and integrated circuits. Recently, all optical logic gates have received considerable attention for their applications in optical communication networks, due to their importance in addressing, switching, encryption, data encoding, signal regeneration, header recognition and contention resolution. In recent years different schemes have been demonstrated for the designing of all optical logic gates based on linear optical effects such as, interferometry [1], semiconductor optical amplifier (SOA) [2] and Mach-Zehnder interferometer (MZI) [3] and nonlinear processes which include electro-optical effect [4,5], thermal-optical effect [6], two-photon absorption [7] and third-order nonlinear effect [8,9]. Logic gates are capable of performing many logic functions and have numerous applications in optical communication, such as, AND logic gate is used to perform address recognition, packet-header modification, and data-integrity verification and also serves as a sampling gate in optical sampling oscilloscopes. XOR gate can perform functions like comparison of data patterns for address recognition, packet switching, data encryption/decryption, parity checking and optical generation of pseudorandom patterns. NOT gate can be used as inverter or switch and XNOR logic gate is used to realize the threshold detector functionality. In this paper, we have proposed the design of all optical logic gates based on two-dimensional photonic crystals composed of triangular lattice of air holes in Si. Till now many logic gate designs have been proposed which consist of Si rods in air [10–13] but those designs are not practical from the point of view of sustainability and fabrication. Photonic crystal composed of air holes in silicon is a more practical structure and has been used in the design of optical logic gates [14,15] and nano photonic devices [16,17]. The proposed optical logic gates are based on the phenomenon of optical interference effect and are designed in two dimensional photonic crystal waveguides composed of air holes in silicon. The simulation results show that the proposed all optical photonic crystal waveguide structure could really function as all optical logic gates. By appropriately choosing the size of the air hole at the center of the four PhC waveguides the optimal performance in terms of response time, bit rate and contrast ratio for the proposed optical logic gates has been obtained.

2. Design and operating principle of all optical logic gates

In this paper, the design for all optical logic gates has been proposed based on the platform of 2D PhC. The proposed two dimensional photonic crystal structure, as shown in Fig. 1 consists of $15a \times 15a$ two dimensional triangular lattice composed of air holes in silicon having refractive index $n = 3.5$. The radius (r) of air holes is $0.3a$, where, 'a' is the lattice constant equal to 0.352 μm. According to the band diagram of the bulk PhC as shown in Fig. 2, light with wavelength range of (1.291–1.715 μm) for TE modes cannot pass through the uniform PhC structure. In the proposed design four waveguides have been created, from which two of them are considered as input ports indicated as port A and port B. As shown in Fig. 1, one port has been indicated as reference port R which is used to create phase difference between input signals resulting into constructive or destructive interference. Output signals are obtained

* Corresponding author. Tel.: +91 9953051499.
E-mail address: dr_rk_sinha@yahoo.com (R.K. Sinha).

http://dx.doi.org/10.1016/j.ijleo.2015.03.003
0030-4026/

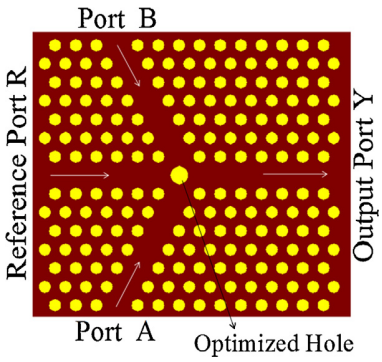

Fig. 1. Schematic representation of all-optical logic gates.

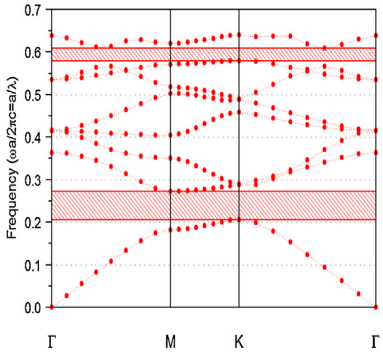

Fig. 2. Band gap structure of the photonic crystal layout.

from the right port indicated as output port Y. Further, in the proposed structure a hole has been introduced at the center of the four waveguides. For the design of all optical logic gates the radius of the central hole is optimized in such a way that for a single input (along with reference signal) as well as both the inputs (along with the reference signal) maximum power is obtained at the output port Y. For the proposed structure, transmittance (T) which is defined as $T = I_{out}/I_{in}$ has also been calculated, where 'I_{out}' is the intensity of light received at the output port Y and 'I_{in}' is the intensity of light launched at the input port. The spectral response of proposed logic gates for TE like polarization of incident light from single input port (with reference signal) as well as for both the input ports (with the reference signal) has been shown in Figs. 3 and 4. Fig. 3 shows the transmittance with respect to the wavelength when the incident light is launched at one of the two input ports with the reference signal having same phase with the input signal. Similarly, Fig. 4 represents the transmittance with respect to the wavelength of

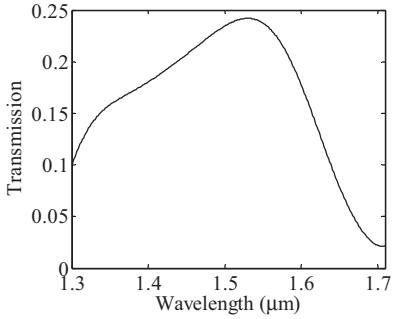

Fig. 3. Variation of transmittance with wavelength from the output waveguide for the single input signal along with the reference signal for TE like polarization of incident light.

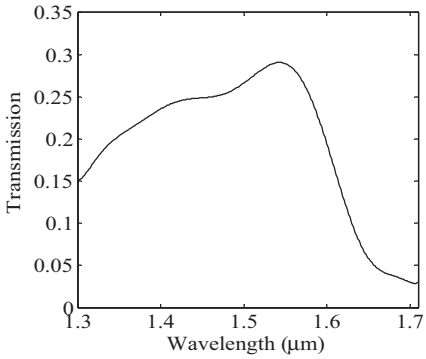

Fig. 4. Variation of transmittance with wavelength from the output waveguide for both the input signals along with the reference signal for TE like polarization of incident light.

incident light launched at both the input ports with the reference signal having same phase as that of the input signals. The contrast ratio defined as $10\log(P_1/P_0)$ (dB) has also been calculated for all optical logic gates, where P_1 represents the power for logic-1 and P_0 represents the power for logic-0. Fig. 5 shows the defect modes that exist within the band gap range. From Figs. 3–5 it has predicted that the optimized structure can be best worked out at the normalized operating wavelength of 1.55 μm which lies in optical communication range. The response time for the proposed structure has also been calculated and plotted [18,19].

3. Optimization of the radius of the hole at the center of the four waveguides

The radius of central hole has been optimized when one of the input signals as well as both the input signals, along with the reference signal are unity and has zero phase difference. From the optimization curve for the radius of the central hole as shown in Fig. 6, it has been observed that as the radius of the central hole increases, the output power increases to a maximum value and then decreases for both the input signals as well as for the single input signal along with the reference signal. Hence the optimized radius of the air hole at the center of four waveguides has been taken as $r_c = 0.44a$.

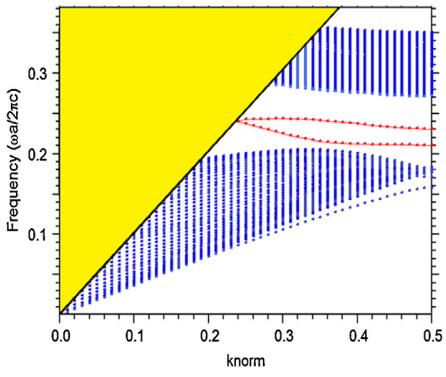

Fig. 5. Dispersion relation for all the four involved PhC waveguides. The black solid line corresponds to the light line and the red dotted lines inside the band gap region correspond to the respective guided modes for TE polarization in all the waveguides. (For interpretation of the references to color in this figure legend, the reader is referred to the web version of this article.)

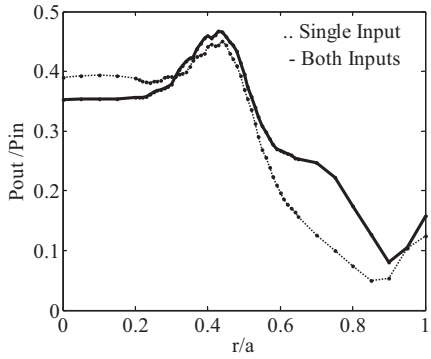

Fig. 6. Normalized power transmittance versus the normalized radius of the central hole in the four PhC waveguides.

4. Simulation and results

After the optimization of the proposed structure to work as all optical logic gates, results have been realized using FDTD method and perfectly matched layer (PML) has been applied to meet the requirements of the courant condition. The input ports A, B and reference port (R) for single input launch as well as for both input launches have been excited by continuous wave (CW) signal with power P_o. Reference signal has been used to optimize the logic output of all the logic gate combinations. For the realization of all the logic gates the radius of central hole has been taken as $r_c = 0.44a$ and the radius of all the other holes as $r = 0.3a$.

4.1. For AND gate

With initial value of $r_c = 0.44a$ and $r = 0.3a$, firstly the function of optical logic AND gate has been demonstrated. In the proposed structure AND gate encompasses of two input signals, a reference signal and an output signal. The AND logic gate operates as follows: (i) when input port A is launched with light having phase angle $\Phi = 0^\circ$ and reference port with light having phase angle $\Phi = 180^\circ$ then logic 0 is obtained at the output port Y. (ii) Similarly, when input port B is launched with light having phase angle $\Phi = 0^\circ$ and reference port with light having phase angle $\Phi = 180^\circ$ then also logic 0 is obtained at the output port Y. (iii) When both the input ports A and B are excited with light signal having phase angle $\Phi = 0^\circ$ and reference port with light also having phase angle $\Phi = 0^\circ$ then logic 1 is obtained at the output port Y. The results are summarized in Table 1 and field distributions for all possible combinations have been shown in Fig. 7. It has been predicted that the gate can operate at a wavelength of 1.55 μm and the calculated value of contrast ratio is found out to be 8.76 dB.

4.2. For OR gate

After the optimization of all the required parameters OR gate has been demonstrated. For OR gate the output is '0' if and only if both the input values are 0 otherwise output values are 1. The operation of OR gate is as follows: (i) when input port A is launched with light having phase angle $\Phi = 0^\circ$ and reference port with light also having phase angle $\Phi = 0^\circ$ then logic 1 is obtained at the output port Y. (ii) Similarly, when input port B is launched with light having phase angle $\Phi = 0^\circ$ and reference port with light having phase angle $\Phi = 0^\circ$ then also logic 1 is obtained at the output port Y. (iii) When both the input ports A and B are excited with light signal having phase angle $\Phi = 0^\circ$ and reference port with light also having phase angle $\Phi = 0^\circ$ then logic 1 is obtained at the output port Y. For the OR gate realization, the presence of same phase angle between the input signal and reference signal results into the constructive interference which helps to satisfy the logic output of the OR gate. The field distribution at steady state as shown in Fig. 8 and Table 2 clearly shows that proposed structure can function as an OR logic gate.

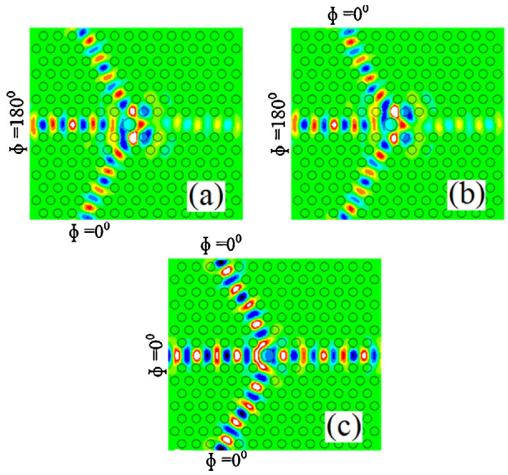

Fig. 7. Field distributions at steady state of the "AND" logic gate for (a) A = 1, B = 0, R = 1; (b) A = 0, B = 1, R = 1 and (c) A = 1, B = 1, R = 1.

4.3. For XOR gate

The output in XOR logic gate is logically "1" if only one of the two inputs is high (1) and logically "0" if both the inputs are high (1) or low (0). The working of XOR logic gate has been explained as follows: (i) when no signal has been launched at the input ports A and B along with the zero signal at the reference port R, output obtained at the port Y is logically "0". (ii) When any of the input ports A and B has been launched with a signal having phase angle $\Phi = 0^\circ$ along with the reference signal having same phase angle $\Phi = 0^\circ$ output obtained at the output port Y is logically "1". (iii) When both the input ports have been excited with the light signal having phase angle $\Phi = 0^\circ$ and reference port with the light having phase angle $\Phi = 180^\circ$ output obtained at the output port is logically "0". The simulation and logic output values shown in Fig. 9 and Table 3 show that the proposed structure could really work as XOR logic gate. The calculated value of contrast ratio for XOR logic gate has been found out to be 8.49 dB.

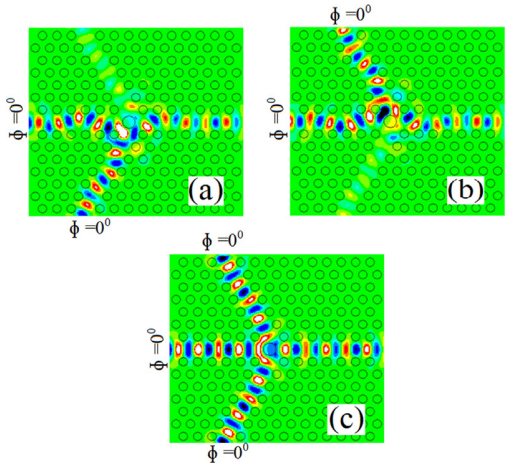

Fig. 8. Field distributions at steady state of the "OR" logic gate for (a) A = 1, B = 0, R = 1; (b) A = 0, B = 1, R = 1 and (c) A = 1, B = 1, R = 1.

Table 1
Truth table for AND logic gate where output Y is in terms of input power P_o.

AND gate				
Input A ($\Phi = 0^\circ$)	Input B ($\Phi = 0^\circ$)	Reference signal (R)	Logic output	Output Y
0	0	0	0	0
0	1	1 ($\Phi = 180^\circ$)	0	$0.17194P_o$
1	0	1 ($\Phi = 180^\circ$)	0	$0.17194P_o$
1	1	1 ($\Phi = 0^\circ$)	1	$0.46638P_o$

Table 2
Truth table for OR logic gate where output Y is in terms of input power P_o.

OR gate				
Input A ($\Phi = 0^\circ$)	Input B ($\Phi = 0^\circ$)	Reference signal (R)	Logic output	Output Y
0	0	0	0	0
0	1	1 ($\Phi = 0^\circ$)	1	$0.44975P_o$
1	0	1 ($\Phi = 0^\circ$)	1	$0.44975P_o$
1	1	1 ($\Phi = 0^\circ$)	1	$0.46638P_o$

Table 3
Truth table for XOR logic gate where output Y is in terms of input power P_o.

XOR gate				
Input A ($\Phi = 0^\circ$)	Input B ($\Phi = 0^\circ$)	Reference signal (R)	Logic output	Output Y
0	0	0	0	0
0	1	1 ($\Phi = 0^\circ$)	1	$0.44971P_o$
1	0	1 ($\Phi = 0^\circ$)	1	$0.44971P_o$
1	1	1 ($\Phi = 180^\circ$)	0	$0.09051P_o$

4.4. For NOT gate

The NOT gate design is like an inverter in which output is inverse of the input. In the proposed structure one input has been taken at the input port A and a reference signal. When input signal is launched at the input port A with phase angle $\Phi = 0^\circ$ and a reference signal with phase angle $\Phi = 180^\circ$ the output obtained at the output port Y is logically '0' and logically '1' when no input signal is launched at the input port but only reference signal is launched with phase angle $\Phi = 180^\circ$. The contrast ratio for NOT gate is 5.42 dB. The Table 4 and field distribution shown in Fig. 10 clearly indicates that the proposed structure can be used as a NOT gate.

4.5. For NAND gate

NAND gate is the inverse of the AND gate where logic output values are inverse of the AND logic output values. In NAND logic gate output is logically '1' if light is launched at any one of the two inputs or zero input launch from both the inputs and it is logically '0' when both the input values are launched along with the reference signal. The working of NAND gate has been explained as follows: (i) when reference signal is launched at the reference port R with phase angle $\Phi = 0^\circ$ and none of the signal is launched at the input ports, or signal with phase $\Phi = 0^\circ$ is launched at either of the input ports A and B, then logic '1' is obtained at the output port Y. (ii) When light with phase $\Phi = 0^\circ$ is launched at both the input ports A and B and reference port R is launched with the signal having phase angle $\Phi = 180^\circ$ then logic '0' is obtained at the output port Y. The results have been summarized in Table 5 where output values are expressed in terms of input power P_o. The contrast ratio for NAND gate is found out to be 9.59 dB. The simulation results shown in Fig. 11 clearly indicate that the structure could really behave as NAND logic gate.

4.6. For NOR gate

NOR logic gate is logically inverse of the OR logic gate where output is '1' when both the inputs are '0'. The operation of NOR logic gate has been demonstrated as follows: (i) when no signal is launched at the input ports A and B and only reference port has been excited with the input signal having phase angle $\Phi = 180^\circ$,

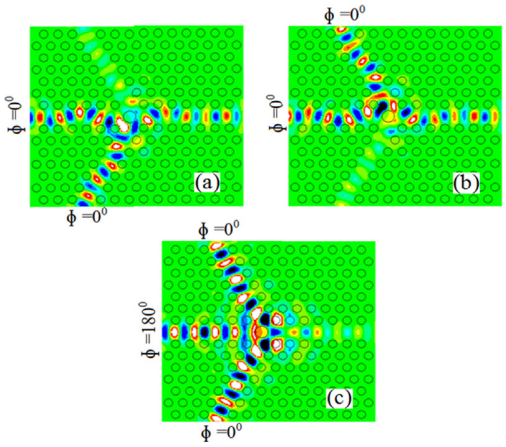

Fig. 9. Field distributions at steady state of the "XOR" logic gate for (a) A = 1, B = 0, R = 1; (b) A = 0, B = 1, R = 1 and (c) A = 1, B = 1, R = 1.

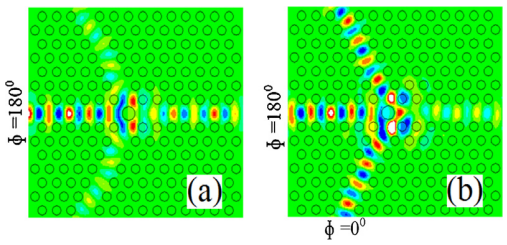

Fig. 10. Field distributions at steady state of the "NOT" logic gate for (a) A = 1, R = 1 and (b) A = 0, R = 1.

Table 4
Truth table for NOT logic gate where output Y is in terms of input power P_o.

NOT gate			
Input A ($\Phi = 0^\circ$)	Reference signal (R)	Logic output	Output Y
0	1 ($\Phi = 180^\circ$)	1	$0.5429P_o$
1	1 ($\Phi = 180^\circ$)	0	$0.1719P_o$

Table 5
Truth table for NAND logic gate where output Y is in terms of input power P_o.

NAND gate				
Input A ($\Phi = 0^\circ$)	Input B ($\Phi = 0^\circ$)	Reference signal (R)	Logic output	Output Y
0	0	1 ($\Phi = 0^\circ$)	1	$0.5429P_o$
0	1	1 ($\Phi = 0^\circ$)	1	$0.4497P_o$
1	0	1 ($\Phi = 0^\circ$)	1	$0.4497P_o$
1	1	1 ($\Phi = 180^\circ$)	0	$0.0905P_o$

Table 6
Truth table for NOR logic gate where output Y is in terms of input power P_o.

NOR gate				
Input A ($\Phi = 0^\circ$)	Input B ($\Phi = 0^\circ$)	Reference signal (R)	Logic output	Output Y
0	0	1 ($\Phi = 180^\circ$)	1	$0.5429P_o$
0	1	1 ($\Phi = 180^\circ$)	0	$0.1719P_o$
1	0	1 ($\Phi = 180^\circ$)	0	$0.1719P_o$
1	1	1 ($\Phi = 180^\circ$)	0	$0.0905P_o$

logic output "1" is obtained at the output port Y. (ii) When either of the two input ports or both the input ports have been excited with light having phase angle $\Phi = 0^\circ$ along with the reference input signal having phase angle $\Phi = 180^\circ$ output obtained at the output port Y is logically "0". The contrast ratio for NOR logic gate is found to be 5.42 dB. The results for the NOR gate have been shown in the Table 6 and Fig. 12. From the Table 6 and field distribution shown in Fig. 12 indicates that the proposed structure could really work as NOR logic gate.

4.7. For XNOR gate

XNOR logic gate is logically inverse of the XOR logic gate, where output is "1" if both the input values are same and "0" if both input values are different. The function of XNOR logic gate is as follows: (i) when both the input ports are either excited with the signal having phase angle $\Phi = 0^\circ$ or not excited with any signal but reference signal has been launched at the reference port R with light having phase angle $\Phi = 0^\circ$, then output obtained at the output port Y is logically "1". (ii) When either of the input ports has been launched with the input signal having phase angle $\Phi = 0^\circ$ along with the reference signal having phase angle $\Phi = 180^\circ$, then output obtained at the output port is logically "0". The contrast ratio for XNOR logic gate is obtained to be 5.42 dB. The field distribution at steady state as shown in Fig. 13 and output values shown in Table 7 clearly indicates that the proposed structure can be used to operate as a XNOR logic gate.

5. Response time

From Fig. 14, which represents the response time for the proposed structure, it has been concluded that the time taken to climb output power from 0 to 90% of the average output power P_{av} in the final steady state is $ct_1 = 35.9\ \mu m$ or $t_1 = 0.419$ ps and it consists of two parts one of which is the time due to transmission delay i.e. $t_{11} = 0.163$ ps and another $t_{12} = 0.256$ ps is the time for the

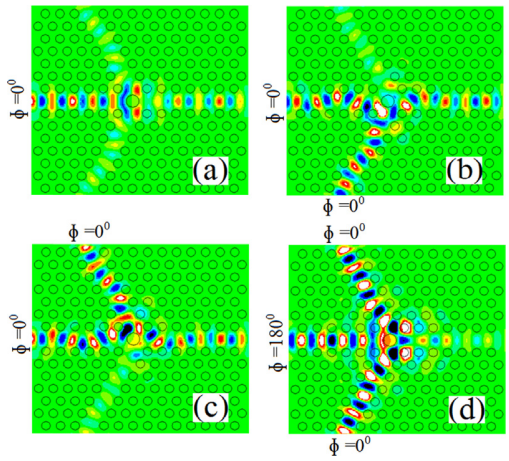

Fig. 11. Field distributions at steady state of the "NAND" logic gate for (a) A = 0, B = 0, R = 1; (b) A = 1, B = 0, R = 1; (c) A = 0, B = 1, R = 1 and (d) A = 1, B = 1, R = 1.

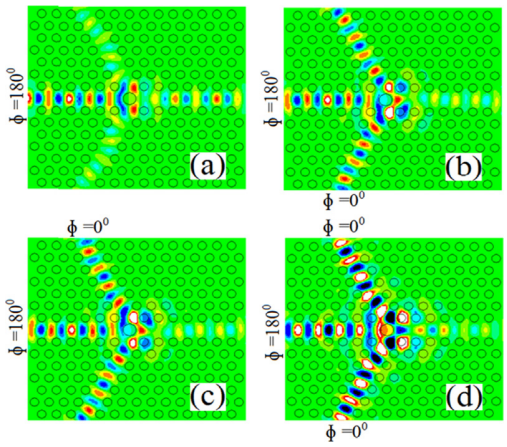

Fig. 12. Field distributions at steady state of the "NOR" logic gate for (a) A = 0, B = 0, R = 1; (b) A = 1, B = 0, R = 1; (c) A = 0, B = 1, R = 1 and (d) A = 1, B = 1, R = 1.

Table 7
Truth table for XNOR logic gate where output Y is in terms of input power P_o.

XNOR gate				
Input A ($\Phi = 0^\circ$)	Input B ($\Phi = 0^\circ$)	Reference signal (R)	Logic output	Output Y
0	0	1 ($\Phi = 0^\circ$)	1	$0.5429P_o$
0	1	1 ($\Phi = 180^\circ$)	0	$0.1719P_o$
1	0	1 ($\Phi = 180^\circ$)	0	$0.1719P_o$
1	1	1 ($\Phi = 0^\circ$)	1	$0.4663P_o$

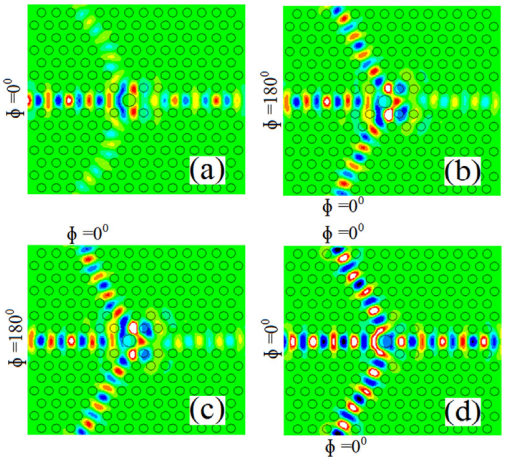

Fig. 13. Field distributions at steady state of the "XNOR" logic gate for (a) A = 0, B = 0, R = 1; (b) A = 1, B = 0, R = 1; (c) A = 0, B = 1, R = 1 and (d) A = 1, B = 1, R = 1.

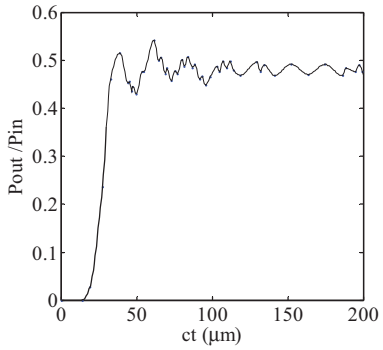

Fig. 14. Time evolution curve of the output power.

output power to climb from 0.1%P_{av} to 90%P_{av}. Since the system operates on linear materials it has been expected that the falling time from average output power P_{av} to 10% P_{av} is approximately equal to t_{12}. Hence, a narrow pulse of width of $2t_{12} = 0.512$ ps can be produced. Hence it has been predicted that the proposed structure has a response period of 1.024 ps and can operate at a bit rate of 0.976 Tbit/s.

6. Conclusion

In this paper, we have proposed the design for all optical logic gates based on optical interference effect in two-dimensional PhC waveguides. The performance of the proposed PhC structure has been analyzed by PWE method and transmission and optimization characteristics have been simulated using FDTD method. The method of determining the operating parameters has been explained and the optimized parameters have been obtained for achieving the contrast ratio for all optical logic gates. The design of the all optical logic gates can operate at very low powers and it is expected that the proposed structure can be effectively used for the design of all optical integrated circuits.

Acknowledgements

The authors gratefully acknowledge the initiatives and support toward the establishment of "TIFAC CENTRE of Relevance and Excellence in Fiber Optics and Optical Communication at Delhi Technological University, formerly Delhi College of Engineering" through "Mission REACH" program of Technology vision-2020, Government of India.

References

[1] P. Sahu, All-optical switch using optically controlled two mode interference coupler, Appl. Opt. 51 (2012) 2601–2605.
[2] J.Y. Kim, J.M. Kang, T.Y. Kim, S.K. Han, 10 Gbit/s all-optical composite logic gates with XOR, NOR, OR and NAND functions using SOA-MZI structures, Electron. Lett. 42 (2006) 303–304.
[3] Y.A. Zaghloul, A.R.M. Zaghloul, Complete all-optical processing polarization-based binary logic gates and optical processors, Opt. Express 14 (2006) 9879–9895.
[4] L. Zhang, Electro-optic directed logic circuit based on micro ring resonators for XOR/XNOR operations, Opt. Express 20 (2012) 11605–11614.
[5] Y. Tian, Proof of concept of directed OR/NOR and AND/NAND logic circuits consisting of two parallel micro ring resonators, Opt. Lett. 36 (2011) 1650–1652.
[6] Q. Xu, R. Soref, Reconfigurable optical directed-logic circuits using micro resonators-based optical switches, Opt. Express 19 (2011) 5244–5259.
[7] T.K. Liang, High speed logic gate using two-photon absorption in silicon waveguides, Opt. Commun. 256 (2006) 171–174.
[8] T. Fujisawa, M. Koshiba, All-optical logic gates based on nonlinear slot-waveguide couplers, J. Opt. Soc. Am. B 23 (2006) 684–691.
[9] P. Andalib, N. Granpayeh, All-optical ultra compact photonic crystal AND gate based on nonlinear ring resonators, J. Opt. Soc. Am. B 26 (2009) 10–16.
[10] Q. Liu, Z. Ouyang, C.J. Wu, C.P. Liu, J.C. Wang, All-optical half adder based on cross structures in two-dimensional photonic crystal, Opt. Express 16 (2008) 18992–19000.
[11] S.K. Tripathy, S. Sahu, C. Mohapatro, S.P. Dash, Implementation of optical logic gates using closed 2D-photonic crystal structure, Opt. Commun. 285 (2012) 3234–3237.
[12] Y. Ishizaka, Y. Kawaguchi, K. Saitoh, M. Koshiba, Design of ultra compact all-optical XOR and AND logic gates with low power consumption, Opt. Commun. 284 (2011) 3528–3533.
[13] Z. Zalevsky, A. Rudnitsky, M. Nathan, Nano photonic and ultra fast all-optical processing modules, Opt. Express 13 (2005) 10272–10284.
[14] P. Rani, Y. Kalra, R.K. Sinha, Realization of AND gate in Y shaped photonic crystal waveguide, Opt. Commun. 298 (2013) 227–231.
[15] C. Husko, T.D. Vo, B. Corcoran, J. Li, T.F. Krauss, B.J. Eggleton, Ultracompact all-optical XOR logic gate in a slow-light silicon photonic crystal waveguide, Opt. Express 19 (2011) 20681–20690.
[16] R.K. Sinha, S. Rawal, Modeling and design of 2D photonic crystal based Y type dual band wavelength demultiplexer, Opt. Quantum Electron. 40 (2008) 603–613.
[17] R.K. Sinha, Y. Kalra, Design of optical waveguide polarizer using photonic band gap, Opt. Express 14 (2006) 10790–10794.
[18] Z. Zang, Numerical analysis of optical bistability based on fiber Bragg grating cavity containing a high nonlinearity doped-fiber, Opt. Commun. 285 (2012) 521–526.
[19] C.J. Wu, C.P. Liu, Z. Ouyang, Compact and low-power optical logic NOT gate based on photonic crystal waveguides without optical amplifiers and nonlinear materials, Appl. Opt. 51 (2012) 680–685.

ISSN (Print) : 2320 – 3765
ISSN (Online): 2278 – 8875

International Journal of Advanced Research in Electrical, Electronics and Instrumentation Engineering

(An ISO 3297: 2007 Certified Organization)

Vol. 4, Issue 4, April 2015

Design of Current-Mode Sinusoidal Oscillators Using Single FTFN

Mukesh Kumr[1], Dharam Vir[2],Dr. Pradeep Dimri[3]

Research Scholar, Department of Electronics Engg, YMCA University of Science & Technology, Faridabad, Haryana, India [1]

HOS, Department of Electronics Engg, YMCA University of Science & Technology, Faridabad, Haryana, India [2]

A.P, Department of Electronics Engg, YMCA University of Science & Technology, Faridabad, Haryana, India [3]

Abstract:This paper presents a current-mode quadrature oscillator. We propose an oscillator that can provide two sinusoidal output currents with 90deg phase difference. It also provides high output impedance that enables the circuit to directly drive load without additional current buffer. The condition of oscillation and frequency of oscillation can be controlled independently and electronically by adjusting the bias currents of the CCTAs. The circuit uses three current controlled transconductance amplifiers (CCTAs) and two grounded capacitors. The proposed circuit uses only grounded capacitors without additional external resistors, the proposed circuit is considerably appropriate to further developing into an integrated circuit. The results of PSPICE simulation program are corresponding to the theoretical analysis. The proposed circuits use single four-terminal floating nullor and, at most, eight passive elements. Two of the oscillator circuits are grounded capacitors and enjoy the independent grounded-element control of the frequency of oscillation and the condition of oscillation. Experimental results are included.

Keywords: Current-Mode Circuits, Sinusoidal Oscillators, CCTA, PSPICE

I. INTRODUCTION

An electronic oscillator produces a repetitive, oscillating electronic signal, often a sine wave or a square wave. Oscillators convert direct current (DC) from a power supply to an alternating current signal. They are widely used in many electronic devices. Common examples of signals generated by oscillators include signals broadcast by radio and television transmitters, clock signals that regulate computers and quartz clocks, and the sounds produced by electronic beepers and video games. Oscillators are often characterized by the frequency of their output signal [1]:

- An audio oscillator produces frequencies in the audio range, about 16 Hz to 20 kHz.
- An RF oscillator produces signals in the radio frequency (RF) range of about 100 kHz to 100 GHz.
- A low-frequency oscillator (LFO) is an electronic oscillator that generates a frequency below ≈20 Hz.

This term is typically used in the field of audio synthesizers, to distinguish it from an audio frequency oscillator. Oscillators designed to produce a high-power AC output from a DC supply are usually called inverters [2].

A. Four Terminal Floating nullor (FTFN) sinusoidal oscillator

The sinusoidal oscillator is an important device, which finds its wide applications in communication, control systems, signal processing, instrumentation and measurement systems. In the literature several active elements like operational amplifier (op-amp), second generation current conveyor (CCII), operational transconductance amplifier (OTA), current feedback operational amplifier (CFOA), four terminal floating nullor (FTFN) etc have been used for realization of oscillators. Among these the FTFN is receiving considerable attention now-a-days. In addition, the use of OTA provides some additional advantage of electronic tunability, high frequency performance and minimize the requirement of external resistors. In 1996, Hou et al. realized a single element control oscillators using a single FTFN in which they introduced six oscillator circuits with four (or three) resistors and capacitors. In 1997, Liu presented a single resistance sinusoidal oscillator (SRCO) using two FTFNs, two resistors and three grounded capacitors but one FTFN is positive and another is negative, which is not good for IC implementation. In 1999, Bhasker proposed a single resistance controlled sinusoidal oscillator using a single FTFN, one buffer, three resistors and two grounded capacitors. In 2001, Cicekoglu presented a general scheme of SRCO's using a single FTFN, five resistors and two grounded capacitors that give eight oscillator circuits. The drawback of this realisation is that it uses a large number of passive elements. In 2002,

ISSN (Print) : 2320 – 3765
ISSN (Online): 2278 – 8875

International Journal of Advanced Research in Electrical, Electronics and Instrumentation Engineering

(An ISO 3297: 2007 Certified Organization)

Vol. 4, Issue 4, April 2015

Bhasker3 proposed a grounded-capacitor SRCO using only one positive FTFN (pFTFN), which uses two grounded capacitors and four resistors. Its drawback is that it cannot use equal valued capacitors. In 2004, Shah et al.8 proposed electronically tunable CM oscillator using FTFN and OTAs which uses one FTFN, two OTA and two capacitors. The drawback of this circuit is that it uses one floating capacitor, which is not good for IC implementation. Again in 2005, Bhaskeret al.9 proposed a new FTFN-based grounded-capacitor SRCO with explicit current mode output and reduced number of resistors using two FTFNs, four resistors and two grounded capacitors. In this paper, a single resistance controlled oscillator (SRCO) is presented which uses one FTFN, one OTA, two resistors and two grounded capacitors. In most of the circuits single types of elements have been used. However the use of two different elements sometimes results in a better circuit realization. In this paper we have used one positive FTFN (pFTFN) and one OTA and all passive components are grounded which is main advantage of our circuit. The frequency of oscillation is controlled using a single grounded resistance that can be replaced by an FET or OTA configured as resistor. The condition of oscillation is adjusted electronically by varying the transconductance of OTA.

II. CIRCUIT DESCRIPTION

The positive FTFN can be characterized by the port relations with vx =vy, ix =iy = 0 and iw =iz.

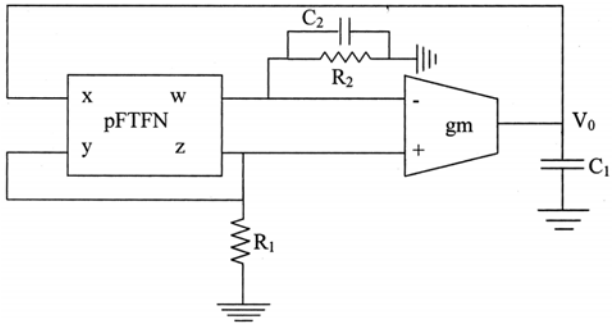

Fig. 1 The circuit for the Oscillator

The circuit above is the circuit for producing the oscillations required in the circuit.

III. DESIGN ISSUE WITH OSCILLATOR

Due to their relatively good phase noise, ease of implementation, differential operation, cross-coupled inductance capacitance (LC) oscillators play an important role in high-frequency circuit design . In thispaper, the time-variant phase-noise model of will be applied toanalyse these oscillators. A simple expression for the tank amplitude is first obtained. The effect of different noise sources in such oscillators is then investigated, and methods for exploiting the cyclo stationary properties of noise are shown. New design implications arising from this approach and experimental results are given. A differential LC oscillator using spiral inductors is demonstrated that dissipates 6 mW of power while running at 1.8 GHz, with a phase noise of 121 dB/Hz at 600-kHz offset.

A. Tank Amplitude

Tank voltage amplitude has an important effect on the phase noise, as emphasized by the presence of q_{max} in the denominator of the expression for the single-sideband phase noise

ISSN (Print) : 2320 – 3765
ISSN (Online): 2278 – 8875

International Journal of Advanced Research in Electrical, Electronics and Instrumentation Engineering

(An ISO 3297: 2007 Certified Organization)

Vol. 4, Issue 4, April 2015

$$\mathcal{L}\{\Delta\omega\} = 10 \cdot \log_{10}\left(\frac{\overline{i_n^2}/\Delta f}{q_{\max}^2} \cdot \frac{\Gamma_{\rm rms}^2}{2\Delta\omega^2}\right)$$

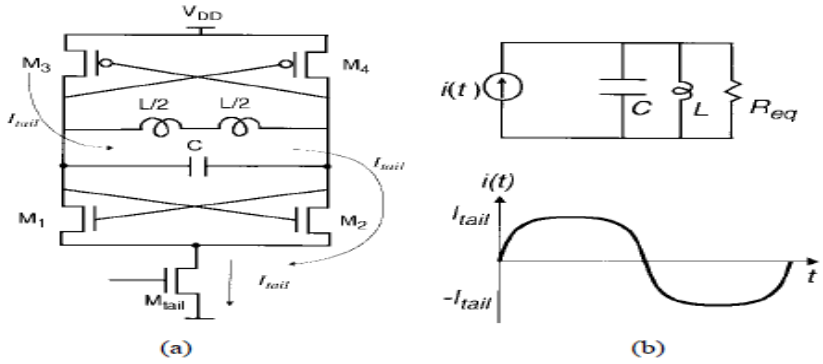

Fig 2 (a) Current flows when the stage is switched to one side. (b) Differential equivalent circuit

It is the power spectral density of the current where it is the rms value of the impulse noise, sensitivity function associated with that noise source, qmax is the maximum signal charge swing, and delta w is the offset frequency from the carrier.

A simple expression for the tank amplitude can be obtained assuming that the current in the differential stage switches quickly from one side to another. Fig. 2(a) shows the current flowing in the complementary cross-coupled differential LC oscillator [3] when it is completely switched to one side. As the tank voltage changes, the direction of the current flow through the tank reverses. The differential pair thus can be modeled as a current source switching between I_{tail} and $-I_{tail}$ in parallel with a resistance±inductance±capacitance(RLC) tank, as shown in Fig. it is the equivalent parallel resistance of the tank.

B. Rectangular Current Waveform

At high frequencies, the current waveform may be approximated more closely by a sinusoid due to finite switching time and limited gain. In such cases, the tank amplitude can be better approximated as

$$V_{\rm tank} \approx I_{\rm tail} R_{\rm eq}.$$

This mode of operation is referred to as the current-limited regime of operation since, in this regime; the tank amplitude is solely determined by the tail-current source and the tank equivalent resistance. Fig. 3.2 shows the simulated node voltages as well as the drain currents of the NMOS transistors, M1 and M2, in this regime of operation. The value of L and C are such that the circuit oscillates at 1 GHz.

ISSN (Print) : 2320 – 3765
ISSN (Online): 2278 – 8875

International Journal of Advanced Research in Electrical, Electronics and Instrumentation Engineering

(An ISO 3297: 2007 Certified Organization)

Vol. 4, Issue 4, April 2015

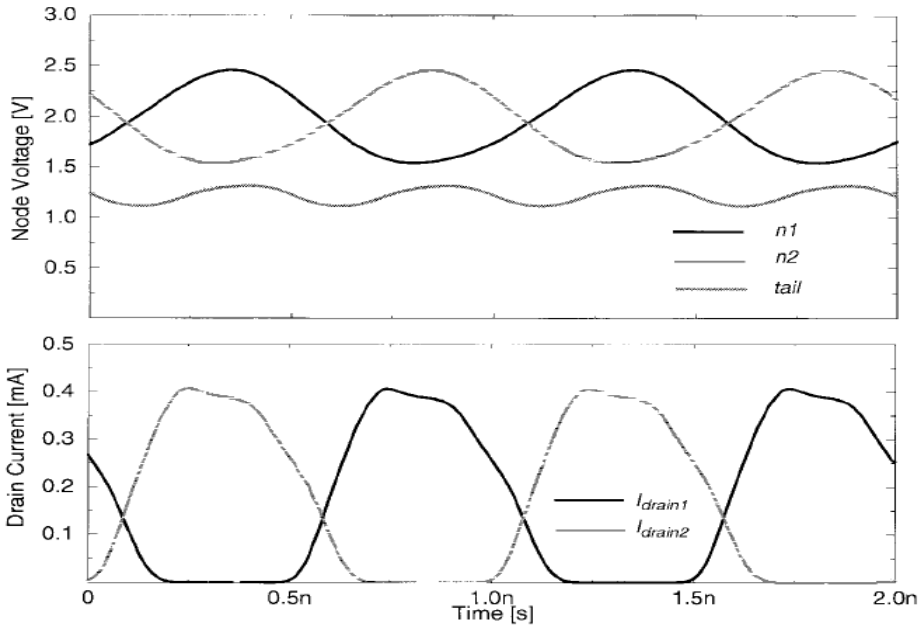

Fig. 3 Simulated voltages and currents in the current-limited regime

Note that 3.2 loses its validity as the amplitude approaches the supply voltage because both NMOS and PMOS pairs will enter the triode region at the peaks of the voltage. Also the tail NMOS transistor may spend most (or even all) of its time in the linear region. This behavior can be seen in the simulated voltages and currents shown in Fig. 3.3 The tank voltage will be clipped at Vdd by the PMOS transistors and at ground by the NMOS transistors. Therefore, for the oscillator of Fig. 3(a), the tank voltage amplitude does not significantly exceed Vdd Note that since the tail transistor is in the triode region, the tail current does not stay constant. Thus, the drain-source voltage of the differential NMOS transistors can drop significantly, resulting in a large drop in their drain current, as shown in Fig. 3 This region of operation is known as the voltage-limited regime. Fig. 3 shows the simulated tank voltage amplitude as a function of tail current for three different values of VddAs can be seen, the tank amplitude is proportional to the tail current in the current-limited region, while it is limited by Vdd in the voltage-limited regime.

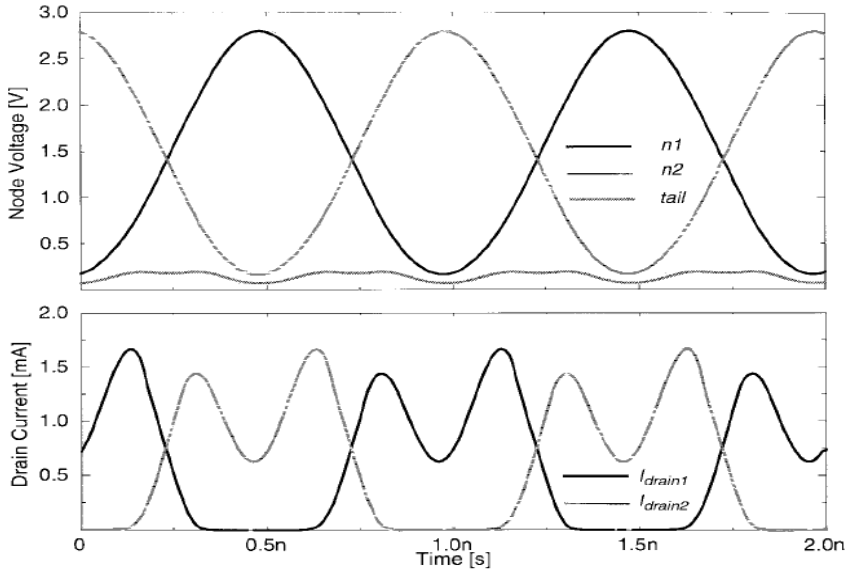

Fig. 4 Simulated voltages and currents in the voltage-limited regime

ISSN (Print) : 2320 – 3765
ISSN (Online): 2278 – 8875

International Journal of Advanced Research in Electrical, Electronics and Instrumentation Engineering

(An ISO 3297: 2007 Certified Organization)

Vol. 4, Issue 4, April 2015

III.DESIGN OF CURRENT MODE SINUSOIDAL OSCILLATOR

This paper presents a current-mode quadrature oscillator using differential different current conveyor (DDCC) and voltage differencing transconductance amplifier (VDTA) as active elements. The proposed circuit is realized from a non-inverting lossless integrator and an inverting second order low-pass filter. The oscillation condition and oscillation frequency can be electronically/orthogonally controlled via input bias currents. The circuit description is very simple, consisting of merely 1 DDCC, 1VDTA, 1 grounded resistor and 3 grounded capacitors. Using only grounded element, the proposed circuit is then suitable for IC architecture. The proposed oscillator has high output impedance which is easy to cascade or dive the external load without the buffer devices. The PSPICE simulation results are depicted, and the given results agree well with the theoretical anticipation. The power consumption is approximately 1.76mW at ±1.25V supply voltages.

A.Design using DDDC

A third order currentmode oscillator, based on DDCC and VDTA. The features of the proposed circuits are that: the oscillation condition can be adjusted independently from the oscillation frequency by electronic method. The circuit construction consists of 1 DDCC, 1 VDTA, 1 grounded resistor and 2 grounded capacitors. The PSPICE simulation results are shown;the electrical behaviours of the ideal DDCC are represented by the following hybrid matrixes which are in correspondence with the theoretical analysis.

$$\begin{bmatrix} V_X \\ I_{Y1} \\ I_{Y2} \\ I_{Y3} \\ I_Z \end{bmatrix} = \begin{bmatrix} 0 & 1 & -1 & 1 & 0 \\ 0 & 0 & 0 & 0 & 0 \\ 0 & 0 & 0 & 0 & 0 \\ 0 & 0 & 0 & 0 & 0 \\ 1 & 0 & 0 & 0 & 0 \end{bmatrix} \begin{bmatrix} I_X \\ V_{Y1} \\ V_{Y2} \\ V_{Y3} \\ V_Z \end{bmatrix}.$$

Fig. 4 Matrix representations of the parameters

The symbol and the equivalent circuit of the DDCC are illustrated in Fig. 5(a) and (b), respectively.

B. Design using VDTA

The circuit symbol of VDTA is shown in Fig. 5, where VP and VN are the input terminals, Z and X is the output ones. Hence, Z is the current output terminal; current through Z terminal follows the difference of the voltages at VP and VN terminals by transconductance gm1. The voltage vZ on Z terminal is transferred into current using transconductance gm2,which flows into output terminal X. The gm1 and gm2 are tuned by IB1 and IB2, respectively. In general, CDTA can contain an arbitrary number of x terminals, providing currents IX of both directions. All terminals of VDTA exhibit high impedance values. The characteristics of the ideal VDTA are represented by the following hybrid matrix:

ISSN (Print) : 2320 – 3765
ISSN (Online): 2278 – 8875

International Journal of Advanced Research in Electrical, Electronics and Instrumentation Engineering

(An ISO 3297: 2007 Certified Organization)

Vol. 4, Issue 4, April 2015

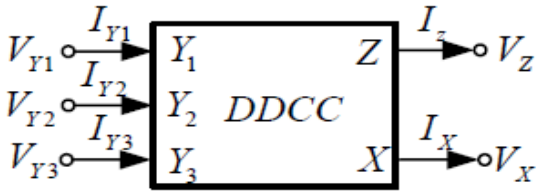

(a)

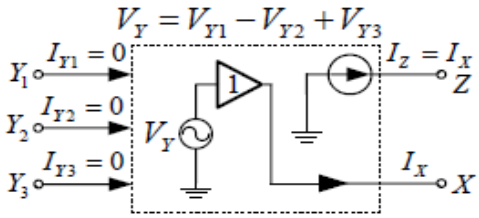

(b)

Fig. 5 DDCC (a) Symbol (b) Equivalent circuit

$$\begin{bmatrix} I_Z \\ I_{X+} \\ I_{X-} \end{bmatrix} = \begin{bmatrix} g_{m1} & -g_{m1} & 0 \\ 0 & 0 & g_{m2} \\ 0 & 0 & -g_{m2} \end{bmatrix} \begin{bmatrix} V_P \\ V_N \\ V_Z \end{bmatrix}.$$

If the VDTA is realized using CMOS technology, gm1 and gm2 can be respectively written as

$$g_{m1} = \sqrt{kI_{B1}},$$

and

$$g_{m2} = \sqrt{kI_{B2}}.$$

Here k is the physical transconductance parameter of the CMOS transistor. IB1 and IB2 are the bias current used to control the gm1 and gm2, respectively.

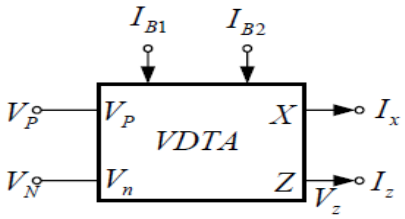

Fig. 6The circuit symbol of VDTA

ISSN (Print) : 2320 – 3765
ISSN (Online): 2278 – 8875

International Journal of Advanced Research in Electrical, Electronics and Instrumentation Engineering

(An ISO 3297: 2007 Certified Organization)

Vol. 4, Issue 4, April 2015

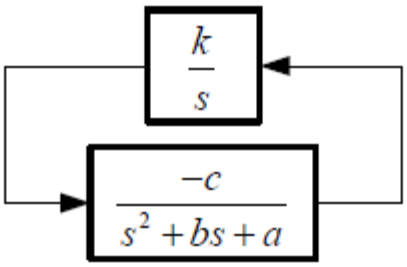

Fig. 7 Block diagram for design of proposed oscillator

C.General structure of 3rd Oscillator

The oscillator is designed by cascading an inverting second order low-pass filter and the lossless integrators as systematically shown in Fig. 6. From block diagram in Fig. 7, we will receive the characteristic equation as

$$s^3 + bs^2 + as + ck = 0$$

The condition of oscillation (OC) and frequency of oscillation (FO) can be written as

$$OC : ab = ck$$

And

$$\omega_{osc} = \sqrt{a}$$

From above Equation, if a = c, the oscillation condition and oscillation frequency can be adjusted independently, which are the oscillation condition can be controlled by b and k, while the oscillation frequency can be tuned by a.

D.Structure of proposed Oscillator

The completed 3rd current-mode quadrature oscillator is shown in Fig. 7. The condition of oscillation and frequency of oscillation can be written as

$$\frac{1}{C_1 R} = \frac{g_{m2}}{C_3},$$

And

$$\omega_{osc} = \sqrt{\frac{g_{m1}}{C_1 C_2 R}}.$$

ISSN (Print) : 2320 – 3765
ISSN (Online): 2278 – 8875

International Journal of Advanced Research in Electrical, Electronics and Instrumentation Engineering

(An ISO 3297: 2007 Certified Organization)

Vol. 4, Issue 4, April 2015

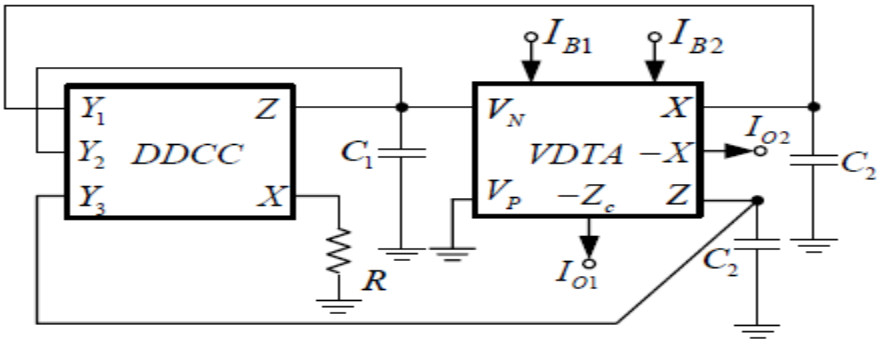

Fig. 8 Proposed Current-Mode Oscillator

If m1 B1 g = kI, m2 B2 g = kIand 1 2 3 C = C = C = C, the condition of oscillation and frequency of oscillation can be rewritten as

$$\frac{1}{R} = \sqrt{kI_{B2}} ,$$

And

$$\omega_{osc} = \frac{1}{C}\sqrt{\frac{(kI_{B1})^{\frac{1}{2}}}{R}} .$$

It is obviously found that, the condition of oscillation and frequency of oscillation can be adjusted independently, which are the oscillation of oscillation can be controlled by settingIB2, while the frequency of oscillation can be tuned by setting IB1. From the circuit in Fig. 8, the current transfer function from Io1 to Io2 is

$$\frac{I_{o2}(s)}{I_{o1}(s)} = \frac{g_{m1}}{sC_2} .$$

For sinusoidal steady state, becomes

$$\frac{I_{o2}(j\omega)}{I_{o1}(j\omega)} = \frac{g_{m1}}{\omega C_2} e^{-j90^\circ} .$$

The phase difference φ between Io1 and Io2 is φ = -90° ensuring that the currents Io2 and Io1 are in quadrature.

E .Output of proposed Oscillator

The working of the proposed oscillator has been verified in PSpice simulation. Internal constructions of DDCC and VDTA used in simulation are respectively shown in Figs. 5 and 6. The PMOS and NMOS transistors have been simulated by respectively using the parameters of a 0.25µm TSMC CMOS technology. The transistor aspect ratios of PMOSand NMOS transistor are indicated in Table I. The circuit was biased with ±1.25V supply voltages, VBB=-0.55V, C1=C2=C3=50pF, IB1=IB2=60µA and R=3.5kΩ. This yields simulated oscillation frequency of 1MHz. Fig. 7 shows simulated quadrature output waveforms. Fig. 8 shows the simulated output spectrum, where the total harmonic distortion (THD) is about 2.95%. The quadrature relationship between the generated waveforms has been verified using Lissagous figure and shown in Fig. 8. The power consumption is approximately 1.76mW.

ISSN (Print) : 2320 – 3765
ISSN (Online): 2278 – 8875

International Journal of Advanced Research in Electrical, Electronics and Instrumentation Engineering

(An ISO 3297: 2007 Certified Organization)

Vol. 4, Issue 4, April 2015

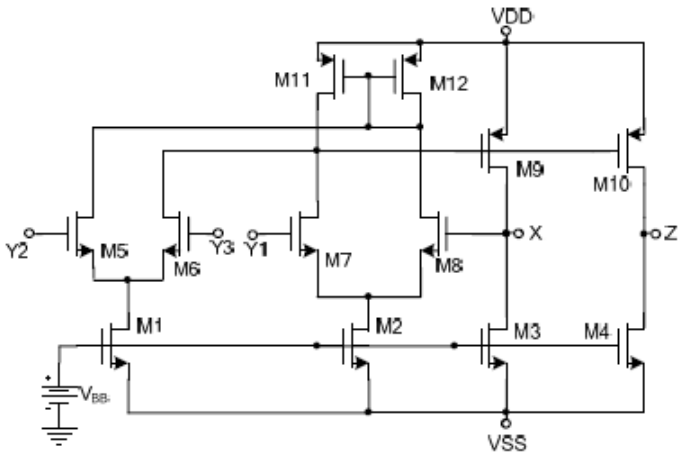

Fig. 9 Internal construction of the CMOS DDCC

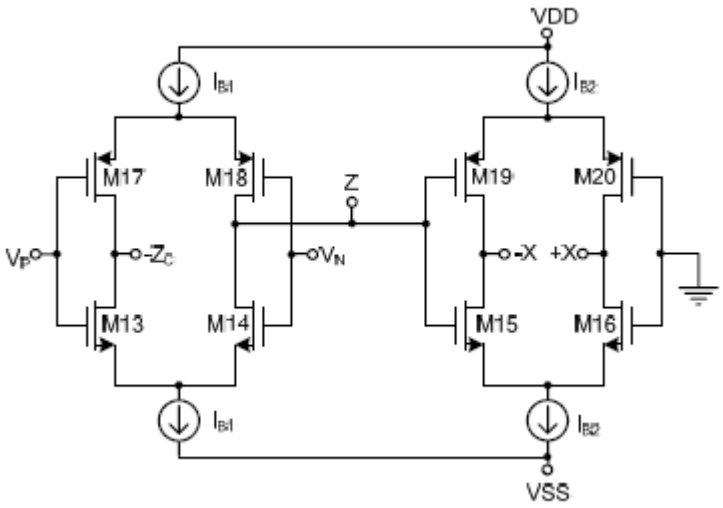

Fig. 10 Internal construction of the CMOS VDTA

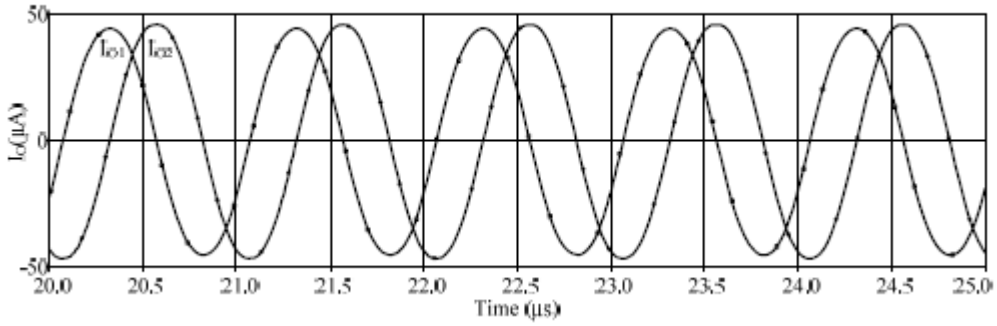

Fig. 11 The simulation result of quadrature outputs

ISSN (Print) : 2320 – 3765
ISSN (Online): 2278 – 8875

International Journal of Advanced Research in Electrical, Electronics and Instrumentation Engineering

(An ISO 3297: 2007 Certified Organization)

Vol. 4, Issue 4, April 2015

F. Practical Design of Proposed Circuit

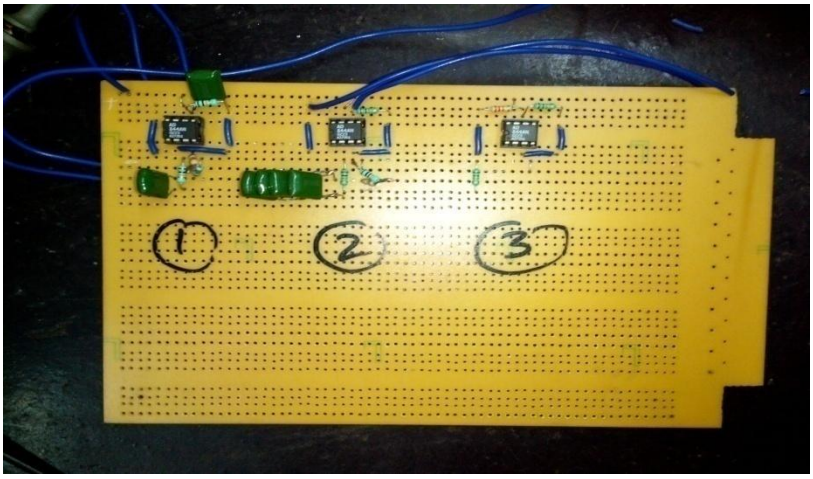

Fig. 12 Practical Design of Proposed Circuit

III. **RESULTS**

The confirm the theoretical analysis, the proposed SCRO circuit was simulated using one PFTFN and one OTA. The PFTFNwas constructed with two ad844 ic's OF Analogue devices inc. and for OTA commercially available IC 3080 was used. The supply voltages were taken as +_15V dc. The passive component were selected as C1=0.01uf, C2 as 0.011uf, R2 as 20 Kohm and gm as 0.5 S. The value of C2 should be equal to 0.01uf, however in spice simulation it has been taken slightly higher i.e. equal to 0.011uf to make the s-term negative in equation so as to get sustained oscillations. It is an established practice in literature using the spice simulation method to verify the results.
The result which is obtained with the help of simulation contains different sections, of all the sections only the parameters obtained in the final report are shown.

Table 5.1 Results for the output obtained

Oscillator circuit	Circuit Parameters				
	C	R = R1=R2=R3 (kΩ)	R4 (start) Exp. (kΩ)	Theor. (kHz)	Exp. (kHz)
Fig.1	0.1µF	10	51.5	0.1949	0.1449
	0.1µF	1	6	1.949	1.549
	1nF	10	57	19.492	17.32
	4.7nF	1	6	41.473	39.259
	1nF	1	6.2	194.924	
Fig.3 (b)	0.1µF	10	23.3	.0398	0.43132
	4.7nF	10	27.5	0.8466	0.8762
	4.7nF	1	2.6	8.466	9.222
	1nF	1	2.6	39.789	
	130pF	1	4.3	306.067	

ISSN (Print) : 2320 – 3765
ISSN (Online): 2278 – 8875

International Journal of Advanced Research in Electrical, Electronics and Instrumentation Engineering

(An ISO 3297: 2007 Certified Organization)

Vol. 4, Issue 4, April 2015

OUTPUT OF RESULTS

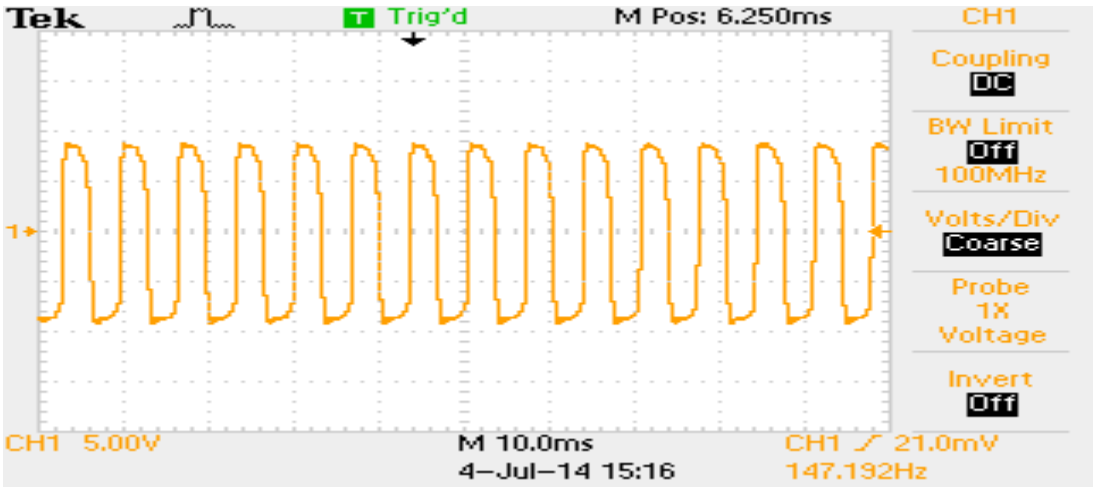

IV. CONCLUSION

In this work an electronically tunable current-mode quadrature sinusoidal oscillator enabling independent current control of oscillation frequency and oscillation condition is realized employing three CDTAs and two grounded capacitors. The proposed circuit is canonical and capable of simultaneously providing two explicit quadrature current outputs. The non-ideal and sensitivity analyses of the circuit have been carried out, and the circuit exhibits a low sensitivity performance.

Verified Outputs

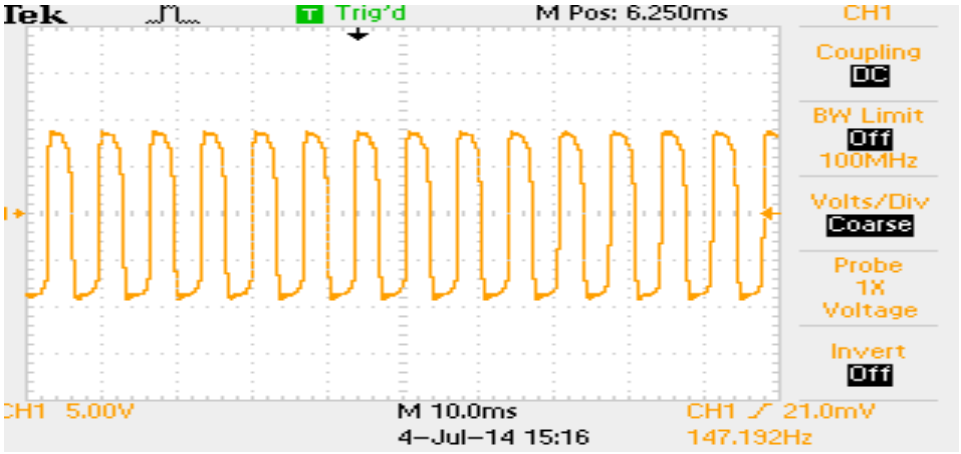

ISSN (Print) : 2320 – 3765
ISSN (Online): 2278 – 8875

International Journal of Advanced Research in Electrical, Electronics and Instrumentation Engineering

(An ISO 3297: 2007 Certified Organization)

Vol. 4, Issue 4, April 2015

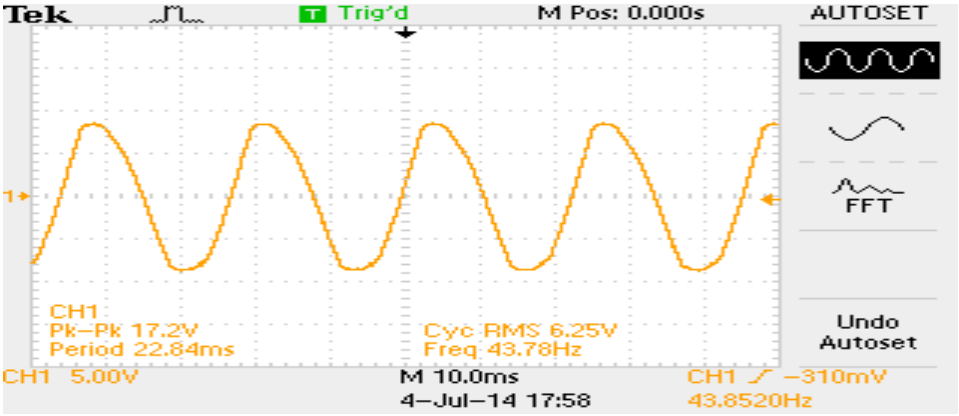

REFERENCES

[1] E. H. Nordholt, "Extending op amp capabilities by using a currentsourcepower supply," *IEEE Trans. Circuits Syst.*, vol. CAS-29, pp.411–414, June 1982.
[2] R. Prokop, V. Musil, "New modern circuit block CCTA and some its applications," The Fourteenth International Scientific and Applied Science Conference - *Electronics ET*'2005, Book 5. Sofia: TU Sofia, pp. 93-98, 2005.
[3] J. H. Huijsing and J. De Korte, "Monolithic nullor—A universal activenetwork element," *IEEE J. Solid-State Circuits*, vol. 12, pp. 59–64, Feb.1977.
[4] M. Higashimura, "Realization of current-mode transfer function usingfour-terminal floating nullor," *Electron. Lett.*,vol. 27, pp. 170–171, Jan.1991.
[5] J. H. Huijsing, "Operational floating amplifier," *Proc. Inst. Elect. Eng.*,vol. 137, pt. G, pp. 131–136, Apr. 1990.
[6] R. Senani, "A novel application of four-terminal floating nullors," *Proc.IEEE*, vol. 75, pp. 1544–1546, Nov. 1987.
[7] A. Uygur and H. Kuntman "CDTA-Based quadrature oscillator design," in Proc. 14th European Signal processing conference *(EUSIPCO 2006)*, September 4-8, 2006.
[8] M. Higashimura, "Current-mode allpass filter using FTFN withgrounded capacitor," *Electron. Lett.*, vol. 27, pp. 1182–1183, June 1991.
[9] S.-I. Liu, "Cascadable current-mode filters using single FTFN," *Electron.Lett.*, vol. 31, pp. 1965–1966, Nov. 1995.
[10] S.-I. Liu and J.-L. Lee, "Insensitive current/voltage-mode filters usingFTFN's," *Electron. Lett.*, vol. 32, pp. 1079–1080, June 1996.
[11] N. A. Shah, S. Z. Iqbal, and M. Quadri, "Current-mode Band-pass Filter Using A Single CDTA," *J. of Active and Passive Electronic Devices*, vol. 4, pp. 1–5, 2009.
[12] M. T. Abuelma'atti, "Cacadable current-mode filters using singleFTFN," *Electron. Lett.*, vol. 32, pp. 1457–1458, Aug. 1996.
[13] Jaikla, W., Siripruchyanun, M. "CCCDTAs-based versatile quadrature oscillator and universal biquad filter". In Proc.of 2007 *ECTI conference*, Thailand, p. 1065-1068, 2007.
[14] U. Cam, A. Toker, O. Cicekoglu, and H. Kuntman, "Current-mode high output-impedance sinusoidal oscillator configuration employing single FTFN," *Analog Integrated Circuits and Signal Proc*., pp. 231-238, vol. 24, 2000.
[15] M. T. Abuelma'atti and H. A. Al-Zaher, "Current-mode sinusoidal oscillators Using Single FTFN," *IEEE Trans.* Circuits and Systems-II: Analog and Digital Signal Proc., vol. 46, pp. 69- 74, 1999.
[16] S. S. Gupta and R. Senani, "Realisation of current-mode SRCOs using all grounded passive elements," *Frequenz*, vol. 57, pp. 26-37, 2003.
[17] M.T. Abuelma'atti, "Grounded capacitor current-mode oscillator using single current follower," *IEEE Trans*. Circuits and Systems-I: Fundamental Theory and Applications, vol. 39, pp. 1018-1020, 1992.
[18] P. Prommee, K. Dejhan, "An integrable electronic-controlled quadrature sinusoidal oscillator using CMOS operational transconductance amplifier," *International Journal of Electronics*, vol. 89, pp. 365-379, 2002.

BIOGRAPHY

Mukesh Kumar received the M.Tech Degree form YMCAUST Faridabad (Haryana) and B.TECH Degree in Electronics and Communication Engg. From Delhi College of Engineering Delhi, 2014, 2009 respectively. In 2001 he started his carrier as Instructor in the field of electronics. Since 2006 he is part of YMCA University of Science & Technology, Faridabad.

ISSN (Print) : 2320 – 3765
ISSN (Online): 2278 – 8875

International Journal of Advanced Research in Electrical, Electronics and Instrumentation Engineering

(An ISO 3297: 2007 Certified Organization)

Vol. 4, Issue 4, April 2015

DharamVir received the M.Tech Degree form MDU Rothak (Haryana) and B.E Degree in Electronics and Communication Engg. From JamiaMilliaIslamia (Central University), New Delhi 2008, 2004 respectively. In 1989 he started his carrier as R&D Engineer in the field of computers and networking. Since 1992 he is part of YMCA University of Science & Technology and presently working as Head of Section (Electronics & Inst. Control) in the Department of Electronics Engineering.

Dr.Pardeep Kumar received the M.Tech Degree from MDU Rothak (Haryana) and B.E Degree in Electronics and Communication Engg. From JamiaMilliaIslamia (Central University), New Delhi 2003, 2010 respectively. In 1991 he started his carrier as Technical Assistant in the field of electronics. Since 1994 he is part of YMCA University of Science & Technology, Faridabad.

IOSR Journal of Environmental Science, Toxicology and Food Technology (IOSR-JESTFT)
e-ISSN: 2319-2402,p- ISSN: 2319-2399.Volume 8, Issue 12 Ver. III (Dec. 2014), PP 64-71
www.iosrjournals.org

Determining the Water Quality Index of an Urban Water Body Dal Lake, Kashmir, India

[1]Raj Shailesh Kanakiya, [2]S.K.Singh, [3]J.N.Sharma
1-Research Scholar, Environmental Engineering Department Delhi Technological University, Delhi, India
2-Professor & Head, Environmental Engineering Department, Delhi, India
3-J.N.Sharma,Supretendent Engineer, J&K pollution Control Board, J&K India

Abstract: *A Water Quality Index (WQI) is a useful statistical tool for simplifying, reporting and interpreting complex information obtained for any water body. A simple number given by any WQI model explains the level of water contamination .A water quality index carried out for Dal lakebased on very important parameters can provide a simple indicator of water quality.The present study deals with the monitoring of variation of seasonal water quality index of Dal lake. The index is used to improve the comprehension of general water quality issues, communicates water quality status and illustrates the need for and the effectiveness of protective practices. It is found that in all cases the change in WQI value follow a similar trend throughout the study period. Water Quality Index of Dal lake for all four basinswere (102.66,120.33,109.35,101.35) for all seasons summer, winter,monsoon thus it is found to be unfit for drinking.*

Keywords: *Dal lake, Water quality index ,Water quality parameters*

I. Introduction

Dal Lake is perceived as vast expanse of water in a pristine landscape where one goes forrecreation. It is a place of experiencing nature by way of boating, camping, fishing, swimming, bird watching, etc. however, when one mentions 'urban lakes' the picture is soon demystified. While urban lakes are different from the common perception of lakes in general they too have value and functions, both ecosystem functions and social values.

The word "Lake" is used loosely to describe many types of water bodies – natural, manmade and ephemeral including wetlands.

The biodiversity of lake and pond ecosystems is currently threatened by a number of human disturbances, of which the most important include increased nutrient load, contamination,acidification, and invasion of exotic species (Bronmark & Hansson, 2002). The ecological stress of the system is reflected by deterioration of water quality and increased levels of biological productivity.

Hydrologic change is the most visible impact of urbanization. Hydrology concerns the quality, duration, rates, frequency and other properties of water flow. Urbanization typically increases runoff peak flows and total flow volumes and damages water quality and aesthetics. Pollutants reach wetlands mainly through runoff. Urbanized watersheds generate large amounts of contaminants, including eroded soil from construction sites, toxic metals and petroleum from roadways, industrial and commercial areas, and nutrients and bacteria from residential areas. By volume, sediment is the most important non-point pollutant. At the same time that urbanization produces large quantities of pollutants, it reduces water infiltration capacity, yielding more surface runoff. Pollutants from urban land uses are, therefore, more vulnerable to transport by surface runoff than pollutants from other land uses.

The organic and inorganic pollutant load in the Dal has accelerated the macrophytic growth which in turn has reduced the water quality and biological oxygen demand (BOD) of the lake and hence has reduced the recreational and aesthetic appeal of the lake

The chemistry of lake water and sediment is a cumulative reflection of catchment geology, weathering and erosional processes as well as anthropogenic inputs. The chemical degradation of silicate and carbonate minerals is various processes, such as dissolution, hydrolysis, oxidation, and reduction (Gupta and Subramanian, 1998).

The basic chemical reactions take place among silicates, carbonates, and rainwater,congruently or incongruently, gives rise to various ions and clay minerals (Freeze and Cherry, 1979).Being an urban type lake, municipal and domestic effluents have altered the surface water composition of Dal Lake, leading to increased eutrophication (Hutchinson, 1999). Moreover, excessive sedimentation rates enhanced by extensive soil erosion due to deforestation and an encroachment by surrounding population have dramatically reduced the lake volume (Chakrapani, 2002). The lake serves as a resource of drinking water, irrigation, fisheries, recreation, tourism, etc.

A Water Quality Index (WQI) is a useful statistical tool for simplifying, reporting and interpreting complex information obtained from any body of water. A simple number given by any WQI model explains the level of water contamination .A water quality index based on some very important parameters can provide a simple indicator of water quality. In general, water quality indices incorporate data from multiple water quality parameters into a mathematical equation that rates the health of a waterbody with number.

Study Area

Dal Lake (Lat. 340 – 6' N, 740-45' E, alt.1583m) situated in the heart of Srinagar city, the summer capital of Jammu Kashmir State is under tremendous anthropogenic pressure. The myriad is ways in which people use the lake along with the numerous pollutant generating activities have stressed the lake ecosystem in diverse ways.

The lake is divided into four basins

Hazratbal, Boddal, Nageen and Gagribal The lake is mainly fed by a large perennial inflow channel, Telbal nala, which drains the largest subcatchment area of about 145 km^2 and contributes to about 80% of the total inflow to the lake (Zutshi and Vass 1978; Trisal 1987, Jellani 2006) as well as a number of small streams,viz,Peshpaw nala, Shalimar nala, Merakhsha nala, Harshikul,etc, around the shore line besides some contribution from groundwater. Within the lake basin itself there are number of springs (Kundangar et al., 1995) which act as permanent water source to the lake. The Nageen basin is the deepest basin (maximum depth of about 6 m), and Gagribal basin the shallowest (maximum depth 2.5m). Of the total area of the lake, 4.1 km^2 is under floating garden or cultivation, 1.51 km^2 is submerged land and 2.25 km^2 under marshy conditions.

II. Materials And Methods

The Survey of the lake and its catchment area is done to know the sampling locations/ sites in the six sub-basins of the lake. The Sampling Sites is shown in the map indicated below. Samples have been collected from these Sites and the Physico –Chemical Analysis is being done in the Boards Laboratory for 12 parameters which are pH, conductivity, Hardness, DO, BOD, TDS, Total Alkalinity, Nitrite , Sulphate ,Chlorides, Calcium, Magnesium.

Various physico-chemical parameters analyzed for water and sediment samples included those for pH (Digital pH meter DPH 504), Electrical conductivity (EC) (Digital EC meter DEM900). Total dissolved solid (TDS) was determined by oven dry method. Biological Oxygen Demand (BOD) was estimated by Azide modification of Winkler method. Total Alkalinity (TA) as HCO^{3-}, Calcium (Ca^{2+}), Magnesium (Mg^{2+}) total hardness (TH), Chloride (Cl), was estimated by standard titrimetry. Sulphate (SO_4^{2-}) by turbidometry, Nitrate (NO_3^{2-}) by Brucine method all using HITACHI UV-VIS spectrophotometer.

Table.1 Description of the Sites

Sr.No	Site	Description
1	Bod-dal	Central Char Chinar
2	Nageen Lake	Central part of Nageen Lake
3	Hazratbal Lake	Near outlet of Hazratbal STP
4	Gagribal Lake	Near Nehru Park

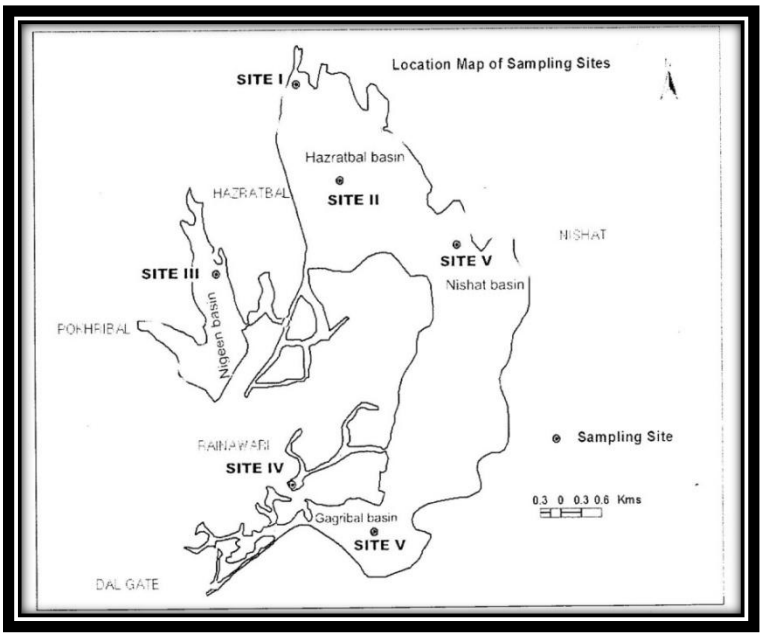

In this study, for the calculation of water quality index, twelve important parameters were chosen. The WQI used here are taken from as recommended by the standards of drinking water quality Bureau of Indian Standards (BIS) .

The weighted arithmetic index method (Brown et. al.,) has been used for the calculation of WQI of the waterbody. Further, quality rating or sub index (qn) was calculated using thefollowing expression.

Qn= 100*[Vn -Vio] / [Sn-Vio]

(Let there be **n**water quality parameters and quality rating or subindex (**qn**) corresponding to **nth** parameter is a number reflecting the relative value of this parameter in the polluted water with respect to its standard permissible value.)

qn=Quality rating for the **nth** Water quality parameter

Vn=Estimated value of the **nth** parameter at a given sampling station.

Sn=Standard permissible value of the **nth** parameter.

Vio= Ideal value of **nth** parameter in pure water. (i.e., 0 for all other parameters except the parameter pH and Dissolved oxygen (7.0 and 14.6 mg/L respectively)

Unit weight was calculated by a value inversely proportional to the recommended standard value **Sn**of the corresponding parameter.

Wn=K/ Sn

Wn= unit weight for the **nth** parameters.

Sn= Standard value for **nth** parameters

K= Constant for proportionality.

The overall Water Quality Index was calculated by aggregating the quality rating with the unit weight linearly.

WQI=Σ qnWn/ ΣWn

Table 2. Water Quality Index (WQI) and status of water quality (Chatterji and Raziuddin2002)

Sr.No	Water Quality Index	Water Quality Status
1	0-25	Excellent water quality
2	26-50	Good water quality
3	51-75	Poor water quality
4	76-100	Very Poor water quality
5	>100	Unsuitable for drinking

Table 3. Drinking Water standards recommending Agencies and unit weights. (All values except pH and Electrical Conductivity are in mg/L)

Sr.No	Parameters	Standard permissible value	Unit Weight
1	pH	8.5	0.2190
2	Electrical Conductivity	300	0.371
3	Total Dissolved Solids	500	0.0037
4	Total alkalinity	120	0.0155

5	Total hardness	300	0.0062
6	Calcium	75	0.025
7	Magnesium	30	0.061
8	Chlorides	250	0.0074
9	Nitrate	45	0.0412
10	Sulphate	150	0.01236
11	Dissolved oxygen	5	0.3723
12	Biological oxygen demand	5	0.3723

Table.No.4. Physico-chemical Characteristics of Sampling sites in all seasons

Sr.No	Parameter	Central Char Chinar			Nageen Central			Hazratbal STP			Nehru Park		
		Feb	Jun	Jul	Feb	Jun	Jul	Feb	Jun	Jul	Feb	Jun	Jul
1	pH	8.20	8.40	8.40	8.10	8.20	8.70	7.50	7.90	8.20	7.40	8.00	8.20
2	Conductivity	220.0	220.0	209.0	350.0	301.0	220.0	285.0	265.0	282.0	143.0	128.0	138.0
3	TDS	143	116	152	192	192	149	184	198	201	83	85	91
4	T.Alkalinity	160.0	212.0	225.0	190.0	309.0	235.0	225.0	218.0	256.0	68.0	76.0	70.0
5	T.Hardness	392	112	142	228	126	120	366	156	184	268	82	104
6	Calcium	36.00	37.00	36.00	38.00	40.00	39.00	38.00	43.00	42.00	45.69	22.40	21.64
7	Magnesium	4.50	3.60	3.80	4.00	5.00	5.00	4.00	6.00	7.00	7.42	6.30	12.15
8	Chlorides	12.0	15.0	16.0	20.0	18.0	18.0	17.0	21.0	24.0	21.0	16.0	12.0
9	Nitrates	450	395	390	480	450	539	435	490	590	420	456	580
10	Sulphates	11.0	7.0	12.0	9.0	19.0	16.0	16.0	14.0	18.0	4.35	11.7	19.20
11	DO	6.8	6.5	6.8	5.4	5.5	5.0	6.0	5.8	5.5	4.3	6	4.3
12	BOD	3.0	2.0	2.0	2.5	2.8	2.0	2.2	1.0	1.0	2.0	2	1.0

Table.No.5 Calculation for Quality Rating

Sr.No	Parameter	Central Char Chinar			Nageen Central			Hazratbal STP			Nehru Park		
		Feb	Jun	Jul	Feb	Jun	Jul	Feb	Jun	Jul	Feb	Jun	Jul
1	pH	80.0	93.3	93.3	73.3	80.0	113.3	33.3	60.0	80.0	26.7	66.7	80.0
2	Conductivity	73.3	73.3	69.7	116.7	100.3	73.3	95.0	88.3	94.0	47.7	42.7	46.0
3	TDS	28.6	23.2	30.4	38.4	38.4	29.8	36.8	39.6	40.2	16.6	17.0	18.2
4	T.Alkalinity	133.3	176.7	187.5	158.3	257.5	195.8	187.5	181.7	213.3	56.7	63.3	58.3
5	T.Hardness	130.7	37.3	47.3	76.0	42.0	40.0	122.0	52.0	61.3	89.3	27.3	34.7
6	Calcium	48.0	49.3	48.0	50.7	53.3	52.0	50.7	57.3	56.0	60.9	29.9	28.9
7	Magnesium	15.0	12.0	12.7	13.3	16.7	16.7	13.3	20.0	23.3	24.7	21.0	40.5
8	Chlorides	4.8	6.0	6.4	8.0	7.2	7.2	6.8	8.4	9.6	8.4	6.4	4.8
9	Nitrates	1000.0	877.8	866.7	1066.7	1000.0	1197.8	966.7	1088.9	1311.1	933.3	1013.3	1288.9
10	Sulphates	7.3	4.7	8.0	6.0	12.7	10.7	10.7	9.3	12.0	2.9	7.8	12.8
11	DO	156.0	162.0	156.0	184.0	182.0	192.0	172.0	176.0	182.0	206.0	172.0	206.0
12	BOD	60.0	40.0	40.0	50.0	56.0	40.0	44.0	20.0	20.0	40.0	40.0	20.0
∑	Qn	1737.1	1555.6	1566.0	1841.4	1846.1	1968.6	1738.8	1801.6	2102.9	1513.2	1507.4	1839.0

Table.No.6 Formation of Water Quality Index

Sr.No	Parameter	Central Char Chinar			Nageen Central			Hazratbal STP			Nehru Park		
		Feb	Jun	Jul	Feb	Jun	Jul	Feb	Jun	Jul	Feb	Jun	Jul
1	pH	17.52	20.44	20.44	16.06	17.52	24.82	7.30	13.14	17.52	5.84	14.60	17.52
2	Conductivity	27.21	27.21	25.85	43.28	37.22	27.21	35.25	32.77	34.87	17.68	15.83	17.07
3	TDS	0.11	0.09	0.11	0.14	0.14	0.11	0.14	0.15	0.15	0.06	0.06	0.07
4	T.Alkalinity	2.07	2.74	2.91	2.45	3.99	3.04	2.91	2.82	3.31	0.88	0.98	0.90
5	T.Hardness	0.81	0.23	0.29	0.47	0.26	0.25	0.76	0.32	0.38	0.55	0.17	0.21
6	Calcium	1.20	1.23	1.20	1.27	1.33	1.30	1.27	1.43	1.40	1.52	0.75	0.72
7	Magnesium	0.92	0.73	0.77	0.81	1.02	1.02	0.81	1.22	1.42	1.51	1.28	2.47
8	Chlorides	0.04	0.04	0.05	0.06	0.05	0.05	0.05	0.06	0.07	0.06	0.05	0.04
9	Nitrates	41.20	36.16	35.71	43.95	41.20	49.35	39.83	44.86	54.02	38.45	41.75	53.10
10	Sulphates	0.91	0.58	0.99	0.74	1.57	1.32	1.32	1.15	1.48	0.36	0.96	1.58
11	DO	58.08	60.31	58.08	68.50	67.76	71.48	64.04	65.52	67.76	76.69	64.04	76.69
12	BOD	22.34	14.89	14.89	18.62	20.85	14.89	16.38	7.45	7.45	14.89	14.89	7.45
∑	WnQn	172.38	164.66	161.28	196.36	192.91	194.83	170.04	170.90	189.83	158.51	155.36	177.82
∑	Wn	1.62	1.62	1.62	1.62	1.62	1.62	1.62	1.62	1.62	1.62	1.62	1.62
	(WnQn)/Wn	106.54	101.77	99.68	121.36	119.23	120.41	105.09	105.62	117.32	97.97	96.02	109.90

Graphical Representation of Seasonal Variation of Water Quality in Dal Lake

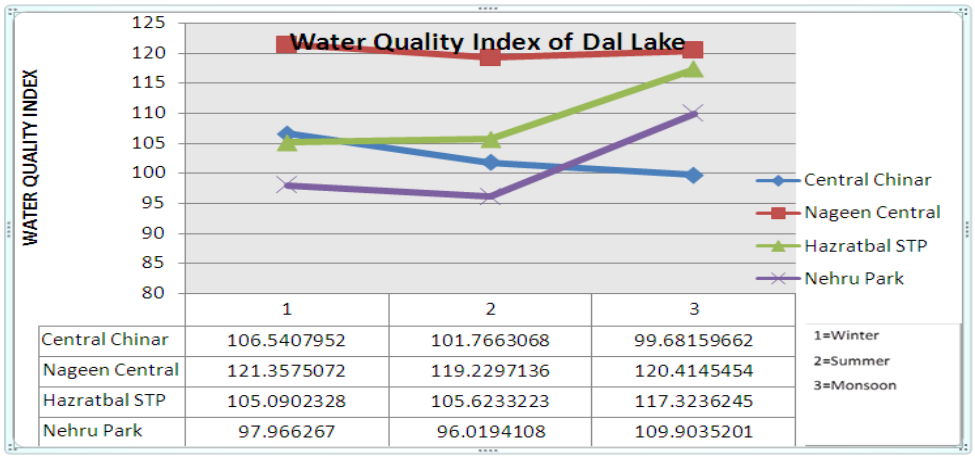

	1	2	3
Central Chinar	106.5407952	101.7663068	99.68159662
Nageen Central	121.3575072	119.2297136	120.4145454
Hazratbal STP	105.0902328	105.6233223	117.3236245
Nehru Park	97.966267	96.0194108	109.9035201

Table.No.8 Average Water Quality Index of Sampling Sites

Sr.No	Sampling Site	Average Water Quality Index
1	Central Chinar	102.66
2	Nageen Central	120.33
3	Hazratbal STP	109.35
4	Nehru Park	101.30

III. Results &Discussion

Water quality Index of the Dal lake is calculated for all seasons viz, rainy season, winter season and summer season . The values of various water related physico-chemical parameters for calculation of Water quality index are presented in Table 3. Season wise
Water Quality Index calculations are depicted in the Table 5,6 and 7.
The Water Quality Index is calculated for four sites Char Chinar,NageenCentral,Hazratbal STP,i.e, are 102.66,120.33,109.35,101.3 respectivelyas per Table.No.8 thus it indicates the water unfit for drinking (Chatterji and Raziuddin 2002).

1. PH

Amongst the 12 parameters selected for forming Water Quality Index for Dal lake,
pH is an important parameter which determines the suitability of water for various purposes. In the present study pH ranged between 7.4 &8.7. Overall average values for three seasons are taken into account the waterbody was found to be slightly alkaline in nature.(Ambasht (1971), Petre (1975), Shardendu and Ambasht (1988), have also made similar observations in their studies on different waterbodies.

2. Conductivity

Conductivity is a measure of capacity of substance or solution to conduct electric current. Conductivity determines the total dissolved solids in the water. Here,the range of Electro Conductivity is average for all other lakes except Nageen where it can be inferred that there
the Conductivity is attributed to high salinity and high mineral content.

3. Total Alkalinity

According to BIS the maximum permissible limit is 120 mg/L. The observed average value of total alkalinity was in greater in range of 160-390 mg/l except for Nehru Park in Gagribal basin. Totalalkalinity values in the study indicates that the water was very hard. Higher values of alkalinityregistered during summer might be due to the presence of excess of free CO_2product as a resultof decomposition process coupled with the mixing of sewage and domestic waste. The low alkalinityduring rainy season may be due to dilution. Jain et. al (1996) also reported similar finding in the study of the Halali Reservoir.

4. Chloride

Chloride is one of the most important parameter in assessing the water quality. Munawar (1970) is of the opinion that higher concentrations of chlorides indicate higher degree of organic pollution. In the present study the concentration of chloride fluctuated between 12 mg/l to 24mg/l .

5. Nitrogen

Nitrogen is an important nutrient for plant and algae growth in the lake. Nitrogen may enter a lake from surface runoff or groundwater sources. Sediments clearly cause nitrogen to undergo a number of changes.

Nitrogen (rather than phosphorus) limits algae growth.The concentration of Nitrogen here is quite high in this study it is in range of 435 mg/l to 580 mg/l.

6. D.O and B.O.D

The measurement of the DO is primary parameter in water pollution studies as it indicates aerobic or anaerobic nature of biological activities in water bodies (Trivedi, 1995).

The dissolved oxygen concentration depends on the physical, chemical and biochemical activities in the water body, and its measurement provides a good indication of water quality. The present study suggests that the concentration ofdissolved oxygen fluctuated between 4.3mg/1 and 5 mg/1. Seasonally, the concentration of dissolved oxygen was more during monsoon and least during summer. Thus indicating variation of dissolved oxygen according to temperature and quantity of water supply This observation is in conformity with the observations of Reddy et.al., (1982)., Ghosh and George (1989), Swarnalatha and Narasingarao (1993) and Venkateswarlu (1993).Bio-chemical oxygen demand is a parameter to assess the organic load in a waterbody.

The BOD concentration ranged between 2 mg/l to 3mg/l indicating the fact that the water body is eutrophic. Seasonally, it was high during summer, being in conformity with the observation of Chatterjee (1992).From all these foregoing observations of the physico-chemical parameters, it can be concluded that the water body shows the characters of eutrophication.

Low dissolved oxygen, high bio-chemical oxygen demand and high nitrate concentration this overall conditions indicate that highly eutrophic condition for the Dal lake.

7. Calcium& Magnesium

The observed average value of calcium was in range of 22 to 40 mg/l, which is below standard permissible limit of 75 mg/l prescribed by BIS. The quantities of calcium in natural water depends geology, types of rock present in the catchment.

While the observed average value of magnesium was in range of 4 to 12 mg/l.Magnesium hardness particularly associated with the sulphate ion has laxative effect on persons unaccustomed to it (Khursid, 1998).

8. Sulphate

Sulphate in lake water is primarily related to the types of minerals found in the watershed and to acid rain. Industries and utilities that burn coal release sulphur compounds into the atmosphere that are carried into lakes by rainfall. In water depleted of oxygen (anaerobic water), sulphate can be reduced to hydrogen sulphide (H_2S).The range of Sulphate is 4.35mg/l to 19.2 mg/l.

9. Algal Bloom

In Dal lake the with the advent of time and due to increased and unabated human incursions within and lake peripheries have witnessed frequent algal blooms. Recurrence of such blooms has become a regular phenomenon in the various basins of the lake. A close relationship was observed between chloride and nitrates which almost coincided with those of high euglenoid population. The reason behind algal bloom can be inferred as lack of water flushing,enrichment of nutrient and building up of free carbon dioxide were the possible causes of the euglenoid bloom in Dal lake.

10. Hardness

Hardness in Dal Lake is higher than permissibleHardness concentration of freshwater bodies of Kashmir Valley has been associated with thick population of plankton, especiallyCyanophyceae (Bhat and Pandit, 2003).In this study in range is 300 to 400 mg/l in certain time of year .The values of total hardness are much fluctuating from that of summer months to winter months

IV. Conclusion

At the outset, the study clearly indicates that the lake water is not fit for drinking consumption .It shall undergo treatment for it to be used for drinking purpose . Thus through Water Quality Index (WQI) we can have overall judgement whether that what purpose does the lake water suffice. In this method we use more systematic approach which gives comparative evaluation of the water quality of sampling stations within a water body . Water Quality index is helpful for public to understand the quality of water as well as being a useful tool in many ways in the field of water quality management.

These results are important so that the local authorities may implement preventive measures to reduce the threat of domestic and industrial discharges as well as agricultural activities discharges and have a check over the land use pattern in the Dal catchment.

References

[1]. Ambasht, R.S., 1971. Ecosystem study of a tropical pond in relation to primary production of different vegetation zones. Hydrobiologia12 : 57-61.
[2]. BIS 1983. Standards for Water for Drinking and other purposes, Bureau of Indian Standards, New Delhi.
[3]. Bhat SA, Pandit AK (2003). Phytoplankton Dynamics in Anchar Lake,Kashmir. J. Res. Dev. 3:71-96
[4]. Brönmark C, Hansson L-A (2002) Environmental issues in lakes and ponds: current state and perspectives. Environmental Conservation .
[5]. Brown, R.M., McCleiland, N.J., Deininger, R.A. and O'Connor, M.F. (1972): A Water Quality Index – Crossing the Psychological Barrier (Jenkis, S.H., ed.) Proc. Int. Conf. on Water Poll. Res., Jerusalem, Vol.6, pp.787-797.
[6]. Chakrapani GJ (2002) Water and sediment geochemistry of major Kumaun Himalayan lakes, India. Environ Geol 43, 99–107.
[7]. Chatterjee, A.A., 1992. Water quality of Nandakananlake. India., J. Environ. Hlth. 34(4): 329-333.
[8]. Chaterjee,C. and Raziuddin, M.2002. Determination of water quality index (WQI) of a degraded river in Asanol Industrial area, Raniganj, Burdwan, West Bengal. Nature, Environment and pollutionTechnology,1(2):181-189.
[9]. Gupta LP and Subramanian V (1998) Geochemical factors controlling the chemical nature of water and sediments in the Gomtiriver. India Env. Geol. 36 (1–2), 102–108
[10]. Ghosh, A. and J.P. George, 1989. Studies on the abiotic factors and zooplakton in a polluted urban reservoir HussainSagar, Hyderabad: Impact on water quality and Embryonic Development of Fishes. Indian J.Environ.Hlth. 31(1): 49-59
[11]. Hutchinson G. E., A Treatise on Limnology, Vol. II, Introduction to Lake Biology and the Limnoplankton, John Wiley and Sons, Inc. New York **(1967)**
[12]. Freeze, R.A., and Cherry, J.A., 1979, Groundwater: Englewood Cliffs, NJ, Prentice-Hall, 604 p.
[13]. Jain S. M., Meenakshi Sharma and Ramesh Thakur. Seasonal variation in Physico–chemical parameters of Halali reservoir of Vidisha district, Indian Journal of Ecobiology8:3, 81 – 188 (1996).
[14]. Jeelani, G, Shah AQ (2006) Geochemical characteristics of water and sediment from the Dal Lake, Kashmir Himalaya: constraints on weathering and anthropogenic activity. Environ Geol. 50, 12–23.
[15]. Khursid. S, Zaheeruddin and A. Basheer. Ind. J. Env. Prot. 18(4): 246-249 (1998)
[16]. Munawar, M., 1970. Limnological studies on fresh water ponds of Hyderabad, India-II, J. Hydrobiologia. 35:127-162.
[17]. Kundankar MRD, Sarwar SG, Shah MA (1995). Limnological characteristics of Hazratbal basin of Dal Lake 1992-93. Technical Report-submitted to Government of Jammu and Kashmir, India.
[18]. Reddy, K.R.P.D. Sacco, D.A Graetz, K.L. Campbell and L.R. Sinclair. 1982. Water treatment by aquatic ecosystem: Nutrient removal by reservoirs and flooded fields. J.Environmental Management, 6(3): 261-271.
[19]. Shardendu and R.S. Ambasht, 1988. Limnological studies of a rural pond and an urban tropical aquatic ecosystem: oxygen enforms and ionic strength. J.TropicalEcology. 29 (2): 98-109.
[20]. Swarnalatha, N. and A. Narasingrao, 1993. Ecological investigation of two lentic environments with reference to cyanobacteria and water pollution. Indian J.
[21]. Microbial. Ecol., 3:41-48.

Effect of different carrier gases and their flow rates on the growth of carbon nanotubes

Aarti Tewari and Suresh C. Sharma

Citation: Physics of Plasmas (1994-present) **22**, 043501 (2015); doi: 10.1063/1.4916057
View online: http://dx.doi.org/10.1063/1.4916057
View Table of Contents: http://scitation.aip.org/content/aip/journal/pop/22/4?ver=pdfcov
Published by the AIP Publishing

PHYSICS OF PLASMAS **22**, 043501 (2015)

Effect of different carrier gases and their flow rates on the growth of carbon nanotubes

Aarti Tewari and Suresh C. Sharma
Department of Applied Physics, Delhi Technological University (DTU), Shahbad Daulatpur, Bawana Road, Delhi 110 042, India

(Received 9 January 2015; accepted 9 March 2015; published online 2 April 2015)

The present paper examines the effect of different carrier gases and their flow rates on the growth of carbon nanotubes (CNTs). A theoretical model is developed incorporating the charging rate of the carbon nanotube, kinetics of all the plasma species, and the growth rate of the CNTs because of diffusion and accretion of ions on the catalyst nanoparticle. The three different carrier gases, i.e., argon (Ar), ammonia, and nitrogen, are considered in the present investigation, and flow rates of all the three carrier gases are varied individually (keeping the flow rates of hydrocarbon and hydrogen gas constant) to investigate the variations in the number densities of hydrocarbon and hydrogen ions in the plasma and their consequent effects on the height and radius of CNT. Based on the results obtained, it is concluded that Ar favors the formation of CNTs with larger height and radius whereas ammonia contributes to better height of CNT but decreases the radius of CNT, and nitrogen impedes both the height and radius of CNT. The present work can serve to the better understanding of process parameters during growth of CNTs by a plasma enhanced chemical vapor deposition process. © *2015 AIP Publishing LLC*.
[http://dx.doi.org/10.1063/1.4916057]

I. INTRODUCTION

Plasma-enhanced chemical vapor deposition (PECVD) has recently emerged as promising carbon nanostructure growth technique.[1–5] PECVD has the advantage of producing low-temperature and vertically aligned carbon nanotubes (CNTs).

The main parameters during PECVD are the growth temperature, substrate bias, externally applied power, growth time, type of catalyst, type of substrate, composition of gases in PECVD, types of feed gas or reducing gas or carrier gas and their respective flow rates, and several others.

Different carrier gases like argon (Ar), ammonia (NH_3), nitrogen (N_2), and hydrogen (H_2) are found to have different effects on the growth density of CNT.[6–11]

Kayastha *et al.*[6] have found that the addition of specific carrier gases could critically modify the growth rate and growth density of multiwall carbon nanotubes (MWNTs). In particular, the addition of Ar to acetylene (C_2H_2) increases the growth density of MWNTs, while the addition of hydrogen (H_2) and nitrogen (N_2) gases decreases the growth density.

Mi *et al.*[7] investigated the effects of ammonia (NH_3) and nitrogen (N_2) as carrier gases on the structure and morphology of CNTs. They observed that the diameter of the CNTs synthesized in NH_3 was larger than that in N_2. Moreover, the alignment of the CNTs grown in NH_3 was better than that in N_2.

Jung *et al.*[8] investigated the growth behaviors in various gas environments of N_2, H_2, Ar, NH_3, and their mixtures. It was also observed that in NH_3 environment much enhanced CNT growth occurs than in the mixture of N_2 and H_2 environment.

Yap *et al.*[9] found that carrier gas could change the growth rate, growth density, and structures of MWNTs. They investigated the growth of CNT under different conditions, e.g., (a) pure C_2H_2, (b) C_2H_2 and Ar, (c) C_2H_2 and H_2, and (d) C_2H_2 and N_2. The addition of Ar dilutes C_2H_2 and reduces the number of C_2H_2 molecules reacting on the iron (Fe) catalyst surface. Both H_2 and N_2 reduce the growth density of MWNTs.

Mi and Jia[10] have grown CNTs arrays on macro porous substrate for different time in the ammonia and nitrogen carrier gases by floating catalyst method. They observed that the CNTs' diameter is smaller in N_2 than that grown in NH_3.

Qian *et al.*[11] found that the size and distribution of carbon spheres become smaller as the ratio of Ar to H_2 in the carrier gas decreases. Also, pure argon favors the growth of carbon spheres, while pure hydrogen does not.

Studies have been done to investigate the effects of flow rate of carrier gases on the growth of CNTs. It is seen that increasing the flow rate of carrier gases affects the growth density and growth rate of CNTs.[12–14]

Toussi *et al.*[12] have investigated three flow rates of carrier gas (Ar = 50 ml/min, 100 ml/min, and 150 ml/min) on the growth of carbon nanotubes. It was seen that as the flow rate of Ar carrier gas was increased, the yield of carbon nanotubes increased.

Malgas *et al.*[13] studied the effect of mixture ratios and nitrogen carrier gas flow rates on the morphology of carbon nanotube structure. They found that at the constant temperature of 750 °C and the higher carrier gas flow rates of N_2, the CNTs with smaller diameters were obtained.

Reynolds *et al.*[14] have investigated the effects of hydrogen flow rate on CNT growth and observed that at a constant methane (CH_4) flow rate of 700 sccm and by varying flow rate of H_2 of 100 and 200 sccm, few CNTs were produced.

Denysenko *et al.*[15] have developed a spatially averaged global discharge model to study the densities and fluxes of the radical neutrals and charged species, the effective electron temperature, and methane conversion factor under various growth conditions. They observed that the densities of molecular and atomic hydrogen decrease with flow rate of argon (J_{Ar}), whereas the densities of hydrocarbon neutrals grow with flow rate of argon (J_{Ar}).

The vertically aligned and low-temperature CNTs so produced by PECVD process have found applications in vertical transistors,[16] field emission devices,[17–21] field ionization applications,[22] and others.

The above works that have been cited[6–14] to study the effects of different carrier gases and their flow rates on the growth of CNT do mention the effects of different carrier gases but do not sufficiently underline the exact processes behind the observed effects. Moreover, they have considered various routes of CNT growth like catalytic chemical vapour deposition,[6] pyrolysis of ferrocene and C_2H_2 mixture,[7] chemical vapor deposition (CVD),[8] thermal CVD,[9] floating catalyst method,[10] and non-catalytic CVD.[11] In the present study, we try to present the possible reasons behind the different observed behaviors of different carrier gases and their consequent results on the growth of CNT. We try to explain the behavior of various carrier gases during CNT growth through a PECVD process by the number density profile of hydrocarbon and hydrogen species created in different carrier gas environments and their repercussions on growing CNT.

In Sec. II, we develop a theoretical model, including the charging rate of the CNT, kinetics of plasma species, i.e., of electron, ions, and neutral atoms, and the growth rate of the CNT on account of diffusion and accretion of ions on catalyst nanoparticle in reactive plasma to study the effects of different carrier gases and their flow rates on the growth of CNT. Results and discussion are given in Sec. III. Finally, conclusion is given in Sec. IV.

II. MODEL

Following Denysenko *et al.*,[15] a cylindrical stainless steel reactor chamber of the plasma source which has the inner diameter (2R) = 32 cm and length (L) = 23 cm is considered. Now, Denysenko *et al.*[15] have considered a large number of possible hydrocarbons in their study, but we in the present paper limit ourselves to a limited number of hydrocarbons. Sode *et al.*[23] have considered various possible combinations of ions in H_2-Ar plasma like Ar^+, H^+, H_2^+, H_3^+, and ArH^+, but the present problem considers CH_3^+, CH_4^+, H^+, H_2^+, H_3^+, Ar^+, N_2^+, and NH_3^+.The present study is therefore applicable to the cases where higher hydrocarbons and a varied combinations of ions in plasma are not considered.

The plasma contains ions of methyl (CH_3^+), methane ion (CH_4^+) denoted as ions A and hydrogen ions ($H^+/H_2^+/H_3^+$) denoted as ions B, and carrier gas ions of argon (Ar), nitrogen (N_2), and ammonia (NH_3) (i.e., Ar^+, N_2^+, and NH_3^+, respectively) are denoted as ions C. A substrate of silicon (Si) over which catalyst of nickel (Ni) is placed is considered in the present paper. In the reactive plasma so considered, CH_4 acts as a carbon source gas.

The main assumptions of the model are:

(1) Plasma containing methyl, methane, hydrogen, argon, nitrogen, and ammonia ions is considered.
(2) Electric field is directed towards x-direction.
(3) Negative substrate potential is applied to the substrate.
(4) A cylindrical stainless steel reactor chamber of the plasma source which has the inner diameter (2R) = 32 cm and length (L) = 23 cm is considered following Denysenko *et al.*[15]
(5) Plasma power ionizes the gas (hydrocarbon, hydrogen, and carrier gas), and highly energetic hydrocarbon, hydrogen, and carrier gas ions initiates the dissociation of catalyst particle to form catalyst nanoparticle, which then seed nanotube growth on them.
(6) These hydrocarbon, hydrogen, and carrier gas ions then travel through the plasma sheath undergoing recombination, adsorption, and desorption loss to the walls and various other processes and eventually diffuses and accretes on nanoparticle to form CNT.

A. The sheath equations

Following Mehdipour *et al.*[24] and Lieberman and Lichtenberg,[25] the sheath equations are:

(1) The continuity equation

$$\left(\hat{i}\frac{\partial}{\partial x}+\hat{j}\frac{\partial}{\partial y}+\hat{k}\frac{\partial}{\partial z}\right)\cdot\hat{i}(n_l u_{lx})=\nu_l n_e. \tag{1}$$

(2) The ion momentum balance equation

$$m_l n_l u_{lx}\frac{du_{lx}}{dx}=en_l E-m_l n_l \nu_{ln} u_{lx}. \tag{2}$$

(3) Poisson's equation (Mehdipour *et al.*[24])

$$\frac{d^2\phi(x)}{dx^2}=-4\pi\sum q_l\delta_l n_l, \tag{3}$$

where l refers to either (i) electron (e), or (ii) CH_3^+, CH_4^+, H^+, H_2^+, and H_3^+ ions, or of (iii) $Ar^+/N_2^+/NH_3^+$ ions, m_l is the mass of species l, n_l is their number density, u_{lx} is the fluid velocity of the particle l, $\phi(x)$ is the sheath potential, ν_l is the ionization frequency, ν_{ln} is the collision frequency with the neutrals and q_l is the charge of species l, δ_l is the *l-th* ion to electron number density ratio, $\sum_l \delta_l = 1$, and $0 < \delta_l < 1$ as electron density is greater in plasma bulk than in sheath.

Now, by using Child Sheath law in cases where the high voltage is applied over longer time scales,[26] the plasma sheath width (λ_s) is given as $\lambda_s = \frac{\sqrt{3}}{2}\lambda_d\left(\frac{2U_s}{k_B T_e}\right)^{\frac{3}{4}}$, where $\lambda_d\left(=\sqrt{\frac{k_B T_e}{n_e e^2}}\right)$ is the Debye length of the plasma and U_s is the substrate bias, k_B is the Boltzmann constant, and T_e is electron temperature.

The ion-neutral collisions have been taken into account in the present model, and these collisions attain significance

at higher pressures. However, our model did not undertake pressure effects into account, but it has been reported that the sheath width decreases as neutral pressure is increased.[24]

B. Charging of the CNT

The equation describes the charge developed on the entire CNT (i.e., spherical tip placed over cylindrical surface), due to accretion of electrons and accretion & diffusion of positively charged ions on the surface of the CNT (i.e., spherical tip over cylindrical surface).

$$\frac{dZ}{d\tau} = I_{iActs} + I_{iActcys} + I_{iBcts} + I_{iBctcys} + I_{iCcts} + I_{iCctcys} - \gamma_e(I_{ects} + I_{ectcys}), \quad (4)$$

where Z is the charge over the entire CNT (i.e., spherical tip and cylindrical surface), $I_{ects} = \pi {r_{ct}}^2 \left(\frac{8k_BT_e}{\pi m_e}\right)^{\frac{1}{2}} n_e(x) \exp\left[Z\alpha_e + \frac{eU_s}{k_BT_s}\right]$ is the electron collection current at the surface of the spherical CNT tip and $\alpha_e\left(=\frac{e^2}{r_{ct}k_BT_e}\right)$, r_{ct} is the CNT tip radius, $n_e(x) = n_{e0}\exp\left[\frac{|e|\phi(x)}{k_BT_e}\right]$ is the electron density in plasma sheath,[27] $\phi(x)$ is the electrostatic potential, γ_e is the sticking coefficient of electrons, $\phi(x) = \phi_0 \exp\left(-\frac{|x|}{\lambda_d}\right)$, ϕ_0 is the negative potential at the surface, $I_{ectcys} = n_e(x) r_{ct} h \left(\frac{2\pi k_BT_e}{m_e}\right)^{\frac{1}{2}} \exp\left[\frac{eV_s}{k_BT_e} + \frac{eU_s}{k_BT_s}\right]$ is the electron collection current on the cylindrical surface of the CNT, V_s is the surface potential on the cylindrical surface of the CNT, h is the height of cylindrical surface of the CNT, m_e is the mass of electron,

$$I_{ijctcys} = n_{ij}(x) r_{ct} h \left(\frac{2\pi k_BT_i}{m_{ij}}\right)^{\frac{1}{2}} \left\{\frac{2}{\sqrt{\pi}}\left(\frac{eV_s}{k_BT_i}\right)^{\frac{1}{2}} + \exp\left[\frac{eV_s}{k_BT_i}\right] erfc\left[\left(\frac{eV_s}{k_BT_i}\right)^{\frac{1}{2}}\right]\right\} \times \exp\left[-\frac{E_b}{k_BT_s}\right]\exp\left[-\frac{eU_s}{k_BT_s}\right]$$

is the ion collection current on the cylindrical surface of CNT, T_i is the ion temperature, m_{ij} is the ion mass (j refers to either A, B, or C positively charged ions as explained earlier), E_b is the energy barrier for bulk diffusion ($\approx$1.6 eV), T_s is the substrate or catalyst temperature,

$I_{ijcts} = \pi {r_{ct}}^2 \left(\frac{8k_BT_i}{\pi m_{ij}}\right)^{\frac{1}{2}} n_{ij}(x)[1 - Z\alpha_i]\exp\left[-\frac{E_b}{k_BT_s}\right]\exp\left[-\frac{eU_s}{k_BT_s}\right]$ is the ion collection current on the spherical CNT, where $n_{ij}(x) = n_{ijo}\left(1 - \frac{2e\phi(x)}{m_i {v_{i0}}^2}\right)^{-\frac{1}{2}}$ is the ion density in plasma sheath,[27] v_{io} is the ion velocity at any point within the plasma, and $\alpha_i\left(=\frac{e^2}{r_{ct}k_BT_i}\right)$.

The following assumptions were considered for solving the currents:

(1) Maxwellian distribution of electrons and ions is considered.
(2) $e\phi(x) \ll k_BT_e$.
(3) $T_e \ll U_s$, i.e., temperature of electrons is lesser than the substrate potential.
(4) The mean free path of the ions is greater than the distance x in the sheath.
(5) For the sheath to perform its function and repel electrons, the potential must be monotonically decreasing with the increase in x. This will occur if $n_i(x) > n_e(x)$ for all x in the sheath.[26]
(6) The high voltage is considered to be applied over longer time scales; therefore, the ions would be accelerated by the electric field.[26]

C. Balance equation of electron density

The equation describes the balance of electron number density in the plasma bulk because of dissociative ionization, recombination with ions, electron collection current, and loss of electrons to discharge wall.

$$\frac{dn_e}{d\tau} = (\beta_A n_A + \beta_B n_B + \beta_C n_C) - (\alpha_A n_e n_{iA} + \alpha_B n_e n_{iB} + \alpha_C n_e n_{iC}) - \gamma_e n_{ct}(I_{ects} + I_{ectcys}) - K^e_{wall} n_e, \quad (5)$$

where β_j is the coefficient of dissociative ionization of the constituent neutral atoms due to external field, $\alpha_j(T_e) = \alpha_{j0}\left(\frac{300}{T_e}\right)^k \mathrm{cm}^3/\mathrm{sec}$ is the coefficient of recombination of electrons and positively charged ions, n_e is the electron number density, n_{iA}, n_{iB}, and n_{iC} are the ion number density of ions A (hydrocarbon), B (hydrogen) and C (carrier), respectively, and $\kappa = -1.2$ is a constant (Tewari and Sharma[28]).

$K^e_{well} n_e = \frac{\gamma_e v_{the} S_{surf} n_e}{4V}$ is the number of electrons lost on the discharge wall per unit time per unit volume, where γ_e is the sticking coefficients of electrons,

$v_{the}\left(=\sqrt{\frac{8T_e}{\pi m_e}}\right)$ is the average thermal velocity of electrons,[15] S_{surf} is the chamber surface area, and V is the volume of the PECVD chamber (in cm^3) whose inner diameter is 2R = 32 cm and length (L) = 23 cm is considered.[15]

The first term on the right side of Eq. (5) is the rate of gain in electron density per unit time because of dissociative ionization of neutral atoms; the second term is the decaying rate of the electron density due to the electron–ion recombination. The third term is the electron collection current at the surface of the CNT (spherical tip placed over the cylindrical surface).[28] The last term denotes the loss of the electrons to the discharge wall.[15]

D. Balance equation of positively charged ion density

The equations describe the balance of positively charged ions in plasma bulk, due to dissociative ionization of neutral atoms, recombination of electrons and ions, ion collection current at CNT surface, their adsorption, desorption, thermal dehydrogenation, and loss to the discharge wall.

$$\frac{dn_{iA}}{d\tau} = \beta_A n_A - \alpha_A n_e n_{iA} - n_{ct}(I_{iActs} + I_{iActcys}) - J_{aiA} + J_{desorptioniA} - K_{wall}^{iA} n_{iA} + \sum_i k_{i1} n_A n_{iC}, \quad (6)$$

$$\frac{dn_{iB}}{d\tau} = \beta_B n_B - \alpha_B n_e n_{iB}(I_{iBcts} + I_{iBctcys}) - J_{aiB} + J_{desorptioniB} + J_{th} - K_{wall}^{iB} n_{iB} + \sum_i k_{i2} n_B n_{iC}, \quad (7)$$

$$\frac{dn_{iC}}{d\tau} = \beta_C n_C - \alpha_C n_e n_{iC} - n_{ct}(I_{iCcts} + I_{iCctcys}) - J_{aiC} + J_{desorptionC} - K_{wall}^{iC} n_{iC} + \sum_i k_{il} n_A n_{iC} + \sum_i k_{i2} n_B n_{iC}, \quad (8)$$

$J_{aij} = \frac{P_i}{(2\pi m_{ij} k_B T_{ij})^{\frac{1}{2}}} \times \frac{n_{ij}}{j_{ij}}$ is the adsorption flux onto the catalyst –substrate surface, P_i is the partial pressure of adsorbing species,[29] $J_{desorptionij} = n_{ij}\nu \exp\left(\frac{-\varepsilon_{ai}}{k_B T_{ij}}\right)$ is the desorption flux of ions from the catalyst -substrate surface, j refers to either A, B, or C ions, ν is the thermal vibrational frequency $\approx 3 \times 10^{13}$ Hz, ε_{ai} is the adsorption energy,[29] and n_{ij} is the ion number density at the catalyst substrate surface.

$J_{th} = n_H \nu \exp\left(\frac{-\delta\varepsilon_{th}}{k_B T_s}\right)$ is the flux of type B ion (namely hydrogen) on account of thermal dehydrogenation. $\delta\varepsilon_{th}$ is the activation energy of thermal dehydrogenation. n_H is the hydrogen ion number density at the catalyst- substrate surface.

$K_{wall}^{ij} = \frac{\gamma_{ij} v_{thij} S_{surf}}{4V}$ denotes the loss of ions j on the discharge wall per unit time per unit volume, γ_{ij} is the sticking coefficients of ions, and $v_{thij} = \sqrt{\frac{8T_{ij}}{\pi m_{ij}}}$ is the average thermal velocity of ions A, B, or C.

The first term in Eqs. (6)–(8) is the gain in ion density per unit time because of ionization of neutral atoms; the second term is the electron-ion recombination. The third term is the ion collection current to the surface of the CNT (spherical tip over the cylindrical surface).[28] The fourth term is the loss of ions because of their adsorption to the catalyst -substrate surface, and fifth term is the gain of ion density due to the desorption of ions from the catalyst-substrate surface into plasma. The term J_{th} in Eq. (7) describes the increase of hydrogen ion number density in plasma because of thermal dehydrogenation. The $K_{wall}^{ij} n_{ij}$ in Eqs. (6)–(8) denotes the loss of the ions to the discharge wall.[15] The last term in Eqs. (6)–(8) is the gain in ion number density due to neutral/ion reactions.[15] The rate of reaction[30] $k_{i1} = 1.05 \times 10^{-10}$ cm^3/s, and rate of reaction[31] $k_{i2} = 2.7 \times 10^{-10}$ cm^3/s.

E. Balance equation of neutral atoms

$$\frac{dn_A}{d\tau} = \alpha_A n_e n_{iA} - \beta_A n_A + n_{ct}(1-\gamma_{iA})(I_{iActs} + I_{iActys}) - n_{ct}\gamma_A(I_{Acts} + I_{Actcys}) + I_A - O_A - \sum_i k_i n_A n_{iC}, \quad (9)$$

$$\frac{dn_B}{d\tau} = \alpha_B n_e n_{iB} - \beta_B n_B + n_{ct}(1-\gamma_{iB})(I_{iBcts} + I_{iBctcys}) - n_{ct}\gamma_B(I_{Bcts} + I_{Bctcys}) + I_B - O_B - \sum_i k_i n_B n_{iC}, \quad (10)$$

$$\frac{dn_C}{d\tau} = \alpha_C n_e n_{iC} - \beta_C n_C + n_{ct}(1-\gamma_{iC})(I_{iCcts} + I_{iCctcys}) - n_{ct}\gamma_C(I_{Ccts} + I_{Cctcys}) + I_C - O_C - \sum_i k_i n_A n_{iC} - \sum_i k_i n_B n_{iC}. \quad (11)$$

Equations (9)–(11) describe the balance of neutral particles in plasma due to recombination of electrons and ions, dissociative ionization of neutral molecules, ion and neutral collection current on the CNT surface, and inflow and outflow into and from the chamber and neutral/ion reactions.

$I_{jcts} = \pi {r_{ct}}^2 \left(\frac{8k_B T_n}{\pi m_j}\right)^{\frac{1}{2}} n_j$ is the neutral collection current at the surface of the spherical CNT tip,

$I_{jctcys} = \pi r_{ct} h \left(\frac{2k_B T_n}{m_j}\right)^{\frac{1}{2}} n_j$ is the neutral collection current on the cylindrical surface of CNT, $\gamma_{ij} = 1$ is the ion sticking coefficient, $\gamma_j = 1$ is the neutral atom sticking coefficient, T_n is the neutral atom temperature, n_j is the neutral atom density, and m_j is the neutral atom mass.

$I_j\left(\frac{cm^{-3}}{s}\right) = \frac{4.4\times 10^{17} J_j[sccm]}{V}$ is the inflow, i.e., the rate at which species j enter the chamber. J_j is the gas inlet flow rate[15] (in standard cubic centimeter). $O_j\left(\frac{cm^{-3}}{s}\right) = \frac{\nu_{pump} n_j}{V}$ is the outflow, i.e., the rate at which species j leave the chamber.[15] ν_{pump} is the pumping rate in cm^3/s. n_j is the number density of species j in cm^{-3}, and V is the volume of the chamber (cm^3).[15] j can either be neutrals of CH_4, H_2 or Ar/N_2/NH_3.

The first term in Eqs. (9)–(11) is the gain in neutral atom density per unit time due to electron–ion recombination; the second term is the decrease in neutral density due to dissociative ionization. The third term is the gain in neutral density due to neutralization of the particles collected at the surface of the CNT. The fourth term is the accumulation of neutral atoms of species A and B on the surface of the CNT.[28] The fifth and sixth terms denote the inflow and outflow of the neutrals into and from the chamber, respectively.[15] The last term denotes the loss in number density due to neutral and ion reactions.[15]

F. Rate equation for energy of catalyst particle

Initially, a catalyst particle Nickel (Ni) of radius 30 nm is considered to be placed over a silicon substrate surface.

Srivastava *et al.*[32] have highlighted in their experimental findings that an increase in microwave power causes more ionization of the gas, which increases the density of plasma species of relatively higher energy. Following experimental results of Srivastava *et al.*,[32] we assume that as the applied rf power increases, it ionizes the gas more which creates more energetic ions, which implies that plasma species of relatively higher energy are created. Since, energy of ions corresponds to the number density and temperature of ions, we

assume that with an increase in rf power the number density and temperature of plasma species increase

$$\begin{aligned} rfpower &= C_p T_s \frac{d}{d\tau}(m_p) \\ &= \left[I_{iActP}\left(\varepsilon^s{}_{iAc} + I_{pA}\right) + I_{iBctP}\left(\varepsilon^s{}_{iBc} + I_{pB}\right)\right. \\ &\quad \left. + I_{iCctP}\left(\varepsilon^s{}_{iCc} + I_{pC}\right)\right] - \left(\frac{3}{2}k_B\right)\left[(1-\gamma_{Ai})I_{iActP}\right. \\ &\quad \left. + (1-\gamma_{Bi})I_{iBctP} + (1-\gamma_{Ci})I_{iCctP}\right]T_s, \end{aligned} \tag{12}$$

where $m_P = \frac{4}{3}\pi {r_P}^3 \rho_P$ is the mass of catalyst particle, r_p is the radius of catalyst particle.

ρ_P is the mass density of catalyst particle, C_p is the specific heat of catalyst particle (Ni) and is 0.44 KJ/Kg°C, and T_s is the substrate temperature. I_{pA}, I_{pB}, and I_{pC} are the ionization energies of atoms A (methane), B (hydrogen), and C (either Ar or NH_3 or N_2), respectively (Tewari and Sharma[28]). In the present problem, we have assumed the substrate and catalyst temperature to be the same. However, Denysenko and Azarenkov[33] have considered the substrate and catalyst temperature to be different in their study and concluded that the substrate-holding platform temperature differs from that of the catalyst nanoparticle temperature mainly due to the temperature variation along the Si substrate.

$\varepsilon^s_{ijc}(Z) = \left(\left(\frac{(2-Z\gamma_{ji})}{(1-Z\gamma_{ij})}\right) - Z\gamma_{ij}\right)k_B T_{ij}$ is the mean energy collected by the ions j (where j refers to ion A, B, or C) at the surface of the catalyst particle[34] and

$$\gamma_{ij} = \left(\frac{e^2}{r_P k_B T_{ij}}\right);$$

$$\begin{aligned} I_{ijctP} &= \pi {r_P}^2 \left(\frac{8k_B T_i}{\pi m_{ij}}\right)^2 n_{ij}(x)\left[1 - Z\gamma_{ji}\right] \\ &\quad \times \exp\left[-\frac{E_b}{k_B T_s}\right]\exp\left[-\frac{eU_s}{k_B T_s}\right] \end{aligned}$$

is the ion collection current at the surface of catalyst particle, j (where j refers to ion A, B, or C).

In Solving Eq. (12), we consider that at rf power of 100 W, and at $\tau = 0$ feeding $n_{iB0} = n_{iA0} = 10^9\,cm^{-3}$, $T_{i0} = 2100\,K$, $T_s = 550\,°C$, $E_b = 1.6\,eV$, $U_s = -50\,V$, and $r_{P0} = 30\,nm$ in expression for I_{iActP}, I_{iBctP}, and I_{iCctP}, we can calculate I_{iActP0}, I_{iBctP0}, and I_{iCctP0}.

Feeding I_{iActP0}, I_{iBctP0}, and I_{iCctP0} and the other parameters, i.e., $\varepsilon^s_{iAc} = 13.2\,eV$, $\varepsilon^s_{iBc} = 13.2\,eV$, and $\varepsilon^s_{iCc} = 13.2\,eV$, $I_{pA} = 11.87\,eV$, $I_{pB} = 13.7\,eV$, and $I_{pC} = 12.21\,eV$ in Eq. (12), we can get the value of catalyst particle radius r_P at any time τ for $T_s = 550\,°C$.

The terms on the right side of Eq. (12) are the rate of energy transferred to the catalyst particle due to the ions collected at the surface of catalyst particle because of ionization of neutral atoms A, B, and C and mean energy collected by the ions at the surface of catalyst particle, and due to the accretion of ions A, B, and C at the catalyst particle site.

The resulting value of catalyst nanoparticle at time τ serves as the initial base radius of the cylindrical part of nanotube.

G. Growth rate equation of the curved surface area of CNT

Following Tewari and Sharma,[28]

$$\begin{aligned} r_P \frac{d(2\pi h)}{d\tau} &= \left(\left\{2n_{CH}\nu\exp\left(\frac{-\delta E_t}{K_B T_s}\right) + 2\theta_{CH} j_{iA} y_d \right.\right. \\ &\quad \left. + 2j_{iA} + \frac{j_{iA}\sigma_{ads} j_{iB}}{\nu} + j_{carbon}\right\} m_{carbon} \\ &\quad + \left\{j_{iA} + \frac{j_{iA}\sigma_{ads} j_H}{\nu} + j_{iA}\exp\left(\frac{-\delta E_t}{k_B T_s}\right)\right\} m_{iA}\Bigg) \\ &\quad \times \frac{D_s \times 2\pi r_p}{\pi r_p^2 \rho_p}\left(\frac{1}{n_{iActcys}}\right) + \gamma_{CH_4}\pi r_P^2 I_{CH_4{}^{ctcys}} \\ &\quad + \gamma_C \pi r_P^2 I_{Cctcys}, \end{aligned} \tag{13}$$

$$\begin{aligned} \frac{d(\pi r_{ct}^2)}{d\tau} &= \left\{j_{iB}\exp\left(\frac{-E_b}{k_B T_s}\right) + j_{iB}\exp\left(\frac{-\delta E_{th}}{k_B T_s}\right) + j_{iB}(1-\theta_t)\right. \\ &\quad \left. + j_{iB} + \theta_{CH}\left(j_{iB} y_d + \nu_0 \nu \exp\left(\frac{-\delta E_i}{k_B T_s}\right)\right)\right\}\frac{h(\tau)}{n_{iB}} \\ &\quad + \gamma_C \pi r_{ct}^2 I_{Ccts}. \end{aligned} \tag{14}$$

Equations (13) and (14) trace the development of the CNT on the catalyst nanoparticle. The height of cylindrical CNT surface is obtained from Eq. (13) in which we consider the growth of the cylindrical part of the CNT and the value of the height of the cylindrical CNT surface at time τ is then fed into Eq. (14) to determine the radius of spherical CNT tip (r_{ct}). Equation (14) specifically calculates the curved surface area of the spherical CNT tip.

Equation (14) accounts only for the nanoparticle tip radius as bottom area is already determined by the catalyst nanoparticle because they seed nanoparticle growth on them. $h(\tau)$ is the height of the CNT at a time τ.

The explanation for all the symbols used in Eq. (13) is given in Table I.

The explanation for all the symbols used in Eq. (14) is given in Table II.

The explanation for all the terms used in Eq. (13) is given in Table III.

The explanation for all the terms used in Eq. (14) is given in Table IV.

III. NUMERICAL RESULT AND DISCUSSIONS

In the present paper, we are studying the effect of different carrier gases and their flow rates on the growth of CNT through the PECVD process. In a PECVD process, the applied power dissociates the feedstock gas (e.g., methane CH_4) and the dissociated species traverse through the plasma sheath following the decomposition of a hydrocarbon gas on the surface of the catalyst and bulk diffusion of carbon into the catalyst particle until saturation to eventually, form carbon nanostructures.

TABLE I. Explanation for all the symbols used in Eq. (13).

S. No.	The notation of various symbols used in Eq. (13)	The explanation for symbols in Eq. (13)
1.	$n_{CH} = \theta_{CH}\nu_0$	The number density or concentration of CH (CH denotes CH_4 species)[24]
2.	$\nu_0 \approx 1.3 \times 10^{15}\text{cm}^{-2}$	The number of adsorption sites per unit area[35]
3.	$j_{carbon} = n_{carbon}v_{thcarbon}/4$	Ion flux of carbon atoms[24]
4.	$v_{thcarbon}$	The thermal velocity of carbon atoms[24]
5.	$j_{iA} = n_{iA}(k_BT_i/m_{iA})^{1/2}$ and $j_{iB} = n_{iB}(k_BT_i/m_{iB})^{1/2}$	Ion flux of type A and B, respectively
6.	$y_d \approx \varepsilon_{icH}/\varepsilon_{dis}$	Ratio of kinetic energy associated with the motion of hydrocarbon ions impinging on the substrate to dissociation energy of CH_4[24]
7.	n_{iB}	Number density of type B ions, i.e., hydrogen ions
8.	ε_{icH}	Kinetic energy associated with the motion of hydrocarbon ions impinging on the substrate[35]
9.	ε_{dis}	Dissociation energy of CH_4
10.	$\sigma_{ads} \approx 6.8 \times 10^{-16}cm^2$	Cross section for the reactions of atomic hydrogen with adsorbed particles[24]
11.	n_{iC}	Number density of C ions (i.e., carrier ions)
12	D_s and $[D_s = D_{s0}\exp(-E_s/k_BT_s)]$, $D_{s0} = va_0^2$ is a constant	Surface diffusion coefficient[35]
13.	$E_s = 0.3$ eV	Energy barrier for diffusion of carbon (C) on the catalyst[35]
14.	$a_0 = 0.34$ nm	Inter atomic distance between carbon atoms
15.	θ_t	Total surface coverage[24]
16.	$\delta\varepsilon_t = 1.3$eV	Energy due to thermal dissociation[35]
17.	γ_{CH_4}	Sticking coefficient of CH_4 neutrals[28]
18.	γ_C	Sticking coefficient of carrier gas, i.e., of either $Ar/N_2/NH_3$
19.	$m_{carbon} = 12$ amu	The mass of a carbon atom
20.	$m_{iA} = 15$ amu for CH_3^+ $= 16$ amu for CH_4^+	The mass of type A (methyl) ions The mass of type A (methane) ions
21.	$h(\tau)$	Height of CNT at time τ
22.	n_{iB}	Number density of type B ions i.e., hydrogen ions
23.	$I_{CH4ctcys}$	Methane neutral atom collection current at the surface of cylindrical CNT[28]
24.	I_{Cctcys}	Carrier gas neutral atom collection current at the surface of cylindrical CNT
25.	$k_B = 1.38 \times 10^{-16}$ ergs/K	Boltzmann's constant
26.	$T_s = 550\,^\circ$C	Substrate temperature
27.	$r_p = 30$ nm	Initial radius of catalyst particle
28.	$\rho_P = 8.908$ g/cm^3	Density of nickel (Ni)
29.	θ_{CH}	Surface coverages of CH_4 species[24]
30.	$\nu = 10^{13}$ Hz	Thermal vibrational frequency[35]
31.	$I_{iActcys}$	Ion collection current of hydrocarbon (i.e., A) the surface of cylindrical CNT[28]

Ions from plasma do usually deposit inhomogeneously on CNTs growing as a forest as reported in Burmaka *et al.*[36] Therefore, in the present model, we assume the inhomogeneous deposition of ions on CNT growing in a reactive plasma medium assisted by the catalyst.

In a PECVD chamber, there are three input gases: hydrocarbon gas, carrier gas, and hydrogen gas. In the present analysis, we investigate the effects of carrier gases on the growth of CNT in a reactive plasma medium. The three different carrier gases, e.g., argon (Ar), ammonia (NH_3), and nitrogen (N_2) are considered. The flow rates of all the three carrier gases are varied individually, keeping the flow rate of hydrocarbon and hydrogen gases constant.

TABLE II. Explanation for all the symbols used in Eq. (14)

S. No.	The notation of various symbols used in Eq. (14)	The explanation for symbols in Eq. (14)
1.	$j_{iB} = n_{iB}(k_BT_i/m_{iB})^{1/2}$	Ion flux of hydrogen (B ion)
2.	T_i	Ion temperature
3.	$E_b \approx 1.6eV$	Energy barrier for bulk diffusion[24]
4.	δE_{th}	Energy due to dehydrogenation of CH_4[35]
5.	θ_t	Total surface coverage[24]
6.	$h(\tau)$	Height of CNT at time τ
7.	r_{ct}	Radius of spherical CNT tip

The calculations have been formed to investigate the dependence of hydrocarbon and hydrogen number density, the height of cylindrical CNT surface, and radius of the spherical CNT tip with time for different flow rates of carrier gases by simultaneous solution of Eqs. (1)–(14) at appropriate boundary conditions.

The initial boundary conditions for the present calculations are at $\tau = 0$, ion number density ($n_{iA0} = 0.5$ ne0, $n_{iB0} = 0.5$ ne0 and $n_{iC0} = 0.5$ ne0), neutral atom density ($n_{A0} = n_{B0} = n_{C0} = 1 \times 10^{14}\text{cm}^{-3}$), electron number density ($n_{e0} = 1.12 \times 10^9$ cm^{-3}), electron temperature (T_{e0}) = 1.5 eV, ion temperature (T_{iA0}) = 2200 K, neutral temperature (T_{n0}) = 2000 K, mass of ion A (m_{iA}) = 15 amu (methyl ion

TABLE III. Explanation for all the terms used in Eq. (13)

S. No.	The mathematical Expression for terms in Eq. (13)	The detailed explanation for terms in Eq. (13)
1.	$2n_{CH}\nu \exp\left(\frac{-\delta E_t}{k_B T_s}\right)$	The generation of carbon atoms on the catalyst surface due to thermal dissociation of methyl ions[24]
2.	$2\theta_{CH} j_{iA} y_d$	Ion-induced dissociation of CH_4[24]
3.	$2j_{iA}$	Decomposition of positively charged hydrocarbon ions
4.	$\frac{j_{iA}\sigma_{ads} j_{iB}}{\nu}$	Interaction of hydrocarbon ions with hydrogen ions[35]
5.	j_{carbon}	Incoming flux of carbon atoms
6.	j_{iA}	Incoming flux of hydrocarbon ions per unit time onto the catalyst particle
7.	$\frac{j_{iA}\sigma_{ads} j_H}{\nu}$	Interaction of adsorbed type A ions with atomic hydrogen from plasma[24]
8.	$j_{iA}(1-\theta_t)$	Adsorption of hydrocarbon ions onto the catalyst-substrate surface[35]
9.	$j_{iA}\exp\left(\frac{-\delta E_t}{k_B T_s}\right)$	Thermal dissociation of CH_4[35]
10.	$\frac{D_s \times 2\pi r_p}{\pi r_p^2 \rho_p}$	The surface diffusion of various species onto the catalyst nanoparticle per unit area per unit mass density[35]
11.	$\gamma_{CH_4}\pi r_P^2 I_{CH_4} ctcys$	Accretion of neutral methane atoms to the cylindrical surface of CNT[28]
12.	$\gamma_C \pi r_P^2 I_{Cctcys}$	Accretion of neutral carrier gas atoms to the cylindrical surface of CNT[28]

CH_3^+) and 16 amu (methane ion CH_4^+), mass of ion B $(m_{iB}) = 1$ amu for (H^+), 2 amu for (H_2^+), and 3 amu for (H_3^+), mass of ion C $(m_{iC}) = 40$ amu for Ar^+, 17 amu for NH_3^+, and 28 amu for N_2^+, coefficient of recombination of electrons and ions $(\alpha_{A0} \approx \alpha_{B0} \approx \alpha_{C0}) = 1.12 \times 10^{-7}\text{cm}^3/\text{s}$, constant $\kappa = -1.2$, and density of Ni $(\rho_P) = 8.908\ \text{g/cm}^3$.

Other parameters used in the calculation are substrate temperature $(T_s) = 550\,^\circ\text{C}$, thermal energy barrier on the catalyst surface (δE_t), energy barrier for bulk diffusion $E_b = 1.6$ eV, energy due to thermal dissociation of methyl ions, dissociation energy of CH_4 $(\varepsilon_{dis}) = 4.2$ eV, Ionization energies of neutral atom A $(I_{pA}) = 8.96$ eV, Ionization energies of neutral atom B $(I_{pB}) = 6.86$ eV, the mean energy collected by the ion A at the surface of catalyst particle $(\varepsilon_{iA}) = 6$ eV, the mean energy collected by the ion B at the surface of catalyst particle $(\varepsilon_{iB}) = 11$ eV, sticking coefficient of electron $(\gamma_e) = 1$, sticking coefficient of ion $(\gamma_{ij}) = 1$, chamber surface area $(S_{surf}) = 3918.72\ \text{cm}^2$, average thermal velocity of electrons $(v_{the}) = 6.48 \times 10^6$ cm/s, chamber volume $(V) = 18488.32\ \text{cm}^3$, and average thermal velocity of ions $(v_{thij}) = 3.67 \times 10^6$ cm/s.

The flow rate of CH_4 (J_{CH4}) and H_2 (J_{H2}) is fixed at 6.0 sccm (standard cubic centimeter) and 12 sccm, respectively. Three different carrier gases N_2, NH_3, and Ar are considered, and their flow rates are individually varied to study the effects of all the three carrier gases and their flow rates on the growth of the CNT by PECVD process. Flow rate of carrier gas (J_C) is varied as 10 sccm, 20 sccm, and 30 sccm.

Fig. 1 displays the variation of the number density of hydrocarbon ions (in cm^{-3}) with time for different flow rates of argon (Ar) carrier gas (i.e., $J_{Ar} = 10$ sccm, 20 sccm, and 30 sccm). It can be seen from Fig. 1 that as the flow rate of carrier gas is increased, the number density of hydrocarbon ions increases. This may be ascribed to the fact that with the increase in carrier gas flow rate, the ions of carrier gas increases and they then react with neutrals of methane giving rise to ions of methyl, thereby increasing their number density within the plasma. The possible governing equation[15] for the above process is

$$Ar^+ + CH_4 \rightarrow CH_3^+ + H + Ar.$$

Figs. 2 and 3 illustrate the variation of the number density of hydrocarbon ions (in cm^{-3}) with time for different flow rates of ammonia (NH_3) carrier gas (i.e., $J_{NH3} = 10$ sccm, 20 sccm, and 30 sccm) and nitrogen (N_2) carrier gas (i.e., $J_{N2} = 10$ sccm, 20 sccm, and 30 sccm). The variation of the number density of hydrocarbon ions with flow rate of carrier gas and explanation for the process obtained in Figs. 2 and 3 for is same as in Fig. 1. When ammonia is taken as a carrier gas, the possible governing equation[37] for the above process is

$$NH_3^+ + CH_4 \rightarrow NH_4 + CH_3^+.$$

TABLE IV. Explanation for all the terms used in Eq. (14)

S. No.	The mathematical expression for terms in Eq. (14)	The detailed explanation for terms in Eq. (14)
1.	$j_{iB}\exp\left(\frac{-E_b}{k_B T_s}\right)$	Hydrogen atom diffusing into catalyst - substrate surface[35]
2.	$j_{iB}\exp\left(\frac{-\delta E_{th}}{k_B T_s}\right)$	Incoming flux of hydrogen due to the dehydrogenation of CH_4[24]
3.	$j_{iB}(1-\theta_t)$	Adsorption of hydrogen ions to the catalyst - substrate surface[24]
4.	j_{iB}	Decomposition of hydrogen ions
5.	$\theta_{CH} j_{iB} y_d$	Ion induced dissociation of CH_4[24]
6.	$\theta_{CH}\nu_0\nu \exp\left(\frac{-\delta E_i}{k_B T_s}\right)$	Incorporation of hydrogen ions due to thermal decomposition of hydrocarbon ions[35]
7.	$h(\tau)$	Height of CNT at time τ
8.	n_{iB}	Number density of type B ions, i.e., hydrogen ions
9.	$\gamma_C \pi r_{ct}^2 I_{Ccts}$	Accretion of neutral carrier gas atoms at the spherical CNT tip

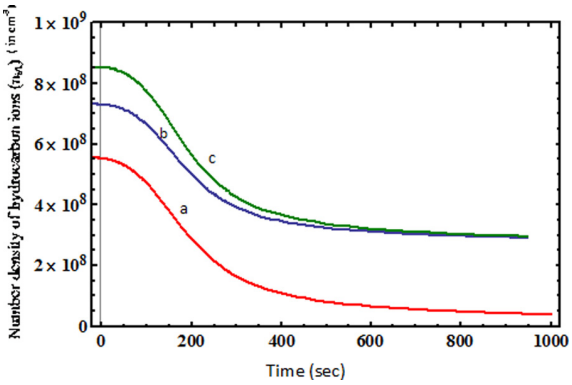

FIG. 1. This figure depicts the time evolution of number density of hydrocarbon ions (in cm^{-3}) for different flow rate of argon carrier gas (where a, b, and c corresponds to $J_{Ar} = 10$ sccm, 20 sccm, and 30 sccm, respectively). The other parameters are given in the text.

Now, when nitrogen is taken as a carrier gas, then possible governing equation is

$$N_2 + CH_4 \rightarrow noreaction.$$

But for N, the possible reaction[38] is

$$N + CH_4 \rightarrow HCN^- + H_2 + H.$$

Figs. 4–6 display the variation of number density of hydrogen ions (in cm^{-3}) with time for different flow rates (in sccm) of argon (Ar), ammonia (NH_3), and nitrogen (N_2) carrier gas. It can be seen from Figs. 4–6 that as the flow rate of carrier gas is increased, the number density of hydrogen ions decreases. This may be ascribed to the fact that with the increase in carrier gas flow rate, the density of both hydrocarbon and hydrogen ions does increase, but hydrogen ions being more reactive than hydrocarbon ions further react with higher hydrocarbon ions in the plasma, thereby increasing the density of hydrocarbon ions but decreasing their own numbers within the plasma. The possible governing equations are

$$Ar^+ + H_2 \rightarrow Ar + H_2{}^+;$$

$$H_2{}^+ + H_2 \rightarrow H_3{}^+ + H;$$

$$H_3{}^+ + C_xH_y \rightarrow C_xH^+{}_{y+1} + H_2.$$

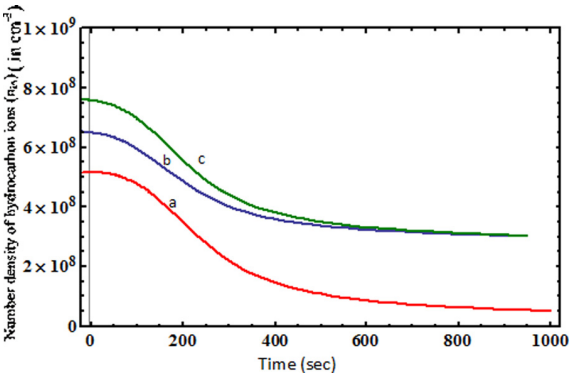

FIG. 2. This figure illustrates the time evolution of number density of hydrocarbon ions (in cm^{-3}) for different flow rate of ammonia carrier gas (where a, b, and c corresponds to $J_{NH3} = 10$ sccm, 20 sccm, and 30 sccm, respectively). The other parameters are given in the text.

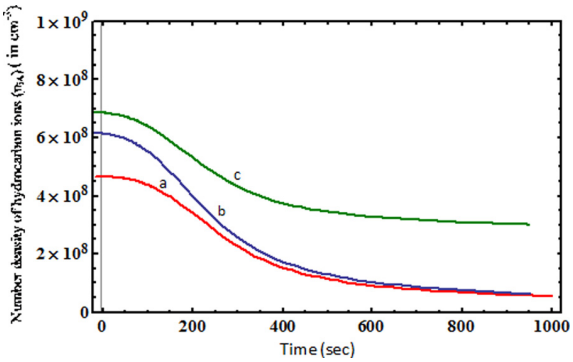

FIG. 3. This figure illustrates the time evolution of number density of hydrocarbon ions (in cm^{-3}) for different flow rate of nitrogen carrier gas (where a, b, and c corresponds to $J_{N2} = 10$ sccm, 20 sccm, and 30 sccm, respectively). The other parameters are given in the text.

From Figs. 1 and 4, Figs. 2 and 5, and Figs. 3 and 6, we can compare the time evolution of densities of hydrocarbon and hydrogen ion with the carrier gas inflow. It can be inferred from Figs. 1 and 4, Figs. 2 and 5, and Figs. 3 and 6 that for the same carrier gas inflow, the hydrogen ion decays faster than the hydrocarbon ion which validates the fact that hydrogen ions are more reactive than the hydrocarbon ions and hence induce the formation of higher hydrocarbons within the plasma.

The increase in the number density of hydrocarbon and decrease in the density of hydrogen with flow rate of carrier gas is in accordance with the results of Denysenko *et al.*[15]

Figs. 7 and 8 illustrate the variation of height (in μm) and radius of CNT (in nm) with time as a function of argon carrier gas inflow rate (i.e., $J_{Ar} = 10$ sccm, 20 sccm, and 30 sccm), respectively. It can be seen from Figs. 7 and 8 that both the height and radius of CNT increase with carrier gas flow rate. This may be ascribed to the fact that as the density of hydrocarbon increases with the carrier gas flow rate, a larger number of hydrocarbon and carbon radicals become readily available for CNT growth, thereby increasing its height. Now, the increase of carrier gas inflow leads to lesser number density of hydrogen ions, thereby reducing the etching effects of hydrogen and hence giving larger radius of CNT tip.

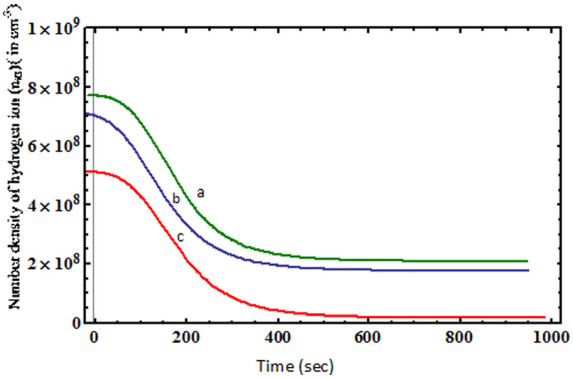

FIG. 4. This figure illustrates the time evolution of number density of hydrogen ions (in cm^{-3}) for different flow rate of argon carrier gas (where a, b, and c corresponds to $J_{Ar} = 10$ sccm, 20 sccm, and 30 sccm, respectively). The other parameters are given in the text.

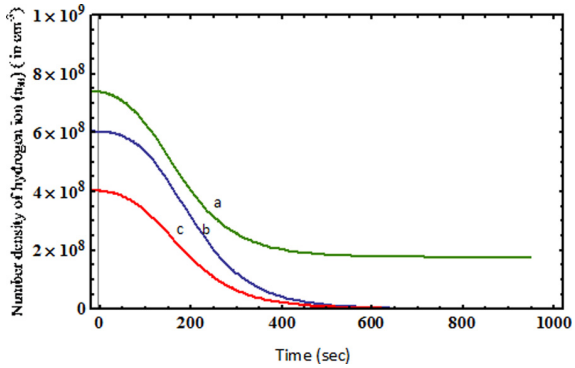

FIG. 5. This figure depicts the time evolution of number density of hydrogen ions (in cm^{-3}) for different flow rate of ammonia carrier gas (where a, b, and c corresponds to $J_{NH3} = 10$ sccm, 20 sccm, and 30 sccm, respectively). The other parameters are given in the text.

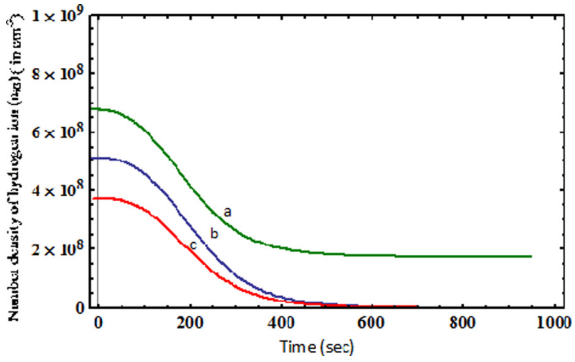

FIG. 6. This figure depicts the time evolution of number density of hydrogen ions (in cm^{-3}) for different flow rate of nitrogen carrier gas (where a, b, and c corresponds to $J_{N2} = 10$ sccm, 20 sccm, and 30 sccm, respectively). The other parameters are given in the text.

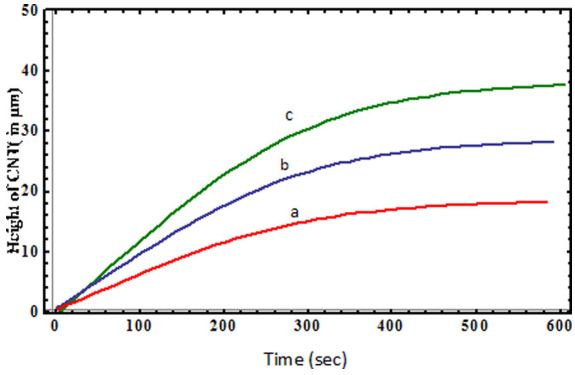

FIG. 7. This figure depicts the time evolution of height of CNT (in μm) for different flow rate of argon carrier gas (where a, b, and c corresponds to $J_{Ar} = 10$ sccm, 20 sccm, and 30 sccm. The other parameters are given in the text.

Fig. 9 illustrates variation of height of CNT (in μm) with time as a function of ammonia carrier gas inflow rate (i.e., $J_{NH3} = 10$ sccm, 20 sccm, and 30 sccm). The height of CNT increases with inflow rate of ammonia. This is because as the density of hydrocarbon increases with the ammonia carrier gas flow rate, a larger number of hydrocarbon and carbon radicals become readily available for CNT growth, thereby increasing its height.

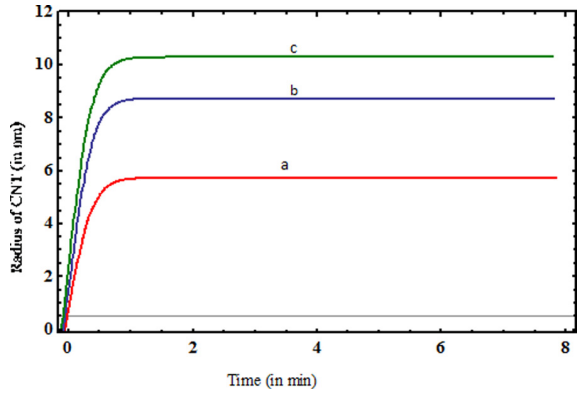

FIG. 8. This figure depicts the time evolution of radius of CNT (in nm) for different flow rate of argon carrier gas (where a, b, and c corresponds to $J_{Ar} = 10$ sccm, 20 sccm, and 30 sccm, respectively). The other parameters are given in the text.

Fig. 10 illustrates the variation of radius of CNT (in nm) with time as a function of ammonia carrier gas inflow rate (i.e., $J_{NH3} = 10$ sccm, 20 sccm, and 30 sccm). The radius of CNT decreases with inflow rate of ammonia. With ammonia gas, the increase of carrier gas inflow leads to lesser number density of hydrogen ions. Now, in ammonia gas environment, there are nitrogen ions also along with hydrogen ions and although reduced hydrogen number density would decrease the etching of CNT by hydrogen ions. However, there would be some etching by nitrogen ions, and hence, the combined effect of etching by nitrogen and hydrogen would eventually result in reducing radius of CNT tip with gas inflow rate.

Figs. 11 and 12 illustrate the variation of height (in μm) and radius of CNT (in nm) with time as a function of nitrogen carrier gas inflow rate (i.e., $J_{N2} = 10$ sccm, 20 sccm, and 30 sccm). The height of CNT decreases with inflow rate of nitrogen. This may be ascribed to the fact that with the nitrogen carrier gas flow rate, a larger number of CN radicals are formed in N_2 environment, which are volatile at room temperatures, and reduces the carbon flux to catalyst particle, thereby producing lesser height and radius of CNTs.[39]

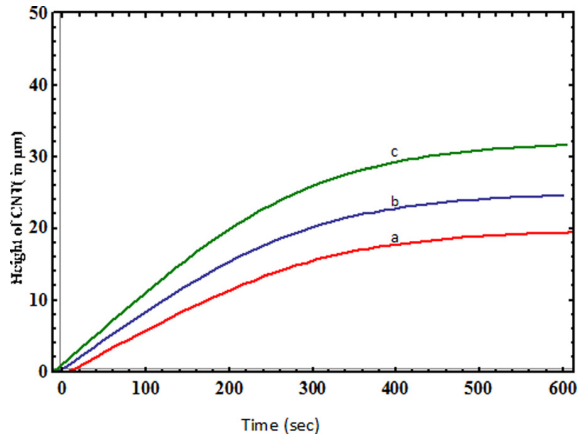

FIG. 9. This figure depicts the time evolution of height of CNT (in μm) for different flow rate of ammonia carrier gas (where a, b, and c corresponds to $J_{NH3} = 10$ sccm, 20 sccm, and 30 sccm, respectively). The other parameters are given in the text.

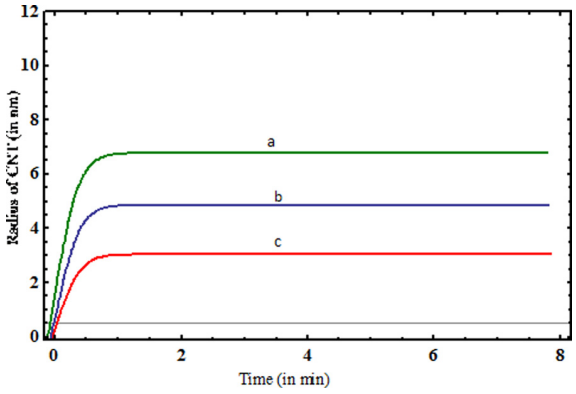

FIG. 10. This figure depicts the time evolution of radius of CNT (in nm) for different flow rate of ammonia carrier gas (where a, b, and c corresponds to $J_{NH3} = 10$ sccm, 20 sccm, and 30 sccm, respectively). The other parameters are given in the text.

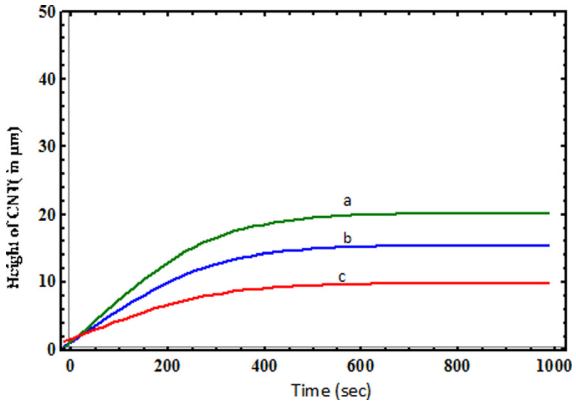

FIG. 11. This figure depicts the time evolution of height of CNT (in μm) for different flow rate of nitrogen carrier gas (where a, b, and c corresponds to $J_{N2} = 10$ sccm, 20 sccm, and 30 sccm, respectively). The other parameters are given in the text.

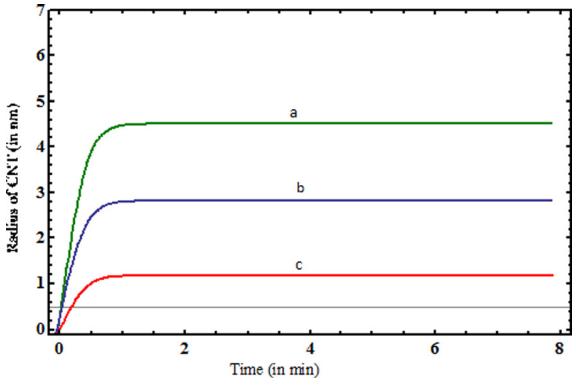

FIG. 12. This figure depicts the time evolution of radius of CNT (in nm) for different flow rate of nitrogen carrier gas (where a, b, and c corresponds to $J_{N2} = 10$ sccm, 20 sccm, and 30 sccm, respectively). The other parameters are given in the text.

Figs. 13 and 14 depict the time evolution of the height of CNT (in μm) and radius of CNT (in nm) for different carrier gases, i.e., Ar, NH_3, and N_2 for a fixed flow rate of 10 sccm for all the three carrier gases. Finally, from Figs. 13 and 14, we can see that the height of CNT (in μm) and radius

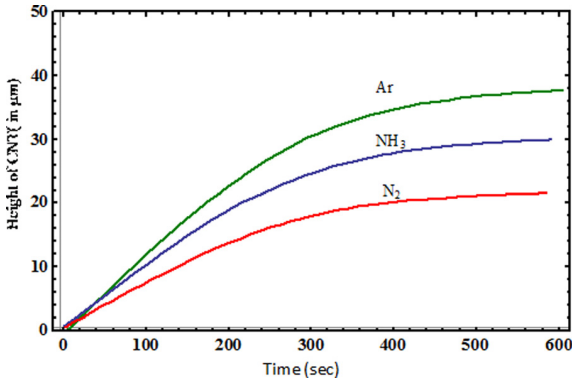

FIG. 13. This figure depicts the time evolution of height of CNT (in μm) for different carrier gases Ar, NH_3, and N_2 for a fixed flow rate of 10 sccm for all the three carrier gases. The other parameters are given in the text.

of CNT (in nm) are largest for argon followed by ammonia and then nitrogen. Thus, one can conclude that argon is the best carrier gas among those considered in the present problem followed by ammonia and then by nitrogen for better growth of CNTs in a reactive plasma medium. The results obtained in the present model comply with the experimental works of Kayastha *et al.*,[6] Mi *et al.*,[7] Jung *et al.*,[8] Mi and Jia,[10] Qian *et al.*,[11] and Malgas *et al.*[12]

IV. CONCLUSION

A theoretical model is developed to investigate the effects of three different carrier gases and their flow rates on the growth of CNT by a PECVD process. The three different carrier gases, e.g., argon (Ar), ammonia (NH_3), and nitrogen (N_2), are considered, and their flow rates are varied to investigate their effects on height and radius of CNTs. The results hold good when the flow rate of CH_4 (J_{CH4}) and H_2 (J_{H2}) is fixed and the substrate and catalyst temperature are assumed to be same. The initial ion number density and neutral atom density for hydrogen, hydrocarbon, and carrier are assumed to be same at 0.56×10^9 cm^{-3} and 1×10^{14}cm^{-3}, respectively. The ion and neutral temperature for hydrogen, hydrocarbon, and carrier are taken to be same at 2200 K and 2000 K, respectively.

The main findings of the work can be summarized as follows:

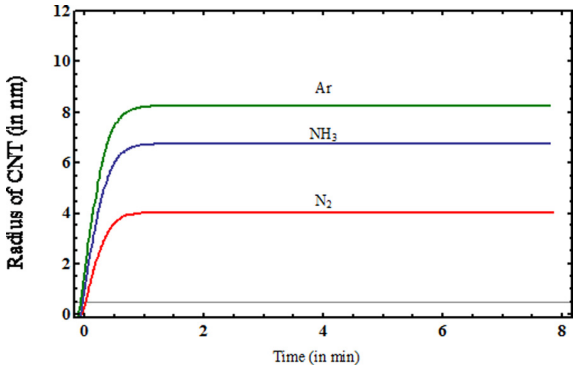

FIG. 14. This figure depicts the time evolution of radius of CNT (in nm) for different carrier gases Ar, NH_3, and N_2 for a fixed flow rate of 10 sccm for all the three carrier gases. The other parameters are given in the text.

(1) With Ar acting as a carrier gas, CNTs with better height and radius are obtained. This is due to the fact that number density of hydrocarbon increases and of hydrogen ions decreases with Ar carrier gas flow rate. The reaction mechanism is governed by Ar^{+}(Argon) + CH_4 (Methane) → CH_3^{+} (Methyl) + H (Hydrogen) + Ar (Argon). The increase in hydrocarbon density, makes carbon radicals readily available for CNT growth which then increases height of CNT. The decrease in hydrogen ion density reduces the etching effects of hydrogen and hence give larger radius of CNT tip.

(2) With NH_3 as a carrier gas, CNTs with better height but smaller radius are obtained. This is because number density of hydrocarbon increases and of hydrogen ions decreases with NH_3 carrier gas flow rate. The possible reaction equation is NH_3^{+} (Ammonia) + CH_4 (Methane) → NH_4 (Ammonia) + CH_3^{+} (Methyl). The increase in the height of CNT with ammonia flow rate is due to the larger availability of carbon radicals with hydrocarbon density. The reduction in radius of CNT is due to the combined etching effects of both hydrogen and nitrogen.

(3) When nitrogen is taken as a carrier gas, both the height and radius of CNT decrease. The possible reaction equation is N (Nitrogen) + CH_4 (Methane) → HCN^{-} (Hydrogen cyanide) + H_2 (Hydrogen) + H (Hydrogen). The reduction in both the height and radius of CNT with the nitrogen carrier gas flow rate is because in N_2 environment, a larger number of CN radicals are formed which are volatile at room temperatures and they reduce the carbon flux to catalyst particle, thereby producing lesser height and radius of CNTs.

[1]V. I. Merkulov, A. V. Melechko, M. A. Guillorn, D. H. Lowndes, and M. L. Simpson, Appl. Phys. Lett. **79**, 2970 (2001).
[2]M. S. Bell, K. B. K. Teo, and W. I. Milne, J. Phys. D: Appl. Phys. **40**, 2285 (2007).
[3]M. Su, B. Zheng, and J. Liu, Chem. Phys. Lett. **322**, 321 (2000).
[4]L. Delzeit, B. Chen, A. Cassell, R. Stevens, C. Nguyen, and M. Meyyappan, Chem. Phys. Lett. **348**, 368 (2001).
[5]L. Delzeit, I. McAninch, B. A. Cruden, D. Hash, B. Chen, J. Han, and M. Meyyappan, J. Appl. Phys. **91**, 6027 (2002).
[6]V. Kayastha, Y. K. Yap, S. Dimovski, and Y. Gogotsi, Appl. Phys. Lett. **85**, 3265 (2004).
[7]W. Mi, J. Y. Lin, Q. Mao, Y. Li, and B. Zhang, J. Natural Gas Chem. **14**, 151 (2005).
[8]M. Jung, K. Y. Eun, J.-K. Lee, Y.-J. Baik, K.-R. Lee, and J. W. Park, Diamond Relat. Mater. **10**, 1235 (2001).
[9]Y. K. Yap, V. Kayastha, S. Hackney, S. Dimovski, and Y. Gogotsi, Mater. Res. Soc. Symp. Proc. **818**, M11.31.1 (2004).
[10]W. Mi and D. Jia, J. Chil. Chem. Soc **55**, 153 (2010).
[11]H.-s. Qian, F.-m. Han, B. Zhang, Y.-c. Guo, J. Yue, and B.-x. Peng, Carbon **42**, 761 (2004).
[12]S. M. Toussi, A. Fakhru'l-razi, A. L. Chuah, and A. R. Suraya, Sains Malays. **40**, 197 (2011).
[13]G. F. Malgas, C. J. Arendse, N. P. Cele, and F. R. Cummings, J. Mater. Sci. **43**, 1020 (2008).
[14]C. Reynolds, B. Duong, and S. Seraphin, J. Undergrad. Res. Phys. **23**, 27 (2010).
[15]I. B. Denysenko, S. Xu, J. D. Long, P. P. Rutkevych, N. A. Azarenkov, and K. Ostrikov, J. Appl. Phys. **95**, 2713 (2004).
[16]W. B. Choi, J. U. Chu, K. S. Jeong, E. J. Bae, J.-W. Lee, J.-J. Kim, and J.-O. Lee, Appl. Phys. Lett. **79**, 3696 (2001).
[17]W. A. De Heer, A. Chatelain, and D. A. Ugarte, Science **270**, 1179 (1995).
[18]W. B. Choi, D. S. Chung, J. H. Kang, H. Y. Kim, Y. W. Jin, I. T. Han, Y. H. Lee, J. E. Jung, N. S. Lee, G. S. Park, and J. M. Kim, Appl. Phys. Lett. **75**, 3129 (1999).
[19]W. I. Milne, K. B. K. Teo, G. A. J. Amaratunga, P. Legagneux, L. Gangloff, J.-P. Schnell, V. Semet, V. T. Binh, and O. Groening, J. Mater. Chem. **14**, 933 (2004).
[20]W. I. Milne, K. B. K. Teo, M. Mann, I. Y. Y. Bu, G. A. J. Amaratunga, N. De Jonge, M. Allioux, J. T. Oostveen, P. Legagneux, E. Minoux, L. Gangloff, L. Hudanski, J.-P. Schnell, D. Dieumegard, F. Peauger, T. Wells, and M. El-Gomati, Phys. Status Solidi A **203**, 1058 (2006).
[21]H. Li, J. Li, and C. Gu, Carbon **43**, 849 (2005).
[22]B. Gruner, M. Jag, A. Stibor, G. Visanescu, M. Haffner, D. Kern, A. Gunther, and J. Fort agh, Phys. Rev. A **80**, 063422 (2009).
[23]M. Sode, T. Schwarz-Selinger, and W. Jacob, J. Appl. Phys. **114**, 063302 (2013).
[24]H. Mehdipour, K. Ostrikov, and A. E. Rider, Nanotechnology **21**, 455605 (2010).
[25]M. A. Lieberman and A. J. Lichtenberg, *Principles of Plasma Discharges and Materials Processing* (Wiley Interscience Publication, USA, 1994).
[26]See http://www.physics.usyd.edu.au/~mmmb/plasma/Chapter5.pdf for Home Page of School of Physics, University of Sydney.
[27]K. Ostrikov and S. Xu, *Plasma Aided Nanofabrication: From Plasma Sources to Nanoassembly* (Wiley-VCH, Weinheim, Germany, 2007).
[28]A. Tewari and S. C. Sharma, Phys. Plasmas **21**, 063512 (2014).
[29]O. A. Louchev, C. Dussarrat, and Y. Sato, J. Appl. Phys. **86**, 1736 (1999).
[30]H. Chatham, D. Hils, R. Robertson, and A. C. Gallagher, J. Chem. Phys. **79**, 1301 (1983).
[31]R. L. Mills, P. C. Ray, B. Dhandapani, R. M. Mayo, and J. He, J. Appl. Phys. **92**, 7008 (2002).
[32]S. K. Srivastava, A. K. Shukla, V. D. Vankar, and V. Kumar, Thin Solid Films **492**, 124 (2005).
[33]I. Denysenko and N. A. Azarenkov, J. Phys. D: Appl. Phys. **44**, 174031 (2011).
[34]M. S. Sodha, S. Misra, S. K. Mishra, and S. Srivastava, J. Appl. Phys. **107**, 103307 (2010).
[35]I. Denysenko, K. Ostrikov, M. Y. Yu, and N. A. Azarenkov, J. Appl. Phys. **102**, 074308 (2007).
[36]G. Burmaka, I. B. Denysenko, K. Ostrikov, I. Levchenko, and N. A. Azarenkov, Plasma Process. Polym. **11**, 798 (2014).
[37]M. A. Everest, J. C. Poutsma, J. E. Flad, and R. N. Zare, J. Chem Phys. **111**, 2507 (1999).
[38]P. A. Gartaganis and C. A. Winkler, Can J. Chem. **34**, 1457 (1956).
[39]Y. K. Yap, S. Kida, T. Aoyama, Y. Mori, and T. Sasaki, Appl. Phys. Lett. **73**, 915 (1998).

International Journal of Current Engineering and Technology
E-ISSN 2277 – 4106, P-ISSN 2347 – 5161

Available at http://inpressco.com/category/ijcet

Research Article

Failure analysis of Magnetorheological Brake

Lijesh K.P.†* and Chiranjit Sarkar‡

†,Mechanical Department, Indian Institute of Technology Delhi, New Delhi, India.
‡Mechanical Delhi Technological University, Delhi, New Delhi, India.

Accepted 01 April 2015, Available online 07 April 2015, **Vol.5, No.2 (April 2015)**

Abstract

Magnetorheological (MR) fluids alter their flow resistance as a function of the magnetic field. The variation in flow resistance is rapid and completely reversible and due to this MR fluids have been used in Braking applications. In the present paper, a MR Brake experimental setup, developed to evaluate the torque performance of MR brake, has been detailed. The measured torque values were compared with the estimated torque values and errors in the experimental values compared to theoretical torque values as a function of rotational speed have been presented. To investigate the reason for the variations, the vibration of MR disc was measured using proximity sensor. Based on the obtained results from proximity sensor the setup was modified. A comparison among the vibration signals measured on test setups (before modification and after modifications) has been presented.

Keywords: *MR brake, roller bearing, vibration, torque.*

1. Introduction

There is a trend to replace conventional hydraulic disk brakes with Magneto-Rheological (MR) brake (Sarkar and Hirani, 2015, Sarkar and Hirani, 2013, Sarkar and Hirani, 2013, Sarkar and Hirani, 2013, Sarkar and Hirani, 2013, Sukhwani, Hirani, 2008, Sukhwani *et al*, 2008, Sukhwani, Hirani, 2008, Sukhwani *et al*, 2009, Sukhwani *et al*, 2007). The MR brake, having time invariant friction performance, is an active system and its response is far better than that of hydraulic disk brakes.

The MR brake consisting a rotating disk, MR fluid (Hirani and Manjunatha, 2007), electromagnet (core+coil), seals, bearings and housing is shown in figure 1. For developing MR fluid, powder (micro-nano size) of material having high magnetic permeability and saturation (for e.g. iron powder) are used (Sarkar, Hirani, 2013). These particles are dispersed in a non-magnetic carrier fluid. Seal (Hirani and Goilkar, 2011, Goilkar and Hirani, 2009, Goilkar and Hirani, 2009, Goilkar and Hirani, 2009, Goilkar and Hirani, 2010), brakes are provided to stop the leakage of the fluid from the housing. The bearings (Hirani *et al*, 1998, Hirani *et al*, 1999, Hirani *et al*, 2000, Hirani *et al*, 2000, Hirani *et al*, 2001, Hirani *et al*, 2001, Hirani, 2004, Hirani, 2005, Hirani, Suh, 2005, Hirani, Samanta, 2007, Hirani, 2009, Hirani, Verma, 2009, Lijesh, Hirani, 2014, Lijesh, Hirani, 2015, Lijesh, Hirani, 2015, Lijesh, Hirani, 2015, Muzakkir *et al*, 2011, Muzakkir *et al*, 2013, Muzakkir *et al*, 2014, Muzakkir *et al*, 2015, Rao *et al*, 2000, Hirani, Samanta, 2007, Shankar *et al*, 2006, Lords, 2012) are required to bear the load of the flywheel (which provides required inertia to the system).

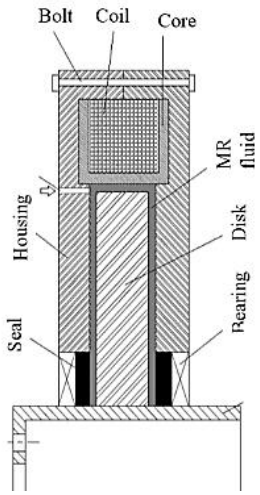

Fig. 1 Asymmetric Sketch of MR Brake

The MR brakes are actuated by passing the magnetic field through the magnetic particles with the help of current carrying electromagnet. On the application of magnetic field, MR fluid changes its state from liquid to semi-solid by aligning magnetic particles in chains. The formation of chain is shown in figure 2. Due to such chaining action, yield strength of fluid increases, friction between disk and housing (Fig. 1) increases and as a result the braking occurs.

*Corresponding author: **Lijesh K.P.**

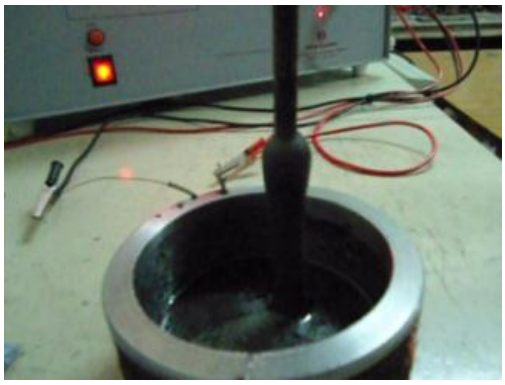

Fig. 2 Chair formation of MR particles with supply of current

Sukhwani, Hirani, (Sukhwani, Hirani, 2008) designed a MR brake for high rotational speed up to 2000 rpm. Sukhwani and Hirani (Sukhwani, Hirani, 2008) concluded that, effectiveness of MR brake reduces at high speeds due to shear thinning of MR fluid. Therefore, to make MR brake more effective at higher speed operation, one needs to think of 'Shear stable MR fluid'. To investigate this phenomenon a MR brake a test setup was developed in the laboratory. Initial study on test setup showed enormous variation between the theoretical and experimental frictional torque values. The measured experimental frictional torque values were higher than the estimated theoretical torque values, which motivated to investigate the test setup. Moreover it was observed that the one of natural frequency of the test setup was close to operational speed of rotating disk. In the present work, experimental investigation is carried out by measuring the displacement of the shaft using proximity sensor at different rotational speed of MR brake and theoretical natural frequency of the system was estimated by using Dunkerley's method (Budynas, Nisbett, 2011). Based on the obtained results the necessary modifications have been incorporated.

2. Braking Torque

The MR brake experimental setup used for the present work is shown in figure 3. It consists of 2 HP DC motor. The speed of the motor is controlled by using the speed controller. A flywheel is mounted between the DC motor and the MR brake through bearing bracket, jaw coupling and flexible coupling. A DC power supply (30 V and 5 A) is used to control the current to the electromagnet of MR brake. The speed of the motor was measured by using tachometer. The experimental torque for the present work was calculated using the instantaneous power drawn from the motor at particular rotational speed.

The theoretical torque for the present work is estimated using following formula (Sukhwani, Hirani, 2008, Sukhwani *et al* 2009, Sukhwani, Hirani, 2008, Sarkar and Hirani (accepted), Sarkar,)

$$T = 2\pi h \tau_{yd}\left(r_2^2 - r_1^2\right) + \frac{4}{3}\eta\pi\omega\left(r_2^3 - r_1^3\right) \quad (1)$$

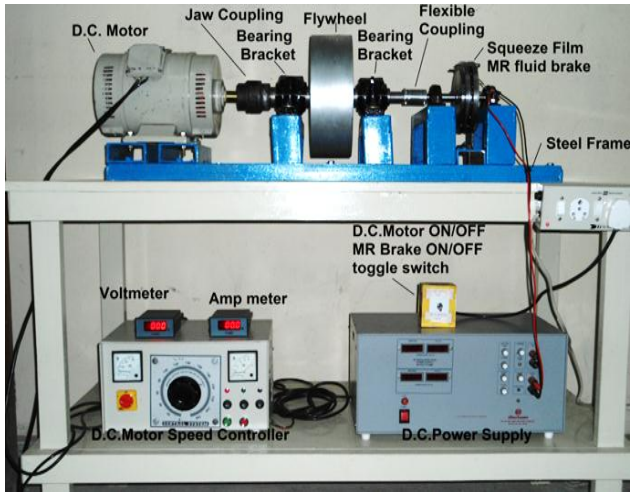

Fig 3 Experimental set for MR brake

Where h is the gap between the rotor and housing filled with MR fluid, τ_{yd} is the yield stress function of magnetic field, η is the viscosity of the MR fluid, ω is angular velocity of the disk brake, r_2 is the outer radius of the disk and r_1 is the radius of the shaft as shown in figure 4.

To study the braking torque of MR brake, r_1=55 mm, r_2=196 mm and h=1mm (parameters used to develop MR brake) were considered. The approximate BH polynomial curve polynomial curve (Budynas, Nisbett, 2011) is given by

$$B = -10^{-11}H^2 + 6\times10^{-6}H + 0.156 \quad (2)$$

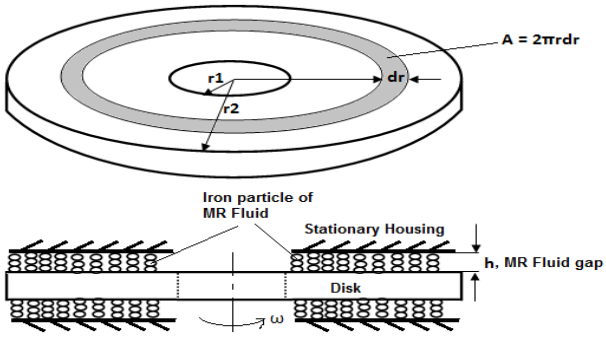

Fig 4 Schematic figure of MR brake

The magnetic field intensity (H=NI/2h) of the MR fluid is in kA/m. The estimated values of torque using equation (1) and experimentally predicted values of torque are plotted in the figure 5. From this figure, huge difference between the experimental and theoretical values as a function of operating speed is observed. In the following section the reason for the deviation in torque values has been detailed.

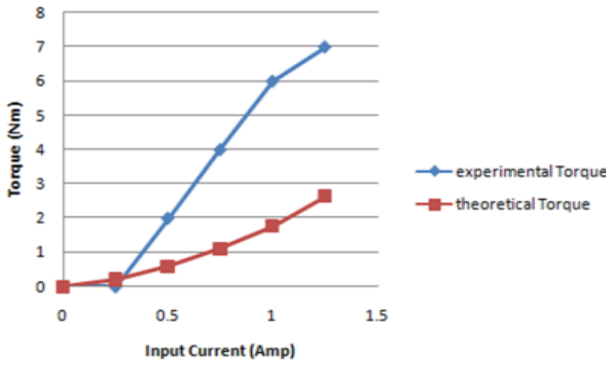

Fig. 5 Experimental and theoretical torques

3. Results and Discussion

To investigate the reason for the variation of the torque, the original setup was modified (as shown in figure 6) to measure the displacement of the disk using proximity sensor.

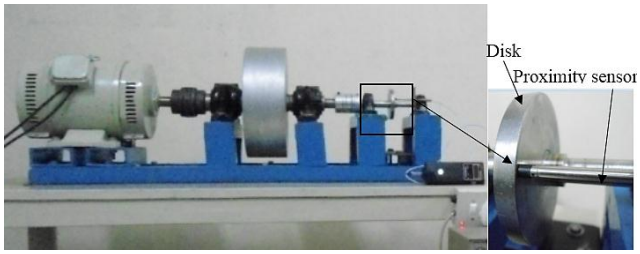

Fig. 6 Modified setup to measure the deflection of disk

The deflection data measured at various speeds using the proximity sensor are plotted in figure 7. From this figure it can be observed the lateral deflection of rotating disc is varying between 0.1 mm to 0.18mm. In theoretical calculations, it is assumed that there will not be any lateral deflection of the disc. To reduce the vibration of the system rubber padding (isolation) was provided as shown in figure 8.

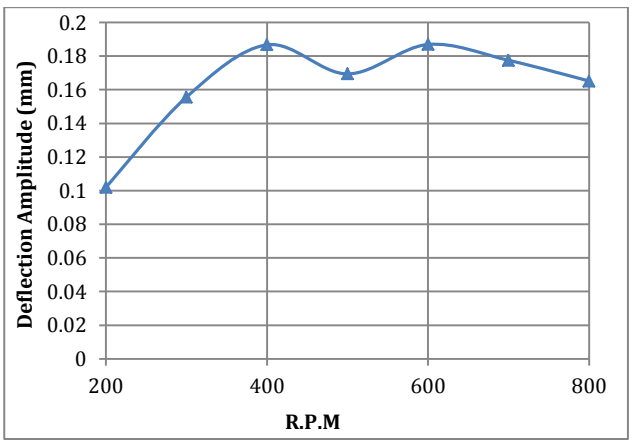

Fig. 7 Proximity sensor signal at different RPM

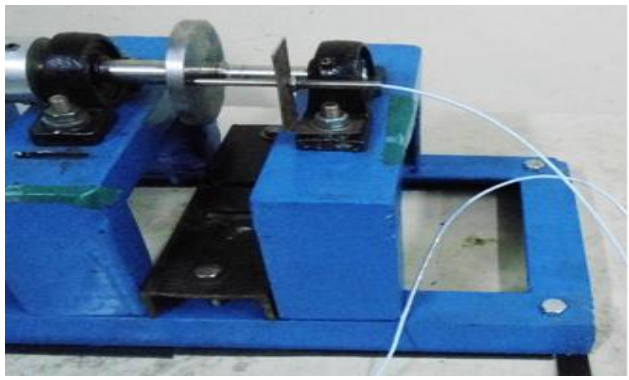

Fig. 8 Rubber padding

In the addition to installing rubber pads, the need to re-grease the bearings was identified. The grease of ball bearing had become black in color (probably due to impurities) as shown in figure 9(a). After completely de-greasing the bearing, the new lithium based grease was applied as shown in figure 9(b).

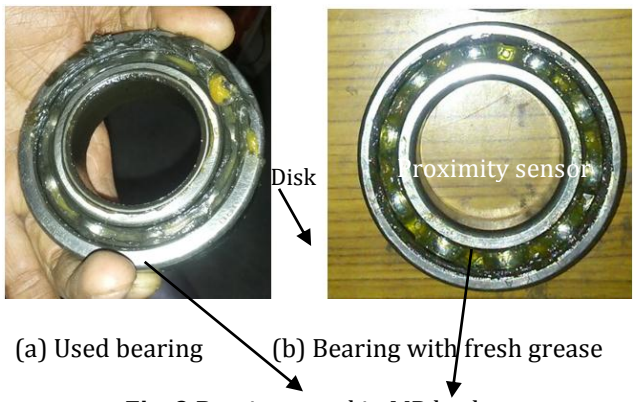

Fig. 9 Bearings used in MR brakes

After using the rubber padding and reapplying the grease in the bearing, the displacement signals were measured. The results are plotted in figure 10. From this figure it can be observed that the vibration of the signal has reduced to great extent, hence proving the rubber pad (isolation) and greasing are necessary for MR brake system.

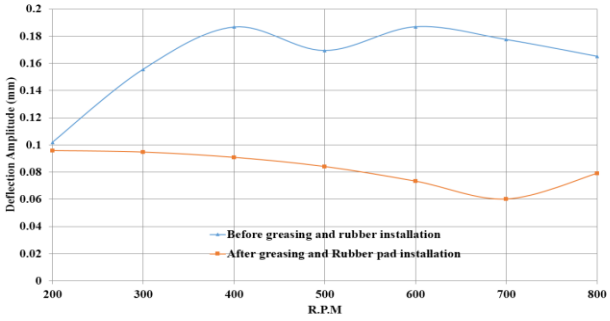

Fig. 10 Proximity sensor signal before and after applying greasing and padding at different RPM

From figure 10 it is observed that the vibration (deflection) is the maximum at 300-400 RPM. To

investigate the reason for such low natural frequency, theoretical study was performed using Dunkerley's method (Budynas, Nisbett, 2011). This method estimates fundamental critical speed of shaft carrying a number of components (gears (Shah, Hirani, 2014, Hirani 2009), pulley, coupling, etc.). The system is divided into number of subsystems based on components. Using this method critical speed of each individual subsystem is estimate by direct formula. To implement this formula, a block diagram of the MR brake system is shown in figure 11.

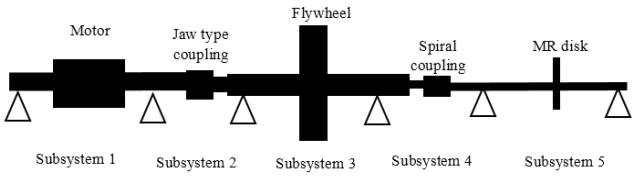

Fig. 11 Subsystems and components of MR brake test setup

In the present system there are total five subsystems. The subsystems 3 is expected to provide more vibration and to reduce the critical speed due to the load of flywheel. To estimate the critical frequency of this subsystem (Fig. 12) following equation is used.

$$f_n = \frac{1}{2\pi}\sqrt{\frac{K}{M}} \tag{3}$$

Where; $K = \frac{P}{\delta}$ and $\delta = \frac{Pl^3}{48EI} \Rightarrow K = \frac{48EI}{l^3}$

and $f_n = \frac{1}{2\pi}\sqrt{\frac{48E\left(\frac{1}{2}mR^4\right)}{Ml^3}} \Rightarrow f_n = \frac{1}{2\pi}\sqrt{\frac{48mER^2}{2Ml^3}} \Rightarrow$

$$f_n = \frac{1}{2\pi}\sqrt{\frac{48\times 209\times 10^9 \times 6\times 0.025^4}{2\times 26\times 0.218^3}}$$

$$\Rightarrow f_n = 1.0514\times 10^3 rad/sec \Rightarrow f_n = 167.27 Hz$$

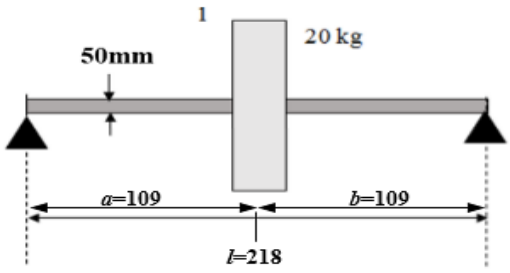

Fig. 12 Free body diagram of sub system 3

The estimated natural frequency of the sub system 3 (ω3) using the equation (3) is 167.27 Hz which is very high compared to the natural frequency occurred in the experimental setup (6.67Hz). This indicates that the subsystem 3 is not the reason for providing low natural frequency. The theoretical study was extended to subsystem 4, consisting a low bending stiffness (can be observed from figure 13) spiral coupling.

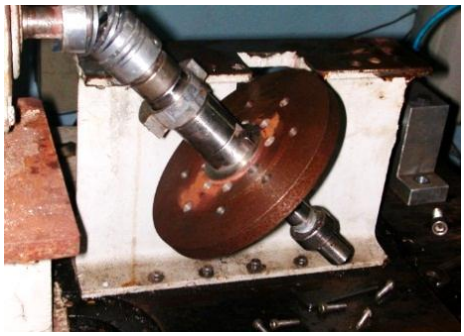

Fig. 13 Failure of Spiral coupling

Due to the low bending stiffness subsystem makes it a weak link. A block diagram of the subsystem 4 is shown in figure 14. The critical frequency estimated for the subsystem 4 having spiral coupling of dimension 60mm length and 40mm diameter, Young's modulus of 10MPa is 9.13Hz.

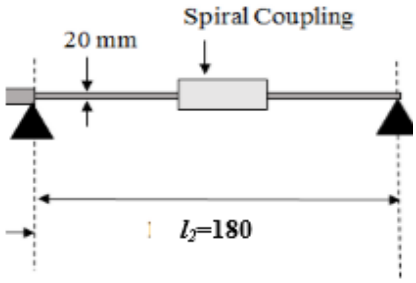

Fig. 14 Block diagram of subsystem 4

Hence from this theoretical study it is concluded that the spiral coupling has reduced the natural frequency of the system. Hence for any system the spiral coupling should not be used or if it is used then the system must be operated lesser the estimated critical speed or appropriate damping system must be provided to reduce the vibration.

Conclusion

To evaluate the performance of the MR brake, a test setup was developed and experiments were performed to measure the frictional torque. The comparison in the theoretical and experimental values of frictional torque revealed errors. Detailed theoretical and experimental investigations were performed and it was found the higher system vibration was the reason for such deviations. The vibration in the system is reduced by

- By providing isolation using rubber padding between the system and foundation
- Application of proper greasing on the ball bearings.
- Replacing the spiral coupling with rigid coupling.

Acknowledgment

This research was supported by Council of Scientific and Industrial Research, New Delhi, India [Grant No. 70(0073)/2013/EMR-II].

References

Sarkar, C. & Hirani, H., (2015), Development of magnetorheological brake with slotted disc, *Proc. IMechE, Part D: Journal of Automobile Engineering*, DOI: 10.1177/0954407015574204.

Sarkar, C. & Hirani, H., (2013),Theoretical and experimental studies on a magnetorheological brake operating under compression plus shear mode, *Smart Materials and Structures*, vol.22. no.11, art. no. 115032

Sarkar, C. & Hirani, H., (2013), Synthesis and Characterization of Antifriction Magnetorheological Fluids for Brake, *Defense Science Journal*, vol. 63, no.4, pp.408-412.

Sarkar, C. & Hirani, H., (2013), Design of a Squeeze Film Magnetorheological Brake Considering Compression Enhanced Shear Yield Stress of Magnetorheological Fluid, *Journal of Physics: Conference Series*, vol.412, no.1, 012045.

Sarkar, C. & Hirani, H., (2014), Effect of particle size on shear stress of magnetorheological fluids, Smart Science, http://dx.doi.org/10.6493/SmartSci.2015.317.

Sukhwani, V. K., Hirani, H., (2008),A Comparative Study of Magnetorheological-Fluid-Brake and Magnetorheological-Grease-Brake, *Tribology Online*, vol 3, no.1, pp. 31-35.

Sukhwani, V. K., Hirani, H., & Singh, T. (2008), Synthesis and Performance Evaluation of MR Grease, *NLGI Spokesman,* vol. 71, no.10.

Sukhwani, V. K. & Hirani, H., (2008),Design, Development and Performance Evaluation of High Speed MR Brake, *Proc. Institute Mech. Engineers., Part L, Journal of Materials: Design and Applications*, vol. 222, no.1, pp. 73-82.

Sukhwani, V. K., Hirani, H., & Singh, T. (2009), Performance Evaluation of a Magnetorheological Grease Brake, *Greasetech India*, vol. 9, no.4, pp. 5-11.

Sukhwani, V. K., Hirani, H., & Singh, T. (2007),Synthesis of Magnetorheological (MR) Grease, *Greasetech* India.

Hirani, H. & Manjunatha, C. S., (2007),Performance Evaluation of Magnetorheological Fluid Variable Valve, *Proc. of the Institution of Mechanical Engineers, Part D, Journal of Automobile Engineering*, vol. 221, no.1, pp. 83-93.

Hirani, H. & Goilkar, S.S., (2011), Rotordynamic Analysis of Carbon Graphite Seals of a Steam Rotary Joint , *Book on IUTAM Symposium on Emerging Trends in Rotor Dynamics*, 253-262, Springer Netherlands.

Goilkar S S, and Hirani H., (2009) ,Design and development of test setup for online wear monitoring of mechanical face seals using torque sensor, *Tribology Transactions*, vol. 52, no.1, pp. 47-58.

Goilkar, S.S. & Hirani, H. (2009), Tribological Characterization of Carbon Graphite Secondary Seal *Indian Journal of Tribology*, vol. 4, no. 2, pp. 1-6.

Goilkar, S.S. & Hirani, H. (2009) Tribological Characterization of Carbon Graphite Secondary Seal *Indian Journal of Tribology*, vol. 4, no. 2, pp. 1-6.

Goilkar, S.S. & Hirani, H. (2010),Parametric Study on Balance Ratio of Mechanical Face Seal in Steam Environment, *Tribology International*, vol. 43, no. 5-6, pp. 1180-1185.

Hirani, H. & Goilkar, S.S., (2009),Formation of Transfer Layer and its Effect on Friction and Wear of Carbon-Graphite Face Seal under Dry, Water and Steam Environments, *Wear*, vol. 226, no. 11-12, pp.1141-1154.

Hirani, H., Athre, K., Biswas, S. (1998), Rapid and Globally Convergent Method for Dynamically Loaded Journal Bearing Design, *Proc. IMechE (UK), Journal of Engineering Tribology*, vol. 212, pp. 207-214.

Hirani, H., Athre, K., Biswas, S. (1999), Dynamic Analysis of Engine Bearings, *International Journal of Rotating Machinery*, vol. 5, no.4, pp. 283-293.

Hirani, H., Athre, K., Biswas, S. (2000), A Hybrid Solution Scheme for Performance Evaluation of Crankshaft Bearings, *Trans. ASME, Journal of Tribology*, vol. 122, no. 4, pp. 733-740.

Hirani, H., Athre, K., Biswas, S. (2000), Transient Trajectory of Journal in Hydrodynamic Bearing, *Applied Mechanics and Engineering*. vol. 5, no 2.

Hirani, H., Athre, K., Biswas, S. (2001), A Simplified Mass Conserving Algorithm for Journal Bearing under Dynamic Loads, *International Journal of Rotating Machinery*, vol. 1, pp. 41-51.

Hirani, H., Athre, K., Biswas, S. (2001), Lubricant Shear Thinning Analysis of Engine Journal Bearings, *STLE, Journal of Tribology Transaction*, vol 44, no. 1, pp 125-131.

Hirani, H., Athre, K., Biswas, S. (2002), Comprehensive Design Methodology for Engine Journal Bearing, *IMechE (UK), Part J, Journal of Engineering Tribology*, vol 214, pp. 401-412.

Hirani, H. (2004), Multi-objective Optimization of a journal bearing using the Pareto optimal concept, *Proc. Institute Mech. Engineers., Part J, Journal of Engineering Tribology*, vol. 218, no. 4, pp. 323-336.

Hirani, H. (2005), Multiobjective optimization of journal bearing using mass conserving and genetic algorithms, *Proc. Institute Mech. Engineers., Part J, Journal of Engineering Tribology*, vol. 219, no. 3, pp. 235-248.

Hirani, H., & Suh, N. P. (2005), Journal Bearing Design using Multi-objective Genetic Algorithm and Axiomatic Design Approaches, *Tribology International*, vol. 38, no. 5, pp. 481-491.

Hirani, H., Samanta, P. (2007), Hybrid (Hydrodynamic + Permanent Magnetic) Journal Bearings, Proc. Institute Mech. Engineers., *Part J, Journal of Engineering Tribology*, vol. 221, no. J8, pp. 881-891.

Hirani, H. (2009),Root cause failure analysis of outer ring fracture of four row cylindrical roller bearing, *Tribology Transactions*, vol.52, no.2, pp.180-190.

Hirani, H., & Verma, M. (2009), Tribological study of elastomeric bearings of marine shaft system, *Tribology International*, vol. 42, no. 2, pp. 378-390.

Lijesh, K. P., Hirani, H., (2014), Stiffness and Damping Coefficients for Rubber mounted Hybrid Bearing, *Lubrication Science*, vol. 26, no.5, pp. 301-314.

Lijesh, K. P., Hirani, H., (2015), Development of Analytical Equations for Design and Optimization of Axially Polarized Radial Passive Magnetic Bearing, *ASME, Journal of Tribology*, vol. 137, no. 1, (9 pages).

Lijesh, K. P., Hirani, H., (2015), Optimization of Eight Pole Radial Active Magnetic Bearing, *ASME, Journal of Tribology*, vol.137, no.2.

Lijesh, K. P. & Hirani, H. (2015), Design and Development of Halbach Electromagnet for Active Magnetic Bearing, *Progress In Electromagnetics Research C*, vol. 56, 173–181.

Muzakkir, S.M., Hirani, H., Thakre, G.D., Tyagi, M.R. (2011), Tribological Failure Analysis of Journal Bearings used in Sugar Mill, *Engineering Failure Analysis*, vol. 18, no. 8, pp. 2093-2103.

Muzakkir, S.M., Hirani, H., Thakre, G.D., (2013), Lubricant for Heavily-Loaded Slow Speed Journal Bearing, Tribology Transactions, vol.56, no. 6, pp. 1060-1068.

Muzakkir, S.M., Lijesh, K. P. & Hirani, H. (2014), Tribological Failure Analysis of a Heavily-Loaded Slow Speed Hybrid Journal Bearing, *Engineering Failure Analysis*, vol. 40, pp.97–113.

Muzakkir, S.M., Lijesh, K. P., Hirani, H., Thakre, G.D. (2015) Effect of Cylindricity on the Tribological Performance of Heavily-Loaded Slow Speed Journal Bearing, Proc. Institute Mech. Engineers., *Part J, Journal of Engineering Tribology*, 2015, vol 229, no.2, pp.178-195.

Muzakkir, S.M. & Hirani, H. (2015), A Magnetorheological Fluid Based Design Of Variable Valve Timing System For Internal Combustion Engine UsingAxiomatic Design, International Journal of Current Engineering Research, Vol.5, No.2 (April 2015), pp 603-612.

Rao, T. V. V. L. N., Hirani, H., Athre, K., Biswas, S. (2000), An Analytical Approach to Evaluate Dynamic Coefficients and Non-linear Transient Analysis of a Hydrodynamic Journal Bearing, *STLE Tribology Transactions*, vol. 23, no.1, pp. 109-115.

Samanta, P., Hirani, H., (2007), A Simplified Optimization Approach for Permanent Magnetic Journal Bearing, *Indian Journal of Tribology*.

Shankar, S., Sandeep, Hirani, H. (2006), Active Magnetic Bearing, *Indian Journal of Tribology*, pp 15-25.

Shah, H. & Hirani, H. (2014), Online Condition Monitoring of Spur Gear, *International Journal of Condition Monitoring*, vol 4, no. 1, pp.15-22.

Hirani, H. (2009), Online Wear Monitoring of Spur Gear, *Indian Journal of Tribology*, vol 4, no.2, pp.38-43.

Lord Corporation, http://www.lord.com/, visited on 20.03.2012.

R.G.Budynas, J.K.Nisbett, (2011), Shigley's Mechanical Engineering Design, Ninth edition, McGraw Hill education (India Private Limited), New Delhi, 2011.

International Journal of Current Engineering and Technology
E-ISSN 2277 – 4106, P-ISSN 2347 – 5161

Available at http://inpressco.com/category/ijcet

Research Article

Frictional Characteristics of Brake Pads using Inertia Brake Dynamometer

Chiranjit Sarkar†* and Harish Hirani‡

†Mechanical Engineering Department, Delhi Technological University, Shahbad Daluatpur, Bawana Road, Delhi – 110042, India
‡Mechanical Engineering Department, Indian Institute of Technology Delhi, Hauz Khas, New Delhi – 110016, India

Accepted 22 March 2015, Available online 05 April 2015, **Vol.5, No.2 (April 2015)**

Abstract

The conventional disc wears out and brake pollutes the environment. In addition, localized heating occurs in the conventional disc brake. To tackle both of these problems, conventional disc brakes can be replaced with magnetorheological (MR) fluids brakes. MR fluids are materials having shear yield stress as a function of magnetic field. On the application of magnetic field, MR particles get aligned and increase shear resistance between relatively moving surfaces. The friction between stator and rotor increases and fulfils the braking function, which means MR fluids can be used as brake friction materials. Understanding of friction behavior is the key factor of satisfactory & reliable working of the brake system. To characterize the friction behavior of MR brake, there is a need to understand the friction behavior of conventional disc brake system. In this research work, experiments have been done to characterize the frictional characteristics of Volvo disk brake system using full-scale brake inertia dynamometer.

Keywords: *Full scale brake inertia dynamometer, Volvo disk brake, Pressure speed sensitivity, bade-recovery behavior.*

1. Introduction

Magnetorheological (MR) brake (Sarkar and Hirani, 2015), (Sarkar and Hirani, 2013), (Sukhwani, *et al*, 2009), (Sukhwani and Hirani, 2008), (Sukhwani and Hirani, 2008), (Hirani and Manjunatha, 2007), (Sukhwani, *et al*, 2007), (Sukhwani, *et al*, 2006), (Gupta and Hirani, 2011), (Muzakkir and Hirani, 2015), (Muzakkir, *et al*, 2015) is a device, where MR fluids are used as brake friction materials. Successful development of MR brake requires an extensive study of the existing brake technologies, working knowledge of MR fluids, broad practice on existing brake inertia dynamometer and theoretical knowledge of electromagnetic field. Therefore in this research work, experiments on existing brake inertia dynamometer using disk pad brake system have been done. The test set up is fully computerized and it can be programmed for any test schedule. The test setup is equipped with 175 kW variable speed (100 rpm to 1550 rpm) DC motor with a feedback system. To maintain complete safety, there is a provision for emergency pneumatic brake.

A good understanding of friction behavior is the key factor of satisfactory & reliable working of the brake system. FMs (Friction Materials) are required to have certain performance characteristics such as, low fade & high recovery of, good pressure – speed sensitivity characteristics etc., to make these material suitable to automotive application. To ensure the required characteristics, FMs are subjected to laboratory and field tests. While vehicle tests are expensive and time consuming; brake inertia dynamometer tests in the laboratory are faster and economic to verify friction material characteristics. IBD incorporating full-size brakes can simulate vehicle tests reasonably well. These dynamometers consisting of motor, inertial wheels & load measuring device can be tuned to simulate the real-test conditions by using a suitable application software package to control of operating parameters viz. braking pressure, RPM, and temperature as per input schedule (s).

Figure 1 shows a block diagram of a full scale IBD. Simply, it consists of a motor controlled by variable speed drive with suitable application package to vary & count speed-up time and measure torque using load cell arrangement. The analog outputs from the various sensors suitably signal conditioned & fed to the interface card of the computer containing application package, make whole arrangement in close loop control. Tribo-evaluation tests conducted on full scale IBD can be mainly categories into: effectiveness (Pressure-speed sensitivity) & fade-recovery (Temperature sensitivity) studies. The first one measures stopping efficiency of FMs subjected to variable load and speed conditions, while fade-recovery study is related to the loss of braking performance at elevated temperatures and the revival

*Corresponding author: **Chiranjit Sarkar**

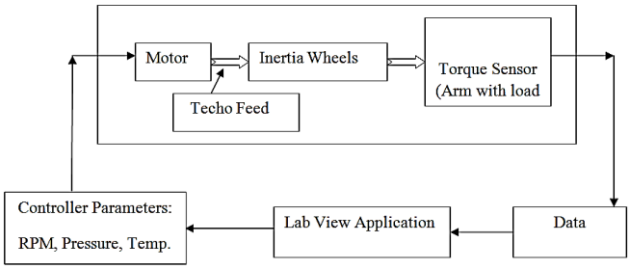

Fig.1 Block diagram of Full scale IBD

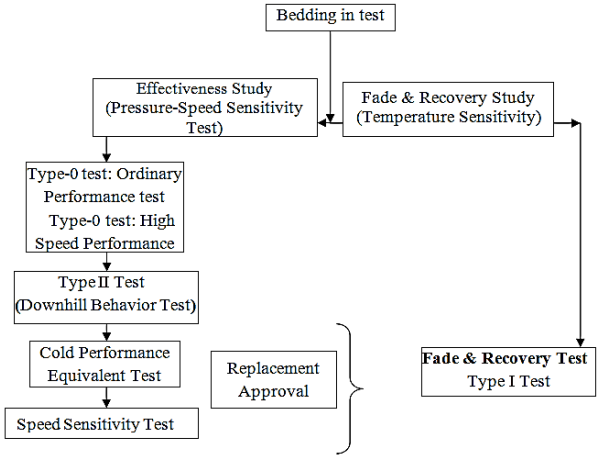

Fig.2 Methodology flow chart

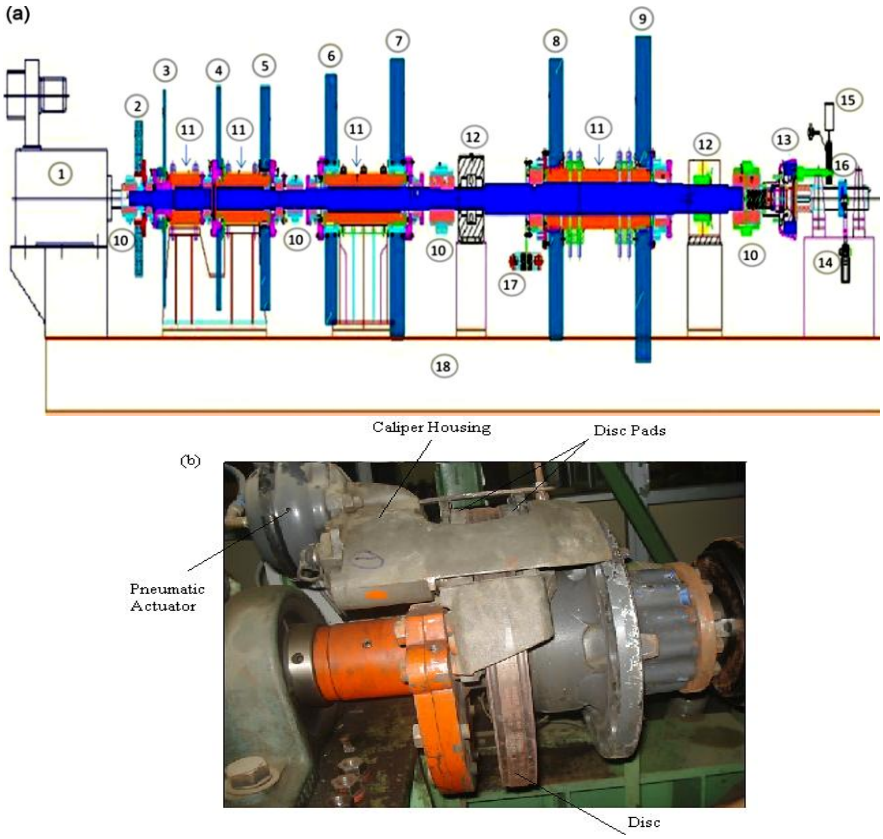

Figure 3 (a) & (b) Schematic of Full scale Inertia Brake Dynamometer :(1) motor, (2) flywheel of 0.5 kg-m sq, (3) flywheel of 2 kg-m sq, (4) flywheel of 4 kg-m sq, (5) flywheel of 8 kg-m sq, (6) flywheel of16 kg-m sq, (7) and (8) flywheel of 32 kg-m sq, (9) flywheel of 64 kg-m sq, (10) couplings, (11) housings, (12) shaft bearings, (13) braking assembly, (14) load cell, (15) air chamber,(16) torque arm, (17) emergency brakes, (18) dyno bed.

Fig.3 Sketch of Inertia Brake Dynamometer (Kumar, *et.al.*, 2009)

of the same at lower temperature. A definite methodology is required to evaluate the performance of friction material. Figure 2 illustrates the methodology followed in the present research work. The first step is to bed the brake as per manufacturer's bedding procedure to ensure at least 80% conformal contact area on the disk pads prior to start of ECE R90 test. The bedded brakes are then subjected to effectiveness test (Type-0, II, cold performance & speed sensitivity). Type-0 test is conducted under two different conditions viz. ordinary (low speed) & high speed conditions. In Type II test disk pads are tested to simulate downhill condition of laden vehicle running with 30Kmph on 2.5% down-gradient of 6 Km in gear disengaged condition. Type I test examines fade & recovery (temperature sensitivity) behavior of FMs.

2. Experimental Study on Inertia Dynamometer

An inertia dynamometer (Dyno) setup, shown in Figure 3 is a fully computerized automatic testing machine for four wheelers capable of performing brake test in both hydraulic as well as in air braking mode. The dynamometer applies variable inertial load on the 175 kW motor and measures the braking force, torque and the coefficient of friction through a computer utilizing Lab view(TM)-based software (version 4.0) connected to it. Its main chassis is of ladder type construction & fabricated out of I-section girders of about 300mm height with adequate diagonal members for rigidity. A fully solid state electronic variable speed drive having tachometer feedback is provided to vary motor speed from 100 RPM to 1550 RPM.

The drive motor is fixed on the separate box type bed which is mounted on the main chassis. The main shaft is directly coupled to the motor through gear coupling. There is provision of getting inertia values from 1.5 Kg-m sq to 153.5 Kg -m sq through careful combination of one fixed & ten attachable inertia wheels (Table 1). The temperature of the disk/drum is monitored by a non-contact IR sensor. The analog output from the sensor is suitably signal conditioned & fed to the interface card of the computer to monitor & control the temperature. The wheel temperature can be kept to desired level with a blower & duct arrangement. Table 2 lists the important technical specification of the inertia dynamometer.

The IBD is instrumented for continuous recording of rotational speed, brake torque, pressure in the brake line, braking time & brake rotor temperature, and number of rotations after brake application. Inertia value (as per ECE R90) norm was calculated considering 55% of the gross vehicle weight (GVW). Hence, wheel load of 4455 Kg with tyre rolling radius of 571 mm had given a total of 148.06 kg-sq m inertia value. Bedding tests were performed as per manufacturer's instruction. Table-3(a) and (b) provides important vehicle parameters & bedding schedule respectively. Gear drive coupling is used to engage and disengage the motor to the main shaft. Inertia is the governing parameter to simulate the braking performance as per the real condition, so the required inertia can be achieved with the help of inertia wheels, the inertia wheel can be engaged to the main driving shaft with the help of wheel drive coupling. The description of inertia wheels are shown in Table 1, if required inertia is 50 kgms^2 then by connecting wheels of inertia value 32, 16, 2 kgms^2 required inertia will be achieved.

The required inertia can be calculated as,
Required inertia = (mass on wheel × rolling radius (tyre radius))/gravity
For four wheeler,
Mass on wheel = ¼(Gross vehicle weight)
For two wheeler,
Mass on wheel = ½ (Gross vehicle weight)

Table 1 Inertia Wheels details

Wheel Type	Inertia Value (Kg-m sq.)	Total Number
Fixed	1.5	One
Attachable	0.5	One
	1.0	One
	2.0	One
	4.0	One
	8.0	Two
	16	Two
	32	One
	64	One

Table 2 Technical specification of IITD Full scale inertia dynamometer

Supplier	Pyramid Precision Engineering Pvt Ltd, Chennai, India
Motor	175 KW, 1500 rpm DC motor with external cooling motor
Max Motor torque	1000 kg-m
Base Speed	1400 rpm
Shaft Speed	1500 rpm
Min inertia	1.5 kg-m sq
Max inertia	1570 kg-m sq
No of wheels	11
Max braking torque	1000 kg-m
Max Pressure (Air)	10 Bar
Max Pressure (Hydraulic)	120 Bar
Gross vehicle weight (GVW) range	1000 kg – 16000 kg
Max. dissipated energy	20 MJ

Table 3(a) Vehicle Test Parameters for Volvo bus disc pad B7R Mark-II

Schedule	ECE R90
Gross vehicles weight (GVW)	16200 kg
Vehicle category	M3
Vehicle model	Volvo bus B7R Mark-II
Inertia	148.6 Kg-m sq
Rolling Radius (Tyre radius)	571 mm
Effective radius	172 mm

Table 3(b) Bedding test schedule

Test condition parameter	Value
Start speed	60Kmph
End speed	0
Controller mode	2bar (air-pressure)
Temperature	0-100˚ C
Wet	False
Pause	False
Blower	On

ECE R 90 test schedule was used in the study to test Volvo disk pad lining. Economic Commission for Europe Regulation 90 (ECE R90) is a European standard for brake components that requires brake manufacturers to conform and guarantee the original equipment standards as far as performance and quality is concerned.

Effectiveness studies (Pressure-speed sensitivity)

Effectiveness studies quantify the influence of operating parameters viz. pressure and speed on the braking performance. Type-0 & speed sensitivity test, specified in ECE R90 schedule, were used to measure performance of Volvo disc pad.

Type-0-Test

In type-0 ordinary performance test, Volvo pads were tested for eight brake applications at spaced intervals of line pressure (2-8 bar) at 60 and 40 Kmph respectively. A similar test was performed in Type-0 high performance for three brake applications at line pressure of 6, 6.5 and 7 bar with speed of 90 and 100Kmph respectively. As the severity of the braking increased consequently stopping distance decreased. However, this brought an increase in the average torque needed to stop the vehicle. Experimental design of this test is shown in Table-5.

Table 4 Vehicle categories according to UN ECE RE90

Vehicle Category		Description
Passenger Vehicle	M	4/3 wheeler, max weight < 1Metric ton
	M1	Carriage seats< 8 in addition the driver's seat
	M2	Carriage seats > 8 in addition the driver's seat, max weight< 5 Metric Ton
	M3	Carriage seats > 8 in addition the driver's seat, max weight> 5 Metric Ton
Goods Vehicle	N	4/3 wheeler, max weight > 1 Metric ton
	N1	Max weight < 3.5Metric Ton
	N2	3.5Metric Ton < Max weight < 12Metric Ton
	N3	Max weight > 12Metric Ton
Trailers	O	Trailers (including semi trailers)
	O1	Max. weight < 0.75Metric Ton
	O2	0.75Metric Ton <Max weight <3.5Metric Ton
	O3	0.75Metric Ton < Max weight < 3.5Metric Ton
	O4	Max. weight > 10 Metric Ton

Speed sensitivity test

Speed sensitivity test examines consistency of braking at specified speed (60, 80 & 110 Kmph) and pressure condition. A total of three snub braking operations with nominal release programmed at each test speeds corresponding to a constant braking pressure of 6.5bar. The experimental design for the test is shown in Table-6.

Fade & recovery behavior (Type-I)

Type-I test highlights effect of temperature on. In real life, heat fading occurs in case of constant brake actuation and make brake inefficient if, it can't fully absorb the developed heat. Brake pads & disc used in effectiveness studies were again reused in this study.

Table 5 Experimental design of Effectiveness test (Type-0)

Description	Braking Speed	Release Speed		Pressure		No of Cycles	Blower
	Kmph	rpm	Kmph	rpm	(bar)		
Type-0 Test (Ordinary performance test)	60	420	0	0	2, 3, 4, 5, 6, 6.5, 7 & 8	1 Stop @ Each Pressure	On
	40	280	0	0	2, 3, 4, 5, 6, 6.5, 7 & 8	1 Stop @ Each Pressure	On
Type-0 Test (High speed performance test)	90	630	0	0	6,6.5,7	3 Stop @ Each Pressure	On
	100	700	0	0	6,6.5,7	3 Stop @ Each Pressure	On

The test starts with three braking stops each at speed of 60 & 40Kmph respectively corresponding to a line pressure of 6.5bar. Temperature of the disc was kept

within 100deg. using air blower. After this, fade test was carried on using twenty snub braking application with speed of 60 (start) & 30Kmph (end). Temperature of the disk allowed rising freely in this segment by keeping air blower in off condition. Finally, after completion of the fade segment, one full braking stop performed at speed of 60 & 40Kmph each keeping blower still in off condition. Table-7 highlights experimental design of Type-I test.

Definition of required terms used in the Type-I test evaluation have been given below-

μ_{max} (fade)=highest recorded during fade test.

μ_{min} (fade)=lowest recorded during fade test.

% fade ratio= (μ_{min} / μ_{max})* 100

Table 6 Experimental design of speed sensitivity test

Description	Braking Speed		Release Speed		Pressure	No of Cycles	Blower
	Kmph	rpm	Kmph	rpm	(bar)		
Speed Sensitivity Test	60	420	30	210	6.5	3 Stop @ Each Pressure	On
	80	560	60	420	6.5	3 Stop @ Each Pressure	On
	110	770	80	560	6.5	3 Stop @ Each Pressure	On

3. Results and Discussions

Test results obtained in Type-0 & Type-I, were analyzed to extract useful information about friction characteristics of Volvo disc pad material. Effect of operating parameters viz. pressure & speed on μ should be as small as possible otherwise consistent braking performance will not be achieved. Plot of μ with respect to applied braking pressure shows Volvo disc pad sensitivity towards pressure. For an ideal FM, this curve should be straight (parallel to X-axis) with minimum undulation. High slope indicates greater sensitivity of μ with pressure. The difference in μ at selected pressure value indicates its sensitivity towards speed. Higher is the difference; consequently higher is the sensitivity of μ towards the speed variation.

The influence of speed on μ is expressed in terms of speed spread (%) which is calculated from the ratio of the μ at selected speed to that at lower speed. Variation in μ and SS (%) with respect to applied pressure (Type-0, ordinary) were shown in Figure-4(a) and 4(b) respectively. Figure 5(a) and 5(b) show corresponding graph of variation in μ_{Avg} & SS (%) with respect to applied pressure respectively (Type-0, high speed). With increase in pressure & speed μ decreased for all the cases. This happens due to fact that with increase in pressure real area of contact increases excessively & disproportionately as polymeric materials (disc FMs) are visco-elastic.

Table 7 Experimental design of Type-I test

Description		Braking Speed	Release Speed		Pressure		No of Cycles	Blower
		Kmph	rpm	Kmph	rpm	(bar)		
Type-I (Fade & Recovery test)	Cold Performance Test	60 & 40	420 & 280	0	0	6.5	3 Stop @ Each Pressure	On
		60	420	30	210	Corresponding to 0.31 g pressure at 1st stop & maintain in rest of cycles.	3 Stop @ Each Pressure	On
	Hot Performance	110	770	80	560	6.5	3 Stop @ Each Pressure	On

This leads to eventually disproportionately low reduction in pressure on the asperities in spite of increase in load. Hence, μ falls down. However, increase in speed affects μ differently. With increase in speed, μ generally doesn't show fixed trends. The μ value increased slightly, showed maximum followed by a sharp decrease in some cases (as in Figure-5(a)). Furthermore, increase in speed brought more frictional heat which easily caused μ to go down as it was highly temperature sensitive (see Figure 4(a) and 5(a)).

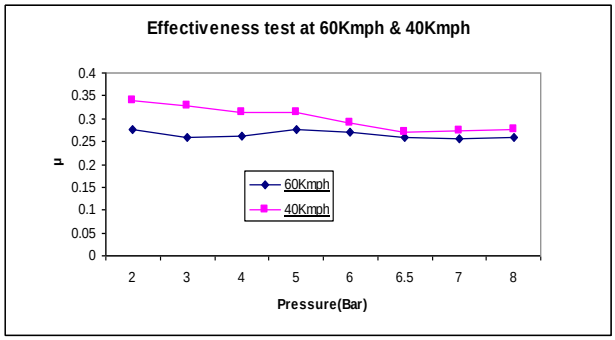

Fig. 4(a) Variation in μ with pressure at 60Kmph & 40Kmph, Type-0 (Ordinary)

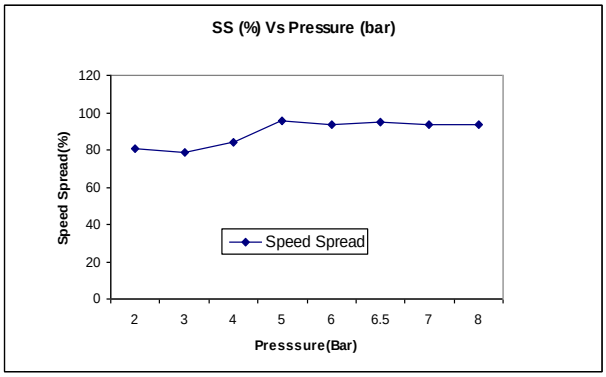

Fig. 4(b) SS (%) with change in pressure from 60 to 40Kmph, Type-0 (Ordinary)

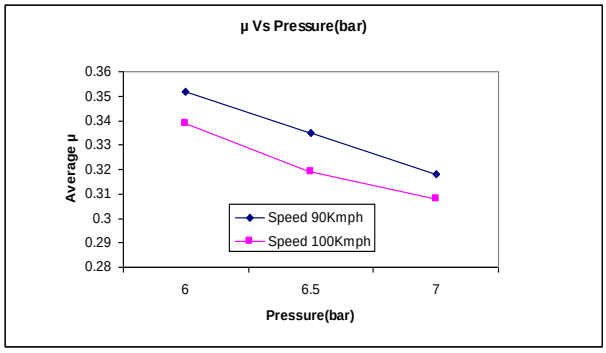

Fig. 5(a) Variation in μ with pressure at 90Kmph& 100Kmph, Type-0 (High performance)

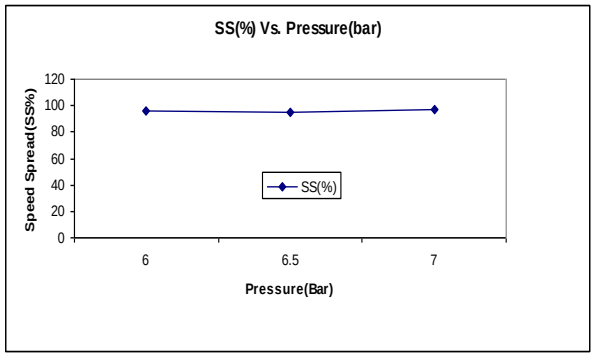

Fig. 5(b) SS (%) with change in pressure from 60 to 40Kmph, Type-0 (High Performance)

Giving a close look on SS (%) Vs pressure graph for both Type-0 tests (ordinary & high performance) brought the fact that stable result obtained at higher pressure region.

Speed Sensitivity Test-

Sensitivity of μ_{Avg} (averaged μ over three brake applications) with respect to speed (Kmph) is shown in Fig-6(a) of Volvo brake pad at test pressure of 6.5 bar. Keeping braking pressure constant (6.5 bar) & varying speed from 60 to 110Kmph brought initially decrement in μ_{Avg} followed by a revival trend. For ideal material, it should be as close to 100 as possible and range should be as small as possible. Variation in SS (%) with speed range was shown in Fig-6(b). a minimum of 86.05% SS drop found which was on good side.

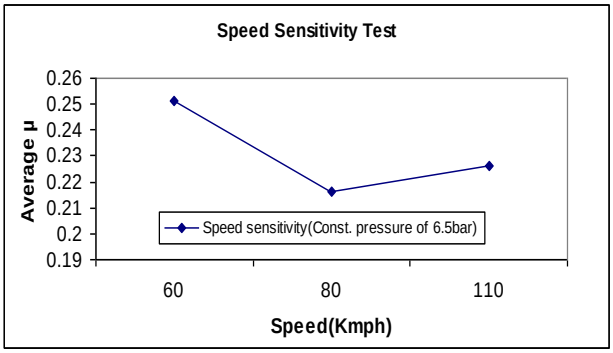

Fig. 6(a) Speed sensitivity of $\mu_{Avg.}$ with respect to speed (Kmph)

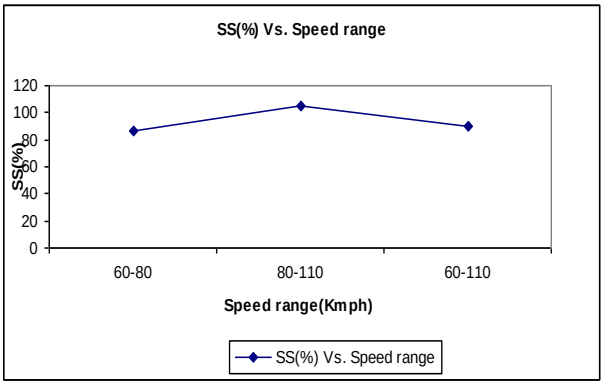

Fig. 6(b) SS (%) Vs. Speed range (Kmph)

Fade behavior study (Type-I)

Figure 7(a) shows fade behavior of Volvo disc pad lining. For an ideal fade curve μ should be in good range (0.3-0.4) and curve should be parallel to X-axis with minimal slope. Performance of FM during fade is decided by a factor called, % fade ratio. That found in this case as 83.43% which was acceptable. Generally fade % ratio in the range of 80-100% are acceptable as per industry norms. The reason behind fade is the

thermal decomposition of ingredients due to accumulation of frictional heat. This test condition was achieved by allowing the disk temperature to rise indefinitely (Figure-7(b)) by applying constant snub braking corresponding to fixed (0.3g) deceleration.

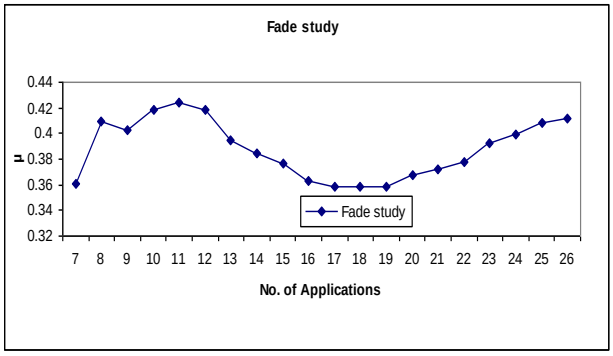

Fig. 7(a) Fade behavior of Volvo disk pad material

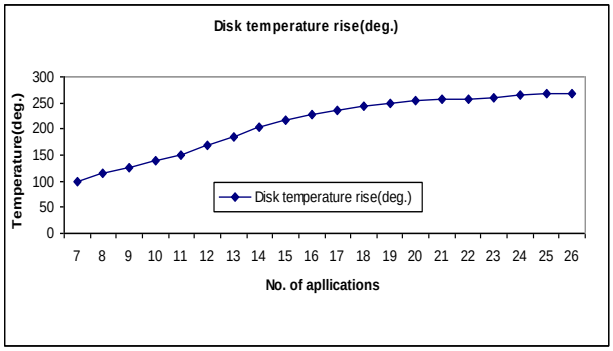

Fig. 7(b) Temperature rise (deg.) in Fade cycle

The experiment on the conventional Volvo brake was performed with the help of standard brake schedule as per the ECE R 90. An ECE R 90 schedule comprises of five major parts viz. bedding in, bedded performance test, high speed performance test, Fade-Recovery test & the speed sensitivity test. The input parameter to the lab view program is test schedule and vehicle parameter e.g., weight of the vehicle, rolling radius and the effective radius of disc brake as shown in the Table 8. The desired inertia can be achieved by connecting the inertia wheel to the main driving shaft with the help of wheel drive coupling. The material of the disc is Pearlitic grey cast iron and for the pad is composite which properties is given in the Table 9.

Table 8 Vehicle test parameters for commercial Volvo bus disk pad

Schedule	ECE R-90
Gross vehicles weight (GVW)	16200 kg
Vehicle model	Volvo bus B7R Mark-II
Inertia	148.6 Kg-m-sec^2
Rolling Radius (Tyre radius)	571 mm
Effective radius (pad on disc sliding radius)	172 mm

Table 9 Physical, chemical and mechanical properties of Volvo bus pads

Parameters	Value
Density (g/cc)	2.24
Acetone extraction (%)	1.25
Hardness ® (ASTM D 785)	95-102
Th. Conductivity (W/m.K) (ASTM-E1461-01)	2.03

Performance test

The performance test examine the behavior of braking torque, stopping distance and disc temperature at average speed with respect to the different applied pressure. The two different speeds (60 Km/hr and 40 Km/hr) and eight different value of pressure (2 to 8 Bar) as per the standard schedule are given below:

Initial speed - 40 and 60 km/hr
Final speed - 0 km/hr
Pressure - 2, 3, 4, 5, 6, 6.5, 7 and 8 bar
No. of cycles - 16 (8 for each initial speed at each operating pressure)
Disc temperature - 100 deg C
Blower - ON

The stopping distance depends upon the braking torque and deceleration rate, higher braking torque and higher deceleration results in lesser the stopping distance. From the Figure 8, it is clear that at the same applied pressure the stopping distance is lesser for the lower speed.

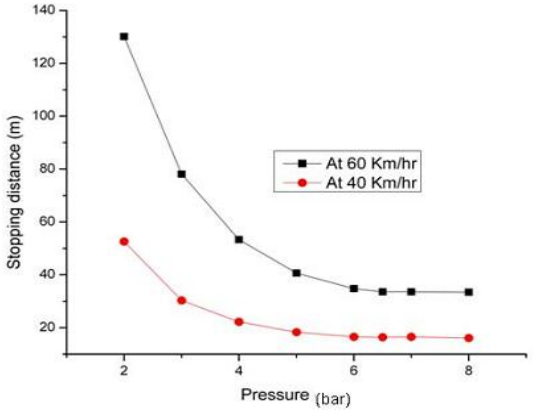

Fig.8 Variation of stopping distance with respect to pressure at different speed

Speed sensitivity test

This test examine the behavior of braking torque, disc temperature and stopping distance when the vehicle is in geared mode and intermediate brake is applied. The final speed of the vehicle is not zero in this test condition, and the test is performed at the operating pressure (6.5 Bar). The test had been performed with the help of standard test schedule which are given below:

Initial speed - 60, 80, 100 km/hr
Final speed - 30, 60, 80 km/hr respectively
Pressure - 6.5 bar for each speed
No. of cycles - 9 (3 cycles at each speed)
Disc temperature - 100 deg C
Blower - ON

Figure 9 shows the behavior of disc temperature and stopping distance at intermediate stopping. The disc temperature is high when the speed of the vehicle is reducing from 110 Km/hr to 80 Km/hr, because more kinetic energy is converted into the heat.

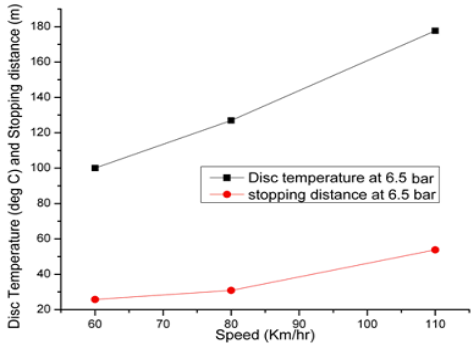

Fig.9 Variation in disc temperature and stopping distance with respect to pressure

High speed performance test

This test examines the behavior of braking torque, disc temperature and the stopping distance with respect to high operating pressure when the vehicle is running at high speed and stop suddenly to zero speed. The test was performed with the help of standard test schedule which is given below:

Initial speed - 90 and 100 km/hr
Final speed - 0 km/hr
Pressure - 6, 6.5 and 7 bar for each speed
No. of cycles - 18 (3 cycles at each pressure corresponding each speed)
Disc temperature - 100 deg C
Blower - ON

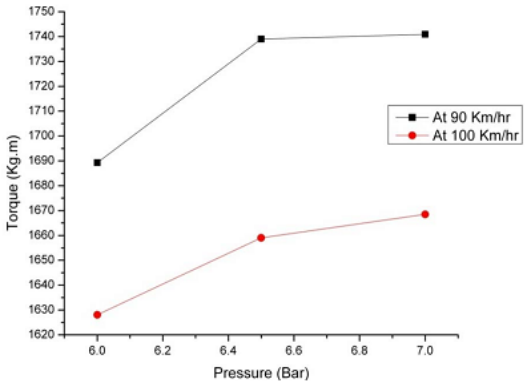

Fig.10 Variation of torque with respect to pressure at high speed

When the speed of the vehicle is constant and operating pressure is increasing then output torque will also increase. At higher speed the output torque is lesser as compare to the lower speed (Figure 10) because at higher speed more heat will generate which reduce the coefficient of friction between disc and pad.

The temperature of the disc will be high at higher speed and higher operating pressure due major loss in kinetic energy. It is clear from the Figure 11 that disc temperature is high at high speed and high pressure.

The stopping distance depends upon the braking torque and braking torque depends upon the applied pressure. It is clear from the Figure 11 that the stopping distance is almost constant with the variation in pressure of 1 bar.

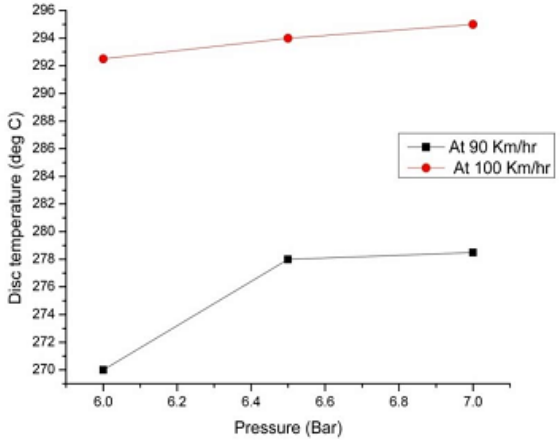

Fig. 11 Variation of disc temperature with respect to pressure at high speed

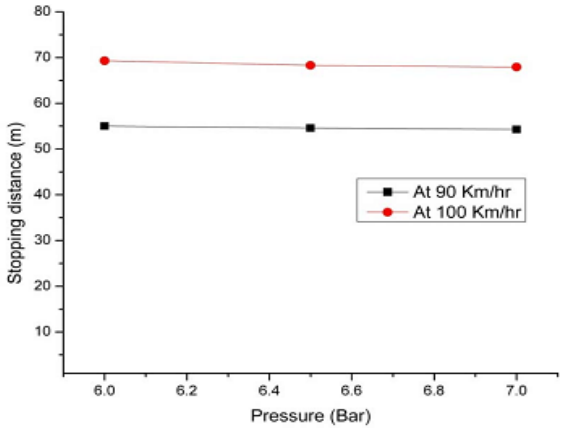

Fig.12 Variation in stopping distance with respect to pressure at high speed

Conclusions

In this research work friction characteristics of Volvo disc brake have been analyzed using Full-scale inertia dynamometer. The following conclusions can be made from this research work.

- The effect of applied braking pressure on coefficient of friction shows Volvo disc pad sensitivity towards pressure.

- With increase in pressure & speed, decreased due to fact that with increase in pressure real area of contact increases excessively and disproportionately as polymeric materials (disc FMs) are visco-elastic.
- Increase in speed brought more frictional heat which easily caused to go down as it was highly temperature sensitive.
- The stopping distance depends upon the braking torque and deceleration rate, higher braking torque and higher deceleration results in lesser the stopping distance.
- The disc temperature is high when the speed of the vehicle is reducing from 110 Km/hr to 80 Km/hr, because more kinetic energy is converted into the heat.
- At higher speed the output torque is lesser as compare to the lower speed because at higher speed more heat will generate which reduce the coefficient of friction between disc and pad.

References

C.Sarkar, H.Hirani, (2015), Design of Magnetorheological Brake using Parabolic Shaped Rotating Disc, International Journal of Current Engineering and Technology (accepted).

C.Sarkar, H.Hirani, (2015), Finite Element Analysis of Magnetorheological Brake using ANSYS, International Journal of Current Engineering and Technology (accepted).

C.Sarkar, H.Hirani, (2015), Transient Thermo Elastic Analysis of Disk Brake, International Journal of Current Engineering and Technology, 5, pp. 413-418.

C.Sarkar, H.Hirani, (2015), Synthesis and characterization of nano-copper-powder based magnetorheological fluids for brake, International Journal of Scientific Engineering and Technology, 4, pp. 76-82.

C.Sarkar, H.Hirani, (2015), Effect of particle size on shear stress of magnetorheological fluids, *Smart Science,* (in press).

C.Sarkar,H.Hirani,(2015),Development of magnetorheological brake with slotted disc, *Proc. IMechE, Part D: Journal of Automobile Engineering*, pp.1-18. DOI: 10.1177/0954407015574204.

C.Sarkar, H.Hirani, (2013), Theoretical and experimental studies on a magnetorheological brake operating under compression plus shear mode, *Smart Materials and Structures*, 22, art. no. 115032.

C.Sarkar, H.Hirani, (2013), Synthesis and characterization of antifriction magnetorheological fluids for brake, *Defence Science Journal*, 63, pp. 408-412.

C.Sarkar, H. Hirani, (2013), Design of a squeeze film magnetorheological brake considering compression enhanced shear yield stress of magnetorheologicalfluid, *Journal of Physics: Conference Series*, 412, 012045.

H.Hirani, C. S. Manjunatha, (2007), Performance evaluation of magnetorheological fluid variable valve, *Proc. of the Institution of Mechanical Engineers, Part D, Journal of Automobile Engineering*, 221, pp. 83-93.

M.Kumar, S.Mallik, J.Bijwe, (2009), Volvo bus disc brake testing on a brake inertia dynamometer, *Proceedings of TRIBO-INDIA conference*, Delhi, pp. 54-57.

S. M. Muzakkir, H. Hirani (2015), A Magnetorheological Fluid Based Design of Variable Valve Timing System for Internal Combustion Engine using Axiomatic Design, *International Journal of Current Engineering and Technology*, 5, pp. 603-612.

S. M. Muzakkir, M. G. Patil, H. Hirani (2015), Design of Innovative Engine Valve: Background and Need, *International Journal of Scientific Engineering and Technology*, 4, pp. 178-181.

S. M. Muzakkir, M. G. Patil, H. Hirani (2015), Design of Innovative Engine Valve, *International Journal of Scientific Engineering and Technology*, 4, pp. 212-217.

S. Gupta, H. Hirani (2011), Optimization of Magnetorheological Brake, ASME/STLE 2011 International Joint Tribology Conference, October 24-26, 2011, Los Angeles, California.

V.K.Sukhwani, H.Hirani, T. Singh, (2009), Performance evaluation of a magnetorheological grease brake, *Greasetech India*, 9,pp. 5-11.

V.K.Sukhwani, H.Hirani, (2008), A comparative study of magnetorheological-fluid-brake and magnetorheological-grease-brake, *Tribology Online*, 3, pp. 31-35.

V.K.Sukhwani, H.Hirani, T.Singh, (2008), Synthesis and performance evaluation of MR grease, *NLGI Spokesman*,71.

V.K.Sukhwani, H. Hirani, (2008), Design, development and performance evaluation of high speed MR brake, *Proc. Institute Mech. Engineers., Part L, Journal of Materials: Design and Applications*, 222,pp.73-82.

V.K.Sukhwani,H.Hirani,T.Singh,(2007), Synthesis of magnetorheologicalgrease,*GreasetechIndia*.

V.K.Sukhwani, V.Lakshmi, H. Hirani, (2006), Performance evaluation of MR brake: an experimental study, *Indian Journal of Tribology*, pp. 67-52.

Impact of Temperature Gradient on the Indian Major Carp Catla catla *Larvae*

J. G. Sharma, S. P. Singh, P. Mittal & R. Chakrabarti

Proceedings of the National Academy of Sciences, India Section B: Biological Sciences

ISSN 0369-8211

Proc. Natl. Acad. Sci., India, Sect. B Biol. Sci.
DOI 10.1007/s40011-014-0419-3

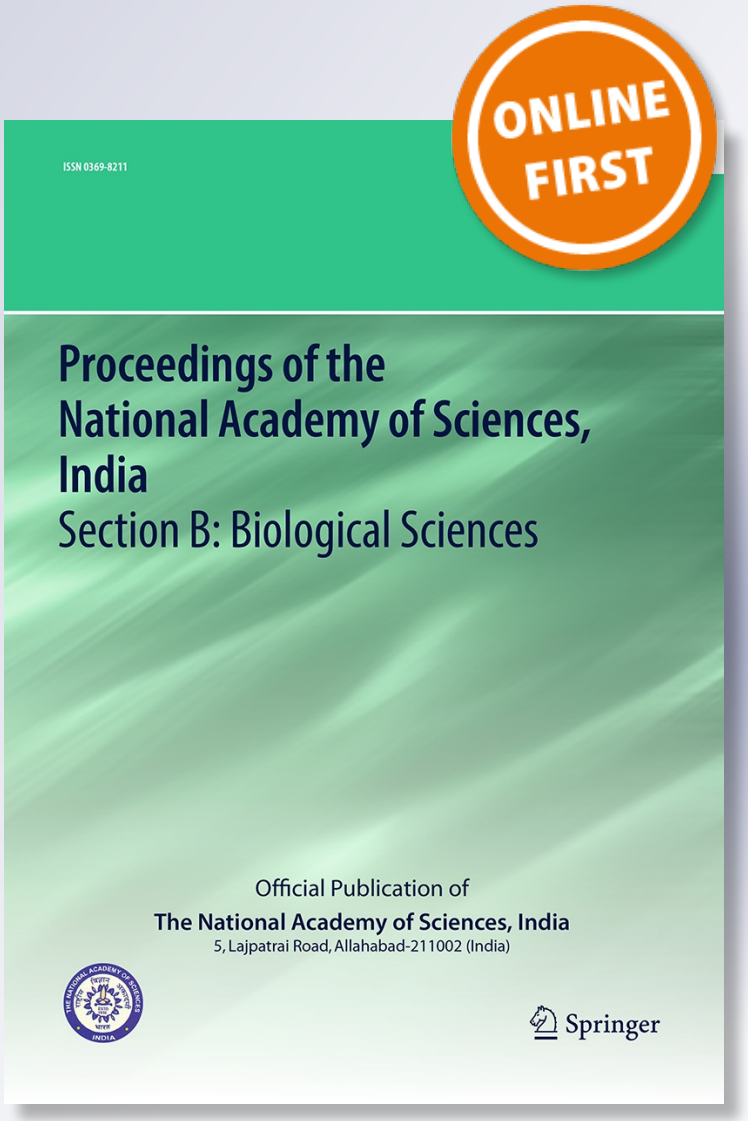

Springer

Proc. Natl. Acad. Sci., India, Sect. B Biol. Sci.
DOI 10.1007/s40011-014-0419-3

RESEARCH ARTICLE

Impact of Temperature Gradient on the Indian Major Carp *Catla catla* Larvae

J. G. Sharma · S. P. Singh · P. Mittal · R. Chakrabarti

Received: 24 December 2013 / Revised: 2 July 2014 / Accepted: 7 August 2014

Abstract *Catla catla* (Family: Cyprinidae) were exposed to 10, 15, 20, 25, 30, 33 and 35 °C following 28 °C acclimation temperature. Temperature change rate was 2 °C/day. Mortality rate of fish was recorded. In 10 °C temperature group, 17 and 65 % mortality was recorded at 14 and 10 °C, respectively. Significantly ($P < 0.05$) higher mortality was recorded in fish exposed at 10–20 °C as compared to other treatments. Cumulative mortality rates were 89, 43, 24, 18, 1, 2, and 3 % in fish exposed at 10, 15, 20, 25, 30, 33, and 35 °C, respectively. In 10 °C temperature group, all fish died within 2 days, whereas in 15 and 20 °C temperature groups, mortality was continued up to 11 days; it was 18 days in 25 °C temperature group. With simple regression analysis for the temperature range ($T < 28$ °C and $T > 28$ °C), percentage changes of mortality per fall and increase of $\Delta T = 1$ °C was calculated in the log-linear regression model framework. When temperature was reduced from 28 °C, the cumulative mortality increment in each 1 °C fall was $e^{.109} = 1.115$ ($P < 0.05$). High R-square value indicated a high variation (96.8 %) in log-transformed mortality for temperature difference. Beta coefficient was less steep when temperature increased beyond 28 °C. The cumulative mortality $e^{.075} = 1.077$ ($P > 0.05$) was obtained for each 1 °C increase of temperature from 28 °C.

Keywords *Catla catla* · Cumulative mortality · Temperature · Time series analysis

Introduction

Fish often experiences various environmental stressors under natural and culture conditions, which results into temporary or chronic disturbance of homeostasis. Water temperature plays an important role in cold-blooded animals. Temperature has long been known as a key environmental factor controlling the physiology, distribution and behavior of fishes [1–4]. Temperature directly influences metabolism affecting all physiological processes viz. food intake, metabolism and nutritional efficiency [5, 6]. Temperature below or above the thermal limit can induce alterations in the fish immune response [7] and influence the development of infectious diseases [8]. Therefore, the basic understanding of thermal physiology of a species is most essential to develop their culture technique. Moreover, in the current scenario, this is also essential to assess the biological effects of different thermal phenomena such as climate change, El Niño, La Niña, overwinters, etc. [9–13].

In India, there is a wide fluctuation of environmental temperature throughout the year. Summer temperature in some areas, especially in northern part is around 45 °C, whereas during winter the mercury drops below 2 °C in these areas. Most of the teleostean species have developed their own specific adaptive mechanisms which enable them to cope up with fluctuations of water temperature and the species survive in the stressful environment [14]. It is assumed that juvenile fishes living at cooler latitudes

J. G. Sharma
Department of Biotechnology, Delhi Technological University, Delhi 110042, India

S. P. Singh · R. Chakrabarti (✉)
Aqua Research Lab, Department of Zoology, University of Delhi, Delhi 110007, India
e-mail: aquaresearchlab@yahoo.co.in

P. Mittal
Department of Mathematics, Satyawati College, University of Delhi, Delhi 1100052, India

Published online: 30 November 2014

should have some capacity to adapt to changing thermal conditions, but this is unclear whether the tropical populations possess sufficient acclimation capacity to accommodate further temperature increase [15]. The understanding of tropical fish responses to temperature change is rudimentary [16]. The lowering of temperature adversely affects the physiological responses of air breathing catfish, *Clarias batrachus* (magur). The food consumption rate and digestive enzyme activities were reduced in the fish at temperature below 25 °C [17, 18].

Catla catla (catla) is one of the most economically important carp species and used in composite culture throughout India. Its natural distribution seems to be governed by temperature dependency rather than latitude and longitude. It is a eurythermal species that grows best at water temperature between 25 and 32 °C. Early-stage larvae remain in surface and sub-surface waters and are strongly phototactic. Adults feed only in surface and midwaters [19]. There is lack of information related to the larval stages. In the present investigation, survival rate of Catla larvae exposed to various temperatures was evaluated using suitable statistical method. This may help to understand the adaptability of this species to various temperatures.

Material and Methods

Experimental System and Maintenance of Larvae

Glass aquarium (50 l each) covered with transparent fiber glass sheet was used as fish culture unit. Each aquarium was connected with a filtration unit (Sera fil bioactive 130, Germany) for the maintenance of reduced level of nitrogenous products in the fish culture unit. The cooling/heating (HAILEA Chiller HC-300A, China/Sera Aquarium Heater 300, Germany) unit was attached with each aquarium to maintain the desirable temperature. Indian major carp *Catla catla* and its larvae were procured from Chatterjee Brothers' Fish Farm, West Bengal having induced breeding facility. Fish were kept in outdoor cemented tanks (165 l) at water temperature 28 ± 2 °C. The fish (0.167 ± 0.02 g) were randomly divided into seven groups and were introduced into experimental aquaria (50 fish/aquarium) maintained in wet laboratory facility. The larvae were acclimated at 28 °C for 7 days. Fish were fed with diet (40 % protein) at the rate of 5 % of body weight throughout the study period. The whole amount of food was divided into two parts and was fed daily at 9.00 a.m. and 5.00 p.m. pH and dissolved oxygen level of water were monitored daily using portable multiple water quality measuring meter (HACH, HQ40 d, USA). pH ranged from 7.60 to 8.04, 7.61 to 8.17, 7.805 to 8.37, 7.87 to 8.41, 7.76 to 8.74, 7.60 to 8.45, 7.62 to 8.47, and dissolved oxygen ranged from 5.57 to 6.15, 5.30 to 6.10, 5.21 to 6.25, 5.56 to 6.18, 5.06 to 6.25, 5.12 to 6.35 and 5.05 to 6.10 mg/l at 10, 15, 20, 25, 30, 33 and 35 °C treatments, respectively throughout the study period.

Table 1 Planned and measured water temperature (±SE) in each treatment during experiment

Treatments (°C)	Planned temperature (°C)	Measured temperature (°C)
10	10	10.56 ± 0.19
15	15	15.23 ± 0.17
20	20	20.02 ± 0.19
25	25	25.36 ± 0.19
30	30	30.07 ± 0.20
33	33	33.05 ± 0.25
35	35	34.87 ± 0.09

Experimental Temperature

Seven different temperatures (Table 1) maintained simultaneously under laboratory conditions were 10, 15, 20, 25, 30, 33 and 35 °C. One group of fish was kept in outdoor condition. Three replicates were used for each temperature. Each experimental temperature was achieved at a rate of change of 1 °C per 12 h (2 °C/day) starting from acclimation temperature of 28 °C. This required 1–9 days to reach the assigned temperature. Duration of experiment was 25 days. The range of temperature selected in the present experiment was based on the environmental temperature which prevailed in various parts of India in different seasons.

Statistical Analyses

Mortality of Fish

Dead fish were collected at regular interval from each tank and their number was recorded. Data were compiled as mean ± S.E. All data were analyzed by using one-way analysis of variance (ANOVA). Statistical significance was accepted at $P < 0.05$ level.

Time Series Analysis

Assuming the ambient temperature (28 °C), simple linear regression of cumulative mortality against the range (Maximum–Minimum) temperatures was performed separately for the "increase" and "decrease" shoulders of temperature/mortality curve, to determine the corresponding

Table 2 Mortality of *Catla catla* versus range of water temperature

Temperature range	Difference	Mortality (%)	LN(M)
T < 28 °C			
28–25 °C	3	18	2.20
28–20 °C	8	24	2.48
28–15 °C	13	43	3.09
28–10 °C	18	89	3.81
T > 28 °C			
28–30 °C	2	1	0.00
28–33 °C	5	2	0.00
28–35 °C	7	3	0.41

slope factor β, or percentage changes of mortality per 1 °C difference of temperature:

$$Ln(M) = Const + \beta(T_{max} - T_{min}) + \varepsilon$$

where, $Ln\ (M)$ = Log-transformed mortality, β = slope factor, T_{max} and T_{min} = maximum and minimum temperature, respectively and ε = residual term

"Decrease" temperatures were defined as reducing T from 28 °C, while the "Increase" implied raising temperature from 28 °C. Log-transformed mortality was used to produce a normal distribution of the dependent variable. In the above regression equation, the temperature intervals between 28 and 25 °C, 28 and 20 °C, 28 and 15 °C, 28 and 10 °C (Table 2) and above 28, i.e. 28–30 °C, 28–33 °C, 28–35 °C (Table 2) were studied separately, because their correlations between *Ln* (M) and T became pronouncedly concave as the absolute value of beta increased.

Results and Discussion

Mortality of Fish

In 10, 15, 20 and 25 °C temperature groups, the water temperature gradually decreased from the acclimation temperature of 28 °C. In 10 °C temperature group, as the temperature reached 16 °C, mortality started; 17 % mortality was recorded at 14 °C and 34 % larvae died immediately as the water temperature became 10 °C. All larvae (65 %) died within 2 days after reaching 10 °C temperature. In 15 °C temperature group, 4 % mortality was recorded at temperature 24–18 °C. As the water temperature further dropped to 15 °C, 16 % mortality of larvae was recorded immediately and the mortality was continued up to 11 days in this group. In 20 °C temperature group, 2 % mortality was found as water temperature became 24 °C; 9 % larvae died immediately as water temperature dropped to 20 °C. Mortality of larvae continued up to 11 days of reaching this temperature (Fig. 1). In 25 °C temperature

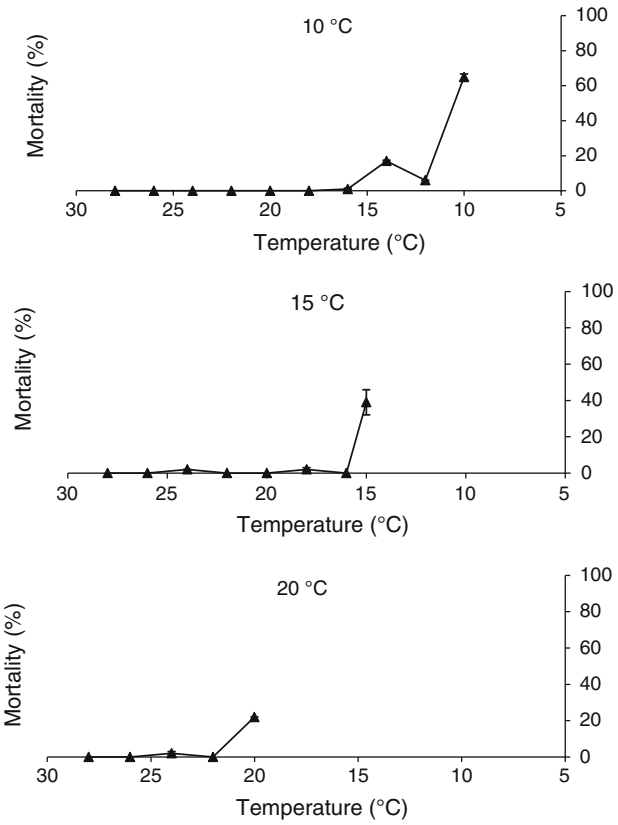

Fig. 1 Mortality of *Catla catla* exposed to the temperature 10, 15 and 20 °C

group, 2 % mortality was recorded on day-4 of reaching 25 °C water temperature and mortality of larvae continued up to 18 days. In 30 °C temperature group, 1 % mortality of larvae was found on day-10 of reaching this water temperature. In 33 °C temperature group, 1 % mortality was recorded within 24 h of reaching this temperature, and further 1 % mortality was found after 4 days. In 35 °C temperature group, 1 and 2 % mortality were recorded on day-2 and day-3, respectively after water temperature become 35 °C. There was no mortality of Catla kept in outdoor condition during the study period.

Among all these treatments, significantly ($P < 0.05$) higher cumulative mortality of Catla was found at lowest temperature of 10 °C as compared to the other groups. Cumulative mortality rates of Catla were 89, 43, 24, 18, 1, 2 and 3 % in 10, 15, 20, 25, 30, 33 and 35 °C temperature groups, respectively (Fig. 2). Though 1–3 % mortality of Catla was recorded in groups exposed to temperature above the acclimation one, there was no significant ($P > 0.05$) difference among these groups. This indicated that the lowering of temperature from 28 °C was more stressful as compared to the raising of temperature for this size group of Catla. Temperature tolerance of fish is dependent upon acclimation temperature [20]. There was 18 °C difference between the acclimation temperature (28 °C) and the

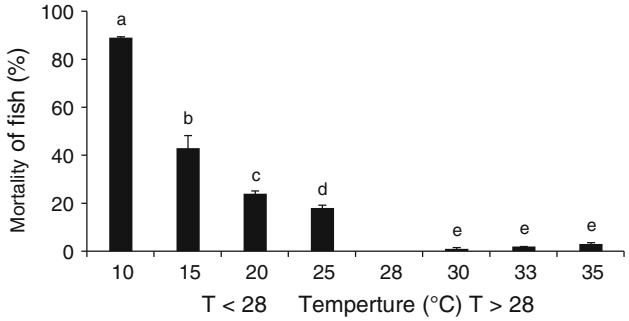

Fig. 2 Cumulative mortality of *Catla catla* (n = 3) exposed to various temperatures

lowest temperature (10 °C) at which the larvae were exposed, whereas there was 7 °C difference between the highest temperature (35 °C) exposed group and the acclimation temperature. As the minimum temperature tolerance limit of adult Catla is ~14 °C, the mortality was highest in larvae exposed at 10 °C. The highest temperature of 35 °C used in the present study was 3 °C higher as compared to the optimum range of temperature of 25–32 °C [19]. The present study showed that at 10 °C temperature all larvae died within 2, whereas at 15 and 20 °C, mortality continued up to 11 days; it continued up to 18 days in 25 °C temperature exposed group. In a similar study, adult *Clarias batrachus* were exposed to a temperature range of 10–35 °C; significantly ($P < 0.05$) higher mortality of fish was recorded at 10 °C as compared to the other temperatures. At 10 °C, 50 % fish died within 5 days of exposure [17]. Lower environmental temperature affected both cellular and humoral responses in fish [21].

With simple regression analysis for the temperature range (T < 28 °C and T > 28 °C), percentage changes of mortality in each fall and increase of $\Delta T = 1$ °C was calculated in the framework of log-linear regression model (Table 3). When temperature was reduced from 28 °C, the cumulative increment of mortality in each 1 °C fall of temperature amounted to $e^{.109} = 1.115$ ($P < 0.05$). High R-square value was observed indicating a high variation (96.8 %) in log-transformed mortality due to difference in temperature. Further, beta coefficient was observed less steep when temperature increased beyond the acclimation temperature of 28 °C. The cumulative mortality of $e^{.075} = 1.077$ ($P > 0.05$) was obtained for each 1 °C increase of the temperature beyond 28 °C. In cold and temperate regions, the temperature-mortality rises as temperature falls below or rises above this "point of maximum comfort" i.e. 28 °C. The above discussion also attempted to establish the range of linear increase in mortality that occurred with each 1 °C drop of outdoor temperature and the effect of cold spells on mortality.

Table 3 Regression results of temperature ranging less and greater than 28 °C

	T < 28 °C		T > 28 °C	
	Constant	Slope	Constant	Slope
Coefficient	1.753	0.109	−0.213	0.075
t-stat	10.643***	7.847**	−0.755	1.347
P value	(0.008)	(0.015)	0.588	0.407

*** $P < 0.01$

** $P < 0.05$

Conclusions

The present study showed that 15 °C temperature was stressful to the larvae of Catla as mass mortality occurred. One degree fall of temperature from 28 °C resulted into 10.7 % mortality of larvae. Being a tropical species, Catla showed adaptability towards higher temperature. Temperature of aquatic environment is important for ensuring survival and failure to adapt temperature fluctuations is generally ascribed to the inability of fish to respond physiologically resulting its mortality.

Acknowledgments Authors are thankful to Indian Council of Agricultural Research, ICAR, New Delhi (NFBSFARA project, AS-2001/2010-11) for financial support.

References

1. Fry FEJ (1947) Effects of the environment on animal activity. University of Toronto, Studies Biological Series No. 55, Publication of Ontario Fisheries Research Laboratory No. 68 p 62
2. Fry FEJ (1971) The effects of environmental factors on the physiology of fish. In: Hoar WS, Randall DJ (eds) Fish Physiology, vol VI. Academic Press, New York, pp 1–98
3. Houston AH (1982) Thermal effects upon fishes. Publication No. NRCC 18 566, National Research Council of Canada, Ottawa
4. Reynolds WW (1977) Temperature as a proximate factor in orientation behavior. J Fish Res Board Can 34:734–739
5. Brett JR (1979) Environmental factors and growth. In: Hoar WS, Randall DJ, Brettin JR (eds) Fish physiology, vol VIII. Academic Press, London, pp 599–675
6. Burel C, Ruyet PL, Gaumet F, Roux AL, Severe A, Boeuf G (1996) Effects of temperature on growth and metabolism in juvenile turbot. J Fish Biol 49:678–692
7. Martins ML, Xu DH, Shoemaker CA, Klesius PH (2011) Temperature effects on immune response and haematological parameters of channel catfish *Ictalurus punctatus* vaccinated with live theronts of *Ichthyophthirius multifiliis*. Fish Shellfish Immunol 31:774–780
8. Le Morvan C, Deschaux P, Troutaud D (1996) Effects and mechanisms of environmental temperature on carp (*Cyprinus carpio*) anti-DNP antibody response and non-specific cytotoxic cell activity: a kinetic study. Dev Comp Immunol 20:331–340
9. Beitinger TL, Bennett WA, McCauley RW (2000) Temperature tolerance of North American freshwater fishes exposed to dynamic changes in temperature. Environ Biol Fish 58:237–275

10. Mora C, Ospina F (2001) Thermal tolerance and potential impact of sea warming on reef fishes from Gorgona Island (Eastern Pacific ocean). Mar Biol 139:765–769
11. Mora C, Ospina F (2002) Experimental effects of La Niña cold temperatures on the survival of reef fishes from Gorgona Island (Tropical Eastern Pacific). Mar Biol 141:789–793
12. Kimball ME, Miller JM, Whitfield PE, Hare JA (2004) Thermal tolerance and potential distribution of invasive lionfish (*Pterois volitans*/miles complex) on the east coast of the United States. Mar Ecol Prog Ser 283:269–278
13. Kimura MT (2004) Cold and heat tolerance of drosophilid flies with reference to their latitudinal distributions. Oecologia 140:442–449
14. Das T, Pal AK, Chakraborty SK, Manush SM, Chatterjee N, Mukherjee SC (2004) Thermal tolerance and oxygen consumption of Indian major carps acclimated to four temperatures. J Therm Biol 29:157–163
15. Eme J, Dabruzzi TF, Bennett AW (2011) Thermal responses of juvenile squaretail mullet (*Liza vaigiensis*) and juvenile crescent *Terapon jarbua* acclimated at near-lethal temperatures, and the implication for climate change. J Exp Mar Biol Ecol 399:35–38
16. Wilson SK, Adjeroud M, Bellwood DR, Berumen ML, Booth D, Bozec YM, Chabanet P, Cheal A et al (2010) Crucial knowledge gaps in current understanding of climate change impacts on coral reef fishes. J Exp Biol 213:894–900
17. Singh SP, Sharma JG, Ahmad T, Chakrabarti R (2013) Effect of water temperature on the physiological responses of Asian catfish *Clarias batrachus* (Linnaeus 1758). Asian Fish Sci 26:26–38
18. Ahmad T, Singh SP, Khangembam BK, Sharma JG, Chakrabarti R (2014) Food consumption and digestive enzyme activity of *Clarias batrachus* exposed to various temperatures. Aquac Nutr. doi:10.1111/anu.12072
19. FAO (2013) http://www.fao.org/fishery/culturedspecies/Catla_catla/en. Accessed 24 Nov 2013
20. Kasim HM (2002) Thermal ecology: a vital prerequisite for aquaculture and related practices. In: Venkataramani B, Sukumarn N (eds) Thermal ecology. DAE Mumbai Publishers, Mumbai, BRNS, pp 222–234
21. Kumari J, Sahoo PK, Swain T, Sahoo SK, Sahu AK, Mohanty BR (2006) Seasonal variation in the innate immune parameters of the Asian catfish *Clarias batrachus*. Aquaculture 252:121–127

INFORMATICS

Human Mutation

OFFICIAL JOURNAL
HGVS
HUMAN GENOME VARIATION SOCIETY
www.hgvs.org

mit-o-matic: A Comprehensive Computational Pipeline for Clinical Evaluation of Mitochondrial Variations from Next-Generation Sequencing Datasets

Shamsudheen Karuthedath Vellarikkal,[1,5§] Heena Dhiman,[2§] Kandarp Joshi,[3,5] Yasha Hasija,[4] Sridhar Sivasubbu,[1,5*] and Vinod Scaria[2,5†]

[1]*Genomics and Molecular Medicine, CSIR Institute of Genomics and Integrative Biology, Delhi, India;* [2]*GN Ramachandran Knowledge Center for Genome Informatics, CSIR Institute of Genomics and Integrative Biology, Delhi, India;* [3]*CSIR Open Source Drug Discovery Unit, Delhi, India;* [4]*Department of Biotechnology, Delhi Technological University, Delhi, India;* [5]*Academy of Scientific and Innovative Research (AcSIR), Anusandhan Bhawan, Delhi, India*

Communicated by Raymond Dalgleish

Received 25 March 2014; accepted revised manuscript 26 January 2015.
Published online 11 February 2015 in Wiley Online Library (www.wiley.com/humanmutation). DOI: 10.1002/humu.22767

ABSTRACT: The human mitochondrial genome has been reported to have a very high mutation rate as compared with the nuclear genome. A large number of mitochondrial mutations show significant phenotypic association and are involved in a broad spectrum of diseases. In recent years, there has been a remarkable progress in the understanding of mitochondrial genetics. The availability of next-generation sequencing (NGS) technologies have not only reduced sequencing cost by orders of magnitude but has also provided us good quality mitochondrial genome sequences with high coverage, thereby enabling decoding of a number of human mitochondrial diseases. In this study, we report a computational and experimental pipeline to decipher the human mitochondrial DNA variations and examine them for their clinical correlation. As a proof of principle, we also present a clinical study of a patient with Leigh disease and confirmed maternal inheritance of the causative allele. The pipeline is made available as a user-friendly online tool to annotate variants and find haplogroup, disease association, and heteroplasmic sites. The "mit-o-matic" computational pipeline represents a comprehensive cloud-based tool for clinical evaluation of mitochondrial genomic variations from NGS datasets. The tool is freely available at http://genome.igib.res.in/mitomatic/.
Hum Mutat 36:419–424, 2015. © 2015 Wiley Periodicals, Inc.

KEY WORDS: mitochondria; haplogroup; heteroplasmy; variation; next-generation sequencing

Introduction

Mitochondrial diseases are one of the most common human genetic disorders [Taylor and Turnbull, 2005]. Pediatric onset of mitochondrial diseases occurs with an estimated incidence of one in 5,000 individuals [Craigen et al., 2013] and estimated prevalence of one in 7,634 [Skladal et al., 2003]. Recent years have seen a tremendous improvement in the understanding of the organization and function of the mitochondria in a variety of biological processes including bioenergetics of the cell, programmed cell death, and also in the predisposition to a wide variety of disease conditions. The human mitochondria encode 37 genes including 13 protein coding genes, 22 transfer RNAs, and two ribosomal RNAs [Shadel, 2008]. The evolution of the organelle has seen a large-scale reduction in the mitochondrial genome with subsequent contributions of components encoded by the nuclear genome [Adams and Palmer, 2003]. The function and integrity of the mitochondria is largely dependent on import of a set of transcripts and proteins encoded by the nuclear genome [Lee et al., 2008]. Recent proteomics experiments have created a compendium of about 1,000 proteins, which are encoded by the nuclear genome and largely found in the mitochondria [Kunkele et al., 1998; Jensen and Johnson, 2001; Wiedemann et al., 2003; Mesecke et al., 2005].

Apart from its functional importance, the peculiar maternal inheritance of the mitochondria has been widely applied as a tool toward understanding migration and population genetics [Pliss et al., 2006; Underhill and Kivisild, 2007]. Recent studies have increasingly shown mitochondrial variations and mitochondrial dysfunction to be associated with a number of pathophysiological conditions including neurological disorders such as Alzheimer's disease [Yan et al., 2013] and metabolic disorders such as type 2 diabetes mellitus [Tang et al., 2005]. The small genome size and availability of tools including tiling microarrays and sequencing has enabled us to understand the diversity of mitochondrial variations [Maitra et al., 2004]. This has been complemented by a number of informatics resources such as MITOMAP [Kogelnik et al., 1996] and MitoLSDB [K et al., 2013], which have systematically curated information from various resources on mitochondrial variations.

The advent of next-generation sequencing (NGS) technology has offered a fresh opportunity to understand mitochondrial variations. Many recent studies have extensively used NGS approaches to identify mitochondrial variants associated with diseases [Craigen et al., 2013; Abaci et al., 2014]. It also provides additional advantages including large depth coverage, which could be effectively used to

Additional Supporting Information may be found in the online version of this article.

Current address: GN Ramachandran Knowledge Center for Genomics Informatics, CSIR Institute of Genomics and Integrative Biology, Delhi 110025, India

†Correspondence to: Vinod Scaria. E-mail: vinods@igib.res.in

‡GN Ramachandran Knowledge Center for Genomics Informatics, CSIR Institute of Genomics and Integrative Biology, Delhi 110025, India.

§These authors contributed equally and would like to be known as joint first authors.

*Correspondence to: Sridhar Sivasubbu. E-mail: s.sivasubbu@igib.res.in

Contract grant sponsor: Council of Scientific and Industrial Research (CSIR), India (grant no. BSC0122–CARDIOMED).

map heteroplasmic variations [Sosa et al., 2012]. In addition, recent exome capture methodologies also incorporate probes from the mitochondrial genome and offers additional opportunities toward understanding mitochondrial variations in clinical settings. With the drastic drop in cost of DNA sequencing, it is expected that affordable mitochondrial sequencing could be effectively employed for patients suffering from mitochondrial disorders [Sosa et al., 2012]. The widespread application of NGS by clinicians is in part limited by the paucity of appropriate systematic computational pipelines for data analysis, which are easy to operate and provide reports in easily interpretable formats. MitoSeek [Guo et al., 2013] is one such tool for NGS data analysis from mtDNA, captured as a by-product of whole-exome or whole-genome sequencing. Although a very expedient resource, it offers just a command-line version that works specifically on large abundance of paired-end sequencing data and does not support single-end data. It reports heteroplasmy, somatic mutations, structural variance, relative mtDNA copy number, and annotations for amino acid changes, without any clinical correlation of the findings. MToolBox is a similar tool that works on command-line [Calabrese et al., 2014]. To this end, mit-o-matic has been created to provide most comprehensive annotation with relevant clinical association that includes haplogroup classification.

In the present work, we describe how a cloud-based data integration platform can leverage the high-quality and clinically relevant information distributed in disparate resources for clinical application toward understanding and annotating mitochondrial variations. As a proof of principle, we use datasets of mitochondrial sequencing from a patient with Leigh disease. To the best of our knowledge, mit-o-matic is to date one of the most comprehensive cloud-based analysis pipelines for clinical annotation of mitochondrial sequencing data from NGS platforms. The resource is freely available at http://genome.igib.res.in/mitomatic/.

Overview of mit-o-matic

mit-o-matic is a comprehensive computational pipeline for annotation of mitochondrial variations from next-generation datasets. It provides automation for alignment of NGS reads to the reference mitochondrial genome, fetching the variants above a set cut-off and creating a descriptive annotation of reported variants. The Web-based interface can accept data in form of FASTQ files directly and perform the analysis entirely online (Option 1), but with a size limitation, which allows an ample coverage of approximately 500× of the mitochondrial genome, which is more than sufficient for most clinical applications. For large datasets above 500× coverage as in very specialized applications, the command-line option can be used for either running the complete pipeline or just parsing an already available pileup file. The parsed pileup files can be stored and used for analysis in future with the "Option 2" on the home page. For each variant, the reference allele, alternate allele, percentage of allele frequency, corresponding gene, amino acid position, and amino acid change with its subsequent effect (synonymous or nonsynonymous) are listed as per the revised Cambridge Reference Sequence (rCRS) [Andrews et al., 1999]. Apart from this, the disease-associated variants are reported with associated phenotype, population frequencies are reported for variants that are not novel, and potential functional consequence is informed for nonsynonymous novel variants. It provides an online user-friendly graphical user interface where the researcher or clinician can avail a comprehensive genetic report on the mitochondrial variations in a dataset. The delivery of computing as a service by integrating various tools and databases for the analysis of mitochondrial variations in the form of a free online user-friendly interface makes mit-o-matic a useful cloud-based data integration platform. An overview of the pipeline is summarized in Figure 1.

Sequence Mapping and Variant calling

The computational pipeline takes in standard high-quality trimmed FASTQ format files for mitochondrial sequences from any of the popular sequencing platforms. The resource supports both single-end and paired-end data from a variety of experimental protocols including amplicon sequencing using two or three sets of primers by different NGS approaches such as duplex sequencing [Schmitt et al., 2012] or direct amplicon sequencing [Huang, 2011; Sosa et al., 2012]. The mtDNA below 500× coverage can be analyzed using the Web-based option, whereas the command-line version can be used for the analysis of whole-exome or targeted-exome containing mtDNA reads. The pipeline provides three options for alignment against the reference rCRS mitochondrial genome sequence modified according to the read length, and supports three popular quality-aware reference mapping algorithms—BWA [Li and Durbin, 2009], BOWTIE [Langmead et al., 2009], and MAQ [Li et al., 2008]. Since the mitochondrial genome is circular, the reference genome has been modified to allow hundred percent mapping of reads on either end. For data with read length of X bp, X-1 bases would be added from the opposite end to start and stop rCRS. The alignments thus generated are reformatted to pileups, and a custom-formatted file is generated that includes frequencies and positions of the mismatches retrieved from the alignments. This file is further provided to the online reporting module of mit-o-matic, which provides a comprehensive annotation of the variations in the sample. An empirical minimum cutoff of 10% variants per site has been used by default to avoid spurious and low-frequency variations [Li et al., 2010]. The frequency of each of the alleles was computed and tabulated with respect to the percentage of reads out of the total against the particular allele. Positions having more than one allele with frequency greater than the cutoff value are referred to as Heteroplasmic sites.

Resources and Analysis Tools Integrated in mit-o-matic

mit-o-matic integrates a number of well-curated datasets and resources for providing the user with a rich annotation of the variants.

Mitochondrial Variations and Annotations

Mitochondrial variants and annotations were primarily derived from MITOMAP [Kogelnik et al., 1996], mtDB [Ingman and Gyllensten, 2006], and MitoLSDB [K et al., 2013]. The variant data were compiled into compatible data files and uploaded into MySQL. This includes variations mapped onto 73 mtDNA function locations and 580 disease associations. The variant database stores 10,416 unique mitochondrial variations from the available resources (MITOMAP [July 11, 2014], MitoLSDB [v.2.0], and mtDB [March 1, 2007]). All the exonic nonsynonymous variations were detected for their potential functional consequences using SIFT [Kumar et al., 2009]. This tool is widely used for predicting the effect of an amino acid

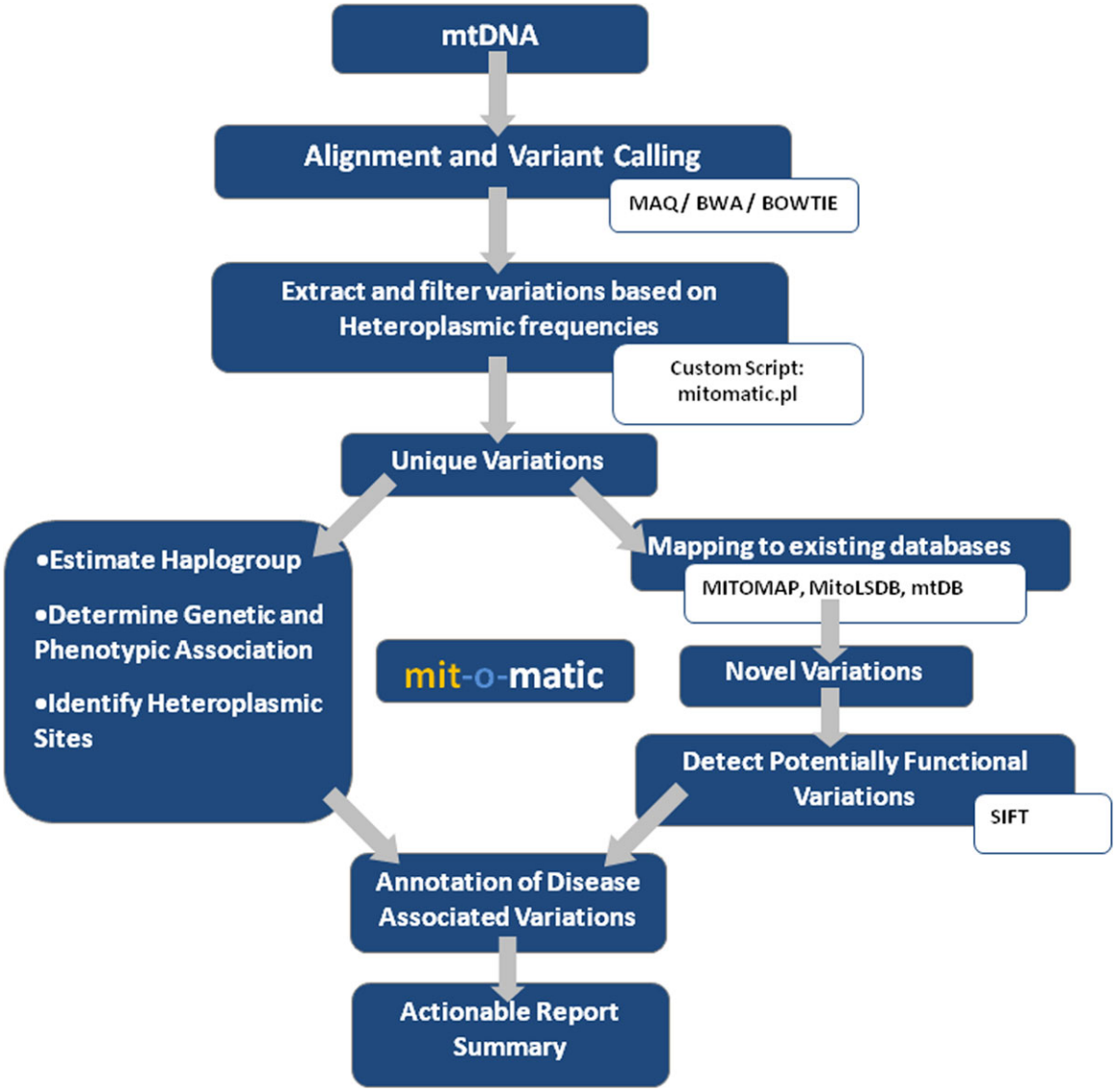

Figure 1. Overview of the computational pipeline.

substitution on protein function on the basis of sequence homology and the physical properties of amino acids.

Frequency of Variations

The frequencies of variations were retrieved from the MITOMAP database, which computes the population frequencies based on 18,363 sequences in GenBank.

Haplogroup Annotations

Haplogroup annotations were performed using a popular approach as described by Fan and Yao (2013). To categorize the mitochondrial variome under most suitable haplogroup, a total of 3,737 haplogroups were derived from a comprehensive phylogenetic tree of global human mtDNA variation. As described in the approach, the variants in a sample were mapped to the variations forming each of the haplogroup and scored, and the best scoring haplogroup was reported by mit-o-matic.

Accuracy Estimation

We randomly introduced 100 mutations in the reference sequence (rCRS) and generated single-end synthetic NGS reads of Illumina platform at discrete coverage values (100×, 200×, 300×, 400×, and 500×) for Q30 phred quality using ART [Huang et al., 2012]. For a given coverage, the reads simulated from the mutated reference genome were mixed with the reads generated from nonmutated reference genome to create FASTQ files with varied maximum allele frequencies (10%–90%) resulting in a dataset consisting of 45 samples. mit-o-matic was run on all these synthetic FASTQ files varying the cut-off values for alternate allele frequency with BOWTIE to check the number of true positive (TP) and false positive (FP) mutations reported by the pipeline. For each coverage data, TP and FP values were plotted across the mit-o-matic frequency cut-off values for all the samples independently (Supp. Fig. S1). We show that the default cut-off (10%) used by Li et al. (2010) provides for extremely accurate analysis of variants. Nevertheless, the tool allows for specialized users to define their default cut-offs based on specific requirements if need arises.

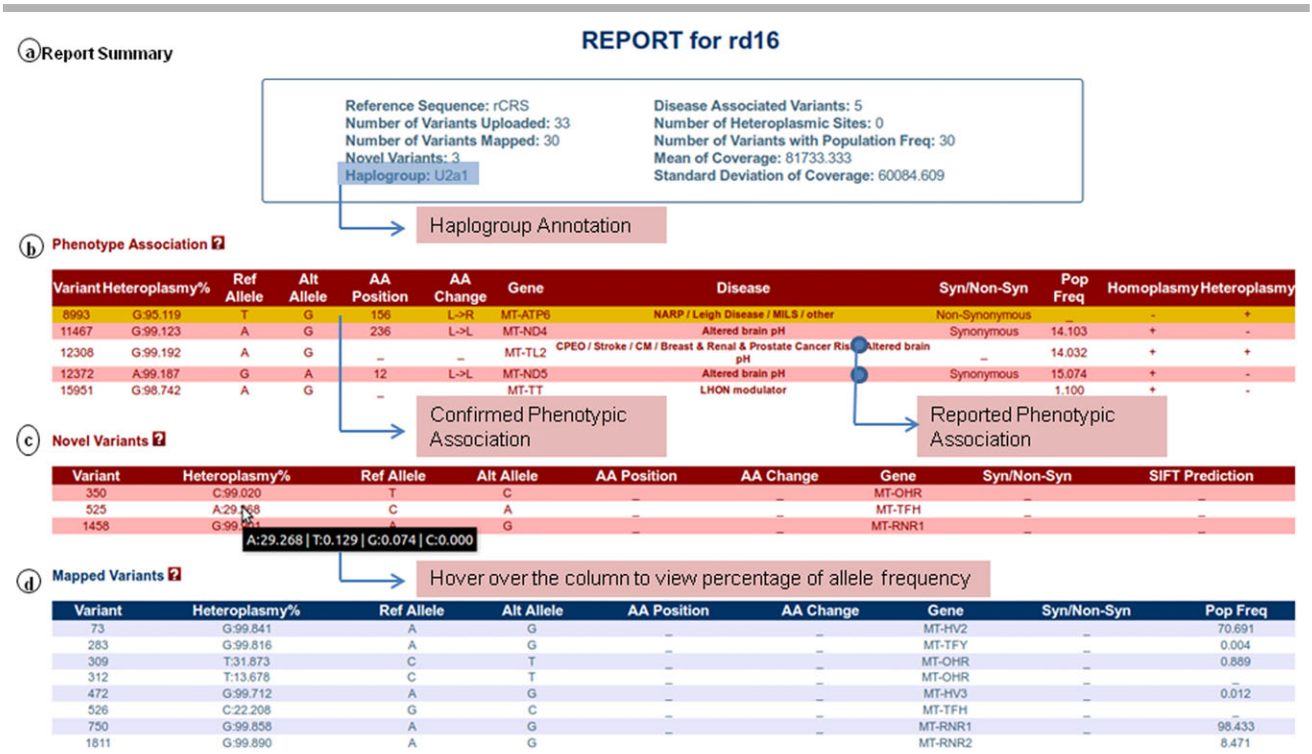

Figure 2. Snapshot of the report page of mit-o-matic. The report summarizes the analysis on top of the page followed by annotations for the variations detected in three different panels. **A:** Summary includes haplogroup, number of heteroplasmic sites, and counts of novel- and disease-associated variants. **B**: Phenotype association section enlists variants with confirmed or reported phenotypic association. **C**: Novel variant section reports all the variations that have not been reported in MITOMAP, mtDB, or MitoLSDB and their corresponding information details are detailed. **D**: Variant map section details variants that have already been reported in the available resources.

Case Study: Application of mit-o-matic for Characterization of Mitochondrial Disorders

To test the utility of mit-o-matic, we used mitochondrial sequence derived from a patient diagnosed with potential Leigh disease and from the patient's mother. Blood sample was taken from individuals abiding all institutional ethical committee rules and regulations. DNA was isolated from 3 ml of blood drawn and amplification of complete mitochondrial DNA was done with the help of long-range PCR (La Taq, Takara) with three overlapping primer sets designed on rCRS [Dames et al., 2013] (Supp. Table S1). All the three PCR products were pooled together to get uniform coverage across the mitochondria by normalizing the number of fragments from each amplicon pool based on the size. Fragmentation for sequencing was done by Covaris SS220 system. Fragmented products were processed further for library preparation using Truseq-DNA sample preparation kit (Illumina, San Diego, California, USA) as per manufacturer's instruction to obtain an insert size of approximately 300 bp. Sequence data were generated using single-end read with a read length of 51 bp on the Genome Analyzer IIx platform (Ilumina).

The sequences from the two samples were mapped onto the modified rCRS reference mitochondrial genome to identify the variants (Supp. Tables S2 and S3). Allelic information was extracted and submitted to the mit-o-matic pipeline for further annotations using the standard pipeline (Table 1). The mit-o-matic pipeline identified a missense mutation from T to G at position 8,993 of the rCRS reference mitochondrial genome, which confirmed phenotypic association with Leigh disease for the patient [Tatuch et al., 1992].

The complete set of variations from the patient's mtDNA matches best to the haplogroup—U2a1. A very low frequency of the variant (T to G at position 8,993) was observed in the mother (0.12%), who shares the same haplogroup with the patient. Position 3,107 represented by "N" is the error nucleotide in the original CRS that is maintained in the revised sequence as a gap [Sondheimer et al., 2011]. The reports of the two cases are summarized as shown in Figure 2.

Table 1. Data Production and Alignment Results for the Patient and the Mother's Sample

	Reads	Mapped reads	Mapping percentage	Coverage
Patient (rd16)	37,776,823	34,699,240	91.85%	106,805.56
Mother (rd22)	5,309,306	4,183,337	78.79%	8,584.31

Conclusions

Mitochondrial variations have been increasingly associated and implicated in a wide variety of human pathophysiological conditions. Conventional methods of mitochondrial variation analysis that include amplicon sequencing using a capillary sequencing approach [Cui et al., 2013] or mitochondrial array-based genotyping [Kassauei et al., 2006] have been developed and employed in clinical practice.

Recent years have seen application of NGS in clinical settings for many diseases. As the use of NGS technology becomes more popular, cost-effective, and well entrenched in clinical settings, one would potentially foresee its applications for diagnosis of mitochondrial disorders as well. Furthermore, the availability of NGS technologies offers a new opportunity to understand mitochondrial variations

at a greater depth [Sosa et al., 2012] with the additional advantage of the possibility to detect low-frequency heteroplasmy sites [Goto et al., 2011]. A number of well-curated resources provide the wealth of mtDNA variations and their phenotypic correlates. However, in general clinical practice, the widespread application of NGS technology for mitochondrial disorders has been hampered by the nonavailability of an integrated computational pipeline. The need of the hour is a pipeline, which could start from mitochondrial sequences, and perform assembly, annotation, and evaluation of clinically relevant variations. mit-o-matic fills in this gap by providing a user-friendly computational pipeline that does not require specialized skills to operate, whereas giving a comprehensive overview of the variants and annotations of the disease-associated variations in a user-friendly and easily interpretable Web interface. It can support any kind of high-quality single-end or paired-end data that have been mapped to the mitochondrial genome, including amplicon sequencing, whole-genome sequencing, and custom enrichment.

The system has been built with future developments in mind, both in terms of usability and applicability. The major future developments would include possibility of integrating the reporting engine with the popular cloud analysis engines such as BaseSpace (http://www.illumina.com/software/basespace.ilmn) and Ion Reporter environments (https://ionreporter.lifetechnologies.com/ir/), which could provide a click-of-a-button ease of mitochondrial variation analysis. We also foresee integration of novel analytical resources and tools for functional annotation of novel mitochondrial variations.

Acknowledgments

The authors thank Dr. Mohd Faruq and Dr. Binuja Varma for their insightful comments, technical help, and reagents.

Disclosure statement: The authors declare no conflict of interest.

Note Added in Proof

During the lengthy revision process for this manuscript, the description of another WES/WGS analysis pipeline tool for mtDNA variants was published, called MToolBox (Calabrese et al., 2014). Our mit-o-matic tool was developed completely independently of MToolBox, without knowledge of its existence.

References

Abaci N, Arikan M, Tansel T, Sahin N, Cakiris A, Pacal F, Sirma Ekmekci S, Gok E, Ustek D. 2014. Mitochondrial mutations in patients with congenital heart defects by next generation sequencing technology. Cardiol Young 25(4):705–711

Adams KL, Palmer JD. 2003. Evolution of mitochondrial gene content: gene loss and transfer to the nucleus. Mol Phylogenet Evol 29:380–395.

Andrews RM, Kubacka I, Chinnery PF, Lightowlers RN, Turnbull DM, Howell N. 1999. Reanalysis and revision of the Cambridge reference sequence for human mitochondrial DNA. Nat Genet 23:147.

Calabrese C, Simone D, Diroma MA, Santorsola M, Gutta C, Gasparre G, Picardi E, Pesole G, Attimonelli M. 2014. MToolBox: a highly automated pipeline for heteroplasmy annotation and prioritization analysis of human mitochondrial variants in high-throughput sequencing. Bioinformatics 30(21):3115–3117.

Craigen WJ, Graham BH, Wong LJ, Scaglia F, Lewis RA, Bonnen PE. 2013. Exome sequencing of a patient with suspected mitochondrial disease reveals a likely multigenic etiology. BMC Med Genet 14:83.

Cui H, Li F, Chen D, Wang G, Truong CK, Enns GM, Graham B, Milone M, Landsverk ML, Wang J, Zhang W, Wong LJ. 2013. Comprehensive next-generation sequence analyses of the entire mitochondrial genome reveal new insights into the molecular diagnosis of mitochondrial DNA disorders. Genet Med 15:388–394.

Dames S, Chou LS, Xiao Y, Wayman T, Stocks J, Singleton M, Eilbeck K, Mao R. 2013. The development of next-generation sequencing assays for the mitochondrial genome and 108 nuclear genes associated with mitochondrial disorders. J Mol Diagn 15:526–534.

Fan L, Yao YG. 2013. An update to MitoTool: using a new scoring system for faster mtDNA haplogroup determination. Mitochondrion 13:360–363.

Goto H, Dickins B, Afgan E, Paul IM, Taylor J, Makova KD, Nekrutenko A. 2011. Dynamics of mitochondrial heteroplasmy in three families investigated via a repeatable re-sequencing study. Genome Biol 12:R59.

Guo Y, Li J, Li CI, Shyr Y, Samuels DC. 2013. MitoSeek: extracting mitochondria information and performing high-throughput mitochondria sequencing analysis. Bioinformatics 29:1210–1211.

He Y, Wu J, Dressman DC, Iacobuzio-Donahue C, Markowitz SD, Velculescu VE, Diaz LA Jr, Kinzler KW, Vogelstein B, Papadopoulos N. 2010. Heteroplasmic mitochondrial DNA mutations in normal and tumour cells. Nature 464:610–614.

Huang T. 2011. Next generation sequencing to characterize mitochondrial genomic DNA heteroplasmy. Curr Protoc Hum Genet Chapter 19:Unit19.8.

Huang W, Li L, Myers JR, Marth GT. 2012. ART: a next-generation sequencing read simulator. Bioinformatics 28:593–594.

Ingman M, Gyllensten U. 2006. mtDB: Human Mitochondrial Genome Database, a resource for population genetics and medical sciences. Nucleic Acids Res 34:D749–D751.

Jensen RE, Johnson AE. 2001. Opening the door to mitochondrial protein import. Nat Struct Biol 8:1008–1010.

K S, Jalali S, Scaria V, Bhardwaj A. 2013. MitoLSDB: a comprehensive resource to study genotype to phenotype correlations in human mitochondrial DNA variations. PLoS One 8:e60066.

Kassauei K, Habbe N, Mullendore ME, Karikari CA, Maitra A, Feldmann G. 2006. Mitochondrial DNA mutations in pancreatic cancer. Int J Gastrointest Cancer 37:57–64.

Kogelnik AM, Lott MT, Brown MD, Navathe SB, Wallace DC. 1996. MITOMAP: a human mitochondrial genome database. Nucleic Acids Res 24:177–179.

Kumar P, Henikoff S, Ng PC. 2009. Predicting the effects of coding non-synonymous variants on protein function using the SIFT algorithm. Nat Protoc 4: 1073–1081.

Kunkele KP, Heins S, Dembowski M, Nargang FE, Benz R, Thieffry M, Walz J, Lill R, Nussberger S, Neupert W. 1998. The preprotein translocation channel of the outer membrane of mitochondria. Cell 93:1009–1019.

Langmead B, Trapnell C, Pop M, Salzberg SL. 2009. Ultrafast and memory-efficient alignment of short DNA sequences to the human genome. Genome Biol 10: R25.

Lee J, Sharma S, Kim J, Ferrante RJ, Ryu H. 2008. Mitochondrial nuclear receptors and transcription factors: who's minding the cell? J Neurosci Res 86:961–971.

Li H, Durbin R. 2009. Fast and accurate short read alignment with Burrows-Wheeler transform. Bioinformatics 25:1754–1760.

Li H, Ruan J, Durbin R. 2008. Mapping short DNA sequencing reads and calling variants using mapping quality scores. Genome Res 18:1851–1858.

Li M, Schonberg A, Schaefer M, Schroeder R, Nasidze I, Stoneking M. 2010. Detecting heteroplasmy from high-throughput sequencing of complete human mitochondrial DNA genomes. Am J Hum Genet 87:237–249.

Maitra A, Cohen Y, Gillespie SE, Mambo E, Fukushima N, Hoque MO, Shah N, Goggins M, Califano J, Sidransky D, Chakravarti A. 2004. The Human MitoChip: a high-throughput sequencing microarray for mitochondrial mutation detection. Genome Res 14:812–819.

Mesecke N, Terziyska N, Kozany C, Baumann F, Neupert W, Hell K, Herrmann JM. 2005. A disulfide relay system in the intermembrane space of mitochondria that mediates protein import. Cell 121:1059–1069.

Pliss L, Tambets K, Loogvali EL, Pronina N, Lazdins M, Krumina A, Baumanis V, Villems R. 2006. Mitochondrial DNA portrait of Latvians: towards the understanding of the genetic structure of Baltic-speaking populations. Ann Hum Genet 70:439–458.

Schmidt O, Pfanner N, Meisinger C. 2010. Mitochondrial protein import: from proteomics to functional mechanisms. Nat Rev Mol Cell Biol 11:655–667.

Schmitt MW, Kennedy SR, Salk JJ, Fox EJ, Hiatt JB, Loeb LA. 2012. Detection of ultra-rare mutations by next-generation sequencing. Proc Natl Acad Sci USA 109:14508–14513.

Shadel GS. 2008. Expression and maintenance of mitochondrial DNA: new insights into human disease pathology. Am J Pathol 172:1445–1456.

Skladal D, Halliday J, Thorburn DR. 2003. Minimum birth prevalence of mitochondrial respiratory chain disorders in children. Brain 126:1905–1912.

Sondheimer N, Glatz CE, Tirone JE, Deardorff MA, Krieger AM, Hakonarson H. 2011. Neutral mitochondrial heteroplasmy and the influence of aging. Hum Mol Genet 20:1653–1659.

Sosa MX, Sivakumar IK, Maragh S, Veeramachaneni V, Hariharan R, Parulekar M, Fredrikson KM, Harkins TT, Lin J, Feldman AB, Tata P, Ehret GB, Chakravarti A. 2012. Next-generation sequencing of human mitochondrial reference genomes uncovers high heteroplasmy frequency. PLoS Comput Biol 8:e1002737.

Tang DL, Zhou X, Zhou KY, Li X, Zhao L, Liu F, Zheng F, Liu SM. 2005. Association of mitochondrial DNA variation with type 2 diabetes mellitus. Zhonghua Yi Xue Yi Chuan Xue Za Zhi 22:636–640.

Tatuch Y, Christodoulou J, Feigenbaum A, Clarke JT, Wherret J, Smith C, Rudd N, Petrova-Benedict R, Robinson BH. 1992. Heteroplasmic mtDNA mutation (T—-G) at 8993 can cause Leigh disease when the percentage of abnormal mtDNA is high. Am J Hum Genet 50:852–858.

Taylor RW, Turnbull DM. 2005. Mitochondrial DNA mutations in human disease. Nat Rev Genet 6:389–402.

Underhill PA, Kivisild T. 2007. Use of y chromosome and mitochondrial DNA population structure in tracing human migrations. Annu Rev Genet 41:539–564.

Wiedemann N, Kozjak V, Chacinska A, Schonfisch B, Rospert S, Ryan MT, Pfanner N, Meisinger C. 2003. Machinery for protein sorting and assembly in the mitochondrial outer membrane. Nature 424:565–571.

Yan MH, Wang X, Zhu X. 2013. Mitochondrial defects and oxidative stress in Alzheimer disease and Parkinson disease. Free Radic Biol Med 62:90–101.

MULTIPLE SECRETVISUAL CRYPTOGRAPHIC SCHEMES USING HALFTONE PATTERN

T.B.Yugendran[1], M. Logesh[2], N. Ezhilvaluthi[3], Mrs.A.Niranjana[4]

[1,2,3,4] *Department of Computer Science and Engineering,*
Easwari Engineering College, Chennai, Tamil Nadu, (India)

ABSTRACT

Visual Cryptography Scheme (VCS) is an encryption method used to encode secret written materials. The idea is to convert the written material into a binary image and encode this image in to n shadow image it is also called as shares of images. The decoding only requires selecting some subset of these n shadow images, making transparencies of them and stacking them on top of each other. Main advantage of this scheme is mathematical computation complexity is reduced to visual cryptographic techniques. Each participant holds a transparency. The pixel expansion and relative contrast are the most critical measurements to evaluate the effectiveness of a VCS. In this paper, VC in addition to Multiple-Secret Visual Cryptographic Schemes (MSVCS) can achieve the minimum pixel expansion and the maximal contrasts.Todevelop a novel and efficient construction for VC using MSVCS. The proposed Visual Cryptograms of Random Grids aims at the minimization of the pixel expansion and maximal contrasts for individual a VC. The Experimental results demonstrate the feasibility, applicability, and flexibility of our construction. The pixel expansions and contrasts derived from our scheme are also better than the previous results.

Keywords -Decryption, Embedded Visual Cryptography Scheme,Encryption,MSVCS And Visual Cryptographic.

I. INTRODUCTION

1.1 Halftone is the reprographic technique that simulates continuous tone imagery through the use of dots, varying either in size or in spacing, thus generating a gradient like effect. "Halftone" can also be used to refer specifically to the image that is produced by this process. Where continuous tone imagery contains an infinite range of colors or greys, the halftone process reduces visual reproductions to an image that is printed with only one color of ink, in dots of differing size or spacing.

1.2 Visual cryptography is to be encrypted in such a way that decryption becomes a mechanical operation that does not require a computer.

In visual secret sharing scheme,an image was broken up into *n* shares so that only someone with all *n* shares could decrypt the image, while any $n - 1$ shares revealed no information about the original image. Each share was printed on a separate transparency, and decryption was performed by overlaying the shares. When all *n* shares were overlaid, the original image would appear. Using a similar idea, transparencies can be used to implement a one-time pad encryption, where one transparency is a shared random pad, and another transparency

acts as the cipher text. Normally, there is an expansion of space requirement in visual cryptography. But if one of the two shares is structured recursively, the efficiency of visual cryptography can be increased to 100%

1.3 Authentication is the process of determining whether someone or something is, in fact, who or what it is declared to be. In private and public computer networks, authentication is commonly done through the use of logon passwords. Knowledge of the password is assumed to guarantee that the user is authentic. Each user registers initially, using an assigned or self-declared password. On each subsequent use, the user must know and use the previously declared password. The weakness in this system for transactions that are significant is that passwords can often be stolen, accidentally revealed, or forgotten.

II. LITERATURE SURVEY

Visual cryptography is one of the techniques used to encrypt the images by dividing the original image into transparencies. The transparencies can be sent to the intended person, and at the other end the transparencies received person candecrypt the transparencies using our tool, thus gets theoriginal image. The proposed Visual cryptography provides the demonstration to the users to show how encryption anddecryption can be done to the images. In this technology, theend user identifies an image, which is not the correct image.That is, while transmitting the image the sender will encryptthe image using our application here sender gets the two ormore transparencies of the same image. An application provides an option to the end user of encryption [1]. The end usercan divide the original image into number of different images.Using our application can send encrypted images that arein the format of GIF and PNG. The encrypted transparenciescan be saved in the machine and can be sent to the intendedperson by other means [source].The performance achievedis any qualified subset of shares can recover the secret image watermarking helps in enables Information hiding, copyright & piracy protection. Here, a technique involving halftone visual cryptography along with watermarking is proposed to achieve visual cryptography via half toning. Digital watermarking is then performed to this halftone image. This ensures that the merits of both visual cryptography and any forbidden subset of shares cannot obtain any information of the secret image other than the size of the secret image [5]. The drawback of print and scan process can introduce noise as well which can make the alignment difficult.

In [2], a method of Information hiding & Piracy protection in Image processing is discussed. Visual cryptography & Digital watermarking are achieved.The performance achieved isdata security has been a challenging task data hiding has a security hole in the encrypted Share file.The main drawback isone type of image format only.Occur due to pixel expansion and Contrast level.

In [3], Phishing is an attempt by an individual or a group to thieve personal confidential information such as passwords, credit card information etc. from unsuspecting victims for identity theft, financial gain and other fraudulent activities. In this paper we have proposed a new approach named as "A Novel Antiphishing framework based on visual cryptography" [4] to solve the problem of phishing. Here an image based authentication using Visual Cryptography is used.

The use of visual cryptography is explored to preserve the privacy of image captcha by decomposing the original image captcha into two shares that are stored in separate database servers such that the original image captcha can be revealed only when both are simultaneously available, the individual sheet images do not reveal the identity of the original image captcha. Once the original image captcha is revealed to the user it can be used as the password. The Performance Achieved is an image based authentication using Visual Cryptography is

used [6].The use of visual cryptography is explored to preserve the privacy of image captcha. The drawback aspect ratio of the recovered image cannot be maintained.The pixel-expansion problem is a major drawback with most VCSs that use the VC-based approach.

DIFFERENCES BETWEEN EXISTING SYSTEM AND PROPOSED SYSTEM

Table: 1 Comparison of Existing and Proposed System

S.No	EXISTING SYSTEM	PROPOSED SYSTEM
1	Maximum Pixel Expansion & Minimum Contrast	Minimum Pixel Expansion & Maximum Contrast
2	No Password Protection	Password Protection
3	Only Single Mode 2 out of 2	Multiple Mode n out of n
4	Only on JPG format Image	JPEG, PNG, PDF & etc.

III. SYSTEM ARCHITECTURE

3.1 Modules

1.1. Halftone Pattern

1.2. Embedded MSVCS

1.3. Stacking (Covering Subsets)

1.4. Authentication

1.5. Tampering

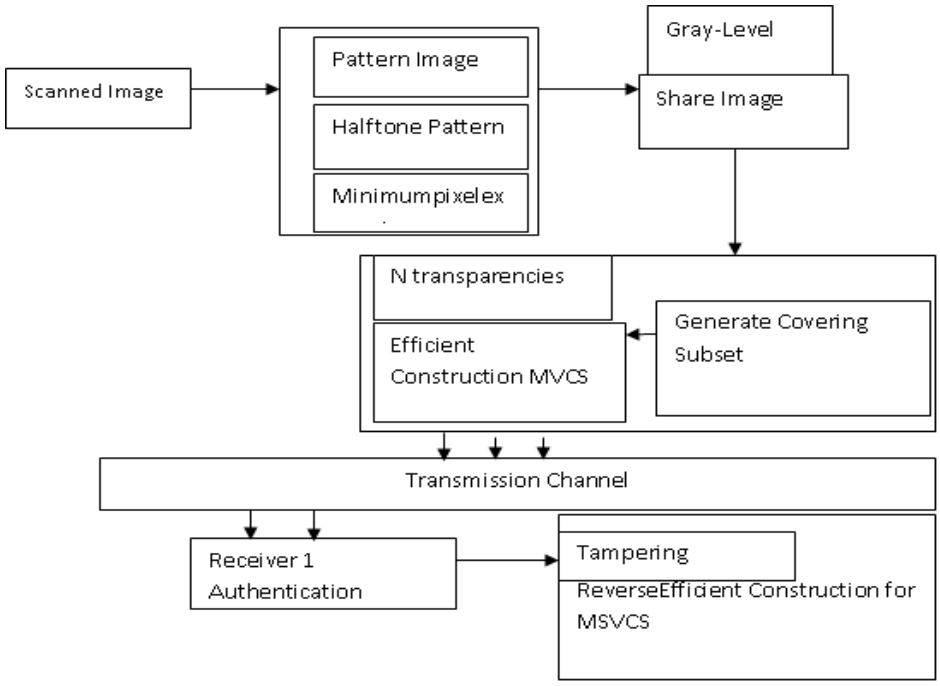

Fig.1 System Architecture Diagram

IV. FUNCTIONAL ARCHITECTURE

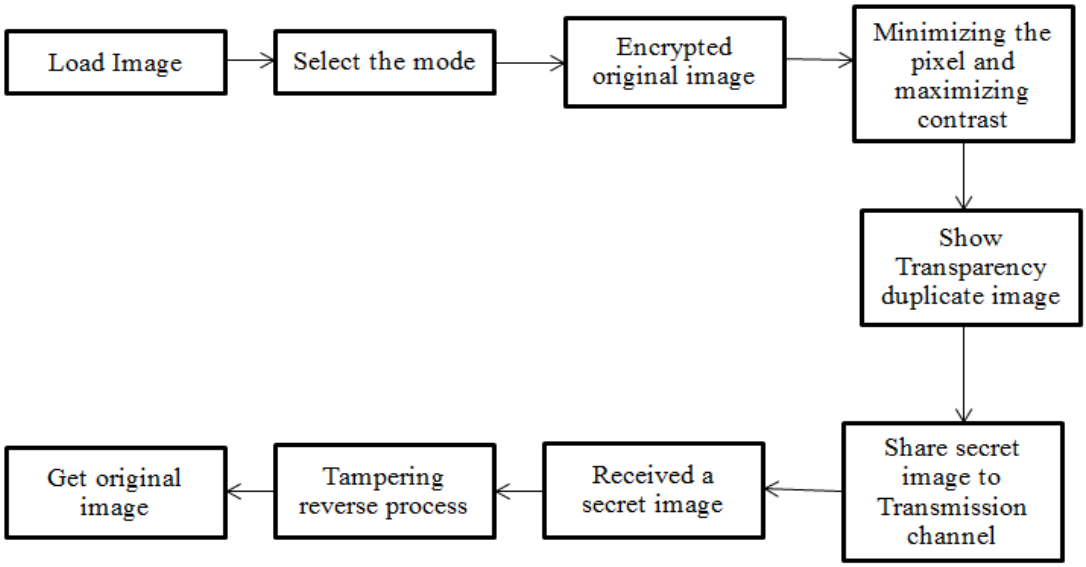

Fig.2 Functional Architecture diagram

V. MODULE DISCRIPTION

5.1. Halftone Pattern

To obtain the original image with only k shares out of n shares, then all the 'n' image shares are necessarily overlaid. When all the image shares that are overlaid are authenticated to be from the same original image.MSVCS share with transparent pixels and pixels from the cover images. MSVCS by using half toning techniques, and hence can treat gray-scale input share images. Their methods made use of the complementary images to cover the visual information of the share images.By using Patterning dithering matrix makes use of a certain percentage of black and white pixels, often called patterns, to achieve a sense of gray scale in the overall point of view.

5.2. Embedded MSVCS

Embedded MSVCS encode a secret image; the dealer takes gray-scale original share images as inputs, and converts them into covering shares which are divided into blocks of sub pixels. Embedded MSVCS contains three main steps:

5.2.1. Generate covering shares.

5.2.2. Generate the embedded shares by embedding the corresponding VCS into the 'n' covering shares information of the original share images are all covered. The stacking results are not necessarily to be all black images. The covering shares have the advantage it's a qualified subsets

5.2.3. Multiple-Secret Visual Cryptographic Schemes (MSVCS) can achieve the minimum pixel expansion and the maximal contrasts.Integer linear program aims at the minimization of the pixel expansion under the constraints for being a MSVCS.

5.3 Stacking (Covering Subsets)

The stacking results of the qualified shares are all black images, the of stacked.All the information of the patterns in the original share images is covered. Hence the visual quality of the recovered secret image is not affected.

5.4 Recipient/Authentication

Authentication has been verified by using Hash Authentication Code algorithm. Authorized user (Recipient) able to access the image, transmitted from Sender.Hash-based Message Authentication Code (HMAC) is a message authentication code that uses a cryptographic key in conjunction with a hash function.

5.5 Tampering

To detect whether or not a digital content has been tampered with in order to alter its semantics, the use of multimedia hashes turns out to be an effective solution.The hash to estimate and prevent the mean square error distortion between the original and the received image.At the cost of additional complexity at the decoder, the proposed algorithm is robust to moderate content-preserving transformations including cropping hash decoding.

VI. HALFTONE ALGORITHM

Halftone is the reprographic technique that simulates continuous tone imagery through the use of dots, varying either in size, in shape or in spacing.Where continuous tone imagery contains an infinite range of colors or greys, the halftone process reduces visual reproductions to a binary image that is printed with only one color of ink. Halftone contact screens can be MAGENTA or GRAY in color. Tint Screen: is used in the platemaking process to create the uniform tone pattern and contains a hard dot structure that is specified by a dot percentage.

1. Highlight = 5-10% in size.
2. Mid-tone = 30-70% in size.
3. Shadow = 90-95% in size
4. Highlights: the whitest tonal value.
5. Mid-tones: the gray tonal values.
6. Shadows: the darkest black tonal value.

VII INPUT & OUTPUT

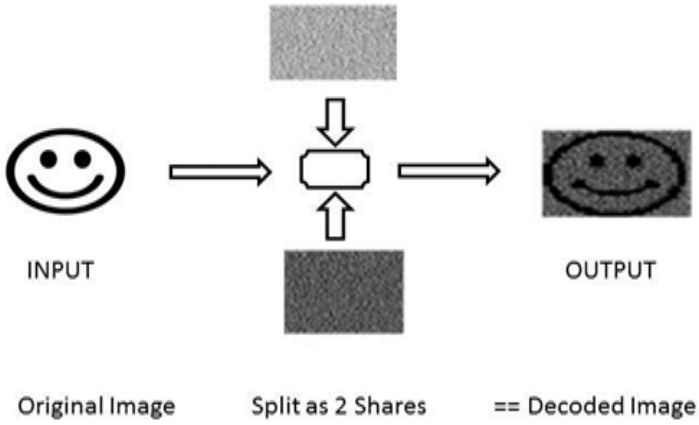

Fig.3 Input and Output Virtual Cryptographic Scheme

OUTPUT

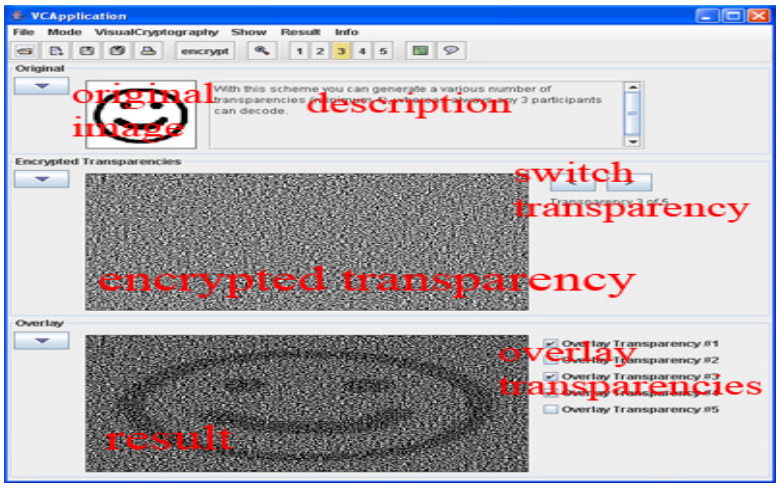

Fig.4 MSVCS Output

VIII. CONCLUSION

To established an efficient construction of n-MSVCS using the skill of linear programming in this paper. The object function aims at minimizing the pixel expansion subject to the constraints satisfying the region incrementing requirements. Unit matrices are introduced as the building blocks and thenumbers of the unit matrices chosen to form the basis matrices of n-MSVCS are set as the decision variables. A solution to these decision variables by our linear program delivers a feasible set of basis matrices of the required n-MSVCS with theminimum pixel expansion. The pixel expansions and contrasts derived from our n-MSVCS are better than the previous results. Since no construction method has ever been reported in the literature, our linear program formulation for n-MSVCS is novel and innovative from both the theoretical and practical points of view. The contrasts of different secret regions can also be designated in the constraints. This enhances the adaptability and flexibility of our MSVCS in practical applications.

IX. FUTURE ENHANCEMENTS

Embedded MSVC has many specific advantages against different well-known schemes, such as the fact that it can deal with gray-scale input images, has smaller pixel expansion, is always unconditionally secure, does not require complementary share images, one participant only needs to carry one share, and can be applied for general access structure. Furthermore, our construction is flexible in the sense that there exist two trade-offs between the share pixel expansion and the visual quality of the shares and between the secret image pixel expansion and the visual quality of the shares.

REFERENCES

[1] N. Anusha and P. Subba Rao, "Visual Cryptography Schemes for Secret Image," Inf. Computat., ISSN: 2278-0181, Vol. 1 Issue 5, July - 2014.

[2] M.Bharathi, R.Charanya and T.Vijayan "Halftone Visual Cryptography & Watermarking" ISSN: 2278-0181, Vol. 2 Issue 4, April - 2013.

[3] Dr.D.C.Joy Winnie Wise, Mr. H.Jeyamohan, A. Sreenivasa, and K.P.Vijaiy, "Visual Cryptography Scheme to Predict Phishing Sites," IJCSEC. Vol.2 ISSN: 2347–8586.Issue.4, July 2014.

[4] G. Ateniese, C. Blundo, A. De. Santis, and D. R. Stinson, "Extendedcapabilities for visual cryptography," Theoretical Computer Sci., vol.250, pp. 143–161, 2001.

[5] G. Ateniese, C. Blundo, A. De. Santis, and D. R. Stinson, "Visual cryptography for general access structures," Inf. Computat., vol. 129, pp.86–106, 1996.

[6] G. Ateniese, C. Blundo, A. De. Santis, and D. R. Stinson, "Constructionsand bounds for visual cryptography," Lecture Notes Computer Science. vol. 1099, pp. 416–428, 1996.

ARTIFICIAL INTELLIGENCE AND EXPERT SYSTEMS

Salil Bhalla[1], Sunandita Singh[2], Sakshi Bhalla[3]

[1]Assistant Professor, [2]Student, Electronics and Communication Engineering Department, Haryana Engineering College, Jagadhri(India)

[3]Technology Consultant, Hewlett Packward, Bangalore (India)

ABSTRACT

The issues and ethical problems that are arising in information system and automation in current time are somewhat different from the ethical problems that are related to future creation of machines with intellectual capabilities for outstripping those of humans. This super intelligence is not just important intention ever made it is also another technological development and more primarily it would lead to an explosive progress in all technological and scientific fields, as super intelligence would manage research with superhuman efficiency. The ethical and moral implications of artificial intelligence are different sides to the arguments and they are obvious. This paper will tell us about the concept and meaning of Artificial Intelligence, its applications, its merits etc. This paper focuses on somewhat different moral and ethical issues of AI and discusses what motivation we ought to give a super intelligence, and introduces considerations related to the development should be accelerated or retarded.

Keywords: Ai Components, Ai Intelligence, Applications, Brainwashing, Expert System, Robotics.

I. INTRODUCTION

The significant aim in research of Artificial Intelligence is to devise machines so that they perform various tasks normally that require human intelligence [1]. AI defines the field as “the study and design of intelligent agents [2]”. An intelligent agent is a system that takes actions which maximizes its chances of success and perceives its environment [3]. AI is the intelligence of robots and machine and also the branch of computer science that aims to create it. Playing good games of chess, learning to improve its own performance, learning to translate languages and proving mathematical theorems are few such things that machine is expected to perform[4][5]. Although each of these tasks have somewhat certain peculiarities that defines it uniquely, many workers who work in this field feel that there are various characteristics which are common to the tasks which require intelligence and they have also tried to work on those problems in which these characteristics were quite visible and those tasks which are somewhat visible and common to many intelligence problems are initial description of a problem and transformation it into a more easily solvable form, heuristic approach and sub-problems associated to it, breakdown of a difficult problem into several other easier problems, and learning them through induction from various past experiences of it.

II. OBJECTIVES OF THE STUDY

· To know the meaning and concept of AI.

- To know the applications where AI is applicable.
- To study the concept of principles in AI.

III. ARTIFICIAL INTELLIGENCE

Artificial Intelligence is that branch of computer science which aims to study the computation requirements for various tasks including reasoning, perception, learning and develops the systems to perform those tasks. This term was coined by John McCarthy in 1955 at Massachusetts Institute of Technology [6] and defined it as, "the science and engineering of making intelligent machines."[7]. Intelligence means to respond flexibly to various situations and to make sense out of contradictory and ambiguous messages. The goals and central problems of AI research includes planning, knowledge, learning, reasoning and perception. Some current popular approaches consists of statistical methods and computational intelligence. The field of AI is interdisciplinary in which number of professions and sciences converges and which includes mathematics, psychology, philosophy, neuroscience and also other specialised fields such as artificial psychology. The field of AI aims to understand and build intelligent entities.

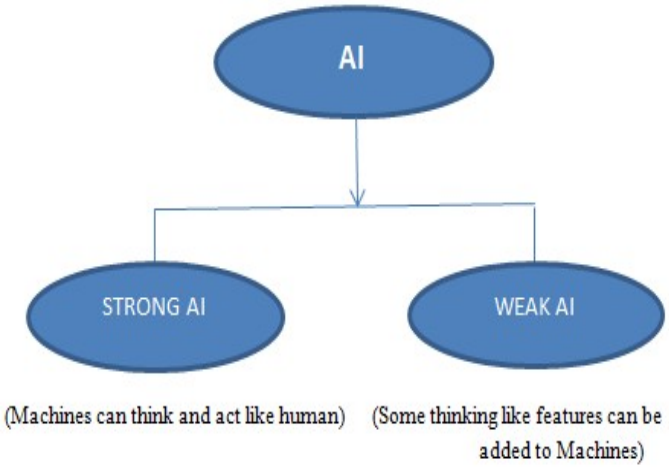

AI Is the field of science that deals with the analysis and synthesis of computational agents that act intelligently. An agent is something that acts in the environment i.e. it does something. We are only interested in what an agent does i.e how it acts to a particular environment. We can judge an agent by its actions. An agent is called to act intelligently when what it does is appropriate for its goals and circumstances, it is flexible to changing environments and changing goals, it makes appropriate choices, and it cannot observe the state of the world directly and it has limited time to act and has a finite memory. A computational agent is that agent who decides about its actions and which can be explained in terms of the computation. This means that decisions can be broken into primitive operation that can be implemented in some physical device. This type of computation can take many different forms. In human beings this type of computation is carried out in the "wetware" and in computers this computations is carried out in the "hardware".

IV. COMPONENTS OF AI

Mainstream thinking in psychology regards human intelligence not as a single ability process but rather as an array of separate different components. Research in Artificial Intelligence has focussed chiefly on the following components of intelligence: learning, reasoning, problem-solving, perception, and language-understanding. [10]

4.1 Learning

Learning can be distinguished into many other different forms which are applied to artificial intelligence. The simplest form is learning through trial and error. For example, a simple computer program used for solving mate-in-one chess problems tries to move randomly until the mate is found. The program then store the solution with the position so that when next time the computer encounter the same position it would recall the solution which is stored previously. Solutions to problems, words of vocabulary etc., these simple memorising of individual items is known as rote learning. Rote learning is relatively easy to implement on the computer. More challenging problem of implementing is called generalization. It involves applying past experience to new situations. This means that learning which involves generalisation makes the learner able to perform better in situations which are not encountered previously. For example, the program that learns the past tense of English verbs by rote will not be able to make the past tense of the word such as jump unless it had been presented previously with jumped, whereas a program that is able to generalize can be able to learn the "add-ed" rule and so can form the past tense of jump based on the experience with similar verbs. Sophisticated modern techniques enable the programs to generalise complex rules from the data.

4.2 Reasoning

To reason is to draw inferences appropriate for the particular situation. Inferences are classified either as deductive or inductive. An example of the former is, "Fred must be in either the museum or the café. He is not in the café; therefore he is in the museum," and of the later, "Previous accidents of this sort were caused by instrument failure; therefore this accident was caused by instrument failure." The most significant difference between these forms of reasoning is that in the deductive case the truth of the premises guarantees the truth of the conclusion whereas in the inductive case the truth of the premises lends support to the conclusion without giving absolute assurance. Inductive reasoning is very common in science, where data are collected and tentative models are developed to describe and predict the future behaviour until the appearance of the anomalous data forces the model to be revised again.

4.3 Problem solving

Problem solving has a general form for example given such and such data and find 'x'. Problem solving in artificial intelligence, may be characterized as a systematic search through a range of possible actions in order to reach some predefined goal or solution. A huge variety of different types of problems is addressed in artificial intelligence. Problem solving methods is divided into two parts-special purpose and general purpose. A special-purpose method is tailor-made for a particular problem and often exploits very specific features of the situation in which the problem is being embedded. In contrast, the general-purpose method is applicable to a wide variety of problems. One example of general-purpose technique used in Artificial Intelligence is means-end analysis—a step-by-step, or incremental, reduction of the difference between current state and final goal. The program selects actions from a list of different means which in the case of, say, a simple robot that might consist of PICKUP, PUTDOWN, MOVEFORWARD, MOVEBACK, MOVELEFT, and MOVERIGHT—until the goal state is reached from the current state.

4.4 Perception

In perception component the environment is scanned by means of various sensory organs which may be real or artificial, and processes analyse the scene and then the scene is decomposed into different objects in various

spatial relationships and their features. Analysis is somewhat complicated by the fact that an object present itself into many other different appearances on various other different occasions and it depends on the angle from which it is viewed, the direction and intensity of illumination in the scene, and how much the object contrasts with the surrounding field, whether or not the parts of it are projecting shadows. Artificial perception is sufficiently well advanced to enable optical sensors to identify individuals, autonomous vehicles like self controlled car device to drive at moderate speeds on the open road, and robots to roam through buildings searching for empty soda cans. One of the earliest systems to integrate perception and action was FREDDY, a stationary robot with a moving television eye and a pincer hand, constructed at the University of Edinburgh, Scotland, during the period 1966–73 under the direction of Donald Michie, who was able to recognise variety of objects from heap of components.

4.5 Language

A language is a system of signs having meaning by convention. Traffic signs, for example, form a mini language, it being a matter of convention that [hazard] means “hazard ahead” in some countries. An important characteristic of full-fledged human language for example English, which distinguishes them from, e.g. bird calls and systems of traffic signs, is their *productivity* A productive language can formulate an unlimited variety of sentences. A productive language is one that is rich enough to enable an unlimited number of different sentences to be formulated within it.

V. APPLICATIONS OF AI

There are various different areas where the Artificial intelligence is applicable. Few of them are as follows-

- Expert System
- Natural Language Processing (NLP)
- Speech Recognition
- Computer Vision
- Robotics
- Automatic Programming

5.1 Expert System

Expert Systems are computer programs that are derived from a branch of computer science research called Artificial Intelligence (AI). Expert system currently is designed to assist experts, not to replace them.

Expert system consists of two main parts. These are knowledge base and the reasoning or inference. The knowledge base of expert systems contains both factual knowledge and heuristic knowledge. Factual knowledge is that knowledge of the task domain that is widely shared, typically found in textbooks or journals, and commonly agreed upon by those knowledgeable in the particular field. Heuristic knowledge is the less rigorous, more experiential, more judgmental knowledge of performance. In contrast to factual knowledge, heuristic knowledge is rarely discussed, and is largely individualistic. It is the knowledge of good practice, good judgment, and plausible reasoning in the field. It is the knowledge that underlies the "art of good guessing." Knowledge representation formalizes and organizes the knowledge. One widely used representation is

the production rule, or simply the rule. A rule consists of an IF part and a THEN part (also called condition and action). The IF part lists a set of conditions in some logical combination. The piece of knowledge represented by the production rule is relevant to the line of reasoning being developed if the IF part of the rule is satisfied; consequently, the THEN part can be concluded, or its problem-solving action taken. Expert systems whose knowledge is represented in rule form are called rule-based systems. They have been used in medical diagnosis, chemical analysis, geological exploration etc.

5.2 Natural Language Processing (NLP)

Natural language processing is an interesting and difficult domain in which to develop and evaluate representation and reasoning theories. All of the problems of AI arise in this domain; solving "the natural language problem" is as difficult as solving "the AI problem" because any domain can be expressed in natural language. The field of computational linguistics has a wealth of techniques and knowledge. It helps to enable people and computers to communicate in a natural language (such as English) rather than in the computer language.

5.3 Speech Recognition

The user communicates with the application through the appropriate input device i.e. a microphone. The Recognizer converts the analog signal into digital signal for the speech processing. A stream of text is generated after the processing. This source-language text becomes input to the Translation Engine, which converts it to the target language text. The goal is to allow computers to understand human speech so that they can hear our voices and recognize the words we are speaking. It simplifies the process of interactive communication between people and computers.

5.4 Computer Vision

By vision, we meant of sensing environment. The goal of computer vision is to give computers this same powerful facility for understanding their surroundings. To do with seeing using information mediated by light in order to interact successfully with the environment As much to do with biological systems as with computers, but there are many different approaches: How do people and animals see? How can we make useful robots that see? What are the general computational structures that underly vision? How do we reconstruct the 3rd dimension from 2-D images? How can we build machines to solve specific tasks involving vision? Very interdisciplinary Artificial Intelligence, Computer Science, Engineering, Psycholog, Neuroscience, Mathematics. AI helps computer to understand what they see through attached cameras.

5.5 Robotics

A robot is an electro mechanical device that can be programmed to perform manual tasks or a reprogrammable multi-functional manipulator designed to move materials, parts, tools or specialized devices through variable programmed motions for performance of variety of tasks. Artificial intelligence and robotics are two closely related areas of study that fall under the field of computer science. AIand robotics specialists design computers and machines that act similar to humans with as little human involvement as possible. An intelligent robot includes some kind of sensory apparatus that allows it to respond to change in its environment.

5.6 Automatic Programming

Programming is the process of telling a computer that exactly what you want it to do. The aim of automatic

planning is to create special programs that act intelligent tools to assist programmers and expedite each phase of programming process

VI. EXPERT SYSTEM ETHICS

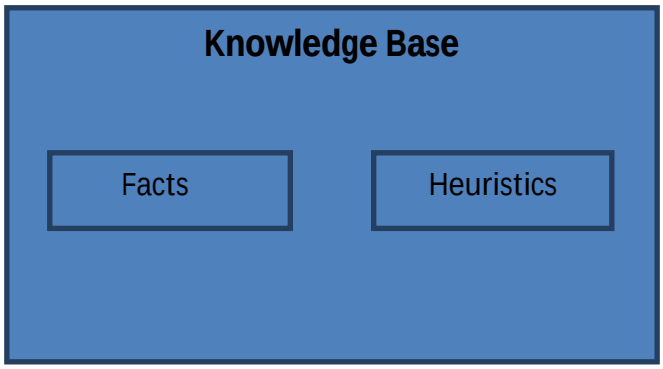

The most important applied area of AI is the field of expert systems. An expert system (ES) is a knowledge-based system that employs knowledge about its application domain and uses a reason procedure to solve various problems that would otherwise require human expertise. The power of expert systems aims primarily from the specific knowledge about a narrow domain stored in the expert system's knowledge base. Expert systems do not have human capabilities. They use a knowledge base of a particular domain and bring that knowledge to bear on the facts of the particular situation at hand. The knowledge base of an expert system also contains heuristic knowledge, the knowledge rules of thumb used by human experts who work in that domain. The applications of expert system include high-risk credit decisions, advertising decision making, and manufacturing decisions. There are various generic categories of expert system applications which include classification, diagnosis, monitoring, process control, design, scheduling and planning, and generation of options. Classification means identifying the object based on stated characteristics. Diagnosis Systems means infering any malfunctioning or disease from the observable data. Monitoring means comparing data from a continually observed system to prescribe certain behaviour. Process Control means controlling a physical process based on monitoring. Design means configuring a system according to specifications. Scheduling & Planning means to develop or modify a plan of action. Generation of Options means generating an alternative solution to a problem. Expert System technologies include Specific expert systems, Expert system shells, Expert system development environments, High-level programming languages.

There are several levels of Expert System technologies available. There are two important things which are to be kept in mind while selecting expert system tools, these are-

1. The tool selected for the project has to match the capability and sophistication of the projected ES, in particular, the need to integrate it with other subsystems such as databases and other components of a larger information system.
2. The tool also has to match the qualifications of the project team.

VII. ROBOTICS AND NEURAL NETWORKS

Artificial intelligence and robotics are two areas of study that are closely related and they fall under the category of computer science. Robotics and artificial intelligence robotics specialists design machines and computers that similar to humans where very little human involvement is possible. It considers the fat that how artificially intelligent beings may be used to benefit humans and how they may be used to harm humans.

7.1The threat to privacy

Aleksandra Solzhenitsyn's The First Circle describes the use of speech recognition technology in the service of tyranny. If an AI program exists that can understand speech and natural languages (e.g. English), then, with adequate processing power it could theoretically listen to every phone conversation and read every email in the world, understand them and report back to the program's operators exactly what is said and exactly who is saying it.

7.2 Robot Rights

Robot rights are those moral obligations of society towards its machines, similar to animals or human rights. These may include the right to life and liberty, freedom of thought and expression and equality before the law. The issue has been considered by the Institute for the Future and by the U.K. Department of Trade and Industry.

7.3 The Threat to Human Dignity

Joseph Weizenbaum argued in 1976 that AI technology should not be used to replace people in positions that require respect and care, such as:

- A customer service representative, (AI technology is already used today for telephone-based interactive voice response systems)
- A therapist, (as was seriously proposed by Kenneth Colby in the 1970s)
- A nursemaid for the elderly, (as was reported by Pamela McCorduck in her book The Fifth Generation)
- A judge, or
- A police officer.

VIII. BRAINWASHING

The above statements are very good example of complexity in programming an artificial brain. The human brain is evolved through millions of years of survival and social behaviour. Imitating human brains working is a huge challenge and by judging the advance of current processor power and complexity it will take several decades more to reach. Once its decided that people want android robots and other machines with an artificially created intelligence sophisticated enough to rival our own. But the question still remains with which ethical and moral values should one install them?

AI shows the same diversity as humans, so what would be the point of creating artificial humans? There are no clear answers. Research is very diverse covering all of the aspects of Artificial Intelligence. We do not even agree on what exactly defined intelligence and already we are creating artificial ones. If we do build android machines with a intended intelligence that think and behave like humans, should not they made absolutely submissive to us?. The super human intelligence that not grant rights can think their human masters and might resist control. The AI's who are granted rights may begin to feel themselves superior to humans and that the rights granted by humans are insufficient. They may view that it is then their decisions of what rights to grant to

humans and not the decision of humans of what rights to grant to them. Many have examined this problem of AI and come to a diverse set of conclusions. IssacAsimov formulated the famous three laws of Robotics which should be the most basic leading behaviour of all Robots. The laws are:-

- A robot may not damage human being or allow a human being to come and harm human.
- A robot must obey instructions given it by human beings except where such orders would conflict with the first law.
- A robot must protect its own existence as long as such protection does not spat with the first and second law. Thus any potential for anti-human action are completely eliminated.

So on a more realistic manner, one should create an artificial intelligence in android or machine form, that would function as an unbiased entity and that this entity's only purpose for eg. Is to teach.

So, then does one give up the obvious benefits of creating AI that can do work of human beings and renounce from doing so? Or does one risk the damage of the species, giving into the desire to improve the quality of human life and to push the limits of human knowledge. Therefore, the issue of which principled, moral and cultural values to instate on our artificially created intelligence goes on. If it cannot even answer a simple "why?", then maybe we should make sure these machines are not intelligent at all. Not capable of making any decision beyond mechanical, programmed movement and certainly not capable of any deductive reasoning and not in any position where it could influence or have control over humans or human society.

XI. CONCLUSION

This paper focuses on the concept that artificial intelligence is becoming a debatable topic these days. The risks in developing super intelligence include the risk of failure to give it the super goal of philanthropy. One way in which this could happen is that the creators of the super intelligence decide to build it so that it serves only this select group of humans, rather than humanity in general. More subtly, it could result in a super intelligence realizing a state of affairs that we might now judge as desirable but which in fact turns out to be a false utopia, in which things essential to human flourishing have been irreversibly lost. We need to be careful about what we wish for from a super intelligence; because we might get it. Many diverse problems have been solved by artificial intelligence programs. Some examples are finding the winning move (or sequence of moves) in a board game, devising mathematical proofs, and manipulating "virtual objects" in a computer-generated world. One deliberation that should be taken into account when deciding whether to promote the development of super intelligence is that if super intelligence is possible, it will likely be developed sooner or later. Therefore, we will almost certainly one day have to take the gamble of super intelligence no matter what. But once in existence, a super intelligence could help us lessen or eliminate other existential risks, such as the risk that advanced nanotechnology will be used by humans in warfare or terrorism, a serious threat to the long-term survival of intelligent life on earth. If we get to super intelligence first, we may avoid this risk from nanotechnology and many others. If, on the other hand, we get nanotechnology first, we will have to face both the risks from nanotechnology and, if these risks are survived, also the risks from super intelligence. The overall risk seems to be minimized by implementing super intelligence, with great care, as soon as possible. Artificial intelligence is making humans redundant and their frirndliness supergoal will cause it to value humanity and individual human beings. An AI coordinating a city could do so in tandem with, not instead of, humans. It is possible for a team of people to control all the traffic lights in a city, but people get bored and sick and quit, and they need breaks for

lunch and cannot work continously. A machine that controls the traffic signals can operate forever, never takes a day off, and never ends a day off, and never needs to be paid. It would be more efficient, and safe.

REFERENCES

[1] Anonymous," Current research and development in scientific documentation, 14," National Science Foundation Washington, D.C., Rept.NSF-66-17.1966.

[2] Poole Mack worth & Goebell1998. P.1

[3] Russell & Norvig 2003, pp.27, 32-58,968-972., Poole &Mack worth&Goebell 1998, pp: 7-21, Luger &Stubbefield 2004, pp.235-240

[4] P.Abrahamas, J.Hansen, and M.Pivar," Final Report, research in sequence analysis,"Information International, Inc.,Cambridge,Mass.,April 1965.

[5] R.J.Solomonoff,"Some recent work in Artificial Intelligence", Proceedings of the IEEE, Vol.54, No.12,December 1966

[6] Tecuci.G.(2012),"Artificial Intelligence. Wires CompStat", 4:168-180.doi:10.10021 wics.200

[7] O'Connor, Kathleen Malone (1994),"The Alchemical creation of life and other concepts of Genesis in medieval Islam. University of Pennsylvania. Retrieved 10 January 2007.

[8] The optimism referred to includes the predictions of early AI researchers (see optimism in the history of AI) as well as the ideas of modern transhumanists such as Ray Kurzweil.

[9] See the Dartmouth proposal, under Philosophy,

[10] R.J.Solomonoff,"Some recent work in Artificial Intelligence", Proceedings of the IEEE, Vol.54, No.12,December1966.

BIOGRAPHICAL NOTES

1. Mr. Salil Bhalla is presently working as Assistant Professor in Electronics and Communication Engineering Department in Haryana Engineering College, Jagadhri, India.

2. Ms. Sunandita Singh is presently pursuing M-Tech in Electronics and Communication Engineering from Haryana Engineering College, Jagadhri, India.

3. Mrs. Sakshi Bhalla is presently working as Technology Consultant in HP (Hewlett Packward), Bangalore, India.

GRAPHENE: A FUTURE POTENTIAL CARBON FIBER MATERIAL

Sapkal Vishal K.[1], Bhamare Punam A.[2], Patil Ulhaskumar V.[3], Awate Swapnil P.[4], Gunjal Shrikant U.[5]

[1, 2] *U. G. Student, Department of Mechanical Engineering, Sandip Foundation's- SITRC, Mahiravani, Nashik, Maharashtra, (India)*

[3, 4, 5] *Asst. Prof. Dept. of Mech. Engg. Sandip Foundation's- SITRC, Mahiravani, Nashik, Maharashtra, (India)*

ABSTRACT

A small amount of Graphene by direct mixing were employed to disperse these nanoparticles into a mono-component epoxy system and used as matrix for advanced composites with woven Glass and Carbon fiber reinforcements. These nanoparticles were added directly into the hosting system and dispersion was carried out by using mechanical stirring. In this study the hybrid polymer composite with Glass fiber, Carbon fiber and epoxy polymer is used. The mechanical characterization results confirm that the composite developed by using graphene nanoparticles represents a fundamental feature in enhancing the tensile elastic modulus and hardness behavior of the composite system, whereas graphene has significant effect on the bending modulus and impact behavior. The optical microscopic study for the fractured samples reveals a significant increase in the fiber-matrix interface adhesion whereas decrease in fiber breakage, fiber pullout and deboning.

Keywords: Epoxy resin, Graphene fillers, Graphene oxide, Hybrid polymer composites, Nano composites, thermosetting resin, Thermal properties.

I.INTRODUCTION

In recent years, composite materials have found increasing applications in construction, aerospace and automotive industries due to their good characteristics of light weight, improved strength, corrosion resistance, controlled anisotropic properties, reduced manufacturing and maintenance costs. However, there is a growing demand to improve on composite materials with reduction in the cost of construction.Everyone agrees that graphene holds massive promise [1]. Possessing a unique portfolio of desirable properties, including excellent conductivity, mechanical strength, gas barrier, thermal and biocompatibility, graphene is an intriguing material.The physical nature of the graphene platelets is important: Factors such as the uniformity, platelet size and the number of graphene platelets in a stack have a fundamental effect on the physical and chemical properties of the grapheme[2], which in turn affects the efficacy of the graphene in its intended use.

II. HISTORY

TABLE 1 HISTORY

SR.NO.	YEAR	TECHNOLOGY
1	1950	Carbon fiber study would start in scientifically.

2	1963	Carbon fiber study will start in industries.
3	1985	Carbon fiber Nano technology with graphene
4	1993	Carbon graphene study will start.

III.CARBON FIBER

Carbon fiber is a material consisting of extremely thin fibers about 0.005–0.010 mm in diameter. The carbon atoms inside the fibers are bonded together in microscopic crystals [3]. There are also other fibers such as glass fiber and aramid fibers. Carbon fiber is mostly occurs in black color.

3.1 Comparison of Carbon Fillers

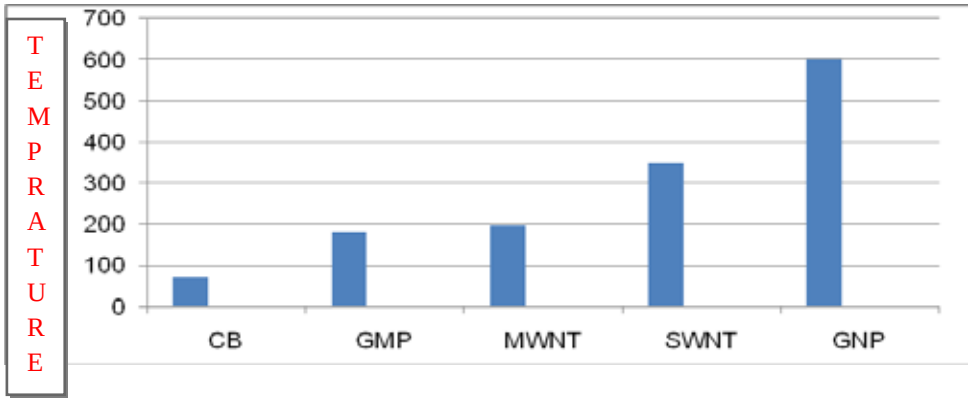

Fig. 1: Graph of Material vs. Temperature

CB- Carbon black

GMP- Graphite microplatelet

MWNT-Multi-WalledCarbon Nanotubes

SWNT- Single-Wall Carbon Nanotubes

GNP- Graphite Nano platelet

3.2 Carbon Fiber Manufacturing Technology

Fig. 2: Manufacturing Technology For Graphene

IV. GRAPHENE

The use of functional graphene is therefore a fundamental part of new product design and should be factored into the plan for the product in the earliest stages of development.

A definitive identification of graphene can be made by analysis of XRD pattern.The XRD pattern of graphite,graphite oxide and graphene are shown in figure 6. XRD pattern of graphite shows an intense peak 2θ = 26·4°.This peak corresponds to 002 plane of graphite withinterlayer spacing of 0·34 nm. In the XRD pattern ofgraphite oxide a new peak appears at 2θ = 13·2°, correspondingto the 002 plane of graphite oxide (Schniepp etal 2003). The interlayer spacing of GO is ~ 0·75 nm,which is significantly larger than that of graphite, due tointercalating oxide functional groups. The mechanism ofexfoliation is mainly the expansion of CO2 evolved intothe interstices between the graphene sheets during rapidheating. The disappearance of native graphite XRD peaksin the XRD pattern of as-prepared graphene sample supportsthe formation of graphene sheets. The SEM imageof graphene sample is shown in figure 7a, where thesheets are highly agglomerated and particles have a fluffymorphology. The TEM image of graphene sample showsa wrinkled paper like structure in low magnification.The selected area diffraction (SAED) pattern ofgraphene sheets is shown in inset of figure 7b. The diffractionpattern indicates the formation of few layers ofgraphene[4].We have measured the d.c. electrical conductivity ofas-prepared graphene sample by four probe setup whichwas ~ 10·6 S/cm at room temperature. The characterizationof graphene sample and investigation of graphene–polymer composites are being carried out and results willbe forthcoming.

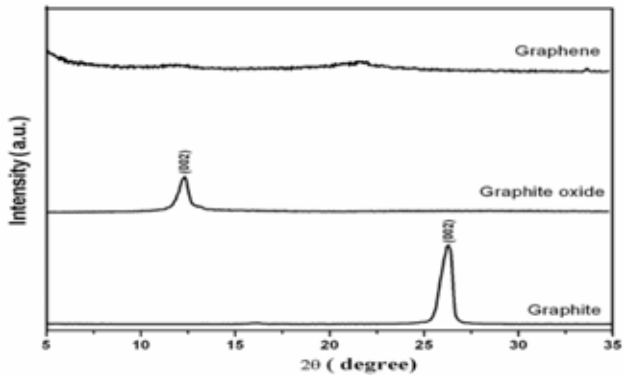

Fig. 3: XRD Patterns of Graphite, Graphite Oxide and Graphene Samples

V. SYNTHESIS OF GRAPHENE

Graphite oxide (GO) was prepared by reacting graphitepowder (5 g) with a mixture of conc. nitric acid (45 ml) and sulphuric acid (90 ml) with potassium chlorate(~ 55 g) at room temperature for 5 days. For thermal exfoliationof graphite oxide, the dried graphite oxide powder (~ 200 m) was placed in a quartz tube (diameter~ 25 mm and length ~ 1·3 m). The sample was flushedwithAir for 15 min and the quartz tube was quickly insertedinto a furnace preheated to 1050°C and held in thefurnace for 30 s. The as-prepared GO was a brownishpowder while the exfoliated version was of light consist enchant shiny black [5].The structural characterization of all the carbon Nano materials were carried out using X-ray diffraction techniqueemploying Expert PRO PANanalytical diffract meter equipped with graphite monochromatic with a Cusource (λ = 1·54 Å, CuKα operating at 45 kV and 40 mA).The as-grown carbons material was characterized byusing scanning (SEM, Philips XL 20), and transmission(TEM, Tacna 20 G2) electron microscopes.

VI. ADVANTAGES

- Carbon fiber has less factor of safety.
- CF has maximum high strength compared withall other fiber material.

- Carbon fiber secure its strength at elevatedambient temperature
- Moisture, acid and solvent at ambienttemperature don't affect carbon fiber.
- Carbon fiber is cheap.
- Light weight at low cost.

VII. LIMITATION

- Manufacturing techniques required to producecarbon fiber are relatively complicated.
- Design of component made of fiber reinforcedplastics is complex. It is necessary to know thedirection of principal stresses in suchcomponents. The fibers are aligned along thedirection of principal stresses.

VIII. APPLICATIONS

- Aerospace engineering.
- Automotive engineering.
- Sports.
- Civil engineering.
- Low-weight high pressure gas storage tank.

IX. FUTURE SCOPE

The future scope of the carbon fiber is soon after university of Manchester physicist's kostyanovosilov & andrejeim discover the wonder material Graphehne-1-atom-thick sheets of carbon that are a one hundred times stronger & much lighter than steel-researchers started incorporating it into polymer composites in the hope of creating materials with greatly improved physical properties. Nearly decade later, efforts to fabricate practical Graphene composites continue apace, but the technology is still in its infancy. Recently, however, a pioneering project began to develop novel Graphene-based Nano composites that one day could truly revolutionize the automotive industry [6]. The 18-month, $1.1-million iGCAuto research collaborative, which is funded by the European Union's 10-years, billion-Euro Graphene Flagship program aims to make high-performance Graphene composites that could reduce the weight of car structures by One-third or more. Advanced composite material are widely viewed as the promising way to make vehicles more fuel-efficient & light weight, but low-mass vehicles tend to perform less vehicle in collisions. So new approaches must be found to enhance the crashworthiness of composites. Graphene composites may be able fill that role. The new iGCAuto consortium comprises a half-dozen research group at the University of Sunderland in Britain, Centro Ricerche FIAT inItaly, Fraunhofer ICT in Germany, Interquimica in Spain, & two Italian Specialist R&D entities, Nanesa, Srl& Delta-Tech SpA.

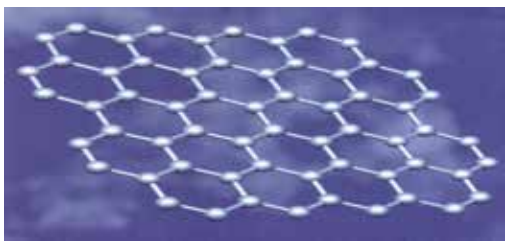

Fig. 4: Structure of Graphene

"Graphene has tremendous application for the automotive industry, and using it to enhance the composite materials in car has considerable potential," said Ahmed Elmarakbi, Prof. of Automotive Engineering at Sunderland, who wrote the original iGCAuto proposal.

"We planned to develop a new way to use Graphene to enhance polymer composites that we hope can save as much as 30% to 50% in automotive structural weight-the chassis and body-in-white-compared to today's steel cars," Elmarakbi said. "In five or six years that improvement could even reach 70%."

The resulting components could not only lesson weight, but also could feature substantially thinner cross section as well.

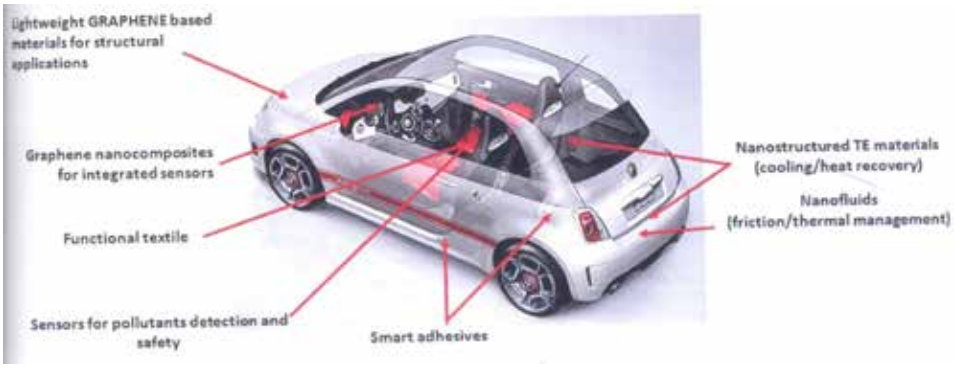

Fig. 5: Future Potential Application of Graphene in Automobiles

The Graphene-based material will be investigated, modeled, & designed to provide improve strength, dimensional stability, thermal behavior, & flame retardance [6]. Fewer smoke emissions is another goal, as is as superior durability-properties that would boost vehicles & occupant safety.

Thus research plans to exploit a novel nanocatalyst and unique Graphene-based nanocomposites materials that were develop by Egyptian scientist Sherif EI-Safety, Chief Researcher at Japan's National Institute for Materials Science, Elkmarakbi said. "Although we're at a very early stage & still have to fully prove the concept, I am growing more confident that our collaboration will be fruitful."

X. CONCLUSION

It has bright future scope because of their low cost, light weight, good mechanical and physical properties like stiffness, high tensile strength etc. from this paper, factor of safety is essential for every component. It depends upon factor i.e. predictable or unpredictable. If predictable, than factor of safety is less and if unpredictable, than factor of safety is high. Carbon fiber is better than all other fibers.The addition of graphene to carbon laminated composites seems to have no influence into stiffness, as the slopes of the stress-strain curves were near constant for all specimen tested. The bending strength, however, wash easily influenced by the formation of graphene pileups into the epoxy matrix and its dispersion around the carbon fibers. The increase on bending strength reached a peak of 140%for the 0.5 % wt. specimens. This enormous increase on bending strength can be attributed to changes on failure mechanism, moving from intra-laminar failure to a mix failure mode where

inter- and intra-laminarfailure are combined in a zigzag pattern. A possible explanation for such behavior is the formation ofstrong bonds at fiber/matrix surroundings due to nanostructures formation.

REFERENCES

[1] Thwe, M. M.; Liao, K.; Comp. Sci. Tech. **2003**, 63, 375. **DOI:** S0266-3538(02)0225-7

[2] Sreekala, M.S.; George, J.; Kumaran, M.G.; Thomas, S.; Comp. Sci. Techno. **2002**, 62, 339. **DOI:** 10.1177/0731684405041717.

[3] AGATE-WP3.1.031027-043-Design Guideline Work Package Title: WBS3.0 Integrated Design Manufacturing, March1, 2002

[4] V. I. Kostikov, "Constructional Materials on the Basis of Carbon in Modern Equipment—Chelyabinsk: Collection of Scientific Works," *Modern Problems of Production and Operation of Carbon Production*, 2005, pp. 8-11.

[5] V. A. Zorin and N. I. Baurova, "Influence of External Factors on the Accuracy of Diagnosing of Road-Building Cars with Use of Carbon Fibers," *Construction and Road Cars*, No. 1, 2009, pp. 50-51.

[6] MOBILITY ENGINEERING, AUTOMOTIVE, AEROSPACE,OFF-HIGHWAY, Volume 1, Issue 5, December 2014.

FUTURE SCADA SYSTEM WITH SMARTER GRID A SMART VISION FOR INDIA

Bharat Nayyar[1], Pratipal Singh[2]

[1]*Department of Computer Science, SKIT, (India)*

[2]*Department of Computer Science, SKIT, (India)*

ABSTRACT

This paper describes a view of SCADA system for future power infrastructure. SCADA is used for distribution of electricity generation on wide area and smart grid is used in integration of information into distribution network. Decentralized energy systems may play an important role for future power systems. SCADA focuses on development of infrastructure, which must support the integration of existing conventional power systems with renewable energy resources. In developing countries, renewable power systems are more complex and use the conventional resources like coal because of which they are widely dispersed power sources. This paper first provides a view of future power delivery and smart grid systems in India and then reviews the present infrastructure of power grid. Based on this review, future grid and future SCADA systems cope with the significant penetration of distribution generation, communication and aged power assets is proposed for wide area monitoring, emergency protection, control demand area, and secure communications. There are many devices connected to the grid and enable us to exchange the information with power system. This will enable the future Indian Smarter Grid and Future of SCADA system.

Keyword : Distribution Generation, Future SCADA, Maintenance, Protection, Smart Grid

I. INTRODUCTION

The main purpose of the Supervisory Control and Data Acquisition (SCADA) system is taking real-time data, monitoring and controlling equipments and processes in the infrastructure with the help of sensors and controllers. A SCADA system for power distribution application is typically a PC- based software package and grid is a term used for transmission of data from distributer to consumer. Few functionalities provided by the software make it smart; that's why it known as smart grid. These functions are self-healing, tolerant to attacks, empower and incorporate the consumer, provide power qualities etc. Energy generation and no storability of electricity is one of the most discussed issues in India. And today's technology is not suitable enough for 21st century. A small scale power generation technology that supplies electric power to the consumer, located on the distribution system near to the consumption place is called Distribution Generation (DG) [1]. India's spending on power infrastructure is growing year by year. According to some surveys India estimated spending $250 billion on power sector generation and $447 billion on infrastructure [2]. The exponential growth of small scale power generation in the last few decades getting more attention, not only has economic advantage, but also environmental impacts [1]. India is a developing country, that's why power sector plays an important role for the Indian economy. Distribution generation consists of dispersed generation including renewable resources like solar, wind, fuel cell and biomass. In the solar energy sector in India, some large projects have been proposed; one of them is running in Thar Desert which generates 700 to 2100 GW [3]. The capacity of wind power in India approx 21200 MW [4].

This paper first discusses about SCADA system for distribution generation with SCADA system in Smart Grid. Then how one can integrate this geographically dispersed generation to the existing power generation plants. And this extendable infrastructure becomes more and more complex. Future SCADA system should handle this so as to ensure the reliability of the clean electricity.

II.DISTRIBUTED GENERATION WITH SCADA IN SMART GRID AND ADVANTAGES AGAINST CENTRALIZED SCADA SYSTEM

In India electricity generation depends mostly on large power plants, mainly using coal (primary energy resource). Raised utilization and demand of primary energy resource is a big issue. The scarcity of the primary energy resource has raised the cost of electricity generation. In the recent decades, small and medium size generation has been gaining more attention. These distribution generations are connected to the distributed system close to the consumer's location and with the emergence of technologies DC grid has changed to AC grid, reducing the loss in the transmission line [9].

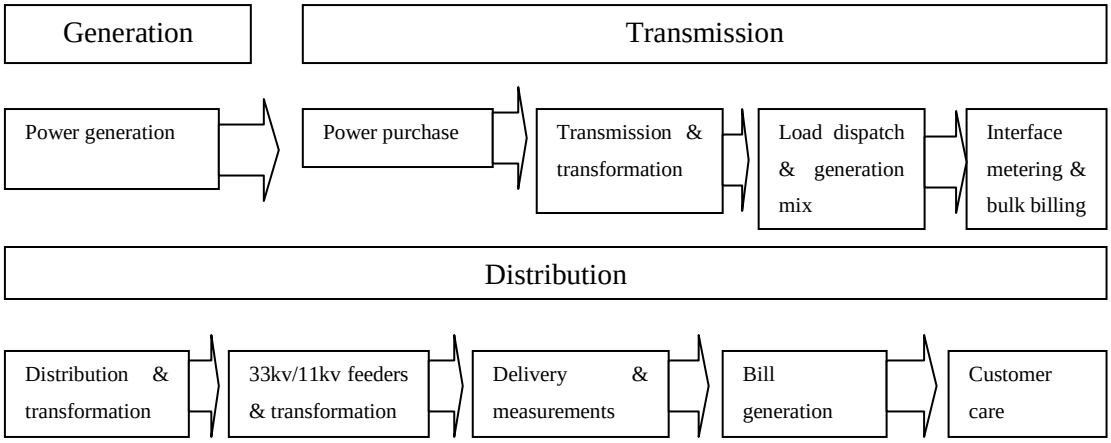

Figure 1: Electricity Value Chain

Large generation station with the vast transmission and distribution grid has come to existence. This interconnection helps to solve the demand and supply problem. Distribution generation can also be defined as a small scale power generation is structural benefits and market related. Structural benefits means how to minimize the cost of the transmission and market benefits means deal with the electricity price volatility, improving power quality and reliability. Restructuring of electric power system creates three major categories, power generation, transmission and generation. There are lots of advantages of distributed generation against the centralized generation. In centralized system in emergency state, only specific area can be under investigation and in decentralized or distributed system make entire control system reliable.

In centralized control system, all the information exchanged between control center and different nodes will be a short period of time. In this case the communication between controllers should work with no error margin, if the error occurs the entire system will collapse. Which means if the some controllers are not working properly, the entire SCADA system will shut down. In distributed control system, the entire system is divided into different control area. And each area owns a local or virtual control system to monitor and control on real time

basis. Which means if a failure occurs on particular area, that area local control system improves that failure and that time only that area will be shut down? So a failure occurred in one control area have less effect on others. That makes it reliable.

SCADA is widely geographically dispersed, we know that. In centralized system the huge database and complex computation make the processing slower. And in distributed system, the task divided into subtasks and these are carried by the local area control center according to control area. These subtasks are processed in distributed computation and this improves the response time.

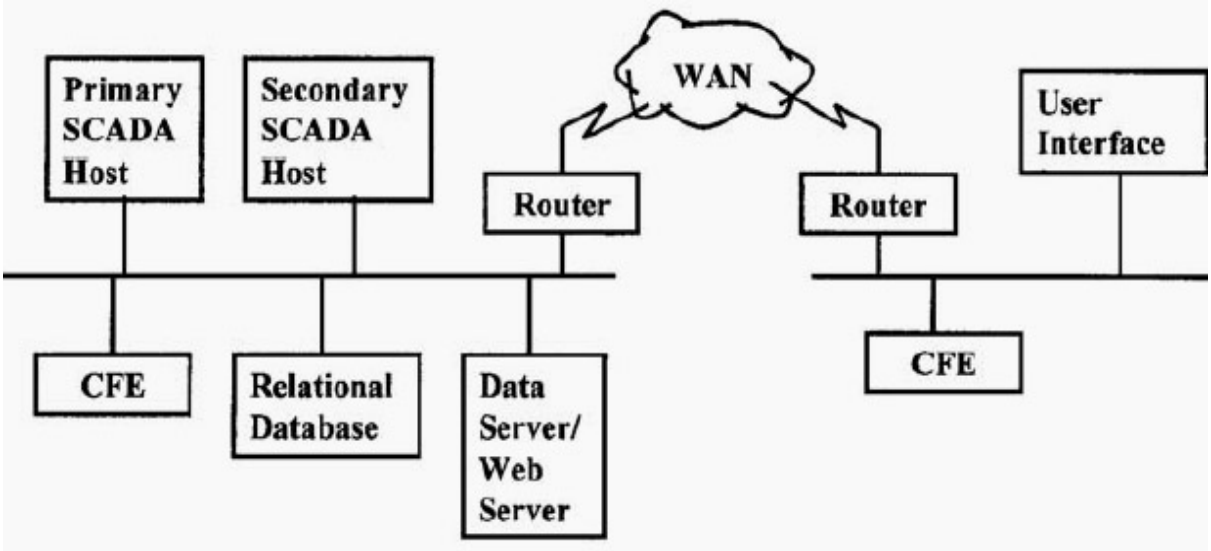

Figure 2: Centralized Control System

If any problem occurs in the main communication system in centralized control system, the whole SCADA does not function properly. And in distributed control, the exchange of data will be within the local area control center. This makes information exchange faster and the data processed locally.

Centralized control system also has High electrical loss, limitation with infrastructure that's why it is not useful for future expansions, vertical structure, in case of failure there is a power cut, high infrastructure cost and unidirectional power flow. Decentralized control system reduce the electrical losses, best for future expansions, failure in one control area covered by central control system and continue from the power grid, bi-directional power flow.

III.INTEGRATION OF DISTRIBUTED GENERATION AND RENEWABLE ENERGY SOURCE

A large amount of our country's infrastructure is dependent on the electricity power. And for generation of electricity we still use the primary energy source that is coal. But from last decade or two, due to scarcity of the primary energy resource has raised the cost of production. Because without this energy source how can we generate electricity? So now we also use the renewable energy source for the electricity generation. So in today's era we use both conventional resource and renewable resource together but the main problem is that how we can integrate this distributed generation and renewable energy source with existing control system? Due

to big change in world climate, rapid increasing of power demand risks the future power systems in general and specially the SCADA system [11].

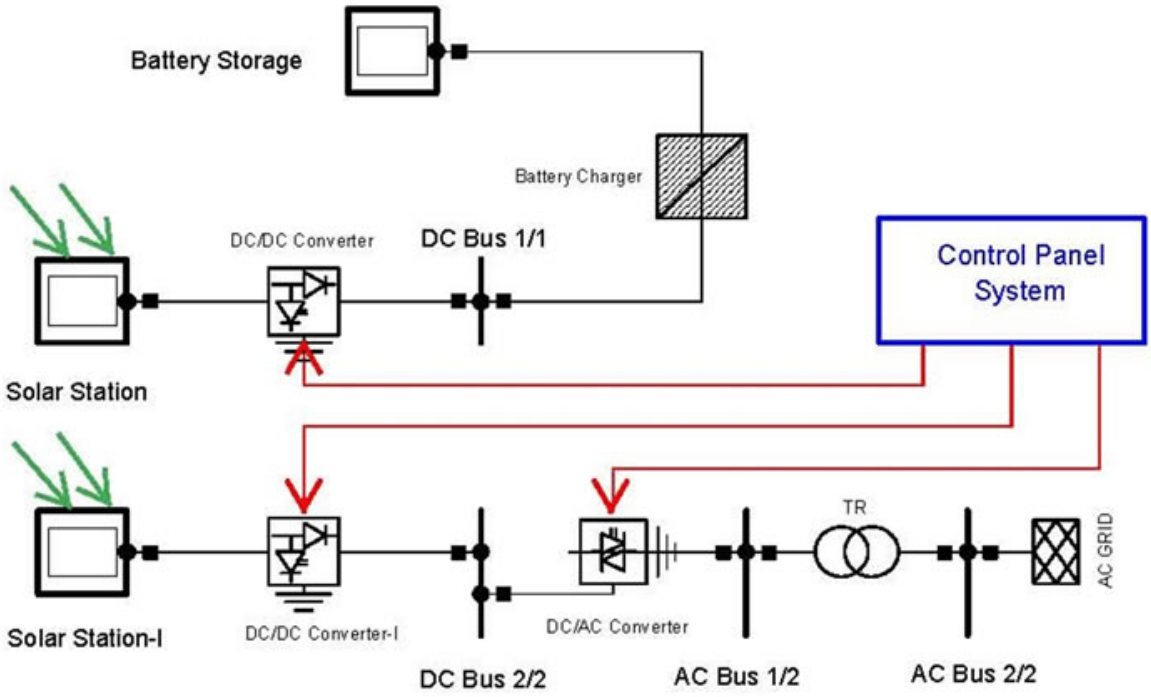

Figure 3: Decentralized Control System in Renewable Energy Source

Renewable energy source is to get the green power generation. These power sources are small in size and located in different places, that makes them to be known as distribution generation [5]. The main aim of the integration is to reduce the cost of energy while increasing the share of renewable energy. The future power grid is a smart grid which can integrate and is able to manage Distributed and Renewable energy source. Using more renewable energy will put upward pressure on unit costs. Renewable energy doesn't have the same operating characteristics, load factors, cost-volume drivers, or dispatch ability as conventional energy, especially base load plants. Renewable energy will stress transmission grids differently and significant investment will be needed to reconfigure bulk power networks.

IV.SMART GRID VISION IN INDIA WITH RENEWABLE ENERGY SOURCE

There are six main factors that will drive the adoption of the smart grid in India. Supply shortfalls, in India, according to official estimates show that the short falls are 12% for total energy and 16% for peak demand. Loss reduction, manage human element in system operations, peak load management, renewable energy. Transform the Indian power sector into a secure, adaptive, sustainable, and digitally enabled ecosystem that provides reliable and quality energy for all with active participation of stakeholders [7]. To support system operators by providing the real time information to make decision on selection generation from renewable energy resources. Indian official estimates increased renewable generation enabled by smart grid could reduce greenhouse gas emission.

In India, some solar plants are running in Rajasthan, Gujarat, Maharashtra, and Madhya Pradesh. In Rajasthan, a 700 to 1200 GW solar power plant is situated. Gujarat contributes 2/3 of the 900 MW in the country [3][6].

Wind power development has been started in 1990s in India. Installed capacity of Indian wind power is nearby 21200MW [4]. Tamil Nadu, Maharashtra, Gujarat, Rajasthan, Andhra Pradesh, Kerala, Orissa are the major wind power plants of India.

V.FUTURE SCADA SYSTEM AND SMART GRID IN INDIA AND CONCLUSION

Distributed computation, monitoring and control will offer an efficient method for power system operators. Distributed generation systems use decentralized control system where local generation plants own a SCADA system. SCADA technology helps the power companies to exchange information and data between different nodes in the entire network. This network comprises of energy management system and distributed management system. The smart grids have computerized systems that give efficient and smooth information exchange for monitoring [8].

REFERENCES

[1] N. Jenkins, R. Allan, P. Crossley, D. Kirschen and G. strbac IET power and energy series 31 “Embedded Generation”.

[2] The smart grid vision for India’s power sector “white paper”.

[3] Solar power in India, "Sustainable production of solar electricity with particular reference to the Indian economy". Renewable and Sustainable Energy Reviews

[4] wind power in India, “World Wind Energy Report 2008".

[5] H. Lee Willies, walter G. Scott; Distributed power generation planning and evaluation.

[6] "Gujarat flips switch on Asia’s largest solar field, leading India’s renewable energy ambitions". Washington Post (New Delhi, India).

[7] Jyotiraditya M. Scindia, Pradeep Kumar Sinha, Sam Pitroda, “smart grid vision and road map for India, ministry of power government of India”.

[8] T.K. Apostolopoulose, G. C. Oikonomou. “a scalable, extensible framework for grid management”. 22nd IASTED international conference Feb, 2004 , Austria.

LOCATION AWARE ROUTING SCHEMES FOR MOBILE ADHOC NETWORKS

Kalpesh P. Popat[1], Dr. Priyanka Sharma[2] , Hardik K. Molia[3]

[1]Research Scholar, [2]Research Supervisor, Gujarat Technological University, Ahmedabad, Gujarat, (India)

[3]Asst. Prof., Dept. of Computer Engineering, Govt. Engg. College, Rajkot, (India)

ABSTRACT

One of the promising wireless network that is based on anytime, anywhere access is the mobile ad hoc network (MANET). A MANET consists of a set of mobile hosts without any support of other devices such as base stations. It is attractive since it can be quickly setup and operated by batteries only. Some critical issues are required to be handled carefully while implementing MANETs in reality. Routing is one of the most critical issues in MANETs. As MANETs allow nodes to be mobile, to change their positions during communication, it may generate issues like route failures and network partitions. The conventional routing schemes are not appropriate in such scenarios. Some advance routing algorithms, such as AODV, DSR, DSDV are proposed which has improved performance significantly. By location awareness, we mean that a host is capable of knowing its current physical location in the three-dimensional world. This paper explores some of the most successful location aware routing schemes.

Keywords: Gedir, Gps, Gpsr, Gra, Lalr, Manet

I. INTRODUCTION

1.1 Network Layer Issues

MANETs support user mobility and so dynamic topologies. As the topology is dynamic, routing is very critical. The traditional routing algorithms don't provide good performance under such scenarios where nodes are continuously changing their locations as well as becoming up and down.[1]

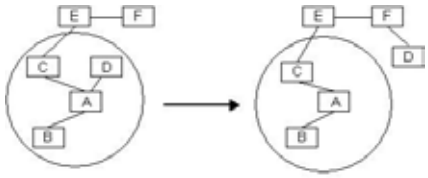

Fig. 1- Node D moves out of Range of A

Fig. 2 shows that some nodes in a MANET become off due to power failure or shut down by the owner. In such case, sometimes network is partitioned in to two or more halves if the node was the only connecting point among them. [1]

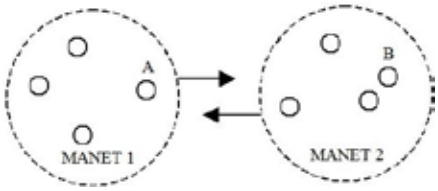

Fig. 2- MANET Partitions

1.2 Routing Architecture

Flat routing keeps information about every node in the MANET without differentiation as per their locations. This strategy is suitable for small MANET to get good performance but it becomes difficult as number of nodes increases. it generates a lot of overload in maintaining information at every node. Hierarchical architecture divides MANET into a set of geographically separated small chunks called the clusters. Every cluster has a set of nodes inside and one of them is selected as cluster head. Routing is performed among cluster heads only.[1]

In proactive routing algorithms, so every node has complete topology of the network to which it belongs. Every node maintains latest toplogy in its own database so it provides fast routing. WRP and DSDV are proactive routing protocols in MANETs.[1]

In reactive routing algorithms, route is searched only when it is needed. So these algorithms are light weighted as compared to proactive algorithms but require more time when a new route is required to be created. DSR and AODV are reactive routing protocols in MANETs.[1]

1.3 Location Awareness

GPS (Global Positioning System) is the most widely used tool to calculate a device's physical location. GPS is a worldwide, satellite -based radio navigation system. The GPS system consists of 24 satellites which transmit navigation messages periodically. Each navigation message contains the satellite's orbit element, clock, and status. After receiving the navigation messages, a GPS receiver can determine its position and roaming velocity. To determine the receiver's longitude and latitude, we need at least three satellites. If we also want to determine the altitude, another satellite is needed. More satellites can increase the positioning accuracy. The positioning accuracy of GPS ranges in about a few tens of meters. GPS receivers can be used almost anywhere near the surface of the Earth. By connecting to a GPS receiver, a mobile host will be able to know its current physical location. This can greatly help the performance of a MANET, and it is for this reason that many researchers have proposed to adopt GPS in MANETs. [2]

II. GPSR (GREEDY PERIMETER STATELESS ROUTING)

2.1 Gpsr

The greedy perimeter stateless routing (GPSR) protocol assumes that each mobile host knows all its neighbors' locations (with direct links). The location of the destination host is also assumed to be known in advance. The GPSR protocol does not need to discover a route prior to sending a packet. A host can forward a received packet directly based on local information. Two forwarding methods are used in GPSR: greedy forwarding and perimeter forwarding. [3]

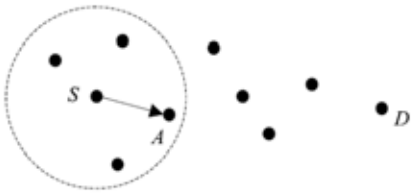

Fig. 3- Greedy Approach

Fig 3. Shows an example of greedy forwarding. When host S needs to send a packet to host D, it picks from its neighbors one host that is closest to the destination host and then forwards the packet to it. In this example, host A is the closest one. After receiving the packet, host A follows the same greedy forwarding procedure to find the next hop. This is repeatedly used until host D or a local maximum host is reached.[3]

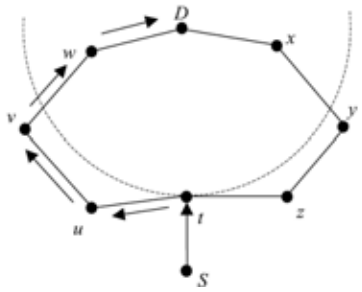

Fig. 4- perimeter forwarding approach

A local maximum host is one that finds no other hosts that are closer to D than itself. In the example in Fig. 4, host t is a local maximum because all its neighbours are farther from D than itself. Therefore, the greedy forwarding method will not work here. When this happens, the perimeter forwarding method is used to forward the packet. The perimeter forwarding method works as follows. The local maximum host first "planarizes" the graph representing the network topology. A graph is said to be planar if no two edges cross. The graph may be transformed into a relative neighbourhood graph (RNG) or a Gabriel graph (GG). Both RNG and GG are planar graphs. After the graph is planarized, the local maximum host can forward the packet according to a right-hand rule to guide the packet along the perimeter of a plane counter clockwise. For example, in Fig. 18.3 at t , we can forward the packet along the perimeter of the plane dxyztuvw counter clockwise. As the packet is forwarded to host w, we know that we are closer to D (as opposed to the location of host t). Then the greedy forwarding method can be applied again, and the packet will reach destination D. Overall, these two methods are used interchangeably until the destination is reached. The GPSR is a stateless routing protocol since it does not need to maintain any routing table.[3]

2.2 Gra

The geographical routing algorithm (GRA) is also derived based on location information. To send or forward a packet, a host first checks route entries in its routing table. If there is one, the packet is forwarded according to the entry. Otherwise, a greedy approach is taken, which will try to send the packet to the host closest to the destination. If the packet runs in to a local maximum host, GRA will initiate a route discovery procedure to discover a route from the host to the destination. This is done by flooding. After the route reply comes back, the route entry will be stored in the host's routing table to use in future. [3]

2.3 Gedir

The geographic distance routing (GEDIR) protocol assumes that each host has the locations of its direct neighbors. Similar to GPSR, the GEDIR protocol also directly forwards packets to next hops without establishing routes in advance. There are two packet-forwarding policies: distance approach and direction approach. In the distance approach, the packet is forwarded to the neighbor whose distance is nearest to the destination. However, in the direction approach, the packet is forwarded to the neighbor whose direction is closest to the destination's direction. The latter can be formulated by the angle formed by the vector from the current host to the destination and to the next hop. [3]

III. LAR (Location-Aided Routing)

The location-aided routing (LAR) protocol assumes that the source host (denoted as S) knows the recent location and roaming speed of the destination host (denoted as D). Suppose that S obtains D's location, denoted

as (Xd, Yd), and speed, denoted as v, at time t0 and that the current time is t1 . We can define the expected zone in which host D may be located at time t1 (refer to the circle in Fig. 5). The radius of the expected zone is R = v(t1 – t0). [4]

From the expected zone, we can define the request zone to be the shaded rectangle as shown in Fig. 6 (surrounded by corners S, A, B, and C). The LAR protocol basically uses restricted flooding to discover routes. That is, only hosts in the request zone will help forward route-searching packets. Thus, the searching cost can be decreased. When S initiates the route-searching packet, it should include the coordinates of the request zone in the packet. A receiving host simply needs to compare its own location to the request zone to decide whether or not to rebroadcast the route-searching packet. After D receives the route-searching packet, it sends a route reply packet to S. When S receives the reply, the route is established. If the route cannot be discovered in a suitable timeout period, S can initiate a new route disco very with an expanded request zone. The expanded request zone should be larger than the previous request zone. In the extreme case, it can be set as the entire network. Since the expanded request zone is larger, the probability of discovering a route is increased with a gradually increasing cost. [4]

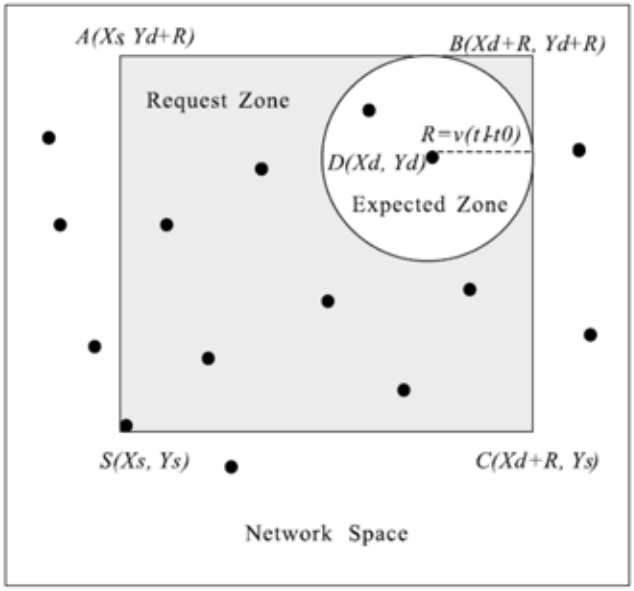

Fig. 5- LALR

IV. CONCLUSION

Algo	Strategy	Information
LAR	Discover route by flooding request packets in request zone	Destination's location and roaming speed
GPSR	Greedy forwarding (distance-based) and perimeter forwarding	Destination's location and all neighbors' locations
GRA	Greedy forwarding (distance-based) and flooding	Destination's location and some neighbors' locations
GEDIR	Greedy forwarding (distance- or direction-based) and flooding	Destination's location and all neighbors' locations

REFERENCES

[1] Hardik K Molia, Rashmi Agrawal , "Exploring the Challenges in MANETs", International Journal of Advanced Networking & Applications 2014

[2] A. Fasbend er et al., Variable and Scalable Security: Protection of Location Information in Mobile IP, Mobile Technology for the Human Race, IEEE 46th Vehicular Technology Conference, 1996.

[3] D. Forsberg et al., Distributing Mobility Agents Hierarchically Under Frequent Location Updates, Sixth IEEE International Workshop on Mobile Multimedia Communications, 1999.

[4] W. Chen, N . Jain, and S. Singh, ANMP: ad hoc network management protocol, IEEE Journal On Selected Areas In Communications, 17(8), 1999.

SWIRL MEASURING EQUIPMENT FOR DIRECT INJECTION DIESEL ENGINE

G.S.Gosavi[1], R.B.Solankar[2], A.R.Kori[3], R.B.Chavan[4], S.P.Shinde[5]

[1,2,3,4,5] *Mechanical Engineering Department, Shivaji University, (India)*

ABSTRACT

Traditional swirl-measurement equipment that adopts a paddle wheel is manually operated to measure the swirl intensity generated from a helical port in an engine cylinder head. The conventional equipment was modified to operate automatically using a pneumatic cylinder to adjust the valve lift. The automatic swirl-measuring equipment was operated in either steady or quasi-steady flow conditions. The surge tank pressure was controlled automatically opening or closing a bypass valve, when the swirl flow was measured in a steady flow whereas, when the swirl flow was in a quasi-steady flow, the surge tank pressure varied naturally adapting to the valve lift in the conditions of closing the bypass valve. Photo sensor is used to measure the paddle speed and differential manometer is used to measure, the pressure at nozzle.

Keywords: Automation, Paddle Wheel Method, Quasi-Steady Flow, Steady Flow, Swirl Flow

1. INTRODUCTION

In order to postpone the energy crisis, one method is to employ the alternative fuels and another is to reducing the fuel consumption of internal combustion engine (ICE). In addition, the global warming effect is an important concern as well. However, the design of an internal combustion engine is a complex. To enhance the efficiency of an engine it is important to optimize thermal efficiency which is obtained at the highest possible compression ratio. But if the compression ratio is too high, there is a chance to have knock, which should be avoided. A solution for this problem is to promote rapid combustion to reduce the time available for the self-ignition to occur. To promote rapid combustion, sufficient large-scale turbulence (kinetic energy) is needed at the end of the compression stroke because it will result in a better mixing process of air and fuel and it will also enhance flame development. However, too much turbulence leads to excessive heat transfer from the gases to the cylinder walls and may create problems of flame propagation. The engine should run at low speeds, in order to have low mechanical losses but the combustion should be fast, enabling good combustion efficiency. Therefore high turbulence should be produced prior to combustion within the cylinder so swirl was induced by the inlet channel within the cylinder head. One of the most important factors that affect diesel engine performance is the rapid mixing of air and fuel in the combustion chamber. The important parameters affecting the air–fuel mixing of diesel engines include fuel injection pressure, injection timing, the architecture of the combustion chamber and the swirl intensity in the combustion chamber. The swirl flow, which induces the intake air to move in a tangential direction during the compression stroke is usually generated in the engine cylinder head. The highly pressurized injected fuel is deflected and dispersed in tangential flow in combustion chamber, which assists the air-fuel mixture in combustion chamber. The swirl flow in the combustion chamber remains an important influencing factor of the mixture formation process in the direct-injection diesel engines. The nature of the swirl flow in an operating engine is extremely difficult to determine instead, steady flow tests are often used to characterize the swirl. There are several swirl-measurements techniques used by manufacturers are the paddle

wheel and impulse method. In the paddle wheel method, the swirl of a charge in a cylinder can find be by calculating the ratio of rotary speed of the paddle in a swirl measurement apparatus, to the engine speed as calculated by measuring the intake air flow rate. For the swirl measurement, the air is sucked by a blower through the port, over the valve lift with an adjustable stroke, past the cylinder liner and the surge tank and finally to a differential flow meter. The valve lift of the cylinder head is controlled automatically. In order to measure swirl in steady state the surge tank pressure is maintained constant by adjusting the bypass valve to either opened or closed. The swirl measuring equipment was modified by closing the bypass valve and controlling the valve lifts which allows quasi-steady flow condition.

1.1 Need Of Measurement Of Swirl:

Fuel droplets cannot be injected and distributed uniformly throughout the combustion space. If air within the cylinder were motionless then there will not be enough oxygen in the burning cone and burning of fuel would be either slow or totally fail. As it would be surrounded by its own products of combustion. Hence an orderly and controlled movement must be imparted to the air, so that a continuous flow of fresh air is brought to rate burning droplet and the products of combustion swept away. The rotational motion of fluid mass within the engine cylinder is called as “swirl”.

- One of the important factor affecting the air-fuel mixture is the swirl intensity inside the combustion chamber.
- Swirl affects the mixing and distribution of charge in the cylinder of diesel engine.
- Low values of swirl are desirable in racing engines.
- High values of swirl are desirable in applications concerned with efficiency and emissions.

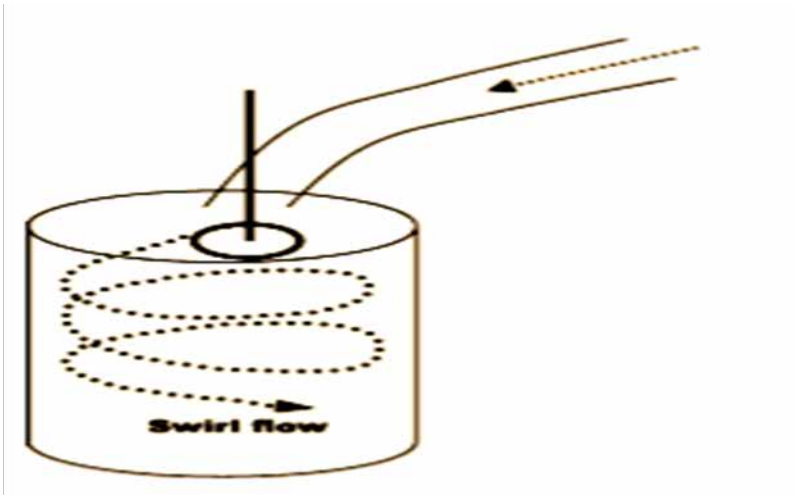

Fig.1: swirling motion in an engine cylinder

II. SWIRL MEASURING EQUIPMENT

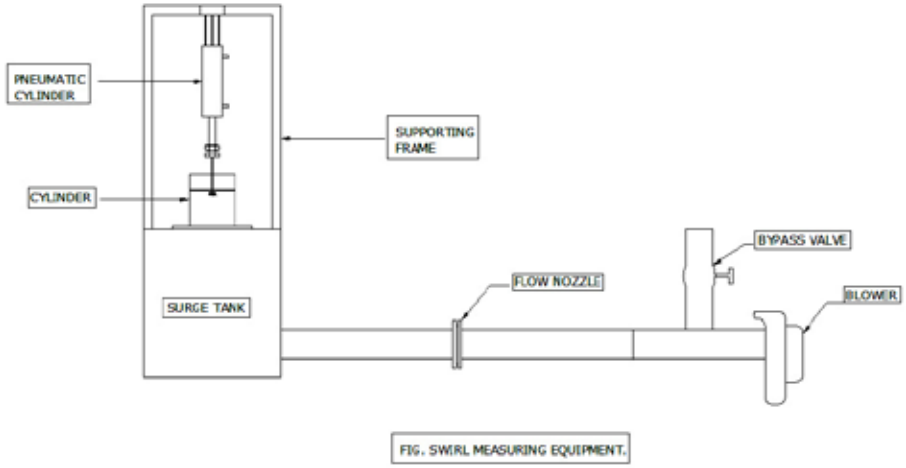

Fig.2: Block diagram of swirl measuring equipment experimental set up

2.1 Construction

The construction of swirl measuring equipment comprises of following parts:

- Surge tank :

The surge tank works as the vacuum creating tank in the swirl measuring equipment. The surge tank is structural member in equipment. The paddle wheel is mounted on the surge tank. The cylinder is also mounted on surface of surge tank. It is also connected to blower through pipe arrangement. The surge tank is used to create vacuum which is an essential requirement of the equipment.

- Cylinder and valve assembly:

The cylinder used in this experiment is Direct Injection Diesel Engine. The cylinder head is mounted on surge tank. The cylinder head consists of valve, actuating spring for the valve, cylinder of standard dimensions. These are one of the important parts in the equipment. The cylinder is made according to the large head engine dimensions.

- Paddle wheel:

The paddle wheel is mounted in the surge tank. The paddle wheel measures the intensity of air swirl. The paddle wheel is attached with sensor and counter for measuring the revolutions of paddle wheel. Paddle wheel is placed exactly below the cylinder head.

- Photo sensor and counter:

The photo sensor is a proximity switch which is kept near the paddle wheel for sensing the revolutions. The measured revolutions are displayed with the help of counter. The electrical input is given to the counter and displays the revolutions. The paddle wheel is equipped with a material which is used by the sensor to sense.

- Pipe assembly:

The one end of pipe is connected to the surge tank and other end is connected to the blower. The pipes are consists of flow nozzle in between them. There is arrangement for measuring the pressure difference before and after the orifice. Bypass valve is also connected with the pipe. The bypass valve is used to maintain constant pressure inside the surge tank.

- Blower:

The blower is connected with one end of the pipe. It creates vacuum inside the surge tank by sucking the air which is present inside of the Surge tank.

2.1 Working of Equipment

The swirl-measurement equipment developed in this study was traditional swirl-measurement equipment using several sensors for essential measurement of swirl. Two differential pressure manometers that measure the intake air flow rate and surge tank pressure, a photo sensor that counts the paddle revolutions, a spring that adjusts the valve lift, and manually operated bypass valve for adjusting surge tank pressure respectively in the traditional swirl-measurement equipment. For the measurement of the swirl ratio of the cylinder head, the Air is sucked by a blower through the port over a valve with an adjusted lift, past the cylinder liner and surge tank, and into the flow nozzle. The pressure drop is maintained uniformly at either 60mm H_2O or 40mm H_2O by controlling the bypass valve to be either opened or closed according to the position of the intake valve lift. A pulse pick-up transmits the paddle wheel rotation to an optical counter. The number of pulses for a given time interval are measured with counters, and the measurement provides the rotation speed ($N_{D)}$ of the paddle wheel. The pressure loss (ΔP) across the flow nozzle is measured with manometer. This procedure is repeated after adjusting the valve lift several times. The valve lift of the cylinder head is controlled by the spring. After the valve lift is adjusted to a large position, the bypass valve is controlled with the manually to obtain the target surge tank pressure. Therefore, the valve movement time interval between consecutive valve lifts cannot be constant when measuring the swirl in a steady flow. When the valve lift was increased continuously with a constant time interval with the bypass valve closed, the intake flow in the cylinder is in quasi-steady state. The valve lift in the quasi-steady flow is adjusted continuously. The spring that adjusts the valve lift. The reason why the spring is used to control the valve lift is due to its exact timing in controlling the interval between consecutive valve lifts. The observations required from the swirl measurement equipment were measured and recorded in a data, while the valve lift was adjusted continuously with a constant time interval. The surge tank pressures, the differential pressure at the flow nozzle are measured at each valve lift. The paddle rotating speed was calculated from cumulating the count of the photo sensor signals during a time interval of the adjustment between consecutive valve lifts.

III. FORMULAE USED

3.1 Mass Flow Rate

The intake air flow rate is measured using the flow nozzle. The pressure difference ΔP across the flow nozzle between the upstream and downstream is measured using the differential manometer in order to calculate the mass flow rate $\dot{m}$ from :

$$m = C_d \times A \times \sqrt{2 \times \rho \times \Delta P} \quad (1)$$

Where,

m = mass flow rate (kg/s)

C_d = coefficient of discharge for flow nozzle = 0.95

A = area of flow nozzle (m^2)

ρ = density of air (kg/m^3)

ΔP = pressure difference (N/m^2)

The swirl estimates the rotation intensity of the cylinder charge, which is very important in the air–fuel mix in the combustion chamber. An equivalent engine speed N (rev/min) corresponding to the intake air flow rate measured with the flow nozzle is obtained by equating the axial flow velocity V_a to the mean piston speed V_m according to,

Axial flow velocity $(V_a) = \frac{m}{\rho A}$ (2)

Mean piston speed $(V_m) = \frac{SN}{30}$ (3)

Equivalent engine speed $(N) = \frac{30m}{\rho SA}$ (4)

3.2 Swirl Ratio

It is the ratio of rotation of paddle wheel placed inside the engine cylinder to the equivalent engine's speed.

$$\frac{N_d}{N} = \frac{N_d \rho A S}{m 30} \quad (5)$$

Where,

N_d =Speed of the paddle (rpm)

N = equivalent engine speed (rpm)

m= mass flow rate (kg/s)

A = area of piston (m^2)

S = engine stroke (mm)

3.3 Specifications of engine cylinder used for experiment

Engine model	-	R6126ZLCD
Type	-	4 stroke, Direct Injection diesel engine
Bore	-	135 mm
Stroke	-	120 mm
Diameter of piston	-	128 mm

3.4 Result Table for Steady state operation

SR NO.	VALVE LIFT (mm)	PADDLE WHEEL SPEED (RPM)	TANK PRESSURE (mm of water)	PRESSURE DIFFERENCE (ΔP in mm of water)	SWIRL NUMBER
1.	2	330	60	10	0.12
2.	4	600	60	20	0.16
3.	6	850	60	22	0.21
4.	8	952	60	24	0.23
5.	10	1012	60	18	0.28
6.	12	1210	60	16	0.36

The maximum swirl ratio is obtained at the maximum valve lift of the cylinder. The limit for the vertical displacement or movement of the valve is in between 2mm to 12 mm. Within this range the swirl ratio can be achieved at various valve lift. The swirl ratio is maximum at the valve lift of 12mm. The swirl ratio is dimensionless number and it is measured in terms of RPM.

IV. CONCLUSION

Swirl measuring equipment is easy to install and operate, resulting in low cost of ownership. Insertion of paddle wheel, lowers installation and maintenance cost. Equipment is developed to measure the swirl of an engine cylinder head. The equipment can be operated in either steady or quasi-steady flows. With the help of swirl number information, we can control the rate of combustion and emissions. With higher number of swirl, faster the combustion takes place, higher is the efficiency and lower the emissions. With the lower number of swirl, lower will be the rate of combustion, lower the efficiency and more will be emissions. We can adjust swirl number according to the application required and enhance the engine performance. For the future enhancement of the project automation is required. For the automation we can use PID controller transducers and stepped motors.

REFERENCES:

[1] Yuh-Yih Wu, Hsien-Chi Tsai, Manh-Cuong Nguyen, “Investigation of realizing SDI with high swirlcharge in a motorcycle engine” INTERNATIONAL JOURNAL OF ENERGY, Issue 2, Vol. 3, 2009

[2] K I Kim and C H Lee, "Development of a new swirl-measurement method for an engine cylinder head by automating the swirl-measuring process" Department of Automotive Engineering, Seoul National University of Technology, Proc. IMechE Vol. 223 Part D: J.

[3] Rajinder Kumar Son and Pranat Pal Dubey" Diesel engine air swirl measuements using AVL TEST RIG", International Journal Of Mechanical Engineering and Technology (IJMET), Volume 4, Issue 1, January-February (2013), pp. 79-91

[4] C. Crnojevic, F. Decool, P. Florent, "Swirl measurements in a motor cylinder" Experiments in Fluids 26 (1999) 542*Ð*548 (Springer-Verlag1999)

[5] M. L. Mathur and R. P. Sharma, Internal Combustion Engine(Dhanpat Rai Publications LTD. New Delhi)

[6] V. Ganesan, I.C. Engines(Tata McGraw-Hill publication LTD. New Delhi)

ROBOTIC ARM CONTROL USING FUSION BAND AND HAND GESTURE RECOGNITION

Gaurav S. Sawarkar

Department of Communication Engineering YCC, Enagpur,(India)

ABSTRACT

Robots make our life easier. Engineering are up to the challenge, and over the past few years they have developed robotic hands with unprecedented strength and sensitivity. Sensor plays an important role in robotics. Robotic application demand sensors with high degrees of repeatability, precision, and reliability. The pick and place operation of the robotic arm can be efficiently controlled using fusion band. This design work is an educational based concept as robotic control is an exciting and high challenge research work in recent years. [1]Our robotic hand controlled wirelessly with fusion band works in synchronization with human hand and has precise and accurate movements with increased range.

Keywords: Accelerometer, CC2500 Wireless Module

I. INTRODUCTION

Robotic tele-operation indicates the remote manipulation of a robot by human operator at a distance. In some specific situation where human can't work directly, robots are used. For most people it is incredibly easy to move their arm. This nature ability can be exploited to give a human operator an easy to use interface to control a robot.

In this project, two sensor fusion input armband devices with the ability to be used by any individual with some level of arm movement and arm voluntary muscle contraction control will be used. The user hand motion will provide a natural and effective way to precisely manipulate the robot with very little training. The devices which will be used are GE-Fusion (Gyro and EMG fusion) and MEA-fusion (Magnetometer, EMG and Accelerometer) Bands, both combined into a small box.

[2]Hand gesture recognition provides an intelligent, natural and convenient way of human computer interaction. Sign language recognition (SLR) and gesture-based control are two major applications for hand gesture recognition technologies. There are two technique used, such as

1.1 Vision Base Gesture Recognition

In vision base gesture recognition, according to technology, computer visions capture the gesture of human hand and display to computer human perform in that time. This technology basically in the field of service robotic there are two gesture recognition methods first is the Temple base approach and natural base approach this is compared and combined with Viterbi algorithm for the recognition of gesture

.

1.2 Motion Capture Sensor Recognition

In motion capture sensor recognition, Accelerometer sensor used to sense the motion of human hand and creates three dimensional analog output voltages. Today accelerometer is small surface mount component. There are three axes X, Y, Z which is labeled in it. And flex sensor is used to control the wrist movement of hand.

II FUSION BAND

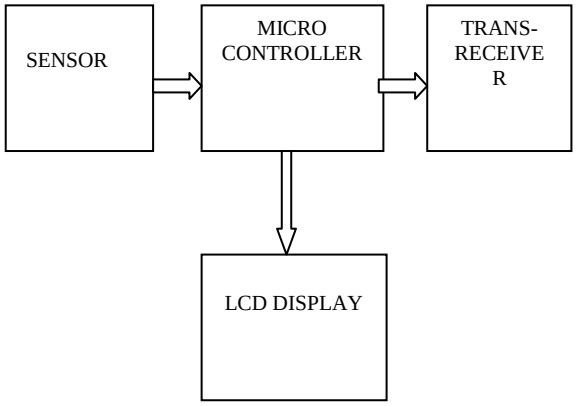

Fig. Block Diagram of Fusion Band

2.1 Sensor

Fig. Accelerometer

EMG (Electromyography) sensor is muscle sensor to enhance control. It is measure very small electrical potential produce during muscle activation. Accelerometer is used to measure the rotation of human body and Magnetometer used to measured angle of body.

2.2 Microcontroller

ATmega16 microcontroller used as the hardware platform. It is controlling unit which all component such as Accelerometer, wireless module, servo motors are interface.

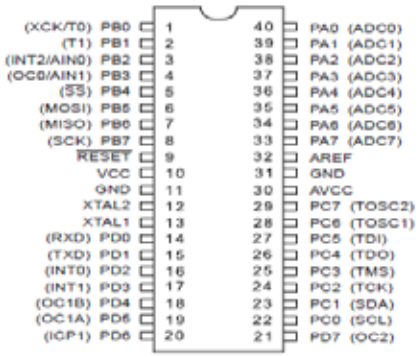

Fig. PIN diagram of ATmega16

2.3 CCC2500 Transreceiver Module

This module can be used for multi way wireless data transmission. It is small size and best range. In this module Up to 250 devices can communicate each other. It work at voltage 4.5 to 5.5Volts and operating range is 30 meter

Fig. CC2500 module

III DISSCUSSION ABOUT FUSION BAND

The device are called GE-Fusion (Gyro and EMG Fusion) and MEA-Fusion (Magnetometer, EMG and Accelerometer)

Bands both are combined into a small box[1]. However by combining sensor, such as combing Accelerometer and EMG sensor for sign language. Combining the Accelerometer and Gyro for motion analysis.

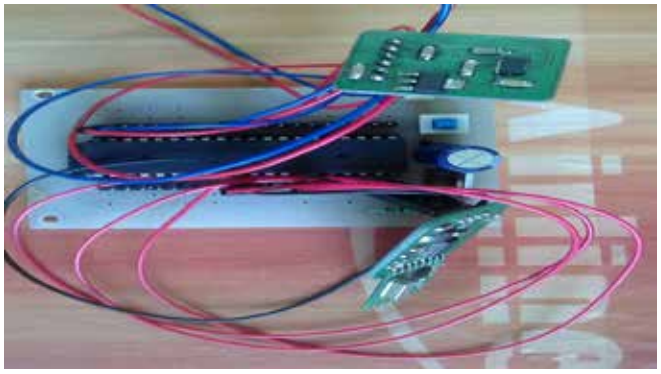

Fig.1

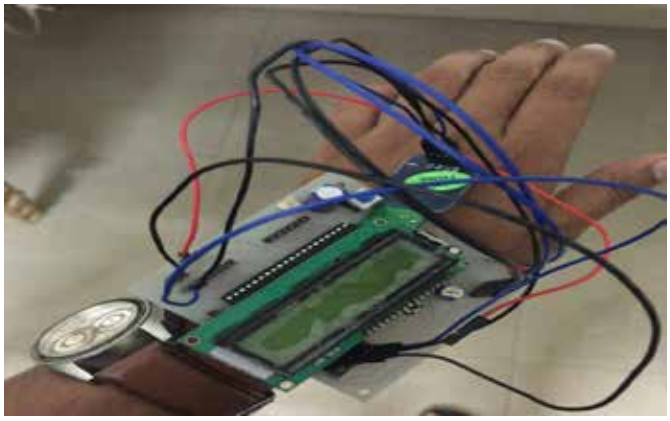

Fig.2

Fig. 1 & 2 fusion band

Yaw and Pitch motion was chosen for control purpose as shown in figure. The robotic arm can be rotate 180 degree of Yaw. To use the Fusion Band a portion of the arm must by movable in yaw (left/right) and pitch (up/down) direction as shown in figure. Fusion Band completely change the way we interacts with industrial machines and robots[1].

Fig. Fusion Band Freedom of Motion [Cut C IEEE 2012]

3.1 Robotic Arm

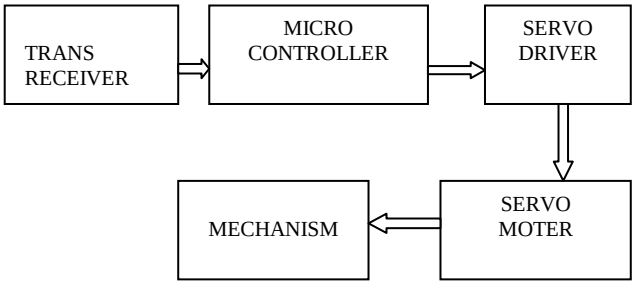

Fig. Block diagram of Receiver part of Robotic Arm

A robotic arm is a type of mechanical arm, usually programmable with similar function to a human arm. Most Robots in the world are design for heavy, repetitive manufacturing work. This task is difficult to handle or boring to human beings. The most manufacturing robot is robotic arm. The robot uses motion sensor to make sure it move just the right amount.

3.3 Servo Motor

Fig. Servo motor

Servo motor are uesd to control the finger movements and wrist movements of the hand. The Rc Servo motor usually have rotation limit from 90 to 180 degree. Servo motor do not rotate continually.

IV EXPECTED OUTCOME

A wireless robotic hand that will be designed to work in synchronization with human hand with precise and accurate movement will also employ a gesture base technique for effective control.

V CONCLUSION AND FUTURE WORK

In this paper, fusion band consists of magnetometer, accelerometer for motion control. Fusion band interface with human hand and capture the motion of human hand. The Fusion band are ideally suited to work with small devices.

In Future research, it include additional feature such as voice recognition to interaction. In future it will be work more range than this paper.

REFERENCE

[1] James Cannan, Huosheng Hu. “A Multi-Sensor Armband based on Muscle and Motion Measurements” IEEE International Conference on Robotics and Biomimetics. [2012]

[2] Wang Wen-hui Yang Ji-hai Vuokko Lantz-Wang Kong-qiao Zhang Xu, Chen Xiang “A Framework for Hand Gesture Recognition”.[2011]

[3] Kostas J. Kyriakopoulos Panagiotis K. Artemiadis “Estimating arm motion and force using emg signals: On the control of exoskeletons” IEEE International Conference on Intelligent Robots and Systems [2008]

[4] Xiang Zhang Weidong Geng Xiubo Liang, Shun Zhang. “Motion based perceptual user interface. [2009]

[5] Rene Winkler Johannes Schumm Martin Kusserow Holger Harms,” Oliver Amft and Gerhard Troester. Ethos: Miniature orientation sensor For wearable human motion analysis” [2010]

[6] Wang Wen-hui Yang Ji-hai Vuokko Lantz-Wang Kong-qiao Zhang Xu, Chen Xiang. "Hand gesture recognition and virtual game control based on 3d accelerometer and emg sensors" IEEE transaction on system [2009]

[7] Nikhil Kadam, Siddhesh Gaiki, Nupur Tupkar, Sakshi Hiwanj. Wirelessly Controlled Robotic Hand [2013]

EFFECT OF DEVELOPED FLUX AND PROCESS PARAMETERS ON HARDNESS OF WELD IN SAW

Gyanendra Singh[1], Vivek Mishra[2],Vijay Shankar Yadav[3]

[1] *Assistant Professor Mechanical Engineeering, Invertis University , Bareilly (India)*

[2,3] *Student, Mechanical Engineering ,Invertis University, Bareilly (India)*

ABSTRACT

In Submerged Arc Welding process flux always plays a vital role. Cost of flux nearly amounts to 50% of the total cost of the overall welding work and after welding the slag hence formed is totally a waste. The ingredients present in flux effects the chemical as well as mechanical properties of the weld bead without the use of different metal or alloy of desired properties. The slag if can be recycled and some ingredients (metal powder) can be added to it then we on one hand can reduce the cost of the process by recycling the waste slag and on the other hand getting the desired property. In the present research, Surface Response Methodology (RSM) is employed for conducting the experiments and analyzing the effect of process parameters (open circuit voltage, travel speed) and weight percentage of Chromium Carbide into the developed flux on the surface hardness of the weld using submerged arc welding process. A significant change in the surface hardness is been observed with the change of percentage of ingredients and process parameters. Therefore the welding cost and pollution caused by dumping of waste slag can be reduced, without any compromise in weld quality, by utilizing the developed flux, prepared from waste slag with the additional benefit of getting the desired properties as needed.

Keywords: Submerged Arc Welding, Flux, Hardness, Response Surface Methodology

I. INTRODUCTION

In submerged arc welding (SAW) produces a coalescence of metals by heating them with an arc between a bare metal wire (electrode) and the metal. The arc and molten metal are “submerged” in a blanket of fusible flux.[1] The primary function of the flux is to protect the weld pool from atmospheric contamination. It facilitates in a slower cooling rate resulting in the desired mechanical properties as well as metallurgical characteristics of the weldment. During welding, a portion of flux melts and gets adhered to the solidified weld pool. This fused flux, generally known as slag, is then detached and removed. The present work uses this waste slag for development of fresh flux and deciding the parameters for hardness in further runs of submerged arc welding.[2, 3]

Flux plays an important role in deciding the weld metal quality.[4] Flux constitutes half of the total welding cost in submerged arc welding. It greatly influence process usability and weld metal mechanical properties [5]. It has been reported that agglomerated fluxes produce weld deposits of better ductility and impact strength as compared with fused fluxes [6,7]. These fluxes are hygroscopic in nature, therefore baking is essential for good weld metal integrity [8]. Data and Bandyopadhyay [9] has performed optimization to determine the amount of waste slag and flux mixture that can be used without sacrificing any negative effect on bead geometry, compared to conventional SAW process, which consumes fresh flux only. Prashad and Dwivedi [10]

investigated the influence of submerged arc welding process parameters on hardness of steel weld bead.

II. EXPERIMENTATION

The Flux used in the present work was firstly prepared from used slag of SAW process. This slag was crushed and Chromium Carbide was added to it with other necessary ingredients and the treated such that the fresh agglomerated flux has been created. Chromium Carbide has a tendency to increase hardness penetration. Chromium Carbide can increase the toughness of steel, as well as the wear resistance. Probably one of the most well-known effects of chromium on steel is the tendency to resist staining and corrosion [11]. Although the excess of carbide will result in the brittleness of the steel, thus the percentage of Chromium Carbide addition should be optimum.

2.1 Identification of Parameters

For defect free, predictable, controllable and higher productive welding, identification of correct welding parameters which control the weld characteristics is essential. These parameters affect the weld metal chemistry, bead shape geometry, metal transfer characteristics, heat input and microstructure of the weld metal [12]. Amongst the welding parameters, arc voltage, travel speed and percentage addition of metal powder for flux were selected as these are independently controllable process variables. Their effect on the hardness of the weld metal was studied. These parameters were selected because these influence the penetration, deposition rate and chemical composition of weld metal. Open circuit voltage was considered in place of arc voltage for investigation because it varies linearly with arc voltage and can be controlled directly.

2.2 Selecting the Range of the Process Variables

The trial runs were conducted to select the range of the welding parameters. The range, covering the lowest and the highest level of the direct welding parameters, was carefully selected so as to maintain the equilibrium between the welding wire feed rate and burn-off rate. The basis of selection of given range for various welding parameters was that the selected range should be within the permissible limit of the parameters of the power source. Also the resultant weld should have good bead appearance, configurations and be free from visual defects viz, undercut, overlap, excessive crown height, surface porosity, non-uniform ripples, macro cracking etc. All the direct and indirect parameters except the ones under consideration were kept constant. The units, symbols, and the range of the factors (parameters) are given in Table 1.

The composition of the base plate which is used is been shown below in Table 2.

Table 1: Range of welding parameters

Parameter	Unit	Range	
		Lower value	Higher value
Metal Powder(m)	% by wt.	0	20
Open circuit voltage (V)	Volts	30	38
Travel speed(c)	m/hr.	22	26

Table 2: Composition of the Base Plate

Material	C	Mn	Si	S	P	Ni	Cr	Cu
Base plate	0.173	0.512	0.173	0.042	0.055	0.017	0.069	0.059

2.3 Conducting the Experiments

For welding purpose TORNADO SAW M-800 welding machine is used. This machine also had the provision for controlling the open circuit voltage, current and travel speed. The welds were laid by using 3.2 mm diameter copper coated M.S wire. The composition of the base plate is given in Table 4. The plate size used for bead on plate welds was 100 × 50 × 6 mm. Chromium Carbide was mixed with crushed slag in different percentages by weight. The welds were laid on the base plate using three passes; two were laid parallel and third was laid on the top of the two. Respond Surface methodology is employed to make design matrix for conducting experiments.

Response (hardness) is measured by the use of Rockwell Hardness Testing Machine in C-scale. The value of response is filled in design matrix and further analysis s done.

2.4. Result and Discussion

2.4.1 Effect of Metal Powder Addition to Flux on Hardness

The average values of hardness for metal powder addition to flux at levels 1, 2 and 3(0, 10, 20), and keeping the other factors (voltage and current) at '0' level are calculated and these values are plotted in Figure 1. It can be seen from the figure 1 that with the increase of metal powder percentage in the flux from 0% to 20%, hardness increases from 1st level to 2nd level and then from 2nd level to third level. An optimal value is reached at nearly 15% of metal powder .

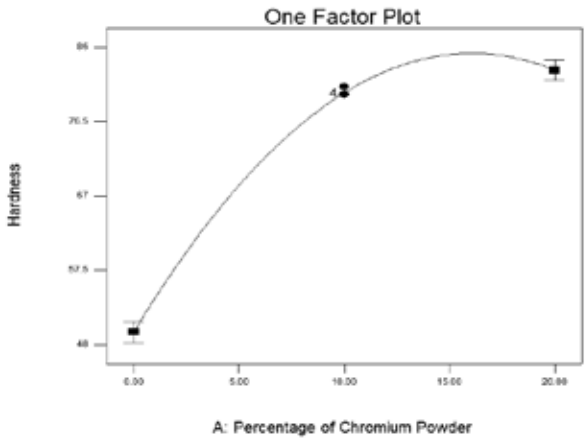

Fig. 1 Metal Powder V/S Hardness Graph, Effect Of Addition Of Metal Powder To Flux On Hardness

Keeping voltage, current and tip to work distance at constant, an increase in metal powder percentage in the flux increases the amount of alloying elements in the flux. During welding, when flux melts more alloying elements enters the weld metal which changes the weld metal composition. The value for hardness initially increases up

to a certain limit then it again decreases due to the excess of carbide in the flux which results in the brittleness of the weld bead.

2.4.2 Effect of voltage on hardness

The average values of hardness for voltage at levels 1, 2 and 3 (30, 34, 38), and keeping the other factors (current and metal powder) at '0' level are calculated and these values are plotted in Figure 2. It can be seen from the figure 2 that with the increase of voltage from 30V to 38V, hardness also increases from 1st level to 2nd level then increases from 2nd level to third level.

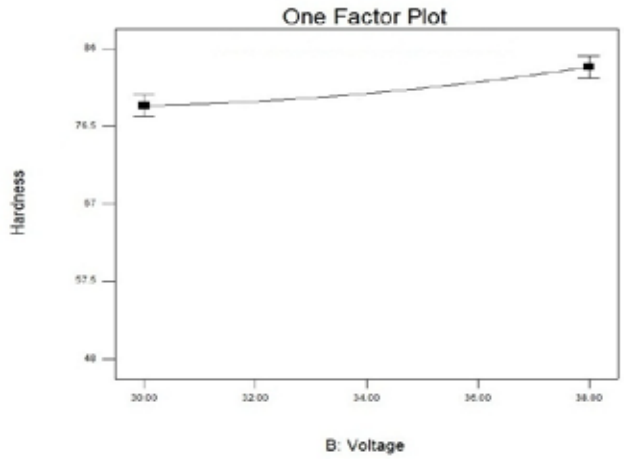

Fig. 2 voltage v/s hardness graph, effect of voltage on hardness

Increasing the arc voltage increases the arc length so that the weld bead width is increased, reinforcement is decreased and flux consumption is increased. Keeping tip to work distance, current and metal powder percentage constant, an increase in welding voltage results in melting of more flux due to which more alloying elements enter the weld metal. Thus arc voltage affects weld metal composition which increases the hardness of the weld metal.

2.4.3 Effect of Travel Speed on Hardness

The average values of hardness for travel speed at levels 1, 2 and 3(22, 24, 26), and keeping the other factors (voltage, percentage of metal powder and current) at '0' level are calculated and these values are plotted in Figure 3. It can be seen from the figure 3 that with the increase of travel speed of SAW machine, hardness increases from 1st level to 2nd level and then from 2nd level to third level.

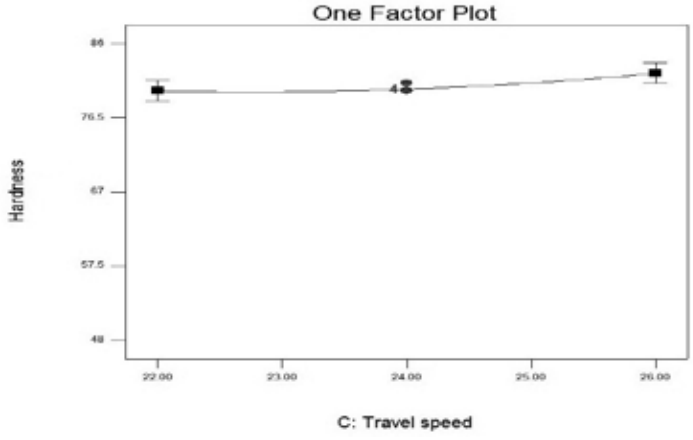

Fig. 3 Travel Speed V/S Hardness Graph, Effect Of Travel Speed On Hardness

Increasing the travel speed of SAW machine decreases the weld wire deposition on the bead and also results in increase in nozzle length to weld bead which results in increase in heat thus flux consumption is increased. Keeping voltage, tip to work distance, current and metal powder percentage constant, an increase in welding speed results in melting of more flux due to which more alloying elements enter the weld metal. Thus travel speed affects weld metal composition which increases the hardness of the weld metal.

III. CONCLUSION

The following conclusion can be drawn on bases of above analysis:-

1. The amount of chromium carbide addition in the flux and the open circuit voltage are found to affect the hardness of the weld metal significantly.
2. Hardness of the weld metal increases with the increase in the arc voltage.
3. Increase in travel speed also increases hardness of the weld metal.
4. An increase in the amount of chromium carbide in the flux increases the hardness of the weld metal upto a certain limit. On further addition of chromium carbide will result in decrease in hardness which may be probably due to being brittleness of the weld bead due to excessive carbide in it.

REFERENCES

1. Kook-soo Bang, Chan Park, Hong-chul Jung, Jong-bong Lee, “Effects of Flux Composition on the Element Transfer and Mechanical Properties of Weld Metal in Submerged Arc Welding”, Met. Mater. Int., Vol. 15, No. 3 (2009), pp. 471~477 doi: 10.1007/s12540-009-0471-3 Published 26 June 2009
2. Saurav Datta, Asish Bandyopadhyay, Pradip Kumar Pal, “Modeling and optimization of features of bead geometry including percentage dilution in submerged arc welding using mixture of fresh flux and fused slag, Springer-Verlag London Limited 2007
3. Livshit LG, Shiryaev AI, “A new ceramic flux for hardfacing”, Welding production, January 1960, pp 25–29
4. C.A. Bulter and C.E. Jackson, “Submerged arc welding characteristics of Cao-TiO2-SiO2 system,” Welding Journal, vol. 46, no. 5, 1967, pp 445-448.
5. Davis. Louise, “An introduction to welding fluxes for mild and alloy steels,” The welding institute, Cambridge, 1981
6. P.S. Vishvanath, “Submerged arc welding fluxes,” Indian Welding Journal, vol.15, no.1, 1982, pp. 1-11.
7. M.L.E. Davis and N. Baily, “Properties of submerged arc fluxes- A fundamental study,” Metal Construction, vol. 65, no.6, 1982, pp. 207-209.
8. Mohan. Narendra and Sunil. Pandey, “Welding current in submerged arc welding,” Indian Welding Journal, 2003, vol. 36, no. 1, 2003, pp.18-22.
9. S. Datta, Bandhopadhayaay, and P.K. Pal, “Modeling and optimization of features of bead geometry including percentage dilution in submerged arc welding using mixture of fresh and fused flux,” International Journal of advanced Manufacturing Technology, vol.36, no. 11, 2008, pp. 1080-1090.

10. K.Parshad, and D.K.Dwivedi, "Some investigations on microstructure and mechanical properties of submerged arc welded HSLA steel joints," International Journal of advanced Manufacturing Technology, vol. 36, no.5, 2008, pp. 475-483.
11. Surian E., Trotti A., Cassanelli A. and Devedia L.A. , " Infuluence of chromium on mechanical properties and microstructure of weld metal from a high-strength SMA electrode', Welding Journal 72(8), 1994 : pp. 45s-54s.
12. Pandey, N.D., Bharti, A. and Gupta, S.R. "Effect of submerged arc welding parameters and fluxes on element transfer behaviour and weld-metal chemistry". Journal of Materials Processing Technology, Volume 40, Issues 1-2: pp. 195-211 (1994).

CURRENT TRENDS IN DOMESTIC SOLAR WATER HEATING - CPC AN AMICABLE ALTERNATIVE, A PROPOSED DISTINCT DESIGN

Jaji Varghese[1], Dr.Samsher[2], Dr.Manjunath.K[3]

[1]*Department of Mechanical Engineering, Aryabhat Polytechnic, D.T.T.E, Delhi, (India)*

[2,3]*Department of Mechanical Engineering, Delhi Technological University,(India)*

ABSTRACT

The use of solar energy for power generation and thermal applications is a well-known concept. For households, the most commonly used is the flat plate collector which is normally fixed in position and to obtain maximum incidence of the solar radiation it has large surface area. These collectors thus have high first time capital and installation cost. High solar fraction and higher temperatures can be attained by use of reflectors. Research studies have been carried out and model validation done with symmetrical and asymmetrical type of reflectors. The better option is to choose a reflector with wider acceptance angle to offset loss of concentration ratio and positioning of tank on the reflector which would become easier. The model studied is batch type heater, as the receiver serves the dual purpose of absorber and storage tank, unlike conventional design which consist of a large number of smaller diameter tubes and separate storage tank. The concentrator i.e. the reflector in this case, is supported on a wooden cradle which comprises the two parabolas of the compound parabolic concentrator.

Keywords: Batch Type, Compound Parabolic, Domestic, Reflector, Solar Water Heaters

I. INTRODUCTION

Inspite of the efforts made by MNES, IREDA and other Govt. & Private agencies the concept of Solar Water Heating for domestic purposes is not widely acceptable. Even the global status report [1] published by REN21 (2010), depicting the average annual growth rates of renewable energy capacity, (2005-2010), the growth in solar water heating system is at standstill, (Year 2005- 16% & year 2010 also 16%) whereas there has been substantial growth in concentrated solar power (25% to 77%) and solar photovoltaic (49% to 72%). The reasons being high first time capital and installation cost; although operating cost is negligible it requires close monitoring as operating cost increases with poor up keeping and maintenance.

For households, generally two types of collectors are available in the market. The collector in most common use is the flat plate collector (FPC) because it is simple in design and has no moving parts but requires large surface area. The FPC are normally fixed in position and do not track the sun and to obtain maximum incidence of the solar radiation it has large surface area. But with large surface area, about 30-50 percent heat losses also occurs and mainly the convective and radiative losses from the front face of the collector. In this system the solar

radiation is asorbed by blackened metallic absorber sheets with built in channels or riser tubes to carry water. The absorber sheets absorb the radiation and transfer the heat to flowing water. The flowing water is then stored in a separate well insulated storage tank. The absorber is enclosed in a insulated outer metallic box covered on the top with glass. These systems are available in multiples of 100 litres per day LPD).

The other is the evacuated tube collector based solar water heater which consists of double layer evacuated borosilicate glass tubes having selective coating on the outer surfaces of inner tubes. These systems are less expensive but life of these systems is less than FPC system. These systems are available in any size i.e. 50, 75, 100, 125, 150 LPD etc.

To obtain higher collection efficiency better alternative is to go for concentrating collectors as it increases the intensity by concentrating the energy available over a large surface on to a smaller surface (absorber). Due to the concentration on a smaller area, the heat loss area is reduced. Further, the thermal mass is much smaller than that of a FPC and hence transient effects are small. The delivery temperatures being high, a thermodynamic match between temperature level and the task occurs. The present work is an attempt in this direction.

II. LITERATURE REVIEW

The success of any solar water heater system is envisaged only if it is capable of delivering hot water when needed and even during non-sunshine hours. The design therefore, should incorporate these two important criteria, a good solar fraction and good heat retention. A good solar fraction can be obtained by improved optical efficiency and heat retention by proper insulation and good thermal storage. Many techniques have been evolved to have good heat retention. To minimise the heat losses apart from the use of good insulation, Chaurasia and John Twidell [2] carried out studies to measure overall loss coefficient with simple glass glazing and with the the use of transparent insulation material (TIM). The effect of using TIM and varying its configuration within the collector has been studied by Reddy and Kaushika [3]. To minimize the nocturnal heat losses Shridhar and Reddy designed and developed a modified cuboid solar integrated-collector-storage (ICS) system with [TIM] transparent insulation material [4]. Abdul Jabbar Khalifa et al. [5] suggested DSWH's system with a back layer of phase change material (PCM), which yielded increase in plate temperature and better heat storage during off-sunshine hours. Hailliot..D et al. [6] evaluated the potential of compressed expanded natural graphite (CENG) and phase change material (PCM) composites to improve the performance of solar domestic hot water (SDHW) systems. Stratification increases the performance of solar systems.[7]. When tanks are horizontally placed, they are usually less stratified than when they are vertical. Carrilleo and Cejudo[6] used TRNSYS software to study a model, an indirect solar domestic hot water system with horizontal storage and a mantle heat exchanger. Soteris and Christos [8] did a simple model validation of a SWH consisting of two flat plate collectors using TRNSYS, the tool was used to optimise the design parameters and annual solar fraction obtained was 79%. Tank volume to collector area (V_t/A_c) ratio has also an important bearing on system performance for thermosyphon systems. Using TRNSYS simulation program, Sharaih and Lof [9] obtained optimum values for tank height and volume, which maximises the annual solar fraction for temperatures ranging from 50-80◦C. The positioning of the auxiliary heater within the tank, is also an important parameter thereby providing good thermal stratification. Shariah and Lof[10] made studies on the effects of auxiliary heater on annual performance of thermosyphon solar water heater simulated under variable operating conditions.

To obtain its wider acceptability in the domestic sector, the need is to improve the water temperature rise during the daily operation and water temperature preservation during the night. To increase the optical efficiency different designs of symmetrical and asymmetrical reflectors have been studied. Extensive study on domestic use of solar water heaters with stationary concentrating reflectors has been performed by Tripanagnostopoulos and Yianoulis [11, 12], presenting a new concept on ICS systems. Helal.O et al. [13] designed an ICS solar water heater based on three parabolic sections. The performance of the system is modelled by a simulation program written in MATLAB programming language and the results compared with the symmetric and asymmetric CPC reflectors of Tripanagnostopoulos model. Senthilkumar and Yasodha developed a three dimensional compound parabolic concentrator, with the CPC reflectors fabricated as horizontal segments instead of vertical segments. [14] Surface errors were thus reduced and optical efficiency increased. Lens walled CPC, a novel design by Yuehong sua et al. [15] with large acceptance angle applied to PV applications can be incorporated in the ICS design. Thermal performance of CPC with large acceptance angle has been studied by Jaji Varghese et al.[16] with mean daily efficiency of 37% and maximum water temperature 60^0C attained. Performance study on an ICS with single tube involute reflector was done by Schmidt and Goetzberger [17]. Such reflector has an acceptance angle of 180°. This means that even diffuse light which is scattered by the transparent insulation material is completely reflected onto the absorber. An annual SF of 0.65 and annual efficiency of 35% was obtained. The concept of using two storage tanks and based on the combination of asymmetric and symmetric CPC reflectors so as to obtain better water temperature stratification has been done by Tripanagnostopoulos and Souliotis. [18]

III. PRINCIPLE OF PROPOSED DESIGN

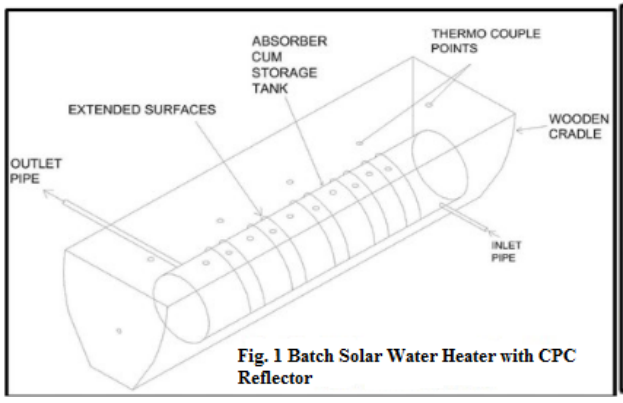

Fig. 1 Batch Solar Water Heater with CPC Reflector

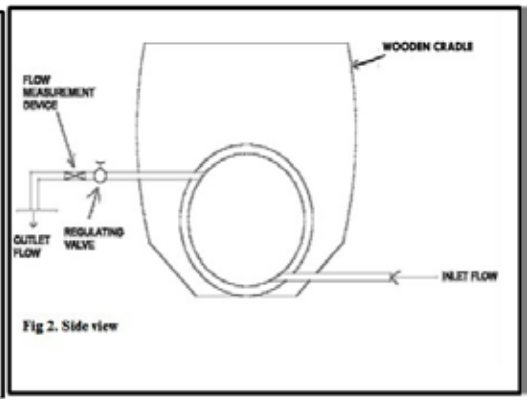

Fig 2. Side view

The present work is an integration of two concepts of solar water heating technology. One is the batch water heater concept (an ancient concept of solar water heating) also referred as built-in- storage water heater where the absorber and storage is a single unit. There is no separate storage tank. The basic principle is that the absorber which is a drum/tank is coated black, (unlike the small diameter tubes in the conventional Flat plate collectors), absorbs the incoming radiation and transmits the heat to water stored in it. The non-illuminated part is backed by insulation. Earlier designs had some portion of the non-illuminated part kept underground.

The other is by the principle of concentrating the radiation on to the receiver (absorber tank) with the help of a reflector also referred as concentrator. The collection efficiency is high and high temperatures can be attained.

The merits of these two systems have been incorporated in the present design. The elimination of separate storage tank (considerably brings down the cost of the system) and incorporating a reflector improves collection efficiency. With a concentrator lesser intercepting area for same temperatures is required which means lesser roof area. The only disadvantage is high night time or nocturnal heat loss which has been now the focus of study and a few methods have been suggested in the paper.

Like the Batch type heater it is a naturally circulated type with the inlet connected to the supply or overhead tank and the outlet regulated by a simple regulating valve. High solar fraction and higher temperatures can be attained by use of reflectors. Most research studies have been carried out and model validation done with symmetrical and asymmetrical type of reflectors with involute profile reflector or with three parabolic sections. But positioning of the tank becomes more cumbersome and compromise has to be done with regard to water temperature stratification and maximum water temperatures. The better option is to choose a reflector with wider acceptance angle to offset loss of concentration ratio and positioning of tank on the reflector which would become easier. Also the design would be easy to fabricate and economically viable. The reflector in this case, is supported on a wooden cradle which comprises the two parabolas of the CPC. The upper end points of the collector are parallel to the central plane of symmetry of the collector thus contributes little to the radiation reaching the absorber, and the CPC can be truncated to reduce its height resulting in saving in reflector area but little sacrifice in performance.

However, such systems suffer from heavy energy losses during night periods or during insufficient radiation. No matter how well insulated the rear and sides of the collector might be; its solar collecting face would constitute a significant source of night time heat loss. As a result, the water temperature would drop by considerable amounts overnight, often leaving little, if any useful energy, the next morning. The thermal protection of the water storage tank is difficult as a significant part of the external surface is used for the absorption of solar radiation contrary to that of the FPC systems, where the hot water is stored in a separate storage tank which is thermally insulated. In this system also referred as integrated collector storage ICS), the opaque thermal insulation can be provided only on the non-illuminated part. Thus, although ICS system has simple construction, installation and operation are less applied than FPC systems as it presents high thermal losses during night or non-sunshine hours. Thus, good thermal heat retention and to suppress nocturnal heat loss is an increasingly important entity in BSWH systems.

In the present design side wall thermal resistance comprises of 4cm wood, 10 cm air gap and 6.5 cm glass wool insulation. The front and back portion are backed by wood and glass wool insulation. To suppress the nocturnal heat loss conventional techniques can be used but the results can be more encouraging if in addition to these conventional techniques, the thermal inertia of the collector can be increased by application of the concept of thermal mass in the design. Thermal mass is a concept in building design that describes how the mass of the building provides inertia against temperature fluctuations, sometimes known as the thermal flywheel effect. This concept has been incorporated in the proposed design by the use of Insulated Concrete Form (ICF). These forms (ICF) are interlocking modular units that are dry-stacked (without mortar) and filled with concrete that stays in place as permanent interior and exterior substrates on walls, floors and roofs. The same can be placed as extended surfaces on the exterior of the tank, thereby increasing the thermal capacity as shown in Fig.1.

IV. CONCLUSION

The advantages of this heater is that it is simple in design as it requires no pumps, blowers, differential thermostats or other externally powered devices and can be built from locally available material with moderate carpentry and plumbing skills. Also the absence of a separate storage tank cuts down the cost considerably.

By utilizing the CPC concept in reflector design, increases the collection efficiency due to increase in the concentration ratio and also minimum of tracking required due to increased acceptance angle. In conventional CPC solar collector to avoid the thermal losses a gap of few millimeters is provided between the small diameter tubular absorber and the reflector. But due to this the optical losses of the collector are increased. In the proposed design, the gap between the absorber and the reflector has less significance, as it is too small compared with the diameter of the cylindrical storage drum. The benefit of thermal mass concept can be envisaged which flattens out the nocturnal heat loss variations to desirable extent.

Also in regions where quality of water is a concern, especially in developing countries, where scaling in the collector systems results in the poor performance. Here it is not a matter of grave concern due to the presence of a larger diameter drum, unlike built in channels or smaller diameter riser tubes in conventional collectors.

Thus this system can be an amicable alternative to the conventional FPC/ETC for domestic purposes.

REFERENCES

[1] Manual of Solar Water Heater, (2013), Delhi energy efficiency and renewable energy management centre, Govt. of NCT, Delhi.

[2] Chaurasia.B.L, John Twidell, Collector cum storage solar water heater with and without transparent insulation material, Solar Energy, Vol.70, No.5, (2001), pp.403–416.

[3] Reddy.K.S, Kaushika.N.D, Comparative study of transparent insulation materials cover systems for integrated-collector-storage solar water heaters, Solar Energy Materials & Solar Cells, Vol.58, (1999), pp.431-446.

[4] Sridhar.A, Reddy.K.S, Transient analysis of modified cuboid solar intergrated collector storage system, Applied Thermal Engineering, Vol.27, (2007), pp.330–346.

[5] Abdul Jabbar Khalifa.N, Kadhim Suffe.H, Mahmoud Sh. Mahmoud, A Storage domestic solar hot water system with a back layer of phase change material, Experimental Thermal and Fluid Science, Vol.44, (2013), pp.174-81.

[6] Haillot.D, Nepveu.F, Goetz.V, Pya.X, Benabdelkarim.M, High performance storage composite for the enhancement of solar domestic hot water systems, Solar Energy, Vol.86, (2012), pp.64–77.

[7] Carrilleo Andres.A, Cejudo Lopez.J.M, TRNSY model of a thermosyphon solar domestic water heater with a horizontal store and mantle heat exchanger, Solar Energy, Vol.72, No. 2, (2002), pp.89–98.

[8] Soteris Kalogiroua.A, Christos Papamarcou, Modelling of a thermosyphon system and simple model validation, Renewable Energy, Vol.21, (2000), pp.471-493.

[9] Shariah.A.M, LOF, The optimisation of the tank volume-to-collector area ratio for a thermosyphon solar water heater, Renewable Energy, Vol.7, No.3, (1996), pp.289-300.

[10] Shariah A.M, Lof.G, Effects of Auxillary Heater on annual performance of thermosyphom SWH simulated under variable operating conditions, Solar Energy Vol. 60, No.2, (1997), pp. 119-126.

[11] Souliotis.M, Quinlan.P, Smyth.M, Tripanagnostopoulos.Y, Heat retaining integrated collector storage solar water heater with asymmetric CPC reflector, Solar Energy, Vol.85, (2011), pp.2474–2487.

[12] Souliotis Chemisana.D, Caouris Y.G, Tripanagnostopoulos.Y, Experimental study of integrated collector storage solar water heaters, Renewable Energy, Vol.50, (2013), pp.1083-1094.

[13] Helal.O, Chaouachi.B, Gabsi.S, Design and thermal performance of an ICS solar water heater based on three parabolic sections, Solar Energy, Vol.85, (2011), pp.2421–2432.

[14] Senthilkumar.S, Yasodha.N, Design and Development of a Three Dimensional Compound Parabolic Concentrator and Study of Optical and Thermal performance, International Journal of Energy Science, Vol.2, 2012, pp.64-68.

[15] Yuehong Sua, Saffa Riffat.B, Gang Peia, Comparative study on annual solar energy collection of a novel lens-walled compound parabolic concentrator (lens-walled CPC), Sustainable Cities and Society, Vol.4, (2012), pp. 35– 40.

[16] Jaji Varghese, Gajanan Awari.K, Mahendra Singh.P, Experimental analysis of a distnct design of a batch solar water heater with integrated collector storage system, Thermal Science, Vol.11, (2007), No. 4, pp.135-142.

[17] Schmidt.C, Goetzberger.A, Single tube integrated collector storage systems with transparent insulation and involute reflector, Solar Energy, Vol.45, (1990), pp.93-100.

[18] Tripanagnostopoulos.Y, Souliotis.M, ICS Solar systems with two water tanks, Renewable Energy, Vol.31, (2006), pp.1698–1717.

DESIGN AND ANALYSIS OF LOW POWER CHARGE PUMP CIRCUIT FOR PHASE-LOCKED LOOP

[1] B. Praveen Kumar, [2]G.Rajarajeshwari, [3]J.Anu Infancia

[1, 2, 3]PG students / ECE, SNS College of Technology, Coimbatore, (India)

ABSTRACT

CMOS is used to construct the integrated circuits with low level of static leakage. With this low level leakage we are designing all the transistor circuits in CMOS logic. To control this static leakage in the circuits the supply voltage is a major concern. Here the step-up converters with charge pump and the level for maintaining its threshold voltage (V_T) is to be analyzed and proposed. Here we are going to propose the novel approach as body bias effect and sub-threshold logic. This will be applied for the step-up converters for energy harvesting applications. The backward control is to be processed for control the internal voltage when the charge transfer switch could be in activation. This will be used to boost the voltages from the circuit for step-up converters. When the supply voltage is to be raise from the fixed voltage level it will be turn OFF the transistor. The maximum level of the converters circuits contain the branch A and branch B which could be contains all p-MOS and n-MOS combinations. The oscillator circuit also to e designed and applied to the proposed six stage charge pump circuit to reduce the power consumption. To reduce the standby mode leakage we are designing the circuit by using power gating logic. These circuits are to be designed and verified by using the TANNER T-SPICE TOOLS.

Keywords: Body Bias, Sub Threshold, Linear Charge Pump.

I. INTRODUCTION

A charge pump circuit provides a voltage that is higher than the voltage of the power supply or a voltage of reverse polarity. In many applications such as Power IC, continuous time filters, and EEPROM, voltages higher than the power supplies are frequently required. Increased voltage levels are obtained in a charge pump as a result of transferring charges to a capacitive load and do not involve amplifiers or transformers. For that reason a charge pump is a device of choice in semiconductor technology where normal range of operating voltages is limited.

Charge pumps usually operate at high frequency level in order to increase their output power within a reasonable size of total capacitance used for charge transfer. This operating frequency may be adjusted by compensating for changes in the power requirements and saving the energy delivered to the charge pump.

The charge pump employs either low quiescent current Burst Mode operation or low noise constant frequency mode. In Burst Mode operation the charge pump VOUT regulates to –0.94 • VIN, and the Charge pump draws only 100µA of quiescent current with both LDO regulators on. In constant frequency mode the charge pump produces an output equal to –VIN and operates at a fixed 500 kHz or to a programmed value between 50kHz to 500kHz using an external resistor. The Charge pump is available in low profile (0.75mm) 3mm x 4mm 14-pin DFN and thermally enhanced 16-pin MSOP packages.

The charge transfer frequency can be adjusted between 50 kHz and 500 kHz using an external resistor on the RT pin. At slower frequencies the effective open-loop output resistance (ROL) of the charge pump is larger and it is able to provide smaller average output current. It can be used to determine a suitable value of RT to achieve a required oscillator frequency. If the RT pin is grounded, the part operates at a constant frequency of 500 kHz.

.

II. EXISTING SYSTEM

2.1 Dickson Charge Pump

The Dickson charge pump and single cascade charge pump, shown in fig 1. , are derived from the ideal diode charge pump architecture. Both circuits output voltage obey equation that can be simplified as in equation.

$$Vout = VDD - Vth(0) + \Sigma [\alpha VDD - Vth(i)] \ldots\ldots. (1)$$

$$Vout = VDD + n (VDD-Vth) \ldots\ldots\ldots\ldots\ldots\ldots\ldots\ldots....(2)$$

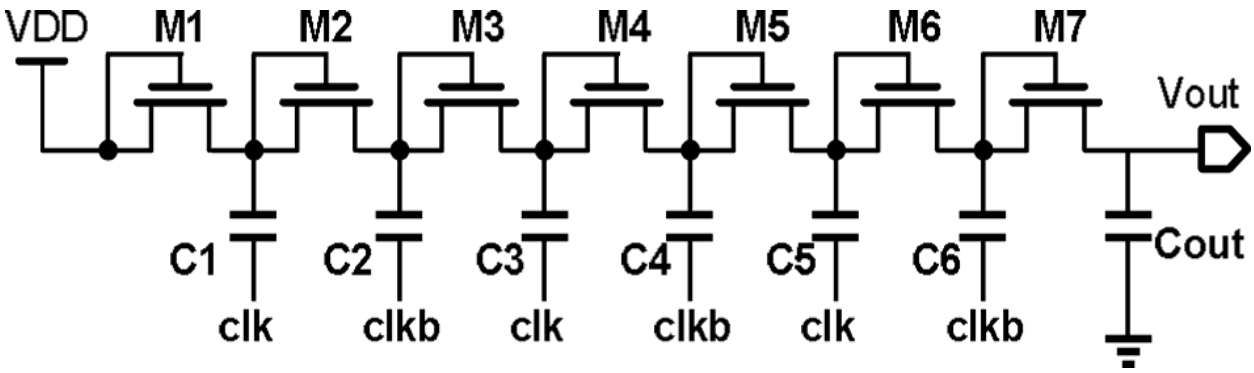

Fig 1. Dickson Charge Pump

The term VDD-Vth is called the voltage gain per unit stage. Note that this gain is additive and not multiplicative as in the voltage doubler architecture. In the Dickson charge pump, as the voltage of each stage increases, the threshold voltage of the diode-connected MOSFET increases due to body effect, and the voltage gain decreases as the number of stages increases. This effect is not present with the single cascade architecture. For large number of stages (>10), the Dickson charge pump has an average voltage gain of 0.25*VDD, while the single cascade circuit produces an average gain of 0.5*VDD.

2.2. Wu Chang Charge Pumps

A charge pump circuit provides a voltage that is higher than the voltage of the power supply or a voltage of reverse polarity. In many applications such as Power IC, continuous time filters, and EEPROM, voltages higher than the power supplies are frequently required.

Increased voltage levels are obtained in a charge pump as a result of transferring charges to a capacitive load and do not involve amplifiers or transformers. For that reason a charge pump is a device of choice in semiconductor technology where normal range of operating voltages is limited. Charge pumps usually operate at high frequency level in order to increase their output power within a reasonable size of total capacitance used for charge transfer.

Six consecutive stages of the charge pump of are shown in Fig. 1. Assume the circuit is in steady-state. When CLK changes from 0 to VDD (when CLKB, the inverse of CLK, falls), the nth stage output, V, increases by CV and the voltages of neighboring stages reduce by the same amount. Consequently, the auxiliary NMOS switch, for the control of nth charge transfer switch, turns on by Vn-Vn-1 = 2CV and the PMOS switch, PMOS, turns off. Thus, V falls from Vn+1 to Vn-1 and turns off NMOS, and Vn-1 and Vn+1 rise to turn on the (n-1) th and (n+1) th charge transfer switches, PMOS and NMOS. Hence, the (n+1)th stage is charged up to the peak voltage of V. Similarly, when CLK falls (CLKB rises), Vn+1 is charged by CV. Thus, the output voltage of the charge pump with n stages is determined.

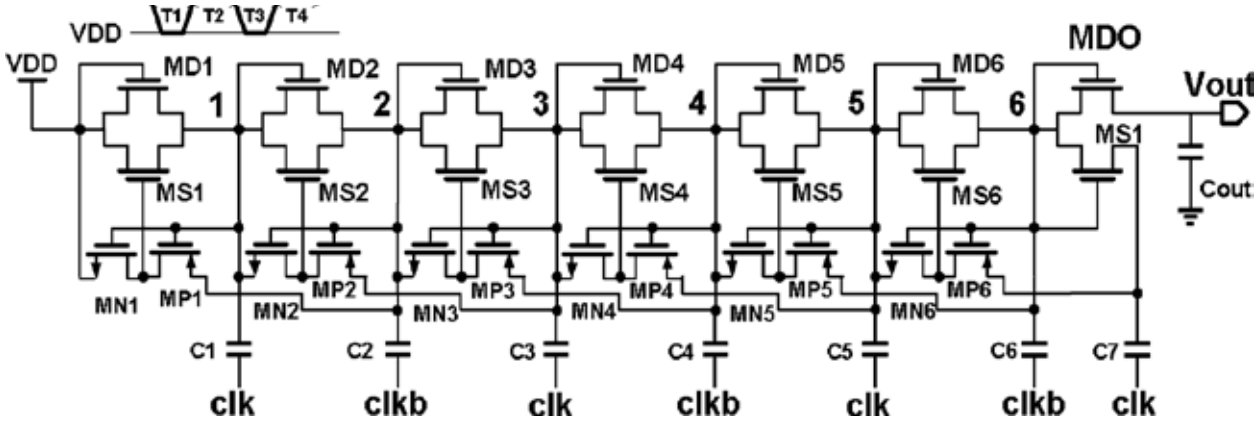

Fig.2 WU CHANG charge pump

Ideally, CV should be close to VDD. However, the parasitic capacitance at each node and the unwanted reverse currents cause CV to be smaller than VDD. Since the parasitic capacitance effect is not significant and can be overcome with ease by increasing unit capacitance Cu, the reverse current effect becomes the dominant loss factor.

2.3. Linear Charge Pumps

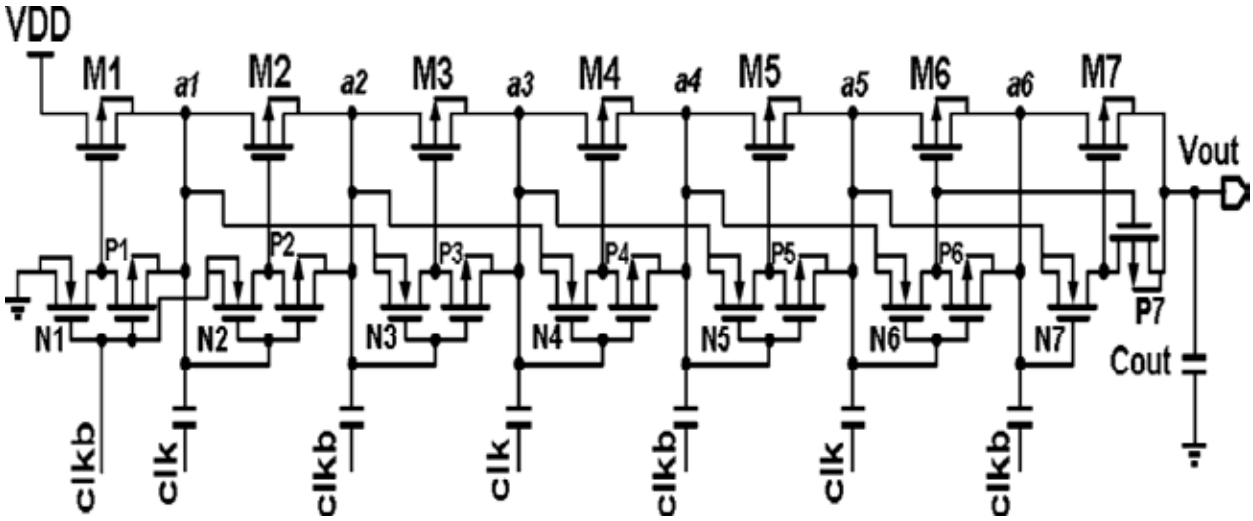

Fig.2 Linear charge pump

The charge pump was not an acceptable solution, until now .The minimum additional requirement was a linear regulator for stabilizing the output voltage. Newer charge pumps are regulated internally and can deliver substantially higher output currents. This way charge pumps are becoming more viable in applications that have been the domain of inductive DC/DC converter. This topic will give an overview on which topologies are used, how charge pumps are regulated and how external capacitors influence the performance of the system.

The main drawback of this topology is constituted by the parasitic capacitances which affect the behavior and performance more than the other topologies. Indeed, as demonstrated in, the reduction of the output voltage with respect to an ideal charge pump (i.e., without parasitic capacitances) strongly increases by increasing the number of stages. Moreover, another critical aspect concerns the switches implementation.

III. PROPOSED SYSTEM

The proposed two branch and six stages of charge pump has been analyzed and this could be uses the body bias effect and the backward control scheme for low power consumption and high amplification. Ignoring leakage effects, this effectively provides double the supply voltage to the load (the sum of the original supply and the capacitor). And also the Charge pumps offer high-efficiency and compact solutions for applications with generally low-output current requirements. This Regulated output charge pumps maintain a constant output with a varying voltage input. This high level of amplification gives the linear output of the all level implementation from the designed circuits. And also this proposed charge pump cannot give any errors or damage during the manufacturing process. The implementation level could be modified when we are designing this charge pump with more number of stages.

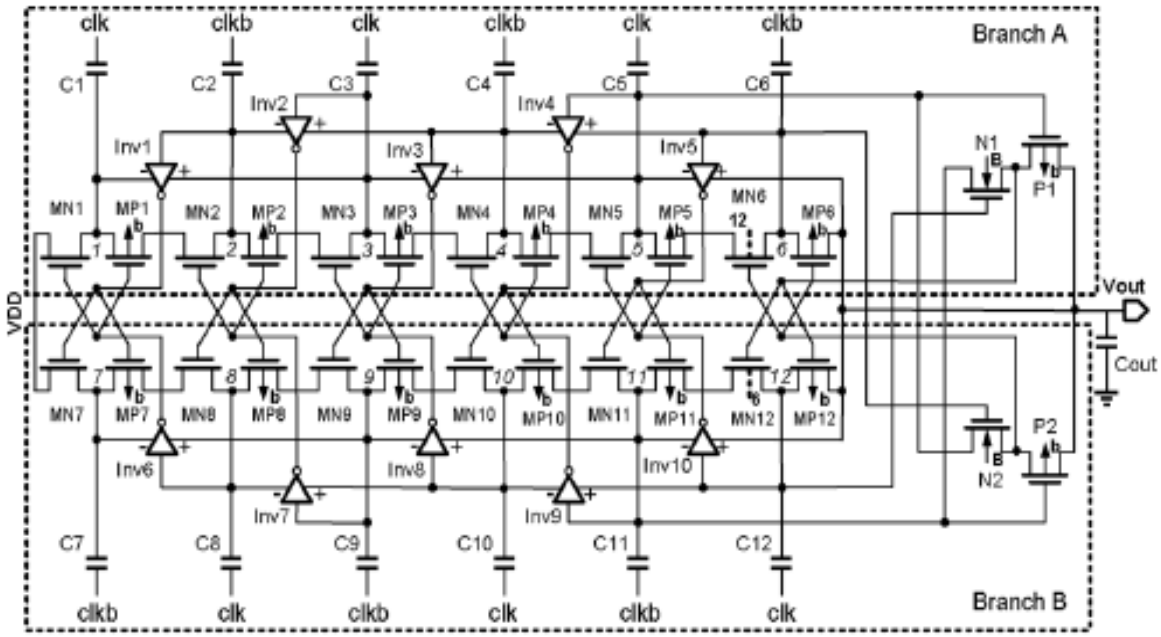

Fig.4 proposed charge pump circuit by using sub-threshold logic

A charge pump circuit provides a voltage that is higher than the voltage of the power supply or a voltage of reverse polarity. In many applications such as Power IC, continuous time filters, and EEPROM, voltages higher

than the power supplies are frequently required. Increased voltage levels are obtained in a charge pump as a result of transferring charges to a capacitive load and do not involve amplifiers or transformers.

IV. SIMULATION RESULT

The new charge pump circuit is designed in TSMC CMOS process, simulated using T-Spice under a 2 mv power supply. This low voltage input supply gives the high amplification stages of the proposed charge pump. The operating frequency is 1000Hz and Fig. shows the charging and discharging result of the new charge pump circuit. The output voltage range is from 995mV up to 1010mV.

The parameter values has been analyzed and tabulated below. This could be a parameter gain of the all charge pump circuits with the input voltage and the output voltage variation of the all other degradations

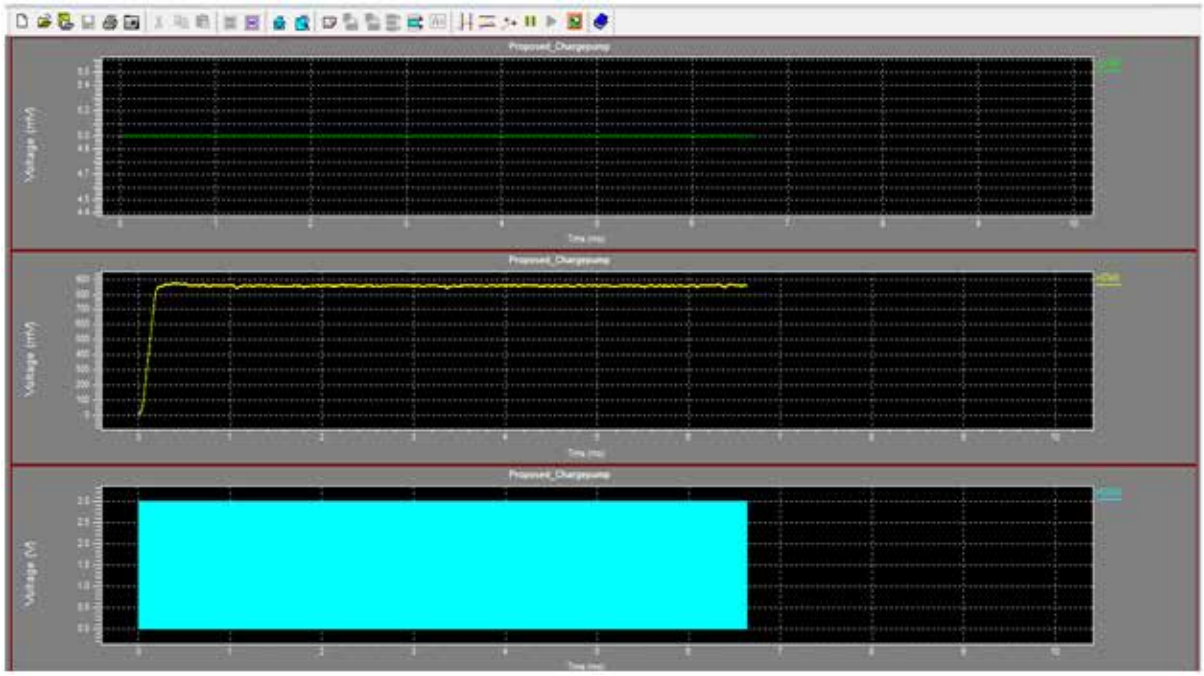

Fig.5 simulation result of proposed system

V. COMPARISION TABLE

CHARGE PUMP	POWER	AMPLITUDE
Dickson charge pump	8.60 W	50 mV
Wu_Chang charge pump	8.04 W	20mV
Linear charge pump	5.84 W	100mV
Proposed charge pump	3.29 W	1000mV

IV. CONCLUSION

Charge pump based on body biasing and the backward control scheme has been proposed in this system. The power and the amplification could be efficient when compared to the other existing charge pump. The low output ripple and high system stability of the dual-phase charge pump circuit are demonstrated by the test chip and get better performance. Therefore, the transient response and driving capability can be improved. Besides, only one closed-loop regulation is utilized to generate the charge pump circuit so as to improve the power conversion efficiency. By using this efficiency calculation the pumping efficiency also calculated and gets the detailed configuration of the proposed charge pump parameter evaluation. The degradation of the amplification could be highly reduces and it could be generated as per the test identification stages proposed in the charge pump design circuit. This circuit could be further used for the implementation of the like PLL based analog devices.

REFERENCES

[1] C.Alippi and C.Galperti, "An adaptive systemfor optimal solar energy harvesting in wireless sensor network nodes," *IEEE Trans. Circuits Syst.—I*, vol. 55, no. 6, pp. 1742–1750, Jul. 2008.

[2] C. Donovan, A. Dewan, H. Peng, D. Heo, and H. Beyenal, "Power management system for a 2.5W remote sensor powered by a sediment microbial fuel cell," *J. Power Source*, pp. 1171–1177, 2011.

[3] C. Donovan, A. Dewan, D. Heo, and H. Beyenal, "Battery less, wireless sensor powered by a sediment microbial fuel cell," *Environmental Science and Technology*, vol. 42, no. 22, pp. 8591–8596, 2008.

[4] P. H. Chen *et al.*, "Startup techniques for 95 mV step-up converter by capacitor pass-on scheme and -tuned oscillator with fixed charge programming," *IEEE J. Solid-State Circuits*, vol. 47, no. 5, pp. 1252–1260, May 2012.

[5] E. J. Carlson *et al.*, "A 20 mV input boost converter with efficient digital control for thermoelectric energy harvesting," *IEEE J. Solid-State Circuits*, vol. 45, no. 4, pp. 741–750, Apr. 2010.

[6] Y. O. Ramadass and A. P. Chandrakasan, "A battery-less thermoelectric energy harvesting interface circuit with 35 mV startup voltage," *IEEE J. Solid-State Circuits*, vol. 46, no. 1, pp. 333–341, Jan. 2011.

[7] J. Holleman *et al.*, "A compact pulse-based charge pump in 0.13 m CMOS," in *Proc. IEEE Custom Int. Circuits Conf.*, 2007, pp. 381–384.

[8] A. Worapishet and J. B. Hughes, "Performance enhancement of switched-current techniques using sub-threshold MOS operation," *IEEE Trans. Circuits Syst.—I*, vol. 55, no. 11, pp. 3582–3592, Dec. 2008.

[9] F. Pan and T. Samaddar, *Charge Pump Circuit Design*. NewYork: McGraw-Hill, 2006.

[10] *Jazz Semiconductor Design Application Manual*. Newport Beach, CA: Jazz Semiconductor Products Inc., 2012.

[11] J.-T. Wu and K.-L. Chang, "MOS charge pump for low voltage operation," *IEEE J. Solid-State Circuits*, vol. 33, no. 4, pp. 592–597, Apr. 1998.

[12] L. Su and D.-S. Ma, "Design and optimization of integrated low-voltage low-power monolithic CMOS charge pumps," in *Proc. Int. Power Electron., Electrical Drives, Automation Motion*, 2008, pp. 43–48.

[13] F. Su andW.-H. Ki, "Gate control strategies for high efficiency charge pumps," in *Proc. Int. Symp. Circuits Syst.*, 2005, pp. 1907–1910.

[14] M.-D. Ker, S.-L. Chen, and C.-S. Tsai, "Design of charge pump circuit with consideration of gate-oxide reliability in low-voltage CMOS process," *IEEE J. Solid-State Circuits*, vol. 41, no. 5, pp. 1100–1107, May 2006.

[15] B. Razavi, *Design of Analog CMOS Integrated Circuits*. New York: McGraw-Hill, 2001.

International Journal of Current Engineering and Technology
E-ISSN 2277 – 4106, P-ISSN 2347 – 5161

Available at http://inpressco.com/category/ijcet

Research Article

Shear Behavior of Magnetorheological Fluid and its effect on MR brake performance

Chiranjit Sarkar†

†Mechanical Engineering Department, Delhi Technological University, Shahbad Daluatpur, Bawana Road, Delhi – 110042, India

Accepted 08 April 2015, Available online 14 April 2015, **Vol.5, No.2 (April 2015)**

Abstract

The aim of this paper is review the viscosity of magnetorheological (MR) fluid as function of shear rate. The different rheological models of shear stress as a function of shear rate have been reviewed. MR fluid has been characterized at various shear rates for different magnetic fields to observe the shear behavior of MR fluid. In order to confirm the shear behavior of MR fluids, experiments have been conducted in MR brake test rig. The results show that with increase in shear rate, there is decrease in braking torque.

Keywords: *MR fluid, MR brake, Shear behavior.*

1. Introduction

Magnetorhelogical (MR) suspensions are known for dramatic change in their apparent viscosity. Due to their variable viscosity, MR fluids are used in engineering applications requiring controllable dynamic performance. One such application is magnetorheological brake in which MR fluid is treated as a brake lining material. This material does not wear-away and provides desirable friction resistance by just controlling the magnetic field passing through it. As MR brake involves electromagnetism and magnetisable friction material, this system can be named as "electromagnetic brake" (Gupta and Hirani, 2011). It is interesting to note that this brake in off state condition can work as bearings (Hirani, 2009, Hirani *et al*, 2000, Hirani *et al*, 1999, Hirani *et al*, 1998, Muzakkir *et al*, 2011, Hirani, 2005, Hirani *et al*, 2001, Muzakkir *et al*, 2013, Hirani 2004, Muzakkir *et al*, 2015, Hirani, Verma, 2009, Hirani, Suh, 2005, Hirani *et al*, 2001, Rao *et al*, 2000, Hirani *et al*, 2000, Hirani *et al*, 2002).

A typical MR fluid consists of 20-40 volume percentage of pure-iron (purity > 99%) particles (size: Ø3-10 micrometers), suspended in a carrier liquid such as mineral oil, synthetic oil, water or glycol. A variety of proprietary additives to avoid gravitational settling, to elude wear and to promote particle suspension, are added to MR fluids. MR fluids exhibit maximum yield strengths of 50-100 kPa for applied magnetic fields of 150-250 kA/m. MR brake has been studied by various researchers (Muzakkir and Hirani, 2015, Muzakkir and Hirani, 2015, Muzakkir and Hirani, 2015, Sarkar and Hirani, 2015), (Sarkar and Hirani, 2013), (Sukhwani, *et al*, 2009), (Sukhwani and Hirani, 2008), (Sukhwani and Hirani, 2008), (Hirani and Manjunatha, 2007), (Sukhwani, *et al*, 2007), (Sukhwani, *et al*, 2006), (Gupta and Hirani, 2011). In their research, shear thinning behaviour of MR fluid (theoretical model and experimental data) was observed. It appears that none of the researchers has measured the shear behaviour using magnetorheometer.

Table 1 Various viscosity shear rate models

Name	Equation	Comment
Bingham[1916]	$\eta = \frac{(\tau - \tau_o)}{\gamma}$	Frequently used model for plastic and viscous materials.
Casson[1959]	$\eta = \frac{\left(\sqrt{\tau} - \sqrt{\tau_o}\right)^2}{\gamma}$	It provides better fit than Bingham but the value of parameters depend on the range of shear rate considered.
Power Law[1921]	$\eta = k\gamma^{n-1}$ For shear thinning n<1 and for thickening fluids n>1.	At high shear rate, it is observed that fluid having n<1 (i.e. pseudo plastic fluid) becomes Newtonian.
Herschel-Bulkley [1926]	$\eta = \frac{(\tau - \tau_o)}{\gamma^n}$	Combination of power law and Bingham model.
De Kee [1975]	$\eta = \frac{\tau - \tau_o}{\gamma e^{\alpha\gamma}}$	-

In application such as MR brake, the true behaviour of MR fluid cannot be obtained. Therefore in the present study, the shear behavior of MR fluid using magnetorheometer as well as MR brake test setup has been presented.

*Corresponding author: **Chiranjit Sarkar**

2. Viscosity-shear rate model of MR fluids

As per Chen, *et al* (2014) MR fluid exhibits Newtonian fluid-like behavior in absence of the external magnetic field, and the constitutive equation is given as

$$\tau = \eta\dot{\gamma} \quad (1)$$

The rheological performance of MR fluid under shearing flowing model in presence of the external magnetic field can be described through Herschel-Bulkey model

$$\tau = \tau(H) + \eta(T)\dot{\gamma}^n \quad (2)$$

Where,$\tau(H)$ represents the dynamic yield stress of MR fluid, which varies along with the strength of the external magnetic field, $\eta(T)$ represents the viscosity of MR fluid as function of the operating temperature T, $\dot{\gamma}$ represents the shear strain rate of MR fluid, and n is constant.

There are a number of similar models presented in the Literature and the most widely used models (Larson, 1999) for viscosity-shear rate relation are summarized in Table 1.Due to lack of any reliable model, expressing shear behaviour of MRF, it is necessary to perform experimental study on MRF using magnetorheometer and setup incorporating MR brake so that the viscosity variation with shear rate can be modelled.

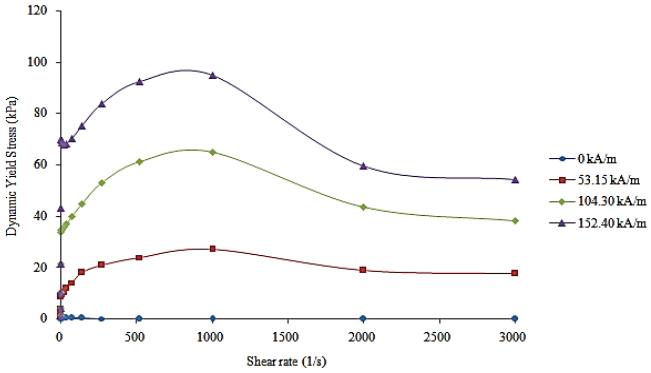

Figure 1 Shear behavior of MR fluids

In the present study, ANTON PAAR modular compact rheometer MCR-102 has been used to measure the shear stress flow curve of MR fluid (85% by iron particles) at different magnetic fields in controlled shear rate (CSR) mode. The measurements were performed in a parallel plate system with a diameter of 20 mm at a gap of 1 mm for various input currents (0.1 to 4.8 A). The resulting flow responses have been examined as a function of magnetic field strength ranging from 0 to 152.4 kA/m. The magnetic field strength (A/m) has been calculated from the magnetorheological cell 70/1T MRD. The operating temperature of 30ºC was maintained. The results of yield strength as function of shear rate are plotted in Figure 1. The maximum value of shear rate is 3000, which is the limitation of used Magnetorheometer. It appears that dynamic yield strength increases with increase in shear rate up to 1000 s^{-1}, but there is decrease in yield strength beyond 1000 shear rate. The trend of shear thinning behaviour (from 0 to 1000 s^{-1} shear rate) remains same even when magnetic field is changed from 53.15 kA/m to 152.40 kA/m. However, there is reduction (figure 1) in dynamic strength with increase in shear rate at zero magnetic field. To confirm the shear thinning behaviour, the dynamic yield stress at different shear rate (up to 1000 s^{-1} shear rate) ranges have been plotted in Figure 2. It shows that the slope of the dynamic yield stress vs. shear rate for different magnetic fields reduces.

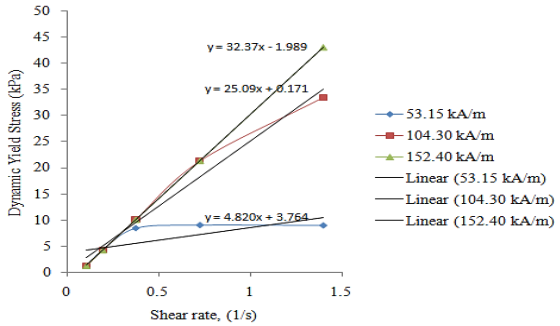

(a) From shear rate 0 to 1.5s^{-1}

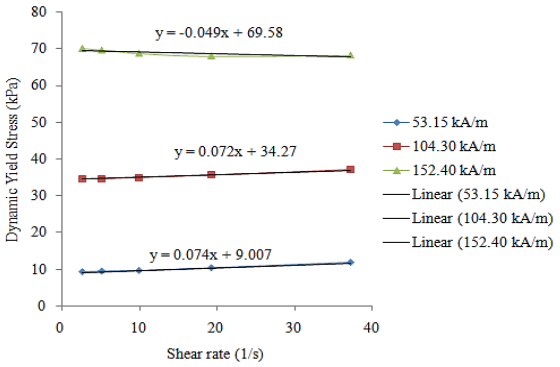

(b) From shear rate 2 to 40s^{-1}

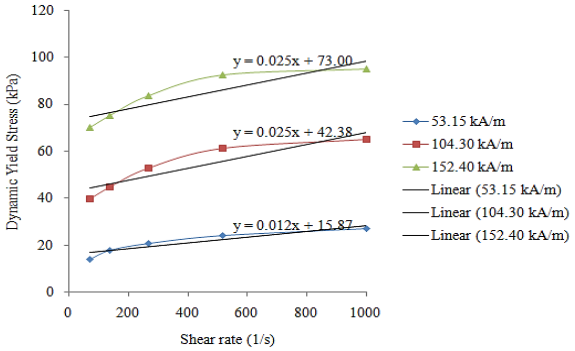

(c) From shear rate 70 to 1000s^{-1}

Figure 2 Shear behavior for different range of shear rate

To study the shear behaviour of MR fluids, the comparison between different available models and synthesised MR fluid model have been plotted in Figure 3.

From this figure it can be concluded that the MR fluid undergoes shear thinning behaviour up to 1000 s^{-1} shear rate, but beyond that it does not follow any particular model. Therefore, it can be concluded that a deeper study is required to model the shear behaviour of MR fluid.

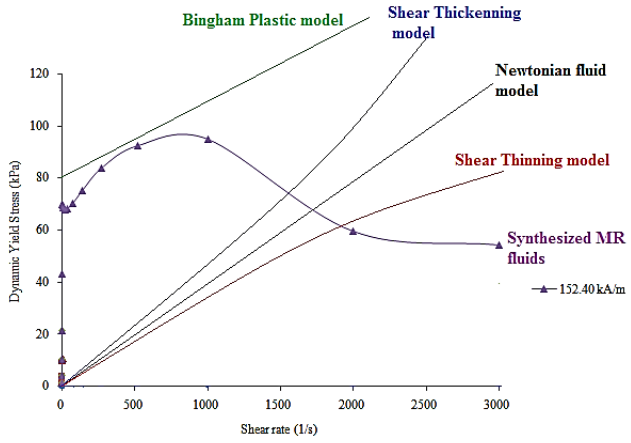

Figure 3 Comparison of MR fluids behaviour with other models

3. Analysis of shear behavior on MR Brake

To understand the rheological behavior of the MR fluid, an experimental study was performed on MR brake. The analysis specially involves study of braking torque vs. temperature at different magnetic field.

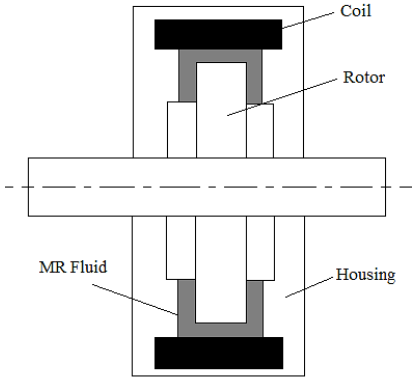

Figure 4 MR brake (Seval, 2002)

3.1. Construction of MR brake

Construction of brake is shown in Figure 4. It consists of rotor fixed to the shaft, which is placed in bearing and can rotate in relation to housing. Between rotor and housing plate, there is a gap filled with MR fluid. Theoretically, a smaller gap will be better because the magnetic flux density in the gap decreases sharply with increasing air gap. In addition, a smaller constant gap can easily maintain a uniform distribution of the magnetic flux in the gap. Practical gap generally range from 0.25 to 2 mm.

Current in the coil, supplied with 12 VDC, creates magnetic field in the gap. Magnetic field strength depends on the current in the coil. Value of the current can be set from 0 to 1 A. Viscosity of the fluid influences torque. When the current in the coil is equal to zero, no magnetic field is generated and brake torque equal to minimum M_{min} is exerted on the shaft. The M_{min} is equal to the torque caused by bearing, seal and viscosity of the carrier liquid. When current is the maximum (1A) then magnetic field is created and brake has highest possible value of the torque M_{max}, that is limited only by maximum current in the coil I_{max} and the construction of the brake.

A heat exchanger was designed and mounted on the circumference of the MR brake to analyze temperature effect on the dynamic viscosity of the MR fluid. The outer diameter of 110 mm was kept and the water was used a circulating coolant to take away heat from MR brake. A schematic block of the experimental set up is shown in Figure 5.

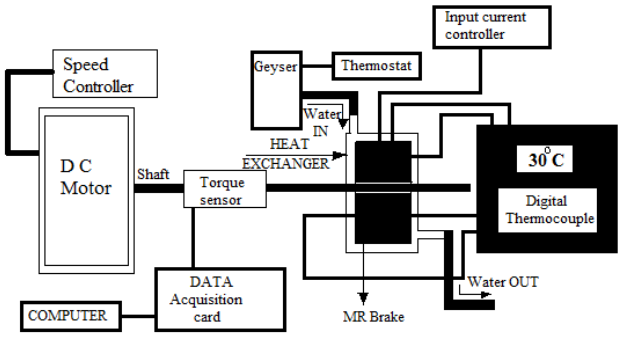

Figure 5. Schematic block of the experimental set up (Sukhwani, *et al*, 2006)

3.2. Experimental set up

An experimental apparatus for evaluating the performance of the MR brake (Lord Corporation MRB 2107-3) was set up. The schematic block diagram is shown in Figure 5. The system is composed of four main parts: DC motor (with associated analog speed regulator), Torque sensor, MR brake and the Heat Exchanger. Torque sensor is connected through a data acquisition card to a computer where values are obtained. The number of samples taken for each reading was 2000 data.

3.3. Procedure

A testing procedure, listed below, was followed

(1) Rotate shaft of MR brake at speed of 200 RPM for 1 min as an initial condition, which stirs the MR fluid in the brake to distribute it evenly. Circulate water at partial opening through the nozzle control gap.
(2) Supply the required current using the 12 VDC power supply source to provide the required current for flux generation.

(3) Control the operating temperature is to the desired level between room temperature to 70ºC.
(4) Measure the torque from the torque sensor. Repeat all sets of reading at 200 and 600 RPM by keeping the temperature constant (i.e. 30˚C). While taking reading it is necessary to check the presence of noise present in the reading. The required values are obtained by averaging all the points.

3.4. Results

To study the shear behavior of MR fluids, the experiments have been done on the experimental set up as described in Sarkar and Hirani (2015). Figure 6 shows the histogram of the braking torque at 200 RPM and 600 RPM. The corresponding shear rates for 200 RPM and 600 RPM are 1000 s^{-1} and 3000 s^{-1}. It shows that with increase in RPM, there is a decrease in braking torque.

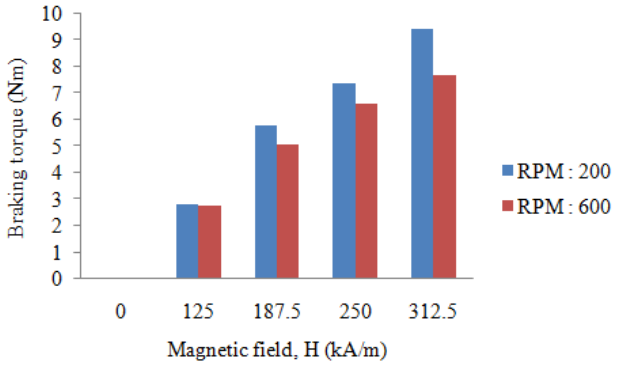

Figure 6 Braking torque at different RPM

Conclusions

In this study, performance of a MR fluid brake has been evaluated to investigate its shear behavior of MR fluid. Following conclusions can be drawn from this study:

1. With increase in speed there is decrease in braking torque.
2. The dynamic yield strength increases with increase in shear rate up to 1000 s^{-1}, but decrease in yield strength beyond 1000 shear rate.
3. If shear rate is larger than 1000 s^{-1}, the MR fluid does not follow any particular model. The trend of shear thinning remains same even when magnetic field is changed from 53.15 kA/m to 152.40 kA/m up to 1000 s^{-1} shear rate. To confirm such behavior of MR fluid, comprehensive study is required.

References

S. Gupta, H. Hirani, (2011), Optimization of magnetorheological brake, *ASME/STLE 2011 International Joint Tribology Conference*, pp 405-406.

H. Hirani, (2009),"Root cause failure analysis of outer ring fracture of four row cylindrical roller bearing", *Tribology Transactions*, vol.52, no.2, pp.180-190.

H.Hirani, K.Athre, S.Biswas, (2000), A Hybrid Solution Scheme for Performance Evaluation of Crankshaft Bearings, *Trans. ASME, Journal of Tribology*, vol. 122, no. 4, pp. 733-740.

H.Hirani, K.Athre, S.Biswas, (1999), Dynamic Analysis of Engine Bearings, *International Journal of Rotating Machinery*, vol. 5, no.4, pp. 283-293.

H.Hirani, K.Athre, S.Biswas, (1998), Rapid and Globally Convergent Method for Dynamically Loaded Journal Bearing Design, *Proc. IMechE (UK), Journal of Engineering Tribology*, vol. 212, pp. 207-214.

S.M.Muzakkir, H.Hirani, G.D.Thakre, M.R.Tyagi, (2011), Tribological Failure Analysis of Journal Bearings used in Sugar Mill, *Engineering Failure Analysis*, vol. 18, no. 8, pp. 2093-2103.

H.Hirani, (2005), Multiobjective optimization of journal bearing using mass conserving and genetic algorithms, *Proc. Institute Mech. Engineers., Part J, Journal of Engineering Tribology*, vol. 219, no. 3, pp. 235-248.

H.,Hirani, K.,Athre and S.,Biswas," (2001), "Lubricant Shear Thinning Analysis of Engine Journal Bearings", *STLE, Journal of Tribology Transaction*, vol 44, no. 1, pp 125-131.

S.M.Muzakkir, H.Hirani and G.D.Thakre, (2013), "Lubricant for Heavily-Loaded Slow Speed Journal Bearing," Tribology Transactions, vol.56, no. 6, pp. 1060-1068.

H Hirani (2004), "Multiobjective Optimization of a journal bearing using the Pareto optimal concept," *Proc. Institute Mech. Engineers., Part J, Journal of Engineering Tribology*, vol. 218, no. 4, pp. 323-336.

H Hirani, T Rao, K Athre and S Biswas, (1997), Rapid performance evaluation of journal bearings, *Tribology international*, vol. 30, no.11, pp. 825-834.

H Hirani, K Athre, S Biswas, (1999), "Dynamically loaded finite length journal bearings: analytical method of solution". *Journal of tribology*, vol. 121, no. 4, pp. 844-852.

S M Muzakkir, K P Lijesh, H Hirani, and G D Thakre, (2015) "Effect of Cylindricity on the Tribological Performance of Heavily-Loaded Slow Speed Journal Bearing, Proc. Institute Mech. Engineers., *Part J, Journal of Engineering Tribology*, 2015, vol 229, no.2, pp.178-195.

K.P.Lijesh, H.Hirani, (2015), "Design and Development of Halbach Electromagnet for Active Magnetic Bearing", *Progress In Electromagnetics Research C*, vol. 56, 173–181.

H Hirani and M Verma, (2009), "Tribological study of elastomeric bearings of marine shaft system", *Tribology International*, vol. 42, no. 2, pp. 378-390.

H Hirani and N P Suh, (2005), "Journal Bearing Design using Multiobjective Genetic Algorithm and Axiomatic Design Approaches", *Tribology International*, vol. 38, no. 5, pp. 481-491.

H Hirani, K Athre and S Biswas, (2001),"A Simplified Mass Conserving Algorithm for Journal Bearing under Dynamic Loads", *International Journal of Rotating Machinery*, vol. 1, pp. 41-51.

T V V L N Rao, H Hirani, K Athre, S Biswas, (2000),"An Analytical Approach to Evaluate Dynamic Coefficients and Non-linear Transient Analysis of a Hydrodynamic Journal Bearing", *STLE Tribology Transactions*, vol. 23, no.1, pp. 109-115.

H Hirani, K Athre and S Biswas, (2000), "Transient Trajectory of Journal in Hydrodynamic Bearing", *Applied Mechanics and Engineering*. vol. 5, no 2.

H Hirani, K Athre and S Biswas, (2002),"Comprehensive Design Methodology for Engine Journal Bearing", *IMechE*

(UK), Part J, Journal of Engineering Tribology, vol 214, pp. 401-412.

Muzakkir, S.M. & Hirani, H. (2015), A Magnetorheological Fluid Based Design Of Variable Valve Timing System For Internal Combustion Engine Using Axiomatic Design, *International Journal of Current Engineering Research,* Vol.5, No.2 (April 2015), pp 603-612.

Muzakkir, S.M. & Hirani, H., (2015), Design of Innovative Engine Valve: Background and Need, *International Journal of Scientific Engineering and Technology*, Volume No.4 Issue No.3, pp : 178-181.

Muzakkir, S.M. & Hirani, H., (2015), Design of Innovative Engine Valve, *International Journal of Scientific Engineering and Technology*, Volume No.4 Issue No.3, pp: 212-217.

C. Sarkar, H. Hirani, (2013), Theoretical and experimental studies on a magnetorheological brake operating under compression plus shear mode, *Smart Materials and Structures*, 22, art. no. 115032.

C. Sarkar, H. Hirani, (2013), Synthesis and characterization of antifriction magnetorheological fluids for brake, *Defence Science Journal*, 63, pp. 408-412.

C. Sarkar, H. Hirani, (2013), Design of a squeeze film magnetorheological brake considering compression enhanced shear yield stress of magnetorheologicalfluid, *Journal of Physics: Conference Series*, 412, 012045.

C. Sarkar, H. Hirani, (2015), Transient thermoelasticanalysis of disk brake, International Journal of Current Engineering and Technology, 5, pp. 413-418.

C. Sarkar, H. Hirani, (2015), Magnetorheological smart automotive engine mount, International Journal of Current Engineering and Technology, 5, pp. 419-428.

C. Sarkar, H. Hirani, (2015), Finite element analysis of magnetorheological brake using ANSYS, International Journal of Current Engineering and Technology, 5, pp. 725-732.

C. Sarkar, H. Hirani, (2015), Design of Magnetorheological Brake using Parabolic Shaped Rotating Disc, International Journal of Current Engineering and Technology, 5, pp. 719-724.

C. Sarkar, H. Hirani, (2015), Synthesis and characterization of nano-copper-powder based magnetorheological fluids for brake, International Journal of Scientific Engineering and Technology, 4, pp. 76-82.

C. Sarkar, H. Hirani, (2015), Effect of particle size on shear stress of magnetorheological fluids, *Smart Science,* (in press).

C. Sarkar, H. Hirani, (2015), Development of magnetorheological brake with slotted disc, *Proc. IMechE, Part D: Journal of Automobile Engineering*, pp 1-18.DOI: 10.1177/0954407015574204.

G. Seval, (2002), Synthesis and properties of Magnetorheological fluids, Dissertation, University of Pitsburgh.

H. Hirani, C. S. Manjunatha, (2007), Performance evaluation of magnetorheological fluid variable valve, *Proc. of the Institution of Mechanical Engineers, Part D, Journal of Automobile Engineering*, 221, pp. 83-93.

J. M. Ginder, L. C. Davis,(1994), Shear Stresses in Magnetorheological fluids: Role of Magnetic Saturation, Applied Physics Letters, 65, pp. 3410-3412

R. G. Larson, (1999), The structure and rheology of complex fluids, Oxford University press, New York.

S. Chen, J. Huang, K. Jian, J. Ding, (2014), Analysis of Influence of Temperature on MagnetorheologicalFluid and Transmission Performance, Advances in Materials Science and Engineering, Article ID 583076, pp 1-7.

V. K. Sukhwani, V. Lakshmi, H. Hirani, (2006), Performance evaluation of MR brake: an experimental study, *Indian Journal of Tribology*, pp. 67-52.

V. K. Sukhwani, H. Hirani, T. Singh,(2007), Synthesis of magnetorheologicalgrease, *Greasetech India*.

V. K. Sukhwani, H. Hirani, (2007), Synthesis and characterization of low cost magnetorheological (MR) fluids, *The 14th International Symposium on: Smart Structures and Materials & Nondestructive Evaluation and Health Monitoring*, 65262R-65262R-12.

V. K. Sukhwani, H. Hirani, (2008), A comparative study of magnetorheological-fluid-brake and magnetorheological-grease-brake, *Tribology Online*, 3, pp. 31-35.

V. K. Sukhwani, H. Hirani, T. Singh, (2008), Synthesis and performance evaluation of MR grease, *NLGI Spokesman*,71.

V. K. Sukhwani, H. Hirani, (2008), Design, development and performance evaluation of high speed MR brake, *Proc. Institute Mech. Engineers., Part L, Journal of Materials: Design and Applications*, 222,pp.73-82.

V. K. Sukhwani, H. Hirani, T. Singh, (2009), Performance evaluation of a magnetorheological grease brake, *Greasetech India*, 9, pp. 5-11.

TARGETED SURVEILLANCE SYSTEM FOR HIGHLY MANEUVERABLE OBJECTS USING FUZZY KALMAN FILTER

Rajesh Rohilla , Vasundhara Dehiya, Rajiv Kapoor

Delhi Technological University
Electronics and Communication Department
Delhi, India

ABSTRACT

In this paper, we describe a novel design for a real-time localization system capable of tracking a highly maneuverable target within a 360 degree range of the camera. The target is defined for surveillance. The approach to tracking includes using a controllable camera which is re-oriented according to the tracked location of the target object. Fuzzy logic is used to determine the direction of motion after using a Kalman filter for tracking. Fuzzy Kalman is thus used for wide area robust tracking for efficient tracking with occlusion handling.

Index Terms— fuzzy controller, robotics, tracking, maneuverable, real time

I. INTRODUCTION

This paper addresses the problem of tracking objects that are moving fast relative to the video frame rate and when the camera not mounted on a rigid surface. Difficulties arise due to variation in motion model, target appearance and noises in measurement.In applications where a single highly maneuverable target is to be tracked over a wide range of area, it is economical to use one camera mounted on a rotatable surface, instead of employing multiple cameras. In this paper, we propose and algorithm with the following features: a)highly maneuverable , b) single target, c) single camera, d)360 degree field, and can handle e) full or partial occlusion of target in an economical way. Due to uncertainty in the motion of the target object, tracking becomes difficult. Drastic motion changes from left to right or target moving out of the range of the camera are some of the issues which cause unexpected movements or jerks in the motion camera. In this paper, our aim is to minimize these drastic movements and obtain a smooth motion for the camera and perform tracking even if the target is lost due to its high speed.

A vast multitude of vision based algorithms are employed for the purpose of tracking of maneuverable targets. Each algorithm involves identification of target object and then tracking of the object. Once tracking is successfully achieved, the action to be taken with the resultant tracking data is dependent on the application. Mobile robots, mounted with a camera, are often used to track the target. Detection of target object is done on the basis of features of the target like colour, intensity, histogram, template etc. which distinguish it from the background. Colour based detection of target is by-far the fastest method for target identification. Another method of target detection is using SURF features [1] which give scale and rotation invariant interest point descriptors for the target. It gives more accurate results than histogram matching and template matching. However, it works when the interest points identifying the target are successfully detected in an image, which is not the case if the target rotates with respect to the camera. Foreground-background analysis is useful in case of stationary cameras [2] . Temporal coherence is also used for creating smart surveillance systems [3] [4] .

However, since the motion of a maneuverable target can be regular or random, filters like Kalman filter and Particle filter, and Fuzzy logic [5] have found plenty of applications in maneuverable target tracking as they have been shown to provide a more accurate path of motion.The earliest such systems[6] utilize a fuzzy based particle filter where fuzzy inference system is calculating the time varying deviation between the actual and predicted position for defined behavior models of the target object. The advantage of using Kalman filter along with Fuzzy logic is that it leads to immediate maneuver detection and more accurate estimation [7]. Later on, more sophisticated algorithms came into development. A fuzzy logic based system was developed which was used for classification of multiple blobs identified in human surveillance applications.

In [8], an Adaptive Fuzzy Particle Filter tracker is implemented which models the target and tracked based on sampling around a predicted position and sample features were scored on the basis of a fuzzy rule . Additional modifications, such as change of colour space from RGB to LAB, are utilized in some works [9] in addition to implementing a fuzzy particle filter. It enhances the robustness of the Particle filter, performed real-time despite drastic changes including background variation, target deformation and partial occlusion. Other works performed face detection and tracking based on fuzzy geometrical face model and motion estimation where facial features were extracted in support region which is determined by fuzzy rules to detect face in the image face [10]. More recent work uses adaptive appearance models where fuzzy particle filter overcomes the uncertainty in various noise models [11]. Focal length

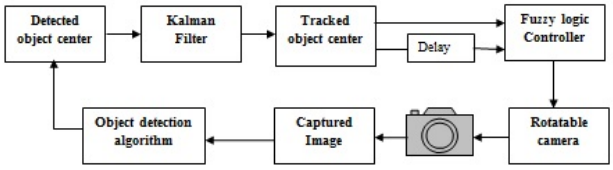

Fig. 1. Block diagram of the system

variation in 3D using two cameras increases the accuracy even more than obtained in 2D [12] .

Over the years, different algorithms have been applied for detection and tracking of target objects as explained in [13] . These algorithms find applications in various fields and perform designated tasks. A real-time object tracking robot whose motion was made autonomous using vision and fuzzy logic control was implemented [14]. Fuzzy clustering algorithms find applications in medical image segmentation which automates the segmentation process with better results in terms of time [15]. Fuzzy theory is used in clustering data association based on improved c-means for multiple-target tracking in crowded environments [16]. GPS navigation is also enhanced to provide improved filter performance by applying an Adaptive fuzzy strong tracking Kalman filter that tuned the weighting factor in real-time according to the change in system dynamic [17]. An extensive survey is presented in [18] and [19] .

Our paper is organized as follows: Section 2 describes the proposed system. Experimental results, showing the efficiency of the proposed method are proposed in Section 3,prior to conclusion in Section 4.

II. SYSTEM DESCRIPTION

Our system consists of three main blocks: initialization and object detection, position prediction and camera control. The video is captured in real-time by the camera and sent to the Control Center (PC) where the target object is detected. A Kalman filter is used to handle the object tracking problem. Using the filter reduces the effect of noise in the input images and reduces drastic changes in motion of the object.

II-A. Initialization and Object Detection

The Initialization step is sets all default values and sets up the conditions that are used to determine what action to take in the absence of target or when it is unable to track the target.Image Capture involves sending real-time video to the Control Center. In this phase, more than one target object may be identified in the image captured by the system. Thus, the algorithm selects the most appropriate object based on the size of the target and tracks the chosen object only. The feature used for detection of the target can be chosen as per the application of the algorithm. We have incorporated two techniques for detection for simulation of the results- color based and SURF features.

For feature-based detection, SURF features are used. The template of target object is loaded. SURF Detector is used to detect the required target object.First the keypoints of the frame and template are calculated, followed by computing the descriptors of the frame and template. The corresponding descriptors are matched and the matches are saved to further processing. Since not all matches correspond to the target object, a condition is imposed on the distance between keypoints. Thus, we obtain only good matches. Keypoints from the good matches are obtained and saved. Comparison is done between the template and good matches to obtain the location of the target object in the given frame. The center of the target object is obtained which is used in the later part of the tracking algorithm.

II-B. Position Prediction

Tracking of detected object is done by applying Kalman Filter to the coordinates of detected target object. Kalman filter uses a system's dynamic model, known control inputs to that system, and multiple sequential measurements to form an estimate of the system's varying quantities that is better than the estimate obtained by using any one measurement alone.

The Kalman filter estimates the state based on a feedback mechanism. The filter predicts the process state at some time and obtains the feedback in the form of measured values. The predictor equations are responsible for projecting forward(in time) the current state and the error covariance estimates to obtain *a priori* estimates for the next step. The predictor equations for projecting the state and error covariance ahead are given as :

$$x_{k+1}^{-} = A_k x_{k+1} + B u_k \tag{1}$$

$$P_{k+1}^{-} = A_k P_k A_k^T + Q_k \tag{2}$$

The measurement update equations are responsible for the feedback and thereby incorporating new input measurements into the predictor equations for an improved estimate. The measurement update equations for computing Kalman gain, updating estimate with new measurement and updating error covariance are given as :

$$K_k = P_k^{-} H_k^T (H_k P_k^{-} H_k^T + R_k)^{-1} \tag{3}$$

$$x_k = x_k^{-} + K(z_k - H_k x_k^{-}) \tag{4}$$

$$P_k = (I - K_k H_k) P_k^{-} \tag{5}$$

The output trajectory obtained after tracking the target object using Kalman filter is smooth and does not vary drastically with change in object position. This is based on the assumption that the change in position of target between two frames is less (which is a very practical assumption). This method gives a tracked path which deals with linear and Gaussian noises. A huge advantage of using the Kalman filter is that it continues to track the target even when it is not detected in the previous step of the algorithm. Since the Kalman uses a predictive method and estimates the next state of the target, it efficiently estimates the next state of the target.

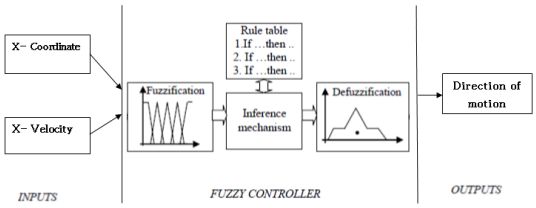

Fig. 2. Block diagram of Fuzzy Inference System

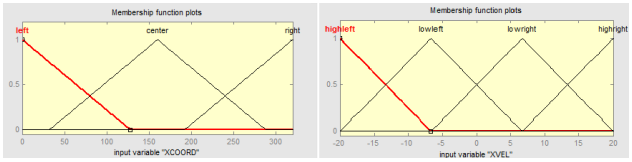

(a)Membership functions of input variables

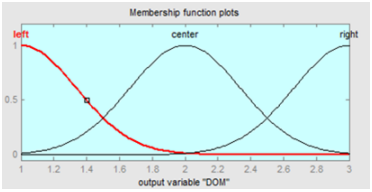

(b)Membership function for output variable

XCoord\ XVel	HIGHLEFT	LOWLEFT	LOWRIGHT	HIGHRIGHT
LEFT	Left	Left	Center	Right
CENTER	Left	Center	Center	Right
RIGHT	Left	Center	Center	Right

(c)Rulebase used for fuzzy controller

Fig. 3. Fuzzy Inference System

II-C. Fuzzy Inference System

The Fuzzy Inference System (FIS) consists of four components: the Fuzzifier, Inference Engine, Rulebase and Defuzzifier. FIS can be essentially viewed as a system that maps input vector to the output vector. Here, our input variables are the tracked x-coordinate of the target, obtained after using the Kalman Filter, and the velocity of motion of target. The output variable is the direction in which the camera must be moved in order to follow the target.

The Fuzzifier takes input values and determines the degree to which they belong to each of the fuzzy sets via membership functions. We have defined three membership functions for x-coordinate namely- left, center and right. For x-velocity, four membership functions have been defined namely- high left, low left, low right and high right. The inference engine defines mapping from input fuzzy sets to the output fuzzy sets. This is based on the rule base, which

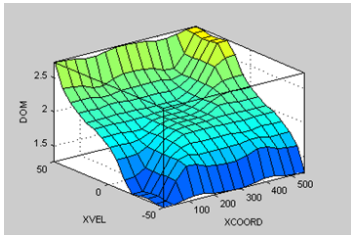

Fig. 4. Surface depicting dependence of input variables with output variables

determines the degree to which the antecedent is satisfied for each rule.The rulebase maps the input variables to output fuzzy sets namely- left, right and center, which represent the direction in which the camera should be moved. Output for all rules is converted into a crisp number by a defuzzifier. 3 We have used Centroid method for defuzzification to return a crisp value. This crisp value is then used to control the direction of motion where 1 correspond to left, 2 to center and 3 to right. Thresholding is done to determine whether the direction must be right, left or right. Unlike rules in conventional systems, a fuzzy rule localizes a region of space along the function surface instead of isolating a point on the surface.

The advantage of applying fuzzy logic in this algorithm is that it considers the ambiguity in location of the target when it lies in the middle of two discrete values, say right and center. The decision concerning the direction in which the camera should be moved is based on multiple factors- location of the target and the velocity with which the target is moving.The dependence of the output variable as a function of the input variables is depicted in the figure.

III. EXPERIMENTAL RESULTS

To check the robustness and accuracy of the proposed algorithm, we set up a robotic platform with a camera mounted on top it. The purpose of the robotic platform was to provide unrestricted view in 360 degree field of view. The target object was initially placed within the frame of the camera. Then it was moved around in free space in a range of 360 degree with different velocities. The direction of motion, as obtained after the Fuzzy Inference System determined the direction in which the robot should move. Motion in right and left direction led to rotation of the robot by a fixed angle, and center referred to no movement of robot.

The variation of motion of the target object, in terms of angle with a reference axis, was plotted with respect to time to study the experimental results. In Figure 5, the target has a constant angular velocity and the tracking is efficient. The camera moves with high accuracy to follow the motion of the target. In another experimental scenario, the target moves with constant angular velocity in clockwise direction and then immediately moves with the same velocity in the reverse direction. These cases demonstrate some of the motion models that may be followed by a highly

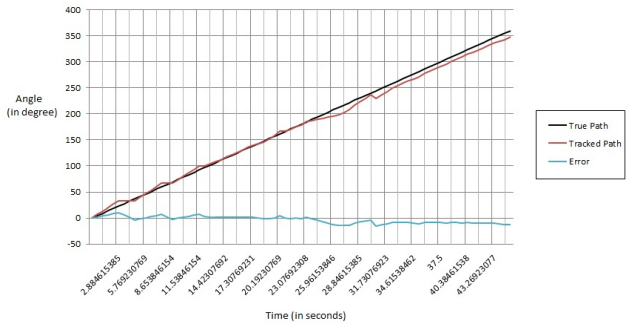

(a)linear motion of the target in a range of 360 degree

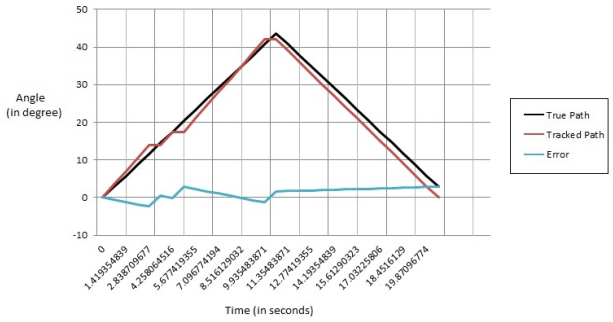

(b)linear motion of the target and then a sharp retracing of path

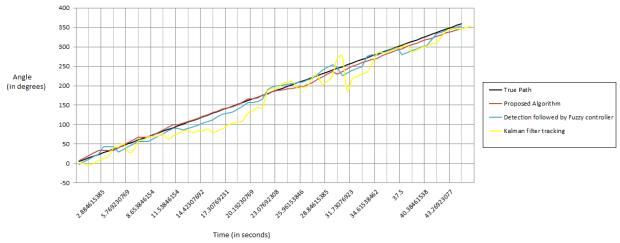

(c)Comparison of tracking achieved by different methods

Fig. 5. Output Graphs

	Proposed Algorithm	Thomas, Ray	Sivabalakrishnan, Manjula
Real-time	Yes	Yes	Yes
Occlusion	Partial and full	-	partial
Use of Fuzzy	Control of direction of motion	Feature estimation	Segmentation of targets in case of occlusion
Detection algorithm	Hue(color-based) and SURF (feature- based)	Fuzzy color histogram in LAB color space	Segmentation in HSV color space
Number of target	Single	multiple	multiple
Range of tracking	360 degree (movable camera)	Stationary camera	Stationary camera

Fig. 6. Qualitative Comparison between the proposed algorithm and existing fuzzy based surveillance algorithms

maneuverable target.As depicted by the graphs, the proposed algorithm for surveillance is highly efficient and accurate with low error.

A huge advantage of this method is that it is successfully able to handle momentary partial and complete occlusion in the particular application scenario where no other target is detected. In case of partial occlusion, the algorithm is still able to detect the visible part of the target on the basis of Hue and the tracking algorithm remains the same. In case of complete occlusion, the tracking algorithm based on Kalman filter predicts the next position of the target and then the fuzzy controller is applied to determine the motion of the camera. When the camera moves, the occluded object again comes into view and tracking is resumed.In case of high velocity changes in the target object, in a manner that the target keeps escaping from the field of view, the algorithm successfully follows the predicted motion of the target, based on the motion model created by Kalman filter till the point when the target was detected. Thus, if the camera loses its target in one frame, it makes an intelligent decision about its new location and proceeds in that direction to track the target. The use of fuzzy logic minimized the need for moving the camera based on every change in position of the target. It is only when the target was moving towards the edge the frame, the camera was moved to obtain the target within the frame.

The proposed algorithm was implemented in real-time and deals with the key challenges faced in tracking of highly maneuverable targets - high maneuverability of target, target specific tracking, efficient utilization of resource(camera) to cover a wide range, and handling or partial and complete occlusion. The extent to which a surveillance system deals with these challenges determine the merit of that algorithm. Many algorithms deal with surveillance systems. Here we have provided a qualitative comparison between our algorithm and that of Thomas, Ray [20] and Sivabalakrishnan, Manjula [21].

A mathematical comparison with existing surveillance algorithms is difficult to achieve because of the movable camera constraint. The direction of the camera changes depending on the target location , resulting in a real-time adaptive tracking system. The system can be qualitatively judged based on its merits in the applications it is desired for.

A comparison of the proposed algorithm is depicted in Fig. 5 (c). The true path and tracked path are depicted by various algorithms to depict the advantages of the proposed algorithm. Tracking algorithms used are a) proposed algorithm based on detection,Kalman filter and fuzzy inference system; b)Detection and fuzzy inference system without Kalman filter; and c) Detection and Kalman filter without fuzzy inference system. It has been observed that tracking in absence of Kalman filter is flawed since it is unable to deal with noisy measurements, leading to incorrect camera motion when detection is flawed. In the case where fuzzy systems are not applied, the camera motion is drastic and jerky since change in camera direction changes the location of target as seen by the camera.Also, it doesn't deal with velocity component of the target.

The proposed algorithm is expected to have applications in monitoring of sporting events . For example,the football is the target object to be tracked and it can be completely

defined by SURF features. A single camera placed at a large distance form the field can be used to track the location of the ball during a game at all times. Other applications include low traffic regions like secluded corridors, high-security vaults or research facilities. Here a single camera facing the door can locate any visitor and follow the motion of the person throughout his work in the secure area. The potential applications and advantages in practical surveillance scenarios are huge.

IV. CONCLUSION

This paper proposes an algorithm to perform surveillance using one camera for a single highly maneuverable target covering a range of 360 degrees using Kalman filter and fuzzy logic. The proposed algorithm was implemented in real-time and successfully tackled some key challenges in tracking of highly maneuverable targets - high manueverability of target, target specific tracking, efficient utilization of resource(camera) to cover a wide range, and handling or partial and complete occlusion. The key aspects of this algorithm are the use of Kalman filter for predictive motion, and the use of velocity component of the tracked object to decide motion of the camera based on Fuzzy Logic, and efficient and economical utilization of resources.

V. REFERENCES

[1] H. Bay, T. Tuytelaars, and L. Van Gool, "Surf: Speeded up robust features," in *Computer Vision–ECCV 2006*. Springer, 2006, pp. 404–417.

[2] Y.-L. Tian, M. Lu, and A. Hampapur, "Robust and efficient foreground analysis for real-time video surveillance," in *Computer Vision and Pattern Recognition, 2005. CVPR 2005. IEEE Computer Society Conference on*, vol. 1. IEEE, 2005, pp. 1182–1187.

[3] I. Cohen and G. Medioni, "Detecting and tracking moving objects for video surveillance," in *Computer Vision and Pattern Recognition, 1999. IEEE Computer Society Conference on.*, vol. 2. IEEE, 1999.

[4] A. Hampapur, L. Brown, J. Connell, A. Ekin, N. Haas, M. Lu, H. Merkl, and S. Pankanti, "Smart video surveillance: exploring the concept of multiscale spatiotemporal tracking," *Signal Processing Magazine, IEEE*, vol. 22, no. 2, pp. 38–51, 2005.

[5] L. A. Zadeh, "Fuzzy sets," *Information and control*, vol. 8, no. 3, pp. 338–353, 1965.

[6] H. Kamel and W. Badawy, "Fuzzy logic based particle filter for tracking a maneuverable target," in *Circuits and Systems, 2005. 48th Midwest Symposium on*. IEEE, 2005, pp. 1537–1540.

[7] M. Bahari, A. Karsaz, and H. Khaloozadeh, "High maneuver target tracking based on combined kalman filter and fuzzy logic," in *Information, Decision and Control, 2007. IDC'07*. IEEE, 2007, pp. 59–64.

[8] P. D. Z. Varcheie and G.-A. Bilodeau, "Adaptive fuzzy particle filter tracker for a ptz camera in an ip surveillance system," *Instrumentation and Measurement, IEEE Transactions on*, vol. 60, no. 2, pp. 354–371, 2011.

[9] L. Qing, X.-D. Xu, and S.-T. Wang, "Fuzzy particle filter for target tracking," *AASRI Procedia*, vol. 3, pp. 191–196, 2012.

[10] P. Hiremath and M. R. Manjunath Hiremath, "Face detection and tracking in video sequence using fuzzy geometric face model and mean shift."

[11] C. Yoon, M. Cheon, and M. Park, "Object tracking from image sequences using adaptive models in fuzzy particle filter," *Information Sciences*, vol. 253, pp. 74–99, 2013.

[12] J. Denzler, M. Zobel, and H. Niemann, "Information theoretic focal length selection for real-time active 3d object tracking," in *Computer Vision, 2003. Proceedings. Ninth IEEE International Conference on*. IEEE, 2003, pp. 400–407.

[13] R. T. Collins, A. Lipton, T. Kanade, H. Fujiyoshi, D. Duggins, Y. Tsin, D. Tolliver, N. Enomoto, O. Hasegawa, P. Burt *et al.*, *A system for video surveillance and monitoring*. Carnegie Mellon University, the Robotics Institute Pittsburg, 2000, vol. 2.

[14] M. S. Uzer and N. Yilmaz, "A real-time object tracking by using fuzzy controller for vision-based mobile robot," *Scientific Research and Essays*, vol. 6, no. 22, pp. 4808–4820, 2011.

[15] O. Oke, T. Adedeji, O. Alade, E. Adewusi *et al.*, "Fuzzy kc-means clustering algorithm for medical image segmentation," *Journal of Information Engineering and Applications*, vol. 2, no. 6, pp. 21–32, 2012.

[16] W. Yue-long and M. Fu-chang, "Data association algorithm based on improved fuzzy c-means for multi-target tracking," in *Electronics and Optoelectronics (ICEOE), 2011 International Conference on*, vol. 3. IEEE, 2011, pp. V3–387.

[17] D.-J. Jwo and C.-M. Huang, "An adaptive fuzzy strong tracking kalman filter for gps/ins navigation," in *Industrial Electronics Society, 2007. IECON 2007. 33rd Annual Conference of the IEEE*. IEEE, 2007, pp. 2266–2271.

[18] A. Yilmaz, O. Javed, and M. Shah, "Object tracking: A survey," *Acm computing surveys (CSUR)*, vol. 38, no. 4, p. 13, 2006.

[19] A. Smeulders, D. Chu, R. Cucchiara, S. Calderara, A. Dehghan, and M. Shah, "Visual tracking: An experimental survey," 2013.

[20] V. Thomas and A. K. Ray, "Fuzzy particle filter for video surveillance," *Fuzzy Systems, IEEE Transactions on*, vol. 19, no. 5, pp. 937–945, 2011.

[21] M. Sivabalakrishnan and D. Manjula, "Fuzzy rule-based classification of human tracking and segmentation using color space conversion." *International Journal of Artificial Intelligence & Applications*, vol. 1, no. 4, 2010.

International Journal of Phytoremediation
Publication details, including instructions for authors and subscription information:
http://www.tandfonline.com/loi/bijp20

The potential of Canna lilyfor wastewater treatment under Indian conditions

A. K. Haritash[a], Ashish Sharma[a] & Kanika Bahel[a]
[a] Department of Environmental Engineering, Delhi Technological University, Shahbad Daulatpur, Delhi (110042) India
Accepted author version posted online: 07 Apr 2015.

To cite this article: A. K. Haritash, Ashish Sharma & Kanika Bahel (2015): The potential of Canna lilyfor wastewater treatment under Indian conditions, International Journal of Phytoremediation, DOI: 10.1080/15226514.2014.1003790

To link to this article: http://dx.doi.org/10.1080/15226514.2014.1003790

Title:

The potential of *Canna lily* for wastewater treatment under Indian conditions

Authors

A. K. Haritash*, Ashish Sharma, Kanika Bahel

Affiliation:

Department of Environmental Engineering

Delhi Technological University

Shahbad Daulatpur, Delhi (110042) India

***Corresponding Author:**

E-mail: akharitash@dce.ac.in; +91-9911710444

The potential of *Canna lily* for wastewater treatment under Indian conditions

Abstract

Low cost treatment of polluted wastewater has become a serious challenge in most of the urban areas of developing countries. The present study was undertaken to investigate the potential of *Canna lily* towards removal of Carbon, Nitrogen, and Phosphorus from wastewater under sub-tropical conditions. A constructed wetland (CW) cell supporting vegetative layer of *Canna lily* was used to treat wastewater having high strength of CNP. Removal of biological oxygen demand (BOD_3) and chemical oxygen demand (COD) varied between 69.8-96.4% and 63.6-99.1%, respectively. *C. lily* could efficiently remove carbon from a difficult to degrade wastewater at COD:BOD ratio of 24.4. Simultaneous reduction in TKN and nitrate pointed to good nitrification rates, and efficient plant assimilation as the dominant nutrient removal mechanism in the present study. Suitable Indian agro-climatic conditions favoured plant growth and no evident stress over the *Canna* plant was observed. High removal rate of 809.8 mg/m^2-day for TKN, 15.0 mg/m^2-day for nitrate, and 164.2 mg/m^2-day for phosphate suggests for a possible use of *Canna*-based CW for wastewater treatment for small, rural, and remote Indian communities.

Keywords: *Canna lily*, Constructed Wetland, CNP

***Corresponding author:** akharitash@dce.ac.in; +91-9911710444

Introduction

Conventional treatment of wastewater is an energy-intensive expensive process which results in production of secondary toxic sludge and requires regular monitoring of skilled personnel. The task is even tougher in developing countries where large volume of wastewater is generated with a diverse nature of pollutants present in it. Removal of nutrients like carbon, nitrogen, and phosphorus (CNP) during tertiary treatment is therefore a challenging task in developing countries since it involves extra input of chemicals and energy (Kivaisi, 2001). The demand for energy and water quality is rising in densely populated developing countries, so it becomes imperative to investigate and devise the low cost and sustainable treatment technologies for wastewater treatment.

Cost-effective treatment of polluted water has become a serious challenge in most of the cities of the world. Urban sprawl has resulted in increased impervious surfaces like roads, rooftops, parking spaces etc. leading to higher surface runoff and mobilization of pollutants (Davis et al., 2009). Urban runoff is designated as a leading impairment source for water bodies and third largest pollution source for lakes (USEPA, 1997), and the effects on receiving waters are quite diverse and complex (Hoffman et al., 2002). Constructed wetlands (CWs) too are reported to be inexpensive and promising tool for nutrient removal (Vymazal, 2007) and stabilization of secondarily treated wastewater with very low energy input rates (Bergdolt et al. 2013). CWs have also been claimed to reduce BOD_5 and *E. coli* for unrestricted urban use and recreational swimming in temperate climate, respectively (Jokerst et al. 2011). There is significant decrese in BOD_5 during conventional secondary treatment of wastewater, but the removal of nitrogen and

phosphate remains limited. Therefore, most of the studies highlight the use of CWs for nutrient removal during the treatment of secondarily treated sewage and stormwater. Presence of excess nutrients, otherwise, may trigger eutrophication in wetlands or other water bodies leading to chocking and other harful environmental effects. Among the best management practices (BMPs) for storm-water management, bioretention system consisting of the surface layer of mulch supporting a layer of vegetation over it, reduces runoff, prevents soil erosion, and improve water quality in a natural aesthetically pleasing manner (Hseih & Davis, 2005). Therefore bioretention systems and constructed wetlands are substantially similar with slight differences of media composition, and regulation of flows in and from the system. An important difference is the infiltration of water in the deep soil in bioretention/biofilteration systems.

The role of macrophytes (Yilmaz & Akbulut, 2011) and emergents in water treatment and removal of pollutants (Mina et al., 2011; Vymazal, 2013) has been documented in several studies, but the studies on *Canna spp*. are limited. An important aspect associated with *Canna* plant is its higher growth rate with significantly high biomass production (Chen *et al*., 2009) which is directly related to nutrient uptake, and tolerance to water stress and chemical fluctuations, making it a suitable candidate for phytoremediation. Another study by Abou-Elela *et al*. (2013) also reported a very high dry biomass accumulation by *Canna lily* compared to *Phragmites australis*, an extensively studied potential plant for wastewater treatment in CWs. Apart from it, the aesthetically pleasing look, and floriculture possibility adds a new dimension to its use in constructed wetlands.

A study by Belmont & Metcalfe (2003) reported that *Canna*, has limited growth and cannot survive in cold winter in northern hemisphere (under temperate conditions) and therefore has a limited use in CWs in such countries. On the other hand, its use in tropical and subtropical countries is expected to yield better results and it can complement the deficient removal rates of conventional treatment systems. The effect of wastewater on growth parameters of *Canna* should also be investigated to ascertain the stress of diverse pollutants, if any, over the plant. Therefore, the present study was initiated to investigate the potential of *Canna lily* in nutrient (CNP) removal from domestic wastewater/sewage under subtropical conditions.

Materials and Methods

Wetland Configuration

A bench scale CW cell (1.1 m length x 0.8 m breadth x 0.35 m depth) located in the campus of Delhi Technological University (DTU) was used during the study. The CW cell was located outdoors in a semi-arid climate with no protection from temperature, sunlight, rainfall, and evapotranspiration to study the removal under natural conditions. The inlet and outlet nozzles were provided to feed raw water and collect the outflow, respectively (Fig. 1). The cell was packed with sand-gravel bed to a depth of 0.35 m and a space of 10 cm over it. The size characterization of sand-gravel packing medium (Fig. 2) represented the graded soil profile with voids in between to facilitate easy root penetration throughout the treatment CW cell. A slope of 1.0 cm was provided along the length to facilitate flow. Fifty (50) plants of *Canna* with mean shoot length of 33.8 ± 4.7 cm were grown in the wetland cell in the month of March

(representing late spring), and an initial period of 15 days was provided to let the plant stabilize in CW cell before undertaking the removal studies. No senescence or death of plants was observed during the initial period of stabilization.

Wastewater Analysis

The wastewater was collected from a collection pond located at 28.7ę N latitude and 77.1ę E longitudes in DTU campus, which receives wastewater from nearby residential blocks and partially from a University hostel. Physico-chemical characterization was done as per the standard methods (APHA, 1998) to determine the average values (n=5) of pH, Total dissolved solids (TDS), Biological Oxygen Demand (BOD_3), Chemical Oxygen Demand (COD), Available phosphate/orthophosphate (AP), Total Kjeldahlôs Nitrogen (TKN), and nitrate. Based on the values determined, synthetic wastewater was prepared in the laboratory using glucose, Pottasium dihydrogen orthophosphate (KH_2PO_4), Ammonium Sulphate [$(NH_4)_2SO_4$], and potassium nitrate (KNO_3) dissolved in groundwater from DTU pump-house(pH 7.5; Na^+ 100 mg/l; K^+ 4.0 mg/l; Ca^{2+} 40 mg/l; Mg^{2+} 19.5 mg/l; CO_3^{2-} 21.6 mg/l; HCO_3^- 310 mg/l; Cl^- 54 mg/l; and SO_4^{3-} 60 mg/l) to simulate the naturally prevailing characteristics of wastewater

Experiments, Data Collection & Statistical Analysis

After an initial period of 15 days for stabilization of Canna lily plants in wetland cell, synthetic effluent having a pH of 7.5, TDS - 2200 mg/l, BOD_3 ï 45 mg/l, COD ï 1100 mg/l, nitrate ï 1 mg/l, TKN ï 50 mg/l, and available phosphate ï 15 mg/l was fed to the system with a total volume of 150 litres initially. Later, 15 litres of synthetic wastewater was fed to the system on regular intervals of 24 hours to make up for the nutrients; and evapotranspiration losses. The

sample of treated wastewater was regularly collected from the outlet and analysed for a period of 30 days. The analysis of the treated wastewater was done as per the standard methods; in triplicates using AR-grade chemicals and reagents. Based on the results obtained, nutrient removal efficiency (percentage basis), and removal rate (mg/m^2-day) of the CW cell were computed. The statistical analysis of data was done on MS-Excel and Minitab 15 software.

Results and Discussion

The growth of *Canna lily* depends on the nutrient availability and agro-climatic conditions. Therefore, the meteorology was monitored regularly throughout the study period (Table 1). The values obtained are classified in semi-arid to arid condition with sufficient availability of sunlight favoring the plant growth, which in turn regulated substantially high uptake/removal of nutrients from wastewater. The values of different parameters monitored in the inlet and outlet of CW cell are given in Table 2.

Removal of Dissolved Solids

The nutrient removal from wastewater depends on the water demand/uptake of the plant. *Canna lily* has a water demand of the order of 1.4 liters/plant/day (Chen et al., 2009) as studied in subtropical to semi-arid climates of Louisiana and California. This demand is 3-5 times more than the other wetland vegetation. Apart from it, meteorological conditions play an important role in regulating evapotranspiration. The semi arid conditions result in higher transpiration and as a result higher uptake of water. Since the average maximum temperature was of the order of 39.2 C, the water uptake was observed to be higher, and so was the removal of dissolved available nutrients. The total dissolved solids (TDS) content in inlet water was 2200mg/l, as

compared to the average level of 708.9 mg/l in outlet. Percentage removal of TDS varied from 63.2 to 74.1 with an average value of 67.8% (Fig. 3). The average removal rate for TDS was 31.9 gm/m^2-day.

Removal of Organic Carbon

Organic carbon in wastewater was monitored in terms of BOD_3 and COD. The BOD_3 in outflow varied from 2 to 13 mg/l with a mean value of 6 mg/l, as against the value of 45 mg/l in inlet. The percent removal ranged from 69.8 to 96.4 with an average value of 87.3% (Fig. 3). The removal rate of BOD_3 was 721.5 mg/m^2-day at a loading rate of 767 mg/m^2-day with a hydraulic retention time (HRT) of 24 hours. The concentration of COD in influent was 1100 mg/l representing it to be high strength wastewater (Metcalf & Eddy Inc., 1991). Percent removal of COD ranged from 63.6-99.1% (Fig. 3) with an average value of 92.8%. The removal rate was 18.1 gm/m^2-day at loading rate of 18.8 gmCOD/m^2-day for a HRT of 24 hours. Average effluent COD concentration was 140 mg/l but it stabilized at around 40 mg/l towards latter half of the study period. Gearheart (1998) too reported the effluent COD concentration of 40 mg/l when the COD loading rate was 14 gmCOD/m^2-day for a wetland treating domestic wastewater. Ayaz & Acka (2001) have reported the same effluent concentration at a loading rate of 40 gmCOD/m^2-day; whereas Reed et al. (1988) had recommended 60 gmCOD/m^2-day for optimum COD removal in a natural system. The present study reports significantly high removal efficiency of *Canna lily* for BOD_3 and COD from a difficult to degrade synthetic effluent with COD:BOD ratio of 24.4, as against the lower removal efficiency of *Typha latifolia* and *Ipomes spp.* based

surface flow wetland system treating industrial effluent with COD:BOD ratio of 17 (Panswad & Chavalparit, 1997).

Removal of Nitrogen

Total nitrogen in wastewater was measured as the sum of Total Kjeldahlôs Nitrogen (TKN) and nitrate. Concentration of nitrite was not determined since it remains very low and insignificant compared to that of ammonium and nitrate in treatment wetlands (Kadlec & Knight, 1996; Belmont et al., 2004). The initial (influent) concentration of TKN was 50 mg/l classifying it as strong wastewater (Metcalf & Eddy, 1991); and the effluent concentration raged between 2.9 to 15.4 mg/l with an average value of 5.3 mg/l. The removal rate was observed to 809.8 mg/m^2-day at a loading rate of 852.3mg TKN/m^2-day for a HRT of 24 hours. The percentage removal varied from 69% to 94% with an average value of 89% (Fig. 3). Percentage removal of similar order has been reported by Ayaz & Acka (2001) to study removal of ammonia by *Canna*. They observed that removal of ammonical nitrogen was around 88% and accounted it for plant assimilation and nitrification. Davis *et al*. (2001) have also suggested 60-80 % removal of TKN by a bioretention media supporting a vegetative layer. Nyakangôo and van Bruggen (1999) reported 87-90% removal of total nitrogen in a constructed wetland to treat domestic wastewater in Nairobi, Kenya. TKN removal in the present study was efficient, and it matches with other studies suggesting a possible use of *Canna*-based CW for wastewater treatment in developing countries. Nitrate concentration in influent was 1 mg/l to supplement plant growth in case nitrification in the experimental system remains limited. Nitrate was reduced to 0.01 to 0.32 mg/l concentration in the effluent with an average value of 0.1 mg/l. Good removal efficiency for

TKN suggests significant nitrification rate facilitating conversion of ammonium ions to nitrate, and subsequent removal of nitrogen. The observed removal rate of nitrate was 15.0mg/m^2-day at a loading rate of 16.0 mg/m^2-day. Average percentage removal of 86% (Fig. 3) with respect to initial concentration was observed during the study. Generally, reduction in concentration of TKN is observed slightly higher than that of nitrate since plant assimilation as well as nitrification of ammonium to nitrate account for TKN removal, whereas removal of nitrate takes place by plant assimilation alone (Chen et al., 2009). Simultaneous reduction in TKN and nitrate points to efficient plant uptake and good nitrification rate in the present study. Since assimilation by plants is efficient, other removal mechanisms do not play a significant role in planted constructed wetland (Zhang et al., 2007; Chen et al., 2009). The percentage removal of nitrogen as observed in our study is higher or almost of the order as observed in other studies. Belmont et al. (2004) had observed 76.7% nitrate removal in cattail based sub-surface flow wetland treating domestic wastewater; and DeBusk *et al*. (1995) too observed about 85% removal of TKN in *floralta limpograss* and *alemangrass* microcosms. They also concluded that *Canna lily* had a significantly high removal rate of nutrients compared to some other emergent macrophytes. Ammonical nitrogen removal of the order of 97-99% has also been observed by Brix *et al*. (2003) and Laber *et al*. (2003) in Denmark and Nepal, respectively, which highlights the use of wetlands in wastewater treatment in different regions of the world.

Removal of phosphate

Phosphate in wastewater was measured as available phosphate (orthophospahte). The initial concentration of orthophosphate was 15.0 mg/l considered as high strength wastewater. The

phosphate concentration in outflow varied between 1.52-3.21 mg/l with an average value of 2.5 mg/l. The percentage removal varied from 77.3 to 91.6% with an average of 82.6% (Fig. 3). The removal rate was observed to be 164.2 mgP/m^2-day at an initial loading of 178.6 mgP/m^2-day after the HRT of 24 hours. DeBusk *et al*. (1995) have also reported similar removal rate of 173 mgP/m^2-day by *Canna lily* based CW treating dairy wastewater. The major removal mechanisms of phosphate might be uptake by plants and adsorption by antecedent substrate (soil and sediments) (Kadlec & Knight, 1996). Most of the studies have reported phosphate removal ranging between 50-80% with respect to initial concentration. Brix et al. (2006, 2011) have reported 46% removal of phosphate from sewage using *Canna* with other two species. Another study by Kimani *et al*. (2012) reported 53 % removal of total phosphate from wastewater from a flower farm. The high removal efficiency of 82.6% might be due to the preferred removal of orthophosphate by plants as observed in the present study. Higher removal rates of available phosphate may also be attributed to higher uptake by *Canna* plants during the initial growth phase before maximum growth is attained as reported in other studies too (Boyd, 1969; Vymazal, 1995). The phosphate removal rate of plants may decrease after attaining maturity and with increasing biomass (DeBusk *et al*., 1995) as observed in bioretention systems. Another reason for higher removal rate could be difference of agro-climatic region favouring higher growth rates of wetland vegetation (Vymazal, 2005) under Indian conditions. Similarly high phosphate removal efficiency of 88% was reported by Nyakangô and van Bruggen (1999) in Nairobi, Kenya attributing to the role of agro-climatic regions. The redox conditions present in wetland might also affect the rate of phosphate removal since aerobic conditions are more favorable for P

sorption and co-precipitation by ligand exchange reactions with hydrous oxides of iron and aluminum (Bostrom *et al*., 1982).

Effect of wastewater on *Canna lily*

Since the nutrients (CNP) are taken up by the plant for its growth and metabolism, it becomes imperative to monitor the growth of the plant and to study its biochemical constituents. The plant growth was monitored in terms of root length, shoot length, and plant density; and the biochemistry of *Canna lily* was studied by determining its Chlorophyll a, chlorophyll b, and carotenoids (Table 3). The growth parameters of the plant revealed 1.2 times increase in plant density, 2.4 times increase in shoot length and 2.8 times increase in root length. A significant increase in the biomass of the plant may be correlated to the utilization/ assimilation of nutrients from the waste water with no adverse physical effect on the growth. The biochemical constituents had an insignificant small change in terms of chlorophyll and carotenoid concentration. Slight decrease in the concentration of chlorophyll a and an increase in chlorophyll b may be attributed to the temperature/ heat stress exerted over the experimental plants in the last phase of the study as reported in other studies too (Shi et al., 2004). The daily maximum ambient temperature raised from 30°C (in initial phase) to 43°C (in final phase) during the study which results in enhanced evapo-transpiration and an elevated stress over the plant. No direct stress of wastewater over the growth of *Canna lily* could be established.

Conclusion

Removal of nutrients (CNP) from wastewater by *Canna lily*-based CW is found to be potentially effective in the present study. Significantly high removal efficiency of *C. lily* stresses upon the

use of such plants in high-strength-wastewater treatment particularly under tropical conditions. Average removal of BOD_3 (87.3%) and COD (92.8%) from wastewater with COD:BOD ratio of 24.4 signifies the use of C. lily for treating selected industrial effluents with high COD:BOD ratio. Simultaneously high removal of TKN and nitrate suggests of good nitrification rates in plant rhizosphere to facilitate conversion of ammonium ions to nitrate and subsequent uptake by the plant. High removal efficiency for TKN, nitrate, and phosphate reflects efficient uptake by plants, which inturn points to plant assimilation as the dominant removal mechanism in the present study. Apart from it, the plant represented no direct physical or bio-chemical stress reflecting of its use in other areas too. Climatic conditions favoring plant growth under Indian conditions make *Canna lily* a suitable wetland plant for nutrient removal particularly for small and remote communities. The study concludes that *C. lily* based CW can be a viable alternative for wastewater treatment especially when nutrients (CNP) are the treatment target.

References

Abou-Elela SI, Golinielli G, Abou-Taleb EM, Hellal MS. 2013. Municipal wastewater treatment in horizontal and vertical flows constructed wetlands. Ecol. Eng. 61: 460-468.

APHA, AWWA, WPCF, 1998. Standard methods for the examination of Water and wastewater, 20th ed. APHA, Washington, D.C.

Ayaz CS, Acka L. 2000. Treatment of wastewater by constructed wetlands in small settlements. Water Sci. Technol. 41: 69-73.

Belmont MA, Cantellano E, Thompson S, Williamson S, Sanchez A, Metcalfe CD. 2004. Treatment of domestic wastewater in a pilot-scale natural treatment system in central Mexico. Ecol. Eng. 23: 299-311.

Belmont MA, Metcalfe CD. 2003. Feasibility of using ornamental plants (Zantedeschia aethiopica) in subsurface flow treatment wetlands to remove nitrogen, chemical oxygen demand and nonphenol ethoxylate surfactants- a laboratory scale study. Ecol. Eng. 21: 233-247.

Bergdolt J, Sharvelle S, Roesner L. 2013. Estimation of graywater constituent removal rates in outdoor free-water-surface wetland in temperate climate. J. Environ. Eng. 139: 776-771.

Bostrom B, Jansson M, Forsberg C. 1982. Phosphorus release from lake sediments. Arch. Hydrobiol. Beih. Ergebn. Limnol. 18: 5ï 59.

Boyd CE. 1969. Production, mineral nutrient absorption, and biochemical assimilation by *Justicia americana* and *Alternanthera philoxeroides*. Arch. Hydrobiol. 66:139-60.

Brix H, Arias CA, Johansen N-H. 2003. Experiments in a two-stage constructed wetland system: nitrification capacity and effects of recycling on nitrogen removal. In: Vymazal, J. (Ed.), Wetlands-nutrients, Metals and Mass Cycling. Backhuys Publishers, Leiden, The Netherlands, pp. 237-258.

Brix H, Koottatep T, Fryd O, Laugesen GH. 2011. The flower and the butterfly constructed wetland system at Koh Phi Phi - system design and lessons learned during implementation and operation. Ecological Engineering 37: 729-735.

Brix H, Koottatep T, Laugesen CH. 2006. Re-establishment of wastewater treatment in tsunami affected areas of Thailand by the use of constructed wetlands. In: Dias, V., Vymazal, J. (Eds.), Proceedings of the 10th International Conference on Wetland Systems for Water Pollution Control, MAOTDR 2006, Lisbon, Portugal, pp. 59-67.

Chen Y, Bracy RP, Owings AD. 2009. Nitrogen and phosphorus removal by ornamental and wetland plants in a greenhouse recirculation research system. Hort. Science. 44(6): 1704-1711.

Davis AP, Hunt WF, Traver RG, Clar M. 2009. Bioretention Technology: Overview of current practice and future needs. J. Environ. Eng. 135: 109-117.

Davis AP, Shokouhian M, Sharma H, Miami C. 2001. Laboratory study of biological retention for urban stormwater management. Water Environ. Res. 73(1): 5-14.

DeBusk TA, Peterson JE, RameshReddy K. 1995. Use of terrestrial and aquatic plants for removing phosphorus from dairy wasewaters. Ecol. Eng. 5: 371-390.

Gearheart RA. 1992. Use of Constructed Wetlands to Treat Domestic Wastewater, City of Arcata, California. Water Sci. Technol. 26: 1625-1637.

Hoffman D, Rattner B, Burton GA, Jr. Cairns J. 2002. *Handbook of Ecotoxicology*, 2nd Ed., CRC-Lewis, Boca Raton, Fla.

Hseih C, Davis AP. 2005. Evaluation and optimization of bioretention media for treatment of urban storm water runoff. J. Environ. Eng. 131: 1521-1531.

Jokerst A, Sharvelle SE, Hollowed ME, Roesner LA. 2011. Seasonal performance of an outdoor constructed wetland for graywater treatment in temperate climate. Water Environ. Res. 83(12): 2187-2198.

Kadlec RH, Knight RL. 1996. Treatment Wetlands, Lewis Publishers, Boca Raton, FL.

Kimani RW, Mwangi BM, Gichuki CM. 2012. Treatment of flower farm wastewater effluents using constructed wetlands in lake Naivasha, Kenya. Indian Journal of Science and Technology. 5: 1870-1878.

Kivaisi AK. 2001. The potential for constructed wetlands for wastewater treatment and reuse in developing countries: a review. Ecol. Eng. 16: 545-560.

Laber J, Haberl R, Langergraber G. 2003. Treatment of hospital wastewater with a 2-stage constructed wetland system. In: Haberl, R., Langergraber, G. (Eds.), Achievments and Prospects of Phytoremediation in Europe. University of Natural Resources and Applied Life Sciences, Vienna, Austria, p. 85 (Book of Abstracts).

Metcalf and Eddy Inc. 1991. Wastewater Engineering. Treatment, disposal and reuse, 3rd ed. McGraw-Hill Inc., NY, 1333 pp.

Mina IA-P, Costa M, Matos A., Calheiros CSC, Castro PML. 2011. Polishing domestic wastewater on a subsurface flow constructed wetland: organic matter removal and microbial monitoring. Int. J. Phytorem. 13: 947-958.

Nyakango LB, van Bruggen MA. 1999. Combination of a well functioning wetland with a pleasing landscape design in Nairobi, Kenya. Wat. Sci. Tech. 40: 249-256.

Panswad D, Chavalparit O. 1997. Water quality and occurrence of protozoa and metazoan in two constructed wetlands treating different wastewaters in Thailand. Wat. Sci. Tech. 36: 183-188.

Reed SC, Middlebrooks EJ, Crites RW. 1998. Natural system for waste management and treatment, Mc-Graw Hill Inc., NY.

Shi L, Wang BZ, Cao XD, Wang J, Lei ZH, Wang ZR, Liu ZY, Lu BN. 2004. Performane of a subsurface-flow constructed wetland in China. J. Environ. Sci. (China). 16(3): 476-481.

U.S. Environmental Protection Agency (US EPA). 1997. Managing Urban Runoff. EPA 841-F-96-004G, Washington D.C.

Vymazal J. 1995. Algae and Element Cycling in Wetlands. Lewis Publishers, Chelsea, Michigan.

Vymazal J. 2005. Horizontal subsurface flow and hybrid constructed wetlands systems for wastewater treatment. Ecological Engineering 25: 478-490.

Vymazal J. 2007. Removal of nutrients in various types of constructed wetlands. Sci. Tot. Env. 380: 48-65.

Vymazal J. 2013. The use of hybrid constructed wetlands for wastewater treatment with special attention to nitrogen removal: A review of recent development. Water Res. 47: 4795-4811.

Yilmaz DD, Akbulut H. 2011. Effect of circulation on wastewater treatment by *Lemna gibba* and *Lemna minor* (floating aquatic macrophytes). Int. J. Phytorem. 13: 970-984.

Table 1. Average meteorological conditions during the study period

Minimum Temperature (C)	24.2±2.5
Maximum Temperature (C)	39.2±3.2
Relative Humidity (%)	37.0±9.2
Wind Speed (m/s)	1.82±0.51
Solar flux (W/m^2)	224.5±4.0
Sunshine hours (hrs)	9-11

Table 2. Values of different parameters during wastewater treatment by *Canna lily*

Parameter / Day	pH	TDS (mg/l)	BOD (mg/l)	COD (mg/l)	Nitrate (mg/l)	TKN (mg/l)	Phosphate (mg/l)
Inlet	**7.5**	**2200**	**45**	**1100**	**1.00**	**50**	**15.00**
Outlet 10-Apr-12	6.8	680	6	1570	0.32	15.4	1.76
11-Apr-12	6.9	710	5	100	0.07	6.8	3.06
12-Apr-12	6.9	730	5	100	0.07	6.3	3.21
13-Apr-12	6.9	750	3	400	0.10	5.4	3.16
16-Apr-12	7.0	690	6	200	0.15	5.3	2.79
17-Apr-12	6.9	660	6	100	0.17	5.6	2.80
18-Apr-12	6.9	770	5	100	0.21	4.4	2.77
19-Apr-12	7.0	800	5	100	0.11	4.6	2.72
20-Apr-12	6.8	675	6	70	0.24	4.4	3.20
23-Apr-12	7.0	690	4	40	0.20	4.5	3.20
24-Apr-12	6.9	720	3	50	0.17	5.5	2.94
25-Apr-12	6.9	668	3	50	0.16	4.3	2.72
26-Apr-12	6.9	730	6	50	0.11	4.8	2.85
27-Apr-12	7.0	780	4	60	0.10	2.9	2.87
30-Apr-12	7.0	810	4	10	0.16	4.8	2.14
01-May-	6.9	720	5	30	0.07	4.1	2.17
02-May-	6.8	610	3	40	0.03	4.8	2.29
03-May-	7.1	780	10	60	0.19	3.7	1.90
04-May-	6.8	620	13	30	0.08	5.2	1.96
07-May-	6.9	770	10	40	0.09	3.3	1.95
08-May-	6.8	570	13	30	0.16	4.1	1.69
09-May-	6.8	780	6	30	0.01	6.7	1.18
10-May-	7.0	620	3	40	0.06	5.9	1.52
11-May-	7.1	680	2	50	0.03	4.5	1.95

Range	**6.8-7.1**	**570-**	**2-13**	**10-**	**0.01-**	**2.9-15.4**	**1.52-3.21**
Mean ± SD	**6.9 ± 0.08**	**708.9 ± 64.76**	**5.7 ± 2.99**	**139.58 ± 314.82**	**0.1 ± 0.07**	**5.3 ± 2.36**	**2.5 ± 0.60**

Table 3. Physical and biochemical Charecteristics of *Canna lily* during the study

Parameter	Initial	Final
Chlorophyll óaô(mg/l)	10.71	9.44
Chlorophyll ôbô(mg/l)	2.44	3.87
Total chlorophyll (mg/l)	13.12	13.27
Carotenoids (mg/l)	0.06	0.07
Average Root length (cm)	21.0	57.7
Average Shoot length (cm)	33.8	80
Density (plants/m^2)	50	59

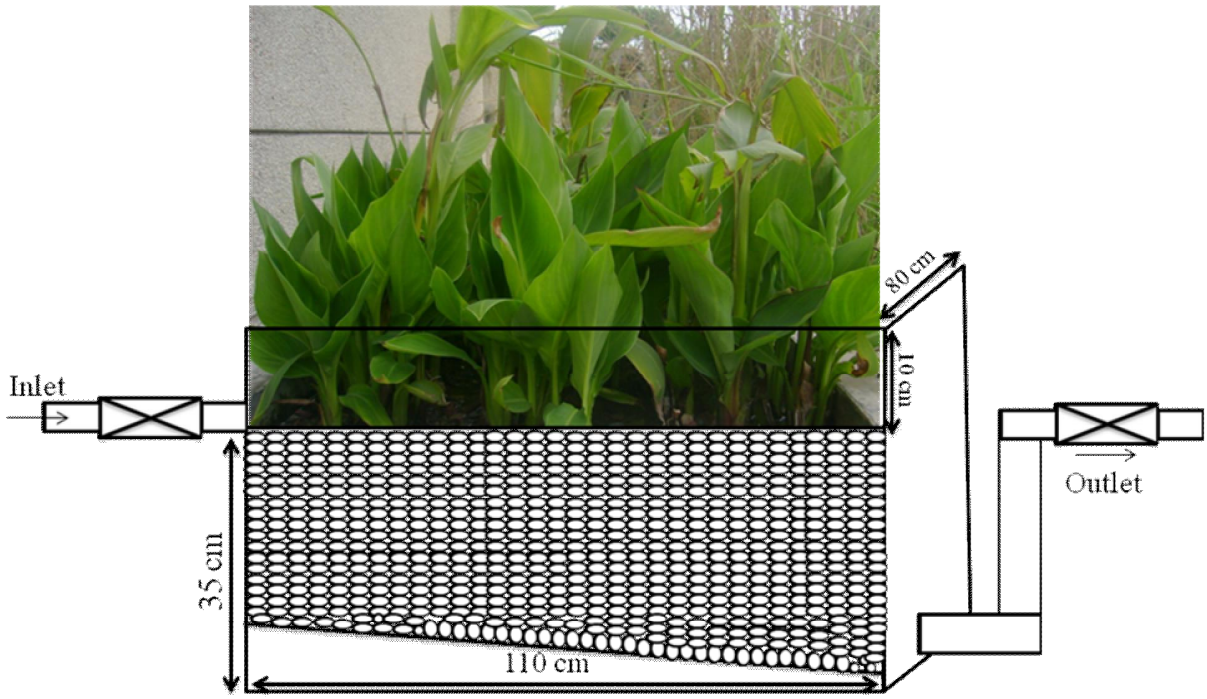

Fig. 1. Configuration of wetland cell used during the study

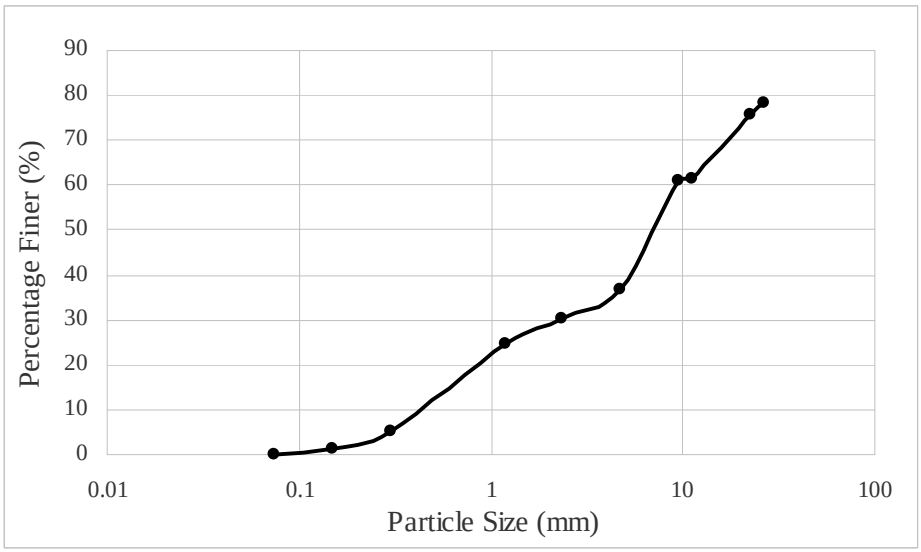

Fig. 2. Particle size distribution of sand-gravel packing medium used in CW cell

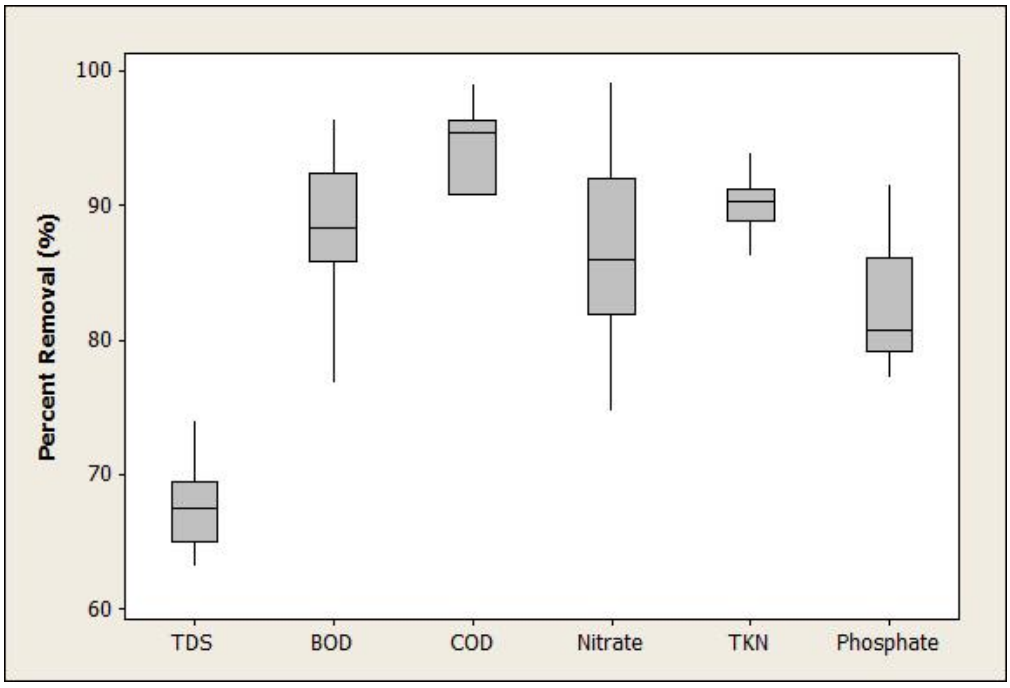

Fig. 3. Percentage removal of CNP by *Canna lily* in constructed wetland

Volume 3, Issue 1 (2015) 118-120 ISSN 2347 - 3258
International Journal of Advance Research and Innovation

Thermo Analysis of Hydrogen Liquefaction System

Devender Kumar *, R. S. Mishra
Department of Mechanical, Delhi Technological University, New Delhi, India

Article Info
Article history:
Received 8 January 2015
Received in revised form
15 January 2015
Accepted 22 January 2015
Available online 15 March 2015

Keywords
Thermodynamics analysis,
Efficiency
COP

Abstract

Hydrogen is rich source of energy but its properties in gaseous state cannot be used efficiently but at the liquid state in can be used in various application but high cost of liquefaction of hydrogen cryogenic system and less efficiency component turned the cryogenic science toward optimization. Second law efficiency analysis system components on demand base parameters, reduces cost of whole system. A mathematical computational program is made on the basis of hydrogen system and second law analysis is done on different input parameters is studied. Second law efficiency of hydrogen system is 19.82 % and COP is 0.9746 is found when inputs are at ambient condition and compressor pressure at 15 bar is provided, but study of graph shows that both start decreasing with further increases of compressor pressure whereas liquefaction mass ratio and Total work done is increases with increase in compressor pressure.

Nomenclature

m=mass flow rate
m_f=Liquefaction mass
h=Enthalpy
s=Entropy
X=Dryness fraction
T=temperature
P=Pressure
$m_{LN_{evop}}$ =mass of liquid nitrogen
$\eta_{2nd\ law}$=Second law efficiency
Ɛ=Effectiveness of heat exchanger
C=Specific heat capacity fluid or gas
W_{net}=Total Work of compression
W_c=Compressor work

1. Introduction

A low temperature environment is termed a cryogenic environment when the temperature range is below the point at which permanent gases begin to liquefy. Permanent gases are elements that normally exist in the gaseous state and were once believed impossible to liquefy. Lack of fossil fuels and increasing need to energy has made us to pay aspecial attention to replacing fossil fuels with renewable resources. Also the fossil fuels and their combustion products were causing global environment problems. These resources of energy are clean and do not pollute the environment. One these sources are hydrogenic energy. Hydrogen derived from renewable energies eventually will contribute to the sustainable development of such countries [1]. Hydrogen combustion produces water vapor that does not make any pollution. Hydrogen is gas form, occupies a large volume and has low density (0.0897 kg/m3) and high pressure [2]. So the dmand of dense form of hydrogen increses but liqifaction of hydrogen is a very slow process and it estimated that The fastest flow that a hydrogen liquefaction system can bear in optimum hydrogen flow is 300 lit/hr[3]. Thus we need to liquefy hydrogen for an easier transportation and safety ,it also studied that thermodynamic performance (t) is low due to existing of nitrogen pre coolers I hydrogen system [4] In hydrogen liquefier the pre-compression of feed gas has generally higher stand-alone exergy efficiency than the cooling and liquefaction sub-process. Decreased feed pressure results in generally higher power consumption but also higher exergy efficiency, and vice versa [5]. Gianluca Valenti et al [6] in research show that the feed, 10 kg s^{-1}, is refrigerated in heat exchangers catalytically promoting the ortho–para conversion down to the low temperature of 20.5 K and at the high pressure of 60 bar with turbo machine expansions show 48% of second law efficiency with low power consumption of hydrogen liquefaction system. SongwutKrasae-in et al [7] showed effect of mutlreferegerant at the hydrogen liquefaction plant. The MR system can be used to cool feed normal hydrogen gas from 25 °C to the equilibrium temperature of −193 °C with a high efficiency. The overall power consumption of the plant is reduced from 5.35 kWh/kg_{LH2}, to minimum of 2.89 kWh/kg_{LH2}.GianlucaValenti et al [8] discuss the influence of the thermodynamic modeling of the fluid on the simulation outcomes. Various hydrogen forms (ortho hydrogen and Para hydrogen) and their mixtures (equilibrium-hydrogen and normal-hydrogen) are studied and described in his research. According to viewpoint of David O. Berstad [9] efficiency and cost is to a large extent dependent on the efficiency of the liquefier so high-efficiency hydrogen liquefier based on mixed-refrigerant (MR) pre-cooling has been developed. Based on his models, a reduction in power consumption obtain in the range of 45–48%. Akihiro Nakano et al [10] proposed a simple estimation method for the liquefaction rate and confirmed that the estimation method well explained the experimental result. A small-scale hydrogen liquefier with a two-stage 10 K Gifford–McMahon cycle (GM) refrigerator is confirmed the estimation method for predicting the liquefaction rate.

Corresponding Author,
E-mail address: devenderdahiya@in.com

2. Thermodynamic Analysis of Hydrogen Liquefaction System

The design is quite critical at low temperatures due to changes in thermo physical properties of hydrogen gas. Fig 1 showed the block diagram hydrogen liquefaction system in which liquefy nitrogen chamber is introduced to reduce the further temperature up to the critical temperature before J-T which is required to liquefy the hydrogen gas.

"Compressor"

$$Wc_{ideal} = m_2 * R * T_1 * ln * (\frac{P_2}{P_1}) \quad (1)$$

$$-Wc = (h_1 - h_2) - T_0 * (s_1 - s_2) \quad (2)$$

"Heat Exchanger A"

$$m_a * h_2 + m_4 * h_{13} = h_3 * m_a + m_4 * h_{14} \quad (3)$$

$$\varepsilon = \frac{m_a * (T_2 - T_3)}{m_a * T_2 - T_{13} * m_{13}} \quad (4)$$

$$P_3 = P_2 \quad (5)$$

"Heat Exchanger B"

$$m_b * h_2 + m_{LN_{evop}} * h_7 = h_4 * m_b + h_8 * m_{LN_{evop}} \quad (6)$$

$$\varepsilon = \frac{m_b * (T_2 - T_4)}{m_b * T_2 - T_7 * m_{LN_{evop}}} \quad (7)$$

"Mixing of two different tem helium"

$$m_3 * c_p * (T_3 - T_5) = m_b * c_p * (T_5 - T_4) \quad (8)$$

"Heat Exchanger C"

$$Q_{LN_{evop}} = m_2 * (h_5 - h_6) \quad (9)$$

$$m_{LN_{evop}} * L_{LN} = Q_{LN_{evop}} \quad (10)$$

$$m_2 * h_5 + m_{LN} * h_{LN} = m_{LN_{evop}} * h_7 + m_2 * h_6 \quad (11)$$

"Heat Exchanger D"

$$m_2 * h_6 + m_4 * h_{12} = h_9 * m_2 + m_4 * h_{13} \quad (12)$$

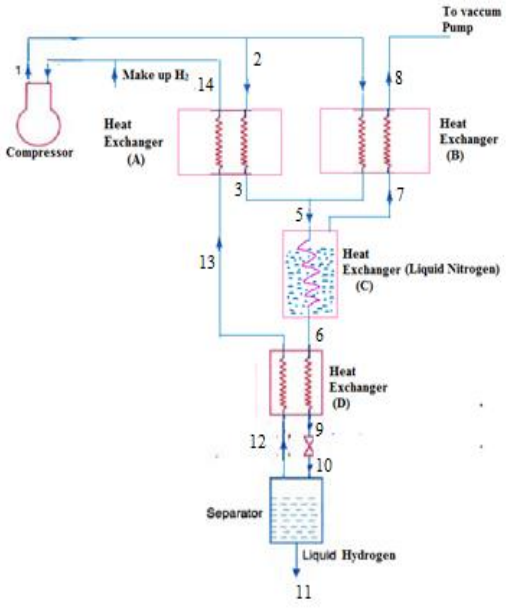

Fig: 1. Block Diagram of Hydrogen Liquefaction System

$$\varepsilon = \frac{m_2 * (T_6 - T_9)}{m_2 * T_6 - T_{12} * m_4} \quad (13)$$

"Expansion Valve"

$$h_9 = h_{10} \quad (14)$$

$$h_{10} = h_{11} + x_{10} * h_{12} \quad (15)$$

Separator"

$$m_2 * h_{10} = h_{11} * m_3 + m_4 * h_{12} \quad (16)$$

3. Result and Discussion

By computational mathematical technique various variable are noticed which are playing high role in hydrogen Liquefaction system and its optimization andto fully understand the effect of these variables on system different values are given and graphs are generated. Fig 1 show the variation of second law efficiency with respect to compressor pressure it show that as increase the compressor pressure after 12 bar the efficiency of system start decreasing whereas Fig 2 show just reverse of this and show increase in liquefaction mass of helium with increase of compressor pressure. Total work is summation of all type of work used in system like compressor work, expander work. Fig 3 shows there not much high fluctuation in variation of total work of system with increase in compressor pressure. At low pressure COP of system is quiet good as comparison with COP at high pressure. Fig 4 show COP of system start decreasing with increase in compressor pressure.

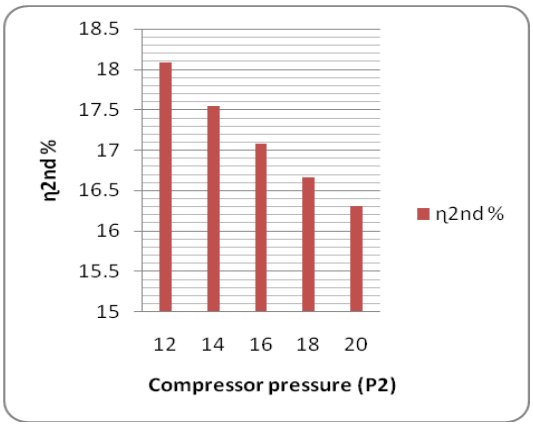

Fig: 2. Variation of Second Law Efficiency to Compressor Pressure

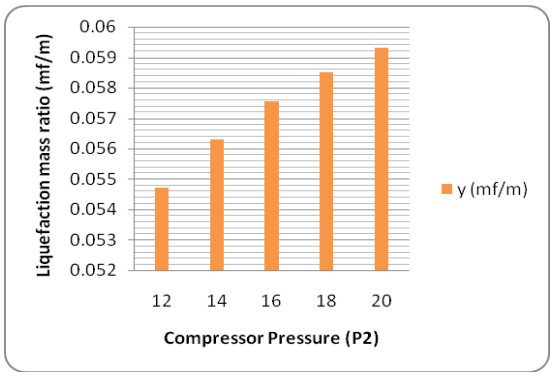

Fig: 3. Variation of Liquefaction Mass Ratio to Compressor Pressure

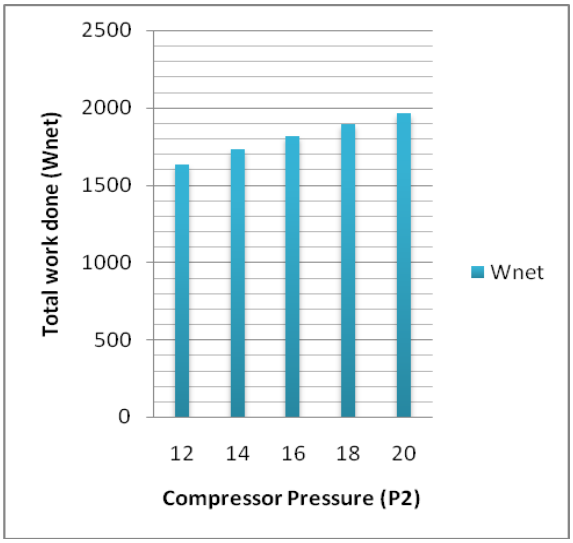

Fig: 4. Variation of Total Work of System to Compressor Pressure

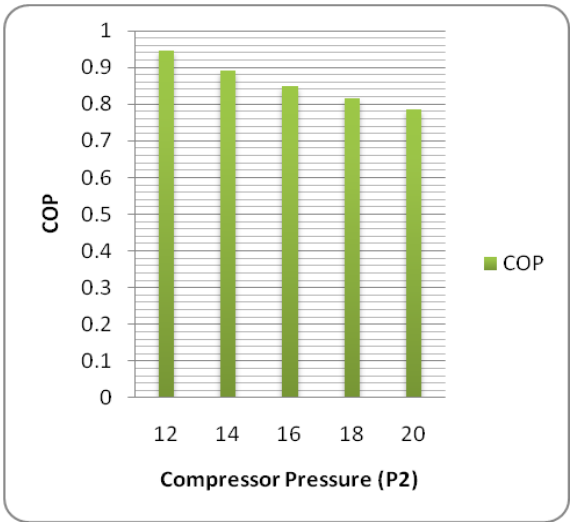

Fig: 5. Variation of COP of System to Compressor Pressure

4. Conclusion

1) Second law efficiency of system is 17.29 % and it start decreasing with further increases of compressor pressure
2) COP of the system is 0.8687 when input at ambient condition and compressor pressure is 15 bar and as like second like efficiency it also start decresing with increases of compressor pressure.
3) Liquefaction mass ratio and Total work done is increases with increase in compressor pressure.

References

[1] T. N. Veziroglu, S. Sumer, 21st Century's energy: Hydrogen energy system, Energy Conversion and Management, 49 (7), 2008, 1820-1831
[2] S. M. Aceves, J. Martinez-Frias, O. Garcia-Villazana, Analytical and experimental evaluation of insulated pressure vessels for cryogenic hydrogen storage, International Journal of Hydrogen Energy, 25(11), 2000, 1075-1085
[3] J. Sargolzaei, Saghatoleslami, Design of cryogenic system for liquefaction of hydrogen, ICHEC 2009
[4] E. E. Ludwig, Applied Process design for chemical and petrochemical plants, Gulf Publishing Company, 4, 2007
[5] O. David Berstad, H. Jacob Stang, Petter Neksa Comparison criteria for large-scale hydrogen liquefaction processes, International Journal of Hydrogen Energy, 34(3), 2009, 1560–1568
[6] G. Valenti, E. Macchi, Proposal of an innovative, high-efficiency, large-scale hydrogen liquefier, International Journal of Hydrogen Energy, 33(12), 2008, 3116–3121
[7] S. Krasae-in, J. H. Stangand Petter Neksa, Simulation on a proposed large-scale liquid hydrogen plant using a multi-component refrigerant refrigeration system, International Journal of Hydrogen Energy, 35(22), 2010, 12531–12544
[8] G. Valenti, E. Macchi, S. Brioschi, The influence of the thermodynamic model of equilibrium-hydrogen on the simulation of its liquefaction, International Journal of Hydrogen Energy, 37(14), 2012, 10779–10788.
[9] David O. Berstad, Jacob H. Stangand Petter Neksa, Large-scale hydrogen liquefier utilising mixed-refrigerant pre-cooling, International Journal of Hydrogen Energy, 35(10), 2010, 4512–4523
[10] A. Nakano, T. Maeda, H. Ito, M. Masuda, Y. Kawakami, A. Kato, M. Tange, T. Takahashi, M. Matsuo, Small-scale hydrogen liquefaction with a two-stage Gifford–McMahon cycle refrigerator, International Journal of Hydrogen Energy, 35(17), 2010, 9088–9094

Volume 3, Issue 1 (2015) 121-123 ISSN 2347 - 3258
International Journal of Advance Research and Innovation

Thermodynamic (Exergy-Energy) Analysis of a Low Pressure Kaptiza Claude System for Liquefaction of Gases

Devender Kumar *, R. S. Mishra
Department of Mechanical Department, Delhi Technological University, Delhi, India

Article Info
Article history:
Received 9 January 2015
Received in revised form
15 January 2015
Accepted 20 January 2015
Available online 15 March 2015

Keywords
Thermodynamics Analysis Claude Kaptiza System,
Energy-Exergy Analysis,
First and Second Law Analysis

Abstract

From various Cryogenics systems, lot of a detailed thermodynamic analysis of cryosystems have been reported in literature however the modification of Claude systems for low pressurefor high yield of liquefied mass of gases is very limited available in literature so far.A comprehensive energy and exergy analysis of Claude Kaptiza cryogenic system for various gases is carried out in this paper by using various properties variables (i.e temperature, pressure etc) in system to find out the more efficient statics of system included exergy destructions in system .Numerical computations have been carried out for various gases in Claude Kaptiza system and it was observed that the inlet variables like pressure temperature and intermediate mass ratio respectively are 3-6 bar,280-290 K and 0.7for optimized result of considered variables such liquefaction mass, liquidation temperature and second law efficiency in low pressure Kaptiza Claude system.

Nomenclature

m= Total mass of gas

m_f=liqified mass of gas

m_4 =mass of air in second heat exchanger

m_8 =mass of air liquefied in the separator

h=Enthalpy

s=Entropy
X=Dryness fraction
T=temperature
P=Pressure
η_{comp}=Efficiency of compressor (approx. 80%)
$\eta_{expander}$= Efficiency of expander (approx. 80%)
$\eta_{2nd\ law}$=Second law efficiency
Ɛ=Effectiveness of heat exchanger (approx. 80%)
C=Specific heat capacity fluid or gas

W_t=Work of reversible isothermal compression

W_c=Shaft work supplied to compressor per unit mass

R=Universal gas constant

W_{net} =Net work done in system

1. Introduction

It's a natural phenomenon that heat flow from high temperature to low temperature and the reverse process without any aid or external work is impossible and if so it just the violation of second law of thermodynamics A device which is which act as intermediate device is called refrigerator. The difference between refrigeration and cryogenics systems lies in the achievable temperature with the dividing line being of -100oF or -74^{o}C [1]. Now a day the process industries are faced with an increasingly competitive environment, ever changing market conditions and government regulations. Yet they a still have to increase productivity and profitability.

Corresponding Author,
E-mail address: devenderdahiya@in.com

In order to have a means of comparison of liquefaction systems through the figure of merit and exergy efficiency. Most of system is ideal in the thermodynamic sense, but it is not ideal as far as practical system is concerned. The perfect cycle in thermodynamics is the Carnot cycle [2]. Today a cryogenics industry is a billionaire industry and lots of research is going on to achieve best one improved process. Cryogenic process to liquefy air which is further extent to extract various particular gas like oxygen, nitrogen, feron etc. Always various analyses is done to identify the loop hole of process and to rectify it to their upper level. electro caloric cooling is a transiting to new cooling principle's is critical and one of the most promising alternatives may be [3].Various particular part are taken under study to increase overall performance of cryogenic system e.g A good exergetic design of a heat exchanger would allow for an increase in the global efficiency of the process, by defining a thermodynamic cycle in which the exergetic losses would be limited [4] apart from this other parts like expander, mass ratio and input variables are considered to improve cryosystems.

2. Thermo analysis of Claude Kaptiza system for liquefaction of gases:

Compressor Work:

$\eta_c=W_t/W_{comp}$ (1)
$W_t=mRTlnP_2/P_1$ (2)
$-W_c=m*(T_1*(s_1-s_2)-(h_1-h_2)$ (3)
$W_{reversible}=W_{actual}-T_0 s_{gen}$ (4)
$W_{net}=W_c+W_e$ (5)

Expander:

$T_8/T_3 = (〖P_8/P_3)^{(((Y-1)/Y)\eta_{expander})}$ (6)
$W_e=m_e*h_3-m_e*h_e$ (7)

"Control volume except compressor"

$m*h_2=W_e+(m-m_f)*h_1+h_f*m_f$ (8)
$y=m_f/m$ (9)

"Work done per mass of gas"

$z=-W_{net}/m$ (10)

"Work done per mass of liq gas"

t=-W_net/m_f (11)

Coefficient of performance of system

COP= ((h_1-h_f)/W_net) (12)

Second law analysis:

$$\eta_{2nd\ law} = ((((h_f - h_1) - T_0 * (s_f - s_1))/(W_{net}) * m_f) * 100)$$

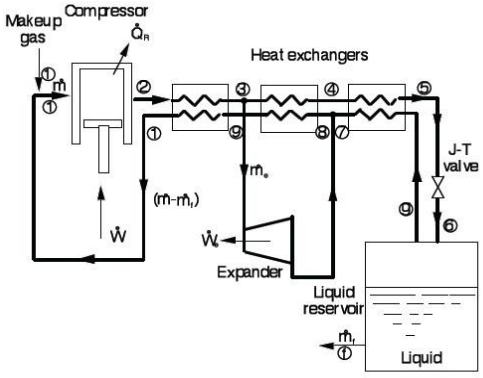

Fig: 1. Block Diagram of Kaptiza System

A complete analysis of Kaptiza Claude cycle is performing with the help of numerical computation technique for various gases. Kaptiza Claude cycle as shown in Fig 1 is taken for analysis. Kaptiza Claude system is almost same as simple Claude system except arrangement of first expander. In Kaptiza system expanderis situated in between the first and second heat exchanger other than this it also consist a compressor, expander, two heat exchangers with throttle valve and separator. The fluid which has to liquefy first fed to compressor in its gaseous form at atmospheric pressure and temperature which circulate from all system and in last fractional mass of total mass get liquefied and remaining again fed in system with additional mass to recirculate in system again. Various results are drawn for particular inlet temperature, pressure and intermediate pressure for low pressure side of expander for different six type gases such oxygen, argon, methane, air, fluorine and nitrogen are considered for study.

3. Results and Discussion

Various results are drawn on the basis of numerical equations of system. In fig 2 variation of liquefaction temperature with inlet pressure as we increases the pressure Liquefaction temperature rises but after crossing 10 bar the increment in liquefaction temperature is start reducing and its slope with inlet pressure start become straighten. Fig 3 show fall of liquefaction mass with increase of inlet temperature and it also show that at 330 k the liquefied mass of methane and argon is same. Fig 4 shows decreases in liquefaction mass with increase of inlet pressure. Fig 5-7 show variation in second law efficiency with intlet temperature, intermediate mass and inlet pressure respectively. Graph analysis of these 5-7 fig shows that second law efficiency is decreases with increase of inlet temperature while with increases of intermediate mass second law efficiency increases whereas it again decreases with increase of inlet pressure. Fig 8 -9 show variation in COP of system with inlet pressure and temperature. They show that increase in pressure is beneficial for system and COP of system is increases with increase in inlet pressure while its increment with increase in inlet temperature is very less. From above graph study it determined that increment and decrement in a very concern range of various variables is good for optimization of Kaptiza Claude System

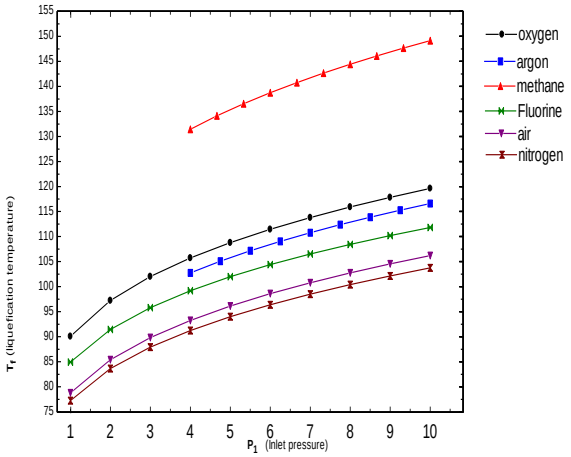

Fig: 2. Variation of Liquefaction Temperature with Inlet Pressure

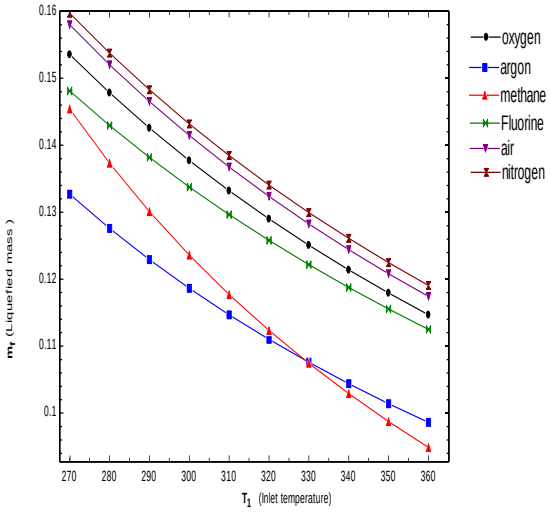

Fig: 3. Variation of Liquefied Mass with Inlet Temperature

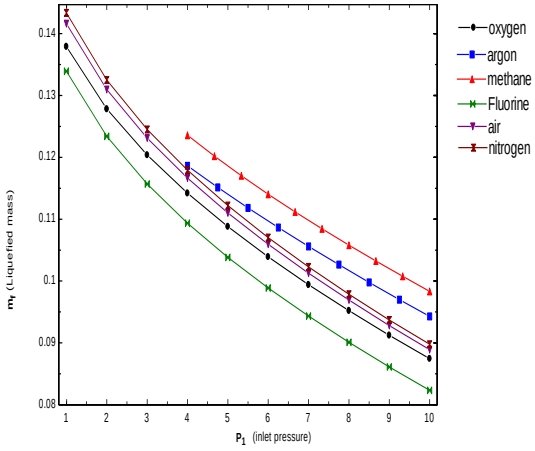

Fig: 4. Variation of Liquefied Mass with Inlet Pressure

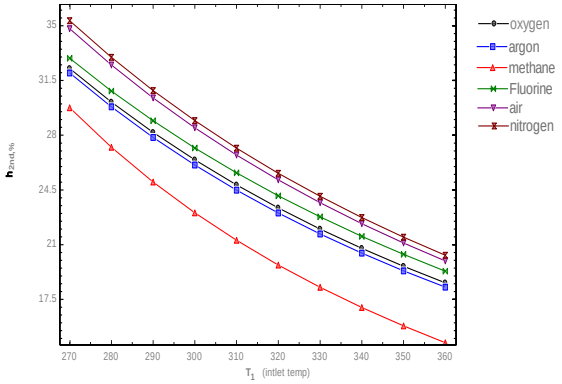

Fig: 5. Variation of 2nd Law Efficiency with Inlet Temperature

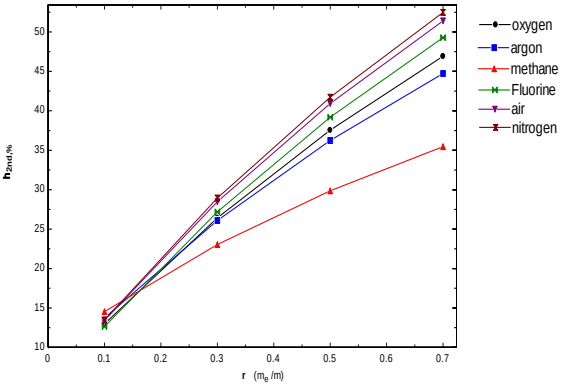

Fig: 6. Variation of 2nd Law Efficiency with Intermediate Mass Ratio

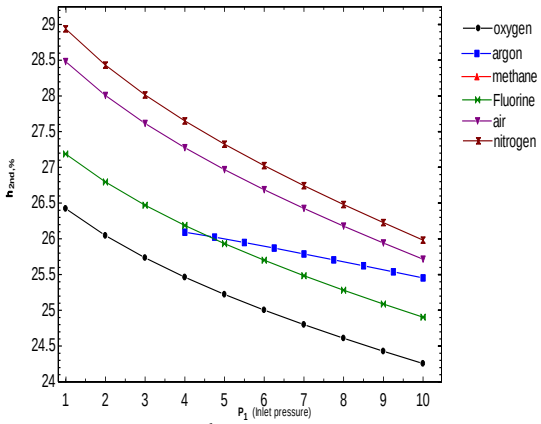

Fig: 7. Variation of 2nd Law Efficiency with Inlet Pressure

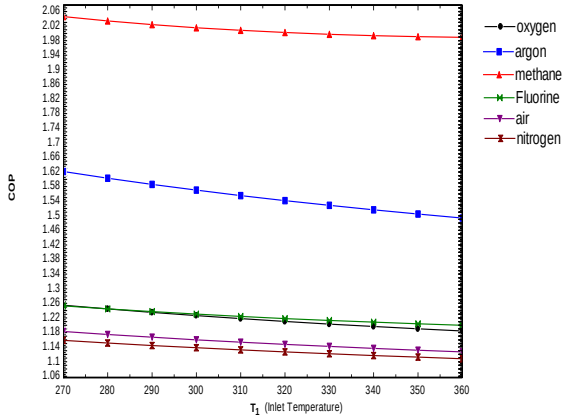

Fig: 8. Variation of COP with inlet Temperature

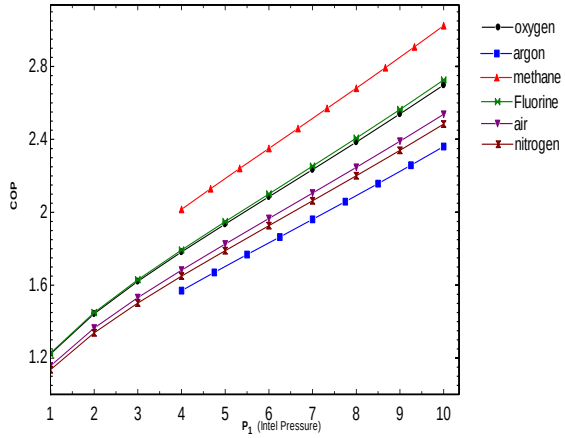

Fig: 9. Variation of COP with Inlet Pressure

4. Conclusion

From above study following results are concluded

1. The optimize range of inlet variables like pressure temperature and intermediate mass ratio respectively are 3-6 bar,280-290 K and 0.7for good result of considered variables such liquefaction mass, liquidation temperature and second law efficiency.
2. Intermediate pressure of low pressure side expander should be in minimum range for high second law efficiency.
3. Increase in inlet temperature decrease the COP, second law efficiency, liquefaction mass.

References

[1] A. M. Papadopoulos, C. J. Koroneos, Refrigeration and Cryogenic systems, Air conditioning– Energy consumption abd environmental quality, Encyclopedia of life supports systems (ELOSS),

[2] S. M. Dash, Study of cryogenic cycles with aspen – hysys simulations, Department of Mechanical Engineering National Institute of Technology Rourkela, 2008-09

[3] Yu. V. Sinyavskii, Electrocaloric refrigerators: A promising alternative to current low-temperature Apparatus, Chemical and Petroleum Engineering, 31(6), 1995, 295-306

[4] R. Agrawal, D. W. Woodward, Efficient cryogenic nitrogen generators: An exergy analysis, Gas Separation & Purification, 5(3), 1991, 139-150

Sharma et al., J Thermodyn Catal 2015, 6:1
http://dx.doi.org/10.4172/2157-7544.1000139

Thermodynamics & Catalysis

Review Article Open Access

Microalgae as Future Fuel: Real Opportunities and Challenges

Monica Sharma[1*], Nitin Thukral[1], Navneet Kaur Soni[1], Sagar Maji[2,3]

[1]Department of Biotechnology, Delhi Technological University, Main Bawana Road, Shahbad Daulatpur, Delhi-110042, India
[2]Department of Mechanical Engineering, Delhi Technological University, Main Bawana Road, Shahbad Daulatpur, Delhi-110042, India
[3]G.B. Pant Govt. Engineering College, Okhala Industrial Estate, Phase-III, NewDelhi-110020, India

Abstract

Depleting reserves and souring prices of petroleum and oil have daunting effect on the economy of many developed and developing nations and forced researchers, government and federal agencies to opt for development of alternate fuels. In recent years, there is renewed interest in the field of algal biofuel production owing to its ability to grow in non-agriculturalable waste land and municipal wastewater/agricultural runoff water. Previous decade was attributed in developing new open culture/ reactor design for enhanced microalgal biomass production, efficient harvesting and pretreatment systems for commercial algal biofuel production. The true potential of algal biofuel spurs debate between algae experts and external observer over economics and environmental sustainability. Currently, no commercial algal energy generation system, which can surpass crop based energy content, is available. In present review, efficient culturing, operational strategies, reactor design and technological advancement in processing of algal fuel have been reviewed in graphical abstract

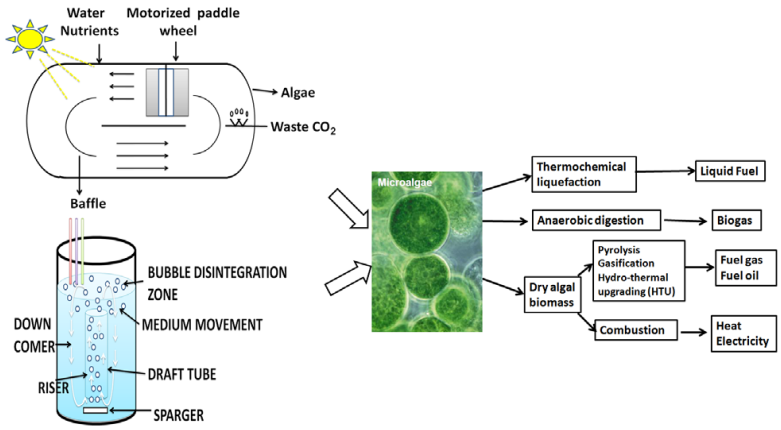

Keywords: Biofuel; Algal fuel; Biorefinery; Microalgae

Introduction

Depleting fossil fuel reserves, global warming and increased global demand for energy pushed the world to a stage where finding a new renewable green alternative fuel is inevitable. Presently the United States and China are the largest worldwide oil consumers (>10 million barrel per day) followed by Japan (4.7) and India (3) (US Energy Information Administration). It is estimated that by the year 2020, there will be 60 fold increases in the demand for oil worldwide. The fossil oil discovery has declined steadily (from 55 billion barrel per year to 10 billion barrel) since 1960's and extractions from unconventional natural sources (deep wells, oil shale and tar sands) are difficult and much more expensive [1].

The noteworthy progress has been made in improving technologies for biological conversion/biofuel production though capital costs for biofuel facilities are relatively high. Although commercial momentum is building, but this emerging industry is still facing many challenges. However, issues like improvement in understanding of the fundamental principles of biofuel efficiency, its scale up technology development and how it will change the automobile sector must be addressed.

The photosynthetic organisms are the most energy efficient systems present in nature and they can form valuable renewal raw material using photoautotrophic mode. Among these photosynthetic organisms algae form a fascinating group of ubiquitous organisms that has high biomass yield, high lipid or/and starch content, that can easily grow on effluents like wastewater and carbon dioxide on waste land. Algae based fuels are environmental friendly because they convert the CO_2 produced from burning of fuel again to algal biomass. There have been lot of controversies about carbon neutrality of biofuels because calculation of the carbon neutrality is a complex and imprecise method based highly on the assumptions. However, virtually all carbon neutral fuels actually require burning of fossil fuel in pre or post production

***Corresponding author:** Monica Sharma, Assistant Professor, Delhi Technological University, Main Bawana Road, Shahbad Daulatpur, Delhi-110042, India, Tel: +91-9717386785; E-mail: monashimla@gmail.com

Received November 11, 2014; **Accepted** February 12, 2015; **Published** February 16, 2015

Citation: Sharma M, Thukral N, Soni NK, Maji S (2015) Microalgae as Future Fuel: Real Opportunities and Challenges. J Thermodyn Catal 6: 139. doi: 10.4172/2157-7544.1000139

stages (process equipments, harvesting, transport of feed stock to the biorefinery, converting the feedstock into ethanol/biodiesel, and further transporting the biofuel to a petroleum refinery or service station). But the overall CO_2 emmision/production is less as compared to other fuels [2-4] .

Due to its chemical characteristics, algal fuel resembles gasoline and mix freely with fossil fuels and they could be used in existing automobile infrastructure. Biomass productivity of the algae is ten times as compared to crops and it could be cultivated in the desert. These characteristics make them attractive raw material for bioenergy production (Figure 1). Earlier the oil productivity was predicted to be more than 100 tons/ha per year (~10 Kg/m^2 per year), although till recent times only 40-60 tons/ha per year (~4-6 Kg/100 Kg/m^2 per year) was achieved commercially and 30 tons of biodiesel/ha per year (~3 kg/m^2 per year) was produced in subtropical or tropical regions [5].

Currently few companies are developing technologies for sustained algal biomass production for producing biofuels but raw data and technological facilities used in the process is not accessible, may be due to patenting issues. Nevertheless the large investment from venture capital, Government grants, collaboration between US large companies and academic institutions in last decade in algae biomass production fueled the idea that algae certainly hold some promise as future fuel [6,7]. In present manuscript we will discuss technological advancement achieved in previous years and the potential of algae as future fuel along with the challenges ahead.

Why algae as a renewable resource?

The agriculture practice is changing drastically in many countries e.g. in Indonesia tropical forest were destructed to grow fuel crops like palm oil and hence posed adverse ecological impact. These crops demand enormous agricultural land, water and fertilizers and yield less than 500-5,000 L of biodiesel per hectare [8]. In comparison algae can be grown on effluents and agricultural and municipal runoff water often can be used in conjugation with wastewater treatment and hold promise as a suitable raw material.

Algae contain carbohydrates and lipids as the main components of biomass. Algae has >50% of its mass in the form of carbohydrate, hence algal dry biomass is an important source to produce fermentable sugar from cellulose and hemicellulose which can be easily converted into bioethanol [9].

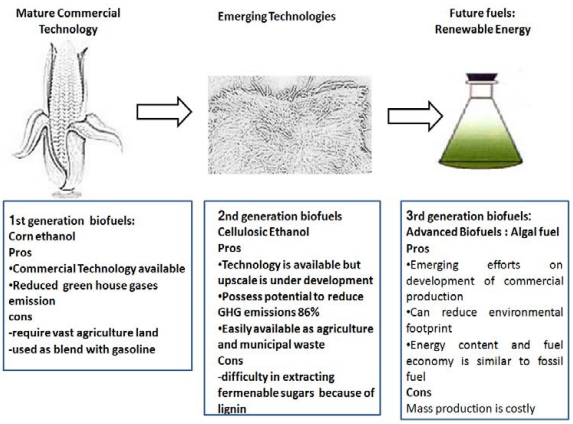

Figure 1: Biofuels Technology

Algae has a unique cell wall composed of mainly polysaccharides and no lignin as compared to other lignocellulosic waste which pose considerable restriction to get fermentable sugars from agricultural waste. A major breakthrough came when Deng and Coleman reported that genetically engineered green algae can be exploited for ethanol production from sunlight e.g. NREL (National Renewable Energy Laboratory) uses *Chlorophyceae* (green algae) and diatoms [10]. Green algae grow rapidly in nitrogen at 30°C, while diatoms require silicon for growth. Algenol Ltd. attracted significant funding when they transformed cyanobacteria to cyanobacterila strain using recombinant DNA technology which got the ability to transform the photosynthetically synthesized sugar into ethanol and also excrete it into the growth medium [11].

Algal oil usually consist of shorter chains and highly saturated lipids (C14:0, C16:0 and C16:1) which are generally favorable for fuel production. Lipid content of algae varies from 2-60% of dry weight (*Chlorella* sp. 28-32%, *Cylindrotheca* sp. 16-37%, *Phaeodactylum tricornutum* 20-30%). In diatoms *Hantzschia* and *Nitzschia* produce about 66% (dry weight) and 28-50% (dry weight) of oil (Table 1). Some algae like *Schizochytrium* sp. And *Botryococcus braunii* can accumulate ~75% of lipid and it can be converted to Straight Vegetable Oil (SVO) or biodiesel [12]. Microalgal oil yield per acre is about 10-25 times (5.87-13.69 L/m^2) as compared to rich plant oil source like palm oil (0.5949 L/m^2). The increased lipid content of algae can be achieved either by strain selection (having high growth rate and oil content) in open culture and closed bioreactors or by manipulating conditions [13]. In algae environmental stress like nutrient deficient environment often results in increase lipid accumulation >60% [14-16], however, these algal oils are unsaturated and hence cannot be used directly in sensitive engines.

Botryococcus braunii is well known cosmopolitan planktonic fresh water microalga, because of its ability to produce hydrocarbon in the form of triterpenes, which gets accumulated on the outside of the cell [17,18]. Generally hydrocarbon consists of 20-60% of algal dry mass and maximum production up to 86% has also been reported [19,20]. It produces three major types of hydrocarbons: botryococcenes, alkadienes and alkatrienes (C23-C33 alkenes). The *Botryococcus* hydrocarbons are non-edible and are very different in chemical constituents of vegetable oil. These hydrocarbons cannot be directly trans-esterified because these triterpenes do not possess the free oxygen atom which is required for trans-esterification reaction but they can produce octane (gasoline/petrol) by hydro-cracking in refinery. On hydro-cracking, Botryococcenes hydrocarbon results into a fuel with high octane value as compared to alkadienes and alkatrienes [21]. Many research groups are studying *B. braunii* growth profile in high salt concentration, N-availability and phosphate, light intensity and pH 8 [22]. The major drawback is that it show fastidicious growth and extraction is difficult because of thick cell wall, which make them unsuitable for large scale biofuel production. Hydrocracking of these hydrocarbons produce various fuel types like diesel, gasoline and kerosene.

Algae can also be used as a source for hydrogen production which can be achieved by three methods: biophotolysis of water, gasification and Steam reformation (SMR) of methane. They form one of the most promising future fuels because they produce only water as an exhaust product and not NO_x gases. Only algae synthesize hydrogen directly from sunlight and water in the complete anaerobic conditions [23], while other microbes like non-sulphurbacteria and green sulphur bacteria use solar energy to extract hydrogen gas from wide variety of substrates [24].

Name of Algae	Oil (% Dry weight)	Commercial culture system
Ankistrodesmus	28-40	Tank
Botryococcus braunii	29-75	Open raceway pond
Chlorella protothecoides	15-55	Central Pivot Ponds, Raceways, Tubular Photobioreactors
Chlorella sp.	29	Central Pivot Ponds, Raceways, Tubular Photobioreactors
Crypthecodinium cohnii	20	Fermenter (heterotrophic)
Cyclotella	42	-
Cylindrotheca sp.	16-37	-
Dunaliella tertiolecta	36-42	Extensive ponds
Haematococcus	20-35	Open paddle-wheel pond , Tubular Photobioreactors
Hantzschia	66	-
Isochrysis sp.	25-33	-
Monallanthus salina	>20	-
Nannochloris	31 (6-63)	-
Nannochloropsis	46 (31-68)	Raceways
Neochloris oleoabundans	35-54	-
Neochloris oleoabundans	35-54	-
Nitzschia	28-50	-
Phaeodactylum tricornutum	31	Vertical bubble column and airlift photobioreactors
Pleurochrysis carterae		Raceways
Scenedesmus	45	-
Schizochytrium	50-77	-
Spirulina	4-11	Raceways
Stichococcus	33 (9-59)	-
Tetraselmis suecica	15-32	Big bag culture
Thalassiosira pseudonana	21-31	-

Table 1: Representing Alga against the amount of Oil obtained as the% dry weight along with the Commercial Culture system that was used to obtain biofuel.

In *Scenedesmus* and *Chlorella vulgaris*, hydrogenase-dependent hydrogen production was observed when alga was grown in anaerobic conditions [25,26]. Kansai Electric Power Co. Ltd. (Nankoh, Osaka, Japan) established a pilot plant for hydrogen generation by clubbing green algae and photosynthetic bacteria. Arthrospira species are reported to possess highest hydrogen producing activity. Nitrogenase mediated hydrogen production under aerobic conditions was proposed by Asada and Kawamura in *Anabaena* sp. [27]. *Chlamydomonas reinhardtii* produces hydrogen in sulfur deprived medium in biohydrogen reactor [28,29]. Hence for algal hydrogen gas production only closed culture system can be employed. Currently only a fraction of H_2 gas production using algae has been achieved of its theoretical maximum (i.e. 20 g $H_2/m^2/day$) value, making process commercially unviable. In the year of 2013, Grow Energy Co. developed Hydral bioreactors for the commercial production of hydrogen using genetically modified algae [30]. In the same year, in Falkenhagen (Germany), the first commercial 2 megawatt power to gas installation was established which generate 360 m^3 of hydrogen per hour [31].

Culturing techniques of algae

Microalgae are phototrophic organisms that can increase their biomass using light, carbon dioxide, water, and inorganic salts [32]. The optimal growth temperature varies from 15-30°C and agitation is required to prevent algal biomass settlement to the bottom [33]. Respiration during the night hours causes some part of the biomass loss produced during day time [34]. The microalgae usually grow on attached surfaces but it prevent the gas and light penetrance to lower level when it outgrow hence causing the death of underlying layer, thus for mass production usually suspension cultures are preferred. The predicted yield of algal biomass from pilot scale to fermenter scale is mostly erroneously calculated because in high density culture, underlying algae are unable to capture all incoming light to convert it into biomass, hence the specific growth rate drops in comparison to low density cultures. The specific growth rate of exponentially growing cultures can be achieved in heterotrophic cultures under optimized conditions of temperature, light intensity, mixing and CO_2 supply. Using such systems the photosynthetic efficiencies of ~7% may be achieved but it results in increased bioreactor maintenance costs thus making the process economically unviable **[35]**.

Algae are generally cultivated in variable open- culture systems or controlled closed culture systems and both possessing their own advantages and disadvantages. The detail of each system is discussed below:

Land based open culture systems

Land based open culture system operation is limited to areas where low cost water is available due to the low depth and large surface area and water loss through evaporation can become a major issue. Marine waters and wastewaters can serve as good matches for this system, as environmental and sustainability issues would prevent large open pond cultivation using potable water. There is already some experience on large scale production using these types of systems, either in pilot projects partially funded by the government, in wastewater treatment plants, where it is used in secondary or tertiary treatment of sewage, or in commercial scale algal cultivation for the health food market [36].

Shallow unstirred ponds: Shallow and unstirred ponds are the simplest of the land-based open culture system for algae cultivation. Their sizes vary from few m^2 to 2,500,000 m^2 and use CO_2 as carbon source. Although open-culture systems are easy to operate, less expensive and have large production capacity but uses more energy and do not allow control of temperature and lighting conditions. It is more easily prone to invasion by other algae and contamination from bacteria. Slow diffusion of nutrients, dead and living algae sedimentation, flotation and limited usage of available sunlight are some other problems that add to the misery of the open-culture systems [13,14,34,37,38].

Circular/ raceway ponds: The race-away ponds have tried to minimize the limitations by using mechanical agitators to provide aeration. In mechanical agitator, arm move in a circular motion, and a paddle wheel cause the circulation of water through narrow pond (Figure 2). The gas bubbles can be blown and part of this gas is used to as carbon source and rest provide medium agitation. A limited number of species can be maintained in an open system, and hence the locally-occurring strain is preferable in an open system [13,14,34,37,38]. The outdoor commercial production of microalgae was achieved in Arthrospira, Chlorella and Dunaliella genera species only because they show high growth in selective medium (basic or highly saline) and also show reduced contamination issues. Such systems are less energy intensive, easy to operate, cheap and more durable than closed systems [39].

Closed systems

The purpose of the mass algal culture and local weather conditions may make the choice of system obvious. However, the main comparison between the two systems is principally cost and productivity. Earlier closed systems were created by covering the pond with a greenhouse. While this resulted in a smaller systems but many problems associated with pond systems were tackled. It allows more species to be cultivated and extend their growing season at will. Open ponds require larger and more cultivation areas to achieve the same productivity. The low mixing rate of open ponds intensifies the self-shading effect due to cell concentration and the physical structure of open ponds prevent proper aeration, causing a low medium CO_2 partial pressure, thus limiting the productivity rate per unit of area and volume.

The growth rate can be controlled variably in closed systems. Regarding the productivity per unit area or volume, Photo-Bioreactors(PBRs) are said to outperform open ponds. Growing algae in closed bioreactor for bioenergy production is a costly affair for biofuel production. Since the single cell oil (SCO) used in pharma, health and cosmetic industry are high value product (costing €1000 s per kilo), upscaling of algae for commercial use must supply biomass for a competent production price with other renewable and non-renewable energy raw materials. Currently only open systems can be used for large scale culturing of algae with minimal financial and energy input [34,40] but they have their pitfalls. With time many researchers attempted to create different type of bioreactors with better monitoring control to upscale the commercial production of algae.

Types of bioreactors: Photobioreactors: These mainly involve photoautotrophic production using natural or artificial lighting, although conventional stirred bioreactor can be used to culture some microalgae species heterotrophically at high densities in the dark. Photobioreactors on the other hand, are systems that are flexible and can be optimized in accordance with the biological and physiological characteristics of the species being cultivated. Thus, minimizing the contamination and offering better control over culture conditions.

Major limitation of photobioreactor is oxygen build up (due to photosynthesis) until they inhibit and poison the algae [41]. So degassing of the culture is a must and it is achieved by periodically returning the culture to a degassing zone. Carbon starvation and an increase in pH often occur as the algae use carbon dioxide. Therefore, carbon dioxide must be fed periodically into the system so as to successfully cultivate the microalgae during scale-up. Photobioreactors may require cooling during daylight hours and the temperature regulation can be achieved through heat exchangers.

Vertical column Photo bioreactors: Vertical column photo bioreactor is made up of glass or acrylic tubing which allows penetration of light for culture of algae. A gas sparger system, at the bottom of the reactor converts the inlet gas into tiny bubbles, which allows for mixing, mass transfer of CO_2, and removing O_2 produced during photosynthesis. Normally, no physical agitation system is implemented in the design of a vertical column photobioreactor. Vertical photobioreactors can be categorized into bubble column and airlift reactors (Figure 3) based on their liquid flow patterns inside the photobioreactors [42].

Bubble column reactors consists of cylindrical vessels with height to diameter ratio greater than 2. They are less expensive and have higher surface-area-to-volume ratio. They do not have moving parts and heat and mass transfer is maintained by gas bubbling upwards from the sparger. The efficient release of oxygen characterizes a bubble column reactor. Sparger design is important for the performance of the photobioreactor. Perforated plates used assparger for breaking and redistributing coalesced bubbles. Light is supplied from outside the column. Circulation of the liquid from central dark zone to the external light zone creates differential gas flow rate which is critical for the photosynthetic efficiency [43].

Airlift reactors are made of a vessel with two interconnecting zones. The gas mixture flows upward to the surface from the sparger in one tube, called gas riser. The other region, called the down comer, is where the medium flows down toward the bottom and circulates within the riser and the down comer. An airlift reactor based on the circulation mode is further categorized into internal loop or external loop [44]. Residence time of gas in different zones affects gas-liquid

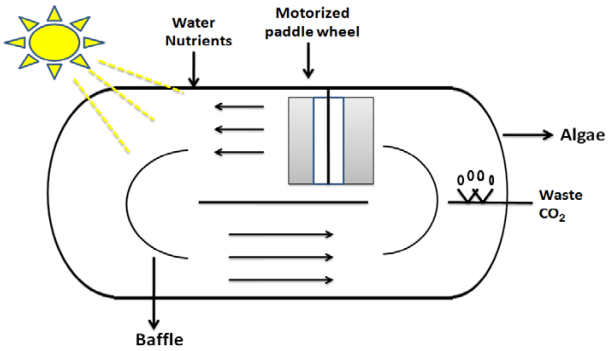

Figure 2: Schematic open race way pond system for algal culture.

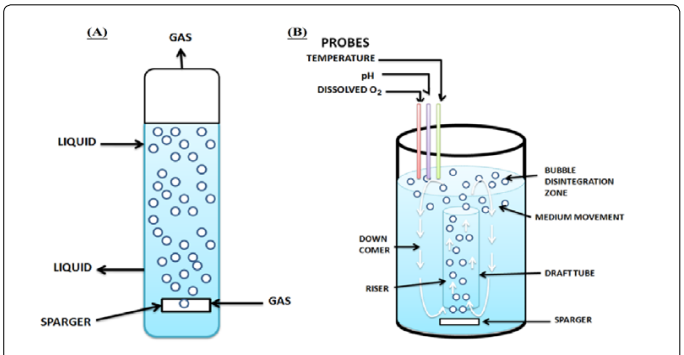

Figure 3: Schematic diagram of vertical bioreactor: A) Bubble column reactor B) Air-lift column reactor.

mass transfer, heat transfer, mixing, and turbulence and thus is critical for controlling the performance. A rectangular airlift photobioreactor have shown better mixing characteristics and better photosynthetic efficiency, however their design are complex and hence suffer difficulty in scale-up.

Flat Plate Photobioreactors (FPP): FPP consist of two rectangular panels made of glass or Perspex spaced about 25 mm or apart, illuminated on both sides and stirred by aeration (Figure 4). The panels may be inclined in some designs to capture optimal amount of radiations and mixing of algal culture is achieved by either by pumping or aeration systems. The aeration helps to remove the oxygen generated during photosynthesis, which is a limiting factor owing to photorespiration. Carbon dioxide can also be added to control growth whereas the temperature is controlled by spraying the water over the panel surface. Though expensive, some systems used heat exchanger for this purpose. However, flat plate systems may also suffers from some problems such as high space requirements, high solar energy, difficult maintenance, and low efficiency in terms of mass production per unit of space [45].

The productivity of FPP highly depends on the space requirements between the panels and the areal productivity constraint for outdoor application. On the other hand, flat plate systems when operated at indoor conditions, the factors such as distance between light sources and panels, temperature effects, illumination of one or both panel sides, light path are crucial. Increasing volume causes increase in hydrostatic pressure, thus making scale-up difficult. Moreover, the hydrodynamic stress may affect the microalgae growth. Though flat panels are very productive but difficulty in scaling up and high cost required to operate, limits its use [46]. Cheaper design was proposed by Rodolfi et al. where they used plastic bags within the rectangular frame [14]. The major limitations are: the scale-up require many compartments and support materials, difficulty in controlling culture temperature, some degree of wall growth and possibility of hydrodynamic stress to some algal strains.

Horizontal Tubular Bioreactors (HTB): Tubular systems are widely used commercial closed-culture systems for algal production. Tubular photo-bioreactors are made of transparent polypropylene acrylic or polyvinyl chloride pipes and have small internal diameters to increase light penetration. An air pump or airlift system is employed for mixing and agitation of the culture. They can be horizontal, vertical, inclined or conical tubular photo-bioreactors (Figure 4). Large illumination area makes them a good candidate for algal culture. However they have some limitations during scale-up. Mass transfer (oxygen build-up) and photo-inhibition becomes a major problem when we go for scale- up. Also, scale-up is done by increasing the diameter of the tubes, thus the cells at the lower part of the tube does not receive enough solar energy required for growth [41].

It is also difficult to control the temperature in the tubular bioreactors, though thermostat or cooling tubes can be used but it is expensive and difficult to implement. In long tubular photobioreactors, gradients of oxygen are formed and CO_2 transfer along the tubes takes place. In HTB increase in pH of the cultures occurs which require frequent re-carbonation of the cultures, which would add to the cost of algal production. HTB also require large land space. But HTB have large illumination surface area and hence suitable for outdoor cultures. They also show fairly good biomass productivities and hence are relatively cheap [46,47]. Helical tubular bioreactor made up of teflon or low density polyethylene named 'Biocoil' was designed in UK and tested successfully at pilot scale (2000 L) for growth of various algae [48].

Of course PBRs have several advantages over open ponds as a cultivation system. However, an open pond is considerably cheaper. The total cost can be analyzed as infrastructure costs (CapEx), maintenance costs and operational costs (OpEx). All these factors favor open ponds. The installation and maintenance costs of PBRs may prove prohibitive for the production of low cost compounds, but acceptable for the nutraceutical industry. Production of compounds such as Carotenoids and some poly-unsaturated fatty acids (PUFAs), such as omega-3 and linoleic acid in a microalgal system, justifies the use of PBRs.

Different PBR designs are being tested and some studies have shown promising results using systems requiring only relatively simple operation and maintenance. Using innovative 110 L flat green wall photobioreactors, a production of 204 mg L^{-1} d^{-1} was reached [14]. Thus, open ponds offer a cheaper operation, but at the expense of productivity. Long term studies with outdoor open ponds have reported productivities ranging from 20 to 50 mg $L^{-1}d^{-1}$ [49,50].

'Big-Bag' systems

Probably the longest used closed culture systems for mass culture of microalgae are the 'big-bag' systems generally used in aquaculture butcheries to feed larval fish, crustaceans, mollusks or rotifers. Although widely used these systems are notorious for the instability of the culture. This instability probably occurs because mixing in these bags is uneven, leading to the build- up of the cells in unmixed areas, which in turn leads to the cell death, especially if the culture is not axenic (bacteria free). To achieve reasonably reliable cultures, it is essential to maintain axenic conditions, a feature that is not essential for the tubular photobioreactors [51].

In recent years, new technological breakthroughs led to designing of unique type of bioreactors. The green solar collector (GSC) uses Fresnel lenses that distribute and focus light efficiently inside a bioreactor [52] (Figure 4). Valcent's HDVB (high density vertical bioreactor) system is a closed circuit process and hence requires little water. Algal growth is precisely controlled by fluid mechanics, gas-liquid mass transfer, and culture is mixed using an airlift pump [53]. Colorado based Solix have develop a clear flat plate photoreactor that utilize the smokestack exhaust from power plant as carbon dioxide source, hence cutting the 90-95% production cost of algal culture [54].

CO_2 enrichment: One approach for raising productivity is CO_2 enrichment. To ensure CO_2 fixation, the carbon concentration mechanisms (CCM), helps the cell locally increases the CO_2

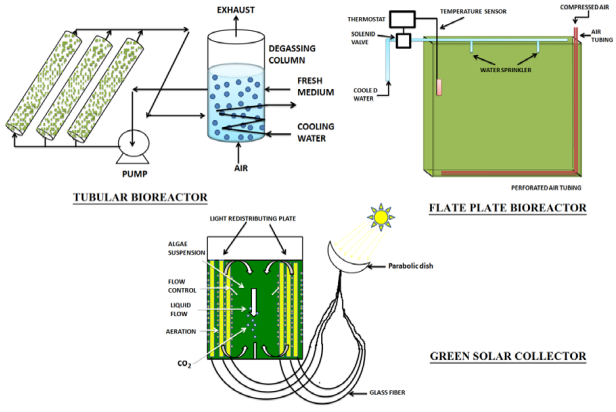

Figure 4: Schematic diagram of closed type systems (bioreactors) for algae culture.

concentration around the Rubisco enzyme to ensure its functioning [36]. This mechanism is wide spread amongst the algae and illustrates the advantages of raising the CO_2 concentration in mass cultures. Indeed, sparging CO_2 into the culture medium is known to increase its cellular concentration and two different approaches are frequently reported, the use of CO_2 to adjust the pH, and CO_2 enrichment as a way to mitigate flue gases [14,55-57]. Of course any feedstock used in large scale production will play an important role on the final price and CO_2 is not an exception. Thus, this type production should optimally be coupled to a bioremediation process.

Moreover, microalgae can effectively convert solar energy into a variety of valuable end products, such as biofuels, food additives, and compounds used in cosmetics and pharmaceuticals [58]. For example, *S.obliquus* [59], *C. vulgaris* [60], and *Chlamydomonas* sp. [61], exhibit both a high CO_2 fixation rate and high lipid/carbohydrate content. Thus, combining microalgae-based CO_2 fixation with biofuel production or bio-based chemical production seems to have a high potential for reducing the level of atmospheric CO_2 while simultaneously producing biofuels or valuable chemicals.

Offshore culture of macroalgae

Macroalgae are long multi-cellular algae (measure in inches/feet) often grown in open ponds and oceans (as seaweed e.g. giant kelp plant). Macroalgae can be grown in offshore systems (i.e. algae culture in the open ocean). Macroalgae hold promise as a raw material for fuel because they produce more biomass per unit area per year. The main species relevant to biofuel production are chlorophyta (genus-Ulva and Caulerpa), red algae (Gigartinales, Halymeniales and Palmariales) and brown algae (order of Fucales, Laminariales and Tilopteridales) [62]. They can be grown on sewage, municipal waste water or agriculture or farm runoff water. In Florida scientist created algal turf scrubber (ATS) in shallow canals having nylon netting on which filamentous algae can form colonies. Studies on algal turf scrubber (ATS) has revealed that the algae can capture around 60-90% of N(nitrogen) and 70--100% of K(potassium) from manure effluents runoff water thus reducing eutrophication of water bodies. On harvesting, the macroalgae can be used as an organic fertilizer [63].

Harvesting and processing of algae

After culturing in open or closed systems, the algal biomass needs to be harvested for further processing. However, harvesting microalgal cells is quite challenging. The microalgae cannot be easily harvested as macroscopic plants, and thus the consequent oil extraction is more complicated. Moreover, algal cultures are very dilute, usually around 1% for autotrophic growth up to 10% for heterotrophic growth [64-65], thus making dewatering a necessary step prior to biomass use. In algae harvesting, dewatering is most capital and energy intensive (-30% of total cost) step. Harvesting from bioreactor is less expensive as compared to open pond system because the biomass productivity can on average be 13 times more than the open pond [34]. In open culture the biomass yield is around 0.5-1.0 gL^{-1}, while in closed system it reach around 5-10 gL^{-1}. Gravity settlement, filtration and centrifugation are the commonly used harvesting method [34]. At times flocculation step or flocculation-flotation is added to aid the harvesting. The choice of harvesting technique is governed by microalgal species used and final product. Uduman et al. summarized the different harvesting techniques used in algae biomass recovery (Figure 5) and concluded that centrifugation is most efficient recovery technique though the cost is high [66]. Many standard techniques have been evaluated for use in mass algal cultivation and their limitations are reviewed in detail elsewhere [33,58,67,68]. The choice of harvest method vary depending on the ultimate use of the biomass like Nutraceutical products require physical processes for harvesting, thus avoiding chemical contamination, and maintaining the product's natural characteristics. As a result the high value of the product gets compensated for the high cost and energy intensity of the method.

Filtration under vacuum can enhance the biomass recovery but they were relatively slower. Alternatively, ultra-filtration results in good recovery, however they require high energy input and filter clogging is frequent making it unsuitable for large scale processes. Mata et al. made use of simple large unit micro strainers as an attractive alternate harvesting strategy [67]. Israel based Algatech Ltd. developed zero energy requiring harvesting step based on sedimentation for *Haematococcus* (efficiency>90%). In recent years, electrocoagulation-electroflotation and ElectroCoagulation (EC) are emerging as cost effective and efficient harvesting systems and have been used for harvesting of *Chlorella vulgaris*, *Phaeodactylum tricornutum* and *Nannochloropsis* sp. with good quality biomass [69-71].

Microalgal harvesting cost can be reduced by harvesting cells by flocculation. In alkaline flocculation, flocculants counterbalance the repelling surface charges on the cells hence cause the algal cells to coalesce to form floc. In such method the flocculant needed in a linear stoichiometeric fashion hence making process very expensive. Schlesinger et al. reported that major hurdle to bulk algal production and harvesting can be tackled by non-toxic inexpensive alkaline flocculation. It is observed that the flocculent amount is governed by a function of logarithm of cell density and in dense cultures like biodigestable sludge, it should reduce the cost of the flocculation below $1.00 per 1000 kg of algal biomass [72].

Strain selection, culturing and harvesting

With existing technology, it is obvious photobioreactors are simply too expensive and for a low value product such as a biofuel open ponds must be used. A simple calculation based on possible solar energy inputs and maximum photosynthetic conversion efficiencies shows that the resulting energy value per square meter allows very little capital expenditure for cultivation facilities. Therefore, although specific laboratory strains have shown to produce high levels of lipids, i.e. *Botryococcos braunii*, but they cannot be used in practice in an open system as there are chances of overrun by indigenous species. Cost effective harvesting is of course a major unsolved challenge, and several

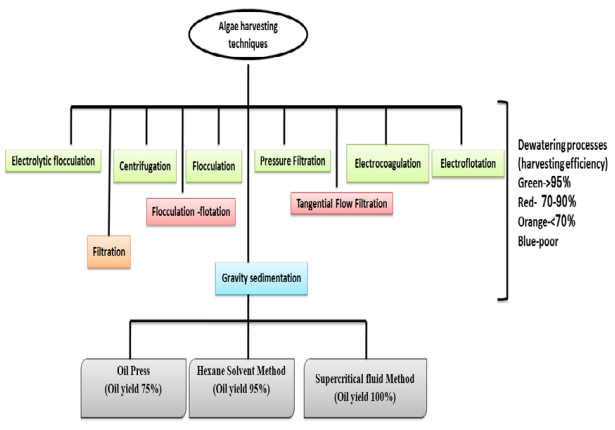

Figure 5: General schema of microalgae harvesting and oil extraction strategies.

new advances have already been discussed in the manuscript [36].

Biofilms

A very little research has gone into to study species that readily form biofilms for biofuels production due to difficulty in maintaining their homogenous suspension cultivation medium. However, several recent studies, with two different systems, have shown that this kind of growth mode can offer the ease of simple mechanical harvesting, leading to slurries with a dry weight content of 9-16%. In one case, algae were grown on a rotating drum imitating an open pond system where harvesting was achieved by simply unspooling and scraping the cotton rope fiber that was used [73]. Another approach, a flat surface which was drip-watered was used to grow algae and were recovered by simple mechanical scraping at the end of growth period. In both cases, not only harvesting method was simplified but the researchers were also able to achieve high rates of biomass production at respectable light conversion efficiencies.

Pretreatment strategy

Microalgal pretreatment is prerequisite for separation of its different useful components, which are further processed to different types of biofuel. Carbohydrate of algal biomass is converted either to ethanol or biogas using fermentation. The biomass is processed in three sequential steps-hydrolysis, acidification and energy generation. Out of these steps hydrolysis is often observed as a rate limiting step. The rigid cell wall and membrane make them resistant to biodegradation or show slower biodegradation during fermentation. For algal oil harvesting expellers/presses, solvent extraction and supercritical CO_2 are conventionally used. For algae having high oil content expeller/pressers are used which mechanically rupture the algal cell (70-75% recovery) [74].

In solvent extraction benzene, ether and hexane are employed to degrade cell walls. Using distillation, oil is recovered from the solvent and this step can be coupled to expellers step for efficient recovery of the oil from biomass (~95%). Supercritical CO_2 penetrated algal cells at high temperature and pressure and cause its rupture (~100%). Supercritical CO_2 treatment are costly, energy intensive, highly sensitive and involves risk due to high pressure requirement [75].

Numerous studies on pretreatment are undertaken including ultrasonication, bead beating, thermochemical, osmotic shock, nano dispersion, enzymatic and microwave treatment [76,77]. Ultrasonication does not require high temperature (like autoclaving and microwave) and expensive chemicals and is therefore most economical [78]. Cell disruption in ultrasonication is achieved either by microbubble cavitation or acoustic streaming [79]. Choi et al. reported enhanced microalgal cell wall disintegration which resulted into increased ethanol and hydrogen production [80]. Grinding of algal biomass resulted in doubling of yield of algal fatty acids extraction. Nano dispersion of crude algal biomass resulted in 62% enhanced yield of total extracted fatty acids [76]. Bremauntz et al. reported that osmotic shock (0.1 M NaCl) pretreatment for 24 h resulted in approx. 30 times increase in fermentable sugar in the *Scenedesmus sp.* Strain [81]. In case of *Botryococcus braunii* osmotic pretreatment enhanced the recovery rate of hydrocarbon >90% than that of untreated sample [48]. Passos et al. investigated the microwave pretreatment on biogas production using microalgae and concluded that microwave pretreatment improved the dissolution and digestibility of microalgae [82]. In enzymatic pretreatment cellulases and lipases are generally used. Enhanced biogas production was achieved when *Botryococcus braunii* and *Nannochloropsis gaditana* were pretreated with bacterial strains having endoglucanase/amylase and cellulase activity [83].

Origin Oil Inc. reported (2010) first single-step extraction of algal oil technology, by using quantum fracturing in combination with electromagnetism and pH modification. After cell rupture algae oil rise and float on the top and removed for skimming and refining. The degraded biomass settles to the bottom of the extraction tank. In this technology, CO_2 injection are used to lowers pH and quantum fracturing cause mechanically distresses in algae cells. Fine-tuned electromagnetic field is then used simultaneously to rupture algae cells. This breakthrough technology can be fine-tuned for range of feedstock and it may result in highly scalable, cost effective oil harvesting system for biofuel generation. Origin Oil Inc. has also innovated and scaled up (up to 200 gallon tank) a technology known as "Live Extraction", where oil is harvested from electrically stimulated live algae continuously [84].

Ames Lab of US Department of Energy also develop a process based on nanospheres for extracting the fuel relevant chemicals Ames lab program director Victor Lin in collaboration with Catilin Inc. and Iowa State University-Center for Catalysis have developed mesoporous nanoparticles which can selectively extract fuel-relevant chemicals from the algal lipid without killing them. These compounds (free fatty acids (FFA) and triglycerides) are converted to biodiesel using commercial T300 catalyst of Catilin. Cavitation Technologies Inc. (CTI) used nanoreactor to create cavitation bubbles in a solvent material and collapse of these bubbles near algal cell wall forms shock waves and liquid jets that results in the cell wall breakage and ultimately cause the contents release into the solvent [85].

Upgrading technology

After harvesting, pretreatment and separation of components, each is converted to suitable bioenergy forms like biodiesel, biogasoline, ethanol, butanol, biohydrogen etc. [86]. PNNL (Pacific Northwest National Laboratory) researchers have developed continuous chemical processes which produce crude oil in less than an hour, and Utah-based Genifuel Corp. got the license for the technology and building pilot plant based on PNNL process. In Brazil, Solazyme Bunge ProdutosRanovaveis Ltd. developed microbial dark fermentation based commercial close bioreactor based plant for conversion of cane sugar to 'tailored oil'. Solazyme in partnership with Chevron has been awarded a grant of $21.8 m from DoE for development of algalfuel demonstration plant for US Navy trails. Soladiesel™ emerged as a superior to ASTM D6751 forjet fuel, D-975 and military specification and clean diesel technology [87].

After oil extraction, the green crude is further subjected to trans-esterification reaction. The green crude is mixed with sodium hydroxide (which act as a catalyst) and alcohol and results in fatty acid methyl esters (FAMEs/biodiesel) and glycerol. The mixture is processed using hydrocracking and hydrogenation and glycerol (by-product) is removed and pure algal biodiesel is harvested and termed as 'Green diesel'.

In recent years hydothermal liquefaction (HTL) has replaced the conventional transesterification method for the production of biodiesel. In this process, elevated temperatures (250-250°C) and pressures (10-20 Mpa) are applied to high moisture algal biomass to break down and reform the chemical molecules into green-crude oil. At such high temperatures and pressure, water acts as a highly reactive medium and promotes the breakdown of chemical bonds, leading to reformation of biomolecules, thus mimicking the natural geological process which produces our current fossil fuels. These conditions make

HTL well suited for the conversion of a wider range of feed stocks like low lipid algae, fast-growing algae that proliferate in wastewater treatment facilities, swine manure, garbage and sewage waste. Thus aiding in reducing environmental pollution, producing bioenergy and preserving valuable water resources. The resulting green-crude oil can have combustion value comparable to crude oil, depending upon the feedstock. It can be further burned in boilers or upgraded to higher value fuel [88,89].

Algal biomass can be converted to variety of fuels using ABE (acetone, butane, and ethanol) Process of Charles Weizmann [90]. In this process the sterilized biomass is fermented with *Clostridium acetobutylicum* at 35-36°C for 58 hours. Fermentation starts after 5-10 hours of lag phase and completes in 48 h, after which mixture is fractal distillated to separate each component. Biobutanol is less energy dense (10%) than gasoline (energy value 114, 000 BTU/Gal) and has higher energy value (110,000 BTU/Gal) as compared ethanol (76,100 BTU/Gal) or methanol (Green Biologics, Website). In most engines, butanol can be used as alternate to gasoline and does not require any modification. It can be blend with gasoline (at 20%), diesel (at 40%) and result in better performance and provide resistance to corrosion than E85 [91]. Bioethanol is another alcohol based biofuel and a Florida based company Algenol developed a breakthrough DIRECT TO ETHANOL® technology which utilize sunlight, algae, non-arable land/ sea water and carbon dioxide/industrial exhaust to produce ethanol and algal biomass. *Porphyridium cruentum* accumulates higher amount of carbohydrates hence have potential as a suitable raw material for ethanol production [92].

Artificial light can be provided by any regular light source such as tungsten or fluorescent bulbs. Low heat generation, the specificity of the wavelength of emitted light, low power consumption and, allowing the restriction of light to photosynthetic active radiation, the influence of different wavelengths and intensities on these microorganisms has led to the use of LEDs. A recent study showed that different wavelengths may have a significant influence on biomass and lipid productivity, as well as on the lipid profile. A strain of *Nannochloropsis* showed a higher growth rate, lipid productivity and different lipid profile under blue light (470 nm) when compared with growth under red (680 nm) or green (550 nm) [93].

Bio-gasoline is produced by directly converting sugar into gasoline using APR (aqueous phase reforming) technique. The carbohydrate solution containing alcohol, glycerol, cellulosic sugar, starch, liquid phase reforming single reactor system at sugar alcohol is fed into temperature of 453.15-538.15 K and 6,800,000 Pa pressure and converted to mixture of oxygenated hydrocarbons, which is further processed using conventional chemical processing to non-oxygenated hydrocarbons. Biogasoline (BG100/100% bio-gasoline) resembles gasoline in its components usually containing hexane and dodecane atoms per molecule and hence can be used as a substitute to gasoline in internal-combustion engines [94]. Owing to its chemical similarity, it can blended with regular gasoline. Though small percentage of octane booster is required by bio-gasoline to match conventional gasoline. In the year 2010, the first bio-gasoline demonstration plant was set up in Madison, WI by Virent Energy Systems, Inc.

Methane is another biofuel that can be produced using algal biomass. Commercial production by either by gasification production of methane is achieved, pyrolysis under high temperature and pressure or by anaerobic digestion.

Economical aspect

The estimation of economic viability of algae based biofuel is a daunting task, primarily because commercial production of algae for bioenergy is not fully explored yet. Secondly the other algal products tend to have a ten times greater value than biofuel (Figure 6). The production system needs to be subjected to a detailed LCA (life cycle assessment), to determine possible environmental impacts, NER (net energy ratio), and an economic analysis before going on for large scale microalgal biofuels production. However, to do this in a meaningful way requires specific inputs on system components, and since many of the outstanding questions raised here; cultivation method (open ponds versus photobioreactors), harvesting technologies, and even extraction and transesterification reactions, remain to be answered, this cannot really be done in a meaningful way at present. An economic analysis which compares the price at the pump of a biofuel with that of a fossil fuel is in fact wrong. A metaeconomic analysis for biofuels is one that takes into consideration indirect costs associated with fossil fuel production and use. A quick overview suggests that there are in fact many hidden costs to fossil fuel use and that the "real" cost of gasoline or diesel is significantly higher than the price paid by the consumer at the pump.

One way to estimate the damage is to look at the cost of adapting to climate change, although this does not provide the actual full costs incurred since this represents less than full mitigation. An initial international study estimated these costs at $49 to 171 billion (USD) per year (UNFCCC, 2007) and it has been argued that this is in fact an underestimate [94]. Of course, these estimates are highly dependent on the accumulated of atmospheric CO_2 burden over time as well as a great deal of uncertainty as to actual impacts. Thus, determining what the competitive cost of a biofuel really should be will require detailed economic analysis. In addition, as mentioned above, detailed costing is not possible given the many uncertainties in the design specifics of a practical algal biodiesel plant. Thus, a realistic cost analysis is impossible at present.

The commercial importance of Microalgae is an untapped resource. Thus production of biogas, biodiesel and other co-products (viz. beta-carotene, PUFA, biofertilizers, among others) can be more environments sustainable and profitable if complemented with wastewater and flue gas treatment. Moreover, Microalgae biomass is also marketed in tablet or powder formulations to be used as food additives in the health food market (e.g. *Arthrospira, Chlorella*, etc.). Algal biomass is also used for preparation of animal feed supplements

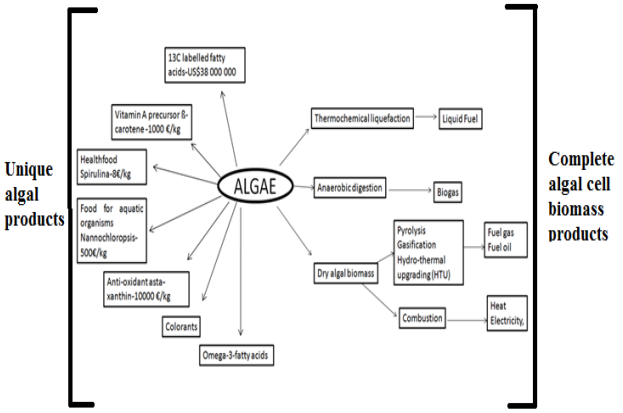

Figure 6: Algal cell biomass products/uses.

and aqua culturing (e.g. Fish feed). Economic viability of commercial algal biofuel production can be achieved if beside fuels rest of high value added products are co-produced via using an integrated biorefinery [95,96].

The capital investment in culturing microalgae and algal oil production costs range from \$10.87 gallon^{-1} to \$13.32 gallon^{-1} [97]. So culturing algae for bioenergy or biofuel production must be clubbed with some high value co-products to make process more economically viable. Researchers are exploring new opportunities in culturing algae in low economic value (e.g. waste land or waste streams) which does not require stringent condition (and capital) and can be used as efficient system to treat waste streams and also decrease greenhouse gas emission.

Using conventional method energy cost per kg of crude oil is estimated to be 1.24 \$/kg while due to single step extraction strategy developed by Origin Oil the energy cost per kg of crude oil dropped to 16.4% of the original cost (0.20 \$/kg).

Challenges

Despite of technological advancements, commercial production of algal biofuel is still too costly because of following factors: cultivation system design requires temperature and growth limiting condition control (CO_2, H_2O sources, energy, nitrogen and phosphorous, sitting and resources) which adds to the cost of production and invasion, instability and fouling of culture results in lower yield of biomass. Algal growth in culture is dilute and therefore requires dewatering before further processing, which is currently an energy intensive and expensive step. After harvesting, algal biomass is processed to carbohydrate (bio-ethanol), lipid (gasoline, biodiesel, jet fuel) and protein (power generation) fractions. Fractionation, extraction technologies and product purification steps used in processing are required to be improved in terms of price, energy input, and scalability.

Biodiesel pose major challenge in terms of cold weather operation and stability. Other challenges are fuel's compatibility with current automobile engine or infrastructure, market share and pricing and co-products market demand. Space management for biomass, fuels, and products handling and storage is an overwhelming issue. Government and industry regulations and standards should be met in terms of GHG emission and pricing.

Current status of microalgae bioenergy in some countries

In November 2006, the U.S. Green Energy Technology Company and Arizona Public Service Company co-operated in November 2006 for the establishment of a microalgae production system in Arizona State. It connected flue gas which contains CO_2 to culture microalgae in a large-scale and finally convert it to biofuel. The yield of biofuel reached 5,000-10,000 gallon per acre per year [98]. In 2010, \$ 6 million funds were allocated to the Arizona State University by the Department of Energy in the U.S. to establish Sustainable Algal Biofuel Consortium (SABC). The U.S. government financially supported many other projects like creating Algae Biofuel Commercialization Consortium (CABC) and Cellana LLC consortium of Kailua-Kona and Hawaii [98].

Countries other than U.S have also started paying attention to microalgae bioenergy development. Chinese Academy of Sciences has successfully developed a large "S" shaped pipe of closed photo biological reactor. Shandong University of Science and Technology, China in 2008 used the thermal power plant and chemical plant flue gas to supply microalgae cultivation CO_2 in the tower dimensional cultivation reactor and finally culture microalgae were used for producing bio-oil. The new Austrian technology company is brewing a huge plan. They invested to microalgae ecological base in the Daqi of Inner Mongolia. 280 hectares of microalgae base has been completed in 2013. Microalgae ecological base will be officially reached industrialization in 2014 [99].

In 2007, Umeå Energi was set to build an algae production plant in the north part of Sweden, headed by Swedish University of Agricultural Science, and the development funding from Umeå Energi, Umeva AB, Ragn-Sells AB and Energi myndigheten. The wastewater reclamation of algae production process, valuable algae biomass production, and CO_2 sequestration from flue gas are the focusing areas under this project [100]. In September 6, 2011, the EU has launched the Algae Development Project (EnAlgae) which focused on the growth and yield information of microalgae and giant algae growing in the North Western Europe.

Conclusion

Microalgae emerged as an ideal bio renewable resource for biofuel production that eventually could replace petroleum-based fuel. Currently, algal based biofuel production is not commercially viable due to the capital intensive bioreactor and post harvesting steps and variable biomass productivity. The algal biofuel production can be economical either by integrated bio refining of high value products or by enhancing biomass/oil productivity by recombinant DNA technology, algal biology and engineering culture system. It is important to develop engineering strategies and optimize them to significantly improve feasibility of microalgae-based biofuel. Other than biofuel, algae find wide applications in various domains e.g. algal biomass after removal of oil can be used as nutrient rich fertilizer (e.g. ATS). It can be used in wastewater-treatment facilities to clean and purify water with little amount of chemicals. Algae can be used as a pollution control agent as they metabolize CO_2 and release oxygen, hence reduces carbon emissions significantly.

References

1. IEEE-Today`s Engineer USA, http://www.todaysengineer.org/2011/Jul/biofuel.asp.
2. Edwards R, Heinz H, larivé JF, Lonza L, Maas H, et al. (2007) "Well-to-Wheels analysis of future automotive fuels and powertrains in the European context". Joint Research Centre (European Commission), EUCAR & CONCAWE.
3. European Environment Agency (2006) Transport and environment facing a dilemma: TERM 2005: indicators tracking transport and environment in the European Union). Copenhagen: European Environment Agency; Luxembourg: Office for Official Publications of the European Communities. ISBN 92-9167-811-2. ISSN 1725-9177.
4. Mortimer ND, Cormack P, Elsayed MA, Horne RE (2003). "Evaluation of the comparative energy, global warming and socio-economic costs and benefits of biodiesel". Sheffield Hallam University. UK Department for Environment, Food and Rural Affairs (DEFRA).
5. Scott EL, Kootstra AMJ, Sanders JPM (2010) Perspectives on bioenergy and biofuels. Sustainable Biotechnology. 179-194.
6. Coyle WT (2010) Next generation Biofuels: Near Term Challenges and implications for Agriculture Economic Research Service. USDA. (BIO-01-01) 26 pp.
7. Lane, Jim (2009) "VC investment in US biofuels reaches \$680.2 million in 2008: a Biofuels Digest special report," Biofuels Digest.
8. Johnston M, Foley JA, Holloway T, Kucharik C, Monfreda C (2009) Resetting global expectations from agriculturalbiofuels. Environmental Research Letters 4.
9. Hamelinck C, Faaij APC (2006) Outlook for advanced biofuels. Energy Policy 34: 3268-3283.

10. Deng MD, Coleman JR (1999) Ethanol synthesis by genetic engineering in cyanobacteria. Applied and Environmental Microbiology 65: 523-528.

11. http://www.algenolbiofuels.com/

12. Dickson AG, Goyet C (2014) Handbook of methods for the analysis of the various parameters of the carbon dioxide system in sea water 197

13. Sheehan J, Dunahay T, Benemann J, Roessler P (1998) A Look Back at the U.S. Department of Energy's Aquatic Species Program-Biodiesel from Algae. Close-out Report. NREL/TP-580-24190: 295.

14. Rodolfi L, ChiniZittelli G, Bassi N, Tredici MR et al. (2009) Microalgae for oil: strain selection, induction of lipid synthesis andoutdoor mass cultivation in a low-cost photobioreactor. Biotechnology and Bioengineering. 102: 100-112.

15. Metting FB (1996) Biodiversity and application of microalgae. Journal of Industrial Microbiology. 17: 477-489.

16. Spolaore P, Cassan JC, Duran E, Isambert A (2006) Commercial applications of microalgae. Journal of Bioscience and Bioengineering. 101: 87-96.

17. Banerjee A, Sharma R, Chisti Y, Banerjee UC (2002) Botryococcus braunii: a renewable source of hydrocarbons and other chemicals. Crit Rev Biotechnol. 22: 245-279.

18. Metzger P, Largeau C (2005) *Botryococcus braunii:* a rich source for hydrocarbons and related ether lipids. Appl Microbiol Biotechnol 66: 486-496.

19. Wijffels RH, Barbosa MJ (2010*)* An outlook on microalgal biofuels. Science 329: 796-799.

20. Rao AR, Ravishankar GA (2007) Influence of CO_2 on growth and hydrocarbon production in *Botryococcus braunii.* Journal of Microbiology and Biotechnology. 17: 414-419.

21. Hillen LW, Pollard G, Wake LV, White N (1982) Hydrocracking of the oils of *Botryococcus braunii* to transport fuels. Biotechnology and Bioengineering 24: 193-205.

22. Qin J (2005) Bio-Hydrocarbons from Algae-Impacts of Temperature, Light and Salinity on Algae Growth. Rural Industries Research and Development, Barton, Australia.

23. Kapdan IK, Kargi F (2006) Bio-hydrogen production from waste materials. Enzyme and Microbial Technology 38: 569-582.

24. Rupprecht J, Hankamer B, Mussgnug JH, Ananyev G, Dismukes C, et al. (2006) Perspectives and advances of biological H_2 production in microorganisms. Appl Microbiol Biotechnol 72: 442-449.

25. Gaffron H, Rubin J (1942) Fermentative and photochemical production of hydrogen in algae. Journal of General Physiology 26: 219-240.

26. Bala K, Murugesan AG (2011) Biological hydrogen production by the algal biomass *Chlorella vulgaris* MSU 01 strain isolated from pond sediment. Bioresource Technology 102: 194-199.

27. Benemann JR, Weare NM (1974) Hydrogen evolution by nitrogen-fixing Anabaena cylindrica cultures. Science 184: 174-175.

28. Wykoff DD, Davies JP, Melis A, Grossman AR (1998) The regulation of photosynthetic electron-transport during nutrient deprivation in *Chlamydomonas reinhardtii.* Plant Physiology 117: 129-139.

29. Melis A (2007) Photosynthetic H_2 metabolism in *Chlamydomonas reinhardtii* (unicellular green algae) Planta. 226: 1075-1086.

30. Grow Energy, CA, USA Press release http://www.growenergy.org/downloads/Hydral- Press022813.pdf

31. E.on Press release http://www.eon.com/en/media/news/press-releases/2013/8/28/eon- inaugurates-power-to-gas-unit-in-falkenhagen-in-eastern-germany.html.

32. Grobbelaar JU (2004) Algal nutrition. In: Richmond A (ed.) Handbook of Microalgal Culture: Biotechnology and Applied Phycology. Blackwell Publishing, Ames, Iowa, pp. 97-115.

33. Grima M, Fernandez FA, Camacho FG, Chisti Y (1999) Photobioreactors: Light regime, mass transfer, and scale up. Journal of Biotechnology 70: 231-247.

34. Chisti Y (2007) Biodiesel from microalgae. BiotechnologyAdvances 25: 294-306.

35. Jorquera O, Kiperstok A, Sales EA, Embiruçu M, Ghirardi ML (2010) Comparative energy life-cycle analyses of microalgal biomass production in open ponds and photobioreactors. Bioresource Technology 10: 1406-1413.

36. Leite GB, Ahmed EM, Abdelaziz, Hellenbeck PC (2013) Algal biofuels: Challenges and opportunities. Bioresour Technol 145:134-141.

37. Carlsson ASV, Beilen JB, Möller R, Clayton D (2007) Micro- and macroalgae utility for industrial applications. Outputs from the EPOBIO project. D. Bowles. York, UK.

38. Pulz O (2001) Photobioreactors: Production systems for phototrophic microorganisms. Applied Microbiology and Biotechnology 57: 287-293.

39. Tredici MR (2010) Photobiology of microalgae mass cultures: understanding the tools for the next green revolution. Biofuels 1: 143-162.

40. Carvalho AP, Meireles LA, Malcata FX (2006) Microalgal reactors: A review of enclosed system designs and performances. Biotechnology Progress 22: 1490-1506.

41. Miro´n AS, Go´mez AC, Camacho FM, Molina GE, Chisti Y(1999) Comparative evaluation of compact photobioreactors forlarge-scale monoculture of microalgae. Journal of Biotechnology 70: 249-270.

42. Miro´n AS, Camacho FG, Go´mez AC, Molina GE, Chisti Y (2000) Bubble Column and Airlift Photobioreactors for Algal Culture. AIChE Journal 46: 1872-1887.

43. Pandey A, Lee DJ, Chisti Y, Soccol CR (2014) Biofuels from algae, Elsevier: Chapter 2.

44. Loubière K, Olivo E, Bougaran G, Pruvost J, Robert R, et al. (2009) A new photobioreactor for continuous microalgal production in hatcheries based in external-loop airlift and swirling flow. Bioengineering Biotechnology 102: 132-147.

45. Slegers PM, Wijffels RH, Straten GV, Boxtel AJB (2011) Design scenarios for flat panel photobioreactors. Journal of Applied Energy 88: 3342- 3353.

46. Oilgaehttp://www.oilgae.com/algae/cult/pbr/typ/flp/flp.html

47. Slegers PM, Beveren PJM, Wijffels RH, Straten, G, Boxtel AJB (2013) Scenario analysis of large scale algae production in tubular photobioreactors. Journal of Applied Energy 105: 395-406.

48. Borowitzka MA (1999) Commercial production of microalgae: ponds, tanks, tubes and fermenters. Journal of Biotechnology 70: 313-321.

49. Das P, Aziz SS, Obbard JP (2011a) Two phase microalgae growth in the open system for enhanced lipid productivity. Renew Energy 36: 2524-2528.

50. Moazami N, Ashori A, Ranjbar R, Tangestani M, Eghtesadi R, et al. (2012) Large-scale biodiesel production using microalgae biomass of *Nannochloropsis*. Biombioe 39: 449-453.

51. Paul NA, Tseng CK, Borowitzka M (2013) Seaweed and Microalgae. In: John SL, Paul CS (eds.) Aquaculture: Farming Aquatic Animals and Plants 2: 268-299.

52. Zijffers JWF, Salim S, Janssen M, Tramper J, Wijffels RH (2008) Capturing sunlight into a photobioreactor: Ray tracing simulations of the propagation of light from capture to distribution into the reactor. Chemical Engineering Journal 145: 316-327.

53. Molina GE, Ace's Ferna´ndez FG, Camacho FG, Rubio FC, Chisti Y (2001) Scale-up of tubular photobioreactors. Journal ofApplied Phycology 12:355-368.

54. Article by Michael Kanellos (2008) http://www.greentechmedia.com/articles/read/can-solix-cut-the-cost-of- making-algae-by-90-5247.

55. Grobbelaar JU (2000) Physiological and technological considerations for optimizing mass algal cultures. J Appl Phycol 12: 201-206.

56. Yoo C, Jun SY, Lee JY, Ahn CY, Oh HM (2010) Selection of microalgae for lipid production under high levels carbon dioxide. Bioresour Technol 101: S71- S74.

57. McGinn PJ, Dickinson KE, Bhatti S, Frigon JC, Guiot SR, et al. (2011) Integration of microalgae cultivation with industrial waste remediation for biofuel and bioenergy production: opportunities and limitations. Photosynth Res 109: 231-247.

58. Yen HW, Hu IC, Chen CY, Ho SH, Lee DJ, et al. (2013) Microalgae-based biorefinery from biofuels to natural products. Bioresour Technol 135: 166-174.

59. Ho SH, Chen CY, Chang JS (2012) Effect of light intensity and nitrogen starvation on CO_2 fixation and lipid/carbohydrate production of an indigenous microalga *Scenedesmus obliquus* CNW-N. Bioresour Technol 113: 244-252.

60. Ho SH, Huang SW, Chen CY, Hasunuma T, Kondo A, et al. (2013) Characterization and optimization of carbohydrate production from an indigenous microalga *Chlorella vulgaris* FSP-E. Bioresour Technol 135: 157-165.

61. Nakanishi A, Aikawa S, Ho SH, Chen CY, Chang JS, et al. (2014) Development of lipid productivities under different CO_2 conditions of marine microalgae *Chlamydomonas* sp. JSC4. Bioresour Technol 152: 247-252.

62. Garofalo R (2009) Algae and aquatic biomass for a sustainable production of 2nd generation biofuels. AquaFUELs-Taxonomy. Biology and Biotechnology 1-258.

63. Thomas D (2002) Seaweeds. The Natural History Museum, London.

64. Wu Z, Shi X (2007) Optimization for high-density cultivation of heterotrophic Chlorella based on a hybrid neural network model. Lett Appl Microbiol 44: 13-18.

65. Gouveia L, Oliveira AC (2008) Microalgae as a raw material for biofuels production. J Ind Microbiol Biotechnol 36: 269-274.

66. Uduman N, Qi Y, Danquah MK, Forde GM, Hoadley A (2010) Dewatering of microalgal cultures: A major bottleneck to algae-based fuels. Journal of Renewable and Sustainable Energy 2: 012701.

67. Mata TM, Martins AA, Caetano NS (2010) Microalgae for biodiesel production and other applications: A review. Renewable and Sustainable Energy Reviews 14: 217-232.

68. Zhu L, Ketola T (2012) Microalgae production as a biofuel feedstock: risks and challenges. Int. J. Sust. Dev. World Ecol. 19: 268-274.

69. Tumsri K, Chavalparit O (2011) Optimizing Electrocoagulation-electroflotation Process for Algae Removal. 2nd International Conference on Environmental Science and Technology IPCBEE vol.6 (2011) © (2011) IACSIT Press, Singapore.

70. Vandamme D, Pontes SCV, Goiris K, Foubert I, Pinoy LJJ, et al.(2011) Evaluation of electro-coagulation-flocculation for harvesting marine and fresh water microalgae. Biotechnol Bioeng 108: 2320-2329.

71. Matos CT, Santos M, Nobre BP, Gouveia L (2013) Nannochloropsis sp. biomass recovery by Electro-Coagulation for biodiesel and pigment production. Bioresource Technology 134: 219-226.

72. Schlesinger A, Eisenstadt D, Bar-Gil A, Carmely H, Einbinder S, et al. (2012) Inexpensive non-toxic flocculation of microalgae contradicts theories; overcoming a major hurdle to bulk algal production. Biotechnology Advances 30: 1023-1030.

73. Christenson LB, Sims RC (2012) Rotating algal biofilm reactor and spool harvester for wastewater treatment with biofuels by-products. Biotechnol. Bioeng 109:1674-1684.

74. Topare NS, Renge VC, Khedkar SV, Chavan YP, Bhagat SL (2011) Biodiesel from Algae Oil as an Alternative Fuel for Diesel Engine. Pharmaceutical Research 2: 116-120.

75. Santana A, Jesus S, Larrayoz Filho RM (2012) Supercritical Carbon Dioxide Extraction of Algal Lipids for the Biodiesel Production. Procedia Engineering 42: 1755-1761.

76. Li Y, Min M, Kong Q, Wang L, Chen Y et al (2009) Effect of various pretreatments on crude algal lipid extraction. American Society of Agricultural and Biological Enginners Annual International Meeting (ASABE) 6: 3584-3591.

77. Jeon BH, Choi JA, Kim HC, Hwang JH, Abou-Shanab Rai, et al. (2013) Ultrasonic disintegration of microalgalbiomassand consequent improvement of bioaccessibility/bioavailability in microbial fermentation. Biotechnology for Biofuels 6: 37.

78. González-Fernández C, Sialve B, Bernet N, Steyer JP (2012) Comparison of ultrasound and thermal pretreatment of *Scenedesmus* biomass on methane production. Bioresource Technology 110: 610-616.

79. Tiehm A, Nickel K, Zellhorn M, Neis U (2001) Ultrasonic waste activated sludge disintegration for improving anaerobic stabilization. Water Resource 35: 2003-2009.

80. Choi JA, Hwang JH, Dempsey BA, Abou-Shanab RAI, Min B, et al. (2011) Enhancement of fermentative bioenergy (ethanol/hydrogen) production using ultrasonication of *Scenedesmus obliquus* YSW15 cultivated in swine wastewater effluent. Energy and Environmental Sciences 4: 3513-3520.

81. Bremauntz P, Fernández-Linares LC, Cañizares-Villanueva RO (2014) Osmotic Stress effectover Carbohydrate Production in a Native Starin of Scenedesmus sp. Natural Resources 5: 5-9.

82. Passos F, Solé M, García J, Ferrer I (2013) Biogas production from microalgae grown in wastewater: Effect of microwave pretreatment. Applied Energy 108: 168-175.

83. Muñoz C, Hidalgo C, Zapata M, Jeison D, Riquelme CR, et al. (2014) Use of Cellulolytic Marine Bacteria for Enzymatic Pretreatment in Microalgal Biogas Production. Appl Environ Microbiol 80: 4199-206.

84. OriginOil™ World biofuels markets (2010) Amsterdam http://wwworiginoilcom/pdf/OOIL_World_Biofuels_Markets_100316pdf

85. The Ames Lab http://www.ameslab.gov [Last accessed April 2014

86. Debirmas M (2009) Biorefineries for biofuel upgrading: A critical review. Applied Energy 86: 151-S161.

87. Solazyme http://www.Solazyme.com [Last accessed May 2013]

88. Alba L, Torri C, Samor C, van der Spek J, Fabbri D, et al. (2012) Hydrothermal Treatment (HTT) of Microalgae: Evaluation of the Process as Conversion Method in an Algae Biorefinery Concept. Energy and Fuels 26 : 642-657.

89. Biller P, Ross A (2011) Potential Yields and Properties of Oil from the Hydrothermal Liquefaction of Microalgae with Different Biochemical Content. Bioresource Technology 102: 215-225.

90. Weizmann C (1919) Production of acetone and alcohol by bacteriological processes. US Patent 1: 315-585.

91. Potts T, Du J, Paul M, May P, Beitle R, et al. (2012) The Production of Butanol from Jamaica Bay Macro Algae. Environmental Progress and Sustain Energy 31: 29-36.

92. Razaghi A, Godhe A, Albers E (2014) Effects of nitrogen on growth and carbohydrate formation in *Porphyridiumcruentum*. Central European Journal of Biology 9: 156-162.

93. Das P, Lei W, Aziz SS, Obbard J (2011) Enhanced algae growth in both phototrophic and mixotrophic culture under blue light. Bioresour Technol 102: 3883-3887.

94. Parry M, Arnell N, Berry P, Dodman D, Fankhauser S, et al. (2009) Assessing the Costs of Adaptation to Climate Change. International Institute for Environment and Development (IIED).

95. LaMonica M (2012) New energy act to fuel flow of 'biogasoline', Tech Culture, CNET.

96. Brennan L, Owende P (2010) Biofuels from microalgae-A review of technologies for production processing and extractions of biofuels and co-products. Renewable and Sustain Energy Reviews 14: 557-577.

97. Sun A, Davis R, Starbuck M, Ben-Amotz A, Pate R, et al. (2011) Comparative cost analysis of algal oil production for biofuels. Energy 36: 5169-5179.

98. Keune N. Algae: Fuel of the Future? National Review Online of the U.S. 08.03.2012. http://www.nationalreview.com/articles/292913/algae-fuel-future-nash-keune

99. Li N (2009) Algae biofuel development suggestions, Science Times, Accessed 2009.

100. Aylott M. (2011). European EnAlgae partnership to unlock the potential of algal bioenergy. http://www.nnfcc.co.uk/news/energetic-algae-project-to-investigate-potential- of-algae-energy-and-fuels. [Last Accessed in October, 2014]

Citation: Sharma M, Thukral N, Soni NK, Maji S (2015) Microalgae as Future Fuel: Real Opportunities and Challenges. J Thermodyn Catal 6: 139. doi: 10.4172/2157-7544.1000139